TOWARDS REAL-TIME POWER MANAGEMENT OF MICROGRIDS FOR POWER SYSTEM INTEGRATION: A DECENTRALIZED MULTI-AGENT BASED APPROACH

by

Christopher Michael Colson

A dissertation submitted in partial fulfillment
of the requirements for the degree

of

Doctor of Philosophy

in

Engineering

MONTANA STATE UNIVERSITY
Bozeman, Montana

November 2012

APPROVAL

of a dissertation submitted by

Christopher Michael Colson

This dissertation has been read by each member of the dissertation committee and has been found to be satisfactory regarding content, English usage, format, citation, bibliographic style, and consistency and is ready for submission to The Graduate School.

Dr. M. Hashem Nehrir

Approved for the Department of Electrical and Computer Engineering

Dr. Robert C. Maher

Approved for The Graduate School

Dr. Ronald W. Larsen

STATEMENT OF PERMISSION TO USE

Christopher Michael Colson

November 2012

DEDICATION

To my wife,
giorraíonn beirt bóthar.

ACKNOWLEDGEMENTS

I extend my sincerest thanks to my committee for their advice and assistance throughout the long process culminating in this document. Especially, I would like to acknowledge Dr. Hashem Nehrir for his dedication to my education and success; his guidance, and advice have been unparalleled. Also, I would like to thank Dr. Bob Gunderson for his deep insights and encouragement. Without both of these fine gentlemen's mentorship, this work would have been unachievable. Further, I thank the National Science Foundation for their fellowship support and the Department of Energy for grant support. Dr. Ratnesh Sharma and Dr. Babak Asghari, both with NEC Laboratories America in Cupertino, CA, provided valuable insight and meaningful discussions leading to improvements during the final stages of this research. Finally, to the men and women of the armed services, especially those operating beneath the waves, it is due to your dedication and service that we may enjoy the luxury of pursuing scientific and technological innovations.

TABLE OF CONTENTS

TABLE OF CONTENTS – CONTINUED

TABLE OF CONTENTS – CONTINUED

LIST OF TABLES

Table Page

LIST OF TABLES – CONTINUED

Table Page

LIST OF FIGURES

Figure Page

LIST OF FIGURES – CONTINUED

Figure Page

LIST OF FIGURES – CONTINUED

Figure Page

LIST OF FIGURES – CONTINUED

Figure Page

LIST OF FIGURES – CONTINUED

Figure Page

LIST OF FIGURES – CONTINUED

Figure Page

LIST OF FIGURES – CONTINUED

Figure Page

LIST OF FIGURES – CONTINUED

Figure Page

LIST OF FIGURES – CONTINUED

Figure Page

LIST OF FIGURES – CONTINUED

Figure Page

GLOSSARY

Alternating current (AC): the conventional form of useful electrical power of sinusoidal form that oscillates direction of current flow at 60Hz.

Apparent power (S): The vector sum of real and reactive powers (see Appendix A).

Cogeneration: A thermal energy recovery process that utilizes a hot stream to transfer energy to a cold stream or conduct useful work. Typically, this process uses waste heat from a thermal source engaged in electricity production to produce additional electricity in combined cycle (CC) processes, or secondary thermal applications, called combined heat and power (CHP), such as heating residential hot water or producing industrial process steam.

Direct current (DC): the form of electrical power of where flow is in a constant direction.

Distributed energy resource (DER): sources of electrical power (< 50MW) connected to local low and medium voltage electrical networks, rather than high voltage wide area power systems, including generations and energy storage technologies.

Distributed generation (DG): the implementation of DER into a local power system, including interconnection and regulation infrastructure.

Energy arbitrage: the practice of, or the derivation of revenue from, storing power purchased at lower cost times and selling it higher price times.

Extra-microgrid: refers to the utility side of the PCC boundary.

Head-space: term derived from fluid dynamics referring to the available capacity margin between generator rated power and generator operating power. This capacity margin is analogous to a tank partially filled with liquid and the volume that remains to be filled.

High voltage (HV): a class of AC voltage levels between 100,000V and 230,000V used to transfer large amounts of electrical power, typically over long distances. Nominal three phase AC voltages are 115kV, 138kV, and 230kV.

Impedance (Z): a measure of the opposition of current flow in a conductor.

Interconnected: an operational mode where a local electrical power system is directly coupled to the wide area power system through one or more PCCs.

Intra-microgrid: refers to the microgrid side of the PCC boundary.

Inverter: a electronically-switched device that converts DC power to AC power.

GLOSSARY - CONTINUED

Islanding: an operational mode where a portion of the power system becomes isolated from the wide area power system. An island remains energized by generation or storage devices within the island.

Low voltage (LV): a class of AC voltage levels less than 1000V used to supply useful loads. Nominal single phase AC voltages are 120/240V; nominal three phase AC voltages are 208V, 480V, and 600V.

Maximum power point tracking (MPPT): an electrical control system that manipulates the output voltage or bus voltage to which a generation source is attached for the purpose of seeking the highest available power output.

Medium voltage (MV): a class of voltage levels between 1000V and 100,000V used for sub-transmission level and distribution of electrical power. Nominal three phase voltages are 4.2kV, 12.5kV, 13.2kV, 69kV [1].

Microgrid: a locally controlled, LV or MV electrical power system that may contain a combination of generation, load, storage devices capable of operating interconnected with the wide area power system or islanded from it.

Multi-agent system (MAS): a collection of autonomous computational entities (agents) which individually perceive and act upon their environment, but collectively interact, cooperate, or compete towards a task or purpose.

Per unit convention (pu): a system that converts power system quantities to fractions of known base quantities used a common references throughout a system. Allow normalization of complex quantities for easier comparison (see Appendix B).

Point of common coupling (PCC): the point of electrical connection between a local electrical power system and a wide area power system.

Real power (P): the portion of electrical power that is useable to perform work. Real power is the average of the product of instantaneous voltage and in-phase current over a period (see Appendix A).

Reactive power (Q): the portion of electrical power that arises when inductive, capacitive, or nonlinear elements are included in the system (see Appendix A). Reactive power represents the energy stored and released in magnetic and electric fields within components that is not available to perform work. Reactive power is the maximum of the product of instantaneous voltage and out-of-phase current over a period (average instantaneous reactive power equals zero).

GLOSSARY - CONTINUED

Single phase (1ϕ): electrical power is transferred by voltages and currents carried over a single conductor.

Three phase (3ϕ): electrical power is transferred by voltages and currents carried over a three nominal conductors.

Watt (W): Unit of power, or energy per unit time (joules/second). Typical usage: 1,000,000W = 1,000kW = 1MW.

Watt-hour (Wh): Unit of energy (joules). Typical usage: 1,000,000,000kWh = 1,000,000MWh = 1,000GWh = 1TWh.

ABSTRACT

The steadily increasing need for electrical power, rising costs of energy, market forces and industry deregulation, an aging infrastructure, tight constraints on new long distance transmission lines, global environmental concerns, and a public demand for greater electrical reliability and security are overwhelming our existing power system. One technology that offers solutions to many of these challenges and addresses smart grid objectives directly is: microgrids. A microgrid is a small (typically several MW or less in scale) power system incorporating distributed generators, load centers, potentially storage, and the ability to operate with or apart from the larger utility grid. Properly managed, assets connected within a microgrid can provide value to the utility power network, improve energy delivery to local customers, and facilitate a more stable electrical infrastructure, benefitting environmental emissions, energy utilization, and operational cost.

While microgrids can achieve significant improvements for customers and utilities alike, microgrid research is in its infancy and, to date, a comprehensive means of managing microgrid operations has not been realized. In this work, two primary efforts are undertaken. First, given the lack of a comprehensive software test bed for microgrids, a simulation environment capable of incorporating microgrid operational concepts, electrical modeling, asset dynamics, and control conditions is developed. Second, using the simulation environment, an enhanced decentralized multi-agent power management and control system is designed and evaluated for the purpose of supervising multi-objective microgrid operations under normal and emergency conditions. Results presented demonstrate effective multi-agent methods that yield improved microgrid performance, as well as facilitate coordinated system decision-making without reliance on a centralized controller. These advancements represent innovation towards the autonomous operation of microgrids, as well as provide important insight into new trade-off considerations associated with multi-objective design for power management.

Microgrids are infrastructure elements that bridge the gap between emerging energy technologies and the existing power system. Simply put, smart grid objectives including higher penetration of renewables, integration of storage, delivery efficiency improvements, more responsive system elements, stronger resiliency, and improved flexibility will be difficult to achieve without microgrids. The simulation environment developed and the power management methodology presented are important steps towards enabling microgrids and realizing their benefits.

CHAPTER 1

INTRODUCTION

1.1 Electrical Energy in the United States

Today, the overwhelming majority of American homes, businesses, and factories rely on a steady supply of electrical power. In 2003, the National Academy of Engineering declared that the electrical infrastructure in the United States is one of the greatest engineering marvels of the 20th century, comprising the single largest interconnected system in the world [1.1]. However, dramatic forces are, and have been, at work changing the fundamental means of supply and distribution of electricity throughout the nation. Unfortunately, rising demand for electricity, an aging delivery infrastructure, and an uncertain energy future are risks to this complex and critical system, further imploring change. The efforts to prepare for the energy future will likely include measures to modernize the electrical grid, enhance the quality and reliability of the energy supply, diversify how the nation sources its immense hunger for electricity, and address the looming crisis of environmental impact of emissions from energy consumption.

This introductory chapter is intended to expose the reader to the myriad of challenges that face the United States electrical power system and how a new technology called microgrids may be an important solution to facing them. Immediately following this chapter, the state-of-art for microgrids is presented. Additionally, in Chapter 2, the contribution to furthering the microgrid state-of-art by the investigations into multi-agent power management and control for microgrids detailed in this dissertation is explained. Approached concurrently or separately, Chapters 1 and 2 highlight the "how" and "why" of modern power systems in the United State, the role microgrids may play, and a new approach to microgrid integration and operation. Ultimately, Chapters 1 and 2 will give the reader a strong basis by which to understand the merits of the work detailed in the chapters that follow.

1.1.1 Background

Being one of the most complex, interconnected systems on the planet, describing the issues that surround electricity generation, transmission, and distribution is complicated. However, some fundamental concepts are presented in this section to give the current state of U.S. electrical power and why new solutions are desperately needed.

In 2011, the most recent year for which comprehensive data is available, the total capacity available to serve domestic electricity demand in the United States was 1,138,638 MW, as indicated by the 2010 nameplate ratings of all electrical generation installed. This installed capacity was divided amongst a diverse assortment of generation sources, as shown in Figure 1.1. The proportions of installed capacity do not tell the whole story, however, when compared to the actual quantities of electricity derived from the installed assets. Today, almost half of the electricity generated in the United States comes from coal, as shown by the proportions of electrical energy actually produced during 2011, in Figure 1.2. It is noted that in 2011, the net electrical energy produced by Hydroelectric Pumped Storage (not shown) was -0.11% indicating overall consumption of electrical energy for that generation sector [1.2].

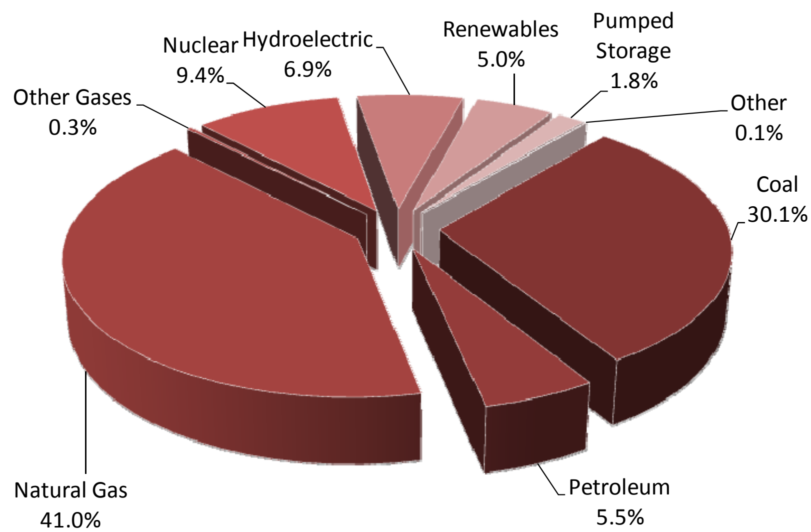

Figure 1.1. 2011 U.S. electric power industry installed capacity by nameplate [1.2].

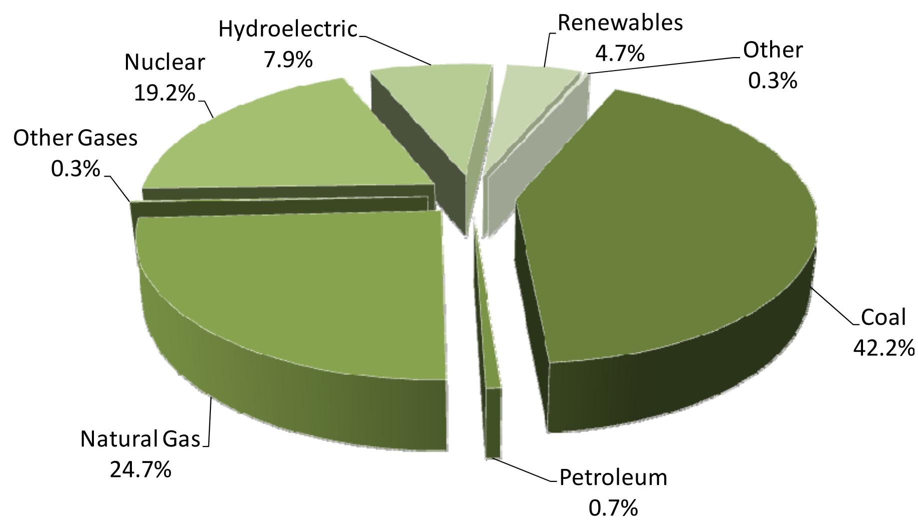

Figure 1.2. 2011 U.S. electric energy produced by generation source [1.2].

The electrical energy produced by the nation’s power plants is consumed by three primary sectors: residential, commercial, and industrial, as well as a very small transportation sector. Currently, the total electricity supply is split about equally between sectors, as shown in Figure 1.3 [1.3]. The revenue derived from each sector, however, shows the premier importance of residential electricity sales, accounting for almost half of all domestic electricity revenue, shown in Figure 1.4 [1.4]. The National Energy Information Administration (EIA), part of the U.S. Department of Energy (DOE), projects that American electricity demand will grow from 3,596 million MW-hrs in 2009 (actual) [1.5] to 4,666 million MW-hrs in 2030 (projected) [1.6]; a 29.8% increase. Growth rates by customer sector are expected to grow 1.7% per year for commercial customers, 0.6% per year for residential customers, and 0.6% per year for industrial customers by 2030 [1.7]. Over the next twenty years, this monumental growth in demand is expected to require $697 billion dollars of investment in new generation alone [1.8]. Going forward, the nation will only become more dependent upon our vital electrical infrastructure. The costs and challenges of maintaining the existing system and expanding to meet future demands will be top issues for lawmakers, regulators, industry professionals, and engineers for the foreseeable future [1.9].

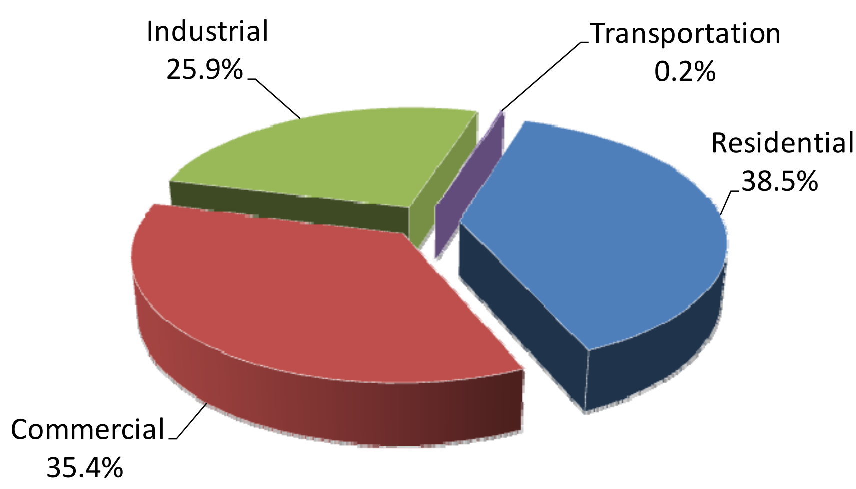

Figure 1.3. 2010 U.S. total electrical energy consuption by sector [1.3].

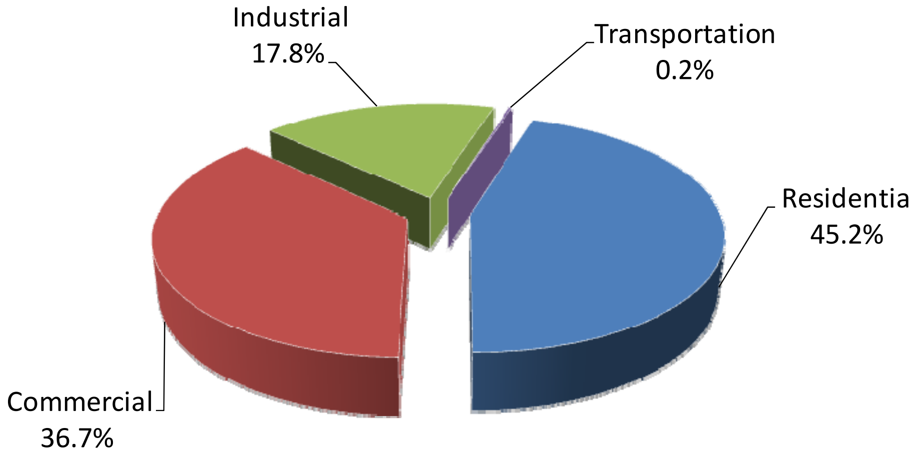

Figure 1.4. 2010 U.S. total revenue from electricity sales by sector [1.4].

The low cost of coal, totaling $40.48 per MW-hr of electricity generated, of which about $25.22 per MW-hr is the actual cost of delivered fuel [1.2, 1.10], and its abundance are the primary reasons why coal continues to be the dominant fuel consumed for electric power production, not only in the United States, but worldwide. As of early 2010, there were 22 coal-fired power plants under construction in the U.S., amounting to 13,755 MW of new nameplate capacity. Building of new coal plant facilities is expected to continue at this level at least through 2015 [1.11]. Unfortunately, even the most advanced coal combustion technologies for electricity generation have significant environmental issues, including the production of carbon dioxide, sulfuric and nitric oxides, and airborne particulate matter. Additionally, existing coal combustion power plants are only able to achieve about a one-third conversion of the chemical potential energy into electricity [1.12]. Natural gas, on the other hand, remains a more expensive fuel despite a drop of over 30% year-to-year in natural gas prices from 2011 to 2012 [1.13]. Natural gas power costs about $57.55 per MW-hr of electricity generated, of which $31.43 per MW-hr accounts for the cost of fuel using the most recent available data from July 2012 [1.2, 1.10, 1.13], but has experienced the largest growth in new capacity implementation over the past decade. In expectation that this trend will continue, the National Petroleum Council projects that over 90% of the new U.S. electrical power plants constructed by 2026 will be fueled by natural gas [1.14]. Conventional electricity production from natural gas almost exclusively involves combustion in turbines roughly 35-45% efficient at converting the energy within natural gas to electricity [1.15]. While the gas combustion process is relatively efficient, it still produces exhaust that is environmentally problematic. High concentrations of gaseous carbon dioxide, sulfur dioxide, and other hydrocarbon products are released from the gas turbine combustion process, as with coal combustion.

Alternatively, nuclear plants generate vast amounts of electrical power without generating adverse environmental emissions and at low cost, about $21.69 per MW-hr of electricity produced. Data on the costs of nuclear fuel and refueling operations, expenses that may occur only every ten to twenty years of plant operational life, are not available. Along with hydro-generation power plants, nuclear power is seen as a viable alternative to fossil fuel combustion plants, such as coal and natural gas. In 2011, there were 104 U.S. commercial nuclear generating units fully licensed to operate at 66 sites, but heavy governmental regulation and widespread negative public perception of nuclear power hampers construction of new centralized plants. Despite huge governmental guarantees, most recently in the U.S. Energy Policy Act of 2005 [1.16], the U.S. had only one new nuclear power plant under construction, the Watts Bar 2 plant, owned by the Tennessee

Valley Authority, as of January 2011. Seventeen additional nuclear plants have been proposed and applications are pending before the NRC, however the earliest that the first plant could come online is 2016 [1.17]. A problematic nuclear safety image and difficult approval process are similar to the obstacles that new large-scale hydro-generation plants face from wildlife and land-use concerns in the United States. In both cases, although each source is expected to grow in capacity over the next 25 years, their overall share of U.S. electrical generation capacity will stagnate or decrease, remaining about 20% for nuclear and a decrease from 7% to 5% for hydroelectric sources [1.18].

Renewables are an alternative to conventional generation. While more costly at present, renewables can offer cleaner energy, be efficiently scaled for use within livable communities, and can eliminate fuel dependence. As of 2011, all renewables, including wind, solar thermal, photovoltaic, biomass, and geothermal generation, but excluding conventional hydroelectric generation, with generating costs varying from $40-$250 per MW-hr, accounted for about 5% of the total installed capacity [1.2]. This is notable for two primary reasons. First, while the proportion of installed renewable generation capacity has more than doubled over the past decade, from 2.0% (1999) to 5.0% (2011), the quantity of electricity produced by renewables has not kept pace. In fact, between 1999 and 2009, while installed nameplate capacity of renewable generators went up 204%, the actual quantity of electrical energy they produced increased only 77%, as shown in Figure 1.5 and Figure 1.6 [1.19]. It is noted that in 1999 and 2009, the net electrical energy produced by Hydroelectric Pumped Storage (not shown) was -0.16%

and -0.11%, respectively, indicating overall consumption of electrical energy for that generation sector.

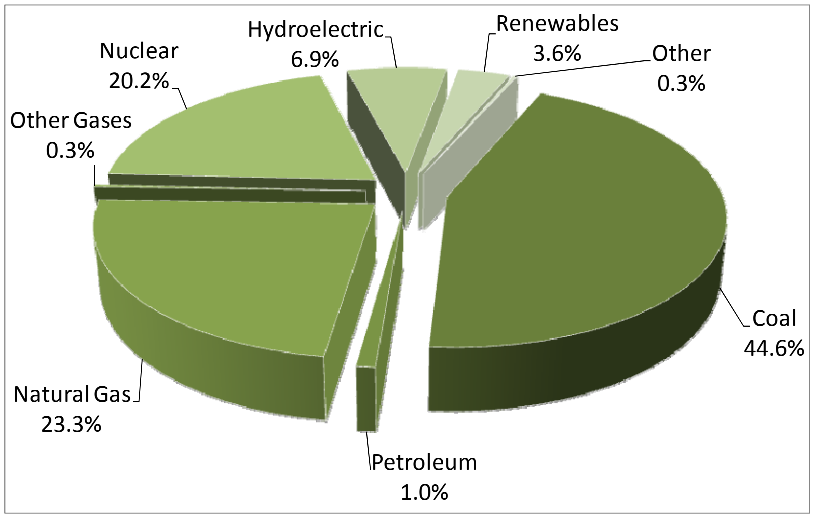

Figure 1.5. 2009 U.S. Electric energy produced by generation source [1.19].

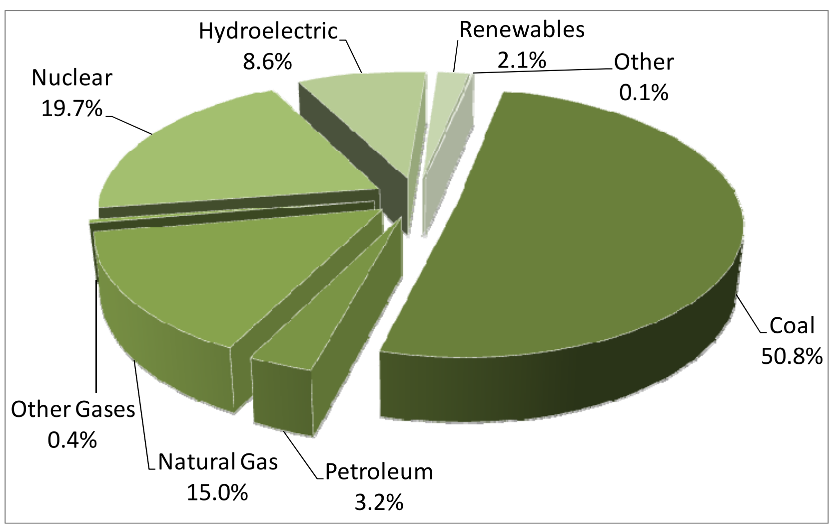

Figure 1.6. 1999 U.S. electric energy produced by generation source [1.19].

The phenomenon of disparate increases in renewable capacity-to-production is primarily explained by a significant drop in overall renewable generation capacity factor, shown in Figure 1.7. It is noted that this data has not been reported by the EIA since 2009 [1.20]. Capacity factor is the ratio of actual electrical energy produced by a generator over a fixed period to the maximum energy the generator could produced, as indicated by its nameplate power rating. The average capacity factor for renewable generators installed in the U.S. declined over the decade because of the huge increases in wind turbine facilities, shown in Figure 1.8. Where utility-scale wind turbines typically exhibit capacity factors between 20-40%, the growth of the wind generation sector caused the average capacity factor for the U.S. renewable generation mix to suffer significantly. In comparison, biomass plants can exhibit 80% capacity factors, while photovoltaic installations show 12-15% [1.21]. The overall effect over the past decade has been large growth of U.S. renewable generation capacity, while modestly increasing the actual production of renewable energy, resulting in capacity-to-production of nearly 3:1. Clearly, the choice to commit capital to new renewable generation is hampered by the perceived need to install three times the nameplate capacity to actually produce equivalent quantities of electrical energy to conventional, non-renewable sources [1.20].

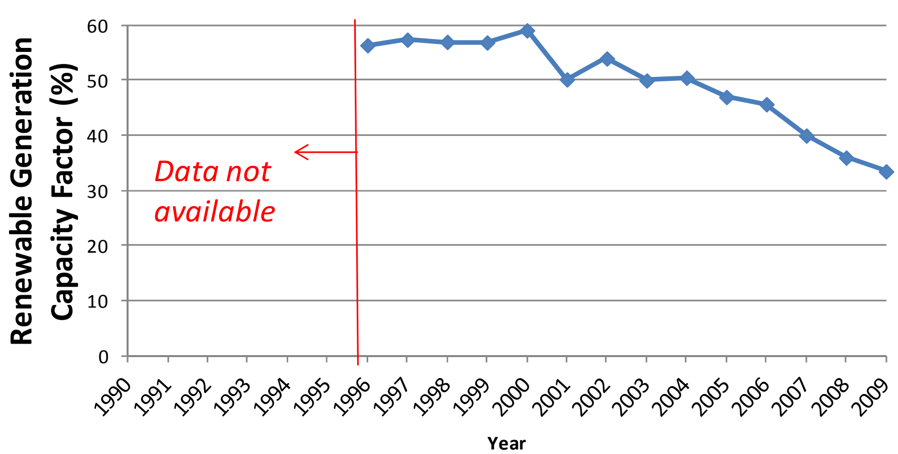

Figure 1.7. 1996-2009 U.S. renewable generation annual capacity factor [1.20].

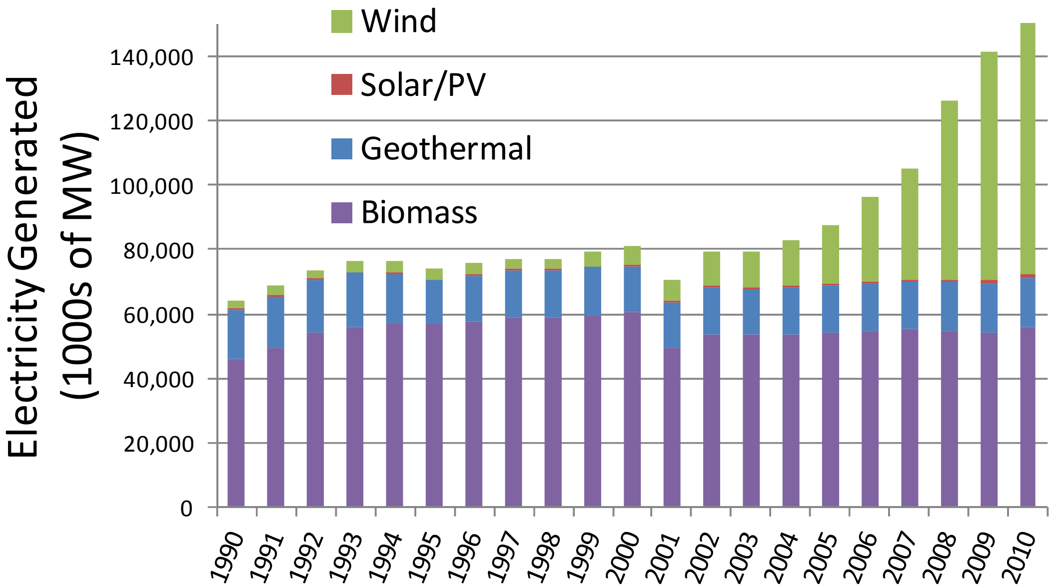

Figure 1.8. 1990-2009 U.S. electric energy produced by renewables [1.20].

One potential solution to improve the capacity factors for installed renewables are distributed energy resources (DER) that produce LV electricity close to the point of use. At the same time, DERs can assist stabilizing the electrical network, provide power during system interruptions, and facilitate capacity growth in a more customized way. Since the latter half of the 1990s, the DOE has defined DERs as utility grid interconnected power-producing facilities up to 50 MW in capacity. In effort to better quantify the population of DER facilities in the U.S., in 2010, the EIA modified its definition of DER to dispersed or distributed generators with nameplate capacities of 1MW or less [1.22]. One of the most important policy roadmaps to describe the future of DER integration in the U.S. was the Grid 2030 vision published by the DOE in 2003. The most unique attribute of Grid 2030 is the establishment of a conceptual design for the future U.S. electrical infrastructure. It lays out a three-tiered framework whereby the national electrical grid would be formulated by a high voltage transmission “backbone”, smaller regional interconnections, and at the lowest level, local distributed mini- and microgrids with DERs [1.23]. Notable because of its forward-looking character, the Grid 2030 document was the first major policy description to emphasize the importance of localized mini- and microgrids to the security, stability, and renewability of the national electrical infrastructure. This concept has remained a key component of U.S. energy policy towards implementation of a comprehensive smart electrical grid, reaffirmed as recently as the U.S. President's National Science and Technology Council smart grid policy of June 2011 [1.24]. However, despite U.S. goals, and while the total capacity of wind and photovoltaic DER installations grew 13 times from 2004 to 2010, they still amounted to just over 2,000 MW, encompassing a 9% share of total U.S. DER capacity, as shown in Figure 1.9. Likewise, the total capacity of DER added during the past decade accounted for only 7-9% of the 249,532 MW of U.S. total electrical generation added during the same period [1.25, 1.26].

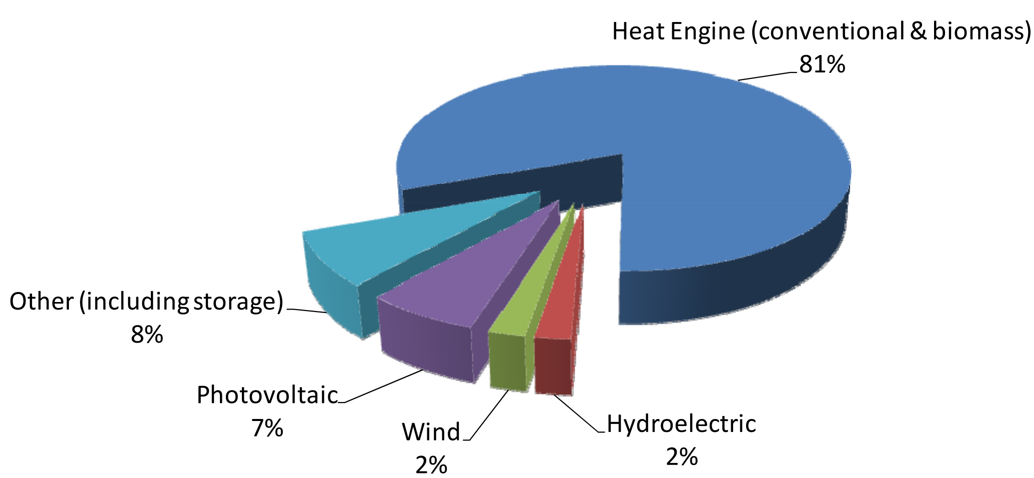

Figure 1.9. 2010 U.S. total DER generation (1MW or less nameplate) by source [1.2].

In the U.S., the nationwide electrical grid network is divided into three major interconnections, Eastern, Western, and Texas; and subdivided into regions by the National American Reliability Corporation (NERC), the privatized, federally-supported standards and enforcement regulatory entity for the electricity industry. Power producers, trading businesses, and municipalities operate within the NERC regions according to applicable state and federal regulations. A major concern for the regional power conglomerates is the ability to balance interregional electricity capacity with the regional demand. Because electricity can be traded in a wholesale manner, similar to commodities, on a spot market basis, power producers with excess supply can sell electrical energy within or across these regions. Projecting forward, each region faces its own set of challenges in ensuring that adequate generation and transmission assets are in place to serve growing demand. Capacity margin is a measure of the percentage of generation supply that exists in excess of electricity demand. On an average basis, capacity margin can indicate the overall, long term health of a NERC region by describing the preparedness of that region for expanding customer consumption. In 2010, only four of the eight NERC regions had total capacity margins equal to or greater than 20%, an accepted safe operating baseline [1.27]. In addition, the ten-year trend of half the regions was flat or downward. This is a troubling sign, as shown in Figure 1.10.

Although the EIA projections of growing residential, commercial, and industrial demand described above are modest on a national level, the trends in capacity margin indicate that some regions will be more deeply affected by the speed by which demand will blossom relative to the quantity of generation is brought online. Moreover, each

NERC region has unique characteristics that make them better or worse fits for renewable technologies, distributed generators, and other infrastructure improvements.

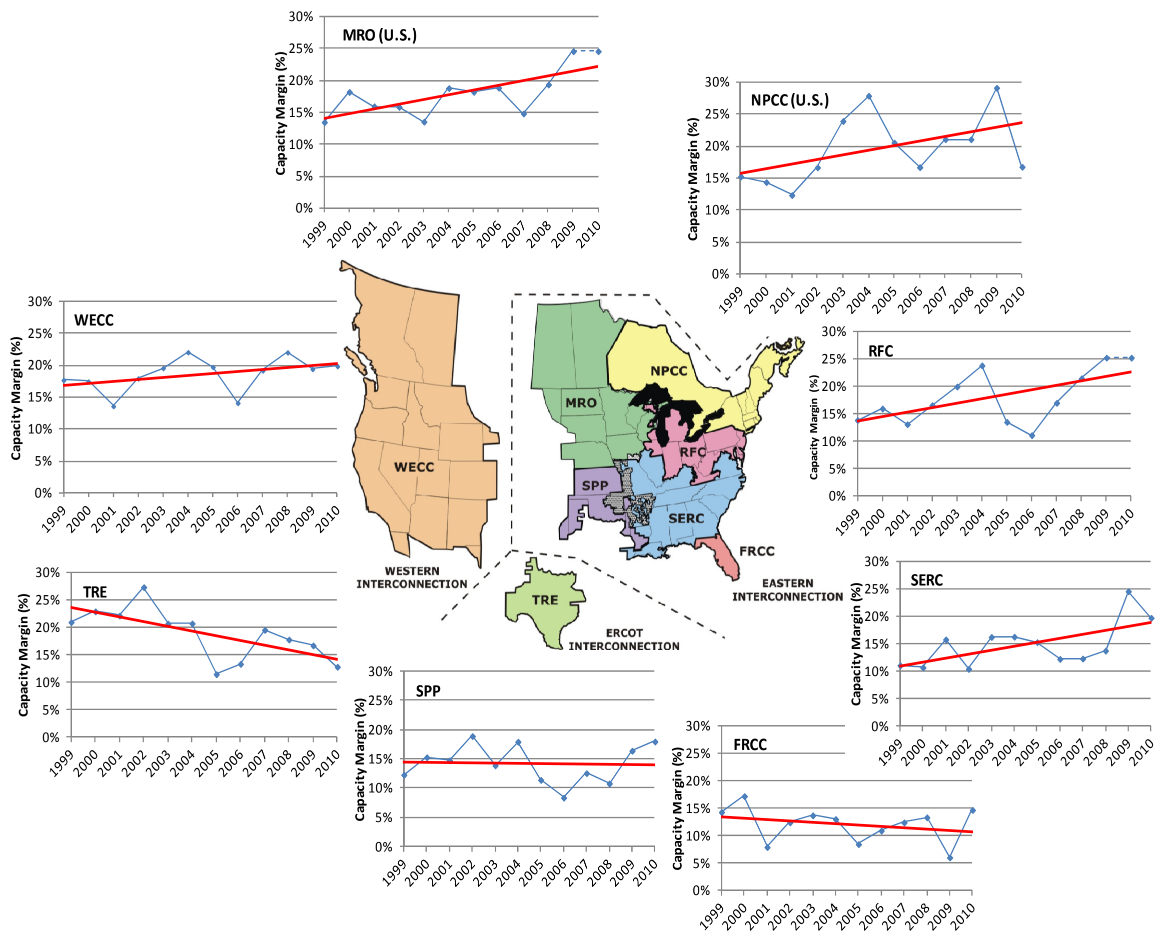

Figure 1.10. Capacity margin trends for U.S. NERC regions [1.2, 1.27].

1.1.2 The Burden of Fossil Energy

No discussion of the state of electrical energy generation, transmission, distribution, and consumption would be complete without surveying the sources from which the energy is derived. Although many innovative and promising technologies for sustainably producing electrical energy without reliance upon fossil fuel sources exist, by a large margin, Americans today continue to rely on carbonaceous fuels for electricity.

1.1.2.1 Sources of American Electrical Energy. Today, almost half of the electricity generated in the United States comes from coal [1.28]. The low cost and abundance of coal are the primary reasons why coal will continue to be the dominant fuel used for electric power production, not only in the United States, but worldwide. Unfortunately, even the most modern coal combustion technologies for electricity generation have significant environmental issues. Additionally, existing coal combustion power plants are only able to achieve about a one-third conversion of the chemical potential energy into electricity [1.29]. Although new coal technologies are in development, it is strategically unwise to expect that coal as a fossil fuel will be a long-term solution to the energy needs of the nation.

Natural gas utilized for electricity production is the fastest growing fuel sector. The National Petroleum Council projects that over 90% of the new electrical power plants that will be constructed by 2026 in the United States will be fueled by natural gas [1.30]. While not disputing this claim, the Administrator of the EIA testified on March 4, 2008 before the U.S. Senate Committee on Energy and Natural Resources that current EIA projections show that “under current laws and regulations, natural gas is expected to lose market share to coal in the electric power sector as result of a continued increase in natural gas prices into the latter half of the projection (2018 and later) and slower growth in electricity demand” [1.31]. Natural gas proponents bolster support for their fuel by pointing out that because natural gas distribution networks already exist, making the possibility of fueling distributed electricity generating sites feasible. Because of this, natural gas has a significant advantage over coal which cannot be easily distributed as an energy source and is best relegated to large, central power production. Conventional electricity production from natural gas almost exclusively involves combustion in gas turbines. Modern gas turbines are about 35-45% efficient at converting the energy within natural gas to electricity [1.32]. While the combustion process is relatively efficient, it still produces exhaust that is environmentally problematic. High concentrations of gaseous carbon dioxide, sulfur dioxide, and other hydrocarbon products are released from the gas turbine combustion process. New reserves and domestic supplies of natural gas have skyrocketed in the past two years, with an increase of almost 8 billion cubic feet per day additional production since 2010 [1.33]. This increase in supply has caused dramatic drop in natural gas prices, amounting to wellhead prices 40% lower in 2012 than in 2010. It is noted that this drop in wholesale natural gas price has only caused residential natural gas prices to trend 4.3% lower over the same period [1.33]. Additionally, prices are forecasted to rebound from the lows in 2012 and trend 10-15% higher in 2013 [1.33].

In the case of conventional combustion-type electricity plants, including combustion-steam and gas turbine technologies, subsystems exist and are commonly employed to recover emission gases. These "scrubber" devices, however, reduce the overall efficiency of the plant and add significant cost. Applying technology that was originally developed for the oil extraction industry, large amounts of research capital are being expended on new large-scale carbon dioxide sequestration techniques. If proven and employed, the carbon emissions from conventional power plants may become less critical. Until better success and cost effectiveness is shown, the limitations of existing combustion power plant technology and concerns over emissions will continue to spur growth in the area of electricity production from alternative means.

1.1.2.2 Concerns with Coal Combustion. Coal burned for electricity is purported to be the cheapest means of deriving electrical power in the world today. As has already been established, if the electrical capacity gains made in the United States over the next 25 years are going to be installed by a smaller class of larger generation corporations, then the least expensive technology is going to dominate. Of course, this technology is coal. It follows, therefore, that a closer evaluation of the true cost of coal be conducted, both from an engineering and policy/planning perspective. Given the most relevant and immediate energy challenge facing the United States today, this is a critically important analysis.

Depending on the terrestrial source, the energy content of coal varies dramatically. Based on the calorific value of class C Subbituminous coal, the most common coal product from the Montana/Wyoming Powder River Basin (PRB) area, the average energy content is: 8,420 BTU/lb or 16.84 million BTU per short ton [1.34]. Coal-fired power plants vary widely in demonstrated First Law of Thermodynamics efficiency and Table I presents the approximate mass of PRB coal that a coal plant would require to generate 1MW-hr of electrical energy, based on its thermal efficiency.

According to the EIA weekly coal report ending October 6th, 2012, the spot market price for PRB (Low-Sulfur) coal was $10.25 per short ton [1.35]. Figure 1.11 shows the fuel costs for coal-fired power plants of increasing thermal efficiencies. Excluding the added costs of fuel transportation, storage, and other expenses, Figure 1.11

demonstrates how cheap electricity from coal is. For comparison purposes, coal mined and burned nearby to the power plant (such as the Colstrip Power Station in Colstrip, MT proximate to PRB coal beds) is analogous to wind farms that harvest local wind resources or photovoltaic arrays that extract the local solar resource. However, given the typical $70 per MW-hr for large-scale wind power or over $90 per MW-hr for photovoltaic power, coal can seem very attractive.

Table 1.1. Characteristics of 1MW-hr (electrical) derived from PRB coal.

Coal Plant Efficiency	BTUs from Coal (1MW-hr, 1W = 3.41BTU/hr)	Pounds of Coal Required (8,420 BTU/lb)
20%	17,050,000	2024.94
25%	13,640,000	1619.95
30%	11,366,667	1349.96
35%	9,742,857	1157.11
40%	8,525,000	1012.47
45%	7,577,778	899.97

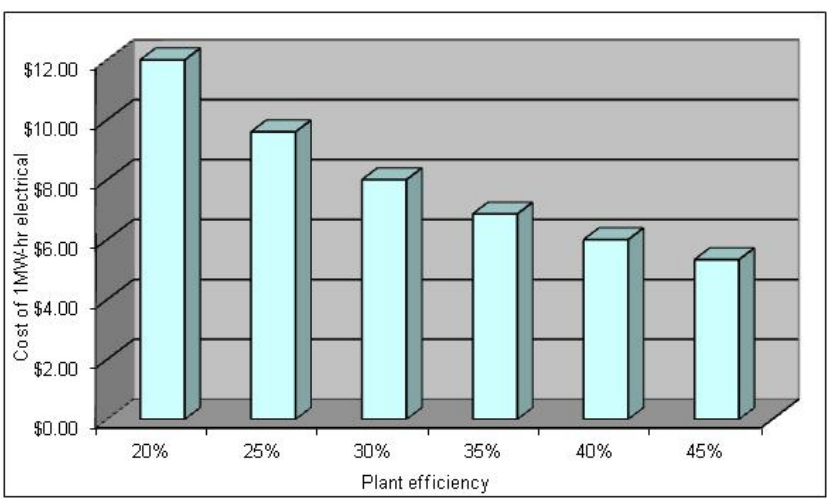

Figure 1.11. Plant efficiency versus cost of 1MW-hr (electrical) derived from PRB coal.

PRB coal is 0.32% Sulfur, 5.2% Ash, 30.2% Water, 30.6% Volatile Matter, and 33.8% Fixed Carbon by weight [1.36]. The primary exhaust products of coal combustion are oxides of: carbon (CO_x), sulphur (SO_x), nitrogen (NO_x), heavy metals, and particulate matter. Of these coal emission components, mercury is a biological neurotoxin, SO_2 and NO_x can cause acid rain, and C02 is the most important greenhouse gas held responsible for climate change [1.37]. Total hydrocarbons (THC) are also a concern, consisting of all volatile and semi-volatile organic compounds that are emitted when organic fuels such as coal are combusted. THCs are of particular concern when emitted because they not only can have a detrimental effect on the atmosphere as greenhouse gases [1.38], but also have a direct negative effect on human health. Of these atmospheric emissions, only CO_2 is not currently regulated by the U.S. Environmental Protection Agency (EPA) under the authority of the amended 1990 Clean Air Act.

According to the Department of Energy, within the U.S., one kW-hr of electricity produced from coal emits 2.095 pounds of CO_2 (also referenced as 212.7 pounds per million BTUs) into the atmosphere [1.39]. According to the EPA, 35.0 pounds of SO_2 and 8.0 pounds of NO_x are emitted per short ton of subbituminous coal burned for electricity production [1.40]. Of the 4,064,702 GW-hrs of electricity produced by the U.S. in 2006, about 1,990,926 GW-hrs were generated from coal [1.41]. In an international context, 17,350,000 GW-hrs of electrical energy was generated by all nations in 2006. The coal-based electricity produced by the U.S. was about 11.5% of this total quantity of electrical power generated by the world. The environmental impact of the U.S. coal-fired electricity industry equated to 2,352,418,430 short tons

(2,134,100,000 metric tons) of CO_2 released into the atmosphere. By interpolation, if every pound of coal burned in the U.S. was from the Powder River Basin in 2006, the U.S. would have maintained approximately a 30.78% average coal plant thermal efficiency based on the amount of CO_2 released and corresponding electricity produced in 2006. Of course, the predominance of coal consumed by the U.S. was in fact higher BTU coal than that of PRB origin. As a result, this reflects that although more BTUs were produced in coal plants in 2006, the actual average plant efficiency in the U.S. was worse than 30.78%. The combined environmental impact of coal plants of various efficiencies is shown in Figure 1.12. It is important to note that all coal combustion power plants in the United States have been statutorily required to comply with the Clean Air Act since 1970, but carbon emissions remain uncovered by these guidelines.

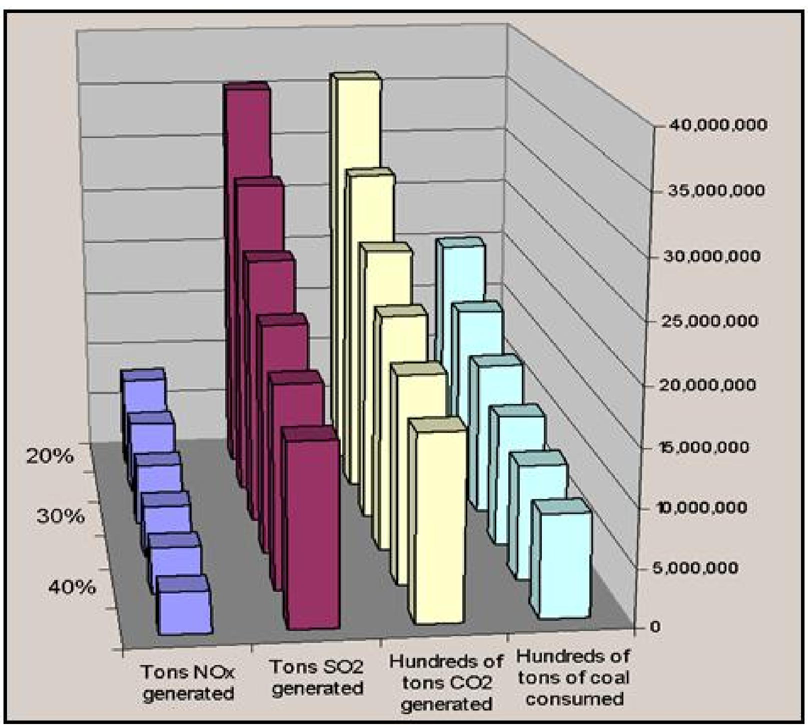

Figure 1.12. Environmental cost of coal based on plant efficiency [1.39, 1.40, 1.41].

Straight-forward compliance with Clean Air Act requirements for power plants can lend a false sense that power plant emissions are "clean". On the contrary, the sheer scale of total power plant emissions can be shrouded by compliance with the SO_x and NO_x emission requirements. For example, the Colstrip Power Plant, located in Colstrip, MT is one of the top-twenty largest coal-fired power plants in the United States. It maintains a combined nameplate capacity between four combustors and turbines of 2.094 GW [1.42]. Despite producing large amounts of airborne carbon, sulfur, and nitric oxides annually, these quantities are consistently in compliance with Clean Air Act and EPA requirements. However, the Colstrip plant continues to be the tenth largest emitter of mercury (1,570 pounds in 2010) in the U.S. [1.43] which is of significant concern for human and environmental well-being, not to mention being the 8^{th} largest CO_2 producing entity in North America in 2005 [1.44].

Within the past decade, carbon dioxide released as a byproduct of power generation has been inculcated as an influential climate change precursor. Despite significant attention globally, it has been virtually impossible to put a price on CO_2 emissions. The key point, however, is that when the cost of carbon is factored in to coal-based electricity, its attractiveness as a fuel is severely diminished. One organization that has attempted to offer guidance in the face of this enormous challenge is the United Nations Intergovernmental Panel on Climate Change (IPCC). This organization is most notable for the 2007 Nobel Peace Prize that it was awarded for work on global issues. In their 2007 report to worldwide policymakers, the IPCC predicts that impacts of climate change are "very likely to impose net annual costs which will increase over time as global temperatures increase". The peer-reviewed estimates of what the IPCC calls the "social cost" of carbon is an average $12 per ton of CO_2, based on 2005 numbers. The IPCC is quick to point out, however, that the estimated range of cost from 100 diverse estimates is from -$3 to $95 per ton of CO_2. It is important to note that negative estimates of cost indicate that CO_2 would in fact have a salable value as a commodity. The IPCC attributes the variability in carbon cost primarily to "differences in assumptions regarding climate sensitivity, response lags, the treatment of risk and equity, economic and noneconomic impacts, the inclusion of potentially catastrophic losses, and discount rates". Of course, these cost estimates do not tell the whole story when, in the context of global climate change, the impact of carbon on different regions and populations are not equal [1.45].

1.1.3 Alternatives to Combustion-based Energy

The case has been made for distributed generation as a means of improving aspects of the electrical grid and consumer power markets. Additionally, the case has been presented as to the hidden cost of what is seemingly the most attractive fuel for electricity production: coal. The next challenge is to evaluate what alternative technologies exist and can be adapted to meet distributed generation goals. For electricity production to move forward, the infrastructure for smaller alternative generators to be distributed close to load consumers and counter the negative effects of centralized dirty power must be developed. Numerous alternative electricity producing systems exist and some have even been incorporated into electrical grids for distributed generation. However, the problem that the nation faces is not simply limited to the fuel that we choose to generate electricity, but how to adapt an electrical transmission and distribution system that is designed for one-way centralized generator-to-load power flow to accept these alternative producers. Concurrently, if we can facilitate alternative generators close to load centers, value can be added by capitalizing on additional properties inherent to them, such as: capturing waste heat from their high temperature exhaust streams for cogeneration purposes or eliminating summer heat loads with innovative installation practices. This section lays out some of the most promising technologies that can be employed as DER and are suitable for microgrid applications.

1.1.3.1 High Temperature Fuel Cells. Fuel cells are electrochemical devices, similar to batteries, which do not lose their voltage potential when supplied with a steady source of fuel. Contrary to other electrochemical devices, with a constant fuel supply, fuel cells can provide significant electrical power without any loss of capability over time. The typical oxidation-reduction reaction that occurs within a fuel cell involves hydrogen, which is broken into free protons and electrons. Similar to a combustion reaction, oxygen is required as the oxidizing agent.

There are several fuel cell technologies that utilize varying materials and operate at different temperature ranges. The two most common types of high temperature fuel cells are the Molten-Carbonate and Solid Oxide. Partly because of their high temperature operation, these fuel cells can achieve 40-60% efficiency at converting the energy of an input fuel to electricity. Efficiencies of this order are comparable or higher than the coal fired steam cycle (88% efficient boiler coupled with a 45% efficient steam turbine equates to about 40% overall) and the gas turbine cycle (about 35% efficient) [1.46].

Furthermore, fuel cells offer several advantages over current generation technologies in that they are smaller, quieter, and because they lack a combustion process, yield only water as a byproduct.

High temperature fuel cells, specifically Solid Oxide Fuel Cells (SOFCs), have the added benefit of being able to utilize bonded hydrogen fuels, such as methane. Due to the unique characteristics within a high temperature SOFC, methane fuel can be internally reformed into hydrogen gas, facilitating the electrochemical reaction. The use of methane, most commonly available as three pound-per-square-inch (3 psi) natural gas (70-90% methane) is very common in homes, businesses, and industry. Higher pressure natural gas distribution pipelines (1300 psi) [1.47] transfer fuel over great distances. In almost all cases, the high pressure natural gas lines are buried and more acceptable to the public than overhead electrical transmission lines. SOFCs can capitalize on distributed natural gas supplies to more efficiently produce electricity apart from central plants.

Fuel cells can be scaled from sizes small enough to be used in automobiles to large enough to be utilized as medium-scale stationary power stations. The electricity produced by fuel cells is direct current (DC). In order for this DC electricity to be utilized on the commercial power grid, it must typically undergo boost DC-DC conversion and inversion to alternating current (AC). Additionally, because of fuel cell characteristic response to increased loading, power shaping and control devices must be utilized for power stability and protection of the fuel cell.

Various aspects of solid oxide fuel cell development are currently being undertaken by numerous companies such as Acumentrics, Altair International, Honeywell, McDermott Technology, Siemens Westinghouse, Ztek Corporation, Delphi, GE Energy, Cummins Power Generation, and others. There are very few production line SOFCs available, but significant investment has been directed towards their development. Although the material and production costs of fuel cells have slowly reduced, their cost currently remains too high for widespread market penetration. This, however, is expected to change over the coming years as material supply and energy demand forces work to bring fuel cell technology into stronger competition.

1.1.3.2 Microturbines. A microturbine is essentially a gas-fired Brayton cycle turbine on a small scale (less than 200 kW net output shaft power). The Brayton turbine cycle requires compression of atmospheric air, the heating of compressed air by fuel combustion, the expansion of the heated air-fuel mixture through a turbine that converts entropy to rotational turbine shaft work, and finally the discharge of exhaust gas to the atmosphere. Typical cycle efficiencies range from 18-35% [1.48].

Microturbines differ from larger combustion turbines in some key ways. First, microturbines typically involve a simple single-stage air compressor and a single-stage turbine assembly. This arrangement is not as efficient or powerful as gas turbines that utilize high compression ratios (13:1/15:1 versus 3:1/4:1 for microturbines) [1.49], but it facilitates a smaller system footprint and simplifies manufacturing. To further simplify microturbine operation, the turbine and generator are coupled by a single shaft with a support bearing between them. Other microturbine designs involve two shaft configurations, but common to both single and dual shaft microturbines are the central bearing. This design simplifies the mechanical operation of the high speed machine.

Dual shaft turbines, also referred to as twin turbine systems, have some advantages over single shaft machines. All turbines operate because of a pressure difference between their inlets and exhaust ports. The larger the pressure difference, the more entropy is converted to useful shaft work. For twin turbine machines, the pressure drop stresses are split between the two turbines effectively reducing the strain on each turbine assembly as compared to a similar pressure difference across a single shaft machine. Twin turbine assemblies offer more flexibility than comparable single shaft machines because of their ability to separate slower turbine speed operations from high speed applications. In other words, the dedicated power turbine within a two turbine machine can be more massive, yet rotate at a lower speed maximizing mechanical efficiency, while a less massive secondary turbine rotates at higher speeds for the benefit of overall system efficiency at auxiliary compression and gasification requirements. Ultimately, when compared at equal shaft power ratings, twin turbine systems offer more design flexibility, slightly better overall efficiency, and more favorable torque/speed characteristics than single turbine machines. These advantages, however, come at greater expense, larger footprint, worse startup characteristics, and more complicated design and fabrication when compared to single shaft construction [1.50].

Currently, the primary developers and manufacturers of microturbines for small-scale electricity or cogeneration uses are: Ingersoll-Rand, Capstone Corporation, ALM Turbine, Elliott Energy Systems, GE Energy Systems, as well as others recognized by the U.S. Department of Energy's Distributed Energy Program. The primary interests of the Department of Energy’s program to foster microturbine development are to [1.51]:

develop higher efficiency, implying fuel-to-electricity conversion efficiency of at least 40%; improve NOx emissions leading to to less than 7 ppm from natural gas fuel; improve material durability achieving a minimum of 11,000 hours of reliable operations between major overhauls and a service life of at least 45,000 hours; reduce the cost of power by lowering system costs to less than $500/kW thereby improving microturbines competitiveness in the power market; and improve fuel flexibility by creating options for multiple fuels including diesel, ethanol, landfill gas, and biofuels.

As with fuel cell technology, the material and production costs of microturbines are coming down. Microturbines have a market penetration lead over fuel cells, mainly due to the scalable nature of the turbine technology and lower capital cost. It remains to be seen whether, in the future, a blend of microturbine and fuel cell applications will become the preferred method of distributed generators.

1.1.3.3 Wind Generation. New installation of wind turbines for the purpose of generating electrical power continues at an astonishing rate. In fact, at the close of calendar year 2011, wind turbine facilities had generated over 50% of the renewable energy in the United States, representing about 1.8% of the total electrical energy consumed that year [1.52]. This growth in wind generation demonstrates a four-fold increase from 2005 and follows a nearly decade-long trend of doubling of wind capacity every 34 months [1.53]. Globally, the trend in wind generation growth is even stronger, with over 38 GW of capacity added in 2009, representing a 31.7% increase over 2008 capacity levels implying the largest percentage gain ever [1.54], followed by the largest one year gain of 40GW of new wind capacity added in 2011 [1.55].

As turbines are brought on-line at an accelerated pace and wind generation technology matures, turbine manufacturers are increasingly investigating better and more robust systems for energy extraction. Lately, interest in PMSGs for large wind turbine design has been rising. This marks a departure from conventional wind generator design that relies on a high-ratio gear box that couples the turbine rotor to the electrical generator rotor. With WECS, the turbine blades attach to the turbine rotor at the hub, transferring the force developed on the blades to the rotor shaft. Although the turbine rotor spins relatively slowly, typically less than 50 RPM for modern large-scale turbines, in conventional turbine systems the gear box steps up this rotational torque to much higher rotational speeds applied at the electrical generator rotor [1.56]. This high speed rotational energy is then converted to electrical energy by means of an electrical generator. As of 2009, nearly three-quarters of utility-grade wind turbine manufactures relied on doubly-fed induction generator (DFIG) technology, by far the most popular technology for wind energy conversion systems (WECS) [1.57]. Commonly, horizontal-axis WECS encompasses the turbine blades, hub link to the turbine rotor, mechanical and gearing systems, the electrical generator, and related electrical components that connect the WECS to the power system [1.58]. However, recent announcements by major industry leaders such as Siemens and General Electric have indicated a new emphasis on PMSG wind generation design, including direct drive arrangements. Primarily, these leading companies are turning to direct drive systems in order to eliminate heavy and maintenance-intensive gear boxes that are very difficult to service in suspended nacelles and especially in off-shore wind assets. By exploiting benefits of PMSGs, wind generator manufacturers are able to directly couple turbine and generator rotors. Additionally, by simplifying the mechanical system, requiring less than half as many parts as a conventional turbine, reduces manufacturing costs [1.59].

Two factors, therefore, stimulate research interest in PMSG technology for wind turbines. First, the significant growth trend of wind generation demonstrates its importance in meeting global needs for electrical power in the future. This is especially true for regions of the United States that hold significant wind resources, such as the Mountain West [1.60]. Secondly, as wind generation technology progresses, it is increasingly evident that PMSG technology has the potential to supplant DFIG technology as the primary means of electricity generation for wind turbines, even at the scale of utility-appropriate turbines. Both of these factors are beneficial for the growth of PMSG wind turbines for microgrid applications, and it follows, that this technology will be the primary one for DER wind turbines in the future.

1.1.3.4 Photovoltaics. Solid-state conversion of solar energy to DC electricity with photovoltaic (PV) cells is a mature technology. With no moving parts and relatively low voltages for individual PV modules, PV can be implemented on nearly any exterior surface with solar exposure. However, the latest laboratory-based conversion efficiency of prototype PV cells remains below 35% and commercially available PV modules remain below 25% efficient [1.61]. These factors imply the need for very large arrays of PV modules to be assembled in order to derive utility-scale quantities of electric power. Due to strong European demand leading to a significant increase in production capacity worldwide, the global production capacity of PV modules has grown from 1.4 GW per year in 2004 to 22.5 GW per year by 2011 [1.62].

This progress has compelled PV module prices to fall in the U.S. from about $5.00 per Watt in 2002 to less than $2.50 per Watt in 2012, although prices are not expected to remain at these low levels beyond 2013 [1.63]. Potentially driven by the low module prices and waning U.S. government programs for new PV projects, a record 1.855 GW of new PV systems were installed in 2011 [1.64]. Although the majority of PV installed during this period was for utility-scale solar facilities, PV remains popular for DER installation for reasons of cost, modularity, and ease of maintenance. While the solar resource at any particular site can be highly variable on an hour-to-hour or day-to-day basis, the annual solar expected production from a site is predictable. Going forward, it is expected that PV will remain a leading DER technology and primary generation source implemented in most hybrid or microgrid systems.

1.1.3.5 Storage Systems. Electrical storage systems allow the accumulation of excess electrical energy generated during periods of low local demand and make it available at periods of high demand. Today, the U.S. integrated power system has virtually no capacity for electrical storage. Primarily, the storage that is available is in the form of pumped-storage hydroelectricity. This involves consuming electrical energy in hydroelectric dam generators (motor action) and transferring downstream water to higher altitude reservoirs for later use. Although the incorporation of storage capacity can facilitate greater power system efficiency and reliability, it has not been cost effective to implement large scale storage. Recently, electrical storage systems have become more attractive for use in conjunction with intermittent renewable, such as wind or photovoltaics. Clearly, storage employed with renewables can reduce the generation capacity necessary during peak demand periods and somewhat mitigate energy flow fluctuations. On a lesser note, storage can reduce the strain on distribution resources, assist frequency regulation, provide voltage support, and improve operating reserves.

Storage technologies used in power system applications hold potential, chemical, or kinetic energies for conversion to electricity at a later time of demand [1.65]. Electric energy storage (EES) devices may be categorized in two major groups: electrochemical and non-electrochemical technologies. The electrochemical EES group is composed primarily of solid-state batteries, including lead-acid or lithium-ion; or flow batteries, including vanadium redox and zinc-bromine devices. Storage technologies that do not rely on chemical potential as the energy storage medium fall into the non-electrochemical category, including pumped hydroelectric, compressed energy storage (CAES), flywheels, and superconducting magnetic energy storage (SMES). Amongst the two categories, various technologies have characteristics that make them more suitable for different applications. The two primary criteria, besides physical and cost factors, that are used for pairing EES to applications relate to power density and energy density. That is, given an EES, how much and how long can it sustain a specified power output. Figure 1.13 gives a representation of various storage technologies and their relative power and energy densities [1.66].

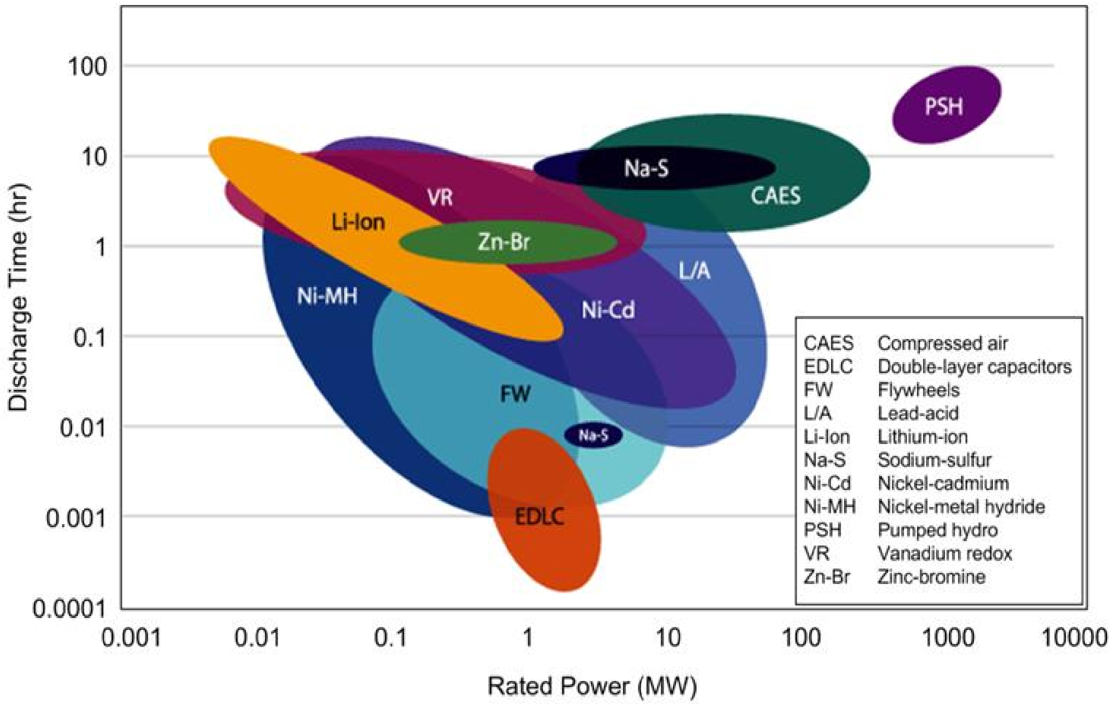

Figure 1.13. Storage technologies power and energy capacities [1.66].

Using information about power and energy density, the suitability of an EES may be further characterized using the following primary power system objectives:

- Improve power quality: characterized by fast response, high power, low energy requirements, most frequently seen for voltage support and frequency regulation applications.

- Provide bridging energy: characterized by high energy demands where power may be required for an extended period, as with generator black starts, contingency reserves, or intermittent renewable generation.

- Improve energy delivery: characterized by smoothing generation intermittency or load demand towards lower operational costs, such as with intermittent renewable or in tiered-pricing energy markets.

For many years, lead-acid storage batteries have been the least costly EES technology for small to medium sized power applications. Recent advances in lithium-ion battery technology is beginning to drive down their cost, as well as making significant improvements over lead acid cycle efficiency (also known as round-trip efficiency), battery life, self-discharge concerns, and EES size and weight. While the per-cycle cost is commonly used to evaluate the capital effectiveness of a potential EES system, there are many other application specific variables that must be considered over the system lifetime, making the EES decision complicated.

Despite the costs, battery storage systems are expected to remain the primary energy storage technology employed in hybrid or microgrid systems in the foreseeable future. As lithium battery technology improves and is scaled for stationary power applications, less versatile lead-acid battery technology is expected to be phased out. However, this transition will take place over the long-term as storage becomes a significant component of emerging power system infrastructure, growing from an insignificant contribution to power system operations today.

1.1.3.6 Cogeneration. The second law of thermodynamics expresses that the "quality" of energy in any system either improves with the input of work or degrades as useful work is extracted. The transfer of system entropy to useful work can only flow in one direction. The total amount of energy that can be extracted from a system is expressed by a combination of the first and second laws of thermodynamics in a quantity called Gibb's Free Energy. Because the total amount of work that can be converted from any themochemical/mechanical/electrochemical system is limited, all energy systems can be compared with only two characteristics: the total amount of available convertible energy and the efficiency of that system at converting it to useful work. This is especially useful when comparing systems that produce electrical energy for commercial, residential, or industrial use. For example, the fuel cell electrochemical process that converts a hydrogen fuel to electrical energy can be compared to the thermal process of a steam boiler and turbine generator that converts coal chemical energy, to thermal energy, to shaft work, and finally to electrical energy. Ultimately, if we know the potential energy of a fuel and the efficiency of a total system process at converting that potential energy to electrical energy, we can compare what would appear to be apples-and-oranges on an apple-to-apple basis.

All thermal energy conversion processes utilize a hot stream to cold stream method for converting fuel energy to electrical energy. Unfortunately, the cold stream often rejects a significant amount of energy that could be converted to useful work to the environment. Another way of looking at this is to consider statistics regarding world electricity production. Although, most of the world's electricity production is by thermal conversion process, the majority of this production does not take advantage of cogeneration methods. As a result, significant amounts of fuel energy are rejected to the environment and not converted to useful work or utilized for a useful purpose. In the coming era of more economically and socially responsible exploitation of energy resources, the world can add significant power generation capacity if it simply examines the heat it rejects from existing electricity producing technology.

Cogeneration, or thermal energy recovery, is the logical solution to the cold stream energy rejection dilemma. Cogeneration processes attempt to utilize the waste heat from a thermal process that produces electricity for additional benefit. Those benefits are diverse and can range from additional electricity production to residential hot water heating to industrial process steam production. While these systems can be very cost effective, they have not been widely implemented and have significant growth potential. As DER generation becomes collocated in residential communities and near commercial centers, it is expected that cogeneration systems will be implemented in conjunction with them, integrating power; heating, ventilation, and cooling (HVAC); as well as secondary heating processes for better service delivery to the customer.

1.1.4 The Need for Diversified Generation

In 1996, there were 3,195 electric utilities in the United States and 65 power marketers. Of these, 2,020 were publicly owned (including 10 Federal utilities), 932 were rural electric cooperatives, and 243 were investor-owned utilities [1.67]. Since the early 1990s, restructuring events have reshaped the electric power industry where numerous electric utilities have merged or been acquired. Some of these electric utilities were directed, through state government mandate, to sell off their generating assets and focus the regulated part of the company on transmission and/or distribution. This process of de-integration consolidated much of the nation’s generating capacity under the ownership of very few corporations. Today, many of the nation's electric utilities exist exclusively for distribution, that is, they purchase wholesale power from other utilities and distribute, on their own distribution lines, the electricity to consumers. In many electricity markets, the intention of deregulators to increase market competition and diversify generating assets has had the opposite effect. The ultimate result has been to concentrate the nation's total utility generation assets in the hands of a small ownership class of utilities. By the end of 1996, there were fewer than 1,000 of the 3,200 utilities in the United States engaged in actual power generation. By 2006, that number had dropped to less than 530 generation-owning companies [1.68], while 3,024 public, investor-owned, cooperative, and municipal companies sold power, purchased from the generators through a complicated transmission and distribution system [1.69]. In 2011, the U.S. power industry had shown a rebound from the effects of divestiture, but the 6,379 regulated power plants, with 16,499 generators in-service, still remained concentrated in the hands of fewer than 1,120 owners; only 620 of which were majority owners (defined by >50% ownership of the power plant) [1.70].

For consumers, generators, and distributors, the market forces of power generation are inescapable. When fewer companies are producing more of a market share of electricity, larger scale and less expensive technology will dominate new generating capacity. While this may benefit rate payers, it does nothing to achieve the national need for a more reliable, secure, and tailored electrical system. Additionally, less expensive technologies that are purchased on massive economies of scale will almost exclusively translate into new coal power plants. This is primarily why the EIA projects 103GW of additional coal-fired power plant capacity will be built in the United States by 2030, encompassing a growth of nearly 6% in share of the total U.S. generating capacity. This anticipated growth in coal capacity is nearly three times greater than the projected growth in added renewable capacity by 2030 (based on the current provisions of the United States Energy Independence and Security Act of 2007, signed into law by President George W. Bush on December 18, 2007) [1.71].

To counter the adverse forces that larger and larger power generation conglomerates have on the electricity market, the solution may be distributed generation (DG). Distributed generation, closely related to DER, describes a dispersed power network that utilizes smaller scale generators located close to where the load is being served. By distributing smaller generating assets instead of relying on large, centralized generation, markets that would otherwise be closed can be opened to diversified electricity producers with a wider array of production methods. This effect can lower consumer costs, reduce environmentally hazardous emissions, improve quality and reliability, and provide system redundancy for power grid security. A smaller scale DG system comprised of DER may be more apt to utilize cogeneration technology which takes advantage of the leftover heat energy that would otherwise be rejected to the environment for useful purposes. Cogenerating power systems can produce process steam for industry, hot water for residential application, or even create additional electricity. Consumers and small electricity producers appear to be the most interested in the use of innovative power generation technologies and their implementation will only occur if distributed generation grows.

As electrical power markets have fully or partially deregulated, opportunities have arisen that make it attractive for companies to invest in technologies that facilitate distributed generation for electricity customers. Moreover, the legal requirements of the

Public Utility Regulatory Policies Act of 1978 (PURPA) established that even small, and presumably distributed, generators of electricity are guaranteed equal access to the electrical grid by means of interconnection. The federal government has repeatedly upheld PURPA's cogeneration and small power producer provisions (Section 210), most recently with the Federal Energy Regulatory Commission (FERC) decision in February 2006, regarding the Energy Policy Act of 2005 [1.72]. In its Final Rule (Order No. 671, Docket RM05-36-000), FERC reaffirmed the interconnection and cogeneration goals of PURPA. This action by FERC effectively stated that small power producers should continue to be encouraged to pursue distributed generation and that combined heat and power (CHP) applications are intrinsically more efficient than separate heat and power production [1.73]. Continued regulatory support encourages the development new distributed generation technology and stymies large electric utilities aims at consolidating the electricity market through centralized generation.

1.2 United States Electrical Energy Future

As social, economic, and political forces propel the nation into the future, it is clear that innovative means of utilizing the electrical infrastructure that currently exists while leveraging emerging technologies for the benefit of the power system, are needed. This section is intended to create a bridges between what has been presented about the state of electricity in the U.S. and connect it with potential solutions for going forward.

1.2.1 Challenges

Based on the brief introduction regarding the status of electrical power generation and delivery in the previous section, the following primary challenges are summarized:

1. New generation capacity is falling behind new electricity demand.

a. Demand for electricity will grow by nearly a third in the next 20 years [1.5].

b. Of the eight U.S. NERC regulatory regions, four have flat or negative capacity margin projections indicating demand is outpacing the integration of additional generation [1.27].

2. New generation capacity may not incorporate high penetrations of renewables.

a. Since 1996, the number of electric utilities in the U.S. that actually own generation assets has decreased from 3,195 [1.67] to 620 majority owners in 2011 [1.70]. Partially due to deregulatory factors, the net result is the concentration of generation assets in for-profit, investor-owned power market corporations [1.69]. This trend implies that the cheapest form of new generation (coal) which yields the largest margins and quickest payback on investment will predominate into the future.

b. Twenty-nine states have passed Renewable Portfolio Standard (RPS) legislation, shown in Figure 1.14. These legislative mandates require that between 15-40% of electricity consumed within the state will originate from a renewable source, with deadlines as early as 2015 [1.74]. So far, California is the only state to come close to meeting a RPS deadline, achieving 17% of state power produced by renewables in 2010 (the 2010 RPS was 20%). Monumental investment, including by non-utility stakeholders, will have to be made to achieving RPS objectives.

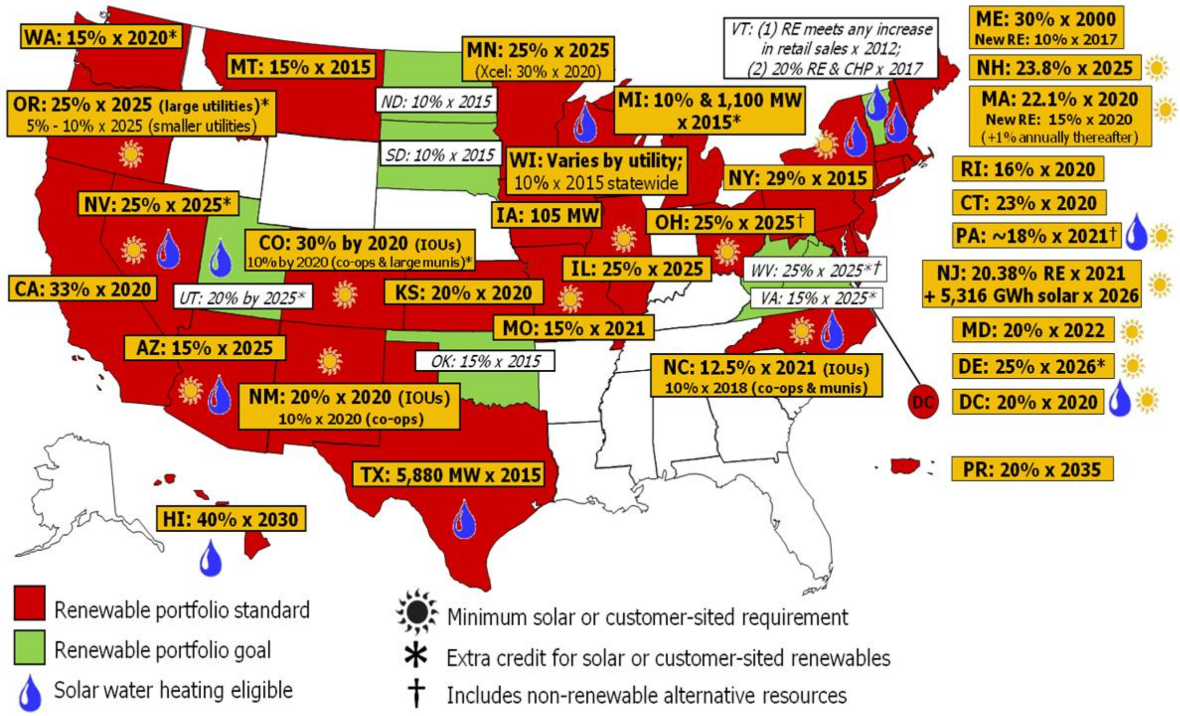

Figure 1.14. United States renewable energy legislative goals & mandates (2011) [1.74].

3. Transmission/distribution assets are outmoded and are near dangerous limits.

a. The power system infrastructure that delivers electricity is degrading rapidly. Nearly 70% of transmission lines and transformers are 25 years or older, while 60% of circuit breakers are 30 years or older [1.75].

b. The vast majority of power system components were installed in the 1960’s and 1970’s prior to microprocessors or high speed communications.

4. Electrical quality and reliability will be more costly and scarce in the future.

a. The power system is being operated in a way that was not foreseen when designed for modern unidirectional flow in the middle part of the 20th century. Wholesale power trade between NERC regions jumped 300% between 2004-2010 (a peak of >400 TWh exchanged in July 2008) indicating massive wheeling (trade) of electricity that pushes a stressed system to its limits [1.76].

b. The reliable delivery of electrical power to consumers is faltering. Since 1991, the number of outages in excess of 100MW and outages that affected more than 50,000 people has doubled every five years [1.77]. This trend shows no sign of abating.

1.2.2 An Infrastructure Solution

The U.S. electrical power system situation is troubling. With demand rising by nearly a third in the face of competing objectives, such as capital cost concerns, the desire to lessen environmental emissions, the need to ensure the security of energy supplies, and enabling better reliability for customer needs, the need for innovative solutions is clear. With a system as complex and interdependent as the national power system, a one-size-fits-all solution to complement existing power system capabilities within the existing centralized generation model, is yet to be seen. However, the case has been made for distributed generation as a means of improving aspects of the electrical grid and consumer power markets. Additionally, microgrids directly address many of the challenges we confront.

1.2.2.1 Microgrids. Microgrids are autonomous power systems, loosely defined by a few MW or less of generation, controllable and non-controllable load centers, and possibly storage systems that integrate together on a localized electrical infrastructure. In periods of emergency, microgrids have the capability to separate, or island, from the utility power system and operate independently, within limits. Upon restoration of normal macrogrid conditions, microgrids can reintegrate and contribute excess power, provide ancillary services, or purchase of electricity from the bulk power system.

As the power system grows to meet future demand, the traditional centralized model that concentrates generation assets centrally and transmits power to distant customers will incur significant costs for new transmission lines, experience strained stability, and present new challenges for overall system flexibility. Microgrids, alternatively, can couple multiple DERs, storage systems, and loads, within a localized framework thereby concentrating these components as a singular power system entity that interconnects with the utility grid in a distributed manner at defined points of common coupling (PCC). This is especially attractive from the system operator's perspective for two primary reasons. First, the microgrid concept concentrates uncertainty caused by renewable generation; rather than many variable DERs independently connected to the utility network, the DERs are combined within the microgrid with limited PCCs. Second, the microgrid conglomerates the interests of microgrid customers and facilitates control of local assets towards their self-interest. In other words, the responsibility for uncertainty incurred by variable generation, shifting load patterns, and changing storage levels is shifted onto the microgrid operator and is served at the local level. In this way, both customer and utility operator benefit. The burden, however, of achieving this operational relationship is shifted to the microgrid power management system. Without an effective supervisory architecture, desirable attributes including safe, efficient, and optimal operation, are difficult to ensure.

The next step towards the future of electricity production is to develop infrastructure technologies, such as microgrids, to enable smaller renewable generation and storage to be distributed close to load consumers and counter the negative effects of centralized power. Unfortunately, it is too easy to focus on simply the fuel type that we choose to generate electricity as comprising the entire problem. Equally or more important, is how we adapt an electrical transmission and distribution system that was designed for one-way centralized generator-to-load power flow to incorporate evolving operational methods with new generation, storage, load, communication, control, and protective technologies. Microgrids are a prime means of addressing these objectives and concurrently achieving broad based system improvements. As an infrastructure component, microgrids, more than any other technology proposed, have the capability to comprehensively reshape the electrical infrastructure towards better energy production, delivery, and utilization. The use of microgrids offers a means of addressing many power system challenges simultaneously. Specifically, microgrids offer solutions to each major challenge facing the future of electrical energy in the U.S., as will be described in the next sections.

1.2.2.2 Improved Integration of New Generation. Viewed from the centralized perspective, there is a great divide between electricity production and electricity consumption. Large central power plants produce electrical energy and it is sent to consumers in unidirectional flow, typically over very long distances. Within microgrids, however, generation and demand are co-located and can have a collaborative relationship, where none exists in the centralized model. A clear example of a electrical supply/demand synergistic relationship that is difficult to achieve with a centralized infrastructure, but inherent to microgrid operations, exists during periods of inadequate generation to meet demand. For centralized power plants, this situation requires the starting and operation of inefficient, costly, and emissions-dense peaking generators to make up for inadequate electricity supply. In the case of microgrids, inadequate supply may commonly occur due to resource curtailment (e.g. photovoltaics experiencing cloud cover), but co-located responsive loads can adjust to compensate for degraded generation. This load response is extremely difficult to achieve on a centralized scale and highlights the microgrid advantages of both distributed control and a localized power system framework. Additionally, storage capacity added within microgrids will complement attached load requirements and assist with mitigating periods of resource curtailment. Ultimately, with increasing electrical demands throughout the entire power system, the implementation of microgrids with distributed generation, responsive loads, and local storage permits a more tailored growth of capacity. This more customized growth has the effect of lowering the necessary total capacity overall and stretches the period over which capacity must be added. In this way the entire power network benefits from a localized, customer-driven microgrid approach to power system growth.

1.2.2.3 Incorporating More Renewable DERs. Microgrids are a prime means for smaller and more distributed renewable systems to incorporate into the power system [1.78]. Rather than utilities being the only entities incentivized to expend capital for new generation assets, microgrids can better facilitate customers, entrepreneurs, cooperatives, private businesses, and other stakeholders to install smaller scale renewables, thereby participating in their own energy future. Utilities, historically, have been opposed to the integration of small renewables, primarily because of their uncertain effects on the entire system when unevenly dispersed throughout. Microgrids, on the other hand, can couple multiple DERs and storage systems within a localized framework. This has the effect of concentrating these components, and any associated intermittency, as a singular power system entity. Rather than the multiple DERs influencing the power system at multiple PCCs, the DERs are concentrated on the microgrid which interconnects with the utility grid in a distributed manner at single PCCs. This is especially attractive from the system operator's perspective because generation fluctuations and subsequent power reversals across the PCC are minimized. From both the perspective of encouraging electricity consumers to become owners of their own renewable generation, and the benefits utilities can realize from supporting distributed renewables throughout their network, microgrid represent a means forward.

1.2.2.4 Relieving Transmission & Distribution Burden. Perhaps the most obvious of the benefits that microgrids offer, by distributing generation closer to the load, significant burdens on the transmission and distribution system can be lifted. Apart from the 83-166 TWh lost annually to transmission inefficiencies alone [1.79] (equivalent to the sum of the energy produced by all renewable generation in the U.S. in 2010 [1.53]), microgrids can provide ancillary voltage support at the end of long radial feeders thereby reducing the burden of voltage regulation on utilities. As demand grows pushing existing infrastructure closer to limits, DER implementation in microgrids can more easily grow with it easing that strain and, in many cases, offsetting the need for new lines. Smaller generation sources distributed throughout the power system are faster to implement. This advantage is not trivial when significant capacity must be added rapidly and new centralized power plants must undergo a lengthy site procurement and construction process, as well as obtain the necessary easements to install new HV transmission lines. In these ways, microgrids can lower the proximity of transmission and distribution to operational limits, delay or offset the need for expensive new lines, and improve loss characteristics and regulation of existing infrastructure.

1.2.2.5 Improved Quality & Reliability at Minimal Cost. The microgrid as an electrical infrastructure component conglomerates the interests of local customers and facilitates control of local assets towards their self-interest. In other words, the responsibility for uncertainty incurred by intermittent generation, shifting load patterns, and changing storage levels is shifted onto the microgrid operator and off the utility. In this way, both customer and utility operator benefit. Electrical quality (limited interruptions, voltage regulation, frequency regulation in the islanded state, and harmonic control) can become more the responsibility of the customer's microgrid rather than the utility. In this way, the bulk power system can naturally evolve into a lower quality, less reliable reservoir of power, while the microgrid sustains improved service to local customers. Given the question of whether to consume significant sums to grow and improve an existing centralized power system to achieve desired quality and reliability standards, or expend a lesser amount to create localized microgrids that achieve the same objectives with additional benefits is clear: invest in growth and microgrid capability.

1.2.2.6 Projecting Microgrid Growth. The need for microgrids is clear and present. Forward-looking utilities and independent power producers have identified this fact and are making strides to implement microgrids. However, much of this work is presently on a small scale and in the demonstration phase. In 2009, Pike Consultants of Boulder, CO predicted that, during 2010 to 2015, almost 3.1GW of new microgrid capacity would come online worldwide. The total market value of this investment in microgrid implementation would surmount $7.8 billion. Of this global prediction, North America was expected to capture $5.8 billion, or 74%, of this market. When these predictions were made by Pike Consultants, they were considered optimistic given the significant economic downturn in global financial markets at the time. After all, this would imply growing operational domestic microgrid installations from 626 MW in 2010 to over 2,352 MW of capacity by 2015. Unfortunately, the EIA does not collect data on hybrid or microgrid installations, and Pike Consultants has not issued a follow-up report assessing their three year old predictions. Despite the lack of empirical evidence regarding how many microgrids are being built and operated in the U.S., the topic has remained in popular press and the focus of new demonstration projects. Going forward it is clear that innovation is required for microgrid designs and control systems. Without this innovation, microgrids can never expect to gain strong utility support, which is crucial for microgrids to be actually implemented.

1.3 Remote Communities, Developing Nations, and Microgrids

So far, the discussion has focused on the particulars of the state of electricity in the U.S. However, the discussion of how microgrids can assist the growth and development of the U.S. electrical infrastructure is not the totality of where microgrids can have an impact. To this end, the discussion of microgrids would not be complete without describing the importance of electrical power delivery to modernizing communities. This is not only limited to communities that are modernizing in the developing world; on the contrary, many industrialized nations retain isolated communities with power systems that are far behind their networked counterparts in terms of reliability, power quality, cost, and environmental impact. Although not the focus of this work, microgrids can have a massive impact on the improvement of electrical service and overall energy delivery to such communities. In Figure 1.15, the two primary paths taken by communities without electrical power towards connection with a modern power system is shown. While the motivations for community-based electrical systems differ whether motivated by economics or service factors, microgrids can expedite system evolution.

Figure 1.15. How communities evolve electrically.

Remote areas and islands are under stress as a result of their dependence on petroleum, the most expensive and least secure fossil fuel. With a few exceptions, the majority of the world's remote areas depend on oil for all of their electricity, heating and cooling, as well as their transportation needs. Moreover, the transportation systems that serve as lifelines to these areas are also dependent on petroleum. The economies of remote areas and islands are therefore extremely vulnerable to rising oil prices, oil price volatility, and supply disruptions. During the past several years, oil prices have achieved historic highs, peaking at $147/barrel in July 2008, and averaging $107/barrel from January-June 2011 [1.80]. These price shocks have created both the opportunity and the necessity for many remote areas to explore renewable energy sources as alternatives to oil. Some remote areas have their own natural gas resources (e.g. Trinidad and Tobago), hydro (e.g. Samoa), and geothermal (e.g. Hawaii) whereas others have taken significant strides to convert to renewable energy systems (e.g. the island of St. Paul in Alaska and the island of Samsø in Denmark). These are important, but atypical cases reflecting the diversity of island and remote areas.

In addition to strengthening the target communities, the energy transition process in remote islands and areas will hold important lessons for centralized grids. This is an important point, often overlooked by large scale regulators, legislators, and power system operators. As nations implement aggressive national renewable energy policies, their continental-scale energy systems will eventually confront the integration challenges that remote islands and areas will face in the near term. For example, as Germany attempts to reach its target of 80% renewable electricity by 2050, its national interconnected power system will require the same utilization of innovative storage, efficiency, and integration strategies that smaller jurisdictions like Hawaii are deploying right now. In other words, the lessons learned from implementing hybrid and microgrid systems are applicable to the broader interconnected power system.

1.4 Loads and Islands

Much has been said about the generation-side of the power system balance. Of course, the quantity, composition, and use of electrical loads makes up the other side of that balance. In this section, a discussion is presented to introduce the topic of electrical loading and its pertinence to hybrid or microgrid systems.

1.4.1 Islanded Power Systems

As mentioned briefly before, by definition, an islanded power system is an operable power network that is isolated from the synchronism of the broader utility grid. Within the island is a composition of generation assets and load. While the generation capacity within the island may not be sufficient to supply all of its loading, the fact that some loads may be energized from island generation is sufficient to make the isolated power system a functional power island. From a safety perspective, utilities typically discourage island formation within the utility network. Primarily, this attitude is a result of concerns stemming from a lack of ability to monitor key electrical parameters from the utility-side near the island and within the island itself. Without automation or remote sensing capabilities, reestablishing an interconnection with the islanded part of the grid is challenging and requires significant care. Overall, until recent revisions of the IEEE

Standard for Interconnecting Distributed Resources with Electric Power Systems (1547), deliberate islanding of DER for the purpose of power a small power network apart from the utility grid was not usually permitted, except in times of extremis. With the revision of 1547.4 in 2011, the standard governing the operation of DER islands has introduced much more flexibility directly applicable to microgrids [1.81].

The primary problem facing islanded power systems is lack of grid rigidity. Especially in smaller networks, without a generator with strongly dominant prime mover inertia, electrical instability arises due to two factors: generation/load mismatch and generator swing. Additionally, depending on the isolated grid configuration, the voltage profile instability can be made worse by long-run feeders without VAR (volt-amps reactive) compensation. If one assumes that the grid configuration is fixed (i.e. already installed) without sufficient grid stabilization (interconnection to a larger grid, sufficient storage, etc.), then either the generator has to be properly controlled, load has to be properly controlled, or both. This presents unique challenges to a small microgrid power system which must account for the potential of high variability in renewable DER generation, as well as the lack of inertia.

1.4.2 Vital Power Applications

Today, many applications require a steady supply of electrical power to support vital operations. Public safety facilities, such as fire houses and police stations, demand constant electricity to power communication assets and computer systems, as well as basic building functions including lights and security systems. Similarly, hospitals must maintain critical electrical equipment for patient telemetry, life support including respiration, and laboratory functions on a constant basis. From an electrical perspective, the characteristics of the electrical devices employed by these applications are fairly consistent: low power (less than 1kW rating per device), often utilize onboard power supplies that convert branch circuit electricity (120VAC or 240VAC) to DC power local to the device, and are intolerant of electricity interruptions. While the importance of maintaining constant electrical power to this equipment is similar to the requirements of industrial applications, there are some key differences. In large manufacturing processes, such as in the semi-conductor or steel industries, constant electrical power is important for maintaining consistent batch qualities, ensuring that automated equipment does not seize while working on expensive materials, and preventing damage to equipment directly. Similarly, for large data centers, a significant cost is incurred when power is lost. However, in these larger scale applications, often several hundred kW to MW capacities at voltage levels from 480VAC to 13.8kV, they can rely on exclusive agreements with the utility to provide rigid electricity. Additionally, on a larger scale, it may be cost effective to employ one or many technologies for ensuring constant electrical power, including large battery storage, quick-start diesel powered backup systems, capacitive compensation, expensive automatic voltage regulation, and multiple feeds from the utility grid.

The proper solution to a power quality problem depends on the type of equipment being protected and the specific power quality issue that needs to be addressed. Especially in rural or isolated applications, the primary power quality problem faced is the inconsistency of the power, rather than more complicated power quality issues, such as low power factor or harmonic distortion of the voltage waveform. Often, because of this specific power quality concern, simple and typically inexpensive uninterruptable power supplies (UPS) are a viable solution. However, UPS systems often lack the flexibility to respond and sustain electrical operations when outages last for many hours. From a system perspective, integrating UPS capabilities into an integrated hybrid microgrid to providing better power and energy management is ideal.

1.4.3 Non-vital Power Applications

Despite most electrical consumer attitudes, the majority of typical electrical loads used in everyday life are not vital. When defining the importance of continuity of power, brief interruptions to lighting, appliances, or entertainment systems do not rise to the level of being life-threatening. Annoying to be sure, any interruption to electrical service can create problems for the consumer, but non-vital loads are ones that can be de-energized without causing significant hardship to the consumer.

Non-vital electrical loads offer the opportunity of capacity margin. In this way, the quantity of non-vital loads that may be turned off at any instant is equivalent to operating generation capacity that is in excess of vital need. From this perspective, non-vital loading has a very real economic value beyond the actual electricity consumed by them. In fact, allowing non-vital loads to be turned on or off by the utility for just this purpose is called Demand Response (DR). In times of extremis, for example during a generator outage where a utility is unable to match sufficient generation to demand, DR can be used to de-energize pre-determined non-vital loads to restore voltage and frequency levels on a power system closer to operational norms. Although not used as frequently, but more so with the advent of higher penetrations of wind power, DR can also be used in reverse where loads are energized when voltage or frequency levels are rising too high due to excess generation or other factors.

Appropriate non-vital loads, when identified can be a valuable commodity for a power system. For microgrids, non-vital loads are important because they can offset the need for significant storage capacity, especially with the employment of renewable DERs. It is expected that, in the future, DR at the distribution level will be a mainstay of the power system. Microgrids are no exception to that prediction, as DR of non-vital loads will be an integral part of microgrid power management.

1.4.4 Power Quality and Reliability

To set the stage for microgrids as a more comprehensive and cost effective solution to ensuring vital power to critical loads, the following discussion of electrical reliability is presented. The dependable flow of electrical power can be described in many ways. Colloquially, the term "power quality" often refers to the constant and reliable delivery of electric power to a user's equipment. However, power quality has specific connotations from a power systems engineering perspective, referring to the actual voltage and current waveform shapes flowing through the electrical system. While the standards vary, in the United States, utility-sourced electric power must meet very strict power quality requirements expressed as voltage and frequency limits, as well as reliability requirements ensuring limited interruptions. Not as closely regulated, but an important attribute of quality power is the absence of harmonic distortion (similar to noise) in delivered power. Harmonics usually originate within the local facility or localized electrical interconnection, introduced by modern power electronic devices used in power supplies, computer equipment, and variable speed motor drives, or items such as welding equipment and fluorescent lighting. Poor power quality, as well as harmonics, can result in undesirable equipment heating, poor motor/compressor efficiency, device malfunctions, communications interference, unexpected circuit breaker trips, flickering lights, and an overall reduction in system capacity. Power quality issues are normally only a large enough concern in larger facilities with significant load. To compensate for poor power quality, equipment may be replaced or capacitive banks may be installed within the facility. Harmonics, on the other hand, are a concern of both large and small capacity systems, leading to solutions including: capacitive compensation, active power filters, capacitor-based dynamic voltage restorers (for large voltage sags < 1 second), and custom designs. Most of these specific power quality issues are normally only a large enough concern to warrant remedial action in large facilities with significant and specialized loads. To compensate for poor power quality, equipment may be replaced, capacitive banks may be installed, or other mitigation actions may be taken within the facility.

On smaller systems, such as a rural health clinic or local hospital, the reliability of electrical supply is of paramount concern. Apart from the power engineering details of power quality, managers of such facilities are primarily concerned with three electrical problems: voltage spikes, voltage sags, and interruptions. Voltage spikes are very straightforward to understand and typically arise due to lighting strikes, generator regulator malfunction, or a confluence of generation and load interactive effects.

Luckily, voltage spikes are infrequent and inexpensive technology is available to protect equipment from them. Voltage sags, alternatively, are more common during periods of inadequate voltage within a facility, causing improper equipment operation or damage. As a way to discriminate the difference between a voltage sag (brownout) and an interrupting event (blackout), the IEEE Standard 1159 defines a voltage sag is as lasting between 1/120 of a second up to a minute. Beyond a minute, for all intents and purposes within a small facility with sensitive equipment, sustained voltage sag can be considered an interruption or outage. A typical cause of voltage sags, assuming that no fault has occurred, is the inadequate supply of electrical power from the generation source. The most common voltage sag protection methods fall into two classes: devices installed directly between the electrical system and the equipment to be protected, or devices installed in parallel with the generation device to support its output when struggling. Examples of the latter are typically more costly and complicated to install, because they must be large enough in capacity to carry the entire facility, both critical and non-critical loads. These solutions may include bypass battery- or flywheel-based backup generation systems or large automatic voltage regulators with fast tap changing transformers in parallel with the generation source. It is much more common for individual pieces or small groups of 120VAC/240VAC single-phase equipment, less than 1kW in capacity, to be protected by an uninterruptable power supply (UPS).

Typical UPS devices are composed of electrical sensing, power conditioning, and storage circuits. The simplest UPS senses when the normal source of electricity has fallen outside of acceptable bounds and switches the load over to being supplied by the storage onboard the UPS. More sophisticated line-interactive UPS devices will also sustain a load during a complete outage, but also utilize multi-tap autotransformers that are capable of utilizing out-of-specification low voltage supplied by the normal supply to power the load with proper electricity. This function is achieved without total reliance on the UPS onboard storage, thus extending the time is can endure an interruption. UPS devices are typically rated in Volt-Amps, which refers to their maximum power capacity, similar to a generator rating. But this only tells half the story; UPS devices, because they include storage, are rated in Watt-Hours which indicates how long the load can be sustained by onboard storage. Many UPS devices allow the implementation of additional storage to increase the Watt-Hour rating, as necessary to the application. When choosing a UPS, both the power demand of the load protected must be considered, but also the desired period during a complete power outage that the load must operate. Currently, UPS prices are about $0.23 per Volt-Amp capacity and $1.39 per Watt-Hour as shown by a collection of commercially available UPS systems reflecting their manufacturer's suggested retail price (MSRP) in Figure 1.16 [1.82].

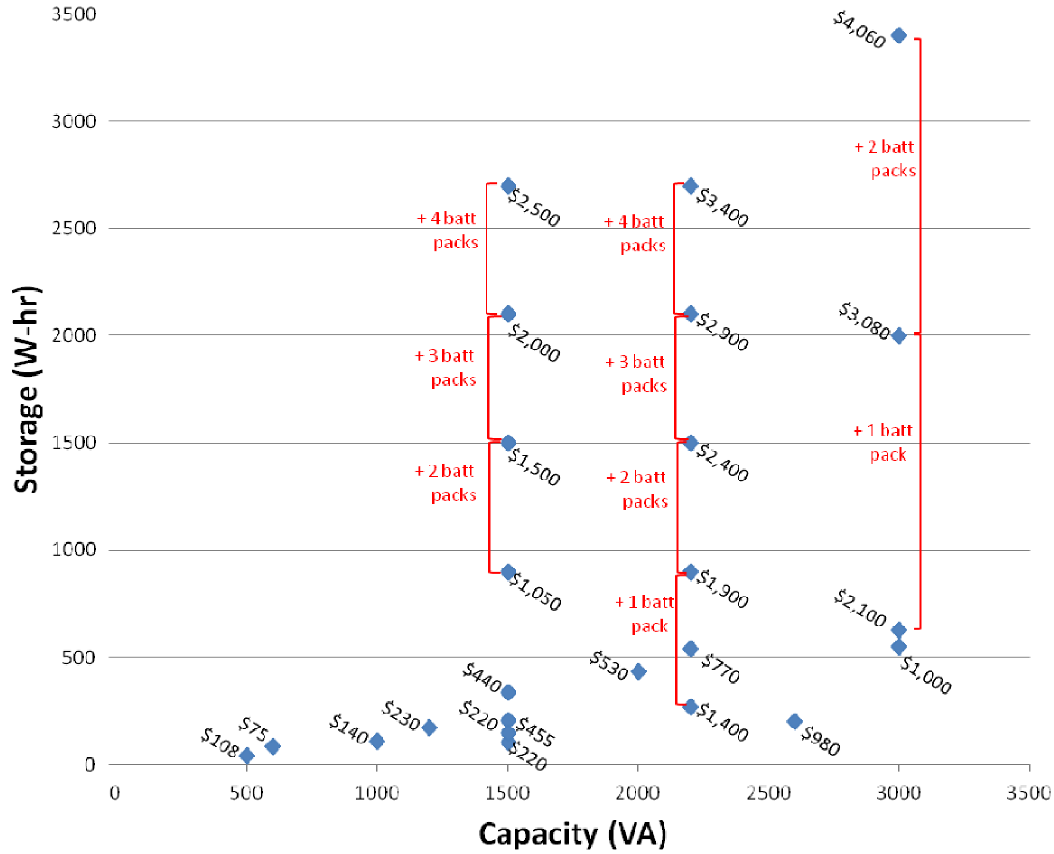

Figure 1.16. Survey of UPS protection for small load applications [1.82].

While it is difficult to measure the general consumer's attitude towards reliability, the analysis of the UPS market does offer some insight. The commercial prices for UPS, shown in Figure 1.16, represent some of the highest costs experienced by the consumer for electrical power devices; roughly \$1 per Wh capacity and \$0.3 per VA rated capacity. When compared to the retail prices for the underlying battery systems, between \$0.239 and \$0.260 per Wh in February 2012 [1.63], the consumer is clearly willing to pay a significant premium for an element of electrical dependability. This willingness to endure high costs for relatively low energy storage may, in no small way, be attributed to the unavailability of other options, such as versatile microgrids. The consumer is left, therefore, to either accept whatever reliability is granted them by the utility power system, or endure high costs to own and operate their own specialized solution. Furthermore, cost estimates vary, but NETL estimates power interruption and power quality issues cost $100 billion per year and will increase 50% within the next few years [1.83]. Microgrids are a clear bridge between these positions. What microgrids can do is directly address the reliability concerns that drive consumers to UPS solutions. At the same time, consumers will benefit from the microgrid capacity to interface with grid-responsive demand-side equipment and facilitate a means for taking advantage of incentive-based price structures. These are significant smart grid objectives, helped by the implementation of microgrids. After all, given the cost that consumers are already paying and Federal Energy Regulatory Commission (FERC) reports that only about 8% of U.S. energy customers can participate in these programs [1.84], microgrids will improve the cost picture and raise levels of service.

1.5 Management Categories

Within the past two decades, some confusing terminology has emerged regarding energy, power, resource, and distribution management which may confuse the reader. This fact has become readily apparent during literature search efforts. Each of these is an important concept because of how each describes the scope of systems, components, and objectives that are managed. Additionally, too often terminology is intermixed, leading to ambiguity. For the purpose of clarity and to highlight where the terminology overlaps, the following definitions are established:

Energy management: the monitoring and manipulation of a complex system of electrical, thermal, and mechanical components and subsystems towards a desired, longer term outcome. Energy management is often concerned with costs including the usage of fuels, the consumption of energy in components and subsystems, heating/cooling/ventilation of facilities, the manipulation of mechanical subsystems, and the optimization of energy flows during operations.

Power management: the monitoring, analysis, and manipulation of set points, operational status, and system characteristics of electrical components within a system. The aim of power management is to affect the immediate operational conditions within an electrical system towards desired, power flows, voltage and frequency parameters, and equipment status. Power management is a component of energy management.

Resource management: the analysis and control of resource procurement and exploitation, including energy, water, and other necessary supplies and materials for operation. Resource management is a component of energy management.

Distribution management: the monitoring, analysis, and manipulation of electrical distribution components towards ensuring the desired delivery of electrical power. Typically involving some automation with human-in-the-loop interfaces, distribution management incorporates power flow, load management, voltage control, system reconfiguration, and emergency actions.

This discussion is relevant because of the intended scope of the work described in latter chapters. For this work, a proposed microgrid power management and control (PM&C) architecture that incorporates aspects of these four management contexts, as shown in Fig. 9, is developed. In many cases, management and control decisions fall into overlapping categories, so for clarity, the PM&C inhabits multiple management domains.

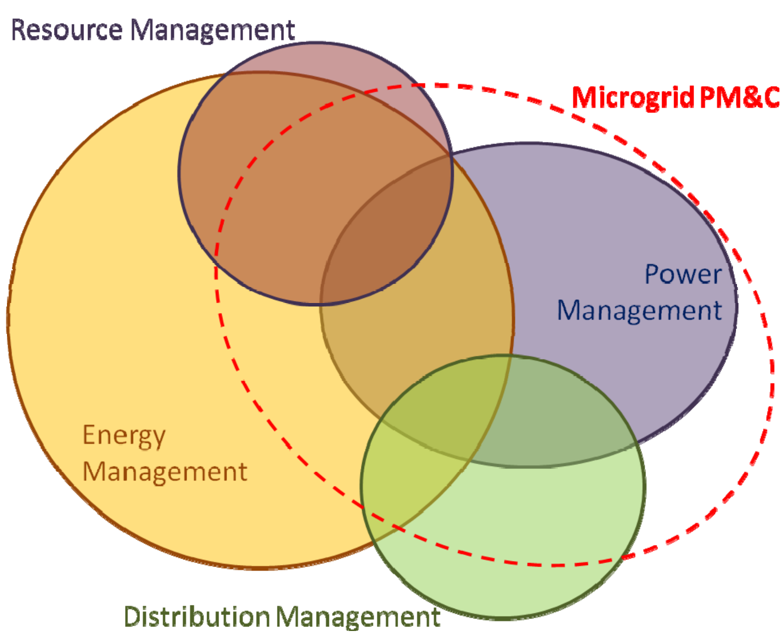

Figure 1.17. Visual representation of the relationships between energy, power, resource, and distribution management.

1.6 Onward

The predominance of this introductory section has been offered for two reasons. Firstly, background has been given to convey to the reader the scale, importance, and immediacy of the challenges facing the United States electrical energy sector today. Secondly, an emerging power system infrastructure concept called microgrids can, in concept, address many or most of these obstacles. Today, however, microgrids only exist in the pilot or demonstration phase. Additionally, in the few existing implementations, they have relied almost exclusively on conventional control systems or human operators to operate them. Clearly, a primary hurdle to broader interest and adoption is the development of safe, reliable, and capable PM&C systems. The PM&C describes the automated supervisory framework that encompasses the computational, communication, and component interface systems that autonomously operate the generation, load, storage, sensory, and direct control assets as a cohesive microgrid. Development of a PM&C is a critical aspect of microgrid research, fundamentally addressing power system structural and operational questions that are not achieved with conventional bulk power system methods. In order for microgrids to move past their current infancy, effective approaches towards PM&C must be realized.

As we advance forward, the U.S. cannot continue to rely on a 20th century power system infrastructure to meet 21st century demands. To be clear, none of the benefits that microgrids offer for power system operations can be realized without safe and effective PM&C architectures, thus highlighting the novelty and importance of the work contained herein. To date, no comprehensive PM&C architecture has been proposed, let alone demonstrated, that is capable of coordinating each of the major asset classes that microgrids employ collectively, nor achieve optimization for multiple objectives based on customer requirements. There is no doubt that this is a complicated problem requiring a comprehensive solution. This work represents a way ahead that will enable microgrids to become key fixtures in our energy future.

REFERENCES CITED

[1.1] George Constable and Bob Somerville, “A Century of Innovation: Twenty Engineering Achievements that Transformed our Lives”, National Academies Press, 2003.

[1.2] Energy Information Administration, "Annual Energy Outlook 2012", U.S. Department of Energy, Report Number: DOE/EIA-0383, 2012.

[1.3] Energy Information Administration, "Electric Power Annual 2010 – Table 7.2", U.S. Department of Energy, Report Number: DOE/EIA-0348, revised 2012.

[1.4] Energy Information Administration, "Electric Power Annual 2010 – Table 7.3", U.S. Department of Energy, Report Number: DOE/EIA-0348, revised 2011.

[1.5] Energy Information Administration, "Electric Power Monthly, December 2010 – Table 5.1", U.S. Department of Energy, Report Number: DOE/EIA-0226, 2010.

[1.6] Energy Information Administration, “Annual Energy Outlook 2011 with Projections to 2035 - Table A8 (Revised Early Release)”, U.S. Department of Energy, DOE/EIA-0383, 2011.

[1.7] Energy Information Administration, “Annual Energy Outlook 2011 with Projections to 2035 - Tables A4, A5, and A6 (Revised Early Release)”, U.S. Department of Energy, DOE/EIA-0383, 2011.

[1.8] M. Chupka, R. Earle, P. Fox-Penner, and R. Hledik, “Transforming America’s Power Industry: The Investment Challenge 2010-2030”, The Edison Foundation, Nov. 2008, available at: http://www.edisonfoundation.net/.

[1.9] Energy Information Administration, "Electric Power Monthly, December 2010 – Table 1.1", U.S. Department of Energy, Report Number: DOE/EIA-0226, 2010.

[1.10] Energy Information Administration, "Electric Power Annual 2009 – Table 8.2", U.S. Department of Energy, Report Number: DOE/EIA-0348, revised 2011.

[1.11] E. Shuster, “Tracking New Coal-Fired Power Plants”, National Energy Technology Laboratory – Office of Systems Analyses and Planning, Jan. 2010, presentation available at: www.netl.doe.gov/coal/refshelf/ncp.pdf.

[1.12] Boyce, Meherwan P., “Gas Turbine Engineering Handbook (3rd Edition)”, Elsevier, 2006, pgs. 86-91.

[1.13] Energy Information Administration, "Electric Power Monthly, July 2012 – Table 4.13.A", U.S. Department of Energy, Report Number: DOE/EIA-0226, 2012.

[1.14] National Petroleum Council. “Balancing Natural Gas Policy - Fueling the Demands of a Growing Economy. Volume I: Summary of Findings and Recommendations”, 2003, available at: http://www.npc.org/reports.

[1.15] J.H. Harker and J.R. Backhurst, “Fuel and Energy”, Academic Press, London, 1981. (et al).

[1.16] 109th U.S. Congress, H.R. 6: Energy Policy Act of 2005, Public Law No: 109-58, Aug. 2005, available at: http://www.govtrack.us/congress/billtext.xpd?bill=h109-6.

[1.17] U.S. Nuclear Regulatory Commission, “Status of License Renewal Applications and Industry Activities - Expected New Nuclear Power Plant Applications”, Dec. 2010, available at: http://www.nrc.gov/reactors/new-reactors/new-licensing-files/expected-new-rx-applications.pdf

[1.18] Energy Information Administration, “Annual Energy Outlook 2011 with Projections to 2035 - Table A9 (Revised Early Release)”, U.S. Department of Energy, DOE/EIA-0383, 2011.

[1.19] Compiled from: Energy Information Administration, "Annual Energy Review – Chapter 8 Tables", U.S. Department of Energy, Report Number: DOE/EIA-0384, 2011.

[1.20] Energy Information Administration, "Electric Power Annual 2009 – Table 5.2", U.S. Department of Energy, Report Number: DOE/EIA-0348, revised 2011.

[1.21] Renewable Energy Research Laboratory, “Wind Power: Capacity Factor, Intermittency, and what happens when the wind doesn’t blow?”, University of Massachusetts at Amherst, available at: http://www.ceere.org/rerl/about_wind/RERL_Fact_Sheet_2a_Capacity_Factor.pdf

[1.22] Energy Information Administration, "Electric Power Annual 2011 – Table 2.1.B", U.S. Department of Energy, Report Number: DOE/EIA-0348, revised 2011.

[1.23] Office of Electric Transmission and Distribution, “Grid 2030 – A National Vision for Electricity’s Second 100 Years”, U.S. Department of Energy, 2003.

[1.24] A. Chopra, V. Kundra, and P. Weiser, editors "Policy Framework for the 21st Century Grid: Enabling Our Secure Energy Future", Executive Office of the President of the United States, National Science And Technology Council, June 2011.

[1.25] Energy Information Administration, "Electric Power Annual 2009 – Table 1.1", U.S. Department of Energy, Report Number: DOE/EIA-0348, revised 2011.

[1.26] Energy Information Administration, "Electric Power Annual 2009 – Table 1.6.C", U.S. Department of Energy, Report Number: DOE/EIA-0348, revised 2011.

[1.27] Energy Information Administration, "Electric Power Annual 2009 – Table 4.2", U.S. Department of Energy, Report Number: DOE/EIA-0348, revised 2011.

[1.28] Energy Information Administration - Office of Integrated Analysis and Forecasting, "Assumptions to the Annual Energy Outlook 2012", U.S. Department of Energy, DOE/EIA-0554, 2012.

[1.29] Boyce, Meherwan P., "Gas Turbine Engineering Handbook (3rd Edition)", Elsevier, 2006, pp. 86-91.

[1.30] National Petroleum Council. "Balancing Natural Gas Policy - Fueling the Demands of a Growing Economy. Volume I: Summary of Findings and Recommendations", 2003.

[1.31] Statement of Guy Caruso, Administrator, Energy Information Administration, U.S. Department Of Energy, Before the Committee on Energy And Natural Resources, United States Senate, March 4, 2008.

[1.32] J.H. Harker and J.R. Backhurst, "Fuel and Energy", Academic Press, London, 1981. (et al)

[1.33] Energy Information Administration, "U.S. Natural Gas Production and Imports", U.S. Department of Energy, DOE/EIA-Short-Term Energy and Winter Fuels Outlook, October 2012.

[1.34] Federal Energy Regulatory Commission, FERC Form 423, "Monthly Report of Cost and Quality of Fuels for Electric Plants - State of Montana", 1999.

[1.35] Energy Information Administration, "Coal News and Markets Report", U.S. Department of Energy, October 2012.

[1.36] James G. Speight, "Handbook of Coal Analysis", John Wiley & Sons, 2005.

[1.37] Damian Flynn, "Thermal Power Plant Simulation and Control", Institution of Engineering and Technology, 2003.

[1.38] U.S. Federal Register, "Control of Emissions of Air Pollution From Nonroad Diesel Engines and Fuel – Final Rule", Vol. 69, No. 124, June 29, 2004, pgs. 38958-38964.

[1.39] U.S. Department of Energy and the U.S. Environmental Protection Agency, "Carbon Dioxide Emissions from the Generation of Electric Power in the United States", July 2000.

[1.40] U.S. Environmental Protection Agency, Emission Factor and Inventory Group (D205-01), "2002 Electric Generating Unit National Emissions Inventory", September 2004.

[1.41] Available at: http://www.eia.doe.gov/cneaf/electricity/epa/epat1p1.html.

[1.42] Puget Sound Energy, "Colstrip Generating Station - Fact Sheet", No: 4153_064, September, 2010.

[1.43] 2010 EPA Toxic Release Explorer, available at: http://iaspub.epa.gov/triexplorer.

[1.44] Commission for Environmental Cooperation (CEC), "North American Power Plant Air Emissions", Montréal (Québec), Canada, 2011.

[1.45] M.L. Parry, O.F. Canziani, J.P. Palutikof, P.J. van der Linden and C.E. Hanson, "Summary for Policymakers. In: Climate Change 2007: Impacts, Adaptation and Vulnerability", Intergovernmental Panel on Climate Change, Cambridge University Press, Cambridge, UK, 7-22.

[1.46] J.H. Harker and J.R. Backhurst, "Fuel and Energy", Academic Press, London, 1981. (et al).

[1.47] Available at: http://www.naturalgas.org/naturalgas/distribution.asp

[1.48] Anne-Marie Borbely and Jan F. Kreider, "Distributed Generation: The Power Paradigm for the New Millennium", CRC Press, Boca Raton, 2001.

[1.49] Available at: http://www.eere.energy.gov/de/microturbines.

[1.50] Michael Modell & Robert Reid, "Thermodynamics and Its Applications", Prentice Hall, Englewood Cliffs, 1983.

[1.51] U.S. Department of Energy's (DoE) Distributed Energy Program, http://www.eere.energy.gov/de/microturbines.

[1.52] U.S. Energy Information Administration, "Electric Power Monthly – Table 1.17.A", December 2011, available online at: http
http://www.eia.gov/electricity/monthly.

[1.53] U.S. Energy Information Administration, "Electric Power Monthly – Table 1.1.A", December 2011, available online at: http http://www.eia.gov/electricity/monthly.

[1.54] World Wind Energy Association (WWEA), "World Wind Energy Report 2009", Bonn, Germany, March 2010.

[1.55] World Wind Energy Association (WWEA), "World Wind Energy Report 2011", Bonn, Germany, May 2012.

[1.56] Hansen, M. Aerodynamics of Wind Turbines. Earthscan Press, 2008.

[1.57] Emerging Energy Research (EER), "Wind Turbine Supply Chain Strategies 2009-2020", Cambridge, Massachusetts, July 2009.

[1.58] F. D. Bianchi, H. D. Battista, and R. J. Mantz, Wind Turbine Control Systems – Principles, Modeling and Gain Scheduling Design. Springer-Verlag London Limited, 2007.

[1.59] P. Fairley, "Wind Turbines Shed Their Gears", *Technology Review*, April 27, 2010.

[1.60] National Renewable Energy Laboratory (NREL), "U.S. Annual Average Wind Speed at 30m Map", available at: http://www.nrel.gov/gis/wind.html

[1.61] M. A. Green, K. Emery, Y. Hishikawa, W. Warta, E. D. Dunlop, "Solar cell efficiency tables (version 39)", *Progress in Photovoltaics: Research and Applications,* Vol. 20, No. 1, pgs. 12–20, January 2012.

[1.62] Mints, P. "Photovoltaic Manufacturer Shipments, Capacity & Competitive Analysis 2010/2011", Navigant Consulting Photovoltaic Service Program Report, NPS-Supply6, April 2011.

[1.63] Solarbuzz Consultants, "Solarbuzz Retail Pricing Environment", NPD Group, released: 07 January 2012, available at: http://www.solarbuzz.com/sites/default/files/facts_figs/SB_Retail_Pricing_120308.xlsx.

[1.64] C. Winneker (editor), "Global Market Outlook for Photovoltaics until 2016", European Photovoltaic Industry Associations, Brussels, Belgium, May 2012.

[1.65] R. Walawalkar and J. Apt, "Market Analysis of Emerging Electric Energy Storage Systems - Final Report", DOE/NETL-2008/1330, July 31, 2008.

[1.66] Electricity Storage Association, "System Ratings – Installed systems as of November 2008", available at: http://www.electricitystorage.org/technology.

[1.67] Energy Information Administration - Office of Coal, Nuclear, and Alternative Fuels, “Electric Trade in the United States - 1996”, U.S. Department of Energy, DOE/EIA-0531/UC-950, 1998.

[1.68] Energy Information Administration, “2006 Generation Capacity Ownership”, Form EIA-860 Database, 2006.

[1.69] Energy Information Administration, “2006 Electric Sales, Revenue, and Average Price Report - Table 10: Class of Ownership, Number of Consumers, Revenue, Sales, and Average Retail Price by State and Utility: All Sectors”, U.S. Department of Energy, 2006.

[1.70] Energy Information Administration, “2011 Generation Capacity Ownership”, Form EIA-860 Database, 2011.

[1.71] “Energy Independence and Security Act of 2007”, H. R. 6, One Hundred Tenth Congress of the United States of America, Dec. 2007.

[1.72] United States Combined Heat and Power Association, “USCHPA Policy Alert: New FERC Policies in Response to EPAct Amendments of PURPA”, Feb 10, 2006. (http://uschpa.admgt.com/press.htm).

[1.73] United States of America, Federal Energy Regulatory Commission, “Revised Regulations Governing Small Power Production and Cogeneration Facilities”, Feb 2, 2006. (http://ferc.gov/whats-new/comm-meet/020206/E-2.pdf)

[1.74] Database of State Incentives for Renewables and Efficiency, Quantitative RPS Data Project Spreadsheet, North Carolina State University, May 2011, available at: http://www.dsireusa.org/.

[1.75] J. Miller, S. Pullins, & S. Bossart, "The Modern Grid", Wisconsin Public Utility Institute & UW Energy Institute presentation to National Energy Technology Laboratory, 29 April 2008.

[1.76] Energy Information Administration, "Wholesale Market Data from Intercontinental Exchange (ICE)", U.S. Department of Energy, 2011, available at: http://www.eia.gov/cneaf/electricity/wholesale/.

[1.77] S. M. Amin, "U.S. Grid Gets Less Reliable", IEEE Spectrum, January 2011, pg. 80.

[1.78] Nikos Hatziargyriou, Hiroshi Asano, Reza Iravani, and Chris Marnay, “Microgrids,” IEEE Power & Energy Magazine, Vol. 5, Issue 4, July/August 2007.

[1.79] K. Forsten & R. Lordan, "Transmission Efficiency Initiative", Technical Report 1017894, Electric Power Research Institute, Oct 2009.

[1.80] U.S. Energy Information Administration, “Gasoline and Diesel Fuel Update”, July 2012, available online at: http http://www.eia.gov/petroleum/gasdiesel.

[1.81] “IEEE Guide for Design, Operation, and Integration of Distributed Resource Island Systems with Electric Power Systems”, IEEE Std 1547.4-2011, 2011.

[1.82] Collected via manufacturer’s internet websites, February 2012.

[1.83] National Energy Technology Laboratory (NETL), “Smart Grid Principal Characteristics Provides Power Quality for the Digital Economy”, DOE/NETL-2010/1412, 2010.

[1.84] United States Department of Energy, “2010 Smart Grid System Report - Report to Congress”, February 2012, pg. 45.

CHAPTER 2

DER AND MICROGRID STATE-OF-ART

Faced with the expectation that global electricity demand will almost double by 2030 and concerns over the costs of new transmission lines, omnipresent system stability issues, and the lack of power system flexibility in meeting localized demand, research efforts are rapidly progressing in areas that seek alternatives to stressed centralized power systems. A logical solution to these challenges is to deploy distributed generation (DG) systems, which are normally small in size (kW to a few MW capacity range), more adaptable in structure, and installed close to customer load demand. Alternative energy distributed generation (AEDG) technology promises to not only provide part of the solution to a growing world's electricity needs, but can provide power in a more customized, efficient, reliable, stable, and clean manner. For clarity, DG and AEDG systems describe the complete power subsystem, implemented in a distributed manner. These DG/AEDG systems may include a single generation asset and its interface to a local power system or the utility grid; or, more broadly, DG/AEDG systems may describe a collection of DER components and power system interfaces working in tandem to provide electrical service. To be clear, the literature sometimes uses DG and DER terms interchangeably, but for specificity: DG describes the means of system implementation (as opposed to conventional or centralized generation) and DER refers to the actual assets themselves (wind turbines, photovoltaics, battery storage, etc.).

This chapter intends to review the literature on two closely related subjects: DER for DG and microgrids. While there are many DER technologies, implementing them into the power system is a topic of great interest. This will compose the first section of this chapter: a literature review of topics surrounding DER integration as DG. Within the past decade, however, there has been increasing interest in an alternative DG approach: microgrids. Rather than viewing DG from a piecemeal perspective, implementing DER in a microgrid framework that acts as a collective DG infrastructure component may be a more comprehensive solution. Therefore, the second section of this chapter will review the latest findings on microgrid systems and look at how actual systems are being implemented worldwide. Finally, the third section of this chapter will illustrate what challenges still remain unaddressed by the state-of-art of microgrid development and will explain what will be accomplished by this work.

2.1 Distributed Energy Resources and Distributed Generation

Worldwide interest in DERs has inspired significant steady progress towards realizing these systems [2.1, 2.2, 2.3, 2.4, 2.5, 2.6, 2.7]. Most DER research to date has focused on two broad areas: the technology itself, such as high temperature fuel cell development; or, issues surrounding DER implementation. For this work, the actual DER technology itself was not as consequential as the questions regarding implementation. Plainly, this is because any strong means or method for integrating DER into the existing grid infrastructure should be technology agnostic. In other words, the customer will ultimately decide what DER technologies are actually installed, if the infrastructure is capable of accepting them. Facilitating a framework to allow this ready integration of current and future DERs is the focus of this work (i.e. through microgrids). To that end, a thorough literature review was conducted to evaluate the state of the art for

DER implementation. This search included reviews of innovative computational techniques, including intelligent methods (sometimes referred to as artificial intelligence), applied towards DER applications. The literature reporting DER research and investigations is categorized in Table 2.1.

The common thread that weaves throughout the references shown in Table 2.1 is the conventional integration of DER into the existing power system. The mindset for much of this literature is to best facilitate the growth and adoption of DER assets without fundamentally disrupting the conventional means of power system operation and control. The body of DER integration work has definitively pushed our understanding and capabilities of the technologies, but in many ways attempts to integrate DER assets into a power system that was never designed or intended to best utilize them. This discrepancy has recently been identified and leads to interest in microgrids, examined in the next section.

Table 2.1. DER implementation literature review by category.

DER Focus Area	**References**
Physical Integration	
Feasibility	[2.8, 2.9, 2.10, 2.11, 2.12, 2.13, 2.14, 2.15]
Planning, sizing, and siting	[2.16, 2.17]
System impacts	[2.18, 2.19, 2.20, 2.21, 2.22, 2.23, 2.24, 2.25, 2.26, 2.27, 2.28, 2.29]
Economics	
Market factors	[2.30, 2.31, 2.32, 2.33, 2.34, 2.35, 2.36]
Market penetration & participation	[2.37, 2.38, 2.39, 2.40]
Emissions and environmental factors	[2.41, 2.42, 2.43, 2.44]
Electronics and Control	
Conventional control	[2.45, 2.46, 2.47, 2.48, 2.49]
Electronics	[2.50,2.51, 2.52, 2.53, 2.54, 2.55, 2.56, 2.57]
Power flow and dynamics	[2.58, 2.59, 2.60, 2.61, 2.62, 2.63, 2.64]
Intelligent Methods	
Physical Integration	[2.65, 2.66, 2.67, 2.68, 2.69, 2.70, 2.71, 2.72, 2.73, 2.74, 2.75]
Economics	[2.76, 2.77, 2.78, 2.79]
Electronics and Control	[2.80, 2.81, 2.82, 2.83, 2.84, 2.85, 2.86, 2.87]
Operations	[2.88, 2.89, 2.90, 2.91, 2.92, 2.93, 2.94, 2.95, 2.96, 2.97, 2.98]

2.2 Microgrids

The earliest mentions of self-sufficient, autonomous power systems apart from the massively interconnected utility power grids came in the late 1990s. This was partially due to improvements in power electronics that allowed better implementation of technologies such as voltage-source inverters for DC DERs, but was also attributed to power industry deregulatory effects that gave rise to the promise of non-utility entities owning and operating independent power systems. In most cases, these independent power systems would be characterized by smaller generation assets, limited scope, and higher penetrations of renewables and technologies enabling better energy management. Two seminal papers from the early 2000s laid out a more cohesive notion of what capabilities and functionality these independent power systems would look like: microgrids [2.99, 2.100]. Two major capabilities were identified that made microgrids unique power system components: the ability to operate either interconnected with or isolated from the utility power system; and, independent and autonomous control that was not dependent upon the utility network for management or control signals for proper operation. When proposed, it was not clear what electrical means was best for coupling multiple DER within microgrid. Electrically, three primary means to achieve multiple asset couplings exist, as shown in Figure 2.1, Figure 2.2, and Figure 2.3. Each of these electrical configurations has positive and negative attributes [2.101]. In Figure 2.1, each DER interacts with the common DC bus through a power electronic interface appropriate to the DER asset. Further, a single inverter connects the common DC bus to the mains AC bus which supplies power to local loads and/or the utility interconnection [2.102, 2.103, 2.104]. The primary benefit of a common DC bus configuration lies in avoiding electrical synchronization between each DER. However, costs and single-point-of-failure reliability are the primary concerns. In Figure 2.2, each DER has a power electronic interface that enables it to connect directly to the common AC bus (mains). The common AC bus configuration is more reliable and relatively less expensive to implement. However, the common AC bus requires each DER asset and interface to be synchronized and bus voltage must be managed. Finally, in Figure 2.3, each DER is connected to a common high frequency AC bus (HFAC) through power electronic interfaces [2.105, 2.106, 2.107, 2.108]. The HFAC is rectified and inverted to supply the mains AC bus. By far, the common HFAC configuration is the most expensive to implement and operate, but is appropriate for some specialized applications where loads may be connected directly to the HFAC bus. Over the past 5-10 years, the majority of the literature that has investigated microgrids has been focused on the common AC bus configuration (Figure 2.2), with a minority dealing with common DC bus configurations (Figure 2.1). For this reason, the common AC bus configuration was used as the primary electrical configuration for design and analysis in this project.

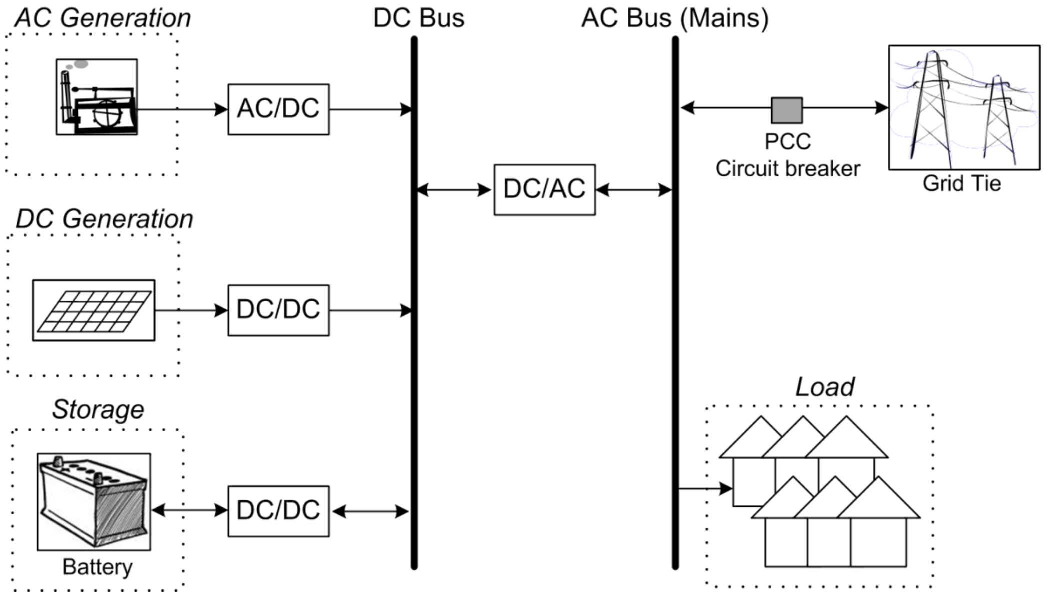

Figure 2.1. Common DC bus configuration for microgrid.

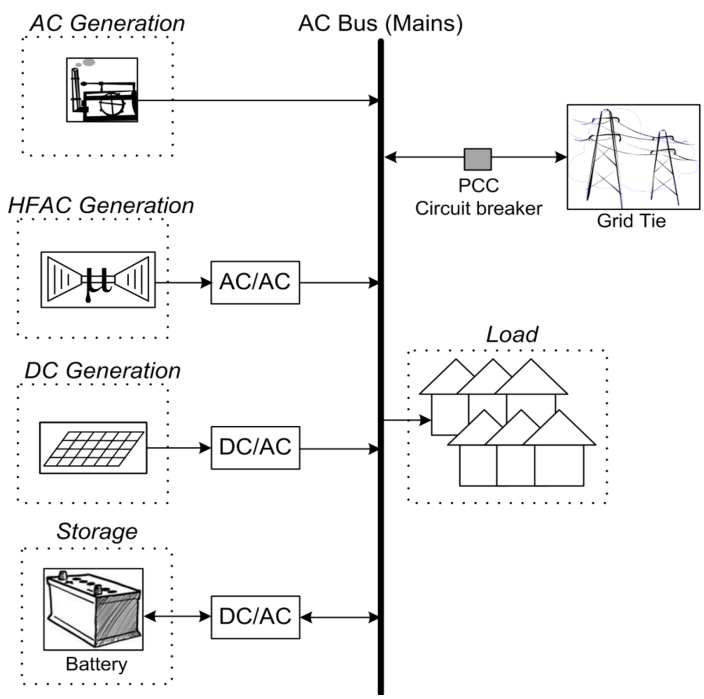

Figure 2.2. Common AC bus configuration for microgrid.

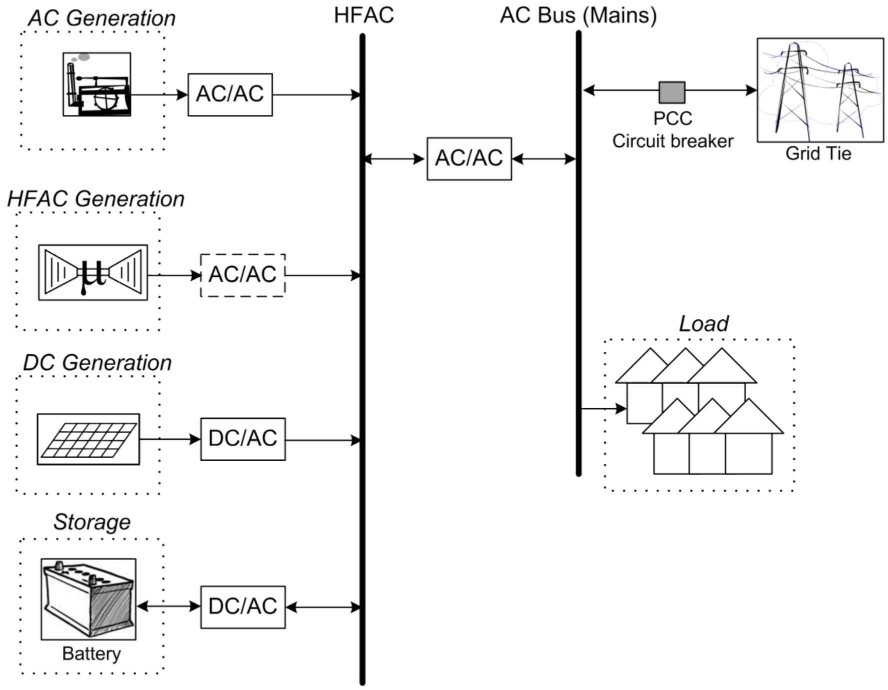

Figure 2.3. Common HFAC bus configuration for microgrid.

A significant amount of literature has been published on microgrids since the year 2000. Most of this work has focused on common AC bus configurations with centralized methods for asset management and control. The key difference between the literature available on DERs and that about microgrids is the maturity of the technology. DERs, including renewable DERs, have been available for conventional applications for over three decades. As opposed to microgrids, DERs are currently implemented all over the world, to varying degrees of penetration on the utility power system. Microgrids, however, firmly reside in the experimental demonstration phase. This developmental status is typified by many different approaches yielding many different outcomes that are hard to compare. The degree of customizability for microgrid applications has lead to few actual microgrid implementations that can be used as ready models for follow-on deployment in other applications. This presents a challenge for the researcher, especially considering that literature announcing innovations for microgrid technology should be as widely applicable as possible, not isolated to a specific microgrid implementation. To that end, a broad literature search was conducted to survey the totality of microgrid research worldwide. In Table 2.2, the microgrid literature is categorized by relevant topic areas.

There are two major areas that appear lacking in the last five years of emerging research on microgrids. First, with the variety of control methods, system configurations, DER assets, and approaches to the merits of microgrids as power system infrastructure components, there is no clear way to simulate these varying aspects comprehensively. This impedes the development of established or standardized microgrid techniques because results are often difficult to repeat or compare. Second, with the few researchers looking into multi-objective decision-making for microgrids, there is a dearth of research on management and control methods that comprehensively take into account goals as different as economic concerns to voltage control. For these two areas, a grand opportunity exists to address both simultaneously.

Table 2.2. Microgrid literature review by category.

Microgrid Focus Area	**References**
Design	
Architecture and design	[2.109, 2.110, 2.111, 2.112]
DER implementation	[2.113, 2.114, 2.115, 2.116]
Siting, sizing, and planning	[2.117, 2.118, 2.119]
CHP integration	[2.120, 2.121, 2.122, 2.123, 2.124]
Operations	
Centralized control	[2.125, 2.126, 2.127, 2.128, 2.129, 2.130, 2.131, 2.132, 2.133]
Fault analysis and protection	[2.134, 2.135]
Demand response	[2.136, 2.137]
Intelligent methods	[2.138, 2.139, 2.140, 2.141, 2.142, 2.143]
Communication	[2.144, 2.145, 2.146]
Power flow	[2.147, 2.148, 2.149]
Multiple objectives	[2.150, 2.151, 2.152]

2.3 Proposed Framework and Simulation Environment

It is clear that a contribution to the state-of-art for microgrids may be made in two ways. Given than many microgrid, and smart grid for that matter, architectures have been proposed, along with different control methods, communications techniques, and system interoperabilities, it is clear that a comprehensive simulation environment is needed to assess the new issues that arise in the use of these systems. This system should be able to incorporate all aspects of microgrid functions, including the electrical network, asset operation and performance, and communications, as well as being flexible enough to allow development and evaluation of innovative control capabilities. Currently, this environment does not exist, nor are their open-source tools that are available to easily implement the desired environment.

The simulation environment is distinctly different from a physical test bed such as those described in [2.153], [2.154], and [2.155]. In these cases, they are both expensive to implement ($250,000 in the case of the Real-Time Digital Simulator used in [2.155]) and limit the development of comprehensive control methods. Primarily, these physically-based microgrid simulators are limited to real-time; that is they may only simulate at the speed of the real world and may not compress time to simulate many hours, days, weeks, or months into faster increments. This makes it very difficult to develop and evaluate complex techniques without a secondary simulation environment anyway. Additionally, in order to incorporate communication and network dynamics for multiple control entities, such as with a MAS, into existing test beds, a separate communication model and interface must be considered. Putting all of these elements together, the environment developed herein will support the development of software agents, control algorithms, and provide a means to test them. While real-time microgrid test beds are ideally suited to small-signal transient analysis and asset interaction studies, they do not meet the needs of microgrid researchers at the current stage of development and state-of-art.

In addition to the contribution of a microgrid simulation environment, new methods of enhanced decentralized control need to be developed. The overwhelming body of microgrid research has been focused on centralized decision-making methods and has, in many ways, been locked in a conventional approach translated from traditional power systems to microgrids. To that end, the focus of this work will be to investigate and develop an enhanced decentralized multi-agent system (MAS) that is capable of making power management decisions for microgrid assets including generation, load, and storage. The flexible MAS will operate in an enhanced decentralized manner utilizing communication pathways, if they exist, to share information amongst agents. In addition to being a new approach towards the multi-objective power management problem for microgrids, the emerging field of cooperation amongst autonomous agents will be explored.

This is an ambitious project: to develop a software-based test bed that incorporates aspects of power system and asset modeling, multi-agent system design, and microgrid management. It will do so in a flexible and modular way paving the way for future innovations in microgrid power management and control, as well as MAS designs.

In summary, the two primary contributions of this work to the state-of-art for microgrid research are:

The development of a comprehensive software-based microgrid simulation environment characterized by:

1. Modularity and scalability for *intra*-microgrid and *extra*-microgrid simulations.
2. Flexible to allow varying levels of detail in models and components, depending on the simulation interests of the researcher.
3. Capable of simulating faster than real-time for the purpose of conducting long-term studies.
4. Based on open-source tools.

The development of a MAS power management system characterized by:

1. Decentralized decision-making enhanced by communication capabilities.
2. Cooperative agents.
3. Evaluate multiple objectives simultaneously.
4. Compatible with the developed microgrid simulation environment and likewise based on open-source tools.

Without capable tools, such as a simulation environment, new methods for microgrid power management cannot be fully realized and evaluated. The purpose of the work described here is to create such a tool and use it to develop a MAS that implements a new way of approaching enhanced decentralized power management for microgrids.

REFERENCES CITED

[2.1] R. Ramakumar, J. J. Bzura, J. Eyer, J. Gutierrez-Vera, T. E. Hoff, C. Herig, J. Iannucci, and M.R. Milligan, "Renewable technologies and distribution systems", *IEEE Power Engineering Review*, Vol. 19, No. 11, 1999, pg. 5.

[2.2] S.N. Singh, "Emerging issues and new challenges in electric power systems", *International Energy Journal*, Vol. 2, No. 2, 2001, pgs. 53-66.

[2.3] X. Li, "Diversification and localization of energy systems for sustainable development and energy security", *Energy Policy*, Vol. 33, No. 17, 2005, pgs. 2237-2243.

[2.4] R. Lawrence, and S. Middlekauff, "The new guy on the block: Applying distributed generation tools in power design systems", *IEEE Industry Applications Magazine*, Vol. 11, No. 1, 2005, pgs. 54-59.

[2.5] L.S. Schell and S. Neff, "Solar Peaking: Distributed photovoltaic generation can ease utility demand", *Energy*, Vol. 30, No. 2, 2005, pgs. 40-42.

[2.6] Editorial, "Distributed generation: Embrace the change", *IEE Power Engineer*, Vol. 18, No. 2, 2004, pgs. 12-13.

[2.7] J. Guerrero, F. Blaabjerg, T. Zhelev, K. Hemmes, E. Monmasson, S. Jemeï, M. P. Comech, R. Granadino, and J. I. Frau, "Distributed generation: Toward a new energy paradigm", *IEEE Industrial Electronics Magazine*, Vol. 4, No. 1, 2010, pgs. 52-64.

[2.8] Y. Fujioka, H. Maejima, S. Nakamura, Y. Kojima, M. Okudera, and S. Uesaka, "Regional power grid with renewable energy resources: A demonstrative project in Hachinohe," *CIGRE 2006*, Paris, August 2006.

[2.9] G. Celli, F. Pilo, G. Pisano, V. Allegranza, R. Cicoria, and A. Iaria, "Meshed vs. Radial MV Distribution Network in Presence of Large Amount of DG", *Proceedings of the IEEE 2004 Power and Energy Society Power Systems Conference*, Vol. 2, Oct. 2004.

[2.10] W. Clark and W. Isherwood, "Distributed generation: Remote power systems with advanced storage technologies", *Energy Policy*, Vol. 32, No. 14, 2004, pgs. 1573-1589.

[2.11] F. Bouffard and D. Kirschen, "Centralised and distributed electricity systems", *Energy Policy*, Vol. 36, No. 12, 2008, pgs. 4504-4508.

[2.12] B. K. Sovacool, "Distributed generation (DG) and the American electric utility system: What is stopping it?", *ASME Transactions on Energy Resources Technology,* Vol. 130, No. 1, 2008, pgs. 120011-120018.

[2.13] T.J. Hammons, “Integrating renewable energy sources into European grids”, *International Journal of Electrical Power and Energy Systems*, Vol. 30, No. 8, 2008, pgs. 462-475.

[2.14] A. Bayod-Rújula, “Future development of the electricity systems with distributed generation”, *Energy*, Vol. 34, No. 3, 2009, pgs. 377-383.

[2.15] K. J. Holmes and L. Papay, “Prospects for electricity from renewable resources in the United States”, *Journal of Renewable and Sustainable Energy*, Vol. 3, No. 4, 2011, pgs. 042701/1-042701/14.

[2.16] S. F. Rivera, “Distributed generation challenges: Air quality, siting, permitting”, *Strategic Planning for Energy and the Environment*, Vol. 20, No. 3, 2000 pgs. 63-66 and 69-80.

[2.17] D. Trebolle, T. Gómez, R. Cossent, P. Frías, “Distribution planning with reliability options for distributed generation”, *Electric Power Systems Research*, Vol. 80, No. 2, 2010, pgs. 222-229.

[2.18] F. Blaabjerg, R. Teodorescu, M. Liserre, & A. V. Timbus, “Overview of control and grid synchronization for distributed power generation systems”, *IEEE Transactions on Industrial Electronics*, Vol. 53, No. 5, Oct 2006.

[2.19] M. Thomson, & D.G. Infield, “Impact of widespread photovoltaics generation on distribution systems”, *IET Renewable Power Generation*, Vol. 1, No. 1, 2007.

[2.20] M. K. Donnelly, J. E. Dagle, D. J. Trudnowski, and G. J. Rogers, “Impacts of the distributed utility on transmission system stability”, *IEEE Transactions on Power Systems*, Vol. 11, No. 2, May 1996.

[2.21] F. D. Kanellos & N. D. Hatziargyriou, “The Effect of Variable-Speed Wind Turbines on the Operation of Weak Distribution Networks *“, IEEE Transactions on Energy Conversion*, Vol. 17, No. 4, Dec. 2002.

[2.22] H. Lund, “Electric grid stability and the design of sustainable energy systems”, *International Journal of Sustainable Energy*, Vol. 24, No. 1, 2005, pgs. 45-54.

[2.23] J. Liu, Jianwei, M.M.A Salama, and R. R. Mansour, “Identify the impact of distributed resources on congestion management”, *IEEE Transactions on Power Delivery*, Vol. 20, No. 3, 2005, pgs. 1998-2005.

[2.24] V.V. Thong, J. Driesen, and R. Belmans, Ronnie “Interconnection of distributed generators and their influences on power system”, *International Energy Journal*, Vol. 6, No. 1, 2005, pgs. 3127-3140.

[2.25] C. Chompoo-Inwai, W.J. Lee, P. Fuangfoo, M. Williams, and J.R. Liao, "System impact study for the interconnection of wind generation and utility system", *IEEE Transactions on Industry Applications*, Vol. 41, No. 1, 2005 pgs. 163-168.

[2.26] R. A. Walling, R. Saint, R.C. Dugan, J. Burke, and L. A. Kojovic, "Summary of distributed resources impact on power delivery systems", *IEEE Transactions on Power Delivery*, Vol. 23, No. 3, 2008, pgs. 1636-1644.

[2.27] G. C. Bakos, "Distributed power generation: A case study of small scale PV power plant in Greece", *Applied Energy*, Vol. 86, No. 9, 2009, pgs. 1757-1766.

[2.28] A. Y. Saber and G. K. Venayagamoorthy, "Efficient utilization of renewable energy sources by gridable vehicles in cyber-physical energy systems", *IEEE Systems Journal*, Vol. 4, No. 3, 2010, pgs. 285-294.

[2.29] T. J. Hammons, "Dispersed generation in modern power systems and its impact in Europe on power system structure and secure operation", *International Journal of Power and Energy Systems*, Vol. 30, No. 1, 2010, pgs. 36-46.

[2.30] T. Moore, "Emerging markets for distributed resources", *EPRI Journal*, Vol. 23, No. 2, 1998, pgs. 8-17.

[2.31] N. I. Meyer, "Distributed generation and the problematic deregulation of energy markets in Europe", *International Journal of Sustainable Energy*, Vol. 23, No. 4, 2003 pgs. 217-221.

[2.32] H.A. Gil & G. Joos, "Models for quantifying the economic benefits of distributed generation", *IEEE Transactions on Power Systems*, Vol. 23, No. 2, May 2008.

[2.33] R. Priddy, "Distributed generation and energy management: Reducing energy costs", *Cogeneration and Distributed Generation Journal*, Vol. 20, No. 3, 2005, pgs. 60-71.

[2.34] D. Mears, J. Iannucci, J. Eyer, and S. Eckroad, "Distributed electricity storage: Foundation for the business case", *IEEE Power and Energy Magazine*, Vol. 3, No. 3, 2005, pgs. 20-24.

[2.35] J. Skea, D. Anderson, T. Green, R. Gross, P. Heptonstall, and M. Leach, "Intermittent renewable generation and the cost of maintaining power system reliability", *IET Generation, Transmission and Distribution*, Vol. 2, No. 1, 2008, pgs. 82-89.

[2.36] S. Wong, K. Bhattacharya, and J. D. Fuller, "Long-term effects of feed-in tariffs and carbon taxes on distribution systems", *IEEE Transactions on Power Systems*, Vol. 25, No. 3, 2010, pgs. 1241-1253.

[2.37] D. A. Ball, W. T. Hanna, and J. A. Stets, “Distributed generation for residential and small commercial markets”, *Proceedings of the American Power Conference*, Vol. 61, 1999.

[2.38] O. Bailey, C. Creighton, R. Firestone, C. Marnay, and M. Stadler, “Distributed energy resources in practice: a case study analysis and validation of LBNL’s customer adoption model”, Lawrence Berkeley National Laboratory (LBNL), Feb. 2003.

[2.39] A. J. Conejo, J. M. Morales, and J. A. Martinez,”Tools for the analysis and design of distributed resources-Part III: Market studies”, *IEEE Transactions on Power Delivery*, Vol. 26, No. 3, 2011, pgs.1663-1670.

[2.40] M. Manfren, P. Caputo, G. Costa, “Paradigm shift in urban energy systems through distributed generation: Methods and models”, *Applied Energy*, Vol. 88, No. 4, 2011, pgs. 1032-1048.

[2.41] A. G. Tsikalakis and N. D. Hatziargyriou, “Environmental benefits of distributed generation with and without emissions trading”, *Energy Policy*, Vol. 35, No. 6, 2007, pgs. 3395-3409.

[2.42] M . Dicorato, G. Forte, and M. Trovato, “Environmental-constrained energy planning using energy-efficiency and distributed-generation facilities”, *Renewable Energy*, Vol. 33, No. 6, 2008, pgs. 1297-1313.

[2.43] S. Karki, M.D. Mann, and H. Salehfar, “Environmental implications of renewable distributed generation technologies in rural electrification”, *Energy Sources, Part B: Economics, Planning and Policy*, Vol. 3, No. 2, 2008, pgs. 186-195.

[2.44] M. F. Akorede, H. Hizam, and E. Pouresmaeil, “Distributed energy resources and benefits to the environment”, *Renewable and Sustainable Energy Reviews*, Vol. 14, No. 2, 2010, pgs. 724-734.

[2.45] R.T. Guttromson, “Modeling distributed energy resource dynamics on the transmission system”, *IEEE Transactions on Power Systems*, Vol. 17, No. 4, 2002, pgs. 1148-1153.

[2.46] K. Sedghisigarchi & A. Feliachi, “Dynamic and Transient Analysis of Power Distribution Systems with Fuel Cells - Part II: Control and Stability Enhancement”, *IEEE Transactions on Energy Conversion*, Vol. 19, No. 2, June 2004.

[2.47] Z. Chen, Y. Hu, and F. Blaabjerg, “Control of Distributed Power Systems” *Proceedings from the CES/IEEE 5th International Power Electronics and Motion Control Conference, IPEMC '06*, Vol. 3, Aug. 2006.

[2.48] J. M. Guerrero, L. Hang, and J. Uceda, “Control of distributed uninterruptible power supply systems”, *IEEE Transactions on Industrial Electronics*, Vol. 55, No. 8, 2008, pgs. 2845-2859.

[2.49] M. Kim, R. Hara, and H. Kita, “Design of the optimal ULTC parameters in distribution system with distributed generations”, *IEEE Transactions on Power Systems*, Vol. 24, No. 1, 2009, pgs. 297-305.

[2.50] K. J. P. Macken, K. Vanthournout, J. Van den Keybus, G. Deconinck, and R. J. M. Belmans, “Distributed control of renewable generation units with integrated active filter”, *IEEE Transactions on Power Electronics*, Vol. 19, No. 5, 2004, pgs. 1353-1360.

[2.51] W. Wongsaichua, W.J. Lee, S. Oraintara, C. Kwan, and F. Zhang, “Integrated high-speed intelligent utility tie unit for disbursed/renewable generation facilities”, *IEEE Transactions on Industry Applications*, Vol. 41, No. 2, 2005, pgs. 507-513.

[2.52] M. A. Kashem, and G. Ledwich, “Energy requirement for distributed energy resources with battery energy storage for voltage support in three-phase distribution lines”, *Electric Power Systems Research*, Vol. 77, No. 1, 2007, pgs. 10-23.

[2.53] J. A. P. Lopes, N. Hatziargyriou, J. Mutale, P. Djapic, and N. Jenkins, “Integrating distributed generation into electric power systems: A review of drivers, challenges and opportunities”, *Electric Power Systems Research*, Vol. 77, No. 9, 2007, pgs. 1189-1203.

[2.54] J. Arai, K. Iba, T. Funabashi, Y. Nakanishi, K. Koyanagi, and R. Yokoyama, “Power electronics and its applications to renewable energy in Japan”, *IEEE Circuits and Systems Magazine*, Vol. 8, No. 3, 2008, pgs. 52-66.

[2.55] C. L. Trujillo, D. Velasco, E. Figueres, and G. Garcerá,Analysis of active islanding detection methods for grid-connected microinverters for renewable energy processing”, *Applied Energy*, Vol. 87, No. 11, 2010, pgs. 3591-3605.

[2.56] M. Liserre, T. Sauter, and J. Y. Hung, “Future energy systems: Integrating renewable energy sources into the smart power grid through industrial electronics”, *IEEE Industrial Electronics Magazine*, Vol. 4, No. 1, 2010, pgs. 18-37.

[2.57] Y. Liao, and C. Lai, “Newly-constructed simplified single-phase multistring multilevel inverter topology for distributed energy resources”, *IEEE Transactions on Power Electronics*, Vol. 26, No. 9, 2011, pgs. 2386-2392.

[2.58] Y. Zhu and K. Tomsovic, “Optimal distribution power flow for systems with distributed energy resources”, *International Journal of Electrical Power and Energy Systems*, Vol. 29, No. 3, 2007, pgs. 260-267.

[2.59] D. Yazdani, M. Mojiri, A. Bakhshai, G. Joós, "A fast and accurate synchronization technique for extraction of symmetrical components", *IEEE Transactions on Power Electronics*, Vol. 24, No. 3, 2009, pgs. 674-684.

[2.60] J. S. Savier, and D. Das, "Energy loss allocation in radial distribution systems: A comparison of practical algorithms", *IEEE Transactions on Power Delivery*, Vol. 24, No. 1, 2009, pgs. 260-267.

[2.61] A. Moreno-Munoz, J. J. G. De-La-Rosa, M .A. Lopez-Rodriguez, J. M. Flores-Arias, F. J. Bellido-Outerino, M. Ruiz-De-Adana, "Improvement of power quality using distributed generation", *International Journal of Electrical Power and Energy Systems*, Vol. 32, No. 10, 2010, pgs. 1069-1076.

[2.62] R. Noroozian, M. Abedi, G. B. Gharehpetian, S. H. Hosseini, "Distributed resources and DC distribution system combination for high power quality", *International Journal of Electrical Power and Energy Systems*, Vol. 32, No. 7, 2010, pgs. 769-781.

[2.63] C. J. Dent, L. F. Ochoa, G. P. Harrison, "Network distributed generation capacity analysis using OPF with voltage step constraints", *IEEE Transactions on Power Systems*, Vol. 25, No. 1, 2010, pgs. 296-304.

[2.64] C. Lee, C. Hsu, and P. Cheng, "A low-voltage ride-through technique for grid-connected converters of distributed energy resources", *IEEE Transactions on Industry Applications*, Vol. 47, No. 4, 2011, pgs. 1821-1832.

[2.65] G. Celli, E. Ghiani, S. Mocci, and F. Pilo, "A multiobjective evolutionary algorithm for the sizing and siting of distributed generation", *IEEE Transactions on Power Systems*, Vol. 20, No. 2, 2005, pgs. 750-757.

[2.66] A. K. Akella, M. P. Sharma, and R. P. Saini, "Optimum utilization of renewable energy sources in a remote area", *Renewable and Sustainable Energy Reviews*, Vol. 11, No. 5, 2007, pgs. 894-908.

[2.67] A. Alarcon-Rodriguez, E. Haesen, G. Ault, J. Driesen, R. Belmans, "Multi-objective planning framework for stochastic and controllable distributed energy resources", *IET Renewable Power Generation*, Vol. 3, No. 2, 2009, pgs. 227-238.

[2.68] Y. P. Cai, G. H. Huang, Z.F. Yang, Q.G. Lin, Q. Tan, "Community-scale renewable energy systems planning under uncertainty-An interval chance-constrained programming approach", *Renewable and Sustainable Energy Reviews*, Vol. 13, No. 4, 2009, pgs. 721-735.

[2.69] A. Alarcon-Rodriguez, G. Ault, and S. Galloway, "Multi-objective planning of distributed energy resources: A review of the state-of-the-art", *Renewable and Sustainable Energy Reviews*, Vol. 14, No. 5, 2010, pgs. 1353-1366.

[2.70] H. Ren, and W. Gao, "A MILP model for integrated plan and evaluation of distributed energy systems", *Applied Energy*, Vol. 87, No. 3, 2010, pgs 1001-1014.

[2.71] Y. M. Atwa, E. F. El-Saadany, M. M. A. Salama, and R. Seethapathy, "Optimal renewable resources mix for distribution system energy loss minimization", *IEEE Transactions on Power Systems*, Vol. 25, No. 1, 2010, pgs. 360-370.

[2.72] W. Ouyang, H. Cheng, X. Zhang, L. Yao, and M. Bazargan, "Distribution network planning considering distributed generation by genetic algorithm combined with graph theory", *Electric Power Components and Systems*, Vol. 38, No. 3, 2010, pgs. 325-339.

[2.73] T. Niknam, S. I. Taheri, J. Aghaei, T. Jamshid; S. Tabatabaei, M. Nayeripour, "A modified honey bee mating optimization algorithm for multiobjective placement of renewable energy resources", *Applied Energy*, Vol. 88, No. 12, 2011, pgs. 4817-4830.

[2.74] H. Oh, "Optimal planning to include storage devices in power systems", *IEEE Transactions on Power Systems*, Vol. 26, No. 3, 2011, pgs. 1118-1128.

[2.75] S. M. Moghaddas-Tafreshi, H. A. Zamani, S. M. Hakimi, "Optimal sizing of distributed resources in micro grid with loss of power supply probability technology by using breeding particle swarm optimization", *Journal of Renewable and Sustainable Energy*, Vol. 3, No. 4, 2011, pgs. 043105/1-043105/17.

[2.76] D. Alfonso, A. Pérez-Navarro, N. Encinas, C. Álvarez, J. Rodríguez, and M. Alcázar, "Methodology for ranking customer segments by their suitability for distributed energy resources applications", *Energy Conversion and Management*, Vol. 48, No. 5, 2007, pgs. 1615-1623.

[2.77] S. Iniyan, K. Sumathy, L. Suganthi, and A. A. Samuel, "Sensitivity analysis of optimal renewable energy mathematical model on demand variations", *Energy Conversion and Management*, Vol. 41, No. 2, 2000, pgs.199-211.

[2.78] H. Ren, W. Gao, W. Zhou, K. Nakagami, "Multi-criteria evaluation for the optimal adoption of distributed residential energy systems in Japan", *Energy Policy*, Vol. 37, No. 12, 2009, pgs. 5484-5493.

[2.79] M. D. Ilic, J. Joo, L. Xie, M. Prica, N. Rotering, "A decision-making framework and simulator for sustainable electric energy systems", *IEEE Transactions on Sustainable Energy*, Vol. 2, No. 1, 2011, pgs. 37-49.

[2.80] S. Sakai, Y. Hayashi, S. Kawasaki, J. Matsuki, Y. Fuwa, and K. Mori, "Experimental multi-objective evaluation of radial and loop distribution network configuration using distribution network equipment", *IEEJ Transactions on Electrical and Electronic Engineering*, Vol. 3, No. 5, 2008, pgs. 530-539.

[2.81] H. Ko, K.Y. Lee, M. Kang, and H. Kim, "Power quality control of an autonomous wind-diesel power system based on hybrid intelligent controller", *Neural Networks*, Vol. 21, No. 10, 2008, pgs. 1439-1446.

[2.82] I. Wasiak, M. C. Thoma, C. E. T. Foote, R. Mienski, R. Pawelek, P. Gburczyk, and G. M. Burt, "A power-quality management algorithm for low-voltage grids with distributed resources", *IEEE Transactions on Power Delivery*, Vol. 23, No. 2, 2008, pgs. 1055-1062.

[2.83] A. Borghetti, M. Bosetti, S. Grillo, S. Massucco, C. A. Nucci, M. Paolone, and F. Silvestro, "Short-term scheduling and control of active distribution systems with high penetration of renewable resources", *IEEE Systems Journal*, Vol. 4, No. 3, 2010 pgs. 313-322.

[2.84] H. Li, F. Li, X. Fangxing; Y. Xu, D. T. Rizy, and J. D. Kueck, "Adaptive voltage control with distributed energy resources: Algorithm, theoretical analysis, simulation, and field test verification", *IEEE Transactions on Power Systems*, Vol. 25, No. 3, 2010, pgs. 1638-1647.

[2.85] N. El Halabi, M. García-Gracia, J. Borroy, and J. L. Villa, "Current phase comparison pilot scheme for distributed generation networks protection", *Applied Energy*, Vol. 88, No. 12, 2011, pgs. 4563-4569.

[2.86] M. A. Pedrasa, T. D. Spooner, and I. F. MacGill, "A novel energy service model and optimal scheduling algorithm for residential distributed energy resources", *Electric Power Systems Research*, Vol. 81, No. 12, 2011, pgs. 2155-2163.

[2.87] W. W. Weaver, "Dynamic energy resource control of power electronics in local area power networks", *IEEE Transactions on Power Electronics*, Vol. 26, No. 3, 2011, pgs. 852-859.

[2.88] A. Keane and M. O'Malley, "Optimal allocation of embedded generation on distribution networks", *IEEE Transactions on Power Systems*, Vol. 20, No. 3, 2005, pgs. 1640-1646.

[2.89] A. Poullikkas "Implementation of distributed generation technologies in isolated power systems", *Renewable and Sustainable Energy Reviews*, Vol. 11, No. 1, 2007, pgs. 30-56.

[2.90] D. Pudjianto, C. Ramsay, and G. Strbac, "Virtual power plant and system integration of distributed energy resources", *IET Renewable Power Generation*, Vol. 1, No. 1, 2007, pgs. 10-16.

[2.91] L. F. Ochoa, A. Padilha-Feltrin, and G. P. Harrison, "Time-series-based maximization of distributed wind power generation integration", *IEEE Transactions on Energy Conversion*, Vol. 23, No. 3, 2008, pgs. 968-974.

[2.92] Y. Chen, C. Shen, and J. Wang, "Distributed transient stability simulation of power systems based on a Jacobian-free Newton-GMRES method", *IEEE Transactions on Power Systems*, Vol. 24, No. 1, 2009, pgs. 146-156.

[2.93] M. A. A. Pedrasa, T. D. Spooner, I. F. MacGill, "Coordinated scheduling of residential distributed energy resources to optimize smart home energy services", *IEEE Transactions on Smart Grid*, Vol. 1, No. 2, 2010, pgs. 134-143.

[2.94] M. Reza, G. Papaefthymiou, P. Schavemaker, W. Kling, and L. Van Der Sluis, "Distributed generation impact on power system transient stability: A stochastic approach", *International Energy Journal*, Vol. 11, No. 2, 2010, pgs. 93-100.

[2.95] B. Klöckl and G. Papaefthymiou, "Multivariate time series models for studies on stochastic generators in power systems", *Electric Power Systems Research*, Vol. 80, No. 3, 2010, pgs. 265-276.

[2.96] A. Schroeder, "Modeling storage and demand management in power distribution grids", *Applied Energy*, Vol. 88, No. 12, 2011, pgs. 4700-4712.

[2.97] C. Cecati, C. Citro, and P. Siano, "Combined operations of renewable energy systems and responsive demand in a smart grid", *IEEE Transactions on Sustainable Energy*, Vol. 2, No. 4, 2011, pgs. 468-476.

[2.98] A. Keane, L. F. Ochoa, E. Vittal, C. J. Dent, and G. P. Harrison, "Enhanced utilization of voltage control resources with distributed generation", *IEEE Transactions on Power Systems*, Vol. 26, No. 1, 2011, pgs. 252-260.

[2.99] C. Marnay, F. Javier Rubio, and A. S. Siddiqui, "Shape of the microgrid", *Proceedings of the IEEE Power Engineering Society Transmission and Distribution Conference*, Vol. 1, 2001, pgs. 150-153.

[2.100] R. H. Lasseter, "MicroGrids", *Proceedings of the IEEE Power Engineering Society Transmission and Distribution Conference*, Vol. 1, 2002, pgs. 305-308.

[2.101] J. M. Carrasco, L.G. Franquelo, J.T. Bialasiewicz, E. Galvan, R.C.P. Guisado, M. Prats, J.I. Leon, and N. Moreno-Alfonso, "Power-electronic systems for the grid integration of renewable energy sources: a survey", *IEEE Transactions on Industrial Electronics*, Vol. 53, No. 4, 2006, pgs. 1002-1016.

[2.102] D. Salomonsson, L. Soder, and A. Sannino, "An adaptive control system for a DC microgrid for data centers", *IEEE Transactions on Industry Applications*, Vol. 44, No. 6, 2008, pgs. 1910-1917.

[2.103] K. Kurohane, A. Uehara, T. Senjyu, A. Yona, N. Urasaki, T. Funabashi, and C. Kim, "Control strategy for a distributed DC power system with renewable energy", *Renewable Energy*, Vol. 36, No. 1, 2011, pgs. 42-49.

[2.104] L. Xu and D. Chen, "Control and operation of a DC microgrid with variable generation and energy storage", *IEEE Transactions on Power Delivery,* Vol. 26, No. 4, 2011, pgs. 2513-22.

[2.105] S.K Sul, I. Alan and T.A. Lipo, "Performance testing of a high frequency link converter for space station power distribution system," *Proceedings of the 24th Intersociety: Energy Conversion Engineering Conference*, Vol. 1, No. 6-11, 1989, pgs. 617 – 623.

[2.106] I .S. Roth, M. Gaudreau, M. A. Kempkes, T. J. Hawkey, and M. J. Mulvaney, "Solid-state high frequency power converters", *Proceedings of the IASTED Multi-Conference- Power and Energy Systems*, Vol. 7, 2003, pgs. 322-326.

[2.107] Z. Ye, Zhihong, T. Wang, G. Sinha, and R. Zhang, "Efficiency comparison for microturbine power conditioning systems", *PESC Record - IEEE Annual Power Electronics Specialists Conference*, Vol. 4, 2003, pgs. 1551-1556.

[2.108] C. Lai, C. Pan, and M. Cheng, "High-efficiency modular high step-up interleaved boost converter for dc-microgrid applications", *IEEE Transactions on Industry Applications*, Vol. 48, No. 1, 2012, pgs. 161-171.

[2.109] D. Jacob, K. Nithiyananthan, "Smart and micro grid model for renewable energy based power system", *International Journal for Engineering Modelling*, Vol. 22, No. 1-4, 2009, pgs. 89-94.

[2.110] X. Zhang, G.G. Karady, and Y. Guan, "Design methods investigation for residential microgrid infrastructure", *European Transactions on Electrical Power*, Vol. 21, No. 8, 2011, pgs 2125-2141.

[2.111] J. Jimeno, J. Anduaga, J. Oyarzabal, and A.G. De Muro, "Architecture of a microgrid energy management system", *European Transactions on Electrical Power*, Vol. 21, No. 2, 2011, pgs. 1142-1158.

[2.112] A. Vaccaro, M. Popov, D. Villacci, and V. Terzija, “An integrated framework for smart microgridsmodeling, monitoring, control, communication, and verification”, *Proceedings of the IEEE*, Vol. 99, No. 1, 2011, pgs. 119-132.

[2.113] D. Pudjianto, C. Ramsay, and G. Strbac, “Microgrids and virtual power plants: Concepts to support the integration of distributed energy resources”, *Proceedings of the Institution of Mechanical Engineers, Part A: Journal of Power and Energy*, Vol. 222, No. 7, 2008, pgs. 731-741.

[2.114] H. Jiayi, J. Chuanwen, and X. Rong, “A review on distributed energy resources and MicroGrid”, *Renewable and Sustainable Energy Reviews*, Vol. 12, No. 9, 2008, pgs. 2465-2476.

[2.115] N.S. Wade, P. C. Taylor, P. D. Lang, and P. R. Jones, “Evaluating the benefits of an electrical energy storage system in a future smart grid”, *Energy Policy*, Vol. 38, No. 11, 2010, pgs. 7180-7188.

[2.116] E. Mashhour, and S.M. Moghaddas-Tafreshi, “Integration of distributed energy resources into low voltage grid: A market-based multiperiod optimization model”, *Electric Power Systems Research*, Vol. 80, No. 4, 2010, pgs. 473-480.

[2.117] M.K. Deshmukh, and S. S. Deshmukh, “Modeling of hybrid renewable energy systems”, *Renewable and Sustainable Energy Reviews*, Vol. 12, No. 1, 2008, pgs. 235-249.

[2.118] A. A. Hussein, S. Harb, N. Kutkut, J. Shen, I. Batarseh, “Design considerations for distributed micro-storage systems in residential applications”, *Proceedings of the International Telecommunications Energy Conference*, 2010.

[2.119] W. Prommee and W. Ongsakul, “Optimal multiple distributed generation placement in microgrid system by improved reinitialized social structures particle swarm optimization”, *European Transactions on Electrical Power*, Vol. 21, No. 1, 2011, pgs. 489-504.

[2.120] A. S. Siddiqui, C. Marnay, J. L. Edwards, R. Firestone, S. Ghosh, and M. Stadler, “Effects of carbon tax on microgrid combined heat and power adoption”, *Journal of Energy Engineering*, Vol. 131, No. 1, 2005, pgs. 2-25.

[2.121] N. J. Kelly, J. A. Clarke, A. Ferguson, and G. Burt, “Developing and testing a generic micro-combined heat and power model for simulations of dwellings and highly distributed power systems”, *Proceedings of the Institution of Mechanical Engineers, Part A: Journal of Power and Energy*, Vol. 222, No. 7, 2008, pgs. 685-695.

[2.122] Y. Yamagishi, H. Sugihara, O. Saeki, and K. Tsuji, "An operational algorithm for residential cogeneration systems based on the monitored daily-basis energy demand", *Electrical Engineering in Japan*, (English translation by Denki Gakkai Ronbunshi), Vol. 170, No. 2, 2010, pgs. 37-45.

[2.123] A. K. Basu, S. Chowdhury, and S. P. Chowdhury, "Impact of strategic deployment of CHP-based DERs on microgrid reliability", *IEEE Transactions on Power Delivery*, Vol. 25, No. 3, 2010, pgs. 1697-1705.

[2.124] M. Jovanovic, V. Turanjanin, V. Bakic, M. Pezo, B. Vucicevic, "Sustainability estimation of energy system options that use gas and renewable resources for domestic hot water production", *Energy*, Vol. 36, No. 4, 2011, pgs. 2169-2175.

[2.125] Y. Ono, N. Uchiyama, T. Nakamura, and Y. Fujita, "Short-term balanced supply and demand control system for microgrids", *Hitachi Review*, Vol. 54, No. 3, 2005, pgs. 141-144.

[2.126] A. G. Tsikalakis, and N. D. Hatziargyriou, "Centralized control for optimizing microgrids operation", *IEEE Transactions on Energy Conversion*, Vol. 23, No. 1, 2008, pgs. 241-248.

[2.127] Y. W. Li, and C. Kao, "An accurate power control strategy for power-electronics-interfaced distributed generation units operating in a low-voltage multibus microgrid", *IEEE Transactions on Power Electronics*, Vol. 24, No. 12, 2009, pgs. 2977-2988.

[2.128] E. Serban and H. Serban, "A control strategy for a distributed power generation microgrid application with voltage- and current-controlled source converter", *IEEE Transactions on Power Electronics*, Vol. 25, No. 12, 2010, pgs. 2981-2992.

[2.129] K. Jong-Yul, J. Jin-Hong, K. Seul-Ki, C. Changhee, H.P. June, K. Hak-Manand N. Kee-Young, "Cooperative Control Strategy of Energy Storage System and Microsources for Stabilizing the Microgrid during Islanded Operation", *IEEE Transactions on Power Electronics*, Vol. 25, No. 12, 2010, pgs. 3037-3048.

[2.130] T. L. Vandoorn, B. Meersman, L. Degroote, B. Renders, and L. Vandevelde, "A control strategy for islanded microgrids with DC-link voltage control", *IEEE Transactions on Power Delivery*, Vol. 26, No. 2, 2011, pgs. 703-713.

[2.131] M. A. Sofla, and G. B. Gharehpetian, "Dynamic performance enhancement of microgrids by advanced sliding mode controller", *International Journal of Electrical Power and Energy Systems*, Vol. 33, No. 1, 2011, pgs.1-7.

[2.132] C. Cho, J. Jeon, J. Kim, S. Kwon, K. Park, and S. Kim, “Active synchronizing control of a microgrid”, *IEEE Transactions on Power Electronics*, Vol. 26, No. 12, 2011, pgs. 3707-3719.

[2.133] H. Karimi, E. J. Davison, and R. Iravani, “Multivariable servomechanism controller for autonomous operation of a distributed generation unit: Design and performance evaluation”, *IEEE Transactions on Power Systems*, Vol. 25, No. 2, 2010, pgs. 853-865.

[2.134] E. Sortomme, S.S. Venkata, and J. Mitra, “Microgrid protection using communication-assisted digital relays”, *IEEE Transactions on Power Delivery*, Vol. 25, No. 4, 2010, pgs. 2789-2796.

[2.135] S. Khomfoi, W. Sae-Kok, I. Ngamroo, “An open circuit fault diagnostic technique in IGBTS for ac to dc converters applied in microgrid applications”, *Journal of Power Electronics*, Vol. 11, No. 6, 2011, pgs. 801-810.

[2.136] C. Álvarez Bel, M. A. Ortega, G.E. Escrivá, and A. G. Marín, “Technical and economical tools to assess customer demand response in the commercial sector”, *Energy Conversion and Management*, Vol. 50, No. 10, 2009, pgs. 2605-2612.

[2.137] S. A. Pourmousavi and M. H. Nehrir, “Demand response for smart microgrid: Initial results”, *IEEE PES Innovative Smart Grid Technologies Conference Europe*, 2011.

[2.138] M. A. Abido, “Environmental/economic power dispatch using multiobjective evolutionary algorithms,” *IEEE Transactions on Power Systems*, Vol. 18, No. 4, 2003, pgs. 1529–1537.

[2.139] A. Ahuja, S. Das, and A. Pahwa, “An AIS-ACO Hybrid Approach for Multi-Objective Distribution System Reconfiguration”, *IEEE Transactions on Power Systems*, Vol. 22, No. 3, 2007, pgs. 1101-1111.

[2.140] X. Li, Y. Song, and S. Han, “Frequency control in micro-grid power system combined with electrolyzer system and fuzzy PI controller”, *Journal of Power Sources*, Vol. 180, No. 1, 2008, pgs. 468-475.

[2.141] B. Ramachandran, S. K. Srivastava, D. A. Cartes, and C. S. Edrington, “Distributed energy resource management in a smart grid by risk based auction strategy for profit maximization”, *Proceedings of the IEEE PES General Meeting*, 2010.

[2.142] B. Ramachandran, S. K. Srivastava, C. S. Edrington, D. A. Cartes, “An intelligent auction scheme for smart grid market using a hybrid immune algorithm”, *IEEE Transactions on Industrial Electronics*, Vol. 58, No. 10, 2011, pgs. 4603-4612.

[2.143] A. Mazza and G. Chicco, “Multi-Objective Distribution System Optimization Using Euclidean Distance Calculations In The Genetic Operators”, *Proceedings of the International Conference on Power and Energy Systems*, 2012, pgs. 14-19.

[2.144] H. Frank and S. Mesentean, “Effcient communication interfaces for distributed energy resources”, *International Journal of Grid and High Performance Computing*, Vol. 2, No. 2, 2010, pgs. 23-36.

[2.145] B. Yoo, S. Yang, H. Yang, W. Kim, Y. Jeong, B. Han, and K. Jang, “Communication architecture of the IEC 61850-based micro grid system”, *Journal of Electrical Engineering and Technology*, Vol. 6, No. 5, 2011, pgs. 605-612.

[2.146] M. Erol-Kantarci, B. Kantarci, and H. T. Mouftah, “Reliable overlay topology design for the smart microgrid network”, *IEEE Network*, Vol. 25, No. 5, 2011, pgs. 38-43.

[2.147] H. Nikkhajoei and R. Iravani, “Steady-state model and power flow analysis of electronically-coupled distributed resource units”, *IEEE Transactions on Power Delivery*, Vol. 22, No. 1, 2007, pgs. 721-728.

[2.148] Z. Yanping and L. Yuping, “A novel newton current equation method on power flow analysis in microgrid”, *IEEE Power & Energy Society General Meeting*, 2009.

[2.149] M. Z. Kamh and R. Iravani, “Unbalanced model and power-flow analysis of microgrids and active distribution systems”, *IEEE Transactions on Power Delivery*, Vol. 25, No. 4, 2010, pgs. 2851-2858.

[2.150] H. Ren, W. Zhou, K. Nakagami, W. Gao, and Q. Wu, “Multi-objective optimization for the operation of distributed energy systems considering economic and environmental aspects”, *Applied Energy*, Vol. 87, No. 12, 2010, pgs. 3642-3651.

[2.151] A.A. Moghaddam, A. Seifi, Alireza; T. Niknam, M. Z. A. Pahlavani, “Multi-objective operation management of a renewable MG (micro-grid) with back-up micro-turbine/fuel cell/battery hybrid power source”, *Energy*, Vol. 36, No. 11, 2011, pgs. 6490-6507.

[2.152] C. Schwaegerl, L. Tao, P. Mancarella, and G. Strbac, “A multi-objective optimization approach for assessment of technical, commercial and environmental performance of microgrids”, *European Transactions on Electrical Power*, Vol. 21, No. 2, 2011, pgs. 1271-1290.

[2.153] K. Hopkinson, X. Wang, R. Giovanini, J. Thorp, K. Birman, and D. Coury, “EPOCHS: a platform for agent-based electric power and communication simulation built from commercial off-the-shelf components", *IEEE Transactions on Power Systems*, Vol. 21, No. 2, 2006, pgs. 548 –558.

[2.154] R.H. Lasseter, J. H. Eto, B. Schenkman, J. Stevens, H. Vollkommer, D. Klapp, E. Linton, H. Hurtado, J. Roy, "CERTS Microgrid Laboratory Test Bed", *IEEE Transactions on Power Delivery*, Vol. 26, No. 1, 2011, pgs. 325-332.

[2.155] J. Jeon, J. Kim, H. Kim, S. Kim, C. Cho, J. Kim, J. Ahn, K. Nam, "Development of Hardware In-the-Loop Simulation System for Testing Operation and Control Functions of Microgrid", *IEEE Transactions on Power Electronics*, Vol. 25, No. 12, 2010, 2919-2929.

CHAPTER 3

FRAMEWORK DEVELOPMENT

While numerous smart grid technological components have made their way to market, a comprehensive framework for integrating the existing power system infrastructure with emerging control, communication, power electronic, and information systems remains elusive. Absent the framework, it is very difficult to meet the challenge of developing the means to endow broader power system flexibility, facilitate better responsiveness to customer objectives, and improve power delivery, while allowing higher levels of renewable generation and enabling technologies. Clearly meeting all smart grid objectives is a tall order, but the difficulty is significantly increased by the lack of a clear direction for future implementation.

Microgrids are seen as a bridging technology to addresses these systematic concerns. What sets microgrids apart from conventional approaches to power system power management is the ground-up approach to local customer autonomous control. Under normal circumstances, microgrids participate in utility-connected power system operations, contributing excess power, providing ancillary services, or purchasing electricity from the bulk power system. Under emergency conditions, microgrids can separate, or island, from the utility power system and operate independently, within limits. Besides operating in an autonomous manner, the microgrid concept allows the local microgrid operator, owner, or group of participants to establish their own operating objectives and operate microgrid equipment towards local goals. In this way, microgrids are seen as a means to aid the growth of distributed renewable generation, facilitate implementation of customer-managed demand response, and raise overall system reliability while at the same time allowing the existing power system infrastructure to grow and evolve in a smart way.

This chapter focuses on the development of the microgrid simulation framework. This includes a discussion of why microgrids are unique from conventional power system operations, details about the scope of the framework, and key aspects of its development. Details of microgrid asset and component models are located separately, in Chapter 5.

3.1 Microgrid Uniqueness

For decades, the traditional power system infrastructure model has been to concentrate generation assets centrally and transmit power to distant customers. As the power system grows to meet future demand, this conventional centralized model can incur significant costs for new transmission lines, cause concern regarding system stability, and present challenges for system flexibility. A logical alternative solution to these challenges is to deploy distributed generation systems, which are normally smaller in capacity, adaptable in structure, and installed close to customer load demand. Microgrids are a distributed solution that can couple multiple DERs, storage systems, and loads, within a localized network concentrating thems as a singular power system entity that interconnects with the utility grid in a distributed manner at defined PCCs.

It is important to note that the microgrid concept goes beyond the conventional means of coupling renewable DER to the power system. While experience has shown that the impact of integrating a limited number of DERs onto the grid is not problematic, this is not so in higher levels of penetration [3.1]. At low penetration, small DERs in limited deployment are too small in capacity to supply power back to the utility, also known as reverse powering [3.2]. Investigations have shown the benefits and drawbacks of broader DER integration for conventional power system performance [3.3] and, overall, uncontrolled connection of DERs to the utility grid is undesirable, especially in large quantities [3.4]. The bottom line is that under a conventional power system model, DERs are very difficult to integrate in high proportions without causing severe instabilities and compromising power system integrity.

Knowing that renewable DERs are difficult to integrate and potentially hazardous to the power system in large numbers, utility planners and system operators have been wary of these technologies. However, microgrids help address this concern directly, making microgrids more attractive to operators and planners, alike. The microgrid concept concentrates uncertainty caused by renewable generation; rather than many variable DERs independently connected to the utility network, the DERs are combined within the microgrid with limited PCCs. This is important because the renewable DERs are concentrated on the microgrid LV AC network, at worst causing voltage fluctuations on one LV/MV transformer on the utility MV distribution network. Those pre-defined microgrid PCCs are much more straightforward to disconnect in emergency situations than many dispersed DERs. Of course, this has described a worst case uncontrolled scenario that is not desirable, nor does it represent the typical operating behavior of a controlled microgrid, but it highlights the immediate infrastructure difference between un-concentrated, large area distribution of LV/MV DER connections to the distribution system, to the concentrated nature of DERs within microgrids.

Related to the DER concentration concept, microgrids also conglomerate the interests of microgrid customers and facilitate control of local assets towards their self-interest. In other words, the responsibility for uncertainty incurred by variable generation, shifting load patterns, and changing storage levels is shifted onto the microgrid operator and is served at the local level. This is very attractive to the utility system operator and planner because uncertainty is difficult to plan for. At the utility level, load-following is achieved by supplementing base-loaded central power plants with large peaking plants. When demand is uncertain, it is difficult to schedule base-loading and increases the reliance on peaking plants, at significantly higher per unit cost and emissions production. By customers being served by microgrid supplies first, in conjunction with a utility connection, much of the fluctuation incurred by resource variability and loading changes can be mitigated at the microgrid level. By facilitating power management at nearly the lowest hierarchical level on the power system, i.e. at the LV microgrid, it lessens the burden for the utility managing the broader power grid. In this way, both customer and utility operator benefit.

Clearly, the positive attributes for the utility operator and planner that are associated with microgrids do come with technological challenges [3.5]. This is particularly true with the microgrid capability to operate interconnected with the utility under normal conditions, but also transition to and from an islanded condition during emergencies. Under normal conditions, an interconnected microgrid must, at the very least, comply with grid rules and operate within established power system guidelines [3.6]. This ensures a high level of service to the local microgrid customers, as well as acceptable real and reactive power support to the utility. The islanded mode, however, is an unconventional power system operating capability, primarily because the microgrid must be able to regulate and sustain its own power delivery [3.7]. Coupling these two modes of operation together into a functional power management and control strategy has not been accomplished to date, and highlights the importance of the work described herein. Further, this work opens new doors that emphasize, ultimately, that economic concerns will dictate the exchange of energy services between the microgrid and electrical grid. The microgrid power management control architecture must be capable of incorporating these considerations and adding value for the customer and utility.

3.2 Scope

An important terminology distinction must be made that is applicable throughout this paper. For clarity, although sometimes used interchangeably in literature, the terms centralized, decentralized, and distributed refer to unique methods of decision-making. Centralized decision-making arises when all information and communication throughout the system is aggregated in a central location. At the central node, decisions are made for each subsystem node within the control boundary. Centralized control architectures reduce the number of individual subsystem controllers in favor of reliance on communication and computational complexity at the central supervisor. Purely decentralized control, on the other hand, requires no communication between subsystems because all control decisions are made with local information only; a controller is assigned to each subsystem. This is not ideal, however, because factors such as stability and the optimality of system-wide objectives cannot be assured [3.8]. Alternatively, an enhanced decentralized (sometimes referred to as hybrid decentralized or distributed) control architecture does not rely on a central supervisor, but is also not purely decentralized. Instead, each subsystem may have its own controller imbued with the capability to communicate with other controllers for the purpose of sharing information. This sharing may allow better decisions to be made without complete reliance on local information alone. Unfortunately, terms for non-centralized control architectures are often used interchangeably in the literature. For the purpose of this work, references to decentralization implies the lack of a central supervisor and the ability of control entities to communicate. As enhanced decentralized control is the primary focus of this work, the hope is that this terminology distinction will prevent confusion between the control architecture, physically distributed assets, and the concept of distributed generation.

Centralized control schemes for power systems are common. This has been feasible as the grid matured due to limited numbers of monitored and controllable components. As the quantity and complexity of system elements grows rapidly, centralized control is increasingly complicated and costly. Alternatively, this work is focused on enhanced decentralized control techniques applied to microgrids. This appears to be a good fit; microgrids are autonomous power system infrastructure components that have the potential for continuous operation with limited need for exterior communication. In this way, they may be controlled independently from the external utility grid network. In continuation of the decentralized control concept, this work seeks to avoid a central controller for the microgrid itself and, instead, distribute decision-making within the microgrid, as well.

Unfortunately, a single platform for conducting multi-agent research for a microgrid system does not currently exist. Many software platforms were investigated, to accomplish this task, but none were ultimately satisfactory. This is not surprising considering the need for the implementation of mathematical models to simulate microgrid components, as well as the ability to create agent algorithms and facilitate an environment for them to "live" and communicate. Subsequently, an open-source simulation environment that can emulate the real-time environment experienced by microgrid agents and their controlled assets was developed.

The key parts of this project will be explained in following sections, but generally involved the creation of appropriate models for microgrid assets and infrastructure, developing distributed agents capable of coordinating microgrid power management and control, and stand-alone simulation of various microgrid scenarios to validate methodologies. Each of these project components will be discussed in detail.

3.3 Approach to Framework

Today, many software packages exist to assist the researcher in developing accurate mathematical models of physical systems. One area of physical system modeling that is particularly challenging is electrical systems. In order to develop a complete electrical system model, it would incorporate quantum, electromagnetic, mechanical, and thermal phenomena, each with varying time-scales, computational complexity, and effect on overall system performance. The relationship between physical phenomena, time-scales, and the desired detail of analyses performed by researchers is displayed in Figure 3.1.

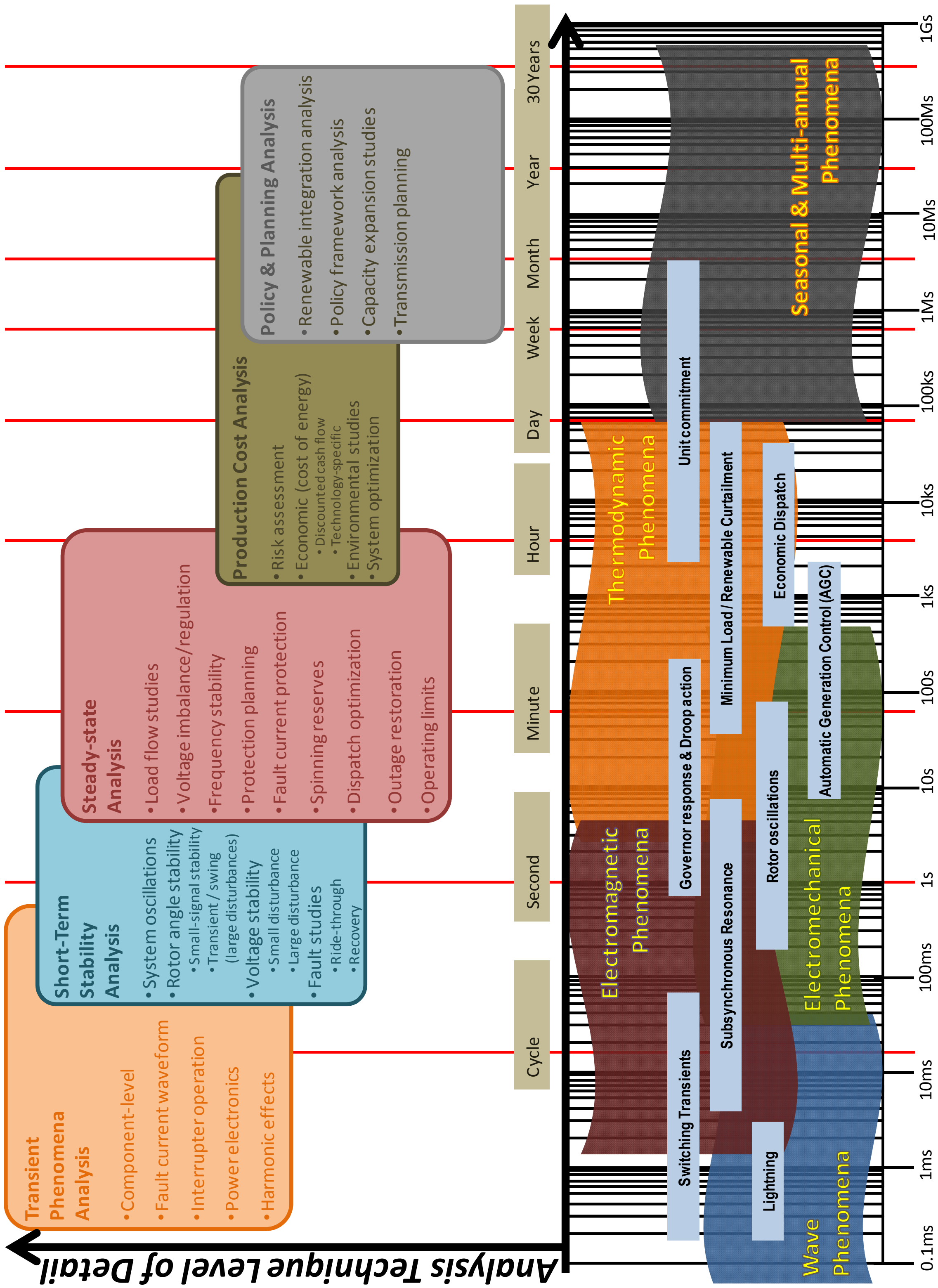

Figure 3.1. Power system phenomenon and analyses.

In many cases, highly dimensional and non-linear characteristics can be linerarized within regions of expected operation or utilize simplifying assumptions, which somewhat eases model development. This fact is capitalized upon by researchers that utilize a variety of software tools when designing and performing analyses of electrical systems. Software, including MATLAB/Simulink, PSPICE, PSS/E, PSCAD, PowerWorld, etc., each allows an analytical focus, when care is applied, that facilitates the proper development of electrical system models that can yield meaningful simulation results given the underlying assumptions. In most cases for power system studies, rather than component level studies, the analytical objective is to evaluate electrical stability. Power system stability is defined by the IEEE/CIGRE Joint Task Force as: "the ability of an electric power system, for a given initial operating condition, to regain a state of operating equilibrium after being subjected to a physical disturbance, with most system variables bounded so that practically the entire system remains intact" [3.9]. Categorically, the analysis of electrical stability, the identification of key factors that contribute to instability and instability mitigation require the classification of stability into appropriate categories which dictate the appropriate level of system detail and analytical techniques for model development [3.10]. Static stability, therefore, describes the effects of gradual small changes to system parameters and focuses on the response of system assets reestablish a tolerable state of operation after such changes. Alternatively, although the term "dynamic stability" is potentially confusing and both IEEE and CIGRE have advised against its usage, it implies the ability of a power system to respond to large disturbances. In other words, when compared to static stability, transient stability is the effect of significant sudden disturbances such as line faults, switching of lines, the application or removal of large loads, etc. on the system's ability to return to a tolerable state of operation.

For the purposes of this study, electrical stability is an important concern. The focus of PM&C is twofold: first, the proper dispatch of microgrid generation, load, and storage assets towards the user-assigned goals is paramount. Secondly, the safe and reliable operation of the microgrid electrical network, including the control assets so that parameters remain within acceptable tolerances is important. In other words, power management primarily describes asset dispatch for static stability. However, for proper microgrid operation, aspects of transient stability are important, especially as sudden events may occur that affect system operation at any time. Therefore, the control component of the PM&C system will address large and fast-acting transient events that impact microgrid operations.

Unfortunately, while many of the commercial software packages offer significant opportunities for customization, some unique aspects of the research project described herein make it infeasible to develop all computational components within a single package. Numerous software packages were investigated as part of this project and many included aspects that were ideal for segments of the microgrid PM&C development, but none allowed the key customization to fully achieve the research objectives. Some of the challenges commercial software presented that led to an interest in developing custom software tools included:

a. Lack of continuous, real time operation.

b. Proprietary or inflexible computational engines.

c. Inability to develop control algorithms.

d. Lack of means to implement agent-based methods.

e. Multi-platform communication issues.

f. Limited access to system data.

g. Lack of support for multi-threaded applications.

h. Inability to develop custom interface for goal-setting.

i. Difficulty with or lack of code conversion.

j. Cost and licensing.

After thorough evaluation, it was decided to design, develop, and implement the proposed multi-agent PM&C framework using the Java Runtime Environment (JRE) and perform algorithm development with the Java programming language. Three primary advantages of the Java platform led to this decision, including: the ubiquity and compactness of the language, the broad availability of virtual machine support on everything from cell phones to servers, and the proven Java Agent DEvelopment Framework (JADE) multi-agent class libraries that allow compliant communication between system agents. Although this development path is more difficult, the advantages for wider implementation and applicability are clear. Subsequently, the project development roadmap, shown in Figure 3.2, annotates how existing commercial software tools are used for this project, as well as independent development.

3.4 Framework Developmental Roadmap

A comprehensive framework for microgrid multi-agent power management and control has not been developed or reported in the literature. Subsequently, very little work was available to build upon and the developmental roadmap, shown in Figure 3.2, was created to provide a path towards achieving the tools and simulation environment necessary.

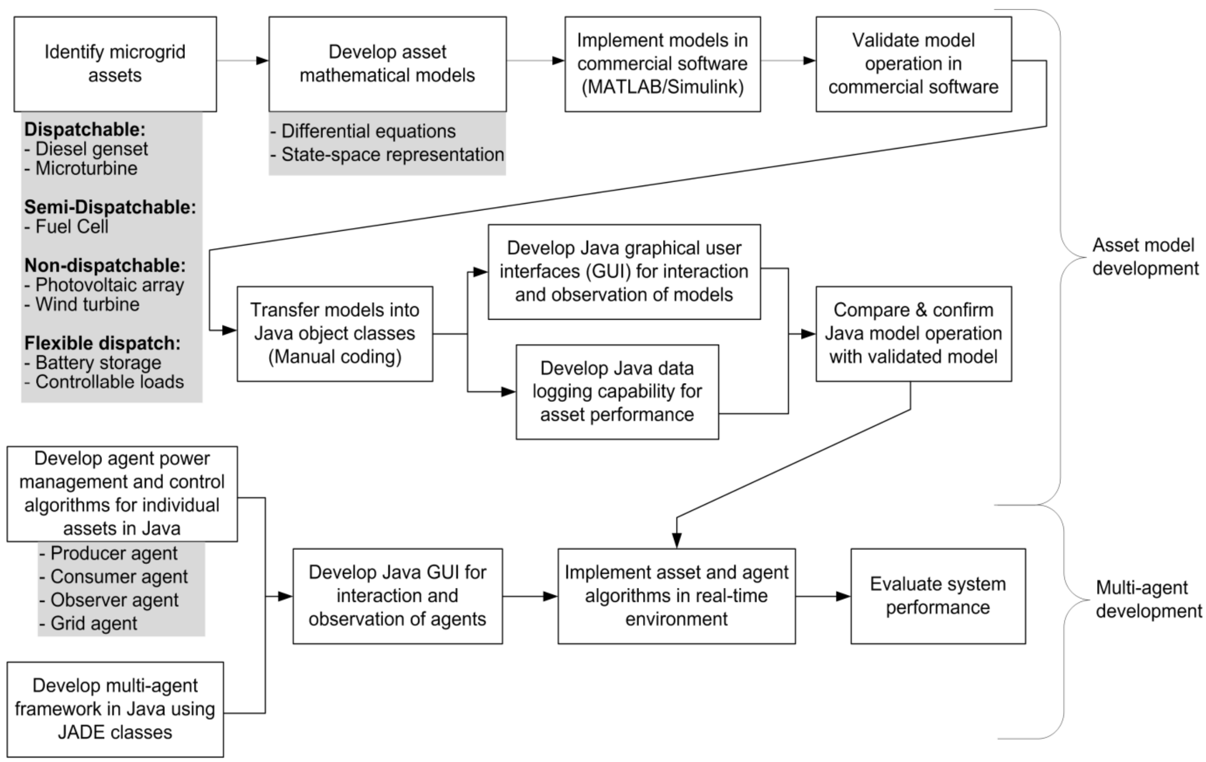

Figure 3.2. Asset model and multi-agent algorithms developmental roadmap.

This straightforward developmental path allowed the components of the complete microgrid simulation to be developed individually and later combined in a common framework.

The simulation environment developed combines the ability to operate component models with control entities, called agents, that guide their operation. Three primary layers, depicted in Figure 3.3, make up the simulation framework are:

Component layer: comprised of the component models. The elements in this layer allow the physical, electrical, mechanical, and chemical aspects of component operation to be calculated.

Control layer: related to the component layer, comprises the direct controls necessary to manipulate a component towards desired operation. In some cases, both the component and control layers may be combined in a single model.

Agent layer: comprised of the higher-level software entities that make operational decisions for assets. The agent layer interacts with assigned components through the control layer.

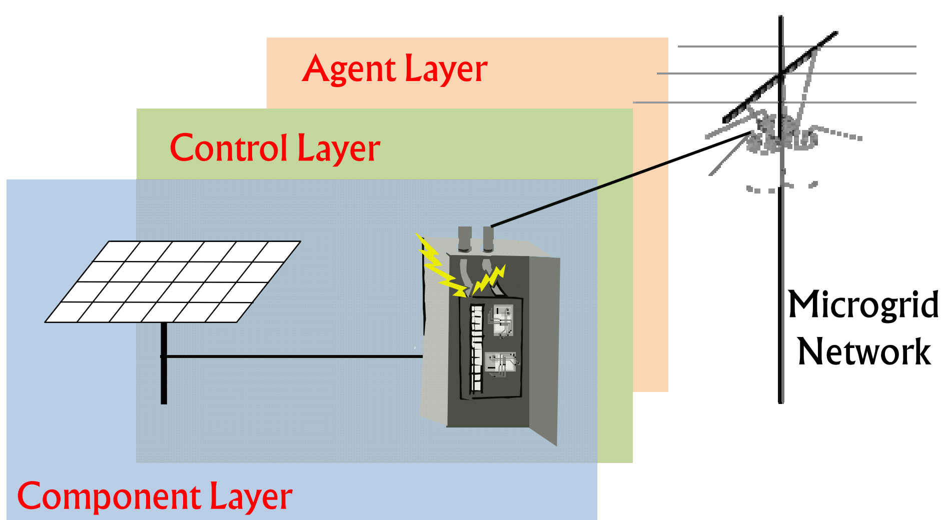

Figure 3.3. Simulation environment framework layers.

Each element within the simulation environment is interconnected with other element in two ways. First, the control agents may interact through a decision-making exchange pathway. This communication path allows the agents to be more than simply decentralized control entities. By enhancing the agents' capability through the decision-making exchange, agents may cooperate towards achieving a better overall outcome for total microgrid system objectives. The second pathway comprised by the simulation environment is the electrical data exchange. This lower hierarchical communication path allows the simulation environment to calculate the electrical conditions on the microgrid. This allows power system modeling that would otherwise not be achievable without aggregating microgrid element data. The two communication pathways are kept separate so as to not compromise the integrity of the enhanced decentralized MAS concept. The connections between microgrid elements are shown in Figure 3.4.

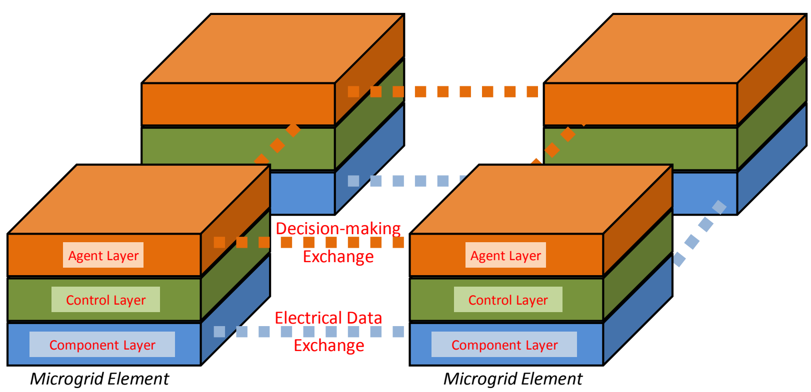

Figure 3.4. Microgrid simulation environment comprised of layered elements.

3.5 JADE

In most cases, the foundational models for microgrid assets were derived from published literature. These models were adapted and modified based on, in some cases, new insight into additional parameters that were required to be modeled for power management purposes. For the individual agent algorithms, these were completely unique, as nothing comparable was found in published literature. However, an important functional part of the agent designs was used from an existing resource. The JADE open-source library objects were originally developed by the Telecom Italia Lab, a R&D branch of the Telecom Italia Group, in 2000. The libraries continue to be maintained for public use, as recently as the 4.2.0 release in June 2012. JADE is simply a set of objects and methods that allow Java programs (referred to as agents) to formalize communication between them. This communication can be local to a single computer or over a communication network, such as TCP/IP, on multiple computers. JADE is a communication protocol that adheres to a strict set of rules for the formatting, sending, and receiving of those messages. JADE does not have any pre-built agents or any pre-written algorithms, just the communication libraries. This was incredibly useful for microgrid agent development because the complex details of communication were not the focus of this project. Subsequently, at the agent level, all agent algorithms developed for microgrid applications adhered to JADE rules for communication.

The Foundation for Intelligent Physical Agents (FIPA) is an IEEE Computer Society standards organization that develops, maintains, and promotes standards for agent-based technology [3.11]. Standards promulgated by FIPA provide interoperability guidelines and communication protocols that encourage the development of systems that can easily interact. Most importantly, compliance with FIPA standards will likely be necessary before implementation of future multi-agent systems (MAS). JADE is a FIPA-compliant platform that specifies a message interaction format that includes performative actions and interaction rules. An example of a market-based microgrid MAS implemented with JADE is shown in [3.12]. JADE allows development of unique Java-based agents that can perform a myriad of tasks while interacting with other agents towards achievement of a desired outcome, within a FIPA-compliant framework.

A JADE-based MAS for microgrid power management is a straightforward implementation. Each component or group of components, within the microgrid is implemented with an associated agent. Upon initialization, the Agent Platform (AP) operates autonomously in the background to support the MAS framework. The microgrid MAS is accessible for communication by other FIPA-compliant platforms, such as from the utility grid, neighboring microgrids, etc. [3.13]. Once initialized, agents attached to microgrid components, or groups of components, can operate independently, according to their programming. The AP directly supports "plug-and-play" connectivity, as agents can come on- and off-line asynchronously and can be easily replicated for fault survivability. Collectively, microgrid agents operate according to user-defined goals and can work independently or cooperatively as their programming dictates, executing their responsibilities in parallel with other agents. Additionally, to support broader parallelism between agent operations, JADE utilizes an event handling concept, called behaviors, to formally dictate how an agent will react to a particular change in state. The concept of behaviors allows JADE agents to more efficiently operate in a real-time environment [3.13]. This attribute allows asynchronous communication, such as the sending and receiving of messages independent of a coordinated clock signal between agents. This, in turn, permits agents to react and cooperate given unpredictable events. In this manner, the agents are not chained to a primary cadence signal or client-server architecture which is characteristic of centralization.

By utilizing the FIPA guidelines for agent-based communication, the interoperability and communication protocols for the microgrid MAS are standardized [3.11]. A fundamental enabling characteristics of a FIPA-compliant MAS is the communication rules, formulated from “performative” messages, that facilitate consistent and efficient communication between agents or other agent platforms. A performative is a concise message header that describes the purpose of the message and indicates the structure of the information that the message contains. Typical performatives include: *INFORM*, *PROPOSE, ACCEPT PROPOSAL, REJECT PROPOSAL, QUERY IF, REQUEST*, *NOT UNDERSTOOD*. By exchanging performative messages, agents can rapidly and asynchronously exchange information for the purpose of forwarding their assigned tasks. Likewise, the performative messaging format can be utilized on the myriad of communication mediums available, but is typically implemented on local area networks.

As a consequence of being crafted in Java, JADE library objects (for example: a method to handle an incoming message) can be quickly integrated into custom algorithms written in Java. In other words, given a custom control program to turn on and off a light switch on command, adding the capability to actuate the light when the control program received a particular message over the internet could be implemented with JADE libraries that "understand" incoming messages directed to it. This does not eliminate the need for the initial control program, but the JADE functionality adds the capability to communicate easily.

The most common general mathematical simulation and analysis software being used worldwide is MATLAB/SIMULINK. As of 2010, the manufacturers of the software, MathWorks Inc., had not developed a means to call JADE libraries (or include them) with MATLAB/SIMULINK. This included the lack of capability to call Java code from within the program, despite the ability to call C, C++, or FORTRAN code directly from MATLAB by creating MEX-files. As of early 2012, MathWorks released support for calling and using Java objects with MATLAB Builder JA which apparently allows creating Java classes from MATLAB m-code, but it is unclear whether complete MATLAB functionality, such as solvers, are accessible. This difficulty in evaluating the MATLAB JA Builder tool highlights a primary reason why the MATLAB software was not idea for this project development: it is proprietary software requiring a license on every machine that uses it. The JA Builder itself is an additional toolbox that must be purchased separately from the MATLAB program. Developing programs that were tied to the MATLAB software, rather than an open-source language such as Java, was undesirable. Additionally, at the outset of design, it was unclear whether the MATLAB/SIMULINK state machine toolbox was adequate to build complicated agent algorithms. For these reasons, development in Java was chosen for this project.

3.6 Decision-making Concept

A MAS is a collection of autonomous computational entities (agents) that possess the ability to perceive aspects of their environment and, in many cases, act upon that environment, within limits. The agents have varying degrees of intelligence based on their roles within the architecture. If so imbued, the agents may pursue goals as to "optimize" certain performance measures within an environment which can be hard to define analytically [3.14]. Additionally, agents may have the capability to interact with other agents. This communication may be simply for the purposes of information passing, or in more complex schemes may involve negotiation or cooperation towards a common goal. This may include interaction whereby agents converge on a course of action by proposing, counter-proposing, accepting, or rejecting operational choices. Additionally, a defining aspect of MAS agents is their perceptual scope of the system situation and highlights a prime difference between centrally managed agent-based systems and those that have dispersed control. Table 3.1 compares centralized and enhanced decentralized MAS schemes. A purely decentralized MAS is not discussed, plainly, because the lack of interaction between agents renders most of the MAS capability moot and is the trivial case.

Centrally-based MAS architectures involve a hierarchy of agents. In a system that incorporates multiple components, system-level control is typically achieved by a central agent with primary decision-making responsibility. This central agent maintains a global operational view, often sourced by information from less sophisticated agents around the system. Decision-making is achieved by the central agent considering the system as a whole and executing behavior that moves it closer to specified objectives. It is widely known that conglomerating all decision-making power centrally speeds the process, often simplifies communication protocols, and may be more economical to implement. However, centralized control can complicate system survivability if the prime agent is lost, can limit the ability of agents without communication to act independently, and incur higher communication overhead that may slow a serialized decision-making process.

Table 3.1. Centralized versus enhanced decentralized MAS.

	Centralized MAS	Enhanced Decentralized MAS
Characteristics	Sophisticated central supervisor; remote agents with limited capabilities dependent on supervisor for decision-making.	No central supervisor; sophisticated distributed agents organize and make decisions collectively.
Communication Infrastructure	Client-server; *n* communication paths†.	*n* minimum communication paths; *n(n-1)/2* maximum if fully networked†.
"Plug & Play"	Entrance and exit from system dictated by supervisor.	Framework facilitates agents to enter and leave the system as conditions permit.
Survivability	System control totally dependent on central supervisor.	Control responsibilities are dispersed and not dependant on a single node.
Reliability	Single node of failure; central supervisor must be redundant.	Decision-making not dependant on a single node.
Synchronization	Central supervisor dictates; control actions issued serially.	Agents act independently; communications and control actions occur asynchronously and in parallel.

†: *n* represents the number of agents within a particular MAS.

An enhanced decentralized MAS is somewhat different. Although similar numbers of agents are assigned to assets and perceptual nodes within the system, there is no singular supervisor that encompasses the prime decision-making power for the group.

The dispersed agents themselves are given a level of intelligence and communication capability that allows them to make decisions independently, as well as coordinate with the group. The primary advantages of decentralizing the microgrid MAS are: dynamic flexibility, asynchronous operation, system survivability, and the potential for lower communication overhead. Each local agent is given a level of intelligence that is consistent with its tasks. While these tasks may be easily quantifiable, with rapidly changing system dynamics, the agents pursue their assigned goals so they meet given performance measures. Additionally, this dynamic environment cannot rely on a synchronous framework as unanticipated events occur. Decentralizing primary functions of control frees agents from dependence on communication traffic as they make decisions and carry out their tasks.

Centralized control schemes for power systems are common, especially with the rise of supervisory control and data acquisition (SCADA) systems [3.15, 3.16, 3.17]. This has been feasible as the grid matured due to limited numbers of monitored and controllable components. It is noted that, as of 2010, only 48% of U.S. substations were automated with SCADA systems while only 78% of U.S. substations had any remote outage detection [3.18]. As the quantity and complexity of system elements grows rapidly, centralized control is increasingly complicated and costly. It has been shown that complex decision-making for large systems that centrally aggregate control can be computationally intensive, cumbersome, and require surmounting numerous technical and communication challenges [3.19]. However, for localized power systems, such as those found aboard modern ships, multiple-objective optimization methods have been shown to be effective [3.20]. Presently, it is unknown whether centralization or decentralization is best suited to microgrid operations, but enhanced decentralized methods appear to be a good fit; microgrids are autonomous power system infrastructure components that have the potential for continuous operation with limited need for exterior communication. In this way, they may be controlled independently from the external utility grid network. In continuation of the enhanced decentralized control concept, the focus of this project is to seek to avoid a central controller for the microgrid itself and, instead, decentralize decision-making within the microgrid, as well.

3.7 *Intra-* versus *Extra*-Microgrid

Microgrids are power system infrastructure components. However, they may appear very differently depending on one's perspective within the power system. Within the microgrid system boundary made up of generation, storage, and load assets, the power management and control focus is local. That is to say that, on the microgrid side of the PCC, details about operation on the macrogrid side of the PCC are reduced to power flow and status of the interconnection. Likewise, from the macrogrid side of the PCC, the inner workings of the microgrid are irrelevant and reduce to the microgrid's power flow contribution and status of interconnection. This boundary distinction is shown in Figure 3.5. From a hierarchical management and control perspective, *intra*-microgrid decision-making is influenced by *extra*-microgrid decision-making, and vice-versa. However, these decision-making processes are made to be separate. Ultimately, the *intra*-microgrid power management and control must be self-serving; providing continuity of electrical service to the local loads first before contributing services to the macrogrid. Local goals drive how *intra*-microgrid assets are operated and towards what objectives. Likewise, if *extra*-microgrid conditions indicate that the macrogrid is in distress, the microgrid will island to preserve its own integrity. This is not to say that microgrids cannot participate in broader macrogrid optimization or reconfiguration. Instead, for the purpose of MAS development at this stage, the lowest hierarchical level (*intra*-microgrid) dominates the decision-making design.

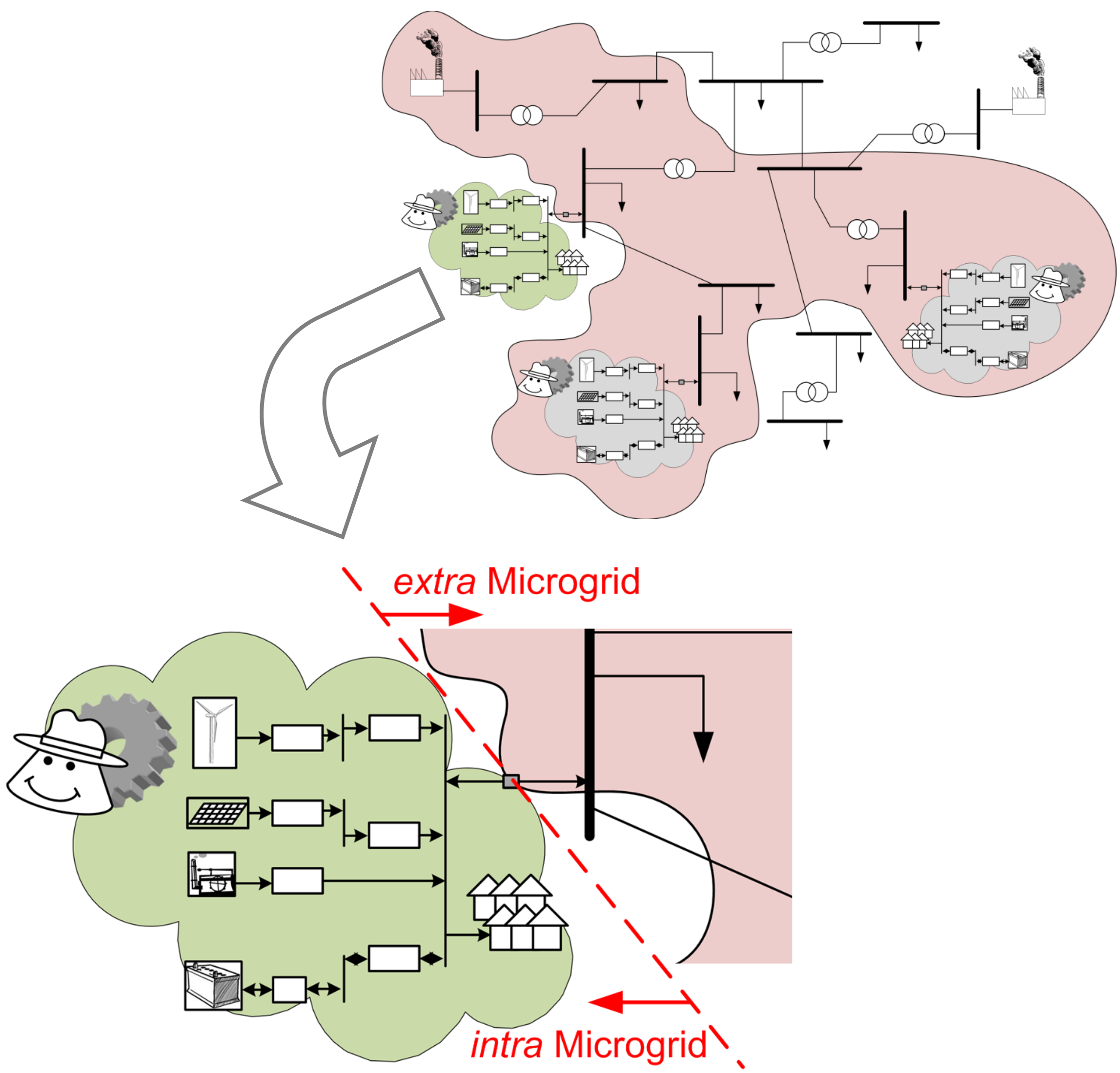

Figure 3.5. *Intra*- and *extra*-microgrid.

3.8 Communication

Communication in automated systems is an enormous field of study that bridges engineering and computer science. Over the past decade, communication capabilities have been increasing in DER and power system applications [3.21]. The means and attributes of communication for control architectures, such as the one developed herein, may greatly affect the performance of the overall system. However, the scope of this project demanded a limit to the investigation of communication effects on system operation. Primarily, because the MAS agents developed utilized TCP/IP communication, many aspects of communication degradation were considered minor and thus not considered. However, for completeness, the following section introduces the topic of communication effects on control architectures. The hope is that using the simulation environment and MAS architecture developed that future work may focus on communication and the related cybersecurity topics.

The two primary communication network topics that affect MAS development are the parametric attributes of the network itself and the network topology. Clearly, the physical construction of the network, including the network nodes, routing components, and physical information transmission media are very important to communication dynamics. Additionally, the network topology which represents the interconnectedness of nodes within the network, is very important in terms of reliability and speed of information dissemination. For the purpose of this project, the network topology was assumed to be complete; that is, that all agents communicating were network neighbors to all other agents. A variation of this topology, not investigated as part of this project, would involve topological bottlenecks where agents were not fully connected. Some recent research, such as in [3.22], has investigated the effect of network topology bottlenecks on information discovery. Information discovery involves the time period required for each agent in the MAS to compile a global set of data about the system simply through the dissemination of information from neighboring agents. Information discovery is very important in MAS systems that require agents to have global information prior to making decisions. This is different, however, from the MAS proposed in this project, primarily because global information from all agents is not required for MAS operation. Additionally, all agents in the developed MAS are neighbors and communication, when used, requires only one step node-to-node. Network topology issues could become more important in complex MAS implementations or in MAS-to-MAS configurations, but these investigations are out of the scope of this project.

Any control architecture that utilizes communication pathways for sensory perception, information sharing, or actuation is subject to an additional domain of uncertainty [3.23]. This uncertainty must be accounted for in the design of the automated system or else unpredictable or undesirable behavior may arise. A means of describing the degree of uncertainty for the purpose of design is called determinism. Determinism is defined as the quality of stable and predictable behavior of communication pathways from state to state [3.24]. In other words, the total communication delay incurred transmitting information from one node to another is bounded by a time t for all nodes in the system. However, communication pathways are mercurial at best and their reliability is described by the Quality of Service (QoS) [3.25]. The key aspects of QoS that affect the determinism of a communication pathway are:

Throughput – the instantaneous rate at which information may pass through a communication pathway (typically measured in bits/sec or data packets/sec) [3.26].

Delay (also known as latency) – an instantaneous measure of the time difference between the transmission and receipt of information. Network delay may arise from a number of sources, the most important of which are: processing delays, the time incurred by computation overhead required to route information through the communication network; queuing delays, the time period incurred while waiting for other information to be routed through common nodes in the network; transmission delay, the time period required to collect and send information at each network node; and propagation delay, related to the physical speed at which the information may be sent through the network medium [3.26, 3.27].

Errors – the frequency of information corruption that requires the information to be resent through the communication pathway. This is closely related to delay and is often not a primary concern in TCP/IP networks [3.26].

Jitter – the variability of delays due to the variability of other information traffic and resources available to pass it through the network [3.26].

Clearly, the QOS experienced by a communication network affects the speed and reliability of the information that is passed between control entities that use it. This may have important implications for MAS that rely on timely or synchronous access to information from other agents. However, the effect of QoS on MAS that communicate asynchronously for non-critical information sharing purposes may be less important. For the enhanced decentralized MAS developed for this work, the ultimate effect of QoS factors remains an open question. To that end, communication network simulation models were evaluated for this project. Specifically, the Java Network Simulator (JNS) was found to have the functionality necessary to simulate simple or complex network topologies [3.28]. JNS is an implementation of the Network Simulator (ns-2), a discrete network event simulator capable of simulating TCP, routing, and multicast protocols over wired and wireless networks [3.29]. The JNS implementation allows nodes, interfaces, and network links to be created easily and included in Java programs. The interface and link classes allow network dynamics to be simulated, mimicking user-defined QoS attributes at different locations within the network. Both may be either simplex (one-way) or duplex (two-way) connections. Interfaces, which connect nodes to links, simulate network entities such as routers, along with the bandwidth and queuing parameters common to them. Links, on the other hand, simulate the physical medium for information transmission such as wires, fiber optics, or wireless signals. Similar to interfaces, links allow the user to define network attributes such as bandwidth, propagation delay, and error rate, mimicking the effects of actual information transmission. Overall, JNS appears to be adequate at simulating network parameters of interest to researchers and is readily implementable alongside the Java simulation environment developed as part of this project.

So far, the discussion of network parameters and topology has been approached from the perspective of functionality. That is, the actual operation of an MAS is affected by how the network is composed and functions. However, there is another aspect of communications that has only recently gained prominence: cybersecurity [3.30]. The notion that information flows within the MAS control architecture could either be exploited for information superiority or be corrupted for the purpose of sabotage are cybersecurity topics [3.30, 3.31, 3.32]. Over the past three to five years, as smart grid concepts have been discussed with more urgency, the effect of hostile actors that could misuse access to power system control architectures has become a serious concern. At present, cybersecurity and how it relates to power system integrity overall has only begun to be investigated [3.33, 3.34]. Additionally, the major standard writing agencies in the United States, namely the IEEE, the North American Electric Reliability Corporation (NERC), National Institute of Standards and Technology (NIST), and the Department of Energy (DOE), have not provided clear guidelines or standards for system interoperabilities or security measures [3.35]. In fact, the conclusion of many industry entities has been to develop their own standards for cybersecurity implementation, leading to a spectrum of what is considered secure [3.35, 3.36]. As time moves forward, cybersecurity issues will become more important as the communication interconnectedness of power system components grows [3.37]. However, at this point, speculating on appropriate cybersecurity countermeasures beyond conventional communication encryption and physical security of network nodes, is inappropriate. What is certain, however, is that cybersecurity concerns will continue to haunt the power system infrastructure in very similar ways that they continue to plague the most broad and mature communication infrastructure in the world: the internet [3.38].

Communication and network attributes are important considerations for the implementation of the MAS developed in this project. However, given the immense diversity of issues and the specific expertise required for communication engineering investigations, these issues are left to future work.

REFERENCES CITED

[3.1] R.A. Walling, R. Saint, R.C. Dugan, J. Burke, and L.A. Kojovic, “Summary of distributed resources impact on power delivery systems”, *IEEE Transactions on Power Delivery*, Vol. 23, 2008, pgs. 1636 – 1644.

[3.2] P. Denholm, “Enabling Technologies for High Penetration of Wind and Solar Energy”, *Proceedings, ASME 5th International Conference on Energy Sustainability,* 2011, pgs. 1451-1458.

[3.3] K. Sedghisigarchi, and A. Feliachi, “Dynamic and Transient Analysis of Power Distribution Systems with Fuel Cells-Part II: Control & Stability Enhancement”, *IEEE Transactions on Energy Conversion*, Vol. 19, 2004, pgs.429-434.

[3.4] E.A. DeMeo, W. Grant, M.R. Milligan, and M.J. Schuerger, “Wind Plant Integration”, *IEEE Power and Energy Magazine*, Vol. 3, 2005, pgs. 38-46.

[3.5] T. Basso and R. DeBlasio, “IEEE 1547 series of standards: interconnection issues”, *IEEE Transactions on Power Electronics*, Vol. 19, 2004, pgs. 1159–1162.

[3.6] J. Zhenhua and R.A. Dougal, “Hierarchical microgrid paradigm for integration of distributed energy resources”, *Proceedings, IEEE Power and Energy Society General Meeting: Conversion and Delivery of Electrical Energy in the 21st Century*, Vol. 1, 2008.

[3.7] G. Celli, F. Pilo, G. Pisano, V. Allegranza, R. Cicoria, and A. Iaria, “Meshed vs. Radial MV Distribution Network in Presence of Large Amount of DG”, *Proceedings, IEEE Power and Energy Society Power Systems Conference*, Vol. 2, 2004 pgs. 709-714.

[3.8] C. Langbort, “Distributed control of complex interconnected systems: a convex approach”, Doctoral Dissertation, Cornell University, Ithaca, NY, 2005.

[3.9] IEEE/CIGRE Joint Task Force on Stability Terms and Definitions, "Definition and Classification of Power System Stability", *IEEE Transactions On Power Systems*, Vol. 19, No. 2, May, 2004.

[3.10] P. Kundur, Power System Stability and Control. New York: McGraw-Hill, 1994.

[3.11] Foundation for Intelligent Physical Agents (FIPA), 2010, available at: http://www.fipa.org/.

[3.12] K. Huang, S.K. Srivastava, D.A. Cartes, and L. Sun, “Market-based multiagent system for reconfiguration of shipboard power systems”, *Electric Power Systems Research*, Vol. 79, 2009, pgs. 550-556.

[3.13] F.L. Bellifemine, G. Caire, D. Greenwood, Developing Multi-Agent Systems with JADE. John Wiley & Sons, West Sussex, England, 2007, chapters 3-4.

[3.14] Gerhard Weiss (Editor), Multiagent Systems, MIT Press, Cambridge, MA, 1999.

[3.15] K. Barnes, B. Johnson, R. Nickelson, "Review Of Supervisory Control And Data Acquisition (SCADA) Systems", Idaho National Engineering and Environmental Laboratory, INEEL/EXT-04-01517, January 2004.

[3.16] A.G. Bruce, "Reliability analysis of electric utility SCADA systems", *IEEE Transactions on Power Systems*, Vol. 13 , No. 3, 1998, pgs: 844-849.

[3.17] K. Stouffer, J. Falco, and K. Kent, "Guide to Supervisory Control and Data Acquisition (SCADA) and Industrial Control Systems Security", NIST Special Publication 800-82, Computer Security Division - Information Technology Laboratory, National Institute of Standards and Technology (NIST), September 2006.

[3.18] By direction of Section 1302 of Title XIII of the Energy Independence and Security Act (EISA), "2010 Smart Grid System Report - Report to Congress", U.S. Department of Energy, February 2012.

[3.19] H. You, V. Vittal, and Z. Yang, "Self-Healing in Power Systems: An Approach Using Islanding and Rate of Frequency Decline-Based Load Shedding", *IEEE Transactions on Power Systems*, Vol. 18, No. 1, 2003.

[3.20] P. Mittra and G.K. Venayagamoorthy, "Implementation of an Intelligent Reconfiguration Algorithm for an Electric Ship Power System", *IEEE Transactions on Industry Applications*, Vol. 47, No. 5, 2011, pgs. 2292-2300.

[3.21] R. Yu, P. Zhang, W. Xiao, and P. Choudhury, "Communication systems for grid integration of renewable energy", *IEEE Network*, Vol. 25, No. 5, 2011, pgs. 22-29.

[3.22] H. Liang, B. J. Choi, W. Zhuang, X. Shen, and A. S. A. Awad, "Multiagent Coordination in Microgrids via Wireless Networks", *IEEE Wireless Communications*, Vol. 19, No. 3, 2012, pgs. 14-22.

[3.23] H. Kopetz, "Software engineering for real-time: a roadmap", *Proceedings of the Conference on the Future of Software Engineering,* 2000, pgs. 201-211.

[3.24] R. Zurawski (editor). The Industrial Communication Technology Handbook. CRC Press, Boca Raton, FL, 2005.

[3.25] Z. Wang. Internet QOS – Architectures and Mechanisms for Quality of Service. Academic Press, San Diego, CA, 2001.

[3.26] J.F. Kurose and K.W. Ross. Computer Networking – A Top-Down Approach (5th Edition). Addison-Wesley, New York, NY, 2010.

[3.27] S. Ci, J. Qian, D. Wu, and A. Keyhani, "Impact of wireless communication delay on load sharing among distributed generation systems through smart microgrids" *IEEE Wireless Communications*, Vol. 19, No. 3, 2012, pgs. 24-29.

[3.28] Available at: http://jns.sourceforge.net/

[3.29] Available at: http://www.isi.edu/nsnam/ns/

[3.30] G. N. Ericsson, "Cyber security and power system communication - essential parts of a smart grid infrastructure", *IEEE Transactions on Power Delivery*, Vol. 25, No. 3, 2010, pgs. 1501-1507.

[3.31] S. Clements and H. Kirkham, "Cyber-security considerations for the smart grid", *Proceedings of the IEEE PES General Meeting*, 2010.

[3.32] I. L. G. Pearson, "Smart grid cyber security for Europe", *Energy Policy*, Vol. 39, No. 9, 2011, pgs. 5211-5218.

[3.33] X. Li, X. Liang, R. Lu, X. Shen, X. Lin, and H. Zhu, "Securing smart grid: Cyber attacks, countermeasures, and challenges", *IEEE Communications Magazine*, Vol. 50, No. 8, 2012, pgs. 38-45.

[3.34] S. Sridhar, A. Hahn, and M. Govindarasu, "Cyber-physical system security for the electric power grid", *Proceedings of the IEEE*, Vol. 100, No. 1, 2012, pgs. 210-224.

[3.35] D. Dolezilek and L. Hussey, "Requirements or recommendations? Sorting out NERC CIP, NIST, and DOE cybersecurity", *Proceedings of the 64th Annual Conference for Protective Relay Engineers*, 2011, pgs. 328-333.

[3.36] Y. Yan, Y. Qian, H. Sharif, and D. Tipper, "A Survey on Cyber Security for Smart Grid Communications", *IEEE Communications Surveys & Tutorials*, In press, 2012.

[3.37] X. Li, X. Liang, R. Lu, X. Shen, X. Lin, and H. Zhu, "Securing smart grid: cyber attacks, countermeasures, and challenges", *IEEE Communications Magazine*, Vol. 50, No. 8, 2012, pgs. 38 – 45.

[3.38] A.H. Mohsenian-Rad and A. Leon-Garcia, "Distributed Internet-Based Load Altering Attacks Against Smart Power Grids," *IEEE Transactions on Smart Grid*, Vol. 2, No. 4, 2011, pgs. 667–674.

CHAPTER 4

MULTI-AGENT SYSTEM

MAS is defined as a collection of autonomous computational entities (agents), which can be effective in broad applications performing tasks based on goals in an environment that can be difficult to define analytically. Often within MAS architectures, autonomous agents work with a limited system-wide perspective and focus on localized task achievement [4.1]. An agent can act upon its environment, as well as interact with other agents that may have conflicting goals, towards an common goal. Agents can be imbued with limited or global perception of situational variables, and likewise, each agent's ability to affect the system environment is dependent on implementation. Although MAS architectures typically use software agents, any collection of computational entities that contains independent agents with the ability to perceive and act upon their environment falls under this concept [4.2], and have proven effective for many challenging tasks [4.3]. Although each agent's ability to affect the system environment is limited to the capabilities of their immediately controllable system or component, agents can communicate information about their goal achievement to other independent agents comprising the MAS. Cooperation arises as agents propose, accept, reject, or counter-propose courses of action based on conferring with other agents, assessing local capabilities, and evaluating native objectives.

In this chapter, the MAS architecture, agent designs, and decision-making framework are presented. The guiding principle of this work was to incorporate flexibility in design leading to an MAS that could be readily modified or changed depending on the desires of the researcher and the decision-making task at hand. The agents developed in this chapter use the JADE messaging framework for their communication. Much of the JADE functionality, such as message structure and ontology, are not explained here. For more details on how the JADE libraries are formulated or object-oriented programming in Java, the reader is directed to [4.4], [4.5], [4.6], [4.7].

4.1 Background

Autonomous agents often work with a limited system-wide perspective within MAS architectures, focusing on their assigned tasks and pursuing solutions towards local goals. If data must be passed between agents, the communication means and protocol is important to the MAS implementation. Within the MAS, agents may propose to accept, reject, or counter-propose courses of action based on communication with other agents, but more broadly, agents exchange information about local goal achievement. Throughout operation, autonomous agents comprise the collective command structure and work together. In this way, the microgrid power management problem is an ideal application of the MAS concept, where more capable self-organized and convergent system behavior can emerge from lower hierarchical agent intelligence. The primary advantages of utilizing a MAS structure for microgrids include: dynamic flexibility, asynchronous operation, system survivability, and potentially lower communication overhead. If appropriately formulated, agents may pursue assigned goals despite losing communication with others within the MAS framework. Communication, therefore, can benefit performance, but is not always necessary. Likewise, communication overhead may be an objective to minimize. It is common for local area network or internet protocol communication to be used for MAS implementations [8] and it is expected that going forward, all available communication protocols including: broadband, power line communications, wireless, and cellular networks, will be used to facilitate MAS interaction. Despite often have conflicting goals, MAS architecture and communications facilitate progress towards common goals while maintaining continuity of operations at a very high level without dependence on a central controller.

4.2 MAS Purpose

The primary purpose of the microgrid power management MAS is to ensure stable delivery of electrical power to its local load customers while optimizing energy production towards an assigned objective(s). Ultimately, key real and reactive power flows on the microgrid are dictated by the generation sources and loads, their system proportion, and how they are operated. The operational objectives is not limited to simply meeting local power demands, but must optimize towards additional constraints such as: emissions concerns, fuel availability and cost, weather conditions, the spot-market price of electricity, etc. Enhanced decentralized management shifts key decision-making to a lower hierarchical level, localized to the component or subsystem. Considerations for MAS architecture include: quantity and variety of controllers, needed communication infrastructure, specificity of control algorithms, and the interaction between controllers affect architecture formulation. The multi-objective, multi-constraint microgrid power management problem is characteristically more complex than for conventional power system operation, with the following operational attributes.

Major objectives:

- Maximize the customer's power availability (e.g. meet consumer's instantaneous load demand).

- Minimize economic factors (e.g. fuel costs, operation and maintenance costs, start-up/shut-down costs, etc.).

- Minimize environmental impact from operating microgrid generators (e.g. emissions, noise, hazardous waste, etc.).

- Maximize the dispatch of shedable loads (e.g. loads capable of reacting to demand response signals).

- Maximize revenue derived from service delivery to the utility grid (including ancillary services, reserves, etc.).

- Minimize energy purchased from outside microgrid.

- Maximize the total efficiency of the microgrid (e.g. kWhrs generated versus kJ fuel consumed).

- Maximize capitalized energy sources (e.g. operational efficiency of kWhrs available versus kWhrs generated).

- Minimize the frequency of power reversals across the PCC interconnection.

- Minimize transient periods during stabilization in the event of a casualty or interruption.

Minor objectives:

- Maximize load factor (e.g. smooth out the peaks and valleys of load and subsequently required generation).

- Minimize the need for storage assets.
- Maximize the microgrid capability to reduce strain on distribution and transmission assets.
- Maximize VAR support to the greater power system.
- Maximize the reduction in line losses.
- Allow the stable, seamless, and adaptable integration of assets onto the microgrid (also known as “plug-and-play”).

Primary constraints:

- Availability of renewable resources (e.g. solar insolation, wind energy, etc.).
- Bus voltage, frequency, and stability requirements.
- Physical electrical characteristics of the microgrid.
- Status of interconnection.

At this stage of development, it is not appropriate to address all of the major and minor objectives simultaneously. Instead, agent algorithms have been developed to focus on some of the objectives to allow the capabilities of the MAS architecture to be demonstrated. One of the best attributes of MAS design is the inherent modular nature of the agents. Adding capabilities to agent decision-making or incorporating other factors for consideration is straight-forward. This flexibility makes MAS power management testing and development appealing.

4.3 Framework Operation

As described in Chapter 3, the microgrid simulation environment and multi-agent development was performed in the Java programming language, utilizing the FIPA-compliant JADE communication libraries. Implementation in this way allowed for flexible and modular design for both the component layer models and the control entities that comprised the agent layer. The simulation environment is capable of operating on any device that can operate a Java Virtual Machine (JVM). The JVM, which is distributed as part of the Java Runtime Environment (JRE), allows Java programs to be executed on many devices, known as cross-platform compatibility. This improves the adoptability of the simulation environment and agents developed as part of this work, enhanced by the fact that the JRE is free and already operating on many devices around the world, eliminating the need for proprietary software.

When the simulation environment is initiated, a virtual boundary known as a container is instantiated. A container is little more than an instantiation of a software class (known as an object) that holds software components (other objects). Within the main container, an agent platform (AP) is created to autonomously operate in the background of the host device. The AP is comprised of two primary parts, the agent management system (AMS) and the directory facilitator (DF). The agent management system (AMS) contains the necessary overhead for agents to interact, including the JADE functionality to allow agents to be instantiated and interconnect their communication. The directory facilitator (DF) is an AP agent that maintains a "phonebook" of instantiated agents. These two functional pieces of software are the core of the JADE infrastructure.

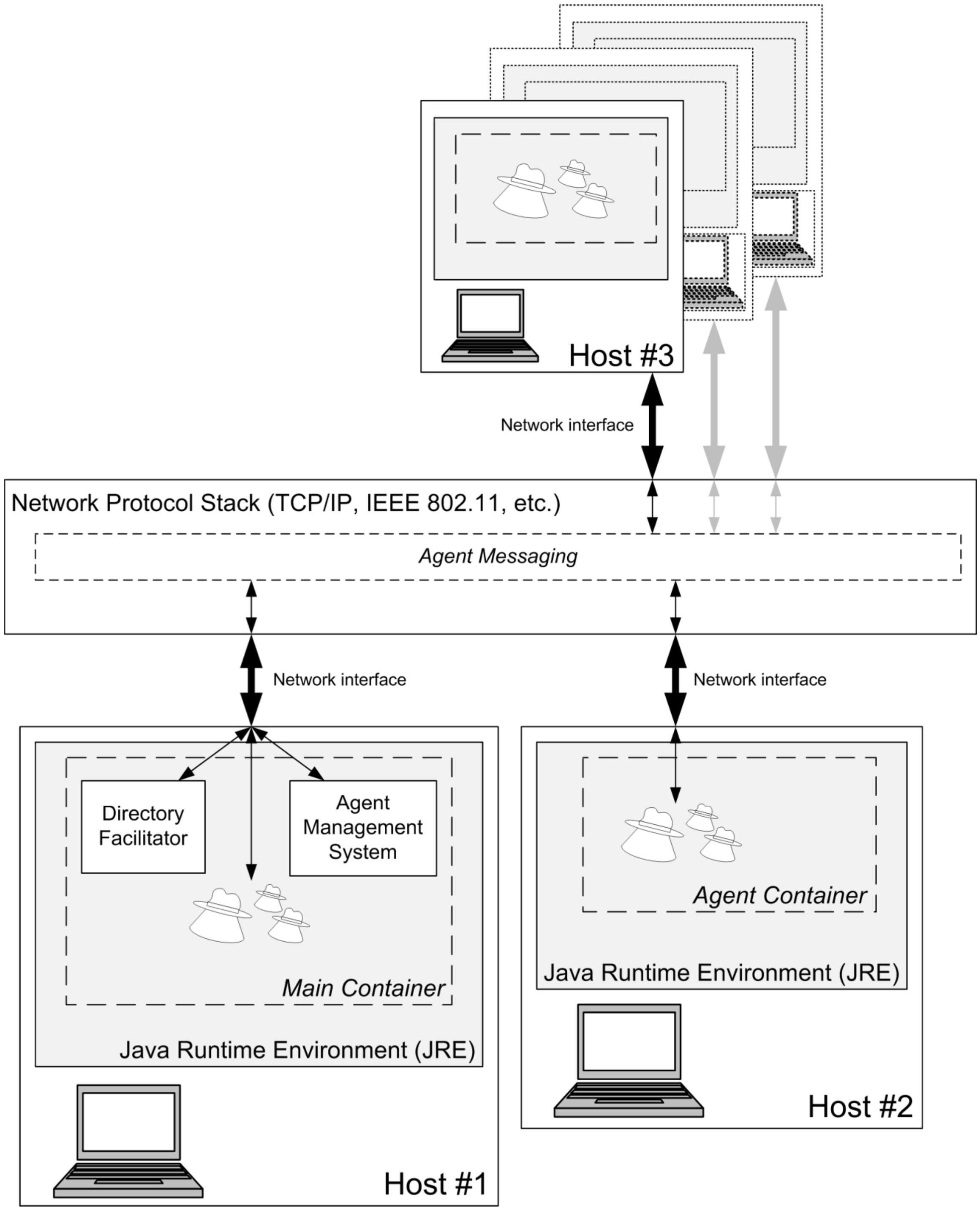

Figure 4.1. Simulation environment diagram.

In addition to the JADE infrastructure, software programs developed to operate as microgrid asset models, electrical system models, optimization methods, and to provide other essential services are instantiated and reside in containers. Only one main container, holding the AP, must exist for the MAS to operate, but the main container may be easily replicated for redundancy [4.4]. When computers or other devices that are JRE-capable are connected through network protocols (such as TCP/IP or IEEE 802.11 wireless), additional containers must be instantiated to hold the simulation environment agents and software. A single device host may operate one or many containers, each with one or more agents. This allows differentiation between software packages that may be directed toward one asset or another, but still utilize the processing capability of a single host device. The functional structure of hosts, containers, and agents for the purpose of operating the microgrid simulation environment is shown in Figure 4.1.

Once instantiated, the AP provides the JADE facilitation infrastructure necessary for agent communication. As discussed in Chapter 3, two communication pathways take advantage of the JADE infrastructure to operate. The decision-making exchange is the medium for microgrid agents to communicate and collaborate. By using this exchange, which is the topic of the bulk of this chapter, the locally-based microgrid asset agents are imbued with broader capabilities than purely decentralized agents. The ability to share information allows the agents to cooperate towards better overall microgrid decisions than would be possible for agents that have no other capacity to gain information other than what is locally available. The electrical data exchange, on the other hand, is simply a simulation environment requirement. In order to solve for microgrid power flow parameters, some electrical information must be aggregated in the background. The electrical data exchange allows electrical data agents to pool asset electrical information to complete this incremental calculation (explained in more detail in 5.9). Different than the agents that utilize decision-making exchange, electrical data exchange agents are software programs that contain the necessary models and JADE functionality to calculate and pass data for microgrid power flow calculation. There are two types of electrical data exchange agents, shown in Figure 4.2: the aggregated electrical agent and the asset electrical agent.

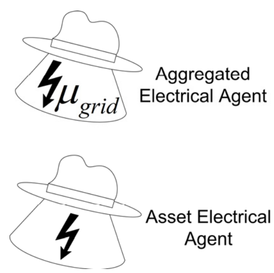

Figure 4.2. Electrical data exchange agents.

The electrical data exchange agents are only agents in the sense that they perform autonomous operations, such as calculating electrical parameters, and communicate according to JADE performatives; they are not used for decision-making nor are they as capable as decision-making agents explained further in the next section. The aggregated electrical agent computes microgrid power flow parameters based on its software circuit model; the asset electrical agents send electrical information about their respective microgrid asset to the aggregated electrical agent. In this way, the aggregated electrical agent maintains the electrical circuit and power flow picture on the microgrid. The aggregator passes microgrid primary AC bus information back to the asset electrical agents that may be used for asset local control. Ultimately, to simulate the electrical characteristics of the microgrid, data aggregation was necessary. However, this occurs in the background and the decision-making agents operating on a separate communication exchange have no access to this information, except through their monitoring of their asset itself (explained in the section below).

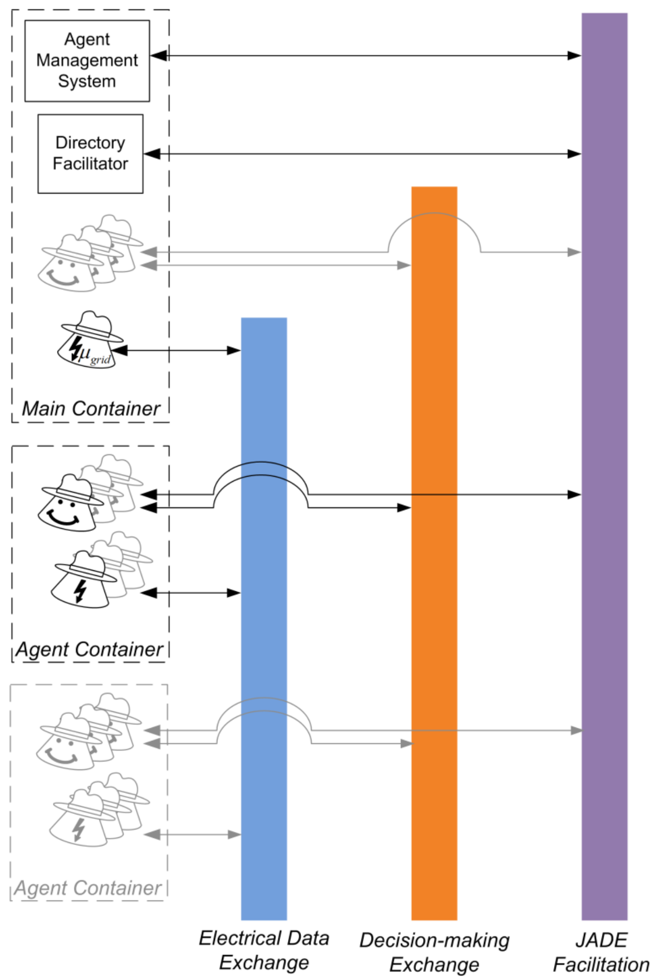

Figure 4.3. Simulation environment communication exchanges.

Together, the two communication pathways, shown in Figure 4.3, allow the simulation environment to incorporate microgrid asset models and the agents responsible for making decisions for the assets. Likewise, this software test bed is modular and expandable, allowing the researcher to incorporate varying levels of modeling specificity as well as experiment with any number of MAS methods and configurations.

4.4 Electrical Data Exchange

In order to simulate the concurrent effects of all microgrid assets on the microgrid electrical buswork, a method that capitalized on the JADE agent framework was devised. For the purpose of simulation, information about asset electrical operational parameters was collated at regular intervals. Within the prescribed interval, the status of the electrical buswork and its parameters was calculated, and made available for asset-specific calculation. This section lays out how this methodology was implemented; for more details on the microgrid electrical model itself, the reader is directed to Chapter 5.

The electrical data exchange served as a communication pathway for microgrid electrical agents. As described in the previous section, electrical data was sensed, calculated, and exchanged by individual asset electrical agents (one per asset) and the aggregated electrical agent (one per microgrid). The aggregated electrical agent, whose sole purpose was to facilitate the electrical model and, thus, the microgrid simulation environment, collects asset sending voltage or impedance information in order to calculate the power flow on the LV microgrid network. The asset electrical agents, when receiving a queuing message, sensed and sent necessary electrical parameters (sending voltage or impedance information) to the aggregated electrical agent. This process, known as the electrical data cycle, is shown in Figure 4.4.

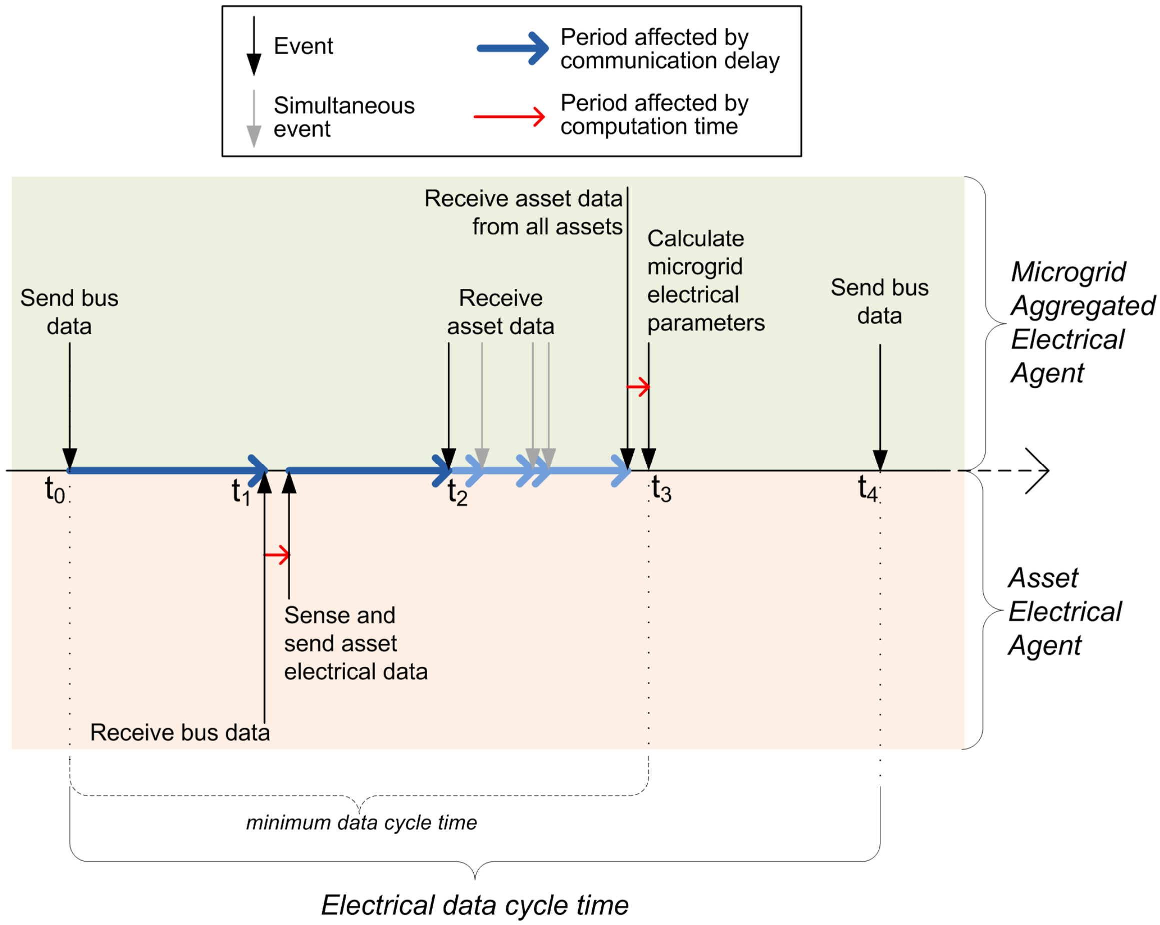

Figure 4.4. Electrical data cycle for microgrid aggregated and asset electrical agents.

The electrical data cycle initiates when the aggregated electrical agent sends the latest microgrid common AC bus voltage (phasor representation) to all electrical agents bound to assets. After a period (t_1 - t_0) affected by any communication delay, the electrical bus data will be received by each asset electrical agent. It is noted that when simulating the microgrid on a single computer or a closed network, that the communication delay (t_1 - t_0) was very short. Additionally, the out-going message sent by the electrical aggregator agent is expected to be received by each asset electrical agent at approximately the same time. When the asset electrical agent receives the bus data, this is an initiating event for the agent to sense and transmit local asset electrical parameters to the aggregated electrical agent. This process involves a small computational overhead, but does not include sensor delay. It is noted that sensor delays were not explicitly incorporated into this method, but could readily be done so.

The message sent by the asset electrical agent to the aggregated electrical agent depends on the type of asset it monitors. For assets that are capable of being producers, i.e. generation and storage assets, the asset electrical agent transmits its sending voltage (phasor representation). For load assets, i.e. consumers, the asset electrical agent sends present connected impedance data (phasor representation). Each of these pieces of data is sufficient to create an accurate picture, once aggregated, of the electrical operation of the microgrid. After the asset electrical agent transmits a message to the aggregated electrical agent containing the electrical parameter, another period of communication delay (t_2 - t_1) is incurred. For consistency, this period (t_2 - t_1) includes the brief computational time that is not affected by communication delay, as shown in Figure 4.4. Between the time that the first response message arrives and the last asset electrical agent responds, the aggregated electrical agent asynchronously collects the electrical parameter of each asset. Once all asset data is received (t_3), the aggregated electrical agent calculates the total LV microgrid power flow. As explained further in the electrical model of Chapter 5, when the microgrid is in interconnected mode, the common AC bus voltage is set by the connection with the utility (simulated by an infinite bus). In this case, the aggregated electrical agent calculates the net power flow of all microgrid assets yielding an interconnection current (phasor representation). When islanded, the balance or imbalance of microgrid asset power flows yields a varying common AC bus voltage (phasor representation). When the number of assets attached to the microgrid is small, the computational time required by the aggregated electrical agent is small. The microgrid electrical information is retained by the aggregated electrical agent until the present electrical data cycle ends (t_4). At that point (t_4), the electrical data cycle repeats.

The total time between cycles (t_4 - t_0) is determined by the experimenter at the outset of simulation. It is noted that the minimum period of an electrical data cycle (t_3 - t_0) is dictated by the sum of the communication delays and computational times for all electrical agents. If this period is short enough, the electrical data period (t_4 - t_0) may likewise be short, leading to smaller electrical simulation increments. Experience has shown that the average time period required for one aggregated electrical agent and three asset electrical agents to complete their actions (t_3 - t_0) is less than 20ms on a closed system. This time period is considered a good estimate of the time performance of the electrical data cycle. This time period is important for more than just the microgrid electrical simulation, but affects the overall simulation, as well. As each asset has its own underlying physical model which is calculated incrementally (described in Chapter 5), the process of each electrical agent posting a new microgrid common AC bus voltage when they receive this information from the aggregated electrical agent serves as the "clock tick". When this occurs, the asset underlying models each independently calculate the next increment of their data. Meanwhile, the decision-making agents (described in the next section) only receive updated asset parameter information when calculation by the asset model is complete for that increment. In this way, the frequency of the electrical aggregator establishes the overall simulation increment time. This is noted, because under most simulation circumstances, the electrical data cycle period is set such that (t_4 - t_0 > t_3 - t_0) and (t_4 - t_0 << 1s). This implies that the microgrid simulation environment may simulate operations faster than the equivalent real time. In other words, given these constraints, using the electrical data cycle as the simulation environment clock, long time periods of microgrid operations may be simulated in less time than required by a real-time simulator. Experience has shown that a full day's worth of disturbance data, such as changing load demand and varying environmental (solar insolation, wind speed), at 1s resolution (86,400 data points) may be simulated in less than 75 minutes for a three-asset microgrid. Extensive speed tests have not been performed on the simulation environment and the electrical data cycle period (t_4 - t_0) has not been pushed below 50ms. This very generous experimental limit has prevented situations where (t_3 - t_0) is not long enough to allow the aggregated electrical agent to collect all of the information from asset electrical agents. This simulation environment question has been left to future work.

The aggregated electrical agent is initialized in the main simulation environment container when the microgrid simulation is started. When a new asset joins the microgrid, the process of instantiation causes the new electrical agent to register itself with the aggregated electrical agent. This process of registration informs the aggregated electrical agent of the asset's type, unique name, and connection impedance. As the microgrid operates, each electrical data agent operates independently, communicating only in accordance with the electrical data cycle. The summary of the programmatic structure for the aggregated electrical and asset electrical agents are shown in Figure 4.5.

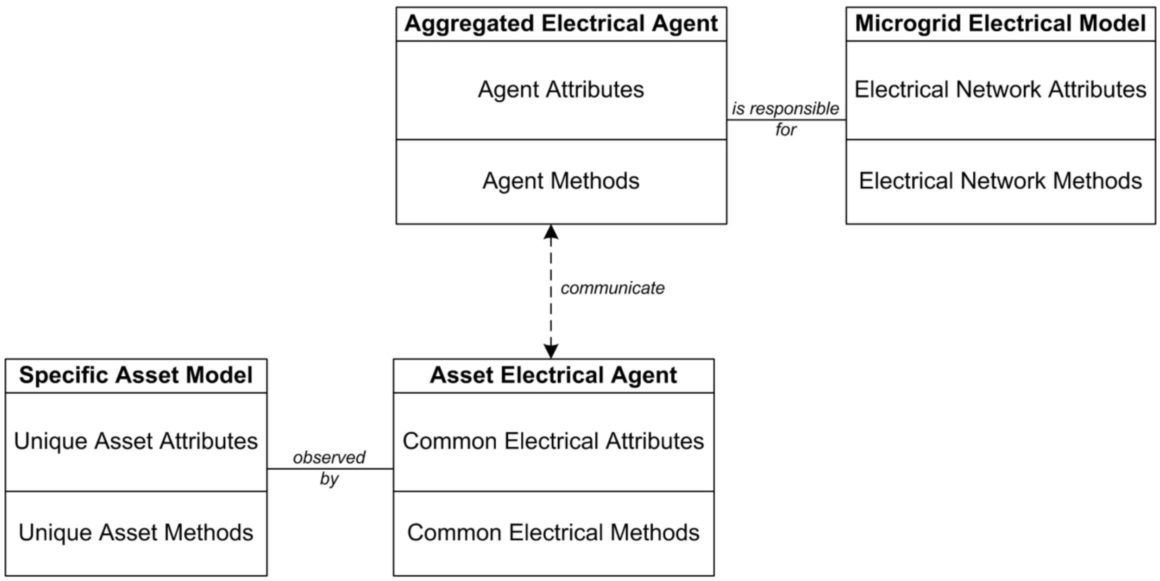

Figure 4.5. Electrical data agent programmatic structure.

Each of the electrical data agents communicate in a straight-forward *INFORM* or *QUERY* format. There is no negotiation between the electrical data agents, as will be described for the decision-making agents in the next section, so communication of this type is not part of their programmatic structure. The electrical data agent structures are shown in Figure 4.6 and Figure 4.7.

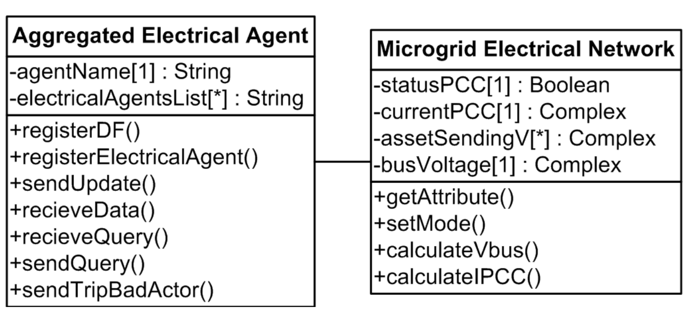

Figure 4.6. Aggregated electrical agent and microgrid electrical network model structure.

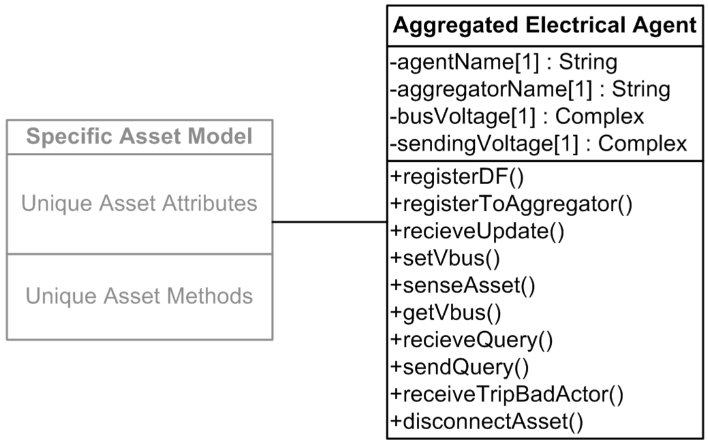

Figure 4.7. Asset electrical agent structure.

Together, the electrical data agents facilitate the simulation of the microgrid electrical network. As this is the basis of the power management interaction between assets on the microgrid, the update of common AC bus parameters is important. It allows the asset electrical agents to provide their associated asset models with the electrical connection data necessary to simulate asset operation. Additionally, the overall microgrid simulation is incremented based on the user-defined electrical data cycle period maintained by the aggregated electrical agent. The underlying set of electrical data agents and their dedicated communication exchange is a key development in creating a suitable simulation environment for LV microgrids.

4.5 Decision-making Agents

The practice of decision-making is a very familiar process for humans. However, attempting to codify the decision-making process in a meaningful, efficient, and useful way is often very challenging. As a consequence, implementing effective autonomous decision-making for automated systems can be difficult. Additionally, implementation is complicated by the need to make judgments rapidly and to seek an ideal conclusion amongst a field of many options and factors. The microgrid power management MAS is an example of an automated decision-making framework that must comprehensively consider complex factors that affects a complex system.

A given microgrid will operate in two distinct states: interconnected or islanded from a larger utility network. The microgrid power management architecture, formulated as a distributed MAS, must adapt to changing conditions within the distinct context of each state. However, from the microgrid asset perspective, the status of the interconnection is not relevant to the job at hand; the asset will perform as directed by its controller. Therefore, when interconnected, the agents must control generation, load, and storage assets primarily from the standpoint of power flows. When islanded, voltage regulation (and to a lesser degree frequency regulation), as well as power balancing, are of critical importance.

A challenge facing microgrid MAS design is how to develop capable agents given immense diversity and uncertainty regarding components the customer may choose to connect to a microgrid. Therefore, to simplify the agent framework and encourage better interoperability, all possible microgrid components are segregated into one of four classifications. By classifying microgrid components, the appropriate agent or combination of agents may be assigned to it. For split AC/DC bus microgrid MAS design, the microgrid component classes are:

Generation: capable of sourcing real and/or reactive power.

Load: consumes real power; leading or lagging power factor.

Storage: can source or consume real power.

Node: connection point with measurable electrical or physical quantities.

The microgrid MAS utilizes three basic agent types: the producer, consumer, and observer agents. For each microgrid component, an agent of appropriate type is assigned to it based on class, e.g. producer agent with a generation asset. In the case of a storage asset, both a producer agent and consumer agent are assigned. This is due to the nature of storage assets that appear to the microgrid as a load when charging or a generator when discharging. In either case, the assigned agents negotiate to determine the best operating point for the asset based on objectives. More generally, it would be unwieldy to design a specific agent for each unique microgrid component, and the agent types are kept as general as possible. Subsequently, in terms of agent design, specific agents are not designed for a specific machine or unique load.

The **Producer Agent** may have the following responsibilities:

- Monitor available real/reactive power from component.
- Monitor actual real/reactive power supplied by component.
- Determine relative per unit cost of power supplied by component.
- Determine an instantaneous performance measure indicating how well the component is achieving optimal operation.
- Give commands to the component regarding startup, shutdown, and quantity of real and/or reactive power to produce.
- Communicate information to other agents and negotiate as necessary.

The **Consumer Agent** may have the following responsibilities:

- Monitor real/reactive power consumed by the component or bank.
- If attached component is controllable or differentiated for demand response, determine the real/reactive power margin (load pick up/shed).
- Give startup, shutdown, or configurational orders to component.
- Communicate information to other agents and negotiate as necessary.

The **Observer Agent** may have the following responsibilities:

- Monitor specific parameters within the microgrid network (e.g. voltage/frequency levels, breaker positions, fuel tank levels, etc.).
- Communicate information to other agents and negotiate as necessary.

For ready identification in the system diagrams throughout this and later chapters, Figure 4.8 shows the icon representation of the agent types.

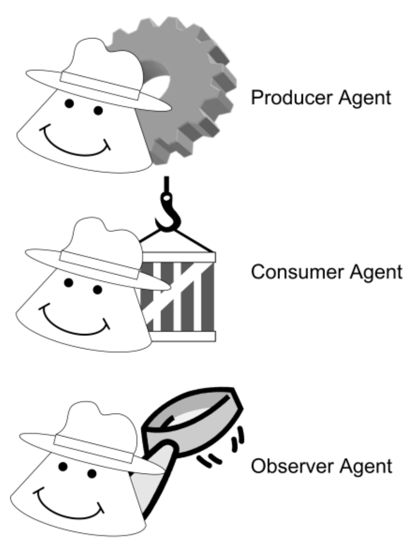

Figure 4.8. MAS decision-making exchange agents.

Every asset in the microgrid system is assigned an agent, depending on the type of asset. For consistency, the asset assigned to each agent shares a common state model, shown in Figure 4.9. When instantiated, an asset begins its life in the operating state (S_1). The operating state represents the normal operation of the asset. At any time, the agent in charge of the asset may direct the asset from S_1 into one of two states: hot-standby (S_2) or off (S_4). Hot-standby is similar to the operating state (S_1), remaining in electrical connection with the microgrid common AC bus, except that the asset operating power is zero. This simulates the state of assets, especially generators, that are placed in a reserve status that can easily be return to service when needed. The off state (S_4) implies that the asset is disconnected from the common AC bus and shutdown. Although not employed in the models used in this work, incorporating minimum shutdown or cooldown times common to some generation devices would utilize the off state. The agent may direct that an asset return to operating status (S_1) from the off status (S_4) after first passing through the hot-standby state (S_2). A special case is the faulted state (S_3). In the event that either the aggregated electrical agent or the asset electrical agent (both utilizing the electrical data exchange) detects a faulted state for the asset, the asset will immediately shift to S_3. This occurs without asset agent action. Similar to the off state (S_4), the asset may only be returned to the operating state (S_1) when faulted (S_3) after passing through the hot-standby state (S_2). The various states of the asset are applicable to consumer as well as producer assets. The asset state flow allows the decision-making agent responsible for it to consider appropriate courses of action based on its objectives .

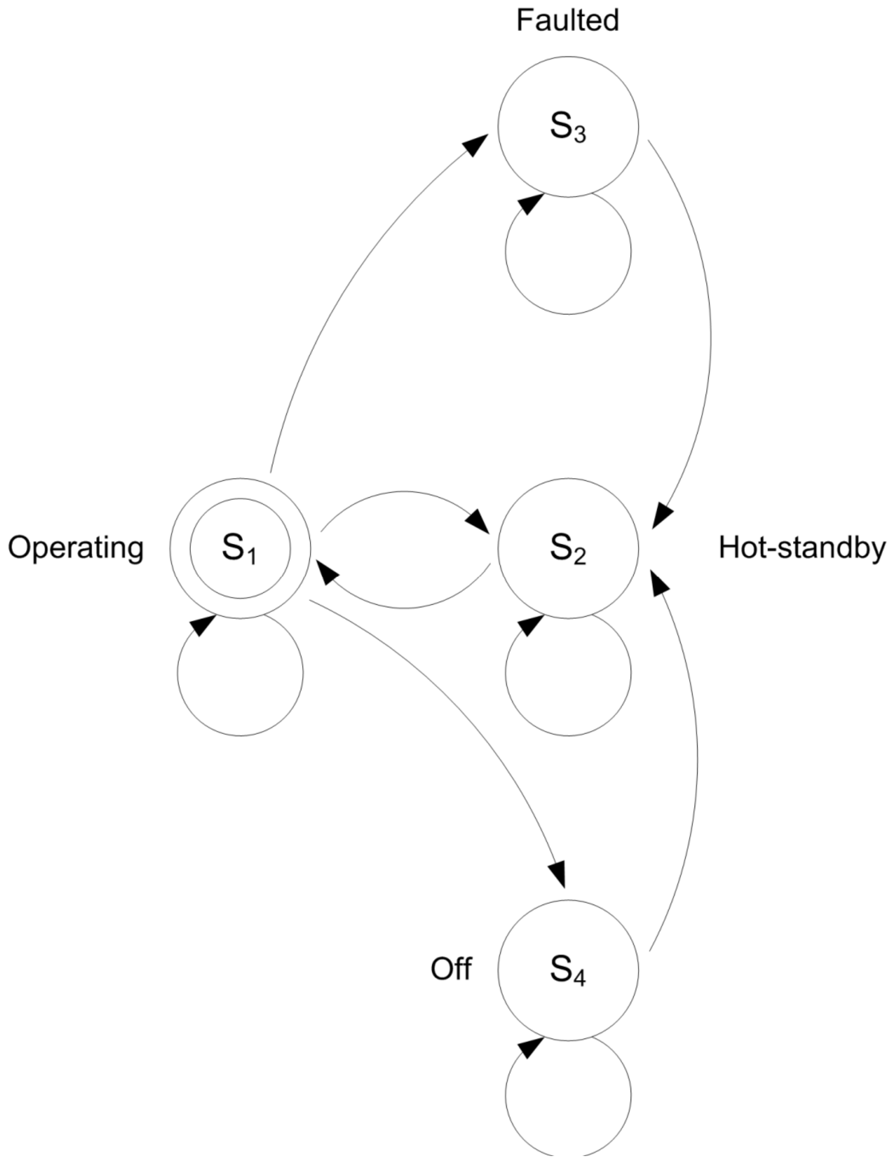

Figure 4.9. Microgrid asset state diagram.

Each agent has a unique, but similar algorithmic structure. Utilizing object-oriented programming principles the basic class structure each consumer and producer agent and asset it is responsible for is shown in Figure 4.10. The observer agent class structure is shown in Figure 4.11.

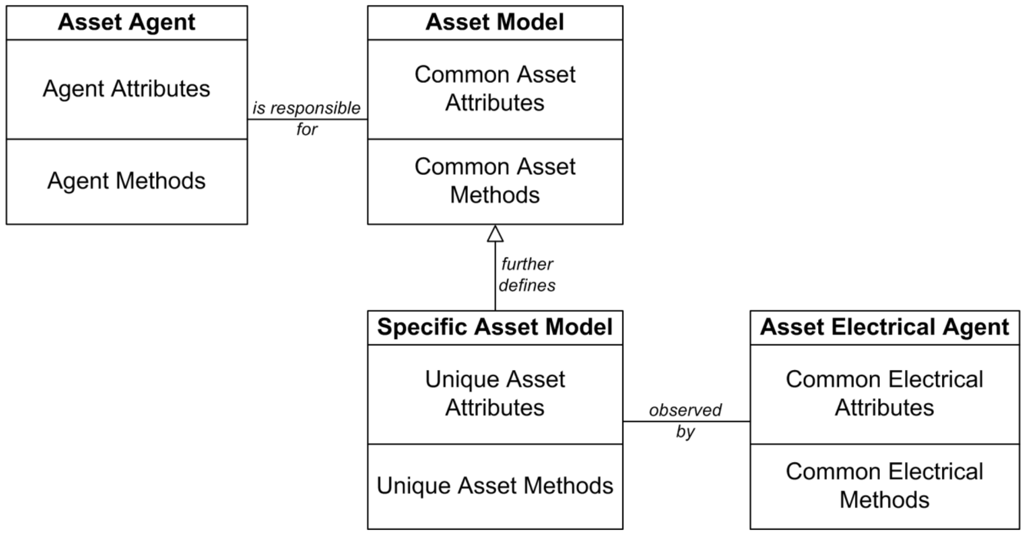

Figure 4.10. Common producer and consumer agent programmatic structure.

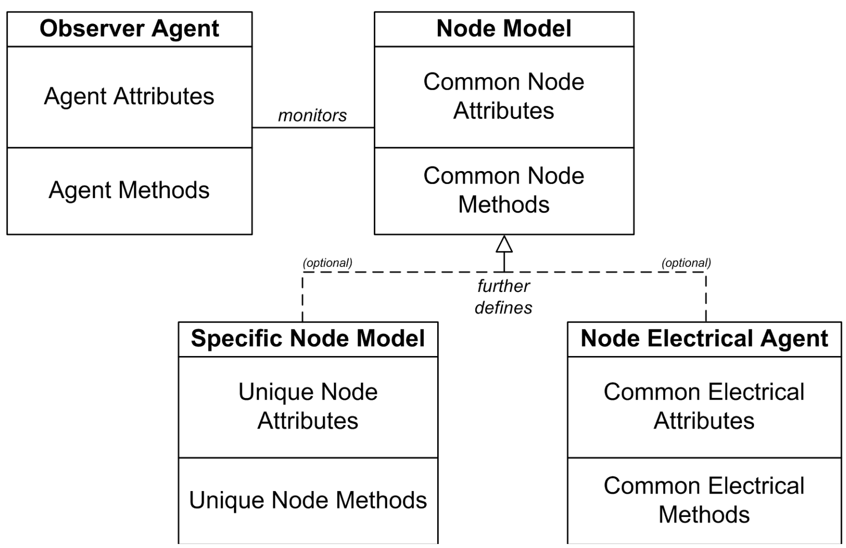

Figure 4.11. Common observer agent programmatic structure.

The common programmatic structure for producer and consumer agents is comprised of four major classes: the agent class, the asset model class, the specific asset model class, and the asset electrical agent class. The agent class contains the methods and attributes that allow it to interact with other MAS agents, obtain information from the asset model object (when instantiated), and make decisions on behalf of the asset it is responsible for. The asset model class is a generalized asset that standardizes information for all microgrid assets. Examples of standard information structure for an asset model object (when instantiated) are: asset type, unique serial identifier, rated power, mode of operation, graphical user interface (GUI) information, etc. When instantiated, an asset model class serves as the superclass for the specific asset model subclass. Within the specific asset model class, the unique attributes and methods associated with the type of asset are defined. This includes the incremental asset model, discussed in Chapter 5, methods to find asset operational parameters, and any asset specific constraints. By differentiating the asset model superclass from the specific asset model subclass, it allows more logical standardization across the framework. For example, although very different microgrid assets, a diesel genset asset and a load bank share some common attributes. Those common attributes are represented within the asset model object (when instantiated), while the specific models and operation of the diesel genset and load assets are represented within the specific asset model subclass. Finally, to support the microgrid electrical network model, parameters calculated and represented by the specific asset model class are observed by the asset electrical agent. This agent acts and communicates on a different hierarchical level as the decision-making agents. The electrical data exchange hierarchy only exists for facilitating the simulation environment and is not observable by the decision-making agents of the microgrid MAS.

The common programmatic structure for the observer agent is comprised of two major classes: the agent class and the node model class; as well as two optional classes: the specific node model class and the node electrical agent class. The agent class contains the methods and attributes that allow the observer to interact with other MAS agents, obtain information from the node model object (when instantiated). The observer agent class does not participate in decision-making, such as the producer and consumer agents, but does interact with MAS agents for the purpose of information passing and negotiation. The node model class represents a generalized node, such as an electrical bus or physical parameter. Additionally, the node model class may include methods that allow it to interpret physical or electrical parameters for the purpose of developing performance information of use to MAS decision-making agents. As the node superclass, the subclass may be further defined in two ways. The first is with a specific node model that may represent physical parameter information such as a fuel tank level or solar insolation intensity. The other subclass option binds a node electrical agent to the superclass. The node electrical agent may interact with the aggregated electrical agent to obtain node electrical information, simulating electrical sensory devices such as a voltage meter or current transducer. The ultimate purpose of observer agents is to act as sensory components that may provide MAS decision-making agents data they need or give the agents a sense of how well a particular aspect of the microgrid is performing. An example of this is for an observer agent monitoring a bus voltage. Rather than simply sensing and reporting the voltage to MAS decision-making agents that may ask for the data, the observer instead may provide a measure of performance. This measure of performance, shown in Figure 4.12, indicates how well the MAS collective is achieving the specified voltage on the observer agent's bus. Information of this type is more useful to decision-making agents and can be used to aid the enhanced decentralized agents towards better overall microgrid system performance.

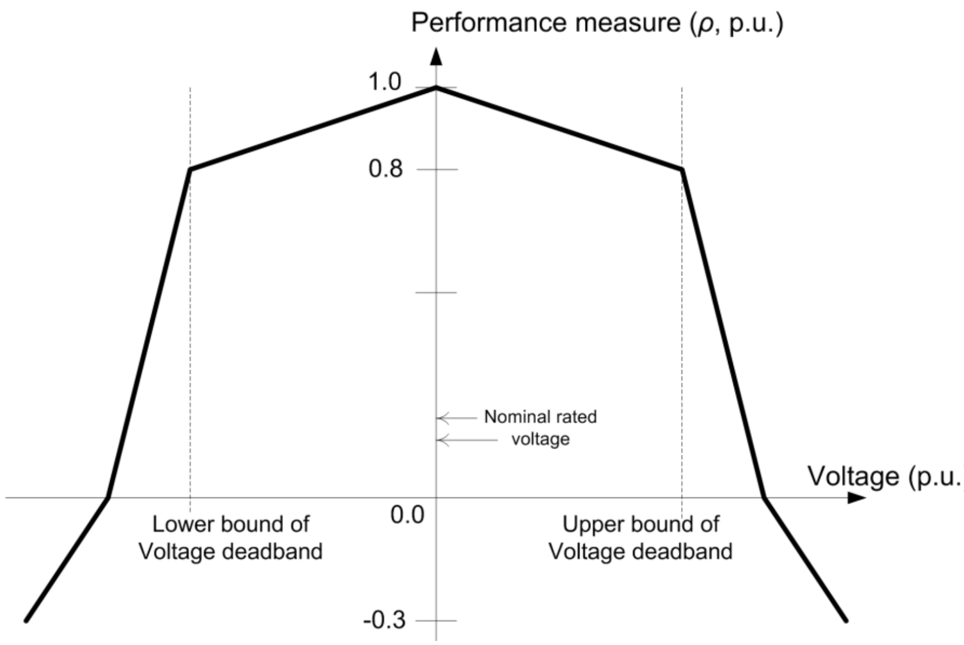

Figure 4.12. Example of an observer agent performance measure.

Using the common structure of Figure 4.10, the unique producer, consumer, and observer agents are presented. For the producer agent, the only major structural difference from agent to agent exists due to the nature of renewable and non-renewable generation assets. As the generation potential of renewable assets is dictated by environmental resource availability (i.e. wind speed, solar insolation, etc.), the specific asset model for the renewable asset contains an additional method to sense its resource. However, this slight difference does not change the overall programmatic structure for the producer agents, shown in Figure 4.13 and Figure 4.14. The consumer agent is shown in Figure 4.15; the observer agent in Figure 4.16.

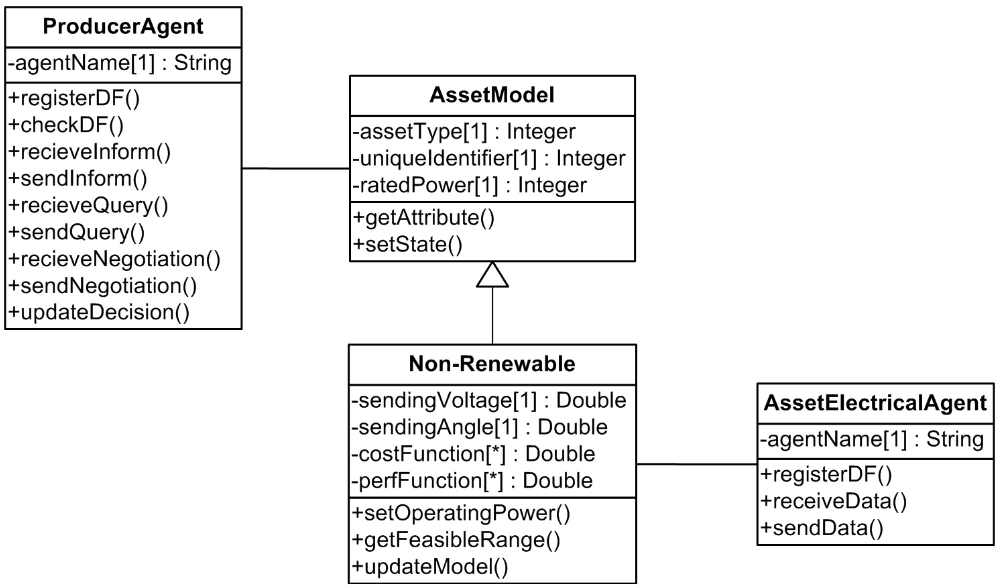

Figure 4.13. Producer agent and asset structure for non-renewable asset.

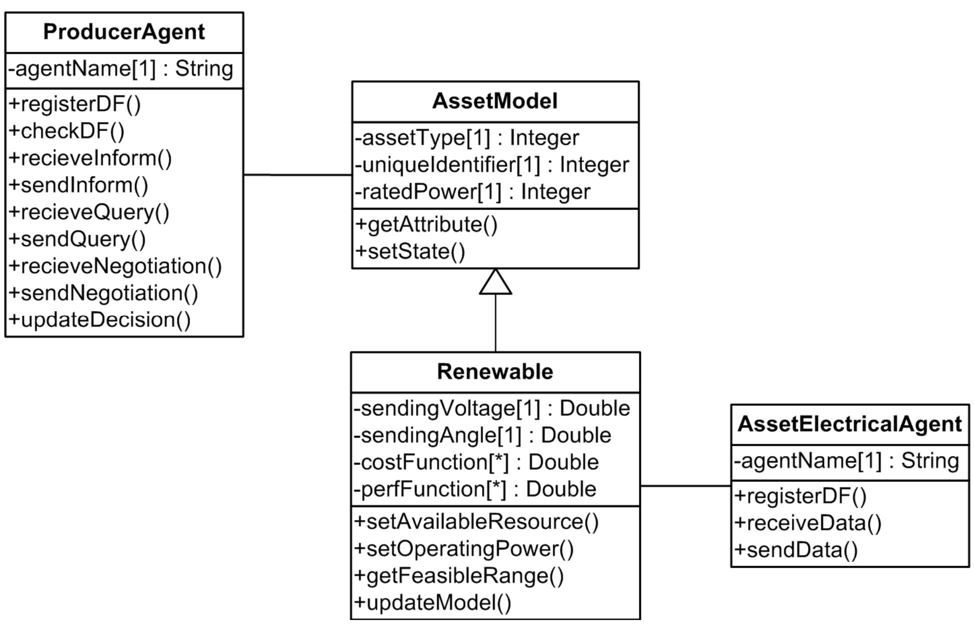

Figure 4.14. Producer agent and asset structure for a renewable asset.

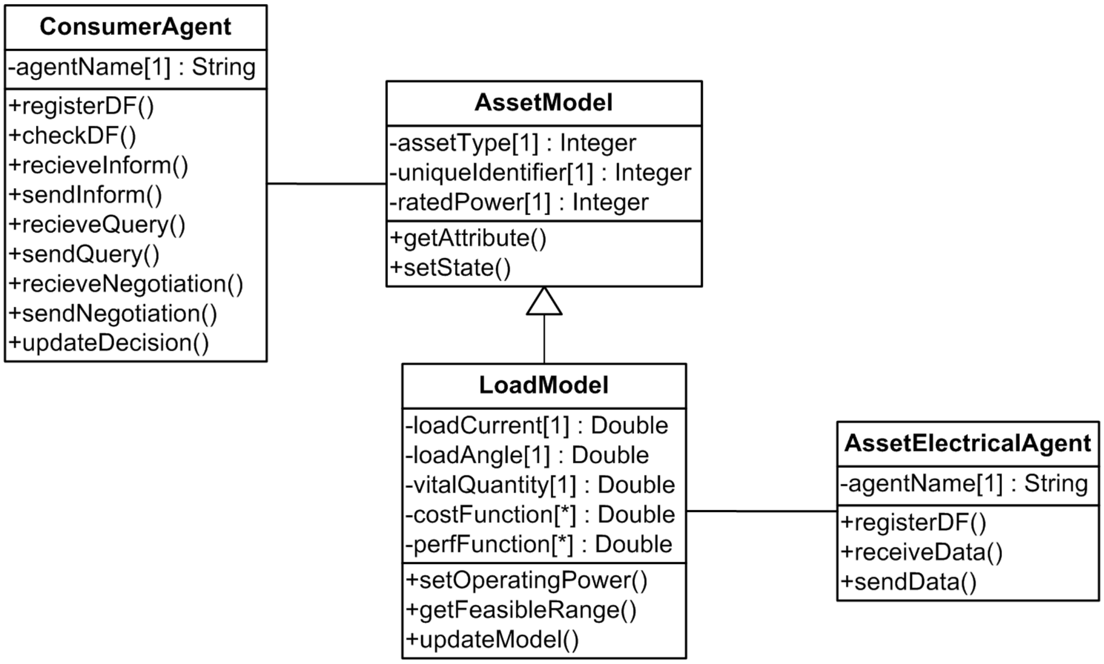

Figure 4.15. Consumer agent and asset structure for a load asset.

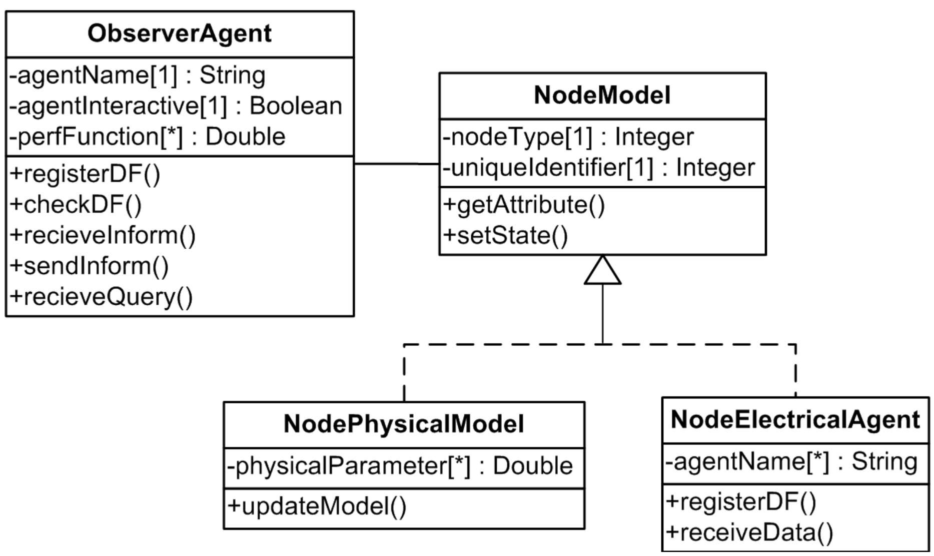

Figure 4.16. Observer agent and structure for node.

The common agent structures allow the MAS to be developed in a consistent and compatible way. The specifics of the asset models are kept separate from the consumer and producer agents for the express purpose of maintaining this framework flexibility. In this way, the decision-making agents are asset agnostic; that is, they may pursue the best cost and performance for their asset without having to be specially customized for that purpose. Likewise, the computational methods used by agents to solve their particular local objective function are equally as interchangeable. It is believed that this is a multi-agent system development best-practice, proven by experience gained developing this simulation environment and microgrid MAS. Additionally, developing MAS PM&C in this way may offer better opportunities for customer adoption, as it is virtually impossible to predict the assets or components that will ultimately be implemented from future microgrid-to-microgrid. Having a flexible MAS PM&C makes that adoption easier.

4.6 Agent Decision Cycle

The decision cycle is an importance concept for MAS operation, shown in Figure 4.17. For the agents that make up the enhanced decentralized MAS, a decision cycle is defined as the amount of time used by each agent to formulate, negotiate, and execute a solution for the operation of its local asset. This is similar in concept to trading cycles used by market agents engaged in economic auctions, such as in [4.9], with two key differences. First, as opposed to market-based auctions that occur at regularly synchronized intervals, the decision cycle is initiated asynchronously by unpredictable events such as spot market price changes, resource availability changes, emergency conditions, etc. Second, the time to complete a cycle varies based on many factors including computation time, intensity of negotiations, latency, and execution time. Ultimately, the decision cycle allows the agents to manage their assigned asset independently and respond to events as they occur, without relying upon a centralized supervisor. Collectively, agents operating autonomously can self-organize and collaborate through negotiation during their decision cycles. This concept allows the MAS to be flexible and responsive while seeking optimal solutions to assigned goals.

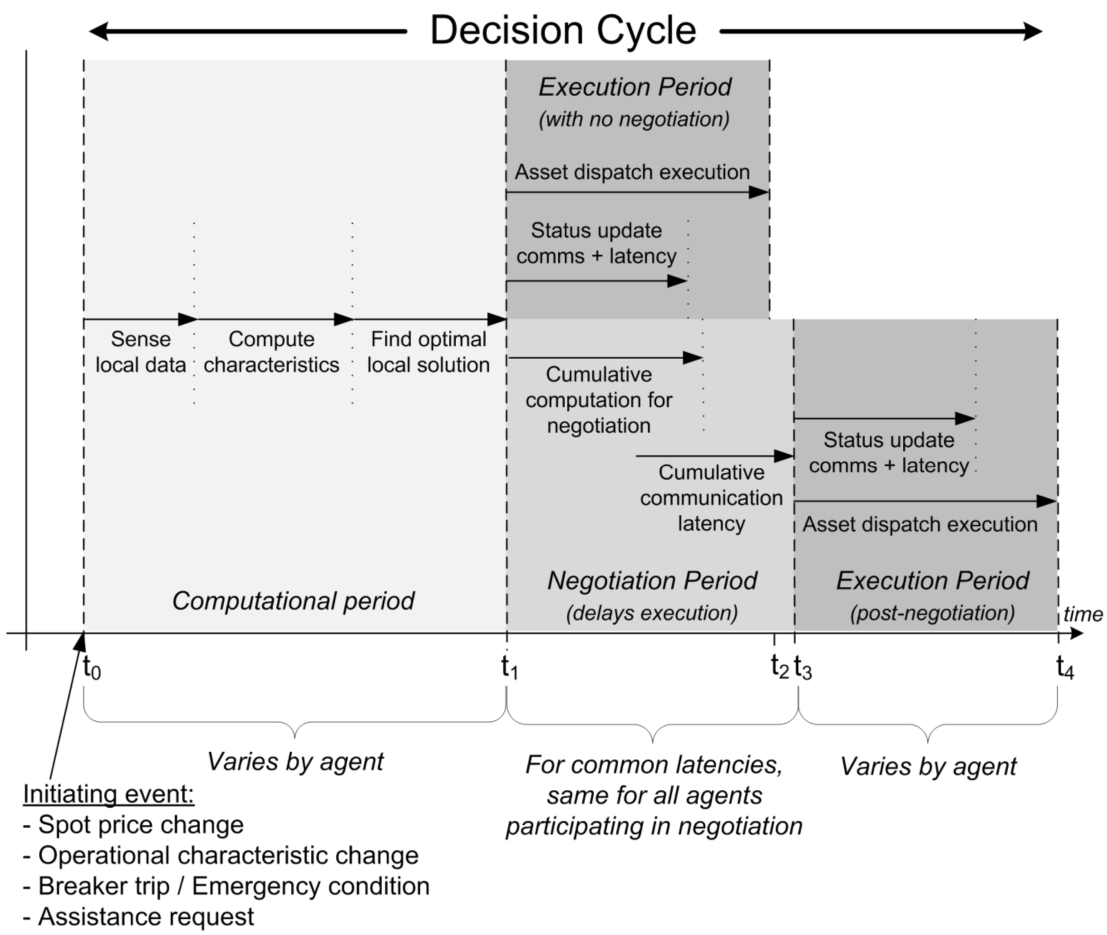

Figure 4.17. Agent decision cycle.

An agent's decision cycle (all t_n references shown in Figure 4.17) initiates asynchronously when an initiating event is perceived by the agent (at t_0). An initiating event may be any perceivable occurrence that disturbs the agent's equilibrium, such as a change in the spot market price of electricity (utility-interconnected operation), a change in an operational characteristic (predominant for renewable sources, including wind speed and solar insolation changes), or an emergency condition. When disturbed by an initiating event, the agent begins a computational period where it senses local conditions and conducts internal computation to determine a solution to its present conditions. The computational period (between t_0 and t_1) may be different for every agent and situationally dependent. The awareness of local conditions and the quality of solution may lead the agent to seek cooperation with other agents, if dictated by the agent's algorithm; otherwise, the agent moves directly to execute its decision. If cooperation is desired, the agent enters a period of negotiation with one or more MAS agents (between t_1 and t_3). This period may be very short due to a lack of response from potential collaborators, or involve many messages passed between agents as they settle upon a mutually agreeable course of action. The agent negotiating behavior is covered in depth in the following protocol methods section. Once negotiation is complete, or if it never began, the agent carries out its local decision during a period of action execution (between t_3 and t_4). The execution period continues until a new initiating event starts the decision cycle to begin again. If no negotiation was conducted, the period of execution follows the computation period directly (between t_1 and t_2).

The simulation environment developed as part of this work uses many different computational processes working simultaneously. The computation of asset parameters occurs separately from the computation of the agents themselves; each which are separate from all other agents and assets. Depending on the complexity of the asset models used and the communication dependency of the agents, the speed by which initiating events may be introduced to the MAS simulation environment varies. This is primarily because of the computational resources required to perform system operation. What has not been fully evaluated in this work, and subsequently is left for the future, is at what frequency of initiating events does the enhanced decentralization of the MAS begin to fail. Theoretically, each agent must have a minimum amount of time ($t_2 - t_0$) to solve its local optimization and execute its decision. This minimum amount of time precludes any negotiation and renders the agent as a purely decentralized one (no enhanced capabilities available through communication). Therefore, there is a maximum frequency of initiating events, equivalent to: $1/(t_2 - t_0)$. However, this maximum frequency would have to be reduced to account for appropriate negotiation periods, when considering the full functionality of the microgrid MAS. It is assumed that if a negotiation period ($t_3 - t_1$) is part of the overall decision cycle period ($t_4 - t_0$), then the maximum frequency of negotiating events would be: $1/(t_4 - t_0)$. This frequency, it is noted, must vary directly with the complexity of agent negotiation and subsequent communication. As JADE message processing itself can transpire in a few milliseconds within a single container on a single host, it is conceivable that this would not be a restrictive limit. However, when communicating between two agents contained in separate containers on separate hosts, it is unknown how the network latency, processing overhead differences, and the intensity of communications (one message pair versus many message pairs transmitted during negotiations) will affect timing. In this work, most development was performed on a single computer with many containers. Typical time between initiating events was significantly longer (1s or greater) than the total time to complete a decision cycle

($t_4 - t_0 < 500$ms). In future work, factors including model complexity, communication delays, and initiating event frequency causing disruptions in decision cycle flow are strong topics of interest.

Each decision-making agent must have the capability to operate autonomously whether or not communication with the MAS is available. When communication is present, the agents may pursue their decision-making with the benefit of collaboration with other agents, as described in the next section. However, as explained in Chapter 3, when communication pathways are not available, the enhanced capabilities of the decentralized MAS revert to a simpler, purely decentralized state. Without communication, the microgrid agents face a challenging power management environment where multiple assets are coupled on a LV network without coordination. If the microgrid is interconnected with the utility, the situation is manageable. This is primarily because the utility rigidly maintains voltage and frequency regulation for the microgrid common AC bus. However, in the islanded scenario without MAS communication, the agents must self-determine how to operate. Normally, from a conventional power management perspective, this would involve operating at a default level, if at all. Using the capabilities of the agents, however, an alternative method is proposed. As the agents are capable of dispatching their asset and monitoring the response of voltage at the common AC bus, the agents may slowly modify asset operation. This is accomplished by hill-climbing towards the optimal dispatch decision, shown in Figure 4.18.

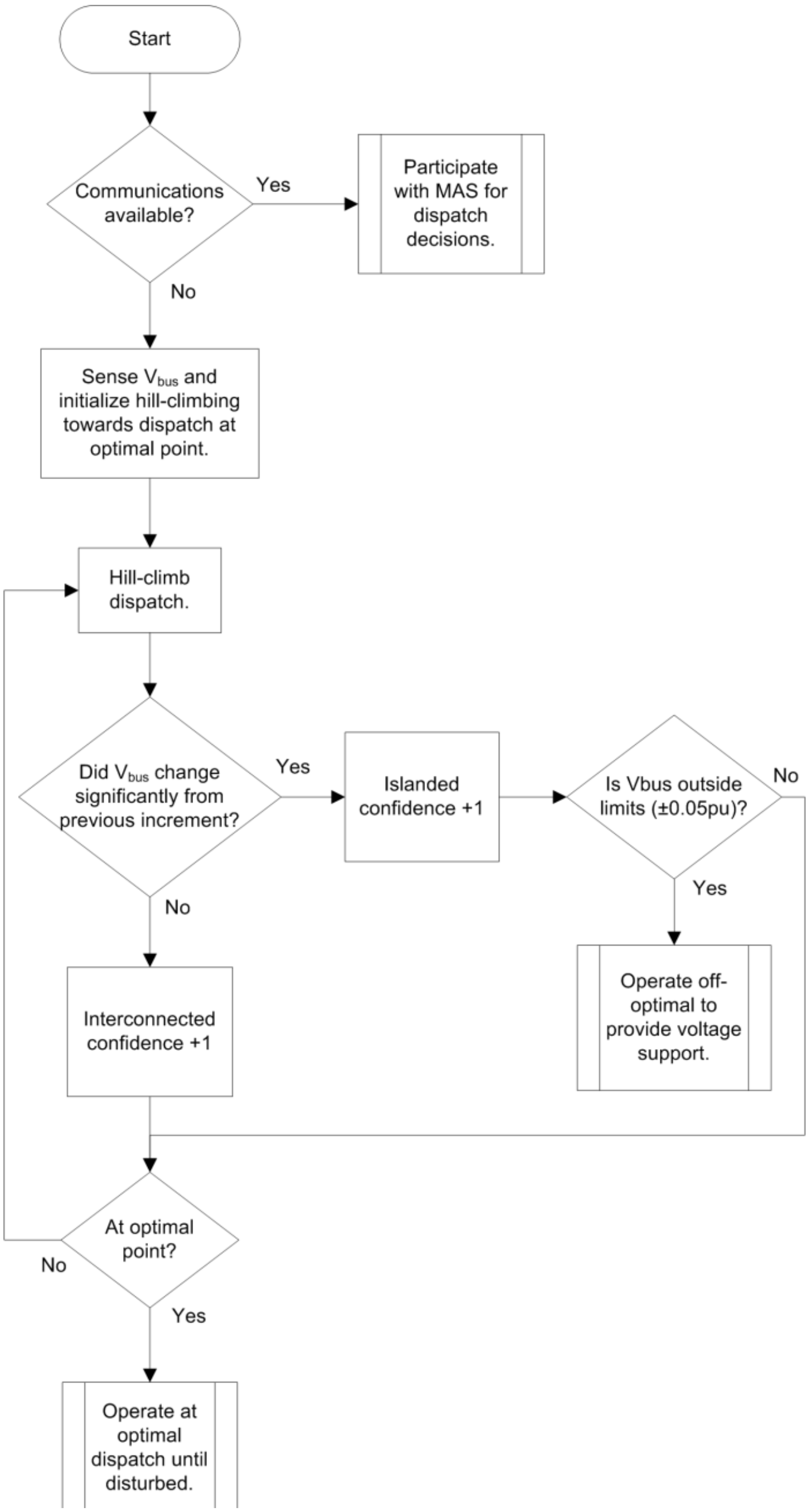

Figure 4.18. Agent operation without communication with the MAS.

After sensing common AC bus voltage (V_{bus}), calculating the optimal operating point given local conditions ($P_{i,optimal}$ for asset i), and initializing the hill-climbing ($P_i = 0$ at $k = 0$) the agent performs hill-climbing dispatch incrementally according to:

$$P_i[k+1] = P_i[k] + \sigma \qquad \left\{0 \le P_i[k] \le P_{i,optimal}[k]\right\} \qquad (4.1)$$

where, $P_i[k]$ is the dispatch in the current increment k; and σ is the hill-climb parameter that determines how large of a step in dispatch power the agent takes between increment k and increment $k+1$. The agent has no exterior means of determining whether the microgrid is interconnected with the utility or islanded when communication with the MAS is unavailable. Therefore, after performing a dispatch hill-climbing step, the agent examines whether V_{bus} has changed appreciably from the previous increment. This is imprecise from a power systems perspective because V_{bus} may be changing due to a number of factors. However, this agent heuristic allows the agent to assess its local impact on common AC bus voltage. Using a simple incremental weighting algorithm, shown by the "Interconnected confidence +1" and "Islanded confidence +1" blocks of Figure 4.18, as the agent is hill-climbing it can adjust its behavior as it becomes more confident in the state of the microgrid. If interconnected, achieving the optimal operational point for the asset is achievable. If islanded, however, the agent must operate suboptimally if V_{bus} falls outside of voltage limits, thereby providing voltage support to the microgrid. This heuristically-guided hill-climbing approach to truly decentralized decision-making agent operation without communications allows the asset to still attempt to operate optimally despite its responsible agent retaining only local parameter visibility.

In the next section, agent protocols for collaboration and coordination when communication is available are described, leading to enhanced rather than purely decentralized decision-making.

4.7 Agent Protocol Methods

Agent protocols are the methods used to communicate with other MAS agents. These protocol methods include interacting with the directory facilitator, sending information to another agent or group of agents, receiving a query for information, or sending and receiving messages necessary to participate in negotiation with another agent or group of agents.

When an agent first connects with the MAS, its first action is to register its existence and basic asset information with the directory facilitator. This action is accomplished with the registerDF() method. At any point during operation, the agent may desire to communicate with another agent, or group of agents, within the MAS. The agent may use an internally maintained record of destination agents to address its impending message properly. However, over time as MAS agents come on and off of the MAS during the course of operation, the agent's internal address record becomes out of date. Therefore, the checkDF() method is available for the agent to query the directory for specific agents of interest, at anytime. Using the directory facilitator in this way ensures that the MAS communication network topology is always fully connected to agents actually present.

Methods such as receiveInform() and sendInform() are self-explanatory. If an agent desires to broadcast information to one or more agents, it may use the sendInform()

method. An example of this method being used would be in the case a producer agent is changing states to hot-standby from operating; it may desire to broadcast this information to each agent in the MAS. The receiveInform() method allows the agent to process incoming informational messages. These methods are slightly different than sendQuery() and receiveQuery() methods. In the case of queries, an agent seeks specific information from another agent or group of agents. It requests that information directly with the sendQuery() method and processes the receipt of the return information with the receiveQuery() method. An example of a message query could occur when a load consumer agent seeks information about head-space from an agent in charge non-renewable generation asset. In this example, the agent receiving the query would respond to the sending agent by invoking the sendInform() method to formulate a message with head-space information in the message body. The inform and query methods allow the agent to interact with other MAS agents, seeking or providing information beyond what is available to the agent locally.

The structure of the sendInform() and recieveInform() methods are shown by Agent N as the sender (solicitor); Agent M as the receiver (solicitee):

Agent N

Known: A_0, B_0.

Create *INFORM* message:

Operating at A_0 yielding B_0.

Send *INFORM* message to Agent M.

The contents of the *INFORM* message states that agent N is currently operating at power A_0 [kW] with a corresponding value of the agent's objective function of B_0. The agent receiving the *INFORM* message (agent M) processes it according to:

Agent M

Received *INFORM* message from Agent N.

Message contents: A_0, B_0.

No reply needed.

The structure of the sendQuery() and receiveQuery() methods are shown by Agent N as the sender (solicitor); Agent M is the receiver (solicitee):

Agent N

Known: A_0, B_0.

Create *QUERY* message:

Operating at A_0 yielding B_0. Interrogative C_0 yielding D_0

Send *QUERY* message to Agent M.

The contents of the *QUERY* message states that agent N is currently operating at power A_0 [kW] with a corresponding value of the agent's objective function of B_0. Additionally, agent N would like to request information about the current operating power (C_0) and corresponding objective function (D_0) of agent M. The agent receiving the *QUERY* message (agent M) processes it according to:

Agent M

Known: C_0, D_0.

Received *QUERY* message from Agent N.

Message contents: A_0, B_0.

Create *INFORM* message:

Operating at C_0 yielding D_0.

Send *INFORM* message to Agent N.

Besides the obvious specificity of the sendQuery() and the receiveQuery() methods, there is no separate method to respond to the query. Instead the solicitee agent responds to its solicitor with an *INFORM* message using the sendInform() method.

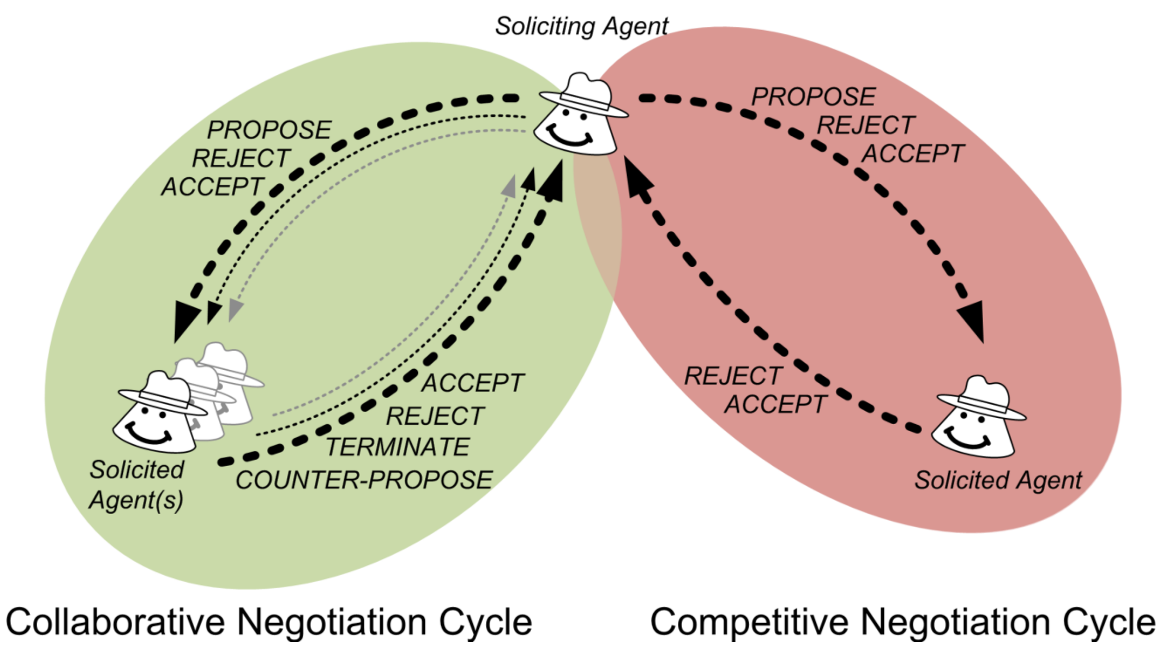

Figure 4.19. Agent negotiation cycles.

The last major type of protocol method for agents allows negotiation. The sendNegotiation() and receiveNegotiation() are more complex than the inform and query methods. For the MAS developed, there are two primary means of negotiation cycles, shown in Figure 4.19. A negotiation cycle is initiated by an agent, according to its algorithm, by formulating a list of agents who are potential proposal solicitees. The negotiation cycle ends with either an accepted proposal or an empty roster of potential solicitees, as dictated by the negotiation conducted, either collaborative or competitive.

The collaborative negotiation cycle, shown in Figure 4.20, takes place when one agent seeks to improve its achievement of its objectives by changing its operating point. When this behavior requires compromise with another asset, such as in power sharing during microgrid islanded operation, an agent may seek to enter into negotiations with another agent. It does so by formulating a message with the sendNegotiation() method as a proposal, according to the following:

Where, Agent N is the sender (solicitor); Agent M is the receiver (solicitee).

Agent N

Known: $A_0, B_0, A_1, B_1, (B_1 - B_0) > 0$.

Create *PROPOSE* negotiation message:

Operating at A_0 yielding B_0. Propose A_1 yielding B_1.

Send *PROPOSE* message to Agent M.

The contents of the *PROPOSE* message states that agent N is currently operating at power A_0 [kW] with a corresponding value of the agent's objective function of B_0. Agent N proposes to operate at A_1 [kW] with a corresponding value of the agent's objective function of B_1. As a rule, the agent will only propose a new operating point (A_1) that yields a better outcome ($B_1 > B_0$).

The agent receiving the *PROPOSE* message (agent M) processes it according to the receiveNegotiation() method as a proposal by:

Agent M

Received *PROPOSE* negotiation message from Agent N.

Known: C_0, D_0.

Find C_1 such that $C_1 = C_0 + \left(A_1 - A_0\right)$.

If $C_1 \in \left\{P_f[k]\right\}$, where $\left\{P_f[k]\right\}$ is the set of discrete operating powers that make up the feasible region at increment k, then calculate D_1, else send *REJECT* message to Agent N.

If $(D_1 - D_0) \geq 0$ or $w_{i,neg}\left|D_1 - D_0\right| \leq \left(B_1 - B_0\right)$, send *ACCEPT* message to Agent N.

Else, if $w_{i,neg}\left|D_1 - D_0\right| < T_i$, send *REJECT* message to Agent N, else send *END NEGOTIATION* message to Agent N.

For the agent receiving the proposal (agent M), the message is processed according to a rule-based algorithm. Given the power change ($A_1 - A_0$) proposed by agent N, agent M verifies that the change is within the feasible range of its operation. If not, the proposal is rejected as infeasible; if it is feasible, agent M evaluates whether the proposal would be beneficial to its own operation. The first check checks whether the proposed power change would yield an improvement in the value of its own objective function ($D_1 > D_0$). The second check evaluates whether the proposed improvement in objective function value (B_1 - B_0) by agent N is equal to or greater than the expected weighted improvement by agent M. The weighting factor ($w_{i,neg}$, which may be unique for each agent i) is an important user-defined variable for agent M; it weights the importance of the agent's own degradation in performance against the improved performance of soliciting agents. In other words, if $w_{i,neg}$ is greater than one, agent M will not agree to the proposal unless agent N can yield a better net improvement in its objectives relative to agent N. This implies that the overall achievement of objectives for the entire microgrid improves despite the degradation experienced by agent M. Conversely, if $w_{i,neg}$ is less than one, this indicates that the user desires agent M to accept proposals even if the net achievement of objectives for the microgrid will be worse in allowing agent N to operate better. In this way, the user has influence on how cooperative agent behavior is when addressing tradeoffs of objective achievement. Of course, if the criteria for accepting the proposal are not met, then the proposal will be rejected. The rejection message from agent M to agent N offers the opportunity for agent N to submit a new and different proposal. However, in before sending the rejection, a final check evaluates the proposal made by agent N against a user-defined negotiation threshold (T_i). The negotiation threshold is used to limit the extent to which negotiation will continue; if the proposal by agent N would cause severe enough a performance degradation for agent N, negotiations are terminated with no opportunity for re-proposal. When received by agent N, a termination message removes agent M from the roster of possible solicitees. Agent N will continue iterating through the roster of solicitee agents until either all solicitees have terminated negotiations or a proposal is accepted. At that point, agent N's negotiation cycle is complete.

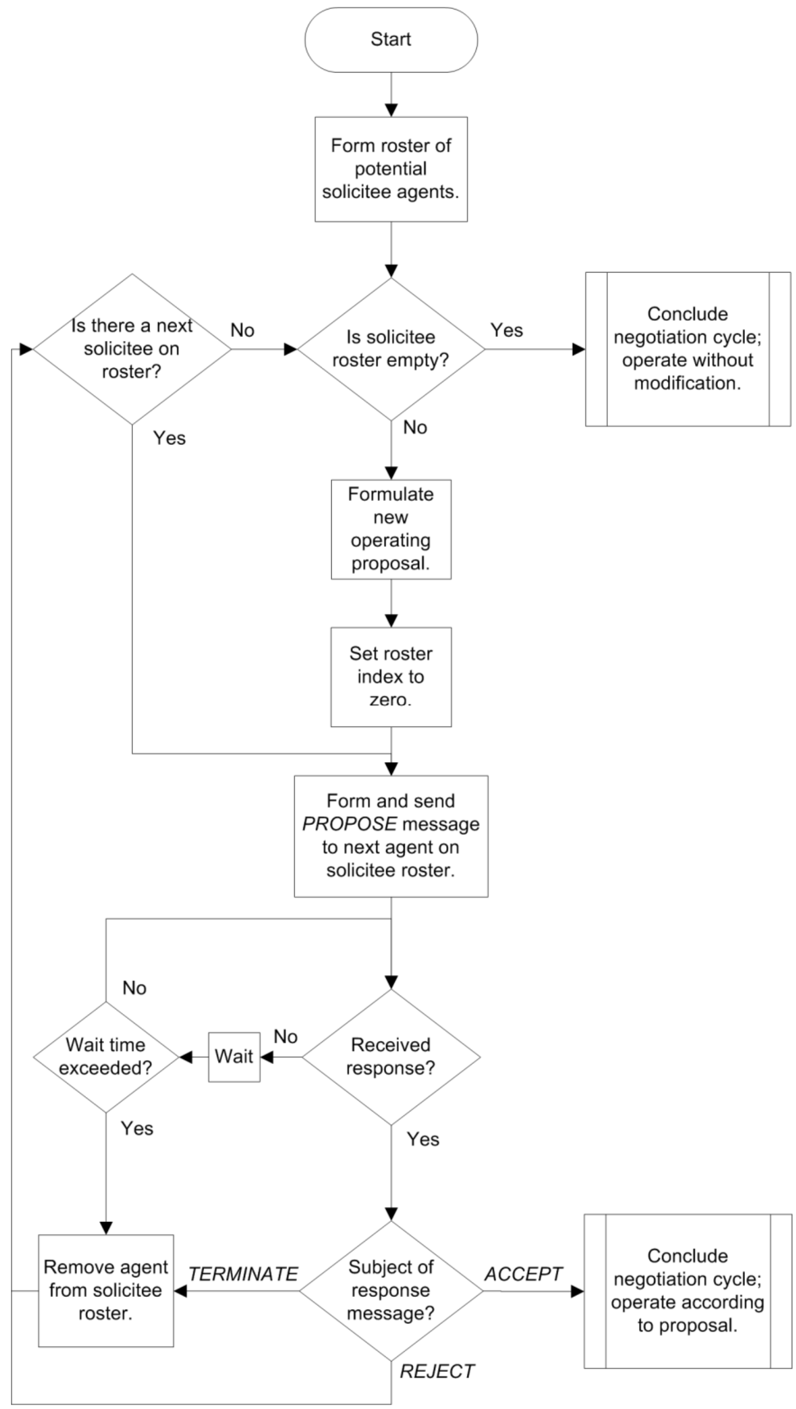

Figure 4.20. Collaborative negotiation cycle.

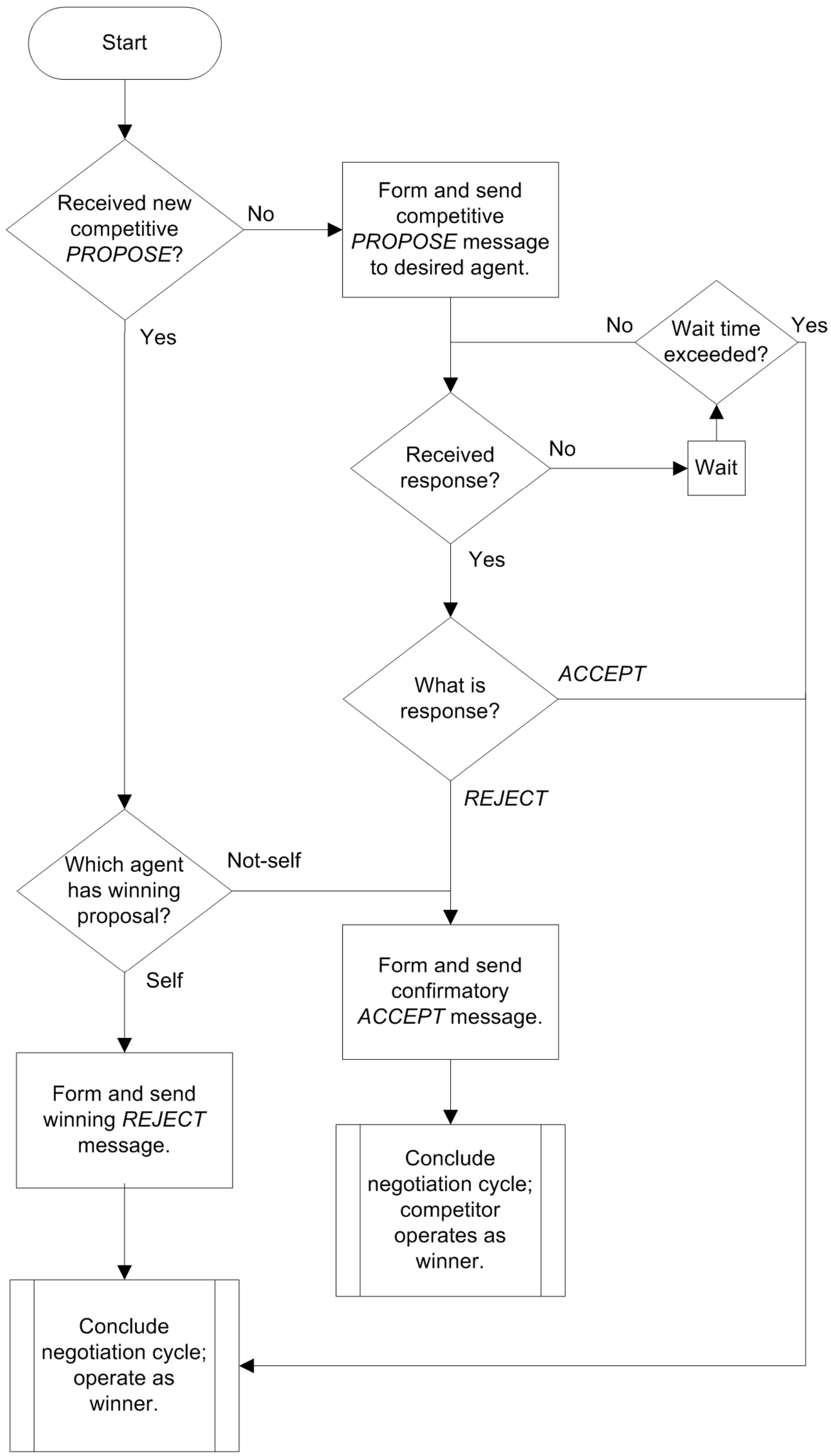

Figure 4.21. Competitive negotiation cycle.

The competitive negotiation cycle, shown in Figure 4.21, is slightly different than the collaborative means. When competitive negotiation takes place, a clear winner and a clear loser are decided through negotiation. This form of negotiation is most commonly associated with agents assigned to the storage asset. Due to the dual-nature of the storage asset that can source or sink microgrid power, during each decision cycle the consumer and producer agents assigned to the storage asset must compete for the right to dispatch it. In this case, the interaction between the two agents must lead to a winning party. For the storage agents, when the decision cycle is reset due to an initiating event, either agent may initiate the competitive negotiation by formulating a sendNegotiation() proposal according to:

Where, Agent N is the sender (solicitor); Agent M is the receiver (solicitee).

Agent N

Known: A_1, B_1.

Create *PROPOSE* negotiation message:

Propose A_1 yielding B_1.

Send *PROPOSE* message to Agent M.

The contents of the *PROPOSE* message states that agent N is proposes to operate at A_1 [kW] with a corresponding value of the agent's objective function of B_1. In this case, prior states of A and corresponding B are not relevant to the negotiations. This is because an initiating event has potentially changed the feasible region of operation for both agents requiring a complete reevaluation of circumstances. Therefore, the proposed actions by both agents conducting negotiations are the only operating points that must be compared.

In the competitive cycle, the agent who receives the proposal has the burden of calculating the winner. The agent receiving the *PROPOSE* message (agent M) processes it according to the receiveNegotiation() method as a proposal by:

Agent M

Received *PROPOSE* negotiation message from Agent N.

Known: C_1, D_1.

If $D_1 \leq B_1$, send *ACCEPT* message to Agent N.

Else, send *REJECT* message to Agent N.

As with the collaborative negotiation cycle, here the agent receiving the proposal (agent M) processes it according to a rule-based algorithm. Given the proposed action (A_1) and corresponding value of the objective function (B_1) proposed by agent N, agent M compares B_1 to the value of its own objective function (D_1). If deemed the superior, agent M will inform the original solicitor (agent N) of winning the negotiations by a confirmatory *ACCEPT* message, agreeing to the proposal. However, if agent M determines it is the winner, agent N will receive a *REJECT* message. In either case, the winning agent will receive an *ACCEPT* message acknowledging that the competitor agent defers the negotiated win to it. Once an *ACCEPT* or *REJECT* message is sent, each agent's negotiation cycle is complete. The competitive negotiation cycle is especially important to the relationship between consumer and producer agents assigned to a storage asset. As such, during each computational increment, one and only one agent is permitted to dictate storage asset operation. As a rule, only the winner of the most recent competitive negotiation cycle is permitted to dispatch the storage asset.

4.8 Agent Operation Methods

When formulating a decision, the primary method used by the agent is updateDecision(). This method has two primary functions: sense information necessary to make a local decision and perform a decision-space search to find the best solution that considers the feasible region. Of information available to the agent, this primarily comes from the specific asset model subclass of the asset model bound to the agent. This information may include the cost and performance function data, feasible range of operation data, and other model specific data. Information derived from communicating with other agents, such as emergency needs, may supplement the data that formulates the search space for the agent's decision-making method. Ultimately, based on the goals assigned by the user and specific decision-making algorithm, the agent uses the updateDecision() method to find a specific operating point for its asset. Part of the updateDecision() method is to command execution of the decided operating point to the asset model and pass this operating point to the appropriate agent protocol, if necessary to communicate the decision to other MAS agents.

Agent decision-making requires analysis of numerous competing goals simultaneously. Multi-objective optimization seeks an optimal solution amidst a combination of objective functions, described by maximizing or minimizing as follows:

$$F(\vec{x}) = \left[f_1(\vec{x}),\ f_2(\vec{x}),\ \cdots,\ f_m(\vec{x}) \right] \tag{4.2}$$

Given:

$$\vec{x} = \left[x_1, \quad x_2, \quad \cdots \quad x_n \right]^T \in R^n \tag{4.3}$$

Subject to:

$$G(\vec{x}) \le 0 \ ,\ G = \left[g_1, \quad g_2, \quad \cdots \quad g_p \right]^T \tag{4.4}$$

where, F is the vector of objective functions containing m objective functions (f_1 to f_m), $\vec{x}$ is the n-length vector of variables to be optimized known as the decision variables, and G represents the p-length vector of inequality constraints. Equality constraints were not applicable to the power management considered in this paper. However, in most cases, a global best of any particular individual objective function may not be a satisfactory solution for the remaining objectives [10]. Because of this, we need to alter our concept of optimality for problems, such as for microgrid power management. Similar to economic systems, Pareto optimal solutions each maximize or minimize the objective function $F(\vec{x})$, but given it is composed of multiple objectives, each Pareto optimal solution implies that any one objective's satisfaction cannot be raised any further without lowering another objective's satisfaction, or vice versa. In other words, many "optimal" solutions exist where the value of $F(\vec{x})$ cannot be improved any further. This topic is discussed further in Appendix D as a primer to innovative computational intelligence methods for solving multi-objective problems.

Many solution-finding methods were investigated, including intelligent computational methods described in Appendix D. For the agents attempting to find optimal dispatch for their assets, the assumption is that they do not have access to the underlying system functions, nor the objective functions of (4.2). Instead, they are presented with a search space of all possible solutions and must choose a single dispatch solution along with its consequences for asset optimality. Therefore, the agents are faced with a search problem, rather than a model-based optimization problem, such as with traditional linear programming. Given this, there are numerous automated methods for finding the optimal solution within a search space, encompassing a large field of topics. Through the experience of developing the simulation environment and the MAS, it rapidly became clear that differentiating the performance of an agent's search algorithm from the overall performance of the MAS was challenging. In this way, there are a number of moving parts, simultaneously affecting each other as the agents pursue their programming. Therefore, it was important to decide what agent-based tools were to be used for simulating a specific purpose. For benchmarking, exhaustive search techniques, including breadth-first search, beam-search, and hill-climbing, were used as agent search methods. Despite being computationally time-intensive, they performed well within necessary time periods for agent decision-making. More advanced search using intelligent methods, specifically metaheuristics shown in Appendix D, were explored for the purpose of qualifying how the time for an agent to make a decision could be improved as the dimensionality and resolution of the search space increased. The question of what search method to employ in the decision-making agent's "brain" will continue to remain a difficult one to fully answer, given the variety of applications the MAS may potentially face. However, from the perspective of the researcher, the simulation environment that has been developed allows agent design modifications and benchmarking to be achieved in a modular and flexible way.

Unfortunately, for the microgrid system conditions can change very rapidly changing the constraints and decision variables. This arises as certain parameters, such as resource availability, spot market price of electricity, microgrid user goals, and other factors change. This means that the Pareto set of solutions in one time increment may be dramatically different from the Pareto set in the next increment. As the MAS operates, cost and performance functions are calculated by the agents for their respective assets at each computational increment. As will be discussed in Chapter 6, a cost measure alone is not adequate to fully define the optimal operation of microgrid assets for the agents responsible for them. Subsequently, each agent determines a performance measure that reflects how well its asset is achieving optimal operation based on its given objectives. The characteristics of the cost and performance functions vary dynamically depending on the asset and conditions including loading, state-of-charge (SOC), discharge history, etc. Cost and performance information may be shared between agents according to the decision cycle, described earlier in this chapter, to assist in cooperation. The concept of the combined objective function for multiple objectives will be explored further in Chapter 6. Additionally, given the flexible nature of the MAS agent structure, the method of solving the combined objective function may depend from agent to agent, depending on the sophistication of the agent. Ultimately, each agent pursues its local solution based on local information, supplemented with information or negotiation from other MAS agents, according to the agents programming.

4.9 Simulation Environment and MAS

This chapter has shown the design and framework of the microgrid simulation environment, along with the agents that interact within it. The next chapter will present microgrid models that were explored as part of instantiating the microgrid simulation environment. While many mathematical models exist for many assets applicable to the MAS, the models shown in Chapter 5 each investigate an aspect of the particular asset that was either missing in the literature or was lacking in available models. The originating purpose, which has been realized, for the simulation environment was to create a framework capable of simulating a microgrid made up of assets that could be collected in a user library. The models of Chapter 5, along with the agents explained in this chapter, comprise a microgrid system toolbox that is readily expandable for follow-on research and development.

REFERENCES CITED

[4.1] G. Weiss. Multiagent Systems. MIT Press, Cambridge, MA, 1999.

[4.2] S. McArthur, E. Davidson, V. Catterson, A. Dimeas, N. Hatziargyriou, F. Ponci, and T. Funabashi, "Multi-Agent Systems for Power Engineering Applications—Part I: Concepts, Approaches, and Technical Challenges", *IEEE Transactions on Power Systems*, Vol. 22, 2007, pgs. 1743-1759.

[4.3] L.Vig and J. Adams, "Multi-robot coalition formation", *IEEE Transactions on Robotics*, Vol. 22, No. 4, pgs. 637-649.

[4.4] F.L. Bellifemine, G. Caire, and D. Greenwood. Developing Multi-Agent Systems with JADE. John Wiley & Sons, West Sussex, England, 2007.

[4.5] Java Agent Development Framework (Telecom Italia), 2012, available at: http://jade.tilab.com/

[4.6] Foundation for Intelligent Physical Agents (FIPA), 2011, available at: http://www.fipa.org/.

[4.7] J. Bloch. Effective Java (Second Edition). Sun Microsystems, Inc., Santa Clara, CA, 2008.

[4.8] H. Fakham, A. Doniec, F. Colas, and X. Guillaud, "A Multi-agents System for a Distributed Power Management of Micro Turbine Generators Connected to a Grid", *IFAC CMTEE*, Vol. 1, 2010.

[4.9] B. Ramachandran, S.K. Srivastava, D.A. Cartes, C.S. Edrington, "Distributed energy resource management in a smart grid by risk based auction strategy for profit maximization", *Proceedings, IEEE Power and Energy Society General Meeting*, 2010.

[4.10] Saul Gass, Linear Programming: Methods and Applications - 5th Edition, Dover Publications, Inc. 2003, pgs. 224-250.

CHAPTER 5

MODELING

It was clear from the outset of investigating how to conduct microgrid simulations and analysis that finding appropriate models for the components that made up the microgrid was going to be complicated. This occurred for a few reasons. First, pre-installed models in software such as MATLAB/SIMULINK or PSPICE are good at simulating many parameters necessary for electrical analysis, but they often lacked full access to the models. This became problematic, for example, when conducting simulations that required visibility of a parameter that the model did not provide. Additionally, as mentioned above, given the limited environments that commercial software packages offered for developing hierarchical control methods, such as multi-agent designs discussed later, it became evident that microgrid components would need to be modeled outside of these software packages. This led to a need to develop models for generation, load, and storage, as well as the power system, to properly implement a power management and control framework for investigation.

The following models were developed for the purpose of serving as stand-alone simulations that could be implemented when necessary for microgrid analysis. When instantiated, the models would calculate their parameters incrementally and have that information available for controllers and observers, alike. By investigating and improving common power system asset models, the resulting models could be used independent from commercial software packages and give greater depth of parameter information important for power management and its evaluation.

5.1 Engineering Practice

When researchers approach modeling, the desire is to develop models that best describe system behaviors of interest to the researcher. Modeling of any system is only as good as the mathematical principles applied to describing it. Likewise, models must be validated by physical or experimental data. From an engineering perspective, models are developed and used with practical applications in mind. After all, engineering is an applied science. To that end, the power engineer does not always have access to good empirical data about a particular asset which complicates model development. The engineer must rely upon manufacturer's specification data, which in many cases, is fairly limited. Examples of this process are common; for instance, an engineer must find and match a component or piece of equipment to a subset of project specifications, and evaluate how that selection will operate within the system. There arises a clear discrepancy for the engineer when conducting this process with models that are notably different than the actual equipment or components under consideration.

The model accuracy and applicability discrepancy was found throughout the conduct of this project, but from a slightly different perspective. Many of the published system or asset mathematical models evaluated for this project were found to be inadequate. This was most often because they were not comprehensive enough to incorporate parameters of interest, such as cost or performance measures, or when simulated, published models did not match published manufacturer's data. Therefore, possibly the strongest contribution of the following asset models is directed at the practicing engineer. The models developed in this section are intended to allow the engineer to use a manufacturer's specification or data sheet directly in order to instantiate an asset model. Too often this is not the case in the literature and causes problems for the engineer. Where possible, details about using manufacturer's data have been highlighted below. Ultimately, the engineer will face difficulty performing practical system studies without good models that reflect operational parameters consistent with manufacturers' reported data. The models presented in this chapter are towards that intended purpose.

5.2 Diesel Generator

The thermodynamics of diesel engine operation, as well as generator set electrical operation are well understood. However, all diesel generators are not created equal. Therefore, using information from sixty commercially available diesel gensets produced by six manufacturers and ranging in size from 6kW to 2,260kW, key generator operating characteristics were compiled and analyzed [5.1]. For proper diesel genset model development, establishing fuel consumption and energy efficiency curves for microgrid assets is very important, as is being able to simulate various diesel capacities for system studies. To that end, the compiled diesel genset data was used to determine parameters that establish default diesel characteristics, based on rated electrical output power capacity. Fuel consumption within a given diesel generator varies nearly linearly with increasing load. Therefore, the following equation described diesel fuel consumption as it varies with load:

$$F = mP_{actual} + bP_{rated} \tag{5.1}$$

where: F is fuel consumption (L/hr); m is fuel curve slope coefficient (L/hr-kW_{actual}); P_{actual} is diesel generator mechanical operating power level (kW); b is fuel curve intercept coefficient (L/hr-kW_{rated}); and P_{rated} is diesel generator nameplate power (kW).

The generator intercept (b) and slope (m) coefficients represent the no-load fuel consumption of the generator divided by its rated capacity and the generator marginal fuel consumption, respectively. These coefficients describe the equation of a line that represents the linear regression of fuel consumption, scaled based on generator capacity. The m and b coefficients were found by first classifying the representative diesel gensets based on rated capacity. Groups of generators were formed based on similarity in characteristics, forming generator classes shown in Figure 5.1 and Figure 5.2. For each generator, a linear regression of fuel consumption and power curves was performed to determine individual slope and intercept coefficients. Then, averages of the coefficients were found across each class, shown in Table I.

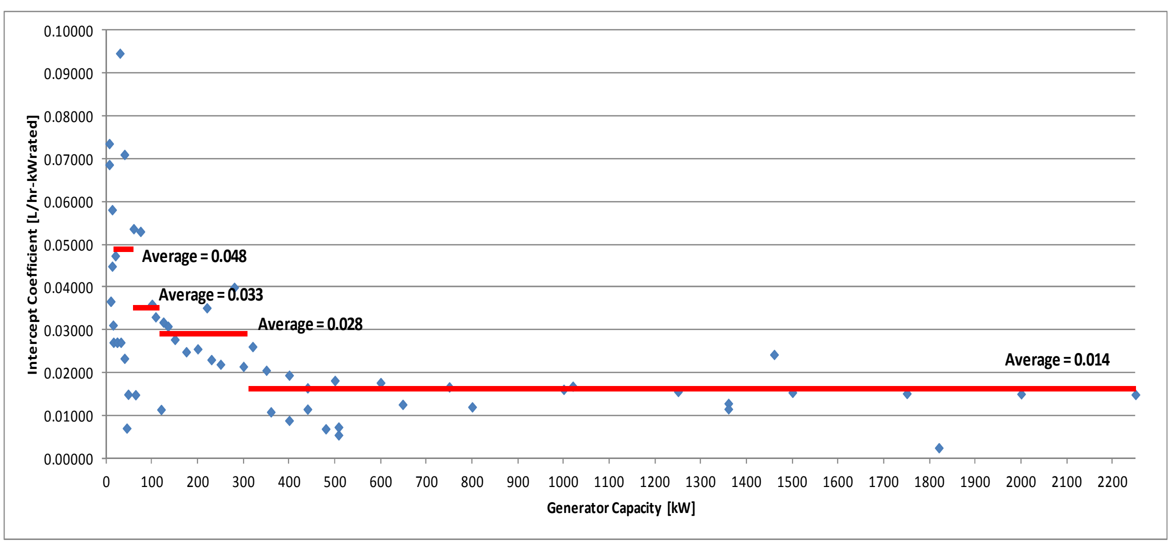

Figure 5.1. Diesel intercept coefficient versus generator rating (fuel flow in L/hr).

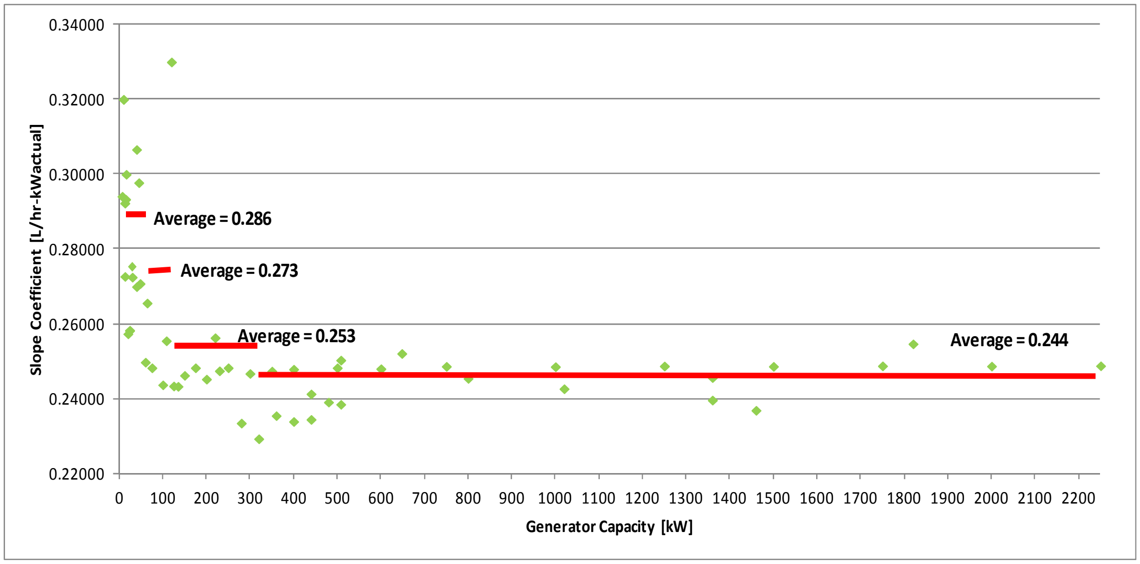

Figure 5.2. Diesel slope coefficient versus generator rating (fuel flow in L/hr).

Table 5.1. Diesel genset fuel curve coefficients based on genset classification.

Classifications of Generators	Intercept Coefficient (based on L/hr)	Slope Coefficient (based on L/hr)
< 30 kW	0.048	0.286
30 - 100 kW	0.033	0.273
100- 300 kW	0.028	0.253
> 300 kW	0.014	0.244

In order to calculate diesel genset efficiency, the following relationship is established:

$$\eta_{diesel} = \frac{P_{out}}{P_{in}} = \frac{P_{actual}}{\dot{m}_{fuel} LHV_{fuel}} \qquad (5.2)$$

where: η_{diesel} is diesel efficiency; $\dot{m}_{fuel}$ is volumetric flow rate of fuel (L/hr); and LHV_{fuel} is fuel volumetric energy content (kJ/L). Lower heating value (LHV) refers to the energy content of a fuel if the reactants are returned to a temperature (appropriate for the system pressure) that yields water in the gaseous state, near its condensation point. Alternatively, higher heating value (HHV) refers to the energy content of a fuel if the reactants are returned to standard temperature, typically 25˚C (298 K) [5.2]. LHV represents a smaller quantity of energy than HHV because the standard enthalpy change of condensation (latent heat of condensation) quantity that would be released from the product water in changing state from gas to liquid is not included. To remain consistent with accepted convention, LHV is used in calculating diesel genset efficiency. When a diesel generator model is instantiated, the model takes on the above default characteristics based on a lookup table referenced by the actual asset rated capacity. Based on the actual rated capacity, a scaled efficiency curve and fuel consumption curve are derived representing the characteristics of the desired generator. Based on the diesel classifications derived, Figure 5.3 shows the efficiency functions that evolve as diesel genset capacity increases.

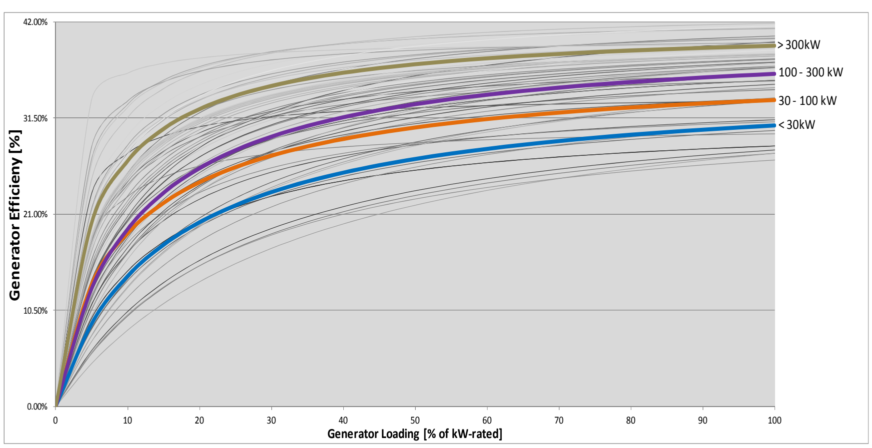

Figure 5.3. Diesel generator efficiency characteristics by rated capacity.

Diesel emissions characteristics were developed from data presented in [5.2, 5.3, 5.4] and are shown in Figure 5.4 and Figure 5.5. Of prime concern for diesel operation were carbon dioxide (CO_2) and total hydrocarbons (THC) exhaust. Carbon dioxide is a well-known constituent that may have a contributory effect on global climate change [5.5]. Total hydrocarbons are all volatile and semi-volatile organic compounds that are emitted when organic fuels (such as petroleum-based fuels, natural gas, ethanols, or biodiesels) are combusted. THCs are of particular concern when emitted because they not only can have a detrimental effect on the atmosphere as greenhouse gases [5.6], but also have a direct negative effect on human health. The fine particulate, known as 2.5 micron particulate matter ($PM_{2.5}$) is known to contribute to premature death from heart or lung disease and is regulated by the U.S. Environmental Protection Agency (EPA) under the authority of the amended 1990 Clean Air Act through the National Ambient Air Quality Standards [5.7]. These two emissions constituents were deemed to be the most important to consider when assessing the environmental impact of diesel operations and were used for quantifying diesel performance in simulation.

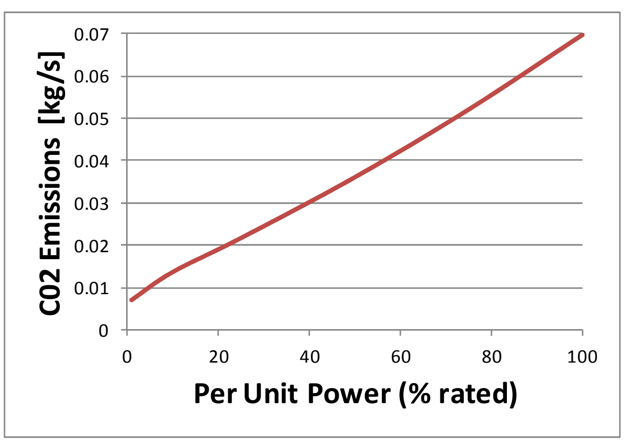

Figure 5.4. CO_2 emissions function for diesel generation.

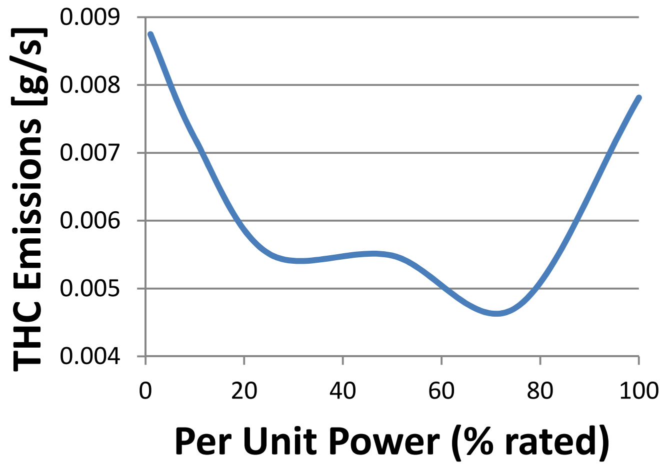

Figure 5.5. THC emissions function for diesel generation.

The diesel generator mechanical model was based on a well-established model used in [5.8] and shown in Figure 5.6. A mechanical torque (τ_{mech}) on the common diesel engine and generator shaft is developed from a difference between a reference rotational speed (ω_{ref}) and actual speed (ω_{act}). While the traditional diesel governor is good at regulating fuel to achieve a near constant shaft speed, the situation is potentially different for diesels employed in microgrids. In microgrid applications, the diesel generator would be expected to participate in system power management and, therefore, must regulate output power as well as shaft speed. To achieve this, a reference mechanical power (P_{mech}) signal and a no-load speed reference (ω_{NL}) signal, both provided by an external reference source, combine in calculation with measures of actual mechanical torque and speed to feed back the ω_{ref} signal. This, along with the calculation of power delivered from the diesel engine to the generator end (P_e), are shown in Figure 5.7. The coefficients for the model used, shown in Table 5.2, are different than those given in [5.8] to account for a smaller capacity diesel with less inertia and faster response. The voltage regulator model, based on the model used in [5.9], is well-known and is shown in Figure 5.8. The coefficients for the voltage regulator model are also given in Table 5.2.

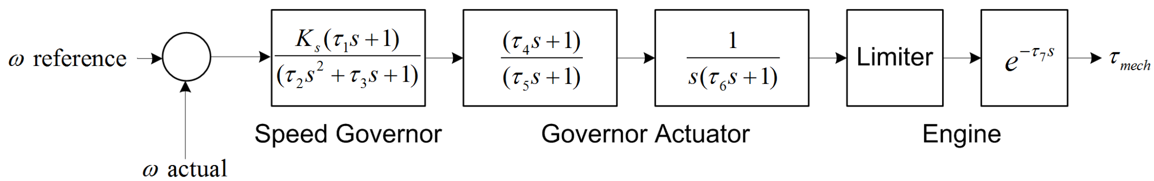

Figure 5.6. Diesel generator mechanical model.

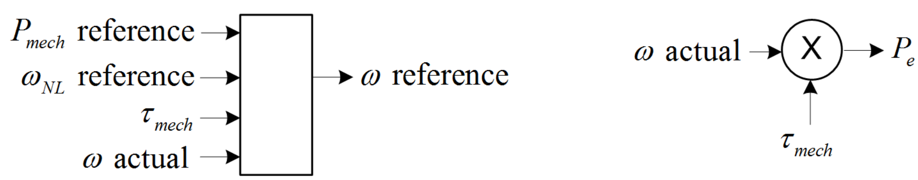

Figure 5.7. Speed reference feedback (left) and generator shaft power (right).

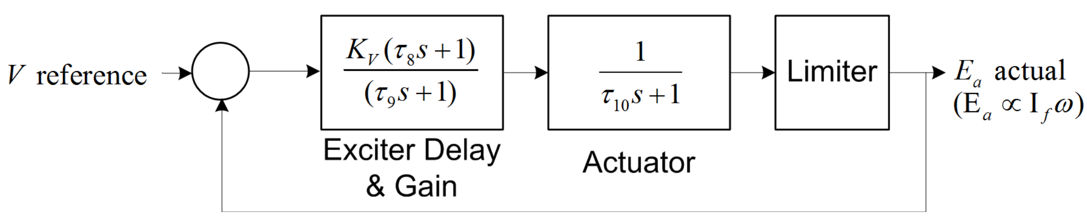

Figure 5.8. Diesel generator voltage regulator model.

Table 5.2. Diesel model coefficients.

Parameter	Value	Parameter	Value
K_s	5	τ_5	0.009
K_v	100	τ_6	0.00384
τ_1	0.2	τ_7	0.8
τ_2	0.002	τ_8	3
τ_3	0.01	τ_9	10
τ_4	0.25	τ_{10}	0.1

The diesel generator interconnection circuit model is based on direct connection to the AC bus, shown in Figure 5.9. This is not mandatory, however, and could be used in an AC/DC-to-DC/AC arrangement with is common for decoupling non-standard frequency AC generators such as microturbines or wind turbines. The generator internal voltage, E_a, sources the synchronous impedance (R_s + jX_s), developing the generator terminal voltage (V_t), which in turn sources armature current (i_a) across the terminal connection impedance (R_t + jX_t) to bus voltage (V_{bus}), according to (all values in RMS):

$$I_a = \frac{V_t - V_{bus}}{R_t + \mathrm{j}X_t} \tag{5.3}$$

$$E_a = V_t + \left(R_s + jX_s\right)I_a \tag{5.4}$$

$$P_e = \left|E_a\right|\left|I_a\right| \tag{5.5}$$

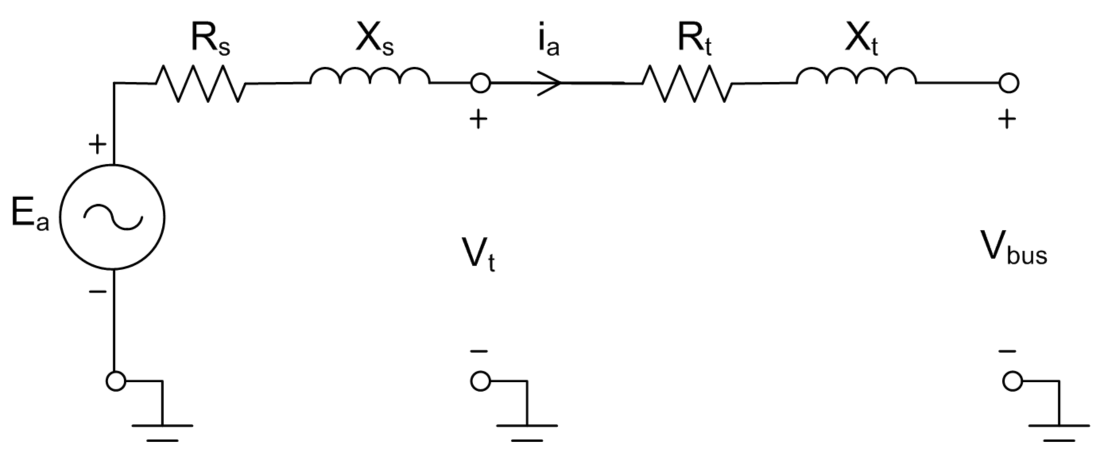

Figure 5.9. Diesel generator interconnection circuit.

This diesel model allows the calculation of internal mechanical and electrical parameters incrementally, as well as fuel flow and emissions information. This information is important for implementation in the microgrid model because it allows the diesel to be dispatched considering many factors, not just constant shaft speed.

5.3 Microturbine Generator

Microturbines (MT) are high rotational speed, low footprint gas turbines that operate based on the Brayton thermodynamic cycle [5.10]. The basic components of the microturbine generation system include the compressor, turbine, recuperator, high speed generator, and power electronics interfacing; the block diagram of the single-shaft MT generator system is shown in Figure 5.10. The MT operates by first compressing inlet air within a radial compressor. Fuel is then mixed with the compressed air in the combustor and burned. Hot combustion gases are expanded in the turbine section producing rotating mechanical power that drives the compressor and a permanent magnet synchronous generator (PMSG) by means of a common shaft. The MT shaft speeds vary widely based on manufacturer, from 50,000 to 120,000 RPM.

Because the direct coupled MT shaft spins at such high speeds, an AC-AC interface is required for coupling the generator to a conventional power system. This is accomplished with power electronics that rectify the high speed AC and then invert the power to 60Hz AC. Although more typically wound for three-phase AC, the same principles apply to single-phase AC, depending on generator and power electronic interface design. Similar to the diesel generator, the MT governor adjusts its fuel flow appropriately to meet generation power demand.

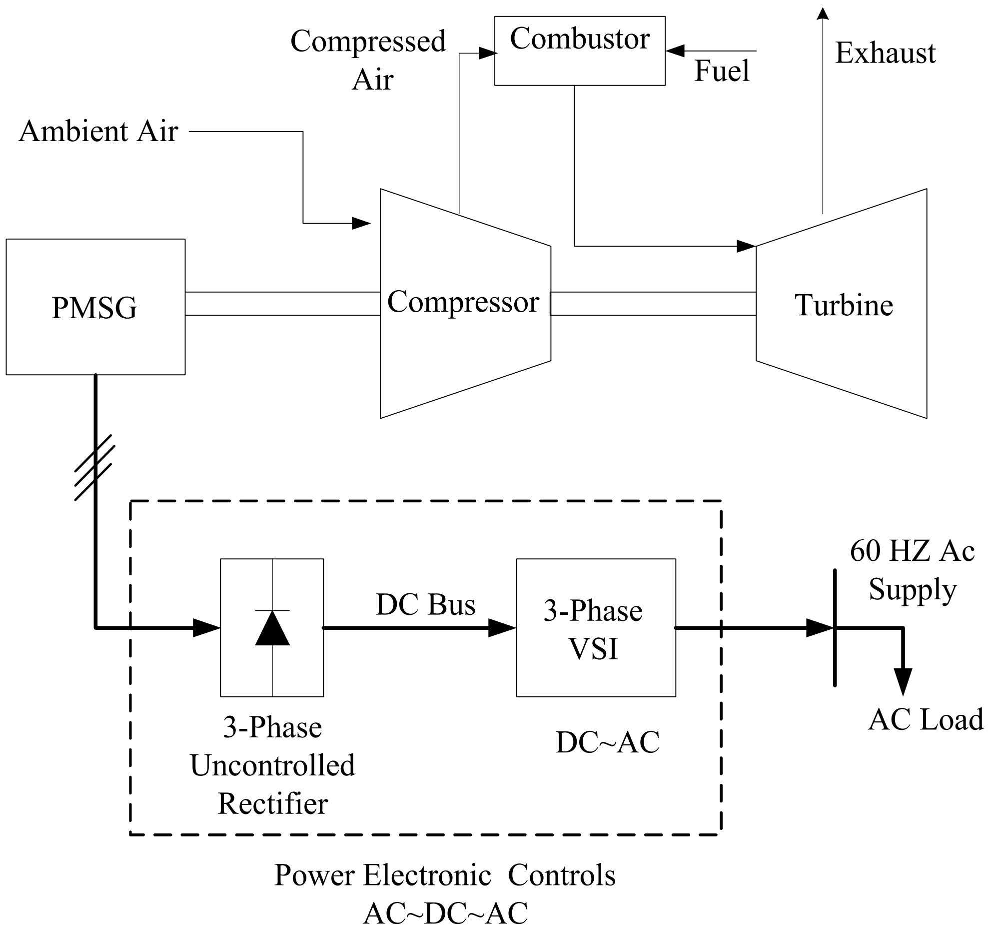

Figure 5.10. Single-shaft MT generator block diagram with PMSG.

The MT model, reported in [5.11], was evaluated for translation into an incremental model suitable for Java implementation. While a good model, it was found to focus primarily on combustor thermodynamics that were difficult to validate against manufacturer’s data. This is not the fault of the model, but rather a consequence of the lack of manufacturer’s data available. Without validation, the model was checked for consistency with heat engine thermodynamics. Interestingly, the MT was found to be about 35% efficient at converting natural gas fuel to AC electrical energy; very similar to the diesel engine and consistent with heat engine energy conversion. It followed that, given the known energy input of the gaseous fuel and the measure of MT system efficiency, the MT operated very much like a diesel, just a different technology. Therefore, knowing that the Carnot principles of the Brayton cycle are very similar to those employed in the diesel model, the diesel model was used in a modified form to simulate MT operation. Fuel governor and voltage regulation operation were adequate stand-ins for analogs in the MT system. It is noted that, in the future, if better manufacturer's data becomes available for MTs that the model reported in [5.11] could be transitioned to an appropriate Java incremental model.

5.4 Photovoltaics

The photovoltaic effect arises from a physical process by which energy from electromagnetic radiation of the sun, known as solar insolation, is converted into useful electrical energy. When certain materials are presented within a solar radiation flux, photons nudge electrons out of their atomic orbits and create free electrons and subsequent vacancies within the material [5.12]. This phenomenon is capitalized upon within sandwiches of thin substrates of doped semiconductor materials, known as photovoltaic cells. By combining an n-layer (semiconductor with a surplus of valence shell electrons) and a p-layer (semiconductor with a deficit of valence electrons, also known as electron holes), a thin region of atoms with filled valence shells develops at the interface between the two layers. This interface junction gives rise to an electric field which accelerates electrons freed by the solar energy interaction towards the n-layer. If the semiconductor pn-junction is connected to an external circuit, the electron flow represents a current that can be harnessed as a source of electric power [5.13]. Individual photovoltaic cells are often combined with numerous other cells into modules that facilitate higher voltage ratings and produce more output power.

Two appropriate models for photovoltaic modules were evaluated. Depending on the desired complexity or the fit to a particular manufacturer's data, either a four parameter (shunt branch omitted) or five parameter model (shunt branch included) can be used. Both models are developed below.

5.4.1 Four-Parameter Model

The four parameter circuit model with shunt resistance neglected, shown in Figure 5.11, can be used to model a photovoltaic array that generates electrical power when exposed to sunlight. The overall photovoltaic model diagram is shown in Figure 5.12.

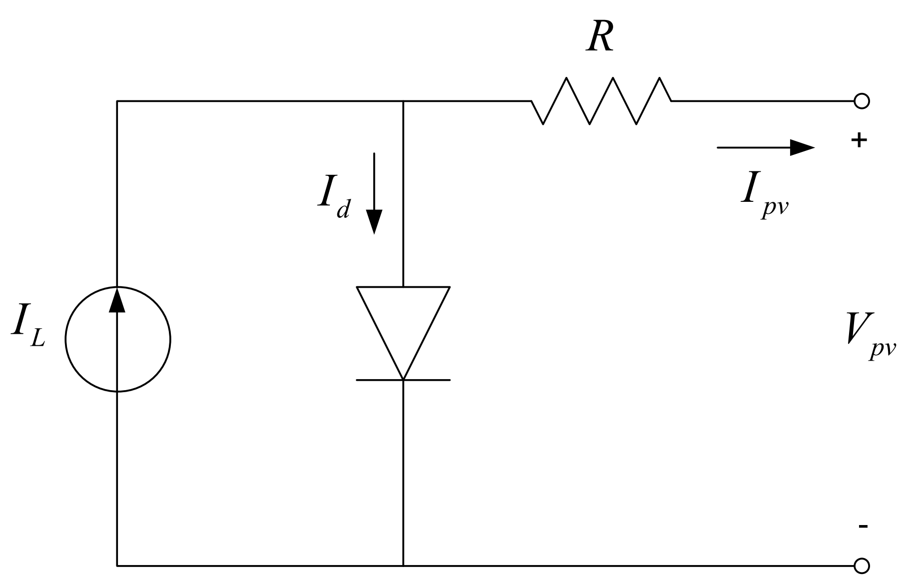

Figure 5.11. Four parameter equivalent circuit model for a photovoltaic cell.

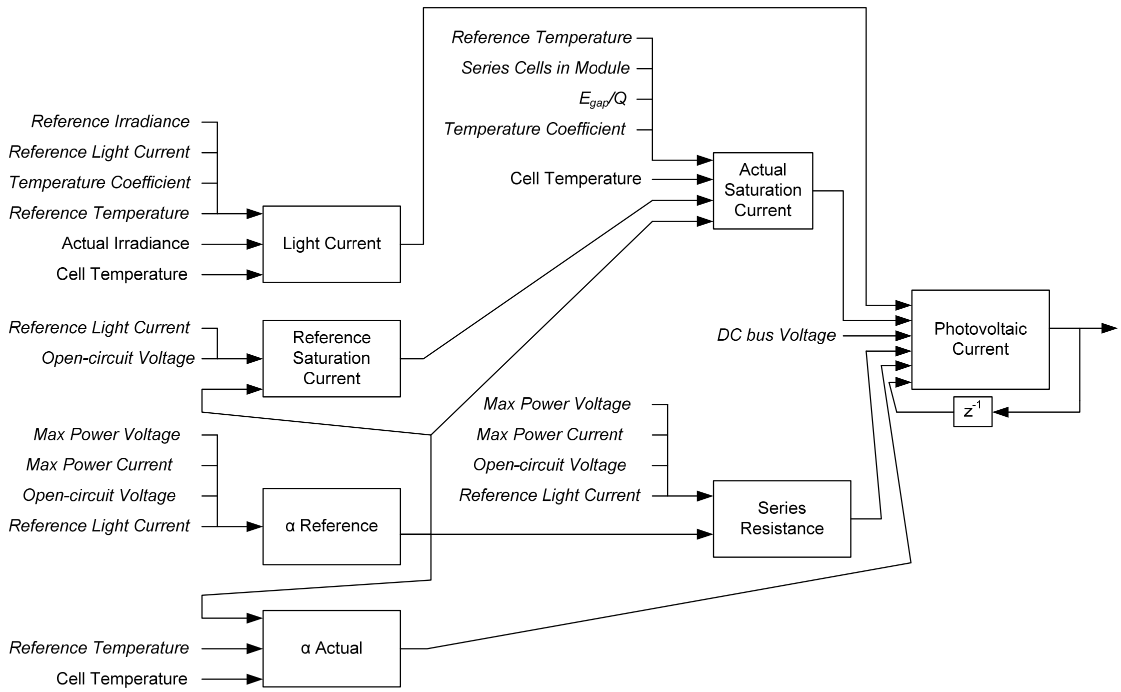

Figure 5.12. Schematic of four parameter photovoltaic cell mathematical model.

The fundamental relationships between the output voltage V_{pv} and the current I_{pv} are represented by the current balance, shown in (5.6). This simplification is found when assuming that the shunt branch current is zero under all conditions [5.14].

$$I_{pv} = I_L - I_D = I_L - I_0 e^{\left(\frac{V_{pv}+I_{pv}R}{\alpha}\right)-1} \tag{5.6}$$

where: I_L is photo or irradiance current (A); I_D is the diode branch current (A); I_0 is saturation current (A); I_{pv} is load current (A); V_{pv} is output voltage (V); and R is series resistance (Ω). The diode branch may be modeled as a current source, controlled by the relative saturation current, dictated by V_{pv}, I_{pv}, and R. The α coefficient represents the thermal voltage coefficient (V), adjusted for photovoltaic temperature, found by:

$$\alpha = \frac{T_c + 273}{T_{c,ref} + 273} \alpha_{ref} \tag{5.7}$$

where, T_c is photovoltaic cell temperature (˚C); $T_{c,ref}$ is reference temperature (normally 25 ˚C); and α_{ref} is the reference thermal voltage coefficient (V). As proposed by [5.15], the α_{ref} coefficient is found by:

$$\alpha_{ref} = \frac{2V_{mpp,ref} - V_{oc,ref}}{\frac{I_{sc,ref}}{I_{sc,ref} - I_{mpp,ref}} + \ln\left(1 - \frac{I_{mpp,ref}}{I_{sc,ref}}\right)} \tag{5.8}$$

where, $I_{sc,ref}$ is short circuit current at the reference conditions (A); $V_{oc,ref}$ is the open circuit voltage of the PV module at reference condition (V); $V_{mpp,ref}$ is maximum power point voltage at the reference condition (V); and $I_{mpp,ref}$ is maximum power point current at the reference condition (A). Each of these values is available on standard product data sheets available from the manufacturers of photovoltaic modules.

The light current, I_L, is a function of temperature and solar irradiance. The air mass ratio represents the mass of air that solar insolation must pass through to reach the photovoltaic panel, relative to the reference air mass if the sun is directly overhead (smallest air mass between the sun and panel). When the air mass ratio is assumed to be 1 (i.e., at reference conditions), I_L may be found by [5.14]:

$$I_L = \frac{\Phi}{\Phi_{ref}} \left[I_{L,ref} + \mu_{I,SC} \left(T_c - T_{c,ref} \right) \right] \tag{5.9}$$

where, Φ is irradiance (W/m^2); Φ_{ref} is reference irradiance (typically 1000 W/m^2); $I_{L,ref}$ is the reference light current often assumed to be equal to the manufacturer's stated reference short circuit current, $I_{sc,ref}$; and $\mu_{I,SC}$ is the temperature coefficient of the short-circuit current (A/°C). Although not always available, $\mu_{I,SC}$ is sometimes listed on the manufacturers data sheet.

The ideality, shape, or completion, factor (n) accounts for the cumulative total of mechanisms that move charge carriers across the photovoltaic diode junction [5.15]. This factor is 1 in an ideal cell, but less than one in an imperfect one. The dimensionless factor may be calculated by observing the relationship between the reference thermal voltage coefficient and cell temperature, by [5.15]:

$$n = \frac{q\alpha_{ref}}{N_s k\left(T_{c,ref} + 273\right)} \tag{5.10)-(a}$$

Or, the following substituting (5.7):

$$n = \frac{q\alpha\left(\dfrac{T_{c,ref} + 273}{T_c + 273}\right)}{N_s k\left(T_c + 273\right)} \tag{5.10)-(b}$$

where, k is the Boltzmann constant (1.3806503×10^{-23} J/K); q is charge of an electron (1.60217733×10^{-19} C); and N_s is the number of photovoltaic cells in series to form the module. The reverse saturation current, I_0, is a function of temperature and can be found by [5.15]:

$$I_0 = I_{0,ref}\left(\frac{\left(T_c+273\right)^3}{\left(T_{c,ref}+273\right)^3}\right)e^{\frac{nN_s e_{gap,ref}}{q\alpha_{ref}}\left[-\left(\frac{T_c+273}{T_{c,ref}+273}\right)+1\right]} \tag{5.11}$$

where, $e_{gap,ref}$ is the electrical band gap of the material (widely published as 1.11-1.17 eV for Si materials [5.16]). It is noted that, by convention, the exponential component comprised of the actual band gap and photovoltaic cell temperature are subtracted *from* the reference-valued component. The reference reverse saturation current is likely not available on the manufacturer's data sheet, but it may be found, as suggested in [5.15] by:

$$I_{0,ref} = I_{sc,ref}\ e^{-\frac{V_{oc,ref}}{\alpha_{ref}}} \tag{5.12}$$

where, $I_{0,ref}$ is saturation current at the reference condition (A).

Finally, according to [5.15], the series resistance within the photovoltaic circuit model may be found by:

$$R = \frac{\alpha_{ref}\ln\left(1-\frac{I_{mpp,ref}}{I_{sc,ref}}\right)+V_{oc,ref}-V_{mpp,ref}}{I_{mpp,ref}} \tag{5.13}$$

Although self-heating of the photovoltaic cell that arises from power dissipation within the series resistance is an important factor in modeling photovoltaic performance, it is known to closely follow insolation according to:

$$T_c = T_{amb} + \Phi\left(\frac{T_{nom} - 20^\circ\mathrm{C}}{0.8}\right) \tag{5.14}$$

where, T_{amb} is the ambient temperature of the surroundings; and T_{nom} is the nominal operating temperature specified by the manufacturer. It is noted that, predominantly, T_{nom} is not equivalent to $T_{c,ref}$.

5.4.2 Five-Parameter Model

The four parameter photovoltaic model is adequate for most simulation tasks. Additionally, it is typical that the values of $V_{oc,ref}$, $V_{mpp,ref}$, $I_{mpp,ref}$, $I_{sc,ref}$, N_s, Φ_{ref}, T_{nom}, $T_{c,ref}$, and $\mu_{I,SC}$ necessary to instantiate the model can be readily obtained from manufacturer data sheets. However, on some occasions the four parameter model does not match stated manufacturer performance. This was especially noted using (5.12) and (5.13), which were satisfactory assumptions, but did introduce errors on larger photovoltaic modules. In those cases, it was found that using a model that did not omit the shunt branch was better suited. The five parameter circuit model diagram with shunt resistance included is shown in Figure 5.13. The overall photovoltaic model diagram is shown in Figure 5.14.

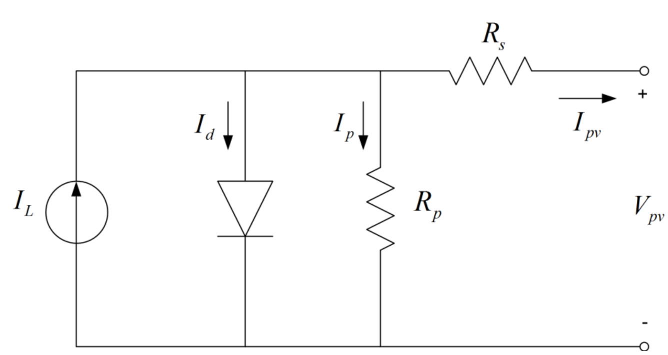

Figure 5.13. Five parameter equivalent circuit model for a photovoltaic cell.

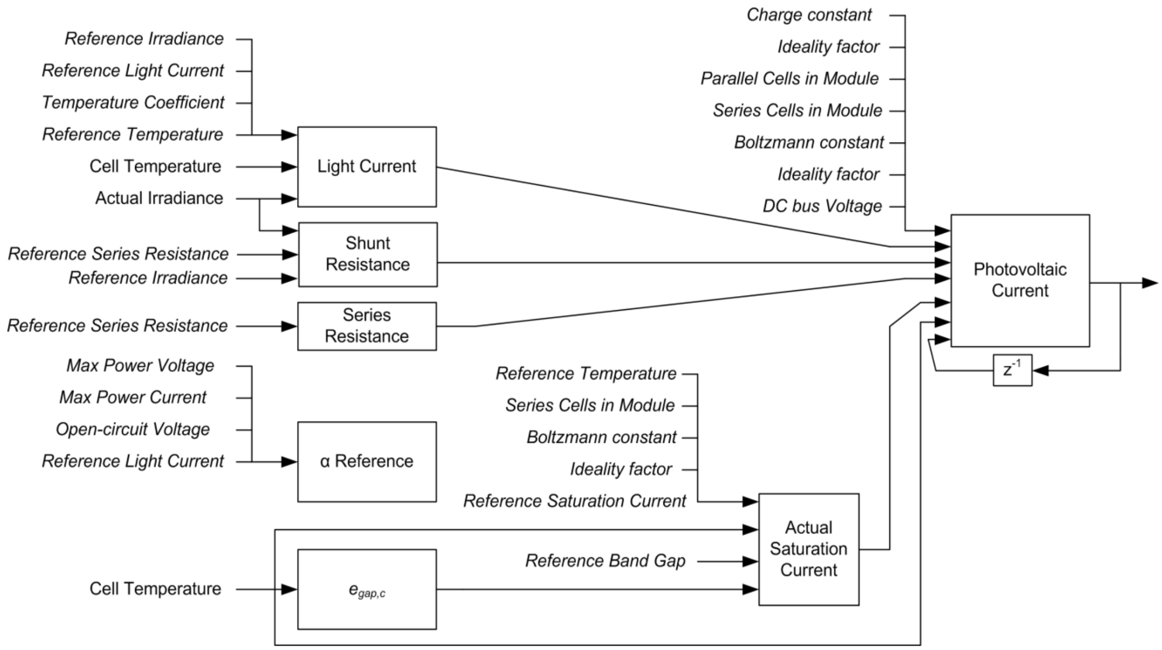

Figure 5.14. Schematic of five parameter photovoltaic mathematical model.

As described above, it was found that on most manufacturers' data sheets the open-circuit voltage ($V_{oc,ref}$), maximum power point voltage ($V_{mpp,ref}$), maximum power point current ($I_{mpp,ref}$), short-circuit current ($I_{sc,ref}$), the number of series and parallel photovoltaic cells per module (N_s and N_p), nominal operating temperature (T_{nom}), and short-circuit temperature coefficient ($\mu_{I,SC}$) were available. In the five parameter model, this gives rise to the following unknown parameters at Standard Reference Conditions (SRC), i.e. $T_{c,ref}$ = 25°C: reference light current ($I_{L,ref}$), reference reverse saturation current (I0,ref), reference ideality factor (n_{ref}), reference shunt resistance ($R_{P,ref}$), and reference series resistance ($R_{S,ref}$). These unknowns can be simplified by observing that $I_{L,ref}$ is very similar to $I_{sc,ref}$ at reference conditions. Additionally, the ideality factor, n_{ref}, is assumed to be independent of temperature and insolation, having a value between 1.1

and 1.3 which favors diffusion as the means of charge carrier transport. Thus, these observations leave the five parameter model with only three unknowns.

Similar to (5.6), the relationships between the output voltage V_{pv} and the current I_{pv} are given by the current balance, shown in (5.15), including the shunt branch current [5.33].

$$\begin{aligned} I_{pv} &= I_L - I_D - I_p \\ &= N_p\left(I_L - I_0 e^{\left(\frac{V_{pv}+I_{pv}R_s\frac{N_s}{N_p}}{\gamma}\right)} - I_0\right) - \frac{V_{pv}+I_{pv}R_s\frac{N_s}{N_p}}{R_p\frac{N_s}{N_p}} \end{aligned} \tag{5.15}$$

where: γ is a ratio of nkT_cN_s / q. Different from the four parameter model, a thermal voltage coefficient (α), is not necessary to calculate. Instead, the shunt resistance parameter (R_p) is calculated according to:

$$R_P = R_{P,ref}\frac{\Phi}{\Phi_{ref}} \tag{5.16}$$

where, $R_{p,ref}$ is the reference shunt resistance; and R_p is the shunt resistance that varies with solar insolation. As noted in [5.14], the series resistance is independent of temperature and insolation, thus $R_S = R_{S,ref}$.

The light current, I_L, a function of temperature and solar irradiance, is calculated according to (5.9). Likewise, the saturation current is calculated similar to (5.11), but incorporating the effect of temperature on band gap, by [5.14, 5.17, 5.18]:

$$I_0 = I_{0,ref}\left(\frac{\left(T_c+273\right)^3}{\left(T_{c,ref}+273\right)^3}\right)e^{\left[-\frac{e_{gap,c}}{nk\left(T_c+273\right)}+\frac{e_{gap,ref}}{nk\left(T_{c,ref}+273\right)}\right]} \tag{5.17}$$

where, the band gap energy of the semiconductor does vary with temperature and is calculated according to [5.19]:

$$e_{gap} = 1.16 - 7.02\times10^{-4}\left(\frac{T_c^2}{T_c-1108}\right) \tag{5.18}$$

Using (5.15) and information from the manufacturer's data sheet, three simultaneous equations may be constructed with only three unknowns. Those equations are:

Open circuit (two unknowns: $I_{o,ref}$ and $R_{p,ref}$):

$$I_L - I_0 e^{\left(\frac{V_{pv}}{\gamma}\right)} - I_0 = \frac{V_{OC,ref}}{R_{p,ref}N_s} \tag{5.19}$$

Short circuit (three unknowns: $I_{o,ref}$, $R_{s,ref}$, and $R_{p,ref}$):

$$I_{sc,ref} = N_p I_L - N_p I_0 e^{\left(\frac{I_{sc,ref}R_{s,ref}\frac{N_s}{N_p}}{\gamma}\right)} - N_p I_0 - \frac{I_{sc,ref}R_{s,ref}}{R_{p,ref}} \tag{5.20}$$

Maximum power point (three unknowns: $I_{o,ref}$, $R_{s,ref}$, and $R_{p,ref}$):

$$I_{mpp,ref} = N_p\left(I_L - I_0 e^{\left(\frac{V_{mpp,ref}+I_{mpp,ref}R_{s,ref}\frac{N_s}{N_p}}{\gamma}\right)} - I_0\right) - \frac{V_{mpp,ref}+I_{mpp,ref}R_{s,ref}\frac{N_s}{N_p}}{R_{p,ref}\frac{N_s}{N_p}} \qquad (5.21)$$

Using these equations, the remaining three unknowns ($I_{o,ref}$, $R_{s,ref}$, and $R_{p,ref}$) may be found and the photovoltaic module parameters calculated incrementally. Photovoltaic self-heating for the five parameter model follows (5.14). The five parameter model was preferable over the four parameter model for most higher capacity photovoltaic modules evaluated [5.18].

5.4.3 Maximizing Photovoltaic Generation

As a renewable source of electrical power, photovoltaic arrays are most often employed in applications where it is desirable to generate as much power from the solar resource as possible, when available. As a result, maximum power point tracking (MPPT) controls are used to manipulate the photovoltaic terminal voltage so as to determine the ideal current level, thereby extracting the highest amount of power available [5.20]. There are several MPPT techniques in use, including look-up table methods, perturb and observe (P&O) methods [5.21, 5.22], model-based computational methods [5.23], hill-climbing and other intelligent methods [5.24, 5.25]. Predominantly, MPPT techniques may be broken into two categories; those which require prior knowledge of photovoltaic parameters and those that do not. The indirect control methods, including open-circuit and short-circuit current methods, demand good performance knowledge of the photovoltaic module in order to seek maximum power.

Direct control methods, such as P&O and hill-climbing, require only sensed voltage, current, and in some cases insolation, to find the optimal power point.

For this study, when the microgrid is interconnected with the utility grid, it is expected that the maximum power production from the photovoltaic will always be desired; either to offset electricity purchases from the utility or to sell excess power to the utility. However, when islanded from the utility, it may be necessary to reduce the amount of power generated by the photovoltaic array to match local load constraints. For most direct photovoltaic controls, MPPT methods do not allow the photovoltaic array to operate significantly off of the point of maximum power. Prolonged operation outside of the controller boundaries will cause the photovoltaic array to become separated from the microgrid. This, of course, is undesirable in any situation where the array could positively contribute to the system. Therefore, an alternative direct control method is proposed for use of photovoltaics on the microgrid.

Much of the MPPT control for the photovoltaic array may be executed by a controller algorithm. In the case of this project, either a separate direct controller may be employed or an agent responsible for the photovoltaic array accomplishes this task. To that end, it is desireable to have two modes of operation: MPPT and reference power (P_{ref}) control. For modeling purposes, the MPPT and P_{ref} controllers are separate algorithms from the agent algorithms, but this is done only for clarity. In this way, the agent directs which control algorithm is in use. Under normal operation, a conventional MPPT method that observes the change in photovoltaic power with respect to the change in photovoltaic DC voltage (dP/dV) is used to extract the maximum amount of power from the photovoltaic array. The *d*P/*d*V controller yields a reference voltage signal ($V_{q,ref}$) that allows the DC/DC converter to adjust the voltage level at the photovoltaic array terminals, thereby controlling the current extracted by the array. When decided by the agent that maximum power tracking is not desirable (according to the goals assigned to the agent responsible for the photovoltaic asset), the agent may shift from the *d*P/*d*V-MPPT controller to the P_{ref} controller. In this mode, the agent supplies a reference power signal (less than the maximum power available) to the P_{ref} controller, which in turn yields a reference voltage signal ($V_{q,ref}$) to the DC/DC converter. This signal directs the DC/DC converter to vary voltage from the open-circuit voltage to achieve the desired reference power. The combination of these controllers and the means of agent interaction are shown in Figure 5.15.

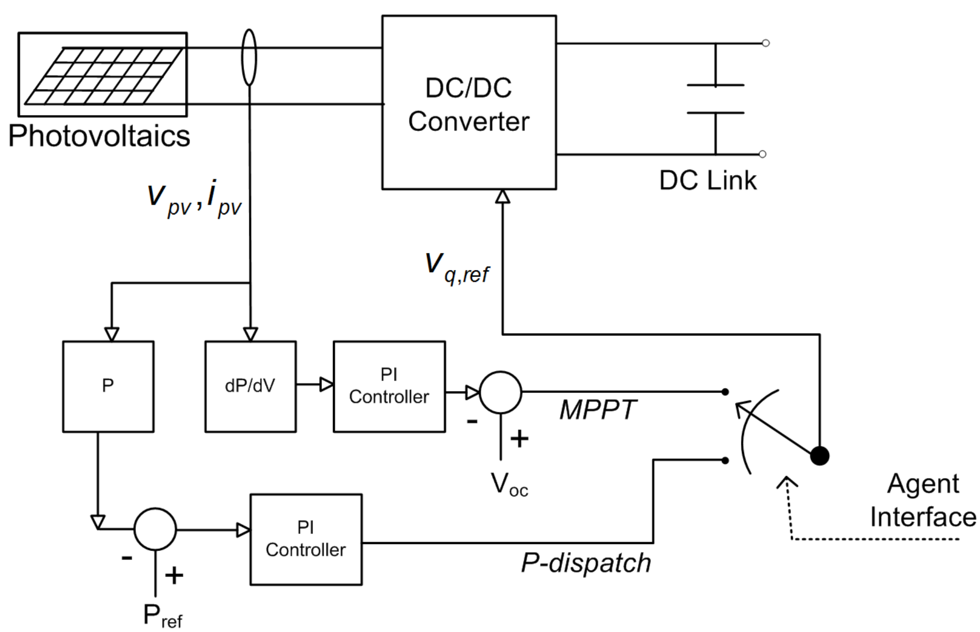

Figure 5.15. DC-side photovoltaic control diagram.

On the AC–side of the DC link, the DC/AC inverter must be controlled in conjunction with the DC/DC converter. This ensures that the power produced by the photovoltaic array is appropriately conditioned for supply to the AC bus. This is similar in principle to the DC/AC control described in more detail for the wind turbine generator in 5.5 . As with the signal flow to the DC/DC converter, the photovoltaic agent determines which reference signals, either P_{ref} or P_{MPPT}, are used for the voltage and current control loops of the inverter. In both cases, reference reactive power (Q_{ref}) is determined by the agent and accompanies the references for real power. Given the nature of a P/Q controllable inverter, the photovoltaic array could be a strong source of reactive power. This could be accomplished by manipulating the phase relationship of DC/AC converter voltage and current. However, although conceivable, this is rarely done in practice because of the toll on circuit components. Instead, for low-inertia components, such as photovoltaics, the quantity of reactive power produced by the DC/AC converter is kept low, at a level to support proper voltage through the expected low impedance interconnection to the AC bus. In Figure 5.16, the AC-side of the photovoltaic interconnection to the AC bus is shown and shows the overall circuit schematic.

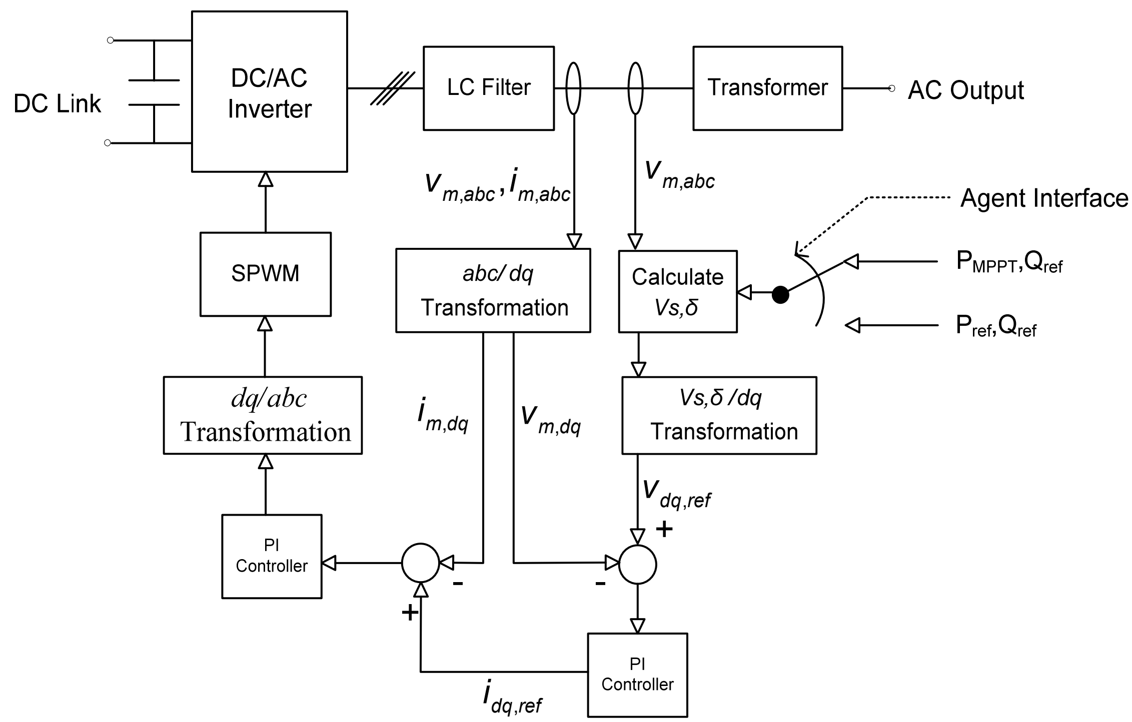

Figure 5.16. AC-side photovoltaic control diagram.

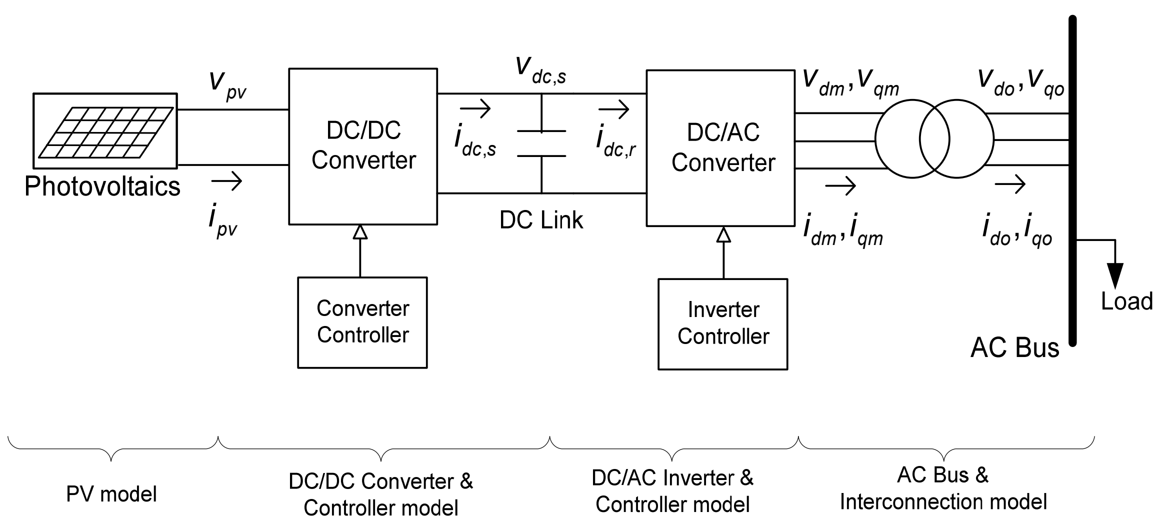

Figure 5.17. Photovoltaic array interconnection system diagram.

5.5 Wind Generation

Permanent magnet synchronous generators (PMSGs) have been the primary choice for small, off-grid wind turbines and the adoption of the technology for large-scale wind turbines is coming. Given that PMSG wind turbines will be more widely adopted in the future of microgrids, it is appropriate to examine their operational considerations. In conventional applications, wind turbines are operated so that they extract the maximum amount of energy from existing environmental conditions. As wind speeds rise, larger amounts of energy are extracted by the turbine blades, converted to electrical energy, and transferred, typically to the power system to which the wind energy conversion system (WECS) is connected. Unfortunately, under this mode-of-operation, in some cases WECS can induce undesirable or unstable conditions on the power system. This effect primarily arises due to the stochastic nature of wind energy, the typical lack of electrical energy storage associated with the power system, and fundamental electrical system dynamics. Simply, in some conventional applications, the power system that the WECS is connected to can suffer from an imbalance between the power injected by the WECS and the power transferred or extracted by the power system. The wind turbines employed in microgrids will not experience the same variable nature of the wind resource, but also must be able to operate within a system that may island itself much more frequently than is expected in conventional applications. Subsequently, alongside the modeling of a PMSG generator for use in a microgrid system, a counterintuitive mode-of-operation control scheme is investigated for wind turbines. Namely, this power management control method allows the power extracted from the wind to follow the demand of the power system; an especially important concept for a small islanded power system, such as a microgrid. With this power management control method, the WECS only generates the power required and does not cause voltage or frequency excursions to occur due to occasions of power imbalance, with or without the benefit of local storage.

The modern development of wind generation technology has been exhaustively covered in the literature [5.26, 5.27, 5.28, 5.29, 5.30, 5.31, 5.32, 5.33, 5.34, 5.35]. Modeling permanent magnet synchronous motor (PMSM) has been explored in the literature, as well, but an extensive treatment of the mathematical model for the generation mode of the permanent magnet synchronous machine is more rare. However, this development is necessary to explore the development of a PMSG control method to facilitate load-following and, thus, is presented here.

5.5.1 Wind Turbine Power Characteristics

The primary purpose of the WECS is to extract energy from prevailing winds and convert it into useful electrical energy to be utilized by a power system. The modes by which wind turbines operate are typically categorized based on two factors for the purpose of control system classification. The initial distinction is whether the turbine is designed to operate at fixed turbine rotational speed, or whether this speed is variable. The second factor is whether the turbine blade orientation with respect to the wind can be adjusted. The angle by which the turbine blades interact with the wind is called pitch angle (θ). Pitch angle is a primary component in how much torque, and subsequently rotational mechanical energy, is developed by the wind turbine. Because turbines can be outfitted with systems that adjust pitch angle during operation, they are classified as either fixed or variable pitch. Consequently, wind turbines are categorized based on four primary modes-of-operation: fixed-speed, fixed pitch; fixed-speed, variable pitch; variable-speed, fixed pitch; variable-speed, variable pitch. The majority of modern, utility-scale turbines fall into the variable speed, variable pitch category [5.27]. Thus, the following discussion focuses on WECS operation that utilizes this predominant wind turbine class.

Wind turbines capitalize on the power available within a wind stream (P_a), defined as:

$$P_a = \frac{1}{2}\rho A v^3 \tag{5.22}$$

where: ρ is the air density in kg/m^3, A is the area swept by the rotor blades in m^2, v is the wind velocity in m/s [5.27, 5.31, 5.32, 5.33]. The proportion of power that is extracted from the wind stream by a WECS is determined by the power coefficient, C_p. The power coefficient is a function of tip speed ratio (TSR or λ) and pitch angle. Tip speed ratio is defined as:

$$\lambda = \frac{\omega_r R}{v} \tag{5.23}$$

where: ω_r is the rotor speed in rad/s, R is the radius of the area swept by the rotor blades in meters [5.27, 5.31, 5.32]. This definition, along with varying pitch angles, gives rise to the power coefficient curves for a wind turbine, shown in Figure 5.18. Further, combining C_p and (5.22) yields the definition of the power extracted by a wind turbine (P_g) [5.27, 5.30]:

$$P_g = \frac{1}{2}\rho A v^3 C_p(\lambda, \theta) \tag{5.24}$$

It is noted that for variable speed, variable pitch wind turbines, TSR and pitch angle have a direct effect on operation and the amount of power extracted from the wind. While the absolute maximum power coefficient for any theoretical turbine (the Betz limit) is 0.593, modern large-scale turbines typically have a C_p in the vicinity of 0.4 to 0.45 [5.27, 5.30]. However, adjustments in any one of three key contributing operational factors (wind speed, pitch angle, rotor speed) will change the amount of power extracted from the wind.

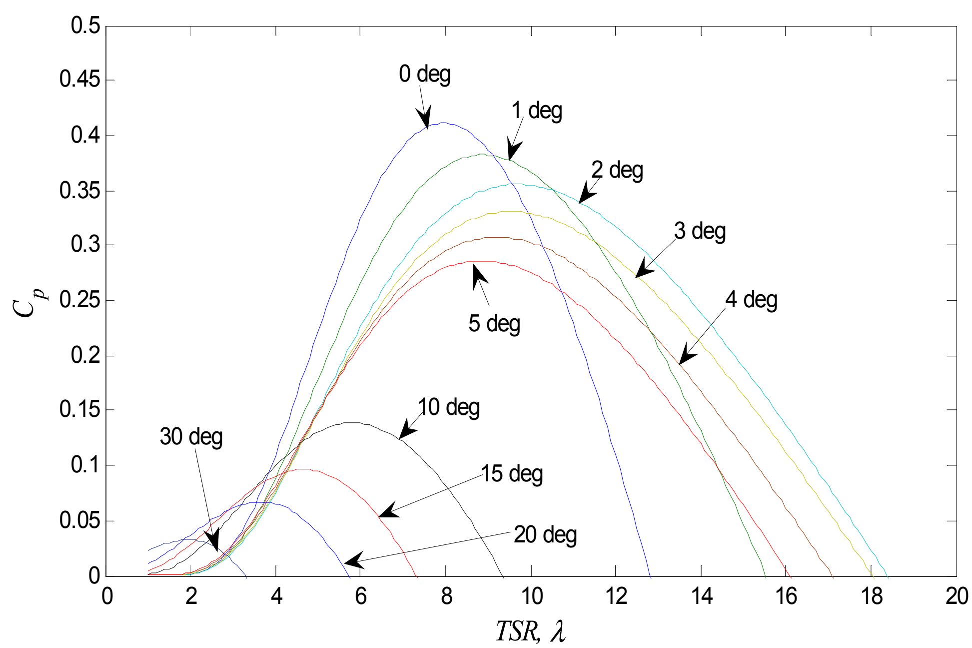

Figure 5.18. Cp versus λ characteristics at different pitch angles (θ).

For variable pitch turbines, a pitch angle controller is used to modify wind flow around the wind turbine blade, thereby controlling torque exerted on the turbine shaft. Below a particular rated wind speed, pitch angle is kept at a constant optimum value (typically 0˚). If wind speed exceeds the rated speed, the controller modifies the turbine blade pitch angle by actuating a mechanical system in the rotor hub. Subsequently, this reduces C_p so that less power is extracted from the wind than is available. Typical pitch control schemes involve modifying pitch angle based on keeping the turbine output power at a constant value, based on machine ratings, as wind speeds rise above a rated value. The C_p versus wind velocity characteristic, shown in Figure 5.19, gives rise to the typical power versus wind velocity operating characteristic for an idealized variable speed, variable pitch wind turbines, seen in Figure 5.20.

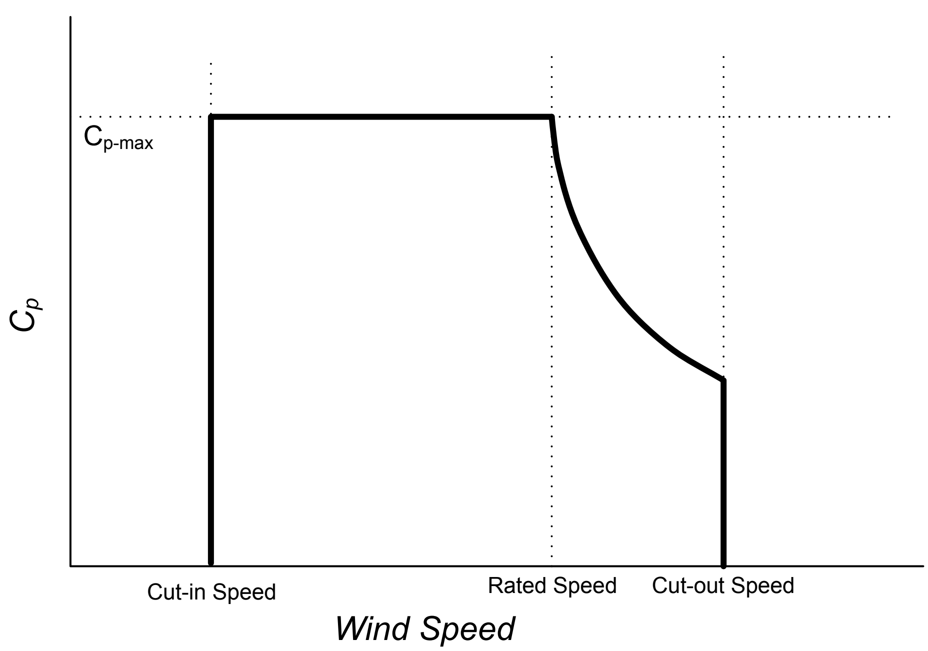

Figure 5.19. C_p versus v characteristic for variable speed, variable pitch turbine.

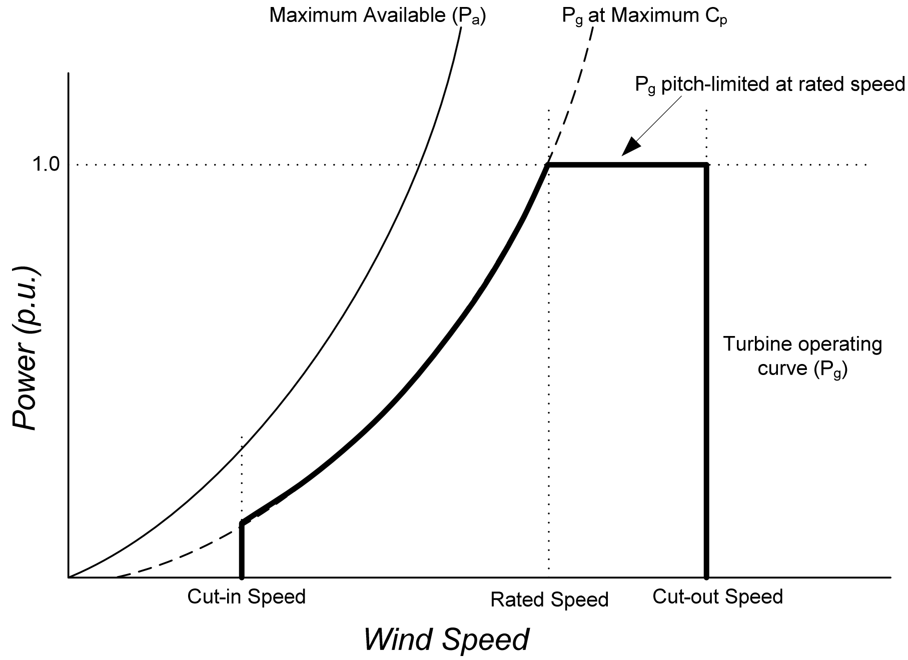

Figure 5.20. Power versus *v* characteristic for variable speed, variable pitch turbine.

As demonstrated in Figure 5.20, the typical variable speed, variable pitch turbine does not engage in power extraction until winds achieve cut-in speed. Additionally, these turbines employ pitch control to limit power at rated wind speed and totally eliminate power extraction at speeds too high to safely operate (cut-out). It is noted that for the typical turbine equipped with pitch control systems, the angle of the turbine blade pitch is not adjusted except above rated speed. Most of the time wind speeds are expected to be below rated speed and, therefore, pitch angle remains at its ideal value for the majority of turbine operations [5.32].

5.5.2 Wind Turbine Model

The dynamic model of the variable speed, variable pitch wind turbine was developed according to the block diagram, shown in Figure 5.21. Given physical and environmental conditions, the wind turbine model imparts a torque onto the common shaft linking it to the PMSG, described by:

$$\tau = \frac{P}{\omega} \tag{5.25}$$

where: τ is torque; P is shaft power; and ω is rotational velocity. The only controller included within the wind turbine model, the pitch angle controller, does not activate until wind speeds above rated speed. At that point, the pitch angle controller compares rated output power (nominal power at rated wind speed) to the actual power output of the turbine, P_g. If the output power of the turbine exceeds the rated power, pitch angle is increased to maintain P_g at rated power. Although key during grid-connected operations, the pitch angle controller is a redundant safety mechanism during load-following operations because WECS power output to the load is limited by the converter and inverter controllers.

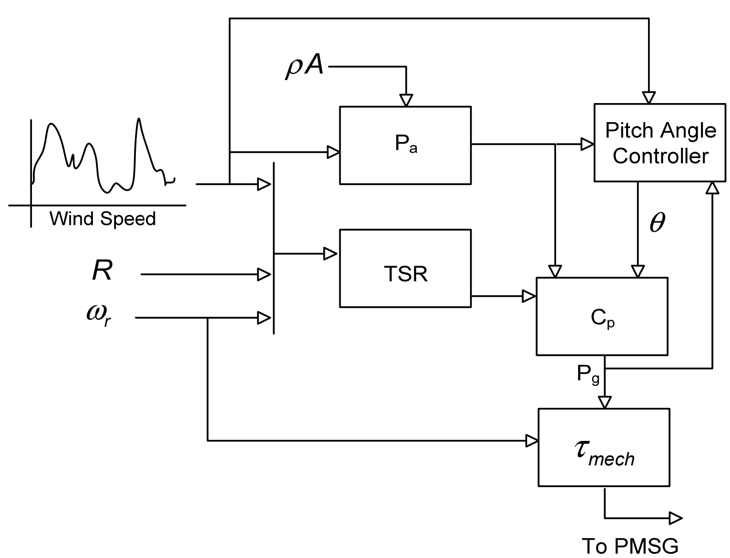

Figure 5.21. Block diagram of wind turbine model.

5.5.3 PMSG Model Development

The PMSG is very similar to the synchronous generator, with the primary difference that the rotor magnetic field is a fixed quantity due to permanent magnets physically attached to it. It is noted that multiple permanent magnetic poles can be incorporated onto the rotor, each which rotate about the rotor axis at the rotor's rotational speed (ω_r). Figure 5.22 shows an idealized rendering of a synchronous machine. The stator (stationary element) contains three sets of armature windings that carry current to an attached source or load. The rotor (rotating element) contains a single set field windings that establish a magnetic field that rotates at an identical speed to the rotor. It is noted that multiple field windings can be introduced onto the rotor. Each additional set of field windings creates an additional two magnetic poles (positive and negative) which also rotate about the rotor axis at the rotor's rotational speed.

Rotor fields and currents flowing in the armature windings yield independent sinusoidal magnetomotive forces (mmf) and magnetic lines of flux within the air gap separating the rotor and stator. The mmf and fluxes interact causing mechanical and electrical conditions to change. Under steady state conditions, the rotor magnetic field is in synchronism with the current flowing through the armature windings. In other words, the interaction between the rotating magnetic field (rotor) and the magnetic field generated by the current-carrying windings (stator) are synchronized, so that they rotate about the rotor axis at the same speed. This magnetic flux linkage between the rotor and stator is key to describe machine operational dynamics.

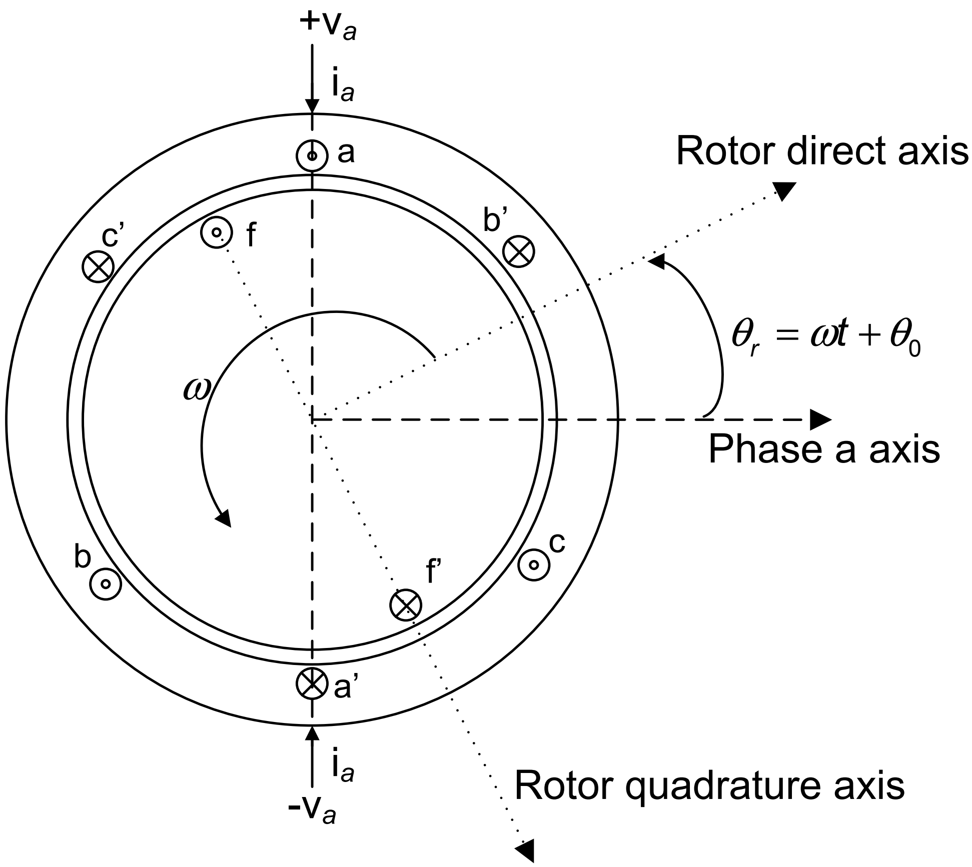

Figure 5.22. Idealized synchronous machine.

Figure note: dots represent windings projected out of the plane of the page, crosses represent windings projected into the plane of the page. The axis that projects into and out of the page, perpendicular to the direct and quadrature axes, is the 'zero-axis' of the *dq0*-reference frame.

Using the well known *abc*-reference frame, flux linkages between the rotor and stator windings are expressed by [5.36]:

$$\begin{bmatrix} \lambda_a \\ \lambda_b \\ \lambda_c \\ \lambda_f \end{bmatrix} = \begin{bmatrix} \mathcal{L}_{aa} & \mathcal{L}_{ab} & \mathcal{L}_{ac} & \mathcal{L}_{af} \\ \mathcal{L}_{ba} & \mathcal{L}_{bb} & \mathcal{L}_{bc} & \mathcal{L}_{bf} \\ \mathcal{L}_{ca} & \mathcal{L}_{cb} & \mathcal{L}_{cc} & \mathcal{L}_{cf} \\ \mathcal{L}_{fa} & \mathcal{L}_{fb} & \mathcal{L}_{fc} & \mathcal{L}_{ff} \end{bmatrix} \begin{bmatrix} i_a \\ i_b \\ i_c \\ i_f \end{bmatrix} \tag{5.26}$$

where: λ represents flux linkage, $\mathcal{L}$ represents the self- or mutual-inductances as they vary with respect to rotor angle (θ_r), and i represents current flowing through respective windings. Self-inductance is indicated by two like subscripts, mutual inductance by dissimilar subscripts. It is noted that at synchronism, the relationship between θ_r and rotor electrical angle (θ_{re}), and likewise, rotor electrical speed (ω_{re}) and ω_r, accords to the number of field poles:

$$\theta_{re} = \left(\frac{poles}{2}\right)\theta_r, \qquad \omega_{re} = \left(\frac{poles}{2}\right)\omega_r \tag{5.27}$$

By virtue of carrying current, each winding within the synchronous machine gives rise to a magnetic field and flux. Each winding, therefore, interacts magnetically with itself and each other winding within the machine. Thus, the flux linkage equations, shown in (5.26), describe the self- and mutual-interactions occurring within the synchronous machine. More specifically however, the inductance quantities ($\mathcal{L}$) contain the information regarding the actual inductive properties that arise from the windings interacting magnetically. For the stator windings (a, b, c), they interact with themselves (inductance quantities represented by $\mathcal{L}_{aa}$, $\mathcal{L}_{bb}$, and $\mathcal{L}_{cc}$), each other ($\mathcal{L}_{ab}$, $\mathcal{L}_{ac}$, $\mathcal{L}_{ba}$, $\mathcal{L}_{bc}$, $\mathcal{L}_{cb}$, and $\mathcal{L}_{ca}$), and the field windings ($\mathcal{L}_{af}$, $\mathcal{L}_{bf}$, and $\mathcal{L}_{cf}$). For the rotor winding (f), it interacts with itself ($\mathcal{L}_{ff}$), and the stator windings ($\mathcal{L}_{fa}$, $\mathcal{L}_{fb}$, and $\mathcal{L}_{fc}$) . In the case of the stator windings, each self-inductance ($\mathcal{L}_{aa}$, $\mathcal{L}_{bb}$, $\mathcal{L}_{cc}$) actually arises from two components: the self-inductance due to the air-gap flux and the leakage flux that fails to self-couple. Because the stator windings are assumed to be symmetric and electrically equivalent, $\mathcal{L}_{aa} = \mathcal{L}_{bb} = \mathcal{L}_{cc}$. For the armature mutual inductances ($\mathcal{L}_{ab}$, $\mathcal{L}_{ac}$, $\mathcal{L}_{ba}$, $\mathcal{L}_{bc}$, $\mathcal{L}_{cb}$, and $\mathcal{L}_{ca}$) however, the situation is slightly different. Assuming that the phase windings are symmetrically distributed 120° apart about the stator casing, the mutual coupling between any two windings are equivalent and only a fraction of the air-gap flux ($\mathcal{L}_{ab} = \mathcal{L}_{ac} = \mathcal{L}_{ba} = \mathcal{L}_{bc} = \mathcal{L}_{cb} = \mathcal{L}_{ca}$). Additionally, the leakage flux component of mutual stator inductance is typically small and therefore neglected. It should be noted that within the stator, stator self- and mutual-inductances are independent of rotor electrical angle (θ_{re}). This is not the case, however, between the stator-and-rotor mutual inductances, as the mmf and air-gap flux varies with respect to the rotor-to-stator position expressed by rotor electrical angle (θ_{re}). Assuming that the rotor and air-gap are cylindrical and symmetric, the stator-and-rotor mutual inductances for each like winding are equal ($\mathcal{L}_{af} = \mathcal{L}_{fa}$, $\mathcal{L}_{bf} = \mathcal{L}_{fb}$, $\mathcal{L}_{cf} = \mathcal{L}_{fc}$). Finally, the rotor self-inductance ($\mathcal{L}_{ff}$) is independent of electrical angle (θ_{re}), but is comprised of both self-inductance due to the air-gap flux and leakage flux components. In summary, the following table is presented [5.36]:

Table 5.3. Table of PMSG inductances.

	Fixed for a given machine	Vary with θ_{re}	Incorporates leakage flux
Self-inductances			
$\mathcal{L}_{aa} = \mathcal{L}_{bb} = \mathcal{L}_{cc}$	X		X
$\mathcal{L}_{ff}$	X		X
Mutual-inductances			
$\mathcal{L}_{ab} = \mathcal{L}_{ac} = \mathcal{L}_{ba} = \mathcal{L}_{bc} = \mathcal{L}_{cb} = \mathcal{L}_{ca}$	X		(Neglected)
$\mathcal{L}_{af} = \mathcal{L}_{fa}$		X	
$\mathcal{L}_{bf} = \mathcal{L}_{fb}$		X	
$\mathcal{L}_{cf} = \mathcal{L}_{fc}$		X	

Using this information, the $\mathcal{L}$ quantities which were initially shown as varying with rotor electrical angle can be more explicitly represented by fixed and varying components (saliency terms are omitted):

$$
\begin{aligned}
&\mathcal{L}_{\mathrm{aa}} = \mathcal{L}_{\mathrm{bb}} = \mathcal{L}_{\mathrm{cc}} = L_{ss} + L_{sl} \\
&\mathcal{L}_{\mathrm{ab}} = \mathcal{L}_{\mathrm{ac}} = \mathcal{L}_{\mathrm{ba}} = \mathcal{L}_{\mathrm{bc}} = \mathcal{L}_{\mathrm{cb}} = \mathcal{L}_{\mathrm{ca}} = L_{ss}\cos(\pm 120^\circ) = -\frac{1}{2}L_{ss} \\
&\mathcal{L}_{\mathrm{af}} = \mathcal{L}_{\mathrm{fa}} = L_f\cos(\theta_{re}) \\
&\mathcal{L}_{\mathrm{bf}} = \mathcal{L}_{\mathrm{fb}} = L_f\cos(\theta_{re} - 120^\circ) \\
&\mathcal{L}_{\mathrm{cf}} = \mathcal{L}_{\mathrm{fc}} = L_f\cos(\theta_{re} + 120^\circ) \\
&\mathcal{L}_{\mathrm{ff}} = L_{ff}
\end{aligned}
\tag{5.28}
$$

where: L_{ss} represents the armature self-inductance due to the air gap flux, L_{sl} is the armature leakage inductance due to leakage flux, L_f is the mutual-inductance due to the air gap flux, and L_{ff} is the sum of the field self-inductance and leakage inductance. These equations expressed in the flux linkage matrix form yields:

$$
\begin{bmatrix} \lambda_a \\ \lambda_b \\ \lambda_c \\ \lambda_f \end{bmatrix} =
\begin{bmatrix}
L_{ss}+L_{sl} & -\frac{1}{2}L_{ss} & -\frac{1}{2}L_{ss} & L_f\cos(\theta_{re}) \\
-\frac{1}{2}L_{ss} & L_{ss}+L_{sl} & -\frac{1}{2}L_{ss} & L_f\cos(\theta_{re}-120^\circ) \\
-\frac{1}{2}L_{ss} & -\frac{1}{2}L_{ss} & L_{ss}+L_{sl} & L_f\cos(\theta_{re}+120^\circ) \\
L_f\cos(\theta_{re}) & L_f\cos(\theta_{re}-120^\circ) & L_f\cos(\theta_{re}+120^\circ) & L_{ff}
\end{bmatrix}
\begin{bmatrix} i_a \\ i_b \\ i_c \\ i_f \end{bmatrix}
\tag{5.29}
$$

It should be noted that three major assumptions are made in this analysis. First, the rotor poles are assumed to be non-salient. In the case of a salient pole machine, the magnetic pole created by the field winding protrudes from the rotor shaft giving rise to a non-sinusoidal mmf distribution in the air-gap. This distorted magnetic field, although symmetric in properly constructed machines, causes a distortion in the flux linkage between the armature and rotor. Although the effects of saliency can be accounted by adding rotor electrical angle dependant quantities to the self- and mutual- inductance quantities of the armature windings, for the purpose of this analysis, the machine poles are assumed to be non-salient. Additionally, the magnetic conductance, referred to as permeance within the air gap is constant and space-related air-gap flux harmonics are neglected. These assumptions are made because modern machines have numerous symmetrically overlaid field and armature components that result in fairly uniform flux densities and harmonic components are mostly cancelled out [5.37].

Knowing that the rotor electrical angle is a key quantity to determining the rotor-to-stator mutual inductances, it is helpful to realize that the analysis of the synchronous machine can be simplified by shifting reference frames. The direct-quadrature-zero (*dq0*) transformation, also known as Park's transformation, permits conversion from fixed-axis *abc* quantities into rotating-axis quantities. For stator quantities, the transformation matrix and inverse transformation matrix are:

$$\begin{bmatrix} S_d \\ S_q \\ S_0 \end{bmatrix} = \frac{2}{3} \begin{bmatrix} \cos(\theta_{re}) & \cos(\theta_{re} - 120°) & \cos(\theta_{re} + 120°) \\ -\sin(\theta_{re}) & -\sin(\theta_{re} - 120°) & -\sin(\theta_{re} + 120°) \\ 1/2 & 1/2 & 1/2 \end{bmatrix} \begin{bmatrix} S_a \\ S_b \\ S_c \end{bmatrix} \quad (5.30)$$

$$\begin{bmatrix} S_a \\ S_b \\ S_c \end{bmatrix} = \begin{bmatrix} \cos(\theta_{re}) & \text{-}\sin(\theta_{re}) & 1 \\ \cos(\theta_{re} - 120°) & \text{-}\sin(\theta_{re} - 120°) & 1 \\ \cos(\theta_{re} + 120°) & \text{-}\sin(\theta_{re} + 120°) & 1 \end{bmatrix} \begin{bmatrix} S_d \\ S_q \\ S_0 \end{bmatrix} \tag{5.31}$$

Using these transformations we can adjust the flux linkage equations above into the rotating reference frame:

$$\begin{bmatrix} \lambda_d \\ \lambda_q \\ \lambda_0 \end{bmatrix} = \frac{2}{3} \begin{bmatrix} \cos(\theta_{re}) & \cos(\theta_{re} - 120°) & \cos(\theta_{re} + 120°) \\ -\sin(\theta_{re}) & -\sin(\theta_{re} - 120°) & -\sin(\theta_{re} + 120°) \\ \frac{1}{2} & \frac{1}{2} & \frac{1}{2} \end{bmatrix} \begin{bmatrix} \lambda_a \\ \lambda_b \\ \lambda_c \end{bmatrix} \tag{5.32}$$

$$\begin{bmatrix} i_d \\ i_q \\ i_0 \end{bmatrix} = \frac{2}{3} \begin{bmatrix} \cos(\theta_{re}) & \cos(\theta_{re} - 120°) & \cos(\theta_{re} + 120°) \\ -\sin(\theta_{re}) & -\sin(\theta_{re} - 120°) & -\sin(\theta_{re} + 120°) \\ \frac{1}{2} & \frac{1}{2} & \frac{1}{2} \end{bmatrix} \begin{bmatrix} i_a \\ i_b \\ i_c \end{bmatrix} \tag{5.33}$$

Because the rotor electrical angle is key to determining the rotor-to-stator mutual inductances, the well known direct-quadrature-zero (*dq0*) transformation permits conversion from fixed-axis *abc* quantities into rotating-axis quantities. After substituting (5.32) and (5.33) into (5.29), block matrix inversion is utilized according to:

$$\begin{bmatrix} A & B \\ C & D \end{bmatrix}^{-1} = \begin{bmatrix} A^{-1} + A^{-1}B(D - CA^{-1}B)^{-1}CA^{-1} & -A^{-1}B(D - CA^{-1}B)^{-1} \\ -(D - CA^{-1}B)^{-1}CA^{-1} & (D - CA^{-1}B)^{-1} \end{bmatrix} \tag{5.34}$$

where: A and D are square matrices; A and $D\text{-}CA^{-1}B$ are non-singular; the inversion can be performed blockwise following the matrix inversion lemma. This significant algebraic manipulation, yields flux linkage and current quantities in the *dq0*-frame of:

$$\begin{bmatrix} \lambda_d \\ \lambda_q \\ \lambda_0 \\ \lambda_f \end{bmatrix} = \begin{bmatrix} L_d i_d + L_f i_f \\ L_q i_q \\ L_{sl} i_0 \\ \frac{3}{2} L_f i_d + L_{ff} i_f \end{bmatrix} \tag{5.35}$$

$$L_d = L_q = \frac{3}{2} L_{ss} + L_{sl} \tag{5.36}$$

where: L_d and L_q are the direct-axis and quadrature-axis synchronous inductances. Clearly, the rotating quadrature reference frame transformation is beneficial, as it eliminates dependence on knowledge of rotor electrical angle.

In order to determine the equivalent circuit in the *dq0*-reference frame, we start in the *abc*-reference frame. Each of the three armature phases are equivalent, so we focus on just one for analysis. Recalling the flux linkage equation for phase a, from above:

$$\lambda_a = (L_{ss} + L_{sl}) i_a - \frac{1}{2} L_{ss} (i_b + i_c) + L_f \cos(\theta_{re}) i_f \tag{5.37}$$

Under balanced current flows, $i_a + i_b + i_c = 0$. Therefore, $i_b + i_c = -i_a$ and the equation for λ_a reduces to:

$$\lambda_a = (\frac{3}{2}L_{ss} + L_{sl})i_a + L_f \cos(\theta_{re})i_f \tag{5.38}$$

The voltage induced into the armature winding by the mmf of the field winding, referred to as the internal voltage (e_a), is equal to time-derivative of the flux linkage (λ_a). Recognizing that the rotor electrical angle is a function of time and that field current is DC ($di_f/dt = 0$), we can substitute and show:

$$\frac{d\lambda_a}{dt} = (\frac{3}{2}L_{ss} + L_{sl})\frac{di_a}{dt} + L_f \frac{d}{dt}\cos(\omega_{re}t + \theta_0)i_f = (\frac{3}{2}L_{ss} + L_{sl})\frac{di_a}{dt} + -e_a \tag{5.39}$$

This induced voltage source is connected to the terminals of the armature through the armature resistance (R_{as}). The air-gap voltage (v_{gs}) results between the self-inductance and leakage inductance of the armature winding. The current that flows through the armature winding is, of course, i_a. Based on this information, we can represent the phase equivalent circuit for the abc-reference frame in Figure 5.23.

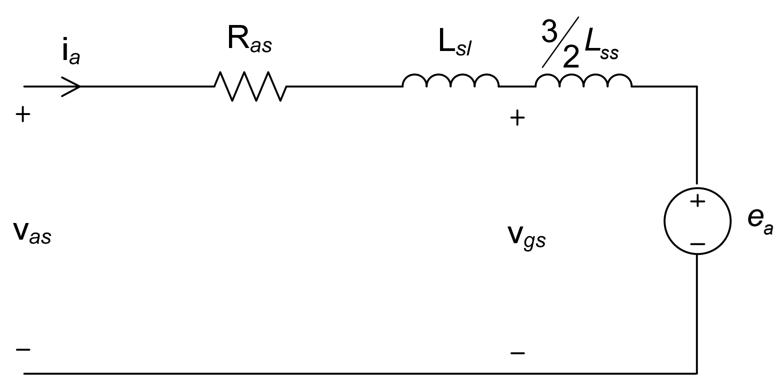

Figure 5.23. Synchronous machine phase equivalent circuit.

The direction of i_a depends on the relationship between the armature terminal voltage (v_{as}) and the internal voltage (e_a). Figure 5.23 shows current flowing into the armature circuit which represents the synchronous machine operating as a motor. When i_a flows out of the armature, the synchronous machine is operating as a generator.

Based on the equations developed and the equivalent circuit, we can represent the armature terminal voltage as:

$$v_{as} = R_a i_a + \frac{d\lambda_a}{dt} = R_a i_a + (\frac{3}{2}L_{ss} + L_{sl})\frac{di_a}{dt} + -e_a \qquad (5.40)$$

In order to convert the abc reference frame phase equivalent circuit to the *dq0*-reference, the time derivatives of the flux linkage equations are useful:

$$\begin{bmatrix} \frac{d\lambda_d}{dt} \\ \frac{d\lambda_q}{dt} \\ \frac{d\lambda_0}{dt} \\ \frac{d\lambda_f}{dt} \end{bmatrix} = \begin{bmatrix} L_d & 0 & 0 & L_f \\ 0 & L_q & 0 & 0 \\ 0 & 0 & L_{sl} & 0 \\ \frac{3}{2}L_f & 0 & 0 & L_{ff} \end{bmatrix} \begin{bmatrix} \frac{di_d}{dt} \\ \frac{di_q}{dt} \\ \frac{di_0}{dt} \\ \frac{di_f}{dt} \end{bmatrix} = \begin{bmatrix} L_d \frac{di_d}{dt} + L_f \frac{di_f}{dt} \\ L_q \frac{di_q}{dt} \\ L_{sl} \frac{di_0}{dt} \\ \frac{3}{2}L_f \frac{di_d}{dt} + L_{ff} \frac{di_f}{dt} \end{bmatrix} \qquad (5.41)$$

Using Park's transform, differentiating with respect to time, back-substituting, front-multiplying the matrix inverse, results in:

$$\begin{bmatrix} v_d \\ v_q \\ v_0 \\ v_f \end{bmatrix} = \frac{2}{3}\begin{bmatrix} \frac{3}{2}R_a & 0 & 0 & 0 \\ 0 & \frac{3}{2}R_a & 0 & 0 \\ 0 & 0 & \frac{3}{2}R_a & 0 \\ 0 & 0 & 0 & 3/2R_f \end{bmatrix}\begin{bmatrix} i_d \\ i_q \\ i_0 \\ i_f \end{bmatrix} + \frac{2}{3}\begin{bmatrix} 0 & -\frac{3}{2}\omega_{re} & 0 & 0 \\ \frac{3}{2}\omega_{re} & 0 & 0 & 0 \\ 0 & 0 & 0 & 0 \\ 0 & 0 & 0 & 0 \end{bmatrix}\begin{bmatrix} \lambda_d \\ \lambda_q \\ \lambda_0 \\ \lambda_f \end{bmatrix} + \frac{2}{3}\begin{bmatrix} \frac{3}{2} & 0 & 0 & 0 \\ 0 & \frac{3}{2} & 0 & 0 \\ 0 & 0 & \frac{3}{2} & 0 \\ 0 & 0 & 0 & \frac{3}{2} \end{bmatrix}\begin{bmatrix} \frac{d\lambda_d}{dt} \\ \frac{d\lambda_q}{dt} \\ \frac{d\lambda_0}{dt} \\ \frac{d\lambda_f}{dt} \end{bmatrix} \quad (5.42)$$

Or simplified:

$$\begin{bmatrix} v_d \\ v_q \\ v_0 \\ v_f \end{bmatrix} = \begin{bmatrix} R_a i_d \\ R_a i_q \\ R_a i_0 \\ R_f i_f \end{bmatrix} + \begin{bmatrix} -\omega_{re}\lambda_q \\ \omega_{re}\lambda_d \\ 0 \\ 0 \end{bmatrix} + \begin{bmatrix} \frac{d\lambda_d}{dt} \\ \frac{d\lambda_q}{dt} \\ \frac{d\lambda_0}{dt} \\ \frac{d\lambda_f}{dt} \end{bmatrix} \quad (5.43)$$

This leads to an expression for terminal voltages (v_d, v_q, v_0) developed at each armature winding and the field winding (v_f) are equal to:

$$\begin{bmatrix} v_d \\ v_q \\ v_0 \\ v_f \end{bmatrix} = \begin{bmatrix} -R_a i_d \\ -R_a i_q \\ -R_a i_0 \\ -R_f i_f \end{bmatrix} + \begin{bmatrix} -\omega_{re} L_q i_q \\ \omega_{re}(L_d i_d + L_f i_f) \\ 0 \\ 0 \end{bmatrix} - \begin{bmatrix} L_d & 0 & 0 & L_f \\ 0 & L_q & 0 & 0 \\ 0 & 0 & L_{sl} & 0 \\ \frac{3}{2}L_f & 0 & 0 & L_{ff} \end{bmatrix}\begin{bmatrix} \frac{di_d}{dt} \\ \frac{di_q}{dt} \\ \frac{di_0}{dt} \\ \frac{di_f}{dt} \end{bmatrix} \quad (5.44)$$

where: R_a is the balanced armature resistance in each stator leg. This gives rise to the key *d*- and *q*-equivalent circuits that represent the PMSG, shown in Figs. 5 & 6. Although these equations and diagrams have been developed for the synchronous machine, in the PMSG model the flux linkage produced by the permanent magnets ($L_f i_f$) is constant, which is to say that i_f is constant and $di_f/dt = 0$.

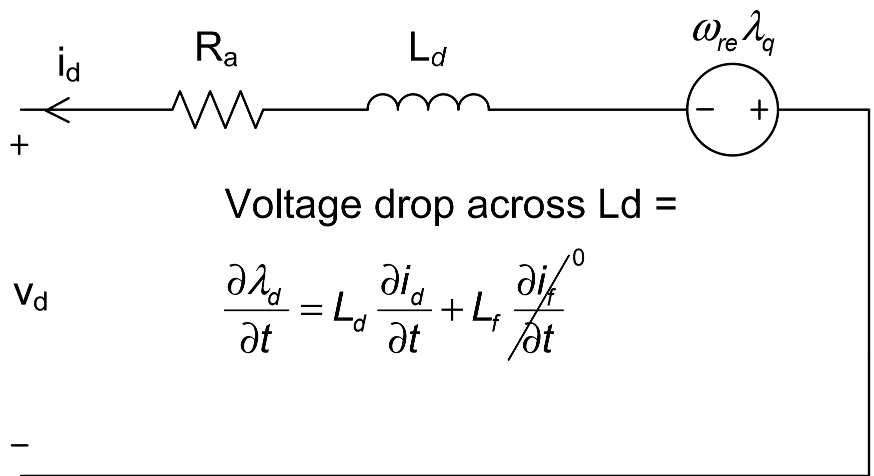

Figure 5.24. *d*-equivalent circuit for PMSG.

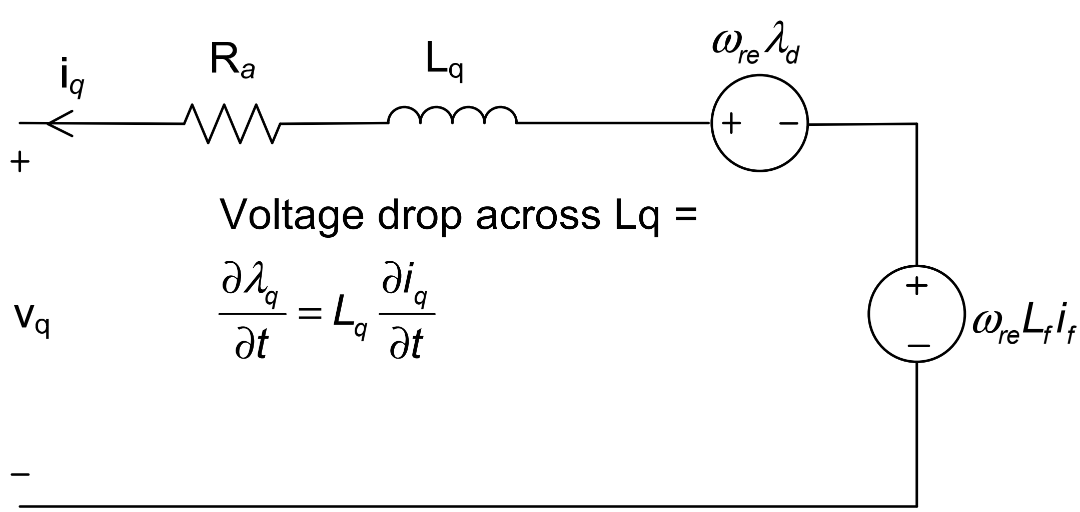

Figure 5.25. *q*-equivalent circuit for PMSG.

The circuit models may be readily implemented as incremental models. In summary, the following enumerates the voltage drops in each equivalent circuit:

<u>*d*-axis:</u>

-$R_a i_d$ (drop across armature resistor)

-L_d (di_d / dt) (drop across d-axis inductance)

-$\omega_{re} L_q i_q$ (*d*-axis voltage induced by speed-related *q*-axis flux)

<u>*q*-axis:</u>

-$R_a i_q$ (drop across armature resistor)

-L_q(di_q / dt) (drop across q-axis inductance)

+$\omega_{re} L_d i_d$ (*q*-axis voltage induced by speed-related *d*-axis flux)

+$\omega_{re} L_f i_f$ (*q*-axis voltage induced by rotor field flux)

Assuming balanced currents in each stator leg, PMSG instantaneous power (p_s) can be found by:

$$p_s = \underbrace{\frac{3}{2} R_a i_d^{\,2} + \frac{3}{2} R_a i_q^{\,2} + 3 R_a i_0^{\,2}}_{Ohmic} +$$

$$\underbrace{\frac{3}{2}(L_d \frac{di_d}{dt} + \cancel{L_f \frac{di_f}{dt}}) i_d + \frac{3}{2} L_q \frac{di_q}{dt} i_q + 3 L_{sl} \frac{di_0}{dt} i_0}_{Magnetic} + \tag{5.45}$$

$$\underbrace{\frac{3}{2} \omega_{re} \lambda_d i_q - \frac{3}{2} \omega_{re} \lambda_q i_d}_{Rotational-Mechanical}$$

Recognizing that the rotational-mechanical power yields the electromechanical torque (τ_{elec}) developed by the PMSG:

$$\tau_{elec} = \frac{p_s}{\omega_r} = \frac{3}{2}\left(\frac{poles}{2}\right)\left(\lambda_d i_q - \lambda_q i_d\right)$$
$$\tau_{elec} = \frac{3}{2}\left(\frac{poles}{2}\right)\left((L_d i_d + L_f i_f) i_q - L_q i_q i_d\right) \tag{5.46}$$

Utilizing the torque produced by the PMSG and the mechanical torque provided by the wind turbine, a mechanical model is used to determine common rotor speed:

$$\omega_r = \frac{1}{J}\int (\tau_{mech} - \tau_{elec} - \tau_{loss}) \, dt \tag{5.47}$$

where, J is the rotor inertia (kg-m^2), τ_{mech} is turbine torque (Figure 5.21), and τ_{loss} refers to frictional losses of the rotor (N-m).

It is logical to ask the question whether existing PMSM models, based on incremental calculations of electrical parameters, would be appropriate for the purpose of simulating the PMSG for the purpose of microgrid analysis. For example, the MATLAB SimPower Systems toolbox contains a Permanent Magnet Synchronous Machine model. Its input is either rotor speed or torque, and it requires connection to a three-phase power system for operation. The model is based on similar characteristic equations as described above, but its operation is mainly geared towards permanent magnet motor operation. It was determined that this model was inadequate for integration into the microgrid modeling for two reasons. First, existing in only SIMULINK, it was not employable in a stand-alone simulation without the use of the MATLAB commercial software. Second, the premise of the model relies on known electrical quantities that may be manipulated in the course of microgrid simulation. In other words, there are two primary ways to look at model development. One method is to see the PMSM as a generator where stator currents arise because of a voltage difference between the internal voltage of the machine and the voltage at the stator terminals. Current flows from the machine to the attached power system or load, as the case may be. Power flow is into the rotor by a prime mover, through the rotor to the generator, through the generator to the load by way of the stator. In the opposite case, when the PMSM is operating as a motor, voltage is not independently present, internal to the machine, because of a lack of power flow into the rotor. In other words, without a prime mover to turn the permanent magnets on the rotor, the machine will not develop an internal voltage. Instead, voltage at the stator induces a torque in the rotor and the counter electromotive force stimulates an internal voltage in the machine. This voltage difference causes stator currents to flow from the attached power system, into the stator of the machine. Power flows from the power system, to the stator, to the rotor, and to the mechanical load on the rotor. The key point in modeling is in which direction the model anticipates power flow. This is "which came first the chicken or the egg" scenario, but highlights an important difference between models.

When the motor is used as the basis for the model, the primary input (either rotor speed or torque) is used to determine the quantity of mechanical power demanded by the rotor. This quantity and the sampled voltage at the stator terminals are used to determine the internal currents of the machine and consequently the other quantities described in the machine equations above. Unfortunately, the stator voltages are determined by the stator terminals voltages. This is unsatisfactory for generator modeling, because in some cases (not the least of which is generator startup) the sampled voltage at the stator is zero.

For generator modeling, it is understood that the voltage difference between the machine and the power system connection determines the current and subsequent characteristics of the operating machine. If open-circuited, the PMSG still maintains a voltage at its stator terminals based on the rotor quantities. This may be a minor point, but it is critical for generator modeling. When electrically loaded, the PMSG's electrical characteristics change (both voltages and currents) to new steady state levels. Therefore, for this model development, stator *dq0* rotating reference frame current quantities are sampled in order to determine how much current has changed in the previous time step. Using the d*i*/d*t* quantities for the previous time step, the stator voltages from the previous time step, and the sampled stator current from the existing time step allows new voltage quantities for the PMSG to be determined. The equations below summarize this process, where *k* represents the current step for the incremental parameter calculation:

$$\begin{bmatrix} v_d(k+1) \\ v_q(k+1) \\ v_0(k+1) \\ v_f(k+1) \end{bmatrix} = \begin{bmatrix} R_a i_d(k) \\ R_a i_q(k) \\ R_a i_0(k) \\ R_f i_f(k) \end{bmatrix} + \begin{bmatrix} -\omega_{re} L_q i_q(k) \\ \omega_{re}\left(L_d i_d(k) + L_f i_f(k)\right) \\ 0 \\ 0 \end{bmatrix} + \begin{bmatrix} L_d & 0 & 0 & L_f \\ 0 & L_q & 0 & 0 \\ 0 & 0 & L_{sl} & 0 \\ \frac{3}{2}L_f & 0 & 0 & L_{ff} \end{bmatrix} \begin{bmatrix} \frac{di_d}{dt}(k) \\ \frac{di_q}{dt}(k) \\ \frac{di_0}{dt}(k) \\ \frac{di_f}{dt}(k) \end{bmatrix} \quad (5.48)$$

$$\begin{bmatrix} \frac{di_d}{dt}(k) \\ \frac{di_q}{dt}(k) \\ \frac{di_0}{dt}(k) \\ \frac{di_f}{dt}(k) \end{bmatrix} = \begin{bmatrix} i_d(k) - i_d(k-1) \\ i_q(k) - i_q(k-1) \\ i_0(k) - i_0(k-1) \\ i_f(k) - i_f(k-1) \end{bmatrix} \tag{5.49}$$

The advantage of this incremental sample-and-calculate model is that changing parameters at the stator terminals caused by fluctuations in connected power system conditions are immediately taken into consideration for the PMSG operating characteristics. By using both stator end information and rotor end information, a proper simulation of PMSG operation may be conducted.

5.5.4 PMSG Power Conversion and Control

The complete WECS dynamic model developed was based on the characteristics of a variable-speed, variable pitch wind turbine as the prime mover, a PMSG, an electrical interface to transfer power to an AC system, and the related control system. The electrical interface between the generator and the power system includes an AC/DC converter, DC link bus, DC/AC converter, and a transformer. Storage is not incorporated into the WECS, however a sufficient capacitance is provided on the DC link bus for proper operation. Subsequently, the WECS model can be used in stand-alone or interconnected applications. Figure 5.26 shows the configuration diagram of the WECS. Variable frequency AC voltage output of the PMSG is converted into DC and then inverted into utility-grade AC. The PMSG produces electrical power at varying voltage and frequency levels. Output currents, and subsequent conditions within the PMSG, rely on the three phase voltage levels at the output terminals of the PMSG. In typical applications, the AC/DC converter (closest to the generator) is a simple, uncontrolled full-bridge rectifier. This arrangement offers limited options with respect to controlling the AC voltage and frequency at the terminals of the PMSG. Alternatively, instead of an uncontrolled rectifier, a controlled switch network converter (using IGBT devices) can be used to connect the steady DC link bus to the PMSG AC bus, as proposed in [5.38]. In effect, this is the same concept as using a controlled voltage source inverter to manipulate the DC link bus voltage into a desired AC voltage applied to the stator terminals of the PMSG. By controlling the stator voltages in this way, the ultimate effect is to adjust the PMSG internal flux linkages and currents to desired results, while accounting for the torque input from the wind turbine.

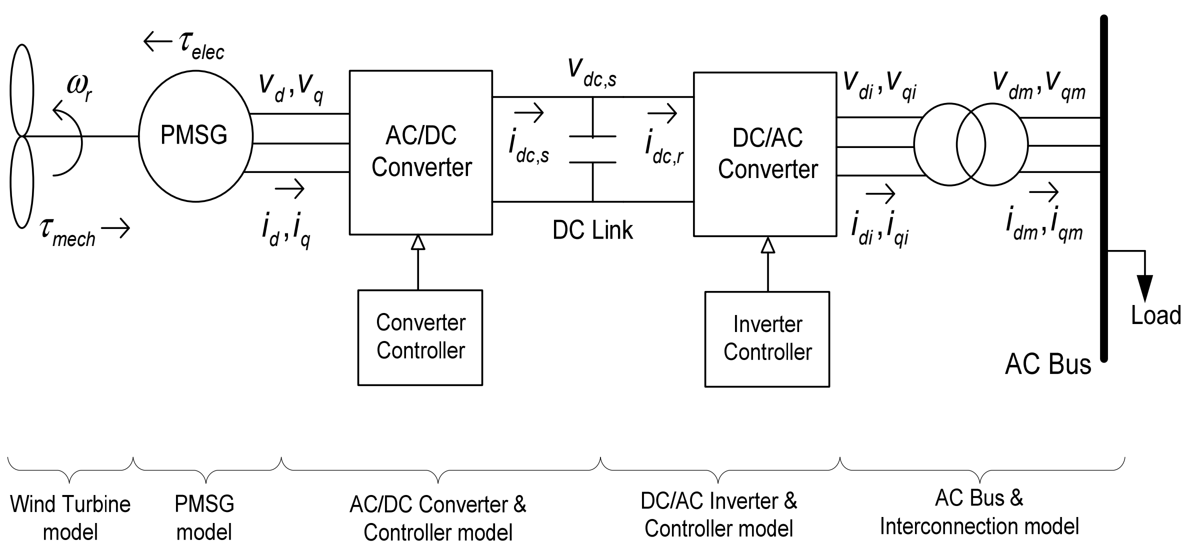

Figure 5.26. WECS model configuration.

As described above, in certain scenarios it is desirable to modulate the amount of power extracted from the wind. However, only three factors dictate *TSR* and C_p, and ultimately P_g: wind speed, pitch angle, and rotor speed. Of these, wind speed, of course, is not controllable. Frequent manipulations of pitch angle can cause undesirable mechanical vibrations and is reserved for limiting power above rated speed. Therefore, only rotor speed control remains as viable to control P_g. As shown in [5.39], rotor speed can be regulated by a nested loop controller for the PMSG-side converter. The rotor speed controller relies on a fast inner current loop to control stator *q*-axis current and a slower outer current loop for stator reactive power control. For the control scheme used here, shown in Figure 5.27, a maximum torque strategy was utilized that dictates $i_{d,ref}$ set to zero [5.39]. The output power of the PMSG-side converter (P_{conv}) is dictated by load demand (P_d+P_l). The value of $C_{p,ref}$ (smaller than $C_{p,max}$) that achieves P_{conv} from the available P_a, is determined by a ratio of the two values. This $C_{p,ref}$, coupled with pitch angle, gives a new TSR operating point. A new rotor speed ($\omega_{r,ref}$), dictated by the new TSR point, is used to determine a rotor speed error. This speed error serves as the primary control signal to determine $i_{q,ref}$, as shown at the top of Figure 5.27. The *dq*-axis current errors are passed to PI compensators that yield voltage references ($v_{d,ref}$, $v_{q,ref}$). These reference voltages determine the sinusoidal pulse width modulation (SPWM) that directs the output of the converter. By using this PMSG-side converter control scheme, electrical parameters within the generator are regulated so that power extracted from the wind is matched to the load demand (load-following).

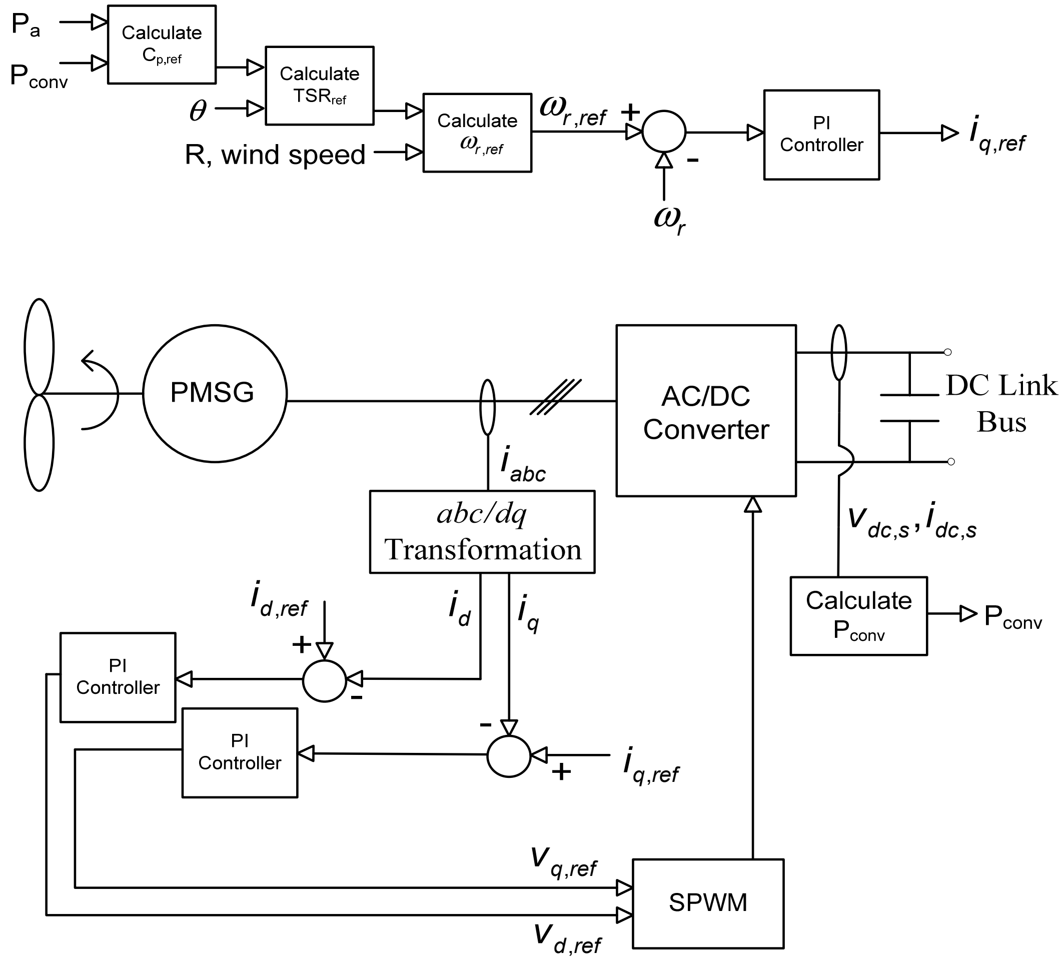

Figure 5.27. Generator-side AC/DC converter control.

Similar to conventional DC/AC voltage source inverters in power system applications, the WECS DC link bus voltage was inverted, filtered, and stepped-up to utility-grade AC. The transformer is assumed ideal, with step-up turn ratio (*N*) such that $v_{abc,o} = Nv_{abc,m}$ and $i_{abc,o} = N^{-1}i_{abc,m}$. The DC/AC inverter was controlled by modifying a scheme reported in [5.40]. Figure 5.28 shows the nested loop controller block diagram. To facilitate use of the inverter for either grid-connected or islanded applications, the interconnection status determined which voltage reference was used for control. When interconnected, the transformed utility (infinite bus) AC bus voltage ($v_{\mathrm{m,abc}}$) is the voltage reference; conversely, when islanded, and a predetermined voltage setpoint ($v_{\mathrm{abc,setpoint}}$) is used. The voltage reference signal, along with AC bus real and reactive power demands (P_{ref},Q_{ref}) determine the required generator "sending" voltage and angle (V_s,δ), according to:

$$|V_s| = \sqrt{\frac{Z^2}{V_r^2}\left(P^2 + Q^2\right) + V_r^2 + 2PZcos(\phi) + 2QZ\sin(\phi)} \qquad (5.50)$$

$$\delta = \phi - cos^{-1}\left(\frac{ZP}{V_r V_s} + \frac{V_r}{V_s}cos(\phi)\right) \qquad (5.51)$$

where: Z is the known interconnection impedance, ϕ is the power factor angle ($\tan^{-1}[Q_{ref}/P_{ref}]$), and V_r is the magnitude of the reference voltage (either $v_{m,abc}$ or $v_{\mathrm{abc,setpoint}}$). The P_{ref} and Q_{ref} signals can be determined either by inspection or dictated by setpoints. Because the V_s and δ signals equate to a three-phase voltage waveform (under balanced conditions) they are converted into a control voltage ($v_{dq,ref}$). This $v_{dq,ref}$ signal is compared to the measured v_{dq} to determine a voltage error signal. This error information feeds a voltage regulator (PI compensator) and yields a current reference signal ($i_{dq,ref}$). This current reference is compared with i_{dq} giving an error signal that is passed to the current controller (PI compensator). The nested loop configuration forms a control system with an inner current control loop and outer voltage control loop, each with an independent PI controller.

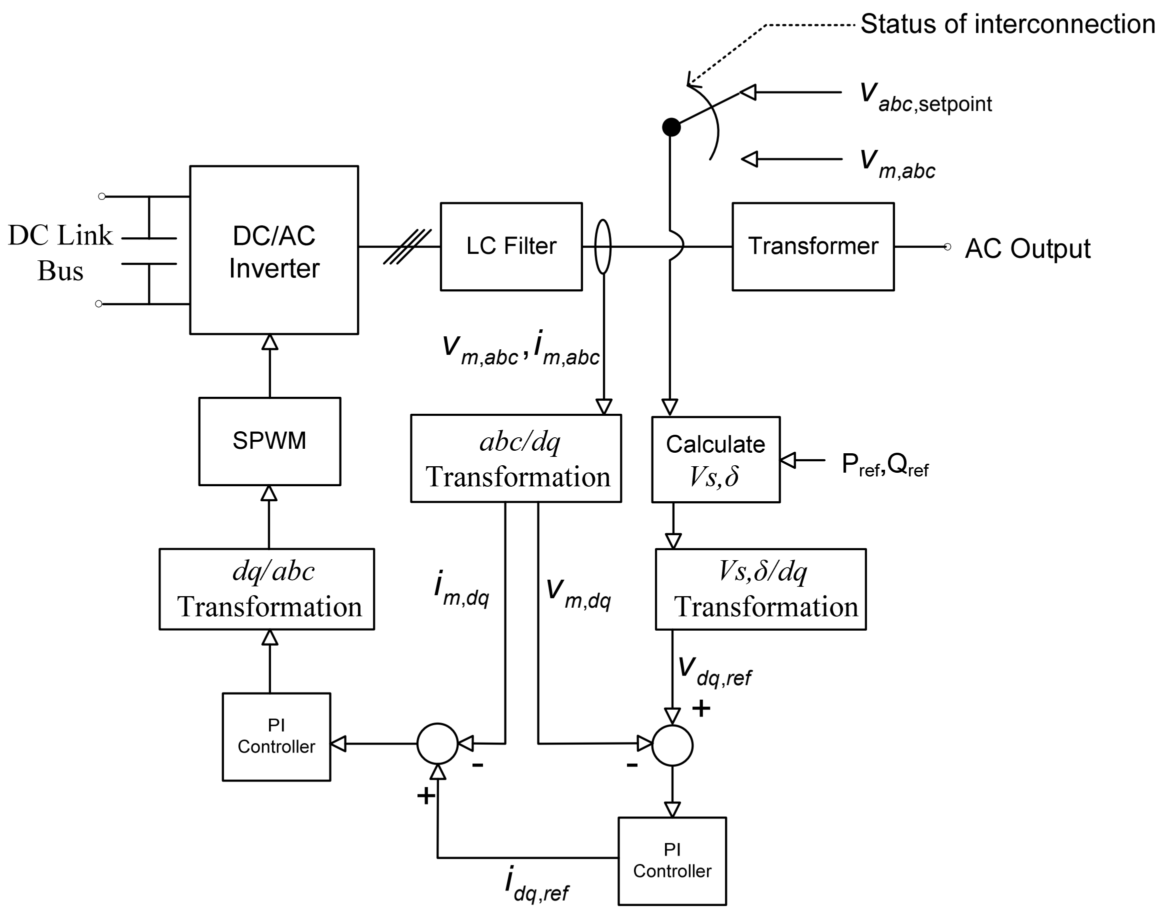

Figure 5.28. Power system-side DC/AC inverter control.

As with the PMSG-side converter, the power system-side inverter receives SPWM control as dictated by the control signals based on regulating *dq* output currents. The unique aspect of using a PMSG-side converter and power system-side inverter decoupled by the DC link bus means that the two AC systems only interact through real power transfer. The use of this inverter control scheme allows the WECS to properly interface with the power system, conveys load demand to the DC link bus, and helps manage AC voltage within limits.

5.5.5 Power Management

The WECS combines the wind turbine with an electrical generator to transfer the rotational mechanical energy developed from the wind to a power system. As an electrical power generation component, WECS can be used in both interconnected power grids and islanded, or isolated, power system applications. In the former, wind turbines are typically operated so that the maximum amount of energy available from the wind is transferred to the grid. In other words, the power accepted by the grid (P_d) is equal to the maximum power that the turbine can extract from the existing wind conditions ($P_{g\text{-}max}$, i.e. when C_p is maintained at $C_{p\text{-}max}$, as in Figure 5.18 and Figure 5.19), minus the losses within the WECS (P_l), i.e. $P_d = P_{g\text{-}max} - P_l$.

For the large interconnected grid, power is wheeled throughout the system to meet overall demands, and voltage and frequency levels are relatively unaffected by the injection of power by an individual wind generating station. Although this concept is generalized, the key point is that for the typical grid-connected WECS, the power received by the grid is determined by how much power is extracted by the WECS. When wind speeds are low, smaller amounts of power are received by the grid. When wind speeds rise, larger amounts of power are transferred. Throughout the typical range of wind speeds (between cut-in and rated wind speeds), the WECS is continuously operated so that C_p is maximized and, resultantly, the maximum amount of power is transferred.

In the islanded case, such as in a microgrid or a remote application, or on a weak feeder, the balance between generation and load must be much more closely attended. Islanded power systems do not have the luxury of wheeling power throughout an extensive network or varying a vast array of complimentary generation sources to maintain an electrically balanced system overall. This is primarily due to their smaller scale, often a lack of electrical storage, and limited flexibility and configuration of locally-connected loads. For islanded applications, a more sophisticated control system is required to properly match electricity supply and demand. The dominant factor in determining the WECS power balance is no longer $P_{g\text{-}max}$, but in fact P_d. Assuming that P_d is not controllable, meaning that demand-response, load-shedding, and dump load control are not present or at least complementary to turbine power control, the amount of power consumed must equal the power produced by the WECS (P_g). Therefore, this gives rise to a new power balance reference. The power extracted by the WECS is equal to the sum of load demand and WECS internal losses, i.e. $P_g = P_d+P_l$. Next, instead of the turbine being operated such that the power coefficient is maximized (previously, $P_g = C_{p,max}P_a$), a new turbine operating point must be found. The new reference power coefficient ($C_{p,ref}$) is equal to the desired power extracted by the WECS divided by the wind power available, i.e. $C_{p,ref} = (P_d + P_l)/P_a$. By determining $C_{p,ref}$ in this way, a new operating point may be determined for the wind turbine. Of course, conventional maximum power transfer can easily be restored by referencing $C_{p,ref}$ to $C_{p,max}$, as with typical grid-connected WECS mode-of-operation. Control of $C_{p,ref}$ for load-following will be further discussed in Section IV.

The turbine power control scheme described for the islanded system is significantly different than is typically employed for grid-connected systems. Under this scheme, when the power available from the wind is greater than the power demand, the

WECS controller must adjust the proportion of power extracted from the wind. This may be somewhat counter-intuitive. After all, this mode-of-operation control scheme stipulates that even though larger amounts of energy exist within the prevailing winds, the WECS controller artificially reduces the amount extracted ($C_{p,ref} < C_{p,max}$). While this effect is certainly undesirable when seeking to maximize wind energy generation, in the islanded case the desire is to ensure stability on the more fragile system. By limiting power produced by the WECS, energy supply matches demand. To be clear, the scheme described above is *necessary* for islanded operations, but *can* be applied to grid-connected systems when load-following or specific power constraints are in effect.

Under real-world operational conditions, a WECS in islanded mode may experience dramatic changes in load. During these load changes, the WECS must modify its output (load follow) to preserve continuity of power. In order to demonstrate the effectiveness of the proposed PMSG-side converter speed controller at reducing the quantity of power produced, a series of simulations were conducted. In Figure 5.29, wind speed remains at a constant 10 m/s and pitch angle is at zero degrees, as the load demand experiences various step changes over 180 seconds. The total power transferred from the wind to the power system follows according to changes in demand. Assuming that sufficient wind power is available ($P_a > P_d + P_l$), the speed controller appropriately senses the need to manipulate shaft rotational velocity based on establishing a new rotor efficiency, as shown in Figure 5.30.

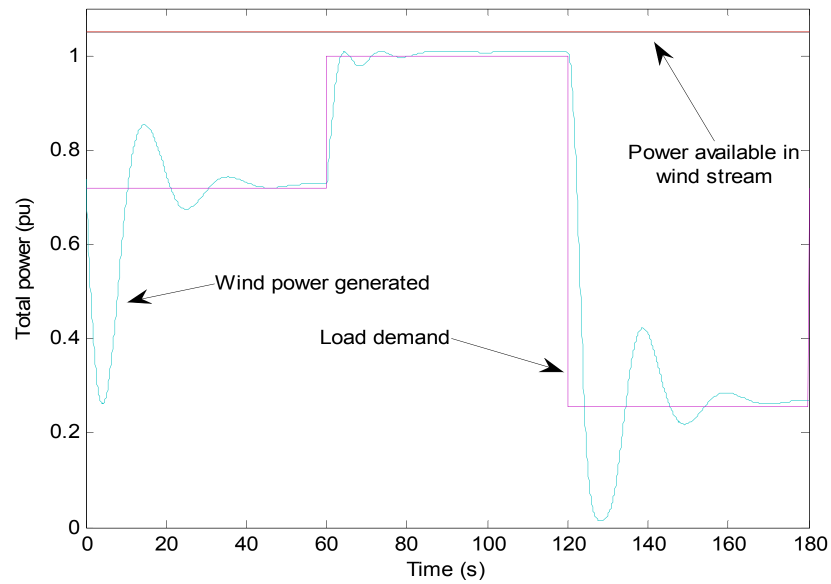

Figure 5.29. Total wind power available, load demand, and power generated.

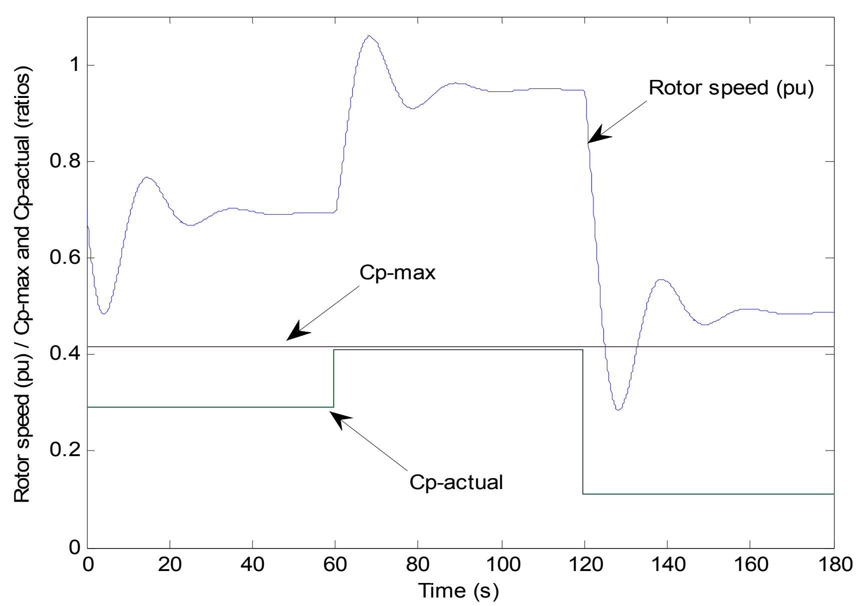

Figure 5.30. Rotor speed, $C_{p,max}$ and actual C_p during load changes.

In order to evaluate the performance of the proposed WECS comprehensively, an islanded microgrid power system with load comprised of a 150-home neighborhood of residential customers was used for simulations. In this scenario, the microgrid which is normally interconnected with a utility power system has become islanded due to a fault on the utility side. Whereas under normal conditions the single 2.0MVA WECS (20% capacity factor) is operated so that it produces the maximum amount of power from the wind possible (C_p is maximized), in this scenario the WECS must perform load-following so as to not cause voltage and frequency excursions on the microgrid system. The microgrid has no storage, but an emergency 300kW diesel generator (DG) with automatic startup is connected in parallel to the WECS. Due to fuel cost and environmental emissions concerns, the DG is only operated during periods when inadequate power is supplied by the wind. To simulate the collection of residential customers, aggregated end-use, time-of-day load curves based on winter weekday usage patterns in the Pacific Northwest region of the United States, described in 5.10.1 , were used. The residential data only reflects real power consumed by all-electric homes in the region; that is, utilizing electric appliances, electric heating/ventilation, and electric hot water heaters. For a more realistic simulation, the residential power factor was set at 0.95 lagging.

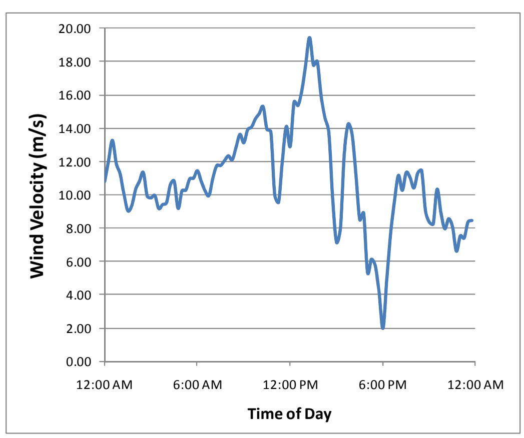

Figure 5.31. 24-hour wind velocity profile (1-minute resolution).

The wind data for this simulation, shown in Figure 5.31, was interpolated from 15-minute interval wind velocity records for a 24-hour period representative of average annual wind speeds at an agricultural station at Deer Lodge, Montana [5.41]. The data was collected at a height of two meters, but corrected to a hub height of 40m, as suggested by [5.42]. Table I annotates the ratings of the WECS considered for this study.

Table 5.4. Specification for 1.5MVA WECS.

Parameter	**Value**
Cut-in speed	3 m/s
Rated speed	14 m/s
Cut-out speed	20 m/s
Blade length	18 m
Air density	1.204 kg/m^3
$C_{p,max}$ ($\theta = 0^o$)	0.41
Stator resistance (R_a)	0.045 pu
dq-axis inductances (L_d, L_q)	0.5 pu
Rotor permanent magnet flux	1.0 pu
PMSG pole pairs	80

The results of the simulation, given in Figure 5.32, show the performance of the WECS system under the scenario proposed. Despite significantly more wind energy available during the majority of the simulated day, the PMSG-equipped WECS regulates the power it generates to match the load on the microgrid AC bus. During periods when wind speeds are too low to provide adequate power to supply microgrid loads (at about

11:15AM, 3:00PM, 4:30-6:45PM, and 8:00-11:00PM), the DG engages automatically to generate the deficit. Overall, this study demonstrates the ability of the load-following controller for the PMSG-equipped WECS to meet proper mode-of-operation requirements in the islanded case. By controlling generator rotational speed electrically, negative effects from variable wind production that can cause significant AC bus instability can be avoided.

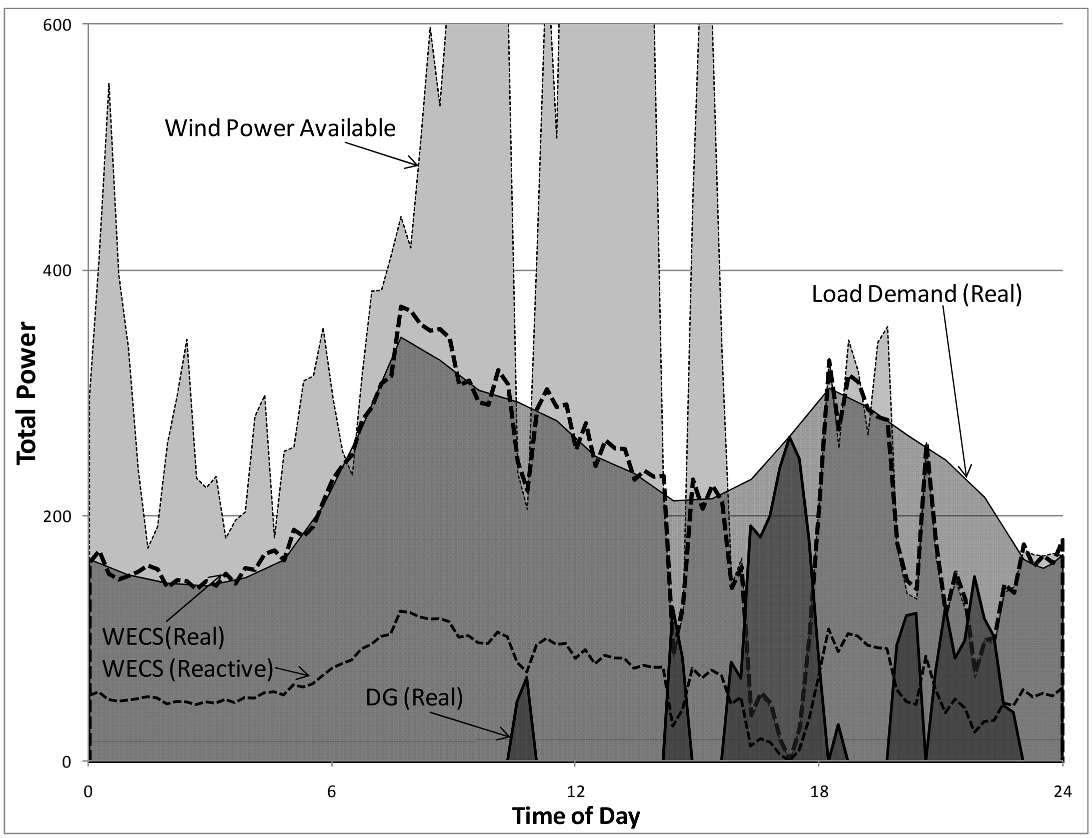

Figure 5.32. 24-hour power supply and demand profiles for 150-residences in islanded microgrid scenario with load-following WECS and DG.

In order for an appropriate incremental model to be used for microgrid simulations, the preceding development was undertaken. The result of this effort yielded a useful model of a PMSG that can be employed in islanded or grid-interconnected modes-of-operation. It is clear that under certain scenarios, such as with an islanded microgrid or on a weak power system feeder, it is desirable for attached wind generation to be curtailed so that voltage and frequency levels do not go out of specification. To that end, and especially as PMSGs become more popular for wind generation, the control methodology shown can be suitable for accomplishing generation-to-load matching.

5.6 Fuel Cell

Fuel cells are direct energy conversion devices that commute the chemical energy of a fuel-oxygen reaction to electrical energy. Energy conversion by electrochemical methods can be more efficient than by combustion, and because of this, fuel cells show potential for implementation in future power generation systems. There are many constructions and chemistries of fuel cells, but in general, they can be divided into two primary classes: low or high temperature of operation. Low temperature fuel cells, such as the polymer electrolyte fuel cell, operate at temperatures less than 300°C and require pure hydrogen as a fuel. High temperature fuel cells, such as the solid oxide fuel cell (SOFC), operate at high temperatures, typically 600-1000°C and, due to this feature, have some unique attributes. High temperature operation allows internal fuel reforming to occur at the anode. This makes high temperature fuel cells very attractive because they can utilize a range of fuels, can be implemented without sources of gaseous hydrogen, and can capitalize on existing natural gas infrastructure. For these reasons, high temperature fuel cells have held greater interest for larger stationary power applications of interest to power system researchers and planners. SOFCs, the most promising of the high temperature fuel cell technologies, has electrochemical reactions that follow [5.43]:

$$H_2 + O^{2-} \rightarrow H_2O + 2e^- \qquad \textit{anode} \qquad (5.52)$$

$$CO + O^{2-} \rightarrow CO_2 + 2e^- \qquad \textit{anode} \qquad (5.53)$$

$$CH_4 + 4O^{2-} \rightarrow 2H_2O + CO_2 + 8e^- \qquad \textit{anode} \qquad (5.54)$$

$$O_2 + 4e^- \rightarrow 2O^{2-} \qquad \textit{cathode} \qquad (5.55)$$

A physically-based dynamic model for a 5 kW tubular SOFC stack, reported in [5.44], was used as a basis for SOFC studies. The model was developed based on SOFC thermodynamic, electrochemical and material diffusion properties, and the mass and energy conservation laws, with emphasis on the fuel cell electrical terminal quantities. Figure 5.33 shows the block diagram upon which the model has been developed. The model input quantities are anode and cathode pressures (P_a and P_c), hydrogen flow rate (M_{H2}), water vapor flow rate (M_{H2O}), dry air flow rate (M_{air}), and initial fuel cell and air temperatures ($T_{fuelinlet}$ and $T_{airinlet}$). The model output quantities are the fuel cell voltage and internal temperature. At any given load current and time, the cell temperature T_{cell} is determined and both the current and temperature signals are fed back to different blocks, which take part in the calculation of SOFC output voltage.

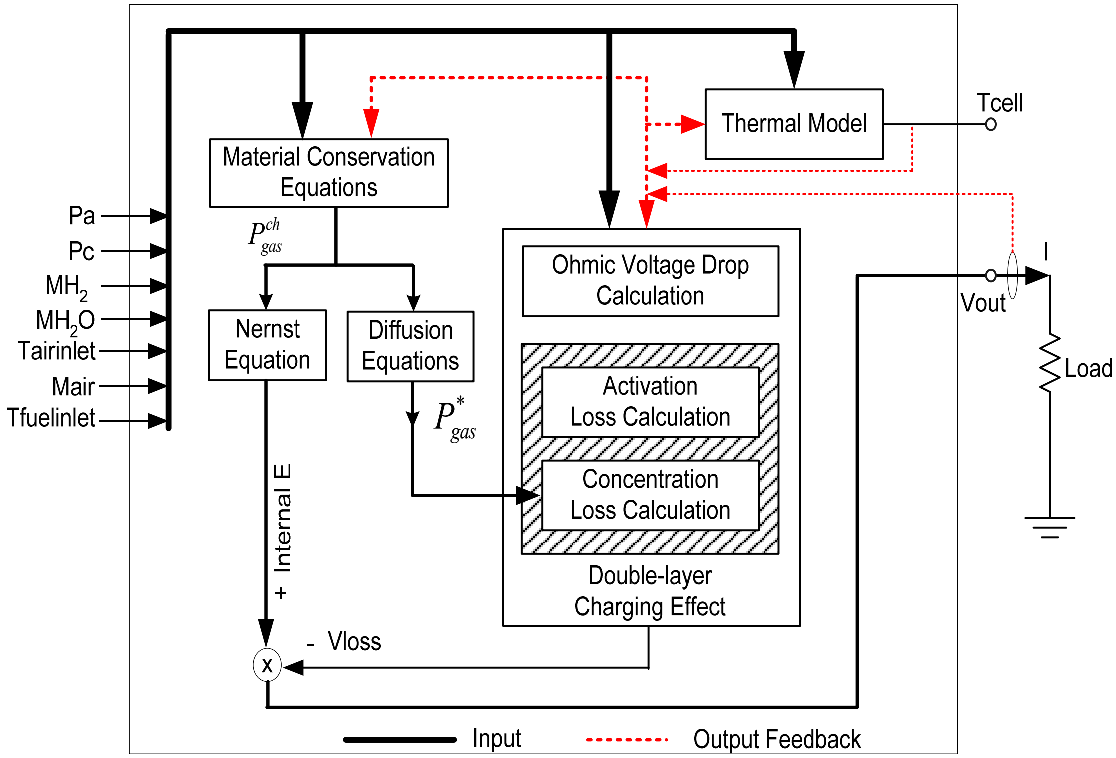

Figure 5.33. Block diagram of SOFC dynamic model [5.44].

The terminal voltage vs. current and power vs. current (V-I and P-I) curves of the SOFC stack model, obtained from the dynamic SOFC stack model reported in [5.44], are shown in Figure 5.34. The operating conditions under which the curves have been obtained are given in the figure. The activation voltage drop dominates the voltage loss within the low-current region. As load current increases, the ohmic voltage drop increases fast and dominates the contribution to the additional voltage reduction. When load current exceeds a certain value (110A for the 5-kW stack at the operating conditions shown in Figure 5.34), the fuel cell output voltage will diminish sharply due to the concentration effects inside the fuel cell.

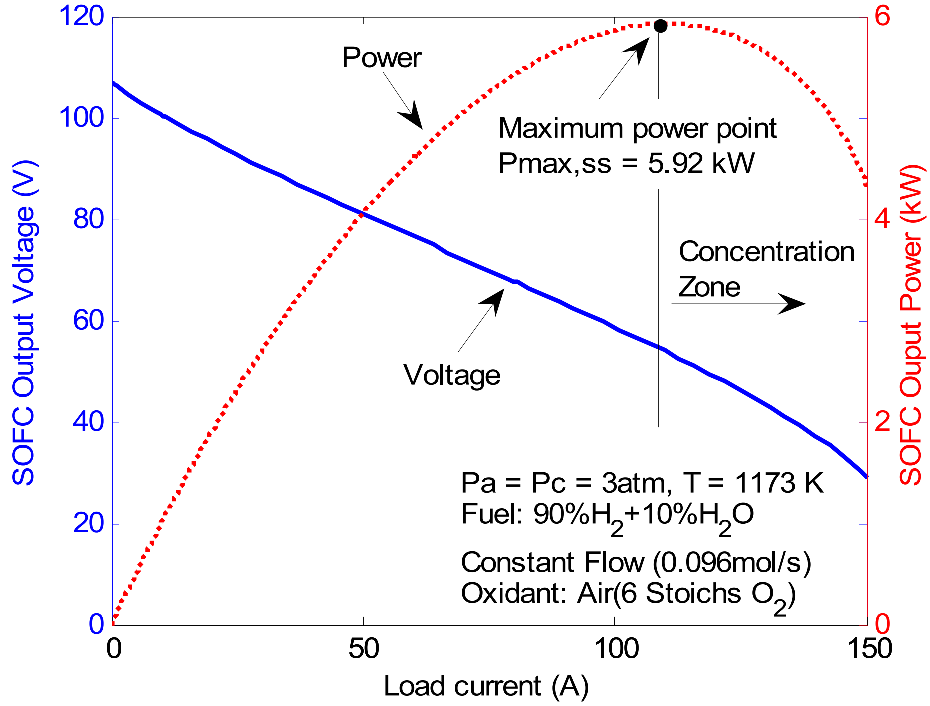

Figure 5.34. V-I and P-I curves of the SOFC model reported in [5.44].

The steady-state response of the dynamic model is similar to that reported in [5.43] and has been validated with operating data from industry sources. For further details about the model, the reader is referred to [5.44].

5.7 Cogeneration: Combined Heat and Power

Many combustion systems, such as internal combustion engines or turbines, produce hot exhaust streams that are typically vented to the atmosphere. This is also true of non-combustion devices such as fuel cells. These exhaust streams are at high temperature and hold the opportunity for significant heat transfer to a secondary medium. However, without proper auxiliary systems, this is energy is typically not captured. Cogeneration refers to coupling additional heat transfer systems to a primary power-producing source for the purpose of extracting energy from the waste heat stream, thereby improving the overall energy conversion of the system. Cogeneration systems are more common at industrial scale, but recently have seen interest for smaller, distributed generation sources. While most cogeneration systems for distributed generators do not produce additional electrical power, they utilize waste heat to offset energy consumption for processes that would otherwise require additional energy input. Cogeneration systems are relatively inexpensive when compared to distributed generation capital costs overall and capitalize on a heat stream that is otherwise wasted. No comprehensive look at distribution-level microgrids would be complete without a discussion of cogeneration systems. Additionally, little research has been focused on smaller cogeneration systems appropriate for distributed generators and, thus, is presented here.

Some high temperature systems, such as SOFCs and microturbines, show significant potential for hybrid heat transfer operations. Hybrid heat transfer applications encompass combined cycle systems and Combined Heat and Power (CHP) systems. In both categories of hybrid systems, high temperature exhaust gases are utilized for further energy extraction. Conventional CC systems are most commonly seen in gas turbine (GT) applications where the unutilized turbine exhaust heat is recovered in a heat recovery steam generator (HRSG). This steam then drives a secondary turbine-generator for additional electricity production. Recently, CC operations, such as with SOFC-GT systems, has been shown as an attractive application for SOFC technology [5.45] On the other hand, CHP systems, also known as cogeneration systems, do not typically generate additional electricity, but instead take advantage of exhaust gas streams for uses such as residential/commercial heating or process steam generation [5.46]. Whether in CC or CHP hybrid configurations, the promise of these systems is higher quantities of extracted energy leading to higher overall system output efficiencies relative to fuel energy input [5.47].

5.7.1 Thermodynamics of Cogeneration Efficiency

Holistically, efficiency is a simple measure of the energy extracted from a system relative to the energy input to the system. Efficiency is an important measure of the performance of system components and can be used to help guide dispatch decisions for systems or groups of systems within a particular power management framework. However, efficiency has many subtleties which must be considered is it is to be used as an appropriate measure of performance for a particular system. For example, SOFCs may commute the chemical energy of a fuel-oxygen reaction to electrical energy at efficiencies between 45% and 65% [5.48, 5.49, 5.50]. However, the boundary conditions of this efficiency calculation are restricted to the inlets and outlets of the anode and cathode channels. It is not possible to sustain operation, much less high efficiency, at this level without auxiliary SOFC systems that utilize a significant quantity of energy to pre-heat, compress and condition inlet gasses in order to maintain the electrochemical process that drives fuel cell electrical generation. In addition, some cases require energy to pre-reform or desulfurize fuel [5.51, 5.52]. In other words, in order to properly model the operations of any complete power source, a system-wide analysis that addresses the electrochemical and thermodynamic operation of the total system and support subsystems is required. To further this discussion, the SOFC is used as a system example, but the principals may be extended to any power source system that yields an exhaust stream with energy extraction potential. While significant literature has been dedicated to determining ideal fuel cell efficiency limited to channel boundaries [5.53, 5.54], the following discussion advances the analysis of components in the context of their actual operation by evaluating the relationship between a coupled high temperature fuel cell and the energy flows required upon input and available to be exploited at the output.

The first law of thermodynamics for an open system, such as a SOFC, relates the difference between the enthalpy flow in/out of the system, to the rates of heat flow and work flow to/from the system. The first law states [5.55]:

$$dQ - dW + \sum_{input\ streams} \dot{n}_i \hat{H}_i = \sum_{output\ streams} \dot{n}_i \hat{H}_i \tag{5.56}$$

where, dQ, dW, and $\hat{H}_i$ represent the rate of system heat flow (joules/sec), rate of system work flow (joules/sec), and specific enthalpy (joules/mol) of the i-th input or output stream, respectively. The $\dot{n}_i$ represents molar flow rate (mols/sec). Neglecting the kinetic and potential energy content of each energy stream, we utilize the definition of enthalpy ($H = U + PV$, where H, U, V, P are specific enthalpy, specific internal energy, and specific volume, respectively and pressure is a non-specific quantity) to simplify (5.56):

$$dH = dQ - dW \tag{5.57}$$

where, dH, dQ, and dW are the rates of enthalpy, heat, and work flow in an open system.

Within the fuel cell system, dW is in the form of output electrical work flow. It is crucial to note, that while the first law describes the conservation of energy, heat and work are fundamentally different than enthalpy in that the former represent modes of energy transfer to and from the system. Work and heat quantities have the same units, but are not simply comparable to enthalpy which represents properties of the system's input and output energy streams.

According to the second law of thermodynamics, the amount of reversible (ideal) heat transfer for a system is expressed by: $dQ_{rev} = TdS$, where dQ_{rev} is the reversible rate of energy transferred as heat (joules/sec), T is temperature (Kelvin), and dS is entropy change (joules/Kelvin-sec). This leads to the definition of Gibbs energy for a constant temperature process:

$$dG = dH - TdS \tag{5.58}$$

where, dG is the Gibbs energy change, which represents the maximum amount of system energy that may be converted to useful work flow (output electrical energy). In the case of SOFCs, Gibbs energy is the maximum amount of electrical energy that could theoretically be extracted from the fuel - oxidizer reaction.

In any context, when system efficiency is analyzed, it is critical to appropriately describe how the efficiency is defined. In terms of the first law of thermodynamics, efficiency is described by ratio of the useful work (electrical energy) that is delivered to the environment from the system to the difference between the system's stream flow energies (enthalpies). The second law of thermodynamics expresses the efficiency as the ratio of the total work flow from the system to the maximum work flow, which is the difference between the Gibbs energy flow of the feed and product streams.

Significant literature has been dedicated to the comparison of a fuel cell process to that of an ideal Carnot heat engine, e.g. [5.56, 5.57]. Heat engines and fuel cells are not directly comparable because of their very different operating principles. Within a heat engine, high temperature energy is delivered from a fuel-air (oxygen) combustion reaction. Some of this high temperature energy is converted to work within the engine, but most of it is rejected to a low temperature heat sink. On the other hand, a fuel cell directly converts fuel-oxygen reaction energy into work without combustion. This aspect of fuel cell operation avoids most of the loss of Gibbs energy experienced in practical heat engines.

First law efficiency, or sometimes referred to as thermal efficiency, is defined as:

$$\eta = \frac{useful\ energy}{total\ enthalpy\ change} \tag{5.59}$$

As previously described, this expression for efficiency can be misleading if taken out of context regarding the relationship between useful energy and work potential. The maximum amount of energy that may be converted to work is exactly equal to the Gibb's energy change of a system. As shown in [5.53], the representation of ideal efficiency for a reversible isothermal reaction occurring within a fuel cell is:

$$\eta_{ideal,electrical} = \frac{-\ Gibb's\ energy\ change}{-\ enthalpy\ change\ of\ reaction} \tag{5.60}$$

Empirical data for the standard enthalpies of formation of the combustion reactants and products are widely published. The standard enthalpy of formation values are very useful for the analysis of the fuel-oxidizer reaction that occurs within a fuel cell [5.55]. An explanation of how the heat of reaction is determined is provided below.

Work potential, also known as exergy, is conserved in perfectly reversible systems, but can be destroyed by irreversible processes [5.58]. Exergy analysis highlights the fundamental difference between a heat engine and the fuel cell: a heat engine transfers heat to useful mechanical work, while the fuel cell as an electrochemical device transfers chemical energy to electrical energy. The combustion process within the heat engine is largely irreversible, and therefore destroys work potential. This process does not occur within the fuel cell and results in a lesser amount of entropy generation.

It can be concluded that fuel cell ideal electrical efficiency, as defined by (5.60), which relates the change in Gibb's energy to the change in the enthalpy reaction, only describes fuel cell ideal electrical efficiency. However, it is useful to understand that CHP applications take advantage of more than just the electrical power produced by high temperature fuel cells. The ideal electrical efficiency defined by (5.60) does not describe the entirety of the thermodynamic system and may not be appropriate for describing CHP applications.

The dynamic SOFC model, briefly described in section II, was used to conduct efficiency studies. Under varying operating conditions, annotated in Table 1, the SOFC model simulations provided data that was used to determine SOFC performance.

Table 5.5. SOFC operating properties for energy studies.

Parameter	**Value**
Number of Cells in Stack	96
Stack Temperature (K)	873 - 1273
Anode input pressure (atm)	1.1
Cathode input pressure (atm)	1.1
Anode H_2 flow rate (mol/s)	0.0096
Cathode H_2O flow rate (mol/s)	0.0001
Oxidant	Not stoichiometrically limited
Mode of operation	Constant fuel supply, utilization varies due to electrochemical and thermal conditions.

As expressed above, the maximum amount of energy that a fuel cell can convert is exactly equal to the change in Gibb's energy for the reaction species. Rather than using the Gibb's energy to determine ideal electrical efficiency, actual SOFC performance data was used to obtain actual electrical efficiency. Utilizing simulated SOFC output voltage and current data, an accurate accounting of the electrical power (electrical energy per unit time) produced by the SOFC could be determined. This data was used according to the following relationship:

$$\eta_{electrical} = \frac{VI}{-\Delta H_{rxn}} \tag{5.61}$$

where V is SOFC output terminal voltage (volts), I is SOFC output current (amps), and

ΔH_{rxn} is the enthalpy flow (joules/sec). It is noted that enthalpy flow represents the total enthalpy flow of the inlet fuel species applied to the SOFC anode. The usage of enthalpy flow is explained later in this section.

A critical aspect of SOFC operation that affects the electrical efficiency, as defined by equation (5.61), is a property of operation called fuel utilization (FU). Because an SOFC is a direct energy conversion device rather than a combustion device, not all available fuel is consumed during operations. In fact, the amount of fuel that is consumed by the SOFC is directly related to its load demands, as shown by Figure 5.35. As a result, to find the true ideal electrical efficiency of the SOFC, it is only appropriate to calculate the enthalpy flow of the actual quantity of fuel that is converted by the SOFC, rather than the total quantity of fuel mass transported to the SOFC anode inlet. Therefore, (5.61) is modified to include the FU percentage, as follows:

$$\eta_{electrical} = \frac{VI}{(-\Delta H_{rxn})(FU)} \tag{5.62}$$

where FU is fuel utilization (%). In the SOFC model, a constant fuel flow is applied, but FU varies dynamically.

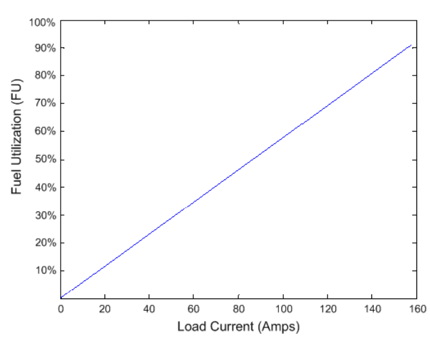

Figure 5.35. Simulated SOFC stack fuel utilization versus load current.

Figure 5.36 shows the simulated electrical efficiency of the SOFC model versus load current for various operating temperatures. The data shows that, at higher currents less energy is converted to useful work in the form of electrical power, however, higher temperature operation has a beneficial effect on SOFC efficiency. In the ideal case, the available amount of Gibb's energy from the hydrogen-oxidizer reaction decreases slightly as temperature increases, but realistic simulations show that higher temperatures provide more favorable thermochemical parameters which overcome the decrease in Gibb's energy. This phenomenon is characterized by the SOFC experiencing improved reaction and mass transport rates, as well as a slightly lower cell resistance, as operating temperature goes up [5.43]. However, as load current increases, SOFC electrical efficiency tends downward and operating temperature tends upward. This phenomenon results from the thermochemical response, which manifests through ohmic, concentration, and charging effect voltage losses, described in [5.44]. As operating temperature rises in response to higher load (within the SOFC rating), and although the electrical efficiency goes down, the higher temperature can be more favorably exploited in CC heat transfer operations downstream. It is noted that due to the fuel utilization effect within the SOFC, electrical efficiency does not appear to go to zero at low load currents. In fact, at zero current, FU is equally zero which results in a zero-over-zero efficiency value. The time step of the SOFC dynamic model is 0.1ns which, given the scale of Figure 5.36, hides the very sudden efficiency rise from zero to approximately 84% in a short time period at time 0+.

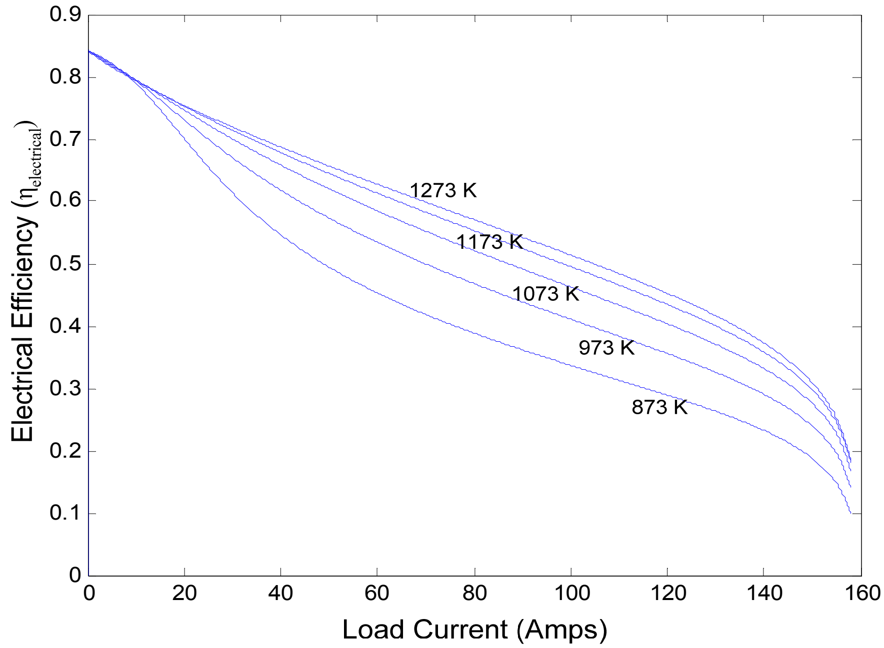

Figure 5.36. Simulated SOFC stack electrical efficiency versus load current at different operating temperatures.

Haynes, in [5.58], correctly asserted that for a proper holistic examination of an operational fuel cell implemented in a hybrid application, the quality and quantity of heat rejected by the high temperature fuel cell must be taken into consideration. This is especially significant for SOFCs which reject considerable high temperature, low pressure exhaust which is valuable for CHP applications, and to a lesser extent, CC applications.

When examining a SOFC in CC operation, both the Gibb's energy and exhaust heat must be combined for a complete picture. Not only will the fuel cell generate electrical energy, but when combined with a reversible heat engine system, heat transfer is harnessed from the fuel cell exhaust gas for conversion to useful work. For SOFC, work potential due to heat transfer is defined as [5.58]:

$$dW_{exhuast} = \left(1 - \frac{T_{sink}}{T_{fuel\ cell}}\right) dQ_{exhaust} \tag{5.63}$$

where, $dW_{exhaust}$ is the rate at which work is performed by the heat engine (joules/sec), T_{sink} is the temperature at which heat engine rejects heat to the environment (K), $T_{fuelcell}$ is the fuel cell exhaust temperature (K), and $Q_{exhaust}$ is the heat flow of exhaust (joules/sec).

Therefore, for any defined duration of time, a complete measure of the fuel cell system work potential can be obtained by combining (5.63) with the Gibbs energy change. As a result, the ideal efficiency expression for a high temperature fuel cell can be written by modifying (5.62) to include $W_{exhaust}$:

$$\eta_{ideal} = \frac{-\Delta G + \left(1 - \frac{T_{sink}}{T_{fuel\ cell}}\right) Q_{exhaust}}{(-\Delta H)(FU)} \tag{5.64}$$

where, η_{ideal} is the ideal SOFC efficiency that incorporates ideal electrical and ideal heat recovery efficiency components in a defined period of time, ΔG is the change in Gibbs energy (joules), and ΔH is the change in enthalpy for the system (joules).

A SOFC is not a heat engine. Literature has discussed the confusion over analyzing fuel cell ideal efficiency under the Carnot and "non-Carnot" contexts, e.g. [5.56, 5.59]. This paper does not attempt to examine theoretical efficiency limits, such as comparing a SOFC to a Carnot heat engine. Instead, actual SOFC characteristics were simulated by dynamic modeling to determine supportable performance and efficiency data, as will be discussed in the forthcoming sections.

Recalling the simplest fuel-oxidizer reaction that takes place within a fuel cell follows the chemical reaction defined by (5.52) - (5.55), standardized enthalpies of formation can be used to determine the enthalpy of reaction (also referred to as enthalpy of combustion) for the fuel/oxygen reaction. For the reaction within a fuel cell, the standard enthalpy of reaction is determined by [5.55]:

$$\hat{H}^0_{rxn} = \sum_{\text{products}} v_i \Delta\hat{H}^0_i - \sum_{\text{reactants}} v_i \Delta\hat{H}^0_i \tag{5.65}$$

where, $\hat{H}^0_{rxn}$ is the standard enthalpy change of reaction (joules/mol), or heat of reaction, v_i is the stoichiometric coefficient of each product or reactant species, $\hat{H}^0_i$ is the standard heat of formation for each reaction species (joules/mol). The standard enthalpy of reaction for the hydrogen-oxidizer reaction that occurs within a fuel cell depends on the resultant state of water: -285.84 kJ/mol (liquid state) and -241.83 kJ/mol (gaseous state) [5.55].

For modeling an open system, such as a fuel cell, calculating the enthalpy flow is useful for evaluating the energy balance described in (5.56). The enthalpy flow is defined as [5.60]:

$$\Delta H_{rxn} = \sum_{\text{products}} \dot{n}_i \hat{H}_i - \sum_{\text{reactants}} \dot{n}_i \hat{H}_i \tag{5.66}$$

where, ΔH_{rxn} is the enthalpy flow for an open system (joules/sec), $\dot{n}_i$ is the molar flow rate of products or reactants (mols/sec), $\hat{H}_i$ is the specific enthalpy for each reaction species (joules/mol).

The enthalpy of reaction for a fuel-oxidizer reaction is referred to as the heating value. From the hydrogen fuel and oxygen reagent, water is produced. The final state of product water determines the appropriate heating value for use when describing the energy content of the fuel. Higher heating value (HHV) refers to the energy content of a fuel if the reactants are returned to standard temperature, typically 25˚C (298 K). Lower heating value (LHV) refers to the energy content of a fuel if the reactants are returned to a temperature (appropriate for the system pressure) that yields water in the gaseous state, near its condensation point [5.2]. LHV represents a smaller quantity of energy than HHV because the standard enthalpy change of condensation (latent heat of condensation) quantity that would be released from the product water in changing state from gas to liquid is not included.

There is significant debate over which heating value is appropriate to use when assessing fuel cells. It may not be appropriate to utilize HHV when calculating the efficiency of a high temperature SOFC due to its high operating temperature. With operating temperatures in the range of 600-1000 ºC between its inlet and outlet ports, water produced at the SOFC anode will not condense to the liquid state until undergoing heat transfer, downstream of the fuel cell. Similarly, the LHV of the hydrogen fuel may not be appropriate for SOFC applications because SOFCs do not operate at temperatures in the vicinity of the condensation point of water.

What contributes to the debate over higher and lower heating values is that the effect of using one or the other may be counter-intuitive. HHV represents a larger magnitude of energy contained within the same amount of fuel. It would seem that a conservative estimate of the energy evolved from a fuel-oxygen reaction would therefore be more in-line with the smaller quantity of energy, i.e., LHV. However, when it comes to efficiency calculations, because the heating value is in the denominator, see (5.60), the smaller the amount of energy contained within a fuel yields a higher efficiency for the given amount of reaction output.

For SOFCs specifically, their operating parameters necessitate an analysis of the enthalpy of the hydrogen-oxygen reaction at non-standard temperatures. It is shown in [5.61] that gas phase heat capacity (Shomate equations) can be used to very accurately determine enthalpies of reaction that occur at a non-standard temperature. According to the gas phase heat capacity equations, the specific enthalpy and specific entropy of reactants and products at non-standard temperatures can be found by [5.60]:

$$\hat{H}_i = \hat{H}_i^0 + \int_{T_0}^{T_f} c_{p,i}(T)\partial T \tag{5.67}$$

$$\hat{S}_i = \hat{S}_i^0 + \int_{T_0}^{T_f} \frac{c_{p,i}(T)}{T}\partial T \tag{5.68}$$

where, $\hat{H}_i$ is the specific enthalpy at T_f (joules/mol), $\hat{H}^0{}_i$ is the standard enthalpy (joules/mol), T_f is the operating temperature (K), T_0 is the standard temperature (298.15K), $c_{p,i}$ is the heat capacity (joules/mol-K)), $\hat{S}_i$ is the specific entropy at T_f (joules/mol-K), and $\hat{S}^0{}_i$ is the standard entropy (joule/mol-K).

The Shomate equations take advantage of empirical gas phase data to determine the change in formation enthalpy of a substance between an initial standard temperature (T_0 = 298 K) and at a non-standard temperature. The equation coefficients take into account this initial temperature (T_0) and utilize only the final temperature, accordingly. This simplifies the equations and calculations for each component species that plays a role in the reaction to [5.2, 5.62]:

$$\hat{H}_i(T) - \hat{H}_i^0 = A \cdot T + \frac{B \cdot T^2}{2} + \frac{C \cdot T^3}{3} + \frac{D \cdot T^4}{4} + \frac{E}{T} + F - H \quad (5.69)$$

$$\hat{S}_i(T) = A \cdot \ln(T) + B \cdot T + \frac{C \cdot T^2}{2} + \frac{D \cdot T^3}{3} + \frac{E}{2 \cdot T^2} + G \quad (5.70)$$

where, $\hat{H}_i(T)$ is the specific enthalpy (joules/mol) of reaction species *i* at non-standard operating temperature *T* (K), $\hat{S}_i(T)$ is the specific entropy (joules/mol-K) of reaction species *i* at non-standard operating temperature *T* (K), and *A, B, C, D, E, F, G,* and *H* are the thermochemical coefficients. By convention and according to the gas phase heat capacity equations, the standard enthalpy, $\hat{H}^0_i$ is equal to the coefficient, *H*. The thermochemical coefficients that satisfy the Shomate equations (5.69) and (5.70) are compound specific and are given in [5.62].

5.7.2 Quantifying Efficiency

The physically-based dynamic SOFC model developed in [5.44] facilitates modeling of multiple physical parameters as they occur within a SOFC. With voltage, current, and temperature data, it is possible to utilize the gas phase heat capacity equations developed above to model SOFC efficiency in real time under varying operating conditions.

Most literature evaluates fuel cell performance merely on the production of electricity and neglects any thermal recovery downstream in a CC configuration, e.g. [5.63, 5.64]. Because of this, the first simulations were run to evaluate only the SOFC electricity generation efficiency. Figure 5.37 gives a comparison of SOFC electrical efficiencies versus load current obtained based on (5.62), from the SOFC dynamic model [5.44]. In the case of the HHV and LHV curves, the published HHV and LHV of hydrogen, multiplied by the molar flow rate of consumed hydrogen was used to obtain the denominator in (5.62). These results are compared to the actual enthalpy flow calculated from SOFC simulation data and used in (5.62). The purpose of showing Figure 5.37 is to demonstrate the utility of determining actual enthalpy flow for modeling purposes. This does not imply that the widely accepted use of LHV and HHV for general fuel-to-work approximations are invalid, conversely, this clearly illustrates how they bracket the efficiency potential of a SOFC.

It is clear from Figure 5.37 that SOFC electrical efficiency is not congruent with either HHV or LHV, but as expected, is somewhere between the two. This demonstrates that at temperatures other than those corresponding exactly to the HHV and LHV, it is not accurate to use either value when calculating efficiency. The actual electrical operating efficiency of a SOFC can therefore be determined as an isolated system.

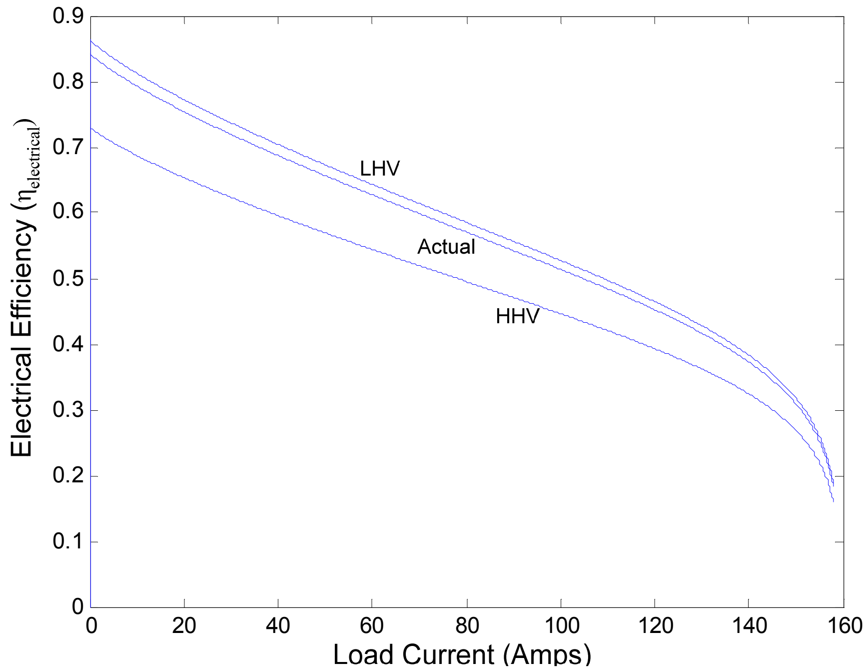

Figure 5.37. Comparisons between dynamically modeled SOFC stack electrical efficiencies utilizing higher heating value, lower heating value, and the calculated enthalpy flow for actual SOFC operating parameters at 1273 K.

To evaluate and quantify cogeneration potential, a simple reversible heat engine model for a thermal recovery system is proposed for analysis of hybrid systems. The heat engine model works on the basis of a hot reservoir that transfers heat to a cold reservoir. As the heat transfer occurs, some work is performed by the heat engine. This combination of heat transfer and work production can be utilized for useful purposes such as generating electricity, pre-heating SOFC inlet gasses, providing process steam, or producing residential hot water, etc. [5.65]. Using knowledge of the SOFC dynamics, shown in Figure 5.37, a SOFC was coupled with two simple cogeneration heat engines to form a hybrid system; one heat engine to simulate the required front-end support subsystems and one heat engine to simulate the heat flow extraction from SOFC exhaust. As previously stated, most CC systems use recovered exhaust heat for additional electricity generation in a bottoming cycle [5.66] and energy that is not extracted by the heat recovery system is then rejected to the environment. This analysis is applicable more broadly, however, evaluating heat flows that can be used for both CC and CHP, as shown in Figure 5.38 In this model, fuel energy and an external source of support energy are inputs to the system; electrical power and work from heat transfer are the useful outputs.

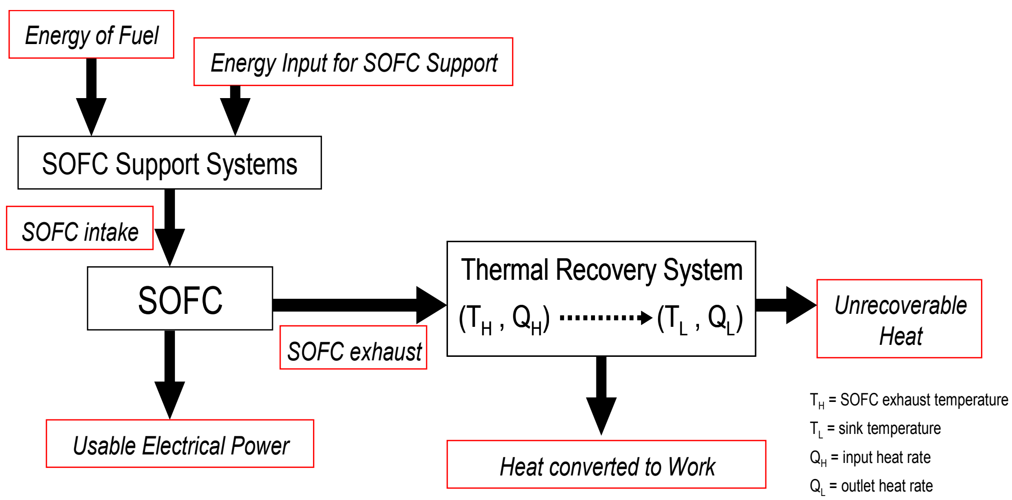

Figure 5.38. Simplified heat flow model for SOFC-CC system.

There exist numerous CC and cogeneration processes that utilize varying means of work extraction from a hot exhaust stream. For this analysis, a generalized model of a heat recovery process for the system was made. The simulated heat recovery system takes in hot SOFC exhaust and transfers its heat to a cold reservoir. As the heat transfer is taking place, the heat recovery system converts an arbitrary 38% of the heat energy present to mechanical work. This is based on a conventional HRSG-turbine system efficiency of 30-40% [5.67]. In an ideal Carnot heat engine, the rate of system work flow

(dW) is equivalent to the difference between the input enthalpy flow (dQ_{hot}) and the output enthalpy flow (dQ_{cold}). Ideal Carnot heat engine efficiency is the ratio of system work flow over the net enthalpy flow, as shown by a manipulation of terms in (5.62). The maximum work flow that may be extracted from a heat engine is bounded by the Carnot limit. Therefore, for this simple non-ideal heat engine model, only 38% of the maximum work flow available between a cold reservoir reference at 390K and the dynamically varying hot SOFC exhaust gas temperature is converted to shaft work. In a static example where hot SOFC exhaust is at 1273K, the 38% model heat engine efficiency conservatively compares to an ideal Carnot efficiency of 69.3%. The initial heat content of each SOFC exhaust product is calculated based on its concentration within the mass flow rate of exhaust. Because specific heat capacity is compound specific and a function of temperature, the gas phase heat capacity equations from [5.62] are utilized in (5.71) to determine the specific heats of each exhaust product ($c_{p,i}$), as the SOFC operating temperature varies under changing load conditions. The total heat flow of the SOFC exhaust gasses are computed according to the sum:

$$d\,Q_{exhaust} = \sum_i \left\{ \int_{T_{sink}}^{T_{fuel\ cell\ \mathrm{exhaust}}} \left[\dot{n}_i c_{p\ ,\ i}(T)\ dT \right] \right\} \tag{5.71}$$

where, $dQ_{exhaust}$ is the exhaust heat flow (joules/sec), $\dot{n}_i$ is the molar flow rate of each exhaust product (mols/sec), $T_{fuel\ cell\ exhaust}$ is the temperature of SOFC exhaust product (K), T_{sink} is the cold sink temperature (K), and $c_{p,i}$ is the specific heat capacity (joules/mol-K) of exhaust species, *i*.

In order to simulate the support subsystems required to sustain an operating SOFC, a lumped model is used. Initial reactants, described by (5.52) - (5.55), are assumed to be at ambient temperature (298K). The compression and pre-heating processes (referred to as support systems) are assumed to be approximately 70% efficient (first-law efficient). Improved support subsystem models are needed for more accurate efficiency evaluation of SOFC-CC operations. Using the support and heat recovery system models, simulations were conducted to determine how much additional work could be extracted from the fuel cell. Figure 5.39 shows a comparison of the electrical efficiency of a SOFC with that of a SOFC-CC system that incorporates the energy lost in conditioning the inlet gasses for SOFC operation.

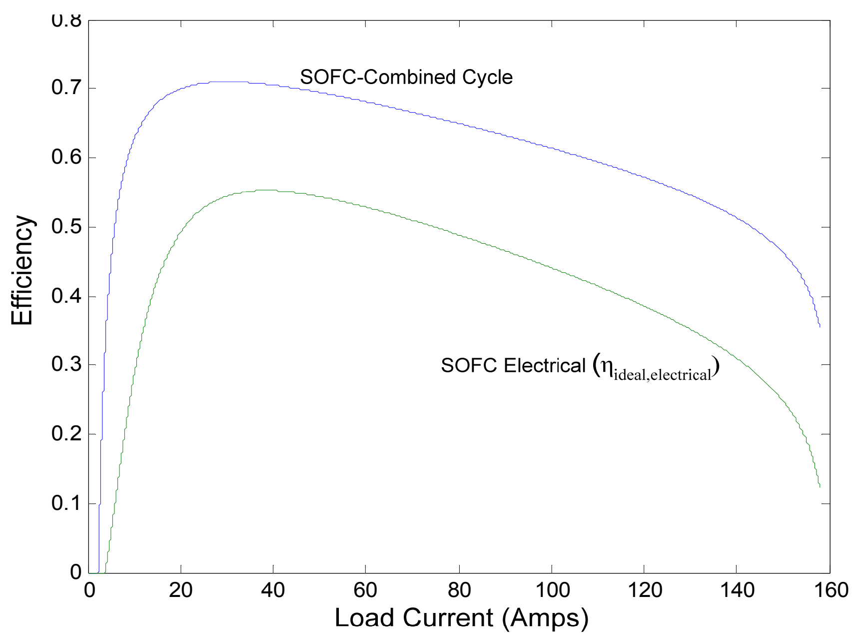

Figure 5.39. Comparison of SOFC stand-alone system electrical efficiency and SOFC-CC system efficiency (both including inlet species preconditioning support).

The results show the inefficiency of operating a hybrid system at low electrical load. The principle of SOFC operation is that energy contained within the hydrogen fuel is partially converted to electrical power. A large quantity of input energy from an external source is still required to support SOFC operations at light electrical loading. This energy far exceeds the electrical power output and heat recovery benefits at low electrical load. However, as the SOFC load increases, the output electrical power rises to a level that, when combined with the gains from heat recovery, far exceed the energy expended in supporting the SOFC operation.

The purpose of Figure 5.39 is to contrast SOFC stand-alone system to that of a SOFC-CC system. In literature regarding fuel cell capabilities, it can be confusing to the reader when presented with electrical efficiency performance of a fuel cell which does not typically take into account the energy consumed in supporting its operations. In Figure 5.39, however, the SOFC electrical efficiency is shown as would be consistent in an actual stand-alone system requiring inlet species support. Figure 5.39 highlights the difference between SOFC electrical and SOFC-CC system efficiencies, especially at low load. While the SOFC does convert fuel energy to electrical energy efficiently, the electrical energy produced is significantly offset by the large amount of energy consumed to sustain SOFC operations at high temperatures. SOFC-CC hybrid operations capitalize on the energy that would otherwise be lost to the environment and make SOFC operations more viable for converting fuel to useful work. Apparent in Figure 5.39 is how beneficial CHP processes can be to the overall energy conversion capability of the SOFC system.

This section has presented the use of a dynamic SOFC model for thermodynamic analysis and efficiency evaluation of SOFC and SOFC-CC systems. This discussion, including that of the appropriate use of fuel heating value, are applicable to all power sources with heat flows that must be considered when evaluating combined system efficiency. Clearly, a CC or CHP heat recovery system can maximize the energy extracted from an inlet fuel and can have significant efficiency benefits. Based on this information, a comparative study was performed in the next section for a hybrid SOFC-CHP plant and the utility supply alternative to a residential load center.

5.7.3 Evaluating SOFC-CHP Benefits

Clearly, concerns about environmental emissions from centralized power plants and the uncertainty of global energy supplies has increased interest in fuel cell technologies for small- to large-scale electricity generation [5.68, 5.69]. In the United States, the average power plant conversion efficiency is 33.2% [5.70], with typical coal and natural gas combustion power plants operating at 20-38% and 30-50% efficient, respectively [5.71, 5.72, 5.73]. As shown above, the efficiency of SOFCs can be significantly higher, especially when combined with CC or CHP capability. Improved fuel-to-electricity efficiency implies a smaller portion of fuel is required to generate equivalent quantities of electrical energy; and, less fossil fuel consumed translates into reduced emissions. In this way, SOFCs alone can be seen as a transitional technology for achieving energy sustainability. Although a hydrogen supply infrastructure does not currently exist for widespread electricity generation, SOFCs promise higher fuel conversion efficiencies even when capitalizing on existing supplies of a relatively clean fossil fuel such as natural gas. In this regard, the benefits of reduced emissions, including less CO_2 produced per kilowatt-hour of electrical energy generated, are immediate. However, in the future, their inherent fuel flexibility allows SOFCs to rapidly shift to hydrogen, a zero-emissions fuel source, when supplies become more available. In similar ways, capitalizing on waste heat to offset energy consumption further enhances the value of SOFC-CHP within a sustainable generation portfolio. These observations and recent research have demonstrated SOFC-CHP potential for large scale power production [5.74].

Using the method developed in section 5.7.2 for evaluating energy flows within a hybrid cogeneration system and appropriately measuring parametric performance, a study was conducted to evaluate a practical application of an SOFC-CHP system for electric power and hot water production, yielding better power production with lower environmental emissions. Specifically, the benefits of a 1.0 MW SOFC-CHP plant for sourcing electrical power and hot water to a residential neighborhood more sustainably and avoiding significant emissions when compared to conventional (typically coal-generated) electricity were evaluated. Although important, the present high capital costs of SOFCs, as well as the absence of carbon production costs in the United States are not considered, but SOFC technology will not experience market acceptance until capital costs drop and the benefits of SOFCs over other technologies (in terms of efficiency, reliability, ease of use, robustness, scalability, etc.) are demonstrated.

5.7.4 SOFC-CHP Electrical-side Design

The physically-based dynamic model for a 5.0 kW tubular SOFC stack, described in Section 5.6 , has been used for simulating the power sources comprising the 1.0 MW power plant. Additional detail on SOFC model development is contained in [5.75]. The 1.0MW power plant size was chosen based on the power necessary to supply a large 500-home residential area or equivalent mixed residential and commercial village community. The 1.0MW power plant most basic power component is the 5.0 kW SOFC stack, comprised of 96 individual fuel cells that combine to yield useful electrical power. Power modules comprised of interconnected 5.0 kW SOFC stacks were combined to achieve larger power capacities. In this case, it was desirable for each SOFC stack to operate near the maximum power point (MPP), shown in Figure 5.34. The MPP for the SOFC stack is roughly 108A at 55 VDC. Taking the nominal stack current of 100 A, a 20-kW power module with a nominal output voltage of 220 VDC is formed by connecting four SOFC stacks in series, as shown in Figure 5.40. Each power module is connected to a common DC bus through individual boost DC/DC converters based on a 5.0 kHz switching frequency for IGBT electronic switches. The DC/DC converters adapt the combined fuel cell module output voltage to a relatively constant DC bus voltage (480 V). A total of fifty SOFC power modules are utilized to achieve nominal power plant capacities of 1.0 MW, shown in Figure 5.40.

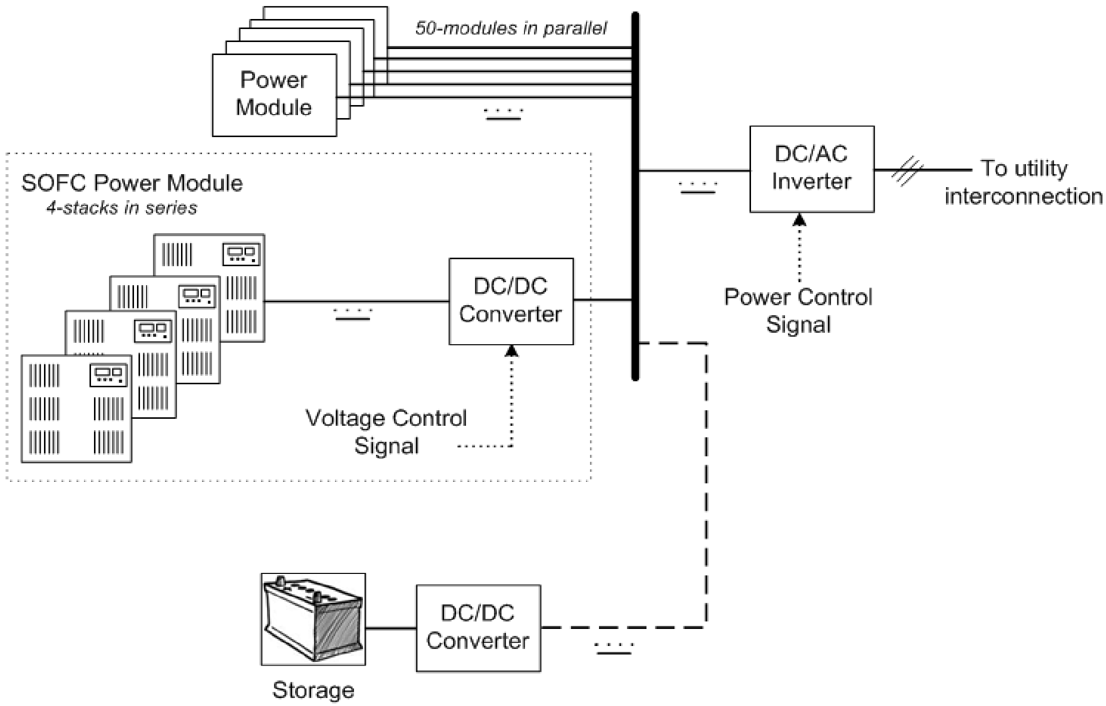

Figure 5.40. System-level diagram of the 1.0 MW SOFC power plant.

The common DC bus feeds a three-arm DC/AC inverter to achieve three-phase AC electrical power. The inverter pulse width modulation (PWM) control signal with a 4860Hz carrier frequency is provided by a V-I controller is discussed below. Power from the inverter is filtered, transformed to utility-grade (12.5 kV) voltage, and is transmitted through a short distribution line to the utility grid. It is assumed that the 1.0 MW SOFC power plant encompasses the SOFC stacks, DC/DC converters, DC/AC inverter, and control and instrumentation circuitry. Exterior to the power plant are the power-filtering, capacitive compensation devices, transformer, and short-run distribution line, as would be consistent with utility interconnection. Power from the inverter is filtered, transformed to utility-grade (12.5 kV) voltage, and is transmitted through a short distribution line to the utility grid. Table 5.6 annotates the parameters used for the components exterior to the SOFC plant to connect to the utility grid. The power plant was designed and simulated without battery storage, but their inclusion is fully possible.

Table 5.6. Power plant interconnection parameters.

Parameter	Design Specification
Output Filtering	
Series resistance	5Ω
Series inductance	100μH
Shunt capacitance	307 μF
Nominal V_{RMS}	208V
Utility Interconnection	
Transformer	208V/12.5kV, 1MVA rated
Coupling resistance	5Ω
Coupling inductance	100mH
Distribution line composition	500 meter ACSR (AWG 6/1)
Distribution line resistance	1.1Ω
Distribution line inductance	0.67mH
Utility Grid Parameters	
Base V_{RMS}	12.5kV
Operating V_{RMS}	0.98pu
Nominal frequency	60Hz

In order to facilitate the SOFC power plant's proper connectivity with the simulated utility grid, the real and reactive power flows between them must be managed. This is achieved by controlling the PWM duty cycle and modulation index signal that operates the inverter. Correspondingly, the inverter output voltage amplitude, angle, and frequency are controlled to meet specified demands. This is made possible by employing a power electronics interface which has the ability to control the power plant signals to match their reference values after a disturbance.

Fuel cells poor susceptibility to load transients is well known [5.76, 5.77]. Rapid current transients of sufficient magnitude can cause fuel cell failure or damage. As explained in [5.44], the total capacitance of an SOFC is roughly equivalent to the combined double-layer charging effect between the porous electrodes within each individual cell of the stack. While the combined stack capacitance can be large, the RC-time constant of the stack remains low because of very small cell resistances. The maximum energy stored within the capacitive electric field due to the double-layer charging effect is equivalent to:

$$E_{dl} = \frac{1}{2} C v^2(t) \tag{5.72}$$

where: E_{dl} is the energy stored due to the double-layer charging effect, C is the equivalent overall stack capacitance and $v(t)$ is the stack terminal voltage. The key point with regards to SOFC performance during rapid power changes is that the quantity of energy stored by the fuel cell is large, but is quickly dissipated during sustained up-power transients.

While the SOFC stack can respond to high frequency transients promptly due to its small time constant and high capacitance, the overall driver of SOFC power performance is dependent on fuel and oxidizer flows. During up-power transients, increased fuel and oxidizer must diffuse through anode and cathode material and chemically react. This process slows the ability of the SOFC to maintain power delivery during a rapid sustained transient, such as a step increase. This characteristic of SOFC performance is currently unavoidable. Here, a method was examined to mitigate the poor SOFC transient response performance. The power electronic control system was designed to slow load transients exhibited by the utility grid before sensed by the SOFC power plant. Additionally, a beneficial consequence of SOFC stack construction was noted, leading to a slightly higher peak capacity of the 1.0 MW SOFC power plant. Through simulations it was noted that, although rated for a nominal 1.0MW capacity, the peak capacity of 50 SOFC power modules is 1.188 MW, giving a slight margin for transient overshoot.

The primary purpose of the power electronics circuitry is to facilitate the conversion of DC electricity from the SOFC power plant to usable AC electricity for the utility grid. Integral to this design is the implementation of a control strategy that ensures the proper power flow management from the SOFC power plant to the utility grid. The controller must sense changes in grid demand and manipulate the SOFC plant output to meet the load. The use of feedback control has the effect of filtering demand transients and slowing the response of the SOFC plant, while ultimately matching its output to the power demands of the utility grid.

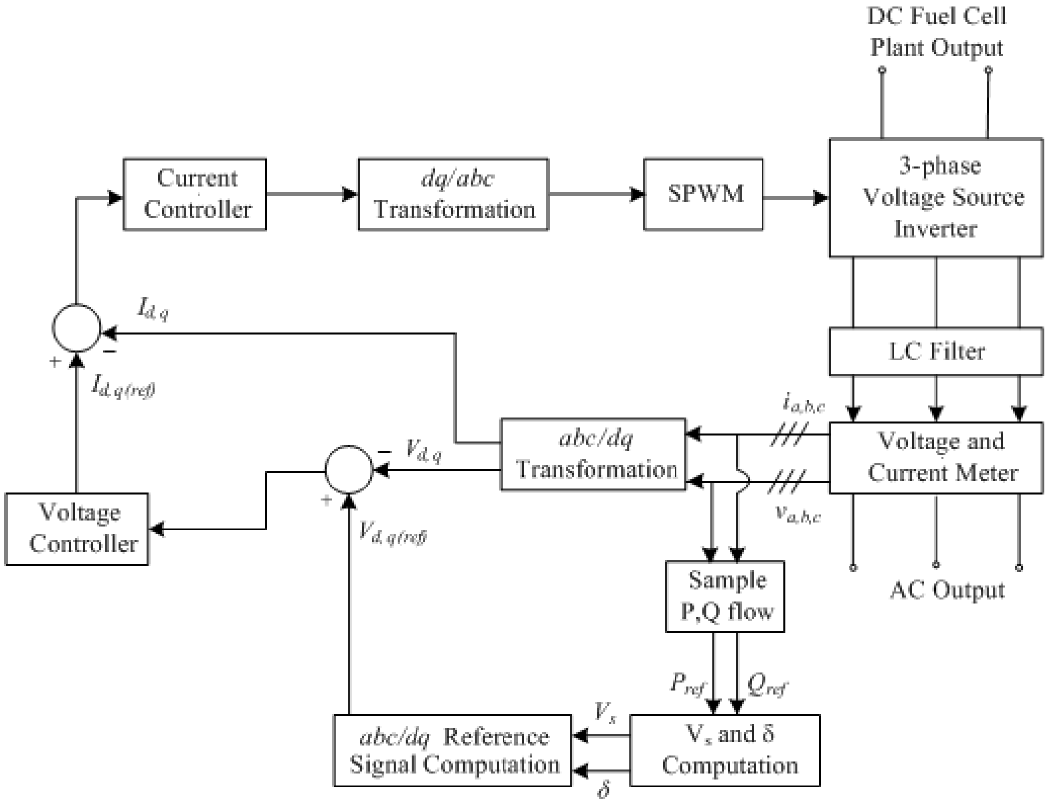

Figure 5.41. Block diagram of the SOFC power plant AC output control system.

The power electronic control circuitry is shown in Figure 5.41 and modifies the control scheme reported in [5.78]. In the figure, the three-phase AC utility bus voltage and current ($v_{a,b,c}$, $i_{a,b,c}$) are measured and transformed into *dq* values ($V_{d,q}$, $I_{d,q}$) through the "*abc/dq* Transformation" block. The real and reactive power demands of the utility grid (P_{ref}, Q_{ref}) are determined by sampling and filtering the balanced three-phase voltages and currents ($v_{a,b,c}$, $i_{a,b,c}$). It can be shown that, based on the *P* and *Q* demands (with power factor angle $\phi = \tan^{-1}(Q/P)$), the sensed utility grid voltage (V_r), and a known interconnection impedance (*Z*), a necessary generator "sending" voltage (V_s) and angle (δ) can be calculated from equations (5.50) and (5.51). It is noted that under balanced conditions $|V_r|$ is equal to each voltage $|v_{a,b,c}|$.

The $V_{d,q,ref}$ signal is created by performing an *abc/dq* transformation on the V_r and δ signals. This $V_{d,q,ref}$ is then compared with the $V_{d,q}$ signal to determine a voltage error signal. This error information is fed into a voltage regulator, which is modeled as a simple PI compensator. These current reference signals are compared with $I_{d,q}$ and the error signal is passed to the current controller, modeled as a simple PI compensator. The combined loop configuration forms a control system with an inner current control loop and outer voltage control loop, each with an independent PI controller.

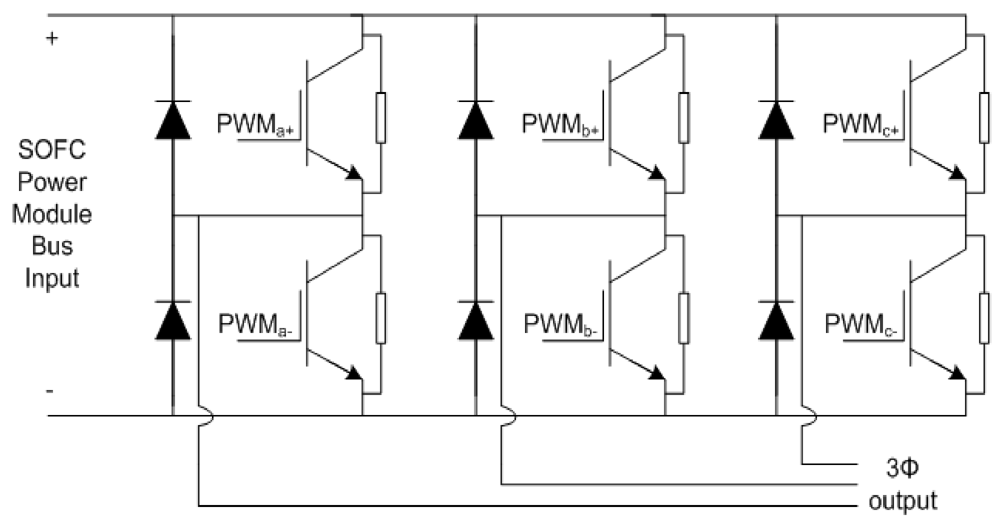

Figure 5.42. VSI schematic for three-phase DC/AC inverter.

The output signals from the current controller, shown in Figure 5.41, are transformed back into *abc* coordinates and used to control sinusoidal pulse-width modulator (SPWM) for proper pulses to the voltage source inverter (VSI) switches. The three-phase VSI has three arms, one for each phase; and each arm/phase has two power electronic switches. The SPWM signals ($PWM_{a,b,c}$) operates on a 4860Hz carrier frequency for control of the IGBT switch devices. The upper and lower switches in each arm are designated with + or –, and receive independent SPWM signals. The three-phase DC/AC VSI schematic is shown in Figure 5.42. This SPWM signal shapes the inverter output voltage for each phase sent to the utility interconnection.

Through simulation, it was shown that additional SOFC power modules improved the plant's margin when responding to large transients. Not only did total plant capacitance rise from added power modules, but when the plant experienced large up-power transients, the effect was spread over more stacks. By dispersing transients over a larger field of stacks, large and rapid changes to fuel and oxidizer flows were reduced. The ultimate effect of adding SOFC plant power modules was to boost the margin between nominal and rated operating conditions; and, this improved overall plant performance which could extend SOFC useful lifespan.

For the purpose of establishing benchmarks, the SOFC-CHP plant was operated interconnected with a utility grid. Although utility power was available to the local grid, this study focused on the ability of the SOFC-CHP power plant to meet the power and hot water demands of the 500-residence case study without requiring support from the utility. As with most generation sources, SOFCs have a region of operation that yields the highest conversion efficiency from fuel-to-electrical energy. It is clear that the economic advantage of operating the SOFC-CHP plant continuously at or near its most efficient operating point and providing excess real/reactive power to the utility is significant. However, while the obvious advantage of this alternative is to minimize transients on the

SOFC-CHP plant, it has the clear disadvantage of causing frequent power reversals across the point of common coupling (PCC). In a dynamic pricing environment where conventional and ancillary power economics can be utilized for dispatch decisions, the opportunity to apply power management optimization to SOFC-CHP plant control may exist. For example, when economically advantageous, the SOFC-CHP plant could provide voltage support by supplying reactive power to a weak radial feeder, or contribute real power for export. These opportunities and modes of power management will be explored further in microgrid discussions in later sections.

5.7.5 SOFC-CHP Thermal Recovery Design

The schematic of the SOFC-CHP thermal system used for benchmarking is shown in. The hot, gaseous exhausts from each SOFC plant stack are aggregated into a common exhaust header. This exhaust passes through a conventional cross-flow, shell-and-tube heat exchanger. The heat exchanger arrangement used takes advantage of unique SOFC exhaust characteristics. In conventional steam exhaust CC applications, exhaust used for work extraction is often at high temperature and pressure. This is not the case for SOFC applications. SOFC exhaust is at relatively high temperature under normal operating conditions (600-1000°C), but its pressure is near atmospheric. This complicates work extraction techniques, such as in a turbine, but is suitable for heat transfer operations in a heat exchanger. Thus, for the purpose of this study, hot exhaust streams resulting from SOFC operations are utilized in a CHP system for the production of residential hot water.

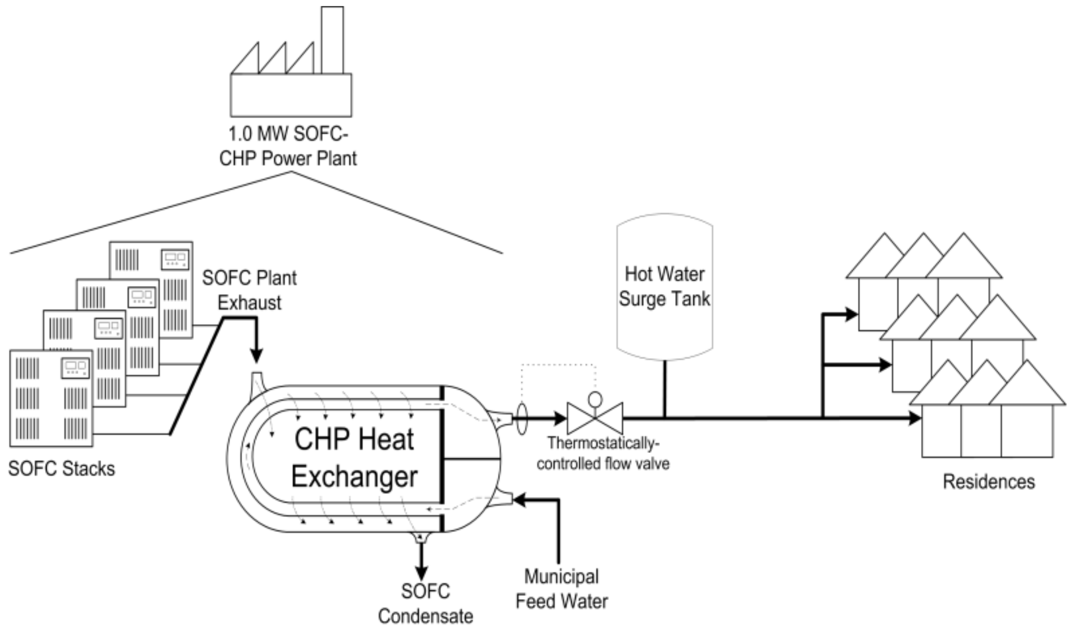

Figure 5.43. CHP system configuration for 1.0 MW SOFC-CHP power plant.

The high temperature exhaust stream passes through the heat exchanger shell and transfers heat to the cooler inner tubing containing the residential hot water, thereby heating it to specified temperatures. Feed water for the residential hot water is supplied to the cold inlet of the heat exchanger from the municipal water supply. It is assumed that the municipal feed water is supplied by underground piping and at a constant 13ºC (about 55ºF). The feed water is circulated around the u-shaped inner tubing of the exchanger by the pressure maintained by the water utility (between 40-80 psi), thereby eliminating the need for local booster pumps. After the SOFC exhaust passes through the heat exchanger transferring heat to the residential hot water, it is expelled to the environment at 200ºC. This value ensures an adequate margin above the saturation temperature (vaporization point) for water contained in SOFC exhaust and prevents pressure fluctuations inside the heat exchanger due to significant condensation.

In order to ensure a constant 50ºC (about 122ºF) hot water supply to the residences, two fluid system arrangements were considered. The first method, although not used for this study, is the more traditional method for producing hot water at desired temperatures by the use of a cold water mixing valve. In this arrangement, as SOFC exhaust heat varies, the quantity of heat transferred in the exchanger varies, but feed water flow through the heat exchanger depends solely on residential demand at the time. As a result, the feed water may become too hot (or too cold) for residential delivery, because of the competing factors: residential hot water demand and SOFC exhaust heat flow. Given these factors, hot water within proper temperature limits must be delivered to the residential customer and is done so by mixing the variable temperature hot water with cooler feed water prior to entering the home. The drawbacks of this arrangement are complexity, inefficiency, and potential periods when residential demand exceeds the heating capability of the SOFC-CHP system.

The alternative fluid system arrangement, used for benchmarking here, is simpler and is shown in Figure 5.43. In this fluid system, a thermostatically-controlled flow valve varies the flow rate of feed water through the heat exchanger. The flow valve controller senses water temperature at the outlet of the heat exchanger and commands valve position, thereby controlling feed water flow. In this manner, the flow valve operates independently of residential hot water demand, at all times maintaining the customer's water temperature at a constant 50ºC. Therefore, if more SOFC exhaust heat is available, the flow valve opens to raise feed water flow rate. If this increased flow is not demanded by residential customers at the time, excess hot water fills the insulated surge tank. As SOFC exhaust heat drops, the flow valve throttles less feed water through the heat exchanger. Correspondingly, if instantaneous demand is higher than the output of the heat exchanger, the surge tank is drawn down. Key to this system arrangement is an appropriately-sized surge tank and heat exchanger to ensure hot water sustainability. In this study, the heat exchanger was designed according to SOFC exhaust parameters [5.79]. The surge tank volume was set at 17,000 gallons, a size reasonable for installation in a residential neighborhood, which is roughly the volumetric capacity of two 18-wheel tanker trucks.

The thermodynamics of the CHP system are described by (5.73) through (5.75) [5.80]. This system arrangement eliminates the possibility of boiling feed water inside the heat exchanger by constantly monitoring hot water outlet temperature and adjusting feed flow rate accordingly.

$$\Delta\dot{Q}_H = \Delta\dot{Q}_C \tag{5.73}$$

$$A\left(T_{outlet} - T_{condensate}\right) = \dot{m}_{feed} \cdot c_{p,HW}\left(T_{HW} - T_{feed}\right) \tag{5.74}$$

$$A = \dot{m}_{SOFC\ exhaust} \cdot c_{p,exhaust} = \sum_{\substack{exhaust \\ components}} \dot{m}_i \cdot c_{p,i} \tag{5.75}$$

where, $\Delta\dot{Q}_H$ is the SOFC exhaust process heat transfer rate, $\Delta\dot{Q}_C$ is the residential hot water (*HW*) process heat transfer rate, A is the sum of the mass flow rates ($\dot{m}_i$) for each SOFC exhaust stream constituent, times the corresponding specific heat capacity ($c_{p,i}$),

T_{outlet} is the uniform exhaust temperature, $T_{condensate}$ is the uniform condenser exhaust temperature, $\dot{m}_{feed}$ is the feed flow rate controlled by the flow valve, $c_{p,HW}$ is the municipal supply feed water specific heat capacity, T_{HW} is the heat exchanger hot water outlet temperature setpoint (60ºC, see below), and T_{feed} is the feed water temperature. When supplied by atmospheric air and hydrogen fuel, SOFC exhaust gases are: water, oxygen, nitrogen, and unconverted hydrogen.

For this CHP system, three primary parameters (SOFC exhaust mass flow rate, exhaust temperature, and feed water flow rate) vary, but must remain balanced thermodynamically. As residential hot water demand varies with use patterns, the surge tank level changes based on the difference between feed water flow rate and demand, shown in equations (5.76) and (5.77).

$$\dot{m}_{surge\ tank} = \dot{m}_{residential\ HW} - \dot{m}_{feed} \tag{5.76}$$

$$l_{surge\ tank} = l_{nominal} + L_c \int_{t_0}^{t_f} \dot{m}_{surge\ tank} \tag{5.77}$$

where, $\dot{m}_{residential\ HW}$ is the mass flow rate of residential hot water demand, $\dot{m}_{surge\ tank}$ is flow rate out of or into the surge tank (positive value is flow out, negative if flow in), $l_{surge\ tank}$ is surge tank water level, $l_{nominal}$ is surge tank initial level, L_c is a conversion factor from mass of water to a proportional volumetric quantity within the surge tank, and t_f and t_0 represent the time values for integration.

It is noted that three primary mechanisms of heat transfer to the environment are considered for CHP system design. First, based on shell and tube design, heat is inevitably lost through the heat exchanger shell. This heat conduction to the ambient air surrounding the exchanger surface is modeled with traditional Newton's cooling laws [5.80]. Second, hot water energy is transferred as heat to supply piping, the surge tank wall, and components that link the SOFC-CHP plant to the residences. This heat loss, primarily by radiative and conductive means, is modeled as 15% of the energy content of the hot water supply. Additionally, heat loss that numerous homes in the United States experience through non-insulated hot water distribution piping is accounted for by simulating as much as a 10ºC (18ºF) temperature drop from where supply piping enters an individual residence and the hot water point-of-use. Correspondingly, the supply temperature set point, based on temperature sensed by the thermostatic flow control valve at the heat exchanger outlet, is set at 60ºC (140ºF).

5.7.6 SOFC-CHP Balance of Plant (BOP)

The SOFC-CHP plant requires secondary subsystems to maintain its proper operation, as described in 5.7.2 . These systems include reagent pre-heating, compressor operations, fuel processing, etc. Typically, the comprehensive analysis of these total system operations is referred to as BOP. Unfortunately, for the few commercially available SOFC systems, details of their support subsystems are not available. However, while these details are not able to be modeled with specificity, the thermodynamics required to support SOFC systems can be. Therefore, preconditioning subsystems needed to operate the SOFC stacks are dynamically modeled in parallel with CHP analysis.

Heat transfer required to conduct pre-heating and fuel-conditioning for anode reagents, as suggested by [5.81] and [5.82], is derived from regenerative heat exchange using a portion of exhaust gases. Although not a true CHP process, by feeding back some exhaust heat to prepare anode reagents for electrochemical conversion in the SOFC stack, significant energy is retained within the system. Regenerative heating significantly improves overall system efficiency and is commonly used in industrial practice, therefore it is considered in the total SOFC-CHP system BOP analysis. Similarly, atmospheric air applied to the cathode is regeneratively pre-heated. Although, some SOFC systems allow cathode reagents at ambient temperatures to be warmed internally within the SOFC [5.81], in this simulation study, supply air is heated to approximately 400ºC prior to use in the SOFC stack, thereby limiting electrochemical performance degradation and avoiding significant thermal shock. The overall support system heat transfer balance is given by:

$$\Delta\dot{Q}_{exhaust} + \Delta\dot{Q}_{input} = \Delta\dot{Q}_{preconditioning} \tag{5.78}$$

where: $\Delta\dot{Q}_{exhaust}$ represents the heat transferred from SOFC exhaust to the preconditioning process; $\Delta\dot{Q}_{input}$ represents the additional heat that must be transferred to the input air steam for preheating, supplied by an exterior source such as auxiliary element heaters; and $\Delta\dot{Q}_{preconditioning}$ is the total amount of heat that must be transferred to SOFC reagents for proper operation.

5.7.7 Hybrid SOFC-CHP Simulations

The aggregate end-use, time-of-day load curves based on seasonal usage patterns in the Pacific Northwest region of the United States for all-electric homes, shown in 5.10.1 and 5.10.2 , were used for the benchmark study; that is, utilizing electric appliances, electric heating and ventilation, and electric water heaters (EWH). In order to develop comparative results, two cases were simulated: total aggregated end-use profiles with EWHs included and total aggregated end-use with EWHs omitted. These cases allowed the performance of the SOFC-CHP plant to be evaluated relative to the performance of conventional electrical generation for supplying power and hot water to residences. As residential loading is not considered to operate at a significant non-unity power factor associated with large inductive loads such as three-phase motors or induction furnaces seen in industrial facilities, the residential power factor was set at 0.95 lagging. Real power followed end-use electricity consumption and, correspondingly, the total apparent power consumed at any time was the vector quantity of real and reactive power.

Simulations with the SOFC stacks under constant hydrogen fuel flow were conducted for four scenarios, weekdays and weekends during the summer and winter. The fall and spring scenarios are less extreme than the winter and summer profiles, and are omitted. Figure 5.44 and Figure 5.45 show two seasonally representative daily profiles (winter weekday and summer weekend) for real/reactive power supplied to the residential neighborhood by the SOFC-CHP plant. Simulations were performed on a singular 24-hour basis and do not take into account previous or following day conditions. At the start of each simulation day, the SOFC-CHP plant is modeled in hot-standby mode, e.g. the plant is operating within its nominal temperature, pressure, and flow limits, but loading is zero. Hence, Figure 5.44 and Figure 5.45 show that reactive power is slow to rise to its demanded level at the beginning of the day and real power overshoots its demanded level due to the large step change of loading commanded at the simulation start.

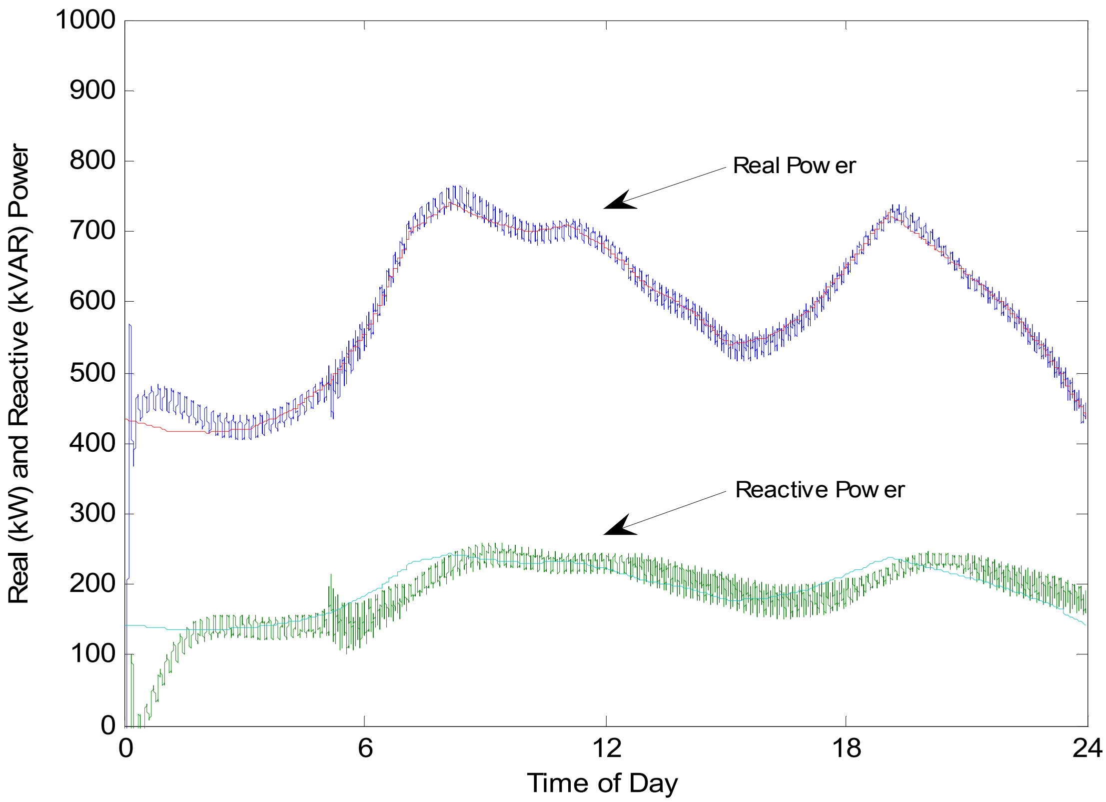

Figure 5.44. Real and reactive power dispatch for the SOFC-CHP power plant in Pacific Northwest 500-home winter weekday load demand scenario.

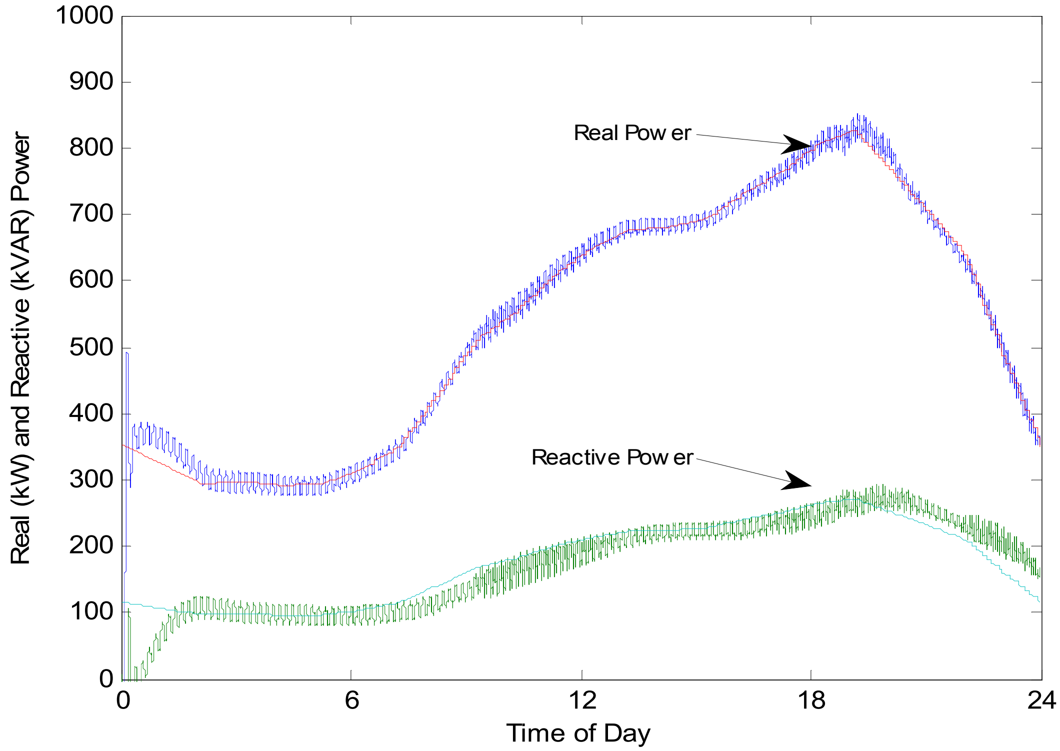

Figure 5.45. Real and reactive power dispatch for the SOFC-CHP power plant Pacific Northwest 500-home summer weekend load demand scenario.

Simulation results demonstrate that residential water demand under each seasonal scenario is met strictly by waste heat produced from SOFC stack operation. Figure 5.46 and Figure 5.47 show two typical daily profiles for residential hot water supplied by the SOFC-CHP plant. Annotated on each figure are residential hot water demand, the available hot water supply, and the insulated surge tank level throughout the simulated day. For all simulations, the initial surge tank level is set at 10% full; and, as described above, do not take into account previous or following day conditions. Figure 5.46 and Figure 5.47 show that the SOFC-CHP plant adequately meets all customer time-of-use hot water demands. Clearly, the daily surplus of hot water in the surge tank indicates that more heat is available from the CHP system than is transferred to the residences.

Additionally, this shows the potential for additional cost savings by expanding the excess CHP hot water service to loads such as: radiant heating, offsetting electricity consumed in space heating, generating process steam, or in other low temperature applications. The SOFC-CHP delivery of hot water is an extremely attractive sustainable alternative considering that otherwise, plant exhaust heat would be expelled to the environment without benefit and additional electricity would be consumed heating domestic hot water.

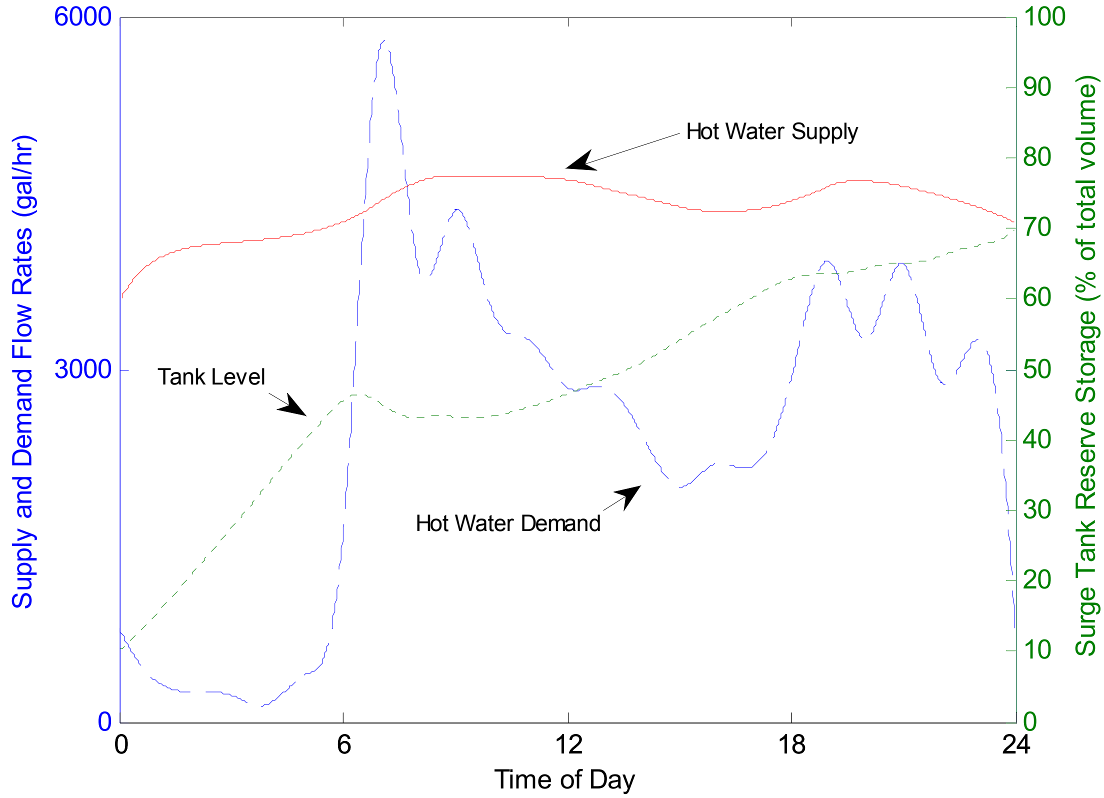

Figure 5.46. Domestic hot water capacity and demand for the SOFC-CHP power plant in a Pacific Northwest 500-home winter weekday demand scenario.

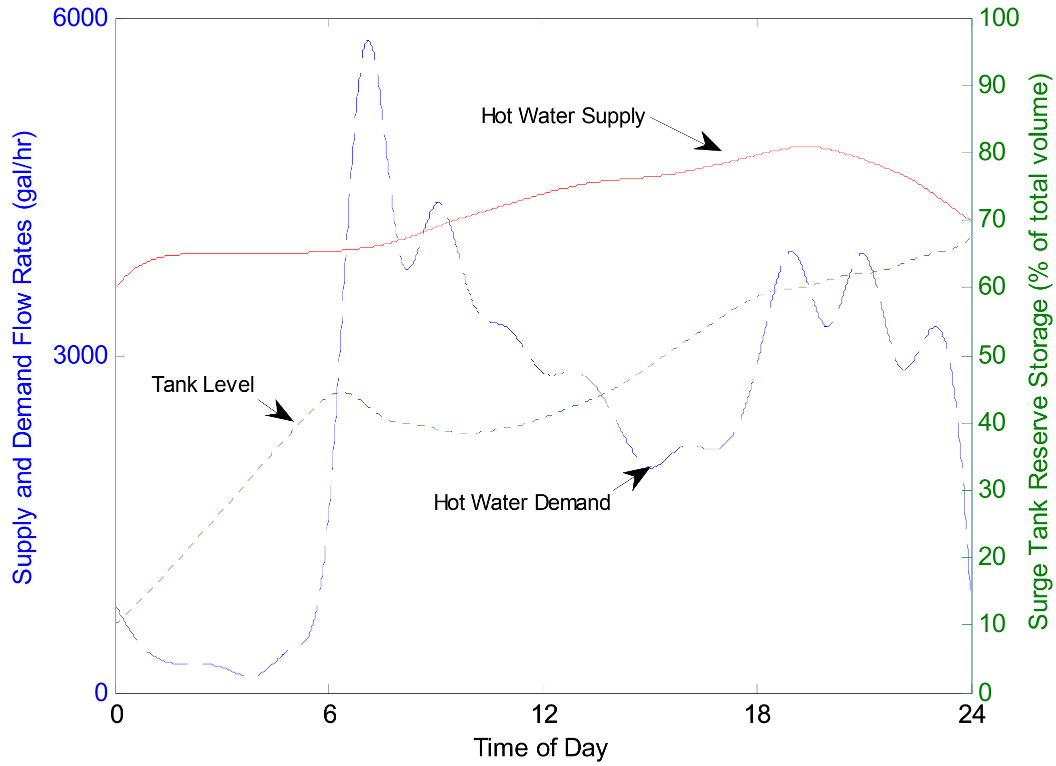

Figure 5.47. Domestic hot water capacity and demand for the SOFC-CHP power plant in a Pacific Northwest 500-home summer weekend demand scenario.

There are two primary advantages for customers who are supplied electricity and domestic hot water from the proposed SOFC-CHP system. First, it is interesting to note that periods of high residential electricity consumption correspond very closely to times of peak hot water usage. This is a significant observation, albeit not unexpected based on domestic habits, but was very consistent for all data reviewed for this study. Due to the strong correlation between periods of peak power and hot water demand (e.g. 8:00 a.m.), reducing the electrical load from EWHs at these times can be dramatic. When considered as a component of total residential demand, EWHs comprise about 11% of installed load [5.83]. However, as shown in Table 5.7, EWHs can make up about 35% of total residential load at times of peak demand. This highlights an obscured benefit of CHP capability: nearly a quarter of average residential electric load can be cut by heating water via CHP, but more dramatically, CHP can reduce residential electrical demand by over a third during the most stressful periods for grid operation.

Table 5.7. Peak end-use demand reduction by CHP in lieu of EWH.

Season	On-peak Average Demand Reduction†	Largest Demand Reduction Percentage (Time-of-Day)
Winter Weekday	27.7%	34.8% (8:00am)
Winter Weekend	26.4%	35.1% (11:00am)
Summer Weekday	24.2%	35.2% (8:00am)
Summer Weekend	24.3%	33.6% (10:00am)

† Peak times-of-day are defined as: 6:00-12:00 a.m. and 5:00-10:00 p.m.

Eliminating significant residential electrical demand during periods of peak grid loading can reduce the need to operate peaking generation plants. Often peaking plants are fossil-fueled, typically coal-fired; reducing peak demand can have a dramatic effect on the per-unit production of environmental emissions and the cost of dispatching these plants [5.84]. In other words, the incremental reduction of electrical load at times of peak demand has a far greater impact on cost and environmental emissions. Primarily, this is due to the expense of operating dirtier plants in inefficient modes to meet demand unmet by base load dispatch. Alternatively, the proposed SOFC-CHP plant assists the power system in two critical ways: during peak demand, leveling the load curve by eliminating EWH power consumed; and, throughout the day, raising overall efficiency by producing power and hot water more sustainably than generators that combust fossil fuels.

The Pacific Northwest region of the United States has a unique blend of generation sources in operation. The Northwest Power Pool Area (NWP), a sub-region of the Western Electricity Coordinating Council (WECC), primarily utilizes hydroelectric power for base load following and supplements base capacity with conventional coal-fired power. Throughout the year, roughly 50-75% of total generated power comes from hydroelectric dams, 30-50% from coal-fired, and 5-15% from other sources, depending on time-of-day [5.85]. Almost exclusively, coal-fired steam and fossil fuel-fired combined-cycle plants make up NWP peaking capacity. By contrast, the East Central Area Reliability Coordinating Agreement (ECAR) region of the U.S. relies on coal-fired plants for nearly 70-85% of base load and almost 100% of peaking supply during both summer and winter [5.85]. Clearly, significant base generator fossil fuel combustion could be offset by the deployment of SOFC-CHP plants, along with large reductions of the dirtiest generation at times of peak electrical loading. Based on this observation, a comparison is drawn between the regional use of conventional generation and generation by a SOFC-CHP plant for the residential study.

For the purpose of this comparative analysis, a simplified avoided-cost model was applied to the NWP and ECAR regions. First, it is difficult to obtain information that quantifies the portion of regional generation that is on-line due to peaking requirements on any given day. Additionally, because dispatch planning is performed prior to the operational period and peaking plants can be brought on-line in times of extremis, it is difficult to make predictions about the proportion of base-loaded versus peaking generation that is offset by operating a SOFC-CHP distributed generation plant. For example, because the Pacific Northwest primarily uses hydroelectricity for load following, on a particular day that does not require peaking plant dispatch, reducing residential demand at peak times only shrinks the amount of hydroelectricity produced. On a different day, if peaking plants are needed, operating the SOFC-CHP plant may predominantly reduce peaking coal-fired plant operations. This dynamic phenomenon varies between regions, as well; unlike in the NWP, any reduction of ECAR loading lowers demand upon coal plants. To account for this effect, this study uses the blend of base and peaking generation operated throughout the year accounted for by regional annual average costs and emissions data. This information is summarized in Table 5.8 and Table 5.9 [5.86], but it is noted that the results shown underestimate both avoided costs and emissions because of the peaking effect described above. Interestingly, Table 5.9 shows that, although the average regional per kW-hr cost is roughly the same between the NWP and ECAR, CO_2 emissions from ECAR generation are almost twice those of the NWP. This reflects the low cost of hydroelectric and coal-fired generation, and the difference of environmental impact between the two sources. The two regions analyzed had some of the lowest electricity costs for residential consumers; below the U.S. average cost of \$0.0945/kW-hr and about half of the cost of electricity in New England (\$0.1344/kW-hr) [5.87].

Table 5.8. Regional generation, emissions, & cost data – 2005 [5.86].

State	Total Generation (MWh)	Total CO_2 Emissions (millions metric tons)	Electricity Cost ($/kWh)†
NWP Subset			
Idaho	10,824,984	0.6	$0.0629
Montana	27,938,778	19.3	$0.0810
Oregon	49,325,003	8.2	$0.0725
Utah	38,165,131	35.9	$0.0752
Washington	101,965,850	14.1	$0.0654
Wyoming	45,567,307	43.4	$0.0748
ECAR Subset			
Indiana	130,371,573	122.6	$0.0750
Kentucky	97,822,419	92.6	$0.0657
Michigan	121,619,771	75.9	$0.0840
Ohio	156,976,323	133.0	$0.0851
W.Virginia	93,626,285	85.3	$0.0621

† Electricity cost for delivery to the residential consumer.

Table 5.9. Regional average emissions and cost data – 2005 [5.86].

Regional Subset	CO_2 Emissions per Generation (metric tons/kWhr)	Electricity Cost ($/kWhr)†
NWP	4.437×10^{-4}	$0.0720
ECAR	8.484×10^{-4}	$0.0744

† Electricity cost for delivery to the residential consumer.

Based on this data and simulation results, the SOFC-CHP power plant allowed each home to eliminate purchases of 3113.4 kWhrs per residence, per annum, from the utility grid. Further, significant emissions were avoided, as annotated for the entire 500-

home neighborhood in Table 5.10. While not considered here, it is noted that other factors such as fuel costs, the capital cost of implementing a power plant, and other expenses vary dramatically between regions and between technologies. Table 5.10 allows data from the NWP and ECAR regions to be compared directly to the SOFC-CHP plant in terms of avoided costs. Clearly, operation of the proposed SOFC-CHP plant avoids significant costs and emissions in the two regions examined.

Table 5.10. Annual savings & avoided emissions with SOFC-CHP.

	NWP	ECAR
Total Operational Cost Savings ($)	$112,084	$115,820
Avoided CO_2 Emissions (tons of CO_2)	690.7	1320.7
Avoided SO_2 Emissions (tons of SO_2)†	5.5	
Avoided NO_x Emissions (tons of NO_x)†	2.1	

† State-specific SO_2 and NO_x emissions information is not available. In lieu of this data, U.S. national averages of 3.53826×10^{-6} and 1.35542×10^{-6} tons per kWh of SO_2 and NO_x, respectively, are used [5.86]. It is noted that use of national averages suppresses emissions impact within the ECAR region and inflates it in the NWP due to their varying reliance on fossil fuels for power.

DER systems, implemented in communities around the nation, are coming. These DERs will be on the scale of 5 MW or less and will be collocated with residential, commercial, and small industrial centers. Here, the methodology, operation, and simulation of a large-scale 1.0 MW SOFC-CHP power plant has been discussed for the purpose of illustrating the type of system that may potentially form the backbone of a decentralized power system comprised of networked DERs. This analysis has demonstrated the feasibility of such as system, and emphasized the improved total system efficiency and emissions reductions they can yield. The simulation results show that for a straight-forward residential case, hundreds of tons of carbon, sulfur, and nitrogen oxide emissions are avoided by reducing demand from conventional, large scale centralized power sources being used today. The benefits, however, go beyond sustainability improvements; it has been shown that the SOFC-CHP plant can have dramatic impacts for both on- and off-peak residential loading, including a reduction of over a third of residential electricity demand at key peak times. This is in addition to a total demand decrease of over 20% annually which is far more than the reported 11% component of average residential loading due to EWHs. The SOFC-CHP system discussed here is a viable example of the type of coupled asset system that will be attractive for microgrids, and therefore, is included in the asset library of this chapter.

5.8 Storage Battery

Storage systems can add significant value to a power subsystem. Besides offering a reservoir of energy for periods of no or low generation, the storage system may serve as a sink for excess energy when a surplus is available. In many applications, aspects of storage system performance are not fully exploited for the purpose of optimizing operation. Two examples of this include round-trip efficiency and storage operational cost. In the case of round-trip efficiency, if considered at all, storage dispatch decisions often use constant average approximations for efficiency, without deference to charge or discharge operation. Clearly, this can introduce errors when calculating how to best dispatch the storage system. Likewise, operational cost is rarely used as a means for assessing storage system performance, and may then only rely on averages. A narrow approach that neglects these factors may also degrade operational performance in real-time, ultimately negatively affecting battery health and longevity. In other words, how a battery system performs over its lifetime is highly dependent upon how it is operated in real-time during each charge and discharge cycle. By using factors such as round-trip efficiency and operational cost, this decision-making process can be improved.

For microgrids there are broader opportunities to integrate locally assigned objectives for power management than exist in conventional utility-supplied end-use applications. However, in order for storage to significantly improve the pursuit of these objectives, additional means of formulating desired performance information must be developed. The following section intends to highlight the importance of cycle-to-cycle round-trip efficiency which can influence battery health and lifespan, as well as the operational cost of storage systems. These factors can improve power and energy management decision-making for hybrid and microgrid applications. Additionally, a method for determining a lead-acid battery model directly from manufacturer data sheets and using this incremental battery models for the purpose of exploring on-line round-trip efficiency and operational cost considerations is shown.

5.8.1 Lead-acid Battery Model

Many hybrid system or microgrid management decisions must be made very quickly given rapidly changing conditions, such as load demand or generation supply, that influence the various systems operating in conjunction. For this purpose, many well-accepted battery system models are inadequate or lack sufficient detail to simulate parameters necessary for a focus on storage system performance. Subsequently, the following has been developed to allow the iterative computation of storage parameters that can be used effectively in real-time power management studies of comprehensive microgrid systems.

For over 100 years, lead-acid batteries have been the most prolific battery storage technology, especially for power system applications [5.88]. Until very recently, lead-acid battery storage systems have been the least costly solution for large scale stationary applications [5.89]. While well understood, there exist a myriad of models available for simulating battery operation, e.g. [5.90, 5.91, 5.92, 5.93]. Unfortunately for the researcher, many battery models rely on laboratory experiments to fit the model to acquired data. This complicates the use of battery models because often the researcher only has battery manufacturer specification or data sheets as guides about battery parameters. In the case of [5.94], a model was developed using manufacturer's data for PSPICE applications. In this paper, the authors have adapted a commonly used lead-acid model, described in [5.95], for the purpose of representing lead-acid battery operations in an iterative computational environment, such as for real-time energy and power management simulations. The model explained below adequately simulates lead-acid battery operation to provide information to an exterior decision-making algorithm which seeks to optimize battery system operations, complementing other assets in a hybrid system or microgrid. Additionally, it is desirable for the process to be repeatable to derive different battery models for many manufacturers, battery sizes, and specifications. Therefore, the following is proposed, drawing upon techniques of [5.95] and [5.96], briefly described below, to achieve this goal.

Initializing the lead-acid battery model requires data from the manufacturer's data sheet to be fit to a capacity function [5.95], shown in (5.79). Using various temperatures, discharge currents, and capacity data points given by the manufacturer, (5.80) and (5.81) may be used to determine the coefficients of (5.79).

$$C(I_t,\theta) = \frac{K_c C_{0*}\left(1+\dfrac{\theta}{-\theta_f}\right)^{\varepsilon}}{1+(K_c-1)\left(\dfrac{I_t}{I_t^*}\right)^{\delta}} \tag{5.79}$$

$$\varepsilon = \alpha(\theta_n - \theta_f) \quad \text{where} \quad \alpha = \frac{1}{C(I_t^*,\theta_a)}\left(\frac{\partial C(I_t^*,\theta)}{\partial \theta}\right) \tag{5.80}$$

$$K_c = \left[\left(\frac{I_t}{I_t^*}\right)^{\delta} - 1\right]\left[\left(\frac{I_t}{I_t^*}\right)^{\delta} - \frac{C_{0*}\left(1+\theta_a/-\theta_f\right)^{\varepsilon}}{C(I_t,\theta_a)}\right]^{-1} \tag{5.81}$$

where, $C(I_t,\theta)$ is the battery capacity [Ah] that varies with terminal current I_t and temperature θ; C_{0*} is the battery capacity [Ah] at rated current at 0°C given by the manufacturer or interpolated; I_t^* is the nominal rated battery current [A] given by the manufacturer, typically the 0.1C (10-hour) rate, positive in the charging direction; K_c and δ are empirically determined coefficients based on various discharge currents and manufacturer reported capacities using (5.81); α is the battery temperature coefficient [°C^{-1}] given by the manufacturer; ε is the battery temperature-capacity coefficient; θ_n is the nominal rated battery temperature [°C] given by the manufacturer; θ_f is the battery rated freezing temperature given by the manufacturer or assumed to be about -30°C; and θ_n is nominal ambient temperature [°C] given by the manufacturer or assumed to be 25°C.

It is common for battery specification sheets to give performance data for varying discharge rates, an example of which is shown in Figure 5.48. However, manufacturers do not provide information about battery voltage recovery upon termination of discharge, which is a key detail for many reported battery modeling techniques that specifically require open-circuit, post-discharge recovery information to determine certain parameters. In lieu of this data being provided in the specification sheet, some assumptions may be made. For example, after a discharge, the open circuit voltage of a lead-acid battery may be reliably predicted, as shown in [5.96], varying approximately 0.2V/cell from fully-charged to fully-discharged. This voltage difference, about 9% of open circuit voltage when fully-charged, may vary slightly depending on lead-acid technology, e.g. vented, valve-regulated, etc.

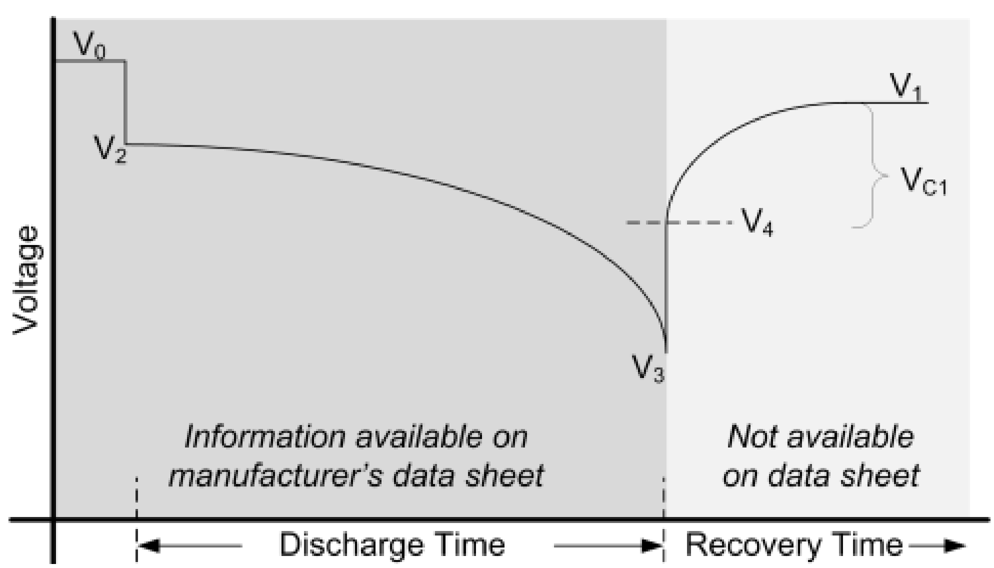

Figure 5.48. Example of discharge curve information shown on a lead-acid battery data sheet, along with post-discharge recovery information often not available.

Information from discharge graphs, such as Figure 5.48, yield information for the lead-acid battery circuit model, shown in Figure 5.49 [5.95]. The circuit model annotates the simulated electrical components that represent battery operation described in the figure. For the purpose of simulation, battery parameters are calculated on an incremental basis. Each computational increment represents a time step determined by the simulation initialization. This method allows the battery to be simulated incrementally in "real-time" alongside other similarly constructed asset models, which is especially pertinent to the multi-objective tasks of microgrid power management.

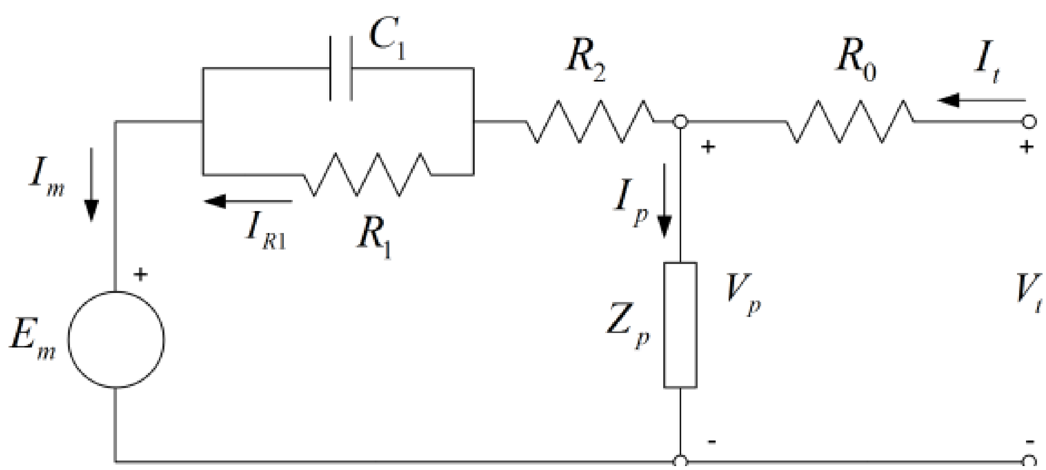

Figure 5.49. Lead-acid battery circuit model.

The third-order circuit model shown in Figure 5.49 is comprised of a series terminal resistance (R_0), a shunt parasitic branch (Z_p), and a main branch composed of a series resistance (R_2) and an RC block (R_1 and C_1 in parallel). Although post-discharge information is rarely available on manufacturer sheets (shown in Figure 5.48), using specifications usually provided allows all relevant voltages shown in Figure 5.48 and Figure 5.49 to be derived directly from manufacturer data, as shown in Table I.

Table 5.11. Voltage equivalent values.

Voltage (Figure 5.48)	Value (Figure 5.48, Figure 5.49)
V_0	$= E_{m0} = V_{OC(open\ circuit), fully-charged}$
V_1	$= V_{OC, post-discharge} = E_{m0}\left[1 - 0.09(1 - SOC)\right]$
V_2	$= V_{t, initially-loaded}$
V_3	$= V_{t, end-of-discharge}$
V_{C1}	$= V_{C0} e^{-\left(\frac{t}{R_1 C_1}\right)}$
V_4	$= V_1 - V_{C0}$

where, E_{m0} is the battery internal voltage when fully charged; V_{C1} is the time-varying voltage across C_1; and V_{C0} is the voltage across C_1 at the instant of post-discharge open-circuiting. Clearly, V_1 is dependent upon how much energy has been released by the battery, represented by a measure of state-of-charge (SOC), which will be discussed further below.

Using the voltage data derived from the specification sheet, the parameters for terminal series resistance (R_0) and main branch series resistance (R_2) can be found by analyzing the instantaneous voltage changes that occur upon initial loading (between V_0 and V_2) and upon stopping discharge (between V_3 and V_4). At these instances, the voltage changes are solely attributed to the voltage drops through R_0 and R_2. In each discharge case, the parasitic loss current (I_p) is very small and I_t can be considered to be flowing ($I_m \approx I_t$) through both R_0 and R_2. In the case of R_0, it varies with SOC, while R_2 only plays a significant role during charging operations and varies with both SOC and I_m, each shown in (5.85) below. Similarly, using information about V_{C0} at a constant discharge at 0.1C, the parameter R_1 may be found. While the battery recovers from the discharge on open-circuit, C_1 discharges through R_1, yielding a small, decreasing voltage, V_{C1} that reduces V_t. As C_1 discharges, the terminal voltage rises to post-discharge battery internal voltage V_1. In the case of R_1, it varies by the status of charge relative to the rated capacity given the discharge history during the unique cycle, shown in (5.84). In other words, the higher the discharge current demanded from the battery, the lower the actual capacity the battery can yield during that cycle. It is noted that, based on convention, discharging yields currents represented by $-I_m$ and $-I_t$. As discussed in [5.96], it is clear that the discharge current prior to the open-circuiting has an effect on the magnitude of V_{C0}. Although slightly different for each lead-acid battery, the empirical relationship between the 0.1C (10-hour) rated discharge rate for the battery and the resulting V_{C0} at the termination of discharge has been found to follow:

$$V_{C0} = a_1\left(\frac{I_t}{I_{t,0.1C}}\right) + a_2 \tag{5.82}$$

$$R_0 = R_{00}\left[1 + A_0(1 - SOC)\right] \tag{5.83}$$

$$R_1 = -R_{10}\ln\left[1 - \left(1 + (K_c - 1)\left(\frac{I_{R1}}{I_t^*}\right)^{\delta}\right)(1 - SOC)\right] \tag{5.84}$$

$$R_2 = R_{20} \frac{e^{A_{21}(1-SOC)}}{1+e^{A_{22}\left(\frac{I_m}{I_t^*}\right)}} \tag{5.85}$$

where, $I_{t,0.1C}$ is the 0.1C (10-hour) rated discharge rate of the battery; a_1 and a_2 are empirically determined coefficients that work well across a range of lead-acid batteries, 0.0183 and 0.0571, respectively; R_{00} is the battery terminal series resistance at full charge; A_0 is a model specific coefficient; R_{10} and R_{20} are base main branch resistances; and A_{21} and A_{22} are model-specific constants. The constant 0.1C rate discharge information is furthermore valuable as it may be assumed that the SOC is <10% upon termination. Using commonly available discharge information, such as the 0.1C and 1C rates shown on the battery manufacturer's specification sheet, R_0 and R_2 may be found according to Table 5.12 and Table 5.13. Often the manufacturer's specification sheet does not have enough detail to provide data to precisely fit the A_{21} and A_{22} parameters, but $A_{21} \approx A_{22} < -5$ has been found to work well.

Table 5.12. Finding circuit resistances at 100% SOC from manufacturer discharge data.

Value	**1C (SOC = 100%)†**	**0.1C (SOC = 100%)†**
Voltage Drop	$V_0 - V_2 = R_0 I_{t,1C}$	$V_0 - V_2 = (R_0 + R_2) I_{t,0.1C}$
R_0	$= R_{00}$	$= R_{00}$
R_2	≈ 0	$= R_{20}\left(1+e^{A_{22}\left(\frac{I_{t,0.1C}}{I_t^*}\right)}\right)^{-1}$

†: by convention, It is negative during discharge.

Table 5.13. Finding circuit resistances at end of discharge from manufacturer data.

Value	**0.1C (SOC < 10%)†**
Voltage Drop	$V_4 - V_3 = \left(R_0 + R_2\right) I_{t,0.1C}$
R_0	$= R_{00}\left[1 + A_0(1 - SOC)\right]$
R_2	≈ 0
A_0	$A_0 = \left(1 - SOC\right)^{-1}\left(\frac{V_4 - V_3}{R_{00} I_t} - 1\right)$
Voltage Drop	$V_{C0} = R_1 I_{t,0.1C}$
R_1	$= -R_{10}\ln\left(\approx 10\%\right)$

†: by convention, It is negative during discharge.

Using these predetermined model parameters, the incremental computation of battery operation may be performed. At the outset of each computational increment, the battery terminal current (I_t) is sensed, along with battery SOC remembered from the previous increment. First, R_0 according to (5) is found. The parasitic branch current (I_p) and main branch current (I_m) are found next according to (5.86) and (5.87) below. Parasitics play their biggest role when charging when V_t rises sufficiently above E_m to compel current reversal in the main branch, leading to $+I_t$ and $+ I_m$ flow from the terminals to E_m. Two observations lead to a modification of the I_p calculation (5.86) from [5.97]. First, the maximum terminal voltage ($V_{t,max}$) allowable during charging operations, typically specified on manufacturer's data sheets, that will avoid battery damage is approximately 2.5V/cell. Second, when the battery approaches fully charged, E_m approaches E_{m0}. Therefore, when charging, V_p is bounded by $V_{t,max}$ and E_{m0}; and the $R_0 I_t$ maximum is about +0.5V/cell. These observations are reflected in (5.86). A scaling factor, a_3, allows parasitic current to be adjusted based on the 0.1C rated current of the battery.

$$I_p = \left(R_0 I_t + E_m\right)\left(\frac{I_{t,0.1C}}{a_3}\right) G_{p0} e^{\left(\frac{(R_0 I_t + E_m)}{V_{p0}} + 2\left(1 - \frac{\theta}{\theta_f}\right)\right)} \tag{5.86}$$

$$I_m = I_t - I_p \tag{5.87}$$

where, G_{p0}, an admittance constant is equal to $2 \times 10^{-12}\ \Omega^{-1}$ [5.95]; V_{p0}, a voltage constant equal to 0.1V [5.95]; and a_3 is the scaling factor equal to 50A which works well for a range of battery capacities. The parasitic branch accounts for irreversible battery reactions, including battery water electrolysis, that draw current (I_p), but do not participate in storage energy transfer. Calculating I_p by (5.86) improves upon methods that assume a constant V_p value across the parasitic shunt.

The next calculations, using R_1, I_{R1}, and I_m from the previous computational increment, are made to update main branch parameters for the current computational increment by:

$$\frac{dI_{R1}}{dt} = \frac{1}{R_1 C_1}\left(I_m - I_{R1}\right) \tag{5.88}$$

$$I_m = I_{R1} + C_1 \frac{dV_{C1}}{dt} = I_{R1} + C_1 \frac{R_1 dI_{R1}}{dt} \tag{5.89}$$

Likewise, K_E, a model-specific voltage-temperature constant, circuit voltages, and a running quantity of charge extracted from the battery are updated by the following [5.95]:

$$K_E = \frac{0.09 E_{m0}}{273 + \theta_n} \tag{5.90}$$

$$E_m = E_{m0} - K_E (273 + \theta)(1 - SOC) \tag{5.91}$$

$$V_t = E_m + I_{R1} R_1 + I_m R_2 + I_t R_0 \tag{5.92}$$

$$Q_e = Q_{e,0} + \int_0^t I_m(t) dt \tag{5.93}$$

where, Q_e is the cumulative quantity of charge [Ah] extracted from the battery and $Q_{e,0}$ is the initial battery charge [Ah].

Finally, using battery parameter information, the quantity of internal heating during this increment may be determined, along with the change in battery temperature [5.95], according to:

$$P_s = I_{R1}^2 R_1 + I_m^2 R_2 + I_t^2 R_0 \tag{5.94}$$

$$\frac{d\theta}{dt} = \frac{1}{C_\theta} \left(P_s - \frac{(\theta - \theta_a)}{R_\theta} \right) \tag{5.95}$$

$$SOC = 1 - \frac{Q_e}{K_c C(I_t^*, \theta)} \tag{5.96}$$

where, P_s is the power [W] consumed in the battery internal heating; C_θ is the battery thermal capacitance [Wh/°C]; R_θ is the battery thermal resistance [°C/W]. The updated battery SOC may be calculated according to (5.96) for use in the next computational increment, knowing the updated charge extracted (Q_e) and battery temperature (θ).

The model described above provides a sufficient level of detail and information to simulate the lead-acid battery for the purpose of optimizing its operation according to additional system considerations. The next sections will explore how to exploit this model for additional information relating to operational cost and round trip efficiency.

5.8.2 Battery Round-trip Efficiency

Round-trip efficiency is defined as the energy into a storage process, relative to the energy derived from that process. Quantifying it is most appropriate when analyzing a single energy storage charge-discharge cycle, where energy has flowed in and then out of the device. Round-trip efficiency may be quantified by:

$$\eta = \frac{E_{out}}{E_{in}} \tag{5.97}$$

where, η is efficiency, E_{out} is energy returned by the storage system, and E_{in} is the energy into the storage system. It is important to highlight that (5.97) masks the contributions of unique charge and discharge processes on the round-trip efficiency of a complete cycle. Each process, whether charging and discharging, exhibits differing energy efficiency characteristics where losses occur during each stage of energy transfer, shown in Figure 5.50. Best calculations of round-trip efficiency may be made by an incremental combination of charging efficiency and discharging efficiency.

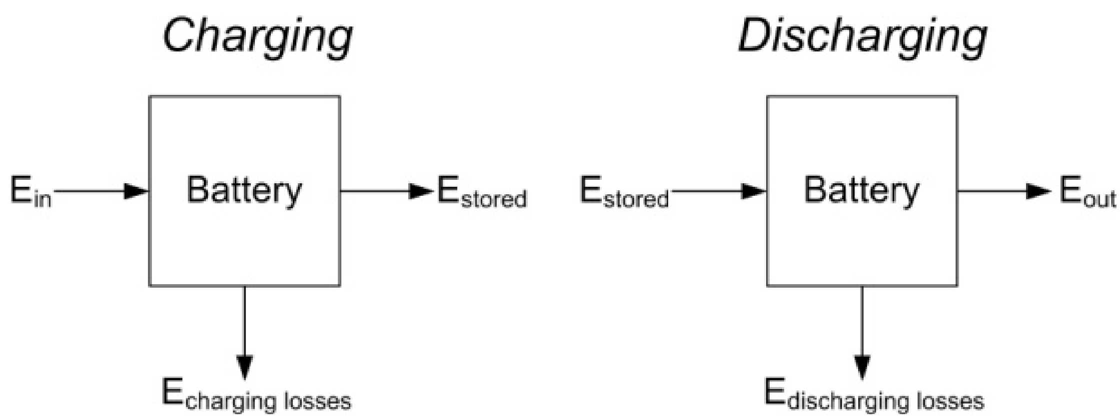

Figure 5.50. Battery energy flows during charging and discharging.

It is highlighted that the simple expression (5.97) masks the contributions of unique charge and discharge processes on the round-trip efficiency of a complete cycle. Each process, whether charging or discharging, exhibits differing efficiency characteristics where losses occur during each stage of energy transfer. Best calculations of round-trip efficiency may be made by an incremental combination of charging efficiency and discharging efficiency.

In a battery storage system, when sending energy to the battery (charging), energy is lost primarily to I^2R through the battery internal impedances and parasitics. While being stored, the predominant loss mechanism is through self-discharge and its magnitude is highly dependent upon the type of battery chemistry. When returning energy (discharging), energy is also lost to I^2R losses through the battery internal impedance, but parasitic are less of a concern. Each of these loss phenomena are evident in the lead-acid model described in 5.8.1 and shown in Figure 5.49. To illustrate these losses, a 500Ah lead-acid electro-thermal model, from 5.8.1 , was used to produce Figure 5.51 and Figure 5.52. These figures show the effects of different constant charge or discharge currents on process efficiencies of energy flow to/from the battery, along with SOC information. The incremental battery model information was used to develop the round-trip efficiency estimates.

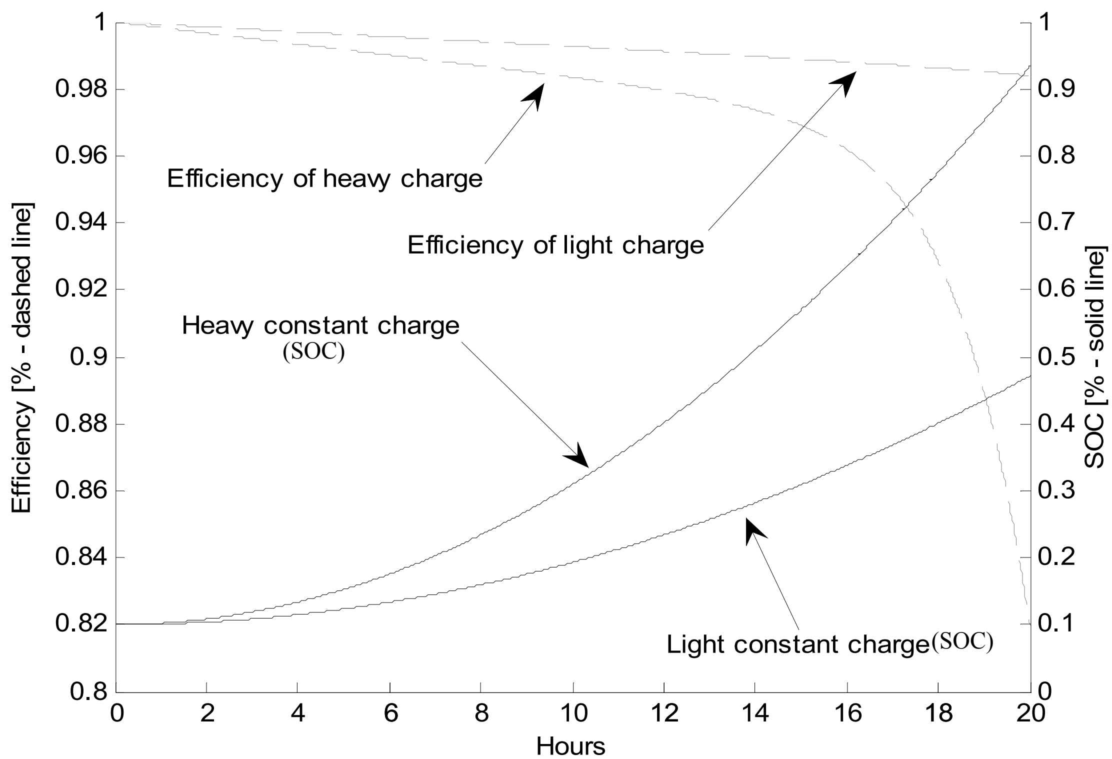

Figure 5.51. Lead-acid battery efficiency & SOC during constant-current charging.

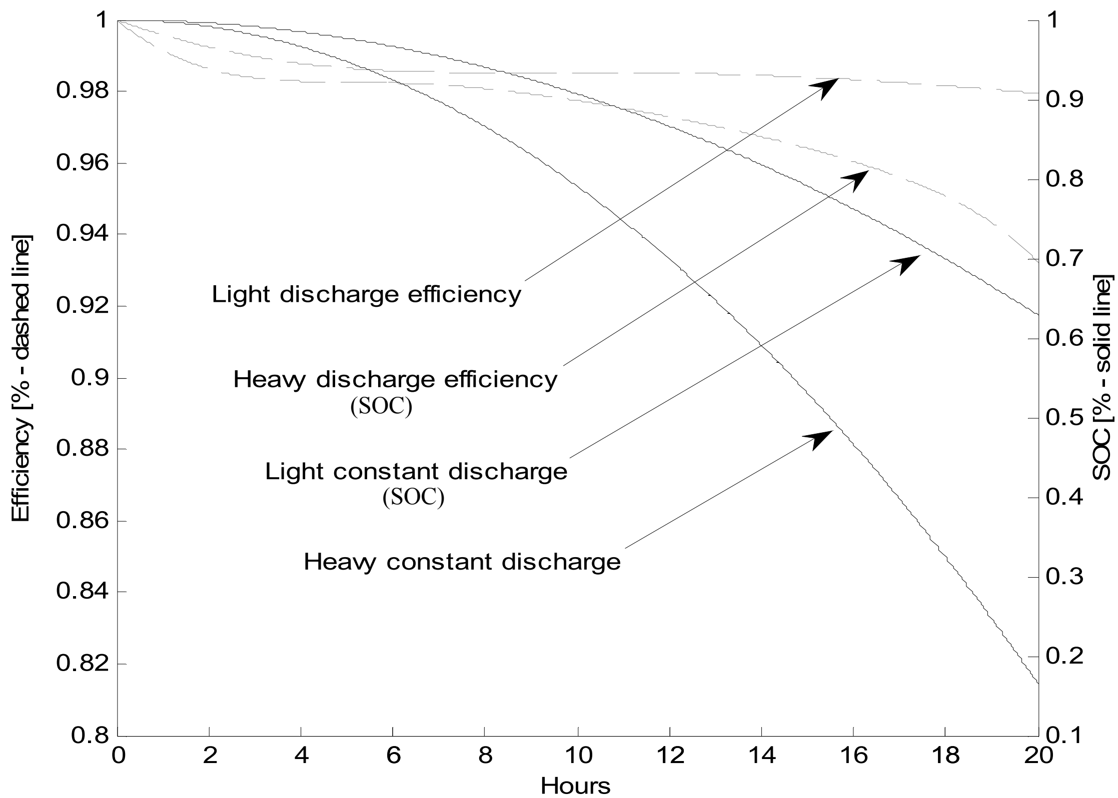

Figure 5.52. Lead-acid battery efficiency & SOC during constant-current discharging.

Intuitively, round-trip efficiency is a useful measure of how well a storage process takes in energy and subsequently releases it. Confusingly, round-trip efficiency figures are routinely reported as averages [5.98, 5.99]. These averages are often inaccurate under actual operating conditions. The best measure of round-trip efficiency would average the charge and subsequent discharge efficiencies for each unique quantity of energy transferred through the battery. However, this is unwieldy. Alternatively, an iterative method to determine battery round-trip efficiency during a single charge/discharge cycle, modifies the calculation of η given above by:

$$\eta_{charge,avg}[n] = \left(\frac{1}{n}\right)\left((n-1)\eta_{charge,avg}[n-1] + \left(\frac{E_{stored}[n]}{E_{in}[n]}\right)\right) \quad (5.98)$$

$$\eta_{round-trip}[n] = \frac{\eta_{charge,avg}[n]}{2} + \frac{1}{2n}\left((n-1)\eta_{discharge}[n-1] + \left(\frac{E_{out}[n]}{E_{stored}[n]}\right)\right) \quad (5.99)$$

where, $\eta_{charge,avg}[n]$ is the running average efficiency during the charging event; $E_{stored}[n]$ is the quantity of energy stored by the battery during the charging event; $E_{in}[n]$ is the energy sent to the battery during the charging event; n is the computational increment; $\eta_{round\text{-}trip}[n]$ is the running average round-trip efficiency during the discharging event; $E_{stored}[n]$ is the energy stored by the battery during the discharging event; and $E_{out}[n]$ is battery energy extracted during the discharging event.

This study yielded some general observations, summarized here. During the charging process, the magnitude of I^2R losses rise as charging rate rises. When discharging, discharging rate has only a small effect on I^2R losses, but does become significant when the energy remaining within the battery nears exhaustion. As shown in Figure 5.52, during shallow SOC discharges, the discharge efficiency remains high within a narrow zone, regardless of discharge rate. Conversely, at higher SOC, charging efficiency, such as shown in Figure 5.51, becomes significantly degraded, primarily due to the rise of parasitic and internal battery heating. Ultimately, the worst drop in efficiency experienced by the battery occurs when charging at high SOCs, regardless of charging rate.

5.8.3 Battery Operational Cost Evaluation

For dispatchable generation sources, it is typical to have fixed and variable operational costs that affect the operational employment of the generator. Fixed costs, which are not dependent upon generator output or status, can include rents, overhaul contracts, and possibly the repayment of sunk financing costs. Variable costs, alternatively, are predominated by operationally dependent factors such as fuel cost and the cost of periodic maintenance. For storage systems, however, the fixed and variable cost makeup of operational expense is quite different. While the cost of storage is a sunk cost, storage systems such as lead-acid or lithium-ion batteries consume no fuel in their operation. This complicates determining a valid variable cost for the operation of a battery storage system, but the following solution is proposed: treat the expected future replacement cost of the battery storage system as a variable cost, spread out over the expected lifetime of the battery. In other words, a battery's lifetime capacity is similar to a fixed amount of fuel [5.100]. When that lifetime capacity is fully consumed, the battery has reached the end of its effective lifespan and must be replaced. This is analogous to refilling the fuel tank. Therefore, by spreading the total lifetime capacity over all of its cycles, an operationally-dependent representation of replacement cost may be utilized, expressing a variable operational cost for battery operations. This proposed method is similar to that described in [5.101] with two key differences. First, rather than finding a cost of energy from the battery on an annualized basis, the operational cost is determined for each computational increment based on battery operational characteristics. Second, the cost of charging the battery is considered in its operational cost, as well as when making the decision to charge or discharge.

The two steps in enabling this cost determination cycle-per-cycle are to: develop a means to predict the effect of present operating conditions on the expected lifetime of the battery and to spread the capital replacement cost across the determined expected lifetime to find the cycle-to-cycle operational cost. While there are many battery lifetime prediction methods, the one used as the basis for this analysis is a weighted Ah-throughput model [5.102, 5.103]. This incremental approach is particularly suitable to operational decision-making because decisions must be made without an entire lifetime of battery data.

A battery has a finite lifespan, quantified by summing together all of the ampere-hours (Ah) discharged during each of its cycles to determine a cumulative Ah capacity for the battery's life. The total charge life of a battery is calculated from manufacturer's specifications by the following:

$$\Gamma_{rated} = L_{rated} DOD_{rated} C_{rated} \tag{5.100}$$

where, Γ_{rated} represents the charge life of a battery (Ah), L_{rated} is the cycle lifetime at rated depth of discharge (DOD_{rated}) and rated discharge current (I_{rated}), and C_{rated} is the Ah capacity at rated discharge current. However, in many cases, a battery is operated differently than the manufacturer specifications.

It is reasonable to assert that the total Ah through a battery during its effective lifetime is directly dependent upon the depth of discharge DOD during each cycle.

Therefore, a relationship can be established between the cycle-to-cycle depth of discharge and its effect on battery effective lifetime. For example, the CERTS microgrid utilizes MK-Powered valve regulated lead acid (VRLA) batteries for its demonstration microgrid (battery model: ES10-12S) [5.104]. Using information from the data sheet [5.105], functions can be readily fit to represent the relationship between battery lifetime and cyclic DOD, given in (5.101), battery capacity as a function of charge/discharge current, given in (5.102), with coefficients shown in Table III.

$$L_{actual} = u_2 \left(\frac{DOD_{rated}}{DOD_{actual}} \right)^{u_0} e^{u_1 (1 - \frac{DOD_{actual}}{DOD_{rated}})} \tag{5.101}$$

$$C_{actual} = u_3 e^{-u_4 I_{actual}} \tag{5.102}$$

where, L_{actual} is the actual battery effective lifetime when operated at DOD_{actual}, which is the actual depth of discharge [%]; DOD_{rated} is the rated depth of discharge [%]; C_{actual} is the actual battery capacity [Ah]; I_{actual} is the actual battery current [A], and u_0, u_1, u_2, u_3, and u_4 are coefficients found from fitting the non-linear function to the data shown in Figure 5.53. It is noted that some battery data sheets, including for the ES10-12S battery, give information about rated DOD up to 100% DOD per cycle over a lifetime. When the manufacturer provides broader performance data, such as for the ES10-12S, better curve fitting can result. In other words, for this case, $L_{rated} = u_2$ (244 cycles, if fully discharged each cycle), whereas the actual nominal L_{rated} = 750 cycles if only discharged 50% per cycle.

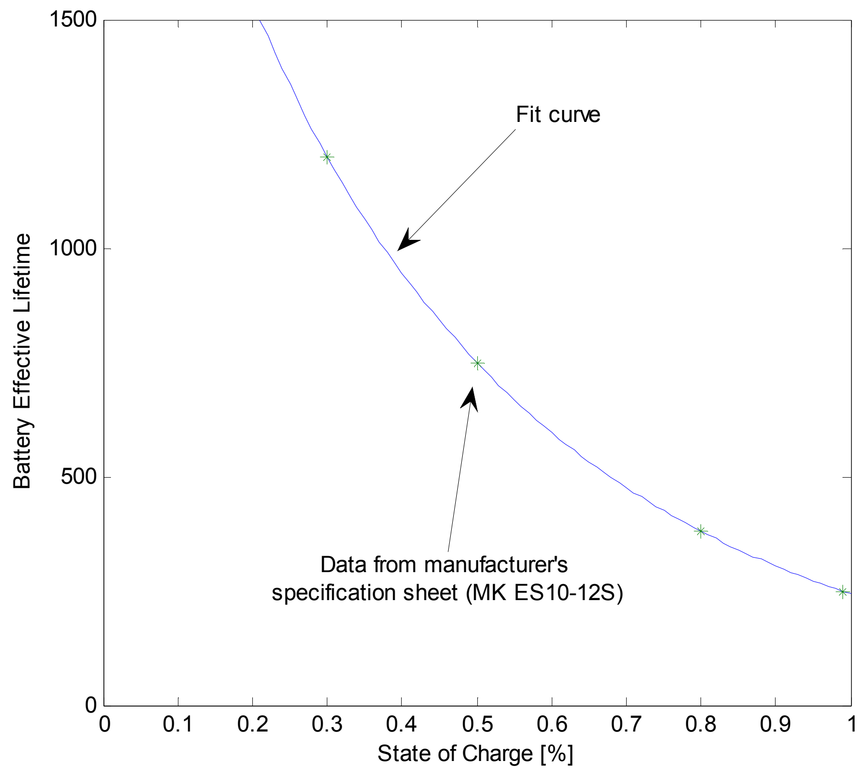

Figure 5.53. Non-linear curve fit for battery effective lifetime to SOC data.

Table 5.14. ES10-12S battery coefficients (derived from [5.105]).

u_0	u_1	u_2	u_3	u_4
0.1576	1.995	247.6	10.74	0.1359

In [5.103], the effective Ah discharge (d_{eff}) in one cycle is defined as the actual Ah discharge, adjusted for the depth and rate of discharge. At I_{rated}, if a battery is discharged to a DOD different than DOD_{rated}, battery lifespan is affected. It follows, therefore, that the ratio of rated lifespan (L_{rated}), in cycles, to the actual lifespan (L_{actual}), indicates an effect on battery lifespan, and is equivalent to the ratio of Ah discharge during a cycle. It is emphasized that this relationship results in a factor that may be computed cycle-to-cycle as actual operation influences battery lifespan, summarized by:

$$\frac{d_{eff}}{d_{actual}} = \frac{L_{rated}}{L_{actual}} = \left(\frac{DOD_{actual}}{DOD_{rated}}\right)^{u_0} e^{u_1(\frac{DOD_{actual}}{DOD_{rated}}-1)} \qquad (5.103)$$

Similarly, when DOD from cycle-to-cycle is held at DOD_{rated}, battery lifespan is affected by variations in discharge current relative to I_{rated}. In other words, the ratio of effective discharge (d_{eff}) to actual discharge (d_{actual}) is affected by the actual discharge current during the cycle. Unfortunately, battery manufacturers rarely give data about various discharge currents over an entire battery lifespan. Alternatively, as postulated in [5.102], the ratio of discharges is equivalent to the ratio of rated capacity (C_{rated}) over the actual capacity (C_{actual}) at the non-rated discharge current. The influence, therefore, of discharging the battery at a non-rated rate is shown by:

$$\frac{d_{eff}}{d_{actual}} = \frac{C_{rated}}{C_{actual}} \qquad (5.104)$$

To unify the effects of DOD and discharge rate on battery lifespan, (5.103) and (5.104) are multiplied together to find:

$$\frac{d_{eff}}{d_{actual}} = \left(\frac{C_{rated}}{C_{actual}}\right)\left(\frac{DOD_{actual}}{DOD_{rated}}\right)^{u_0} e^{u_1(\frac{DOD_{actual}}{DOD_{rated}}-1)} \qquad (5.105)$$

Or, simplified for the MK ES10-12S battery:

$$d_{eff} = 0.9139\left(d_{actual,i}\right)\left(DOD_{actual,i}\right)^{0.1576}\left(e^{\left(0.1359 I_{actual,i} + 3.99 DOD_{actual,i} - 1.995\right)}\right) \quad (5.106)$$

The expression established in (5.105) can be used to determine a cycle-to-cycle estimate for the remaining battery lifespan, which is fundamental for calculations of battery operational cost. Cycles remaining until battery exhaustion are found by:

$$L_{remaining} = L_{rated}\left(1 - \frac{\sum^{n} d_{eff}}{\Gamma_{rated}}\right) \quad (5.107)$$

Or, simplified for the MK ES10-12S battery:

$$L_{remaining} = 750 - 0.2077\sum_{i=1}^{n}\left(d_{actual,i}\right)\left(DOD_{actual,i}\right)^{0.1576}\left(e^{\left(0.1359 I_{actual,i} + 3.99 DOD_{actual,i} - 1.995\right)}\right) \quad (5.108)$$

Clearly, estimates of battery parameters, including (5.105) and (5.107), may be calculated incrementally. This information allows decisions about battery operation to account for factors such as cost and battery lifetime as the following equations show:

$$C_n = u_3 e^{-u_4 I_n} \quad (5.109)$$

$$d_n = I_n \Delta t \quad (5.110)$$

$$DOD_{n+1} = DOD_n + \Delta DOD_n \quad \text{where} \quad \Delta DOD = \frac{d_n}{C_n} \quad (5.111)$$

$$deff_n = d_n\left(\frac{C_{rated}}{C_n}\right)\left(\frac{DOD_{n+1}}{DOD_{rated}}\right)^{u0}\left(e^{u_1\left(\frac{DOD_{n+1}}{DOD_{rated}}-1\right)}\right) \tag{5.112}$$

$$T_{n+1} = T_n + deff_n \tag{5.113}$$

where, C_n is the rated capacity based on the current, I_n, at increment n; d_n is the Ah discharged during increment n; Δt is the period between increments n and $n+1$; ΔDOD is the depth of discharge incurred in increment n, DOD_n is the running calculation of depth of discharge in increment n; DOD_{n+1} is the running depth of discharge at the start of increment $n+1$; $deff_n$ is the effective discharge incurred during increment n; T_n is the total effective discharge over the present life of the battery, initialized when the battery was placed in service.

Next, a decision must be made during increment n how to discharge the battery in the next increment; in other words, where to set I_{n+1}. To achieve this, it was desirable to create a search space of all possible cost outcomes dictated by a choice to discharge at I_{n+1}. The following method allows this search space to be created containing all possible results from the feasible range of currents (0 to I_{rated}). First, the range of possible discharges is estimated for the next increment by:

$$\overline{d}_{n+1,est} = \varepsilon \overline{I}_{n+1,est} \text{ where } \overline{I}_{n+1,est} = \{0, \; .. \; , I_{rated}\} \tag{5.114}$$

where, $\overline{d}_{n+1,est}$ is all feasible Ah discharges estimated for the next increment governed by a range of discharge currents, $\overline{I}_{n+1,possible}$, from 0 to I_{rated} (vector of length m). In the next increment, DOD is unknown, so $\overline{DOD}_{n+1,est}$ is a vector (of length p) that represents the estimated range of DOD from 0 to the rated DOD_{limit} ($\overline{DOD}_{n+1,est} = \{0, \,..\, , DOD_{rated}\}$). These two estimated parameter vectors help establish the estimated effective discharge search space for the next increment, ($deff_{(est\ n+1),\ n}$). The search space is a matrix of size m x p. Using (5.105), the following intermediate equation is developed:

$$deff_{n+1,est} = \bar{d}_{n+1,est}\left(\frac{C_{rated}}{C_{n+1}}\right)\left(\frac{\overline{DOD}_{n+1,est}}{DOD_{rated}}\right)^{u0}\left(e^{u_1\left(\frac{\overline{DOD}_{n+1,est}}{DOD_{rated}}-1\right)}\right) \qquad (5.115)(a)$$

Substituting into the expression:

$$deff_{n+1,est} = \left(\varepsilon\bar{I}_{n+1,est}\right)\left(\frac{C_{rated}}{u_4 e^{-u_5\bar{I}_{n+1,est}}}\right)\left(\frac{\overline{DOD}_{n+1,est}}{DOD_{rated}}\right)^{u0}\left(e^{u_1\left(\frac{\overline{DOD}_{n+1,est}}{DOD_{rated}}-1\right)}\right) \quad (5.115)(b)$$

Rearranging leads to:

$$deff_{n+1,est} = \underbrace{\left(\frac{\varepsilon C_{rated}e^{-u_1}}{u_4 DOD_{rated}^{\ \ u_0}}\right)}_{(1\text{ x }1)}\underbrace{\left(\bar{I}_{n+1,est}e^{u_5\bar{I}_{n+1,est}}\right)^{T}}_{(m\text{ x }1)}\underbrace{\left(\overline{DOD}_{n+1,est}^{\ \ u_0}\, e^{\frac{u_1\overline{DOD}_{n+1,est}}{DOD_{rated}}}\right)}_{(1\text{ x }p)} \qquad (5.115)$$

where, the (mx1) vector is calculated by element-wise evaluation of $\bar{I}_{n+1,possible}$; the (1xp) vector is calculated by element-wise evaluation of $\overline{DOD}_{n+1,possible}$; and the resulting matrix contains all feasible estimates of effective discharge ($deff_{n+1,est}$) in the next increment. Given the search space of estimated effective discharge, the space can easily be converted to reflect cost of each possible discharge solution. This is accomplished by recognizing that given the cost of replacement of the battery (*COR*) may be spread across the rated charge life of a battery (Γ_{rated}) by \$ per Ah. Therefore, using the estimates of effective discharge in the next increment ($deff_{n+1,est}$), the cost of each discharge choice in the matrix may be assigned a cost value by:

$$cost_{n+1,est} = \left(\frac{deff_{n+1,est}}{\Gamma_{rated}} \right) COR \tag{5.116}$$

where, $cost_{n+1,est}$ is the search space (mxp) of estimated costs based on all feasible discharge currents and DODs during the next increment. This search space allows a decision-maker to use estimated costs to evaluate a particular operational choice for the next increment. Of course, (5.116) reflects a flat cost assignment over battery lifetime. In other words, each Ah of charge life has the same cost. However, the algorithm may be modified to suit the particular interest of the decision-maker. For example, using (5.107), which contains information about discharge history, an increasing cost function could be employed which values Ah of charge life more highly towards the end of battery life and correspondingly values Ah more cheaply at beginning of battery life, according to:

$$cost_{n+1,est} = \left(\frac{deff_{n+1,est}}{\Gamma_{rated}} \right) COR \left(1 - \frac{L_{remaining}}{L_{rated}} \right) \quad \{n>1\} \tag{5.117}$$

This illustrates how the method of valuing battery health throughout the life of the battery is up to the decision-maker, depending on their particular interest. Ultimately, this algorithm shown allows battery cost, as well as effective battery lifetime, to be found incrementally as operation deviates from rated conditions. This information is valuable and can be used to make operational choices in a similar manner to dispatchable assets.

5.9 Microgrid Electrical Circuit and Power Flow

The approach to modeling microgrid electrical parameters is similar conventional power system operations, but is influenced by some additional key characteristics. First, as explained in Chapter 2, straight-forward common AC bus configured microgrids are expected to be dominant for applications less than 5MW in total capacity. Given this assumption, microgrids less than 5MW in capacity can be expected to utilize primary generation sources to produce AC power at mainly low (LV) voltage levels, with some short distance distribution at medium (MV) voltage levels [5.106]. Additionally, it is expected that the primary microgrid generator classes are: inverted DC sources (such as PV), rectified and inverted high frequency AC sources (such as microtubines), and conventional rotating AC sources (such as diesels). These generation sources will be relatively close to load centers, giving rise to primarily resistive distribution lines. Microgrid generation assets are predominantly expected to lack significant inertia present for much larger generators. Whereas in larger power systems, generator rotational inertia facilitates voltage/frequency (Vf) droop control for real and reactive power delivery, for microgrid sources without large inertia Vf-droop control is less desirable [5.107]. For more details on power system fundamentals, see Appendix A.

The optimal power flow (OPF) problem has been a conventional power system topic of interest for many years. It focuses on finding generator power set points that minimize the overall cost of generation within a power network subject to capacity and transmission line constraints [5.108]. While the OPF is an important problem for large interconnected HV power systems, the problem is different than the microgrid power dispatch problem formulation. The focus for MAS decision-making incorporates aspects of the OPF, but neglects transmission constraints as they are not applicable to LV microgrids. Additionally, generator constraints are handled implicitly through the development of feasible ranges of operation, discussed further in Chapter 4. Overall, approaches to solving the OPF for large interconnected power systems are instructive, but many of the concepts are co-opted by MAS power management.

The role of the DC link capacitance is very important for inverted DER. The DC link capacitance, which may be either an actual capacitor or in some cases a battery, is the energy storage on the DC connection between the DC output of the DER (or DC-DC converter) and the DC-side of the inverter. When the command signal to the inverter exceeds the output power of the DER source itself, one of two actions must occur: either the DER source increases its power output or the inverter must be commanded to an output power matching that of the DER. During the short period when the DER source output does not match the real power supplied by the inverter, the DC link capacitance discharges supplying the energy deficit. Likewise, if output power of the inverter is less than that supplied by the DER, the DC link absorbs the energy difference. From a modeling perspective, it is important to realize the importance of the DC link to proper DER interface with the common AC bus. If the DC link is not appropriately sized, its reservoir of electrostatic energy storage could be too small to supply or absorb power changes while the inverter and DER controllers are settling. For the modeling in this work, the effect of momentarily exceeding the rating of DERs was prevented with sufficiently large DC link capacitance and avoided the need to consider appropriate circuit protection schemes. More sophisticated models, if developed, could easily be implanted into the simulation environment.

It is well known that real and reactive powers are coupled. This is illustrated by Figure 5.54 and Figure 5.55, and is shown by the following derivation:

$$\bar{I} = \frac{\bar{V}_s - \bar{V}_r}{R + jX} = \frac{|V_s|}{|Z|}\angle\left(\phi_s - \phi_{R+jX}\right) - \frac{|V_r|}{|Z|}\angle\left(\phi_r - \phi_{R+jX}\right) \quad (5.118)$$

$$\bar{I} = \frac{|V_s|}{|Z|}\cos\left(\phi_s - \phi_{R+jX}\right) - \frac{|V_r|}{|Z|}\cos\left(\phi_r - \phi_{R+jX}\right) + j\left[\frac{|V_s|}{|Z|}\sin\left(\phi_s - \phi_{R+jX}\right) - \frac{|V_r|}{|Z|}\sin\left(\phi_r - \phi_{R+jX}\right)\right] \quad (5.119)$$

where, I is the phasor current passed from the sending generator at sending phasor voltage (V_s) to the receiving bus at receiving phasor voltage (V_r) through the connecting impedance Z, which is composed of resistance (R) and reactance (X). Apparent power transferred from the sending generator to the receiving bus is equal to:

$$S_r = V_r I_r^* \quad (5.120)$$

Or, when broken into real and reactive power components:

$$S_r = \underbrace{\frac{|V_s V_r|}{|Z|}\cos\left(\phi_s - \phi_{R+jX}\right) - \frac{|V_r|^2}{|Z|}\cos\left(\phi_r - \phi_{R+jX}\right)}_{P_r}$$
$$\underbrace{-j\left[\frac{|V_s V_r|}{|Z|}\sin\left(\phi_s - \phi_{R+jX}\right) - \frac{|V_r|^2}{|Z|}\sin\left(\phi_r - \phi_{R+jX}\right)\right]}_{Q_r} \tag{5.121}$$

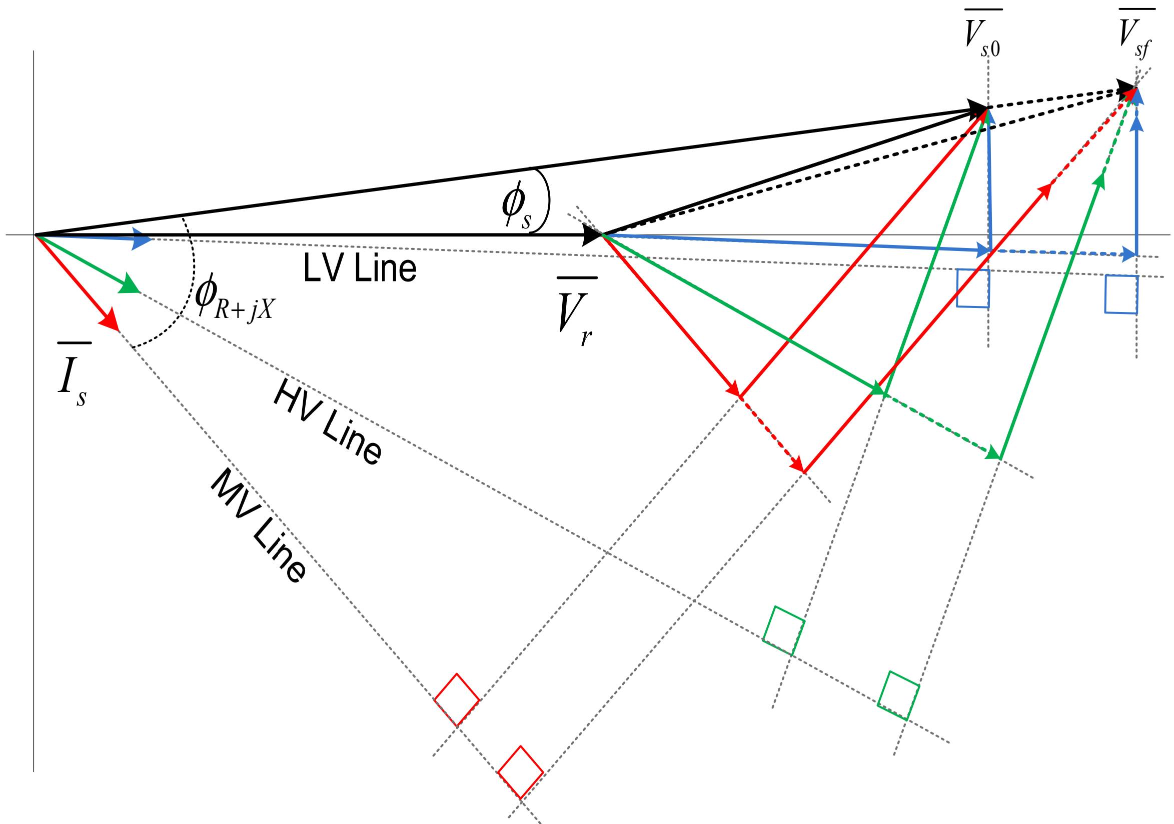

Figure 5.54. Normalized phasor representation for typical LV, MV, HV lines.

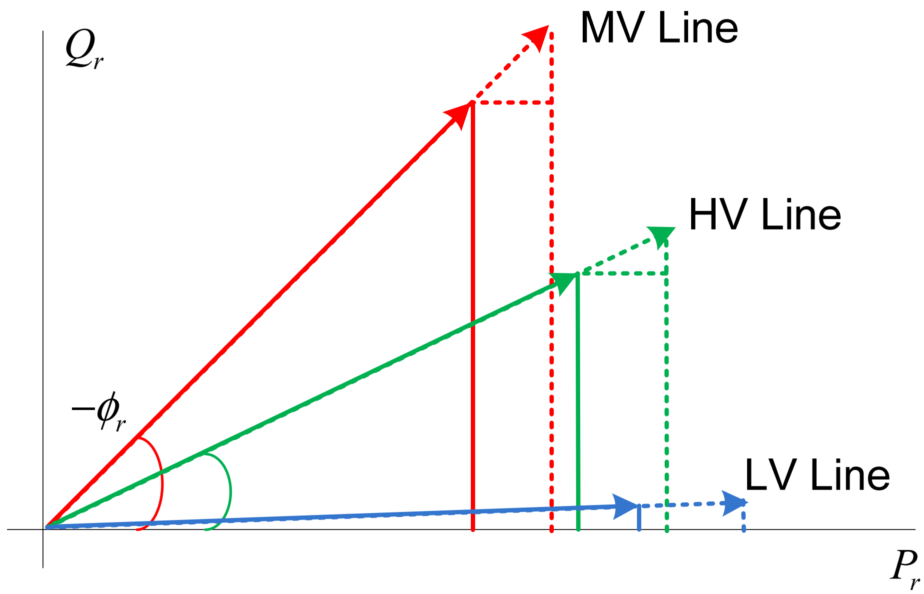

Figure 5.55. Normalized power transferred graph for typical LV, MV, HV lines.

Clearly, when V_r is used as the reference voltage, changes in the angle (ϕ_s) and the magnitude of V_s have coupled effects on P_r and Q_r. This is where knowledge of the microgrid electrical is important for classifying generator changes to V_s and ϕ_s. Typically, in MV and HV networks it is assumed that the resistance of lines is relatively small compared to reactance. This leads to a the well known simplification of (5.121):

$$S_r = \underbrace{\frac{|V_s V_r|}{|Z|}\sin(\phi_s)}_{P_r} \underbrace{-j\left[\frac{|V_s V_r|}{|Z|}\cos(\phi_s) - \frac{|V_r|^2}{|Z|}\right]}_{Q_r} \tag{5.122}$$

This simplification presumes that for small changes P_r is primarily dependent on ϕ_s and Q_r is primarily dependent the magnitude of V_s. This underlines the basis of conventional power system droop control. Droop controllers focus on control of ϕ_s and

V_s to control active and reactive power flow, respectively. Clearly, as can be seen from (5.121), the flow of active and reactive powers are not completely decoupled, but the simplification in (5.122) is operable because they are mostly independent given small changes. However, microgrids may be different and the interconnecting electrical network may not contain the same resistive and reactive balance seen in MV and HV networks. This point is highlighted by the data collected in Table 5.15.

Table 5.15. Power line parameters [5.106, 5.107, 5.109].

IEEE System Voltage Class	Nominal Voltage	R' (Ω/km)	X' (X_L-X_C, Ω/km)	Line XR-ratio
Low Voltage (<1000 V)	0.6 kV	0.642	0.083	0.13
Medium Voltage (1001-100,000V)	13.8 kV	0.161	0.190	1.18
High Voltage (>100,000V)	230 kV	0.05	0.191	3.82

Due to the low XR ratios found in low voltage distribution networks, shown in Table 5.15, manipulations of generator sending voltage (V_s) magnitude has a much greater impact on real power flow on the microgrid than in the MV and HV cases, as shown in Figure 5.54 and Figure 5.55. At transmission levels, reactive power delivery is controlled by sending voltage magnitude, while real power delivery is manipulated by sending voltage frequency [5.109]. From Figure 5.54 and Figure 5.55, it is clear why this is relevant to MV- and HV-level power deliver, but is dramatically less effective for the LV-level. Therefore, this simplifies the electrical system modeling required for simulating microgrid power flow. Additionally, because of the relatively few assets involved, the information flow and computational overhead to arrive a system electrical parameters is achievable quickly.

This discussion has been highlighted because of the potential pitfalls illustrated by the assumption made by conventional droop theory, based on (5.122), if applied to LV microgrids. If connected by primarily resistive lines, rather than (5.122), the simplification of (5.121) becomes:

$$S_r = \underbrace{\left[\frac{|V_s V_r|}{|Z|}\cos(\phi_s) - \frac{|V_r|^2}{|Z|}\right]}_{P_r} \underbrace{-j\frac{|V_s V_r|}{|Z|}\sin(\phi_s)}_{Q_r} \tag{5.123}$$

where, ϕ_{R+jX} is near zero, causing a major change in the calculation or real and reactive powers for LV microgrids. This can be illustrated by focusing on the phasor diagrams that represent the voltage and currents present in a single generator connection to the microgrid common AC bus, shown in Figure 5.56 and Figure 5.58. The corresponding diagrams for real, reactive and apparent power (S_r) received by the common AC bus are shown in Figure 5.57 and Figure 5.59.

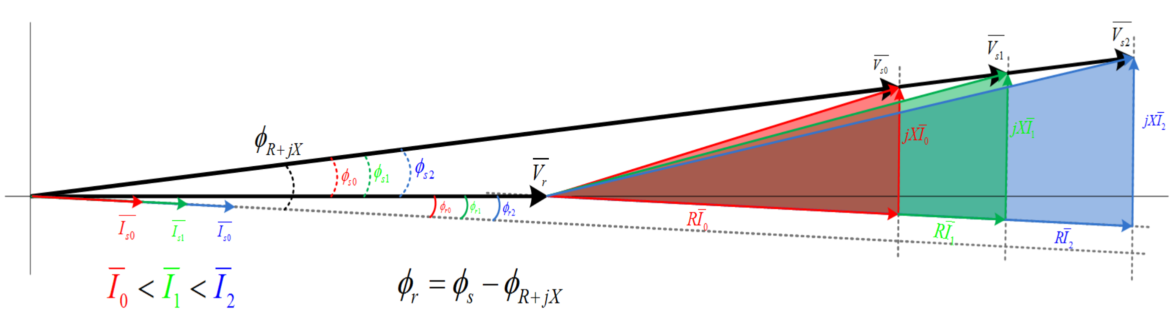

Figure 5.56. Sending voltage magnitude change on voltage and current in LV network.

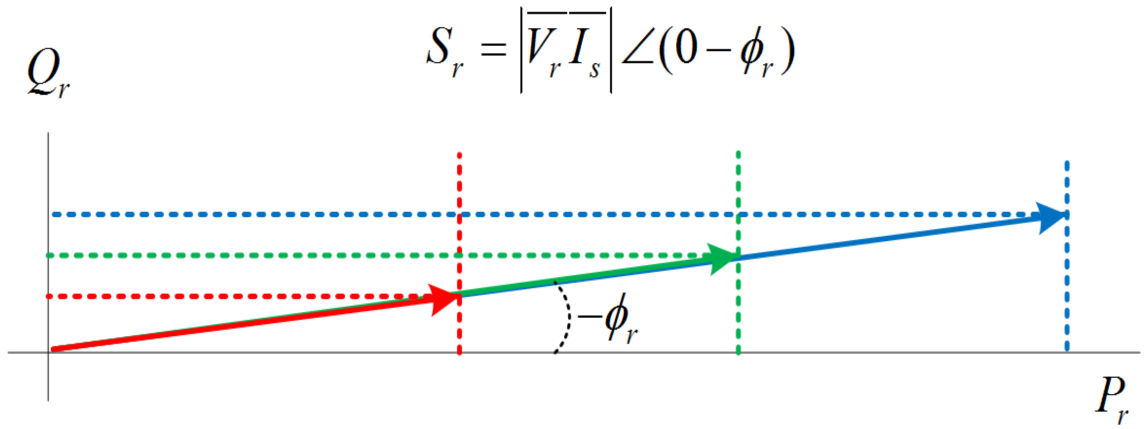

Figure 5.57. Sending voltage magnitude change on receiving real/reactive power in LV network.

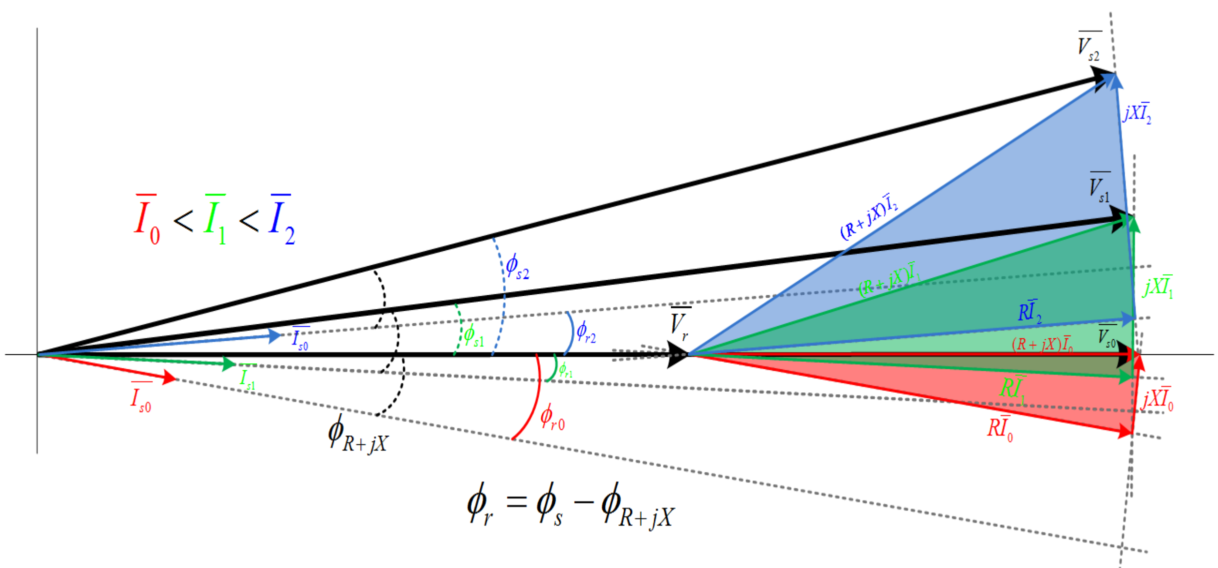

Figure 5.58. Sending voltage angle change on voltages and currents in LV network.

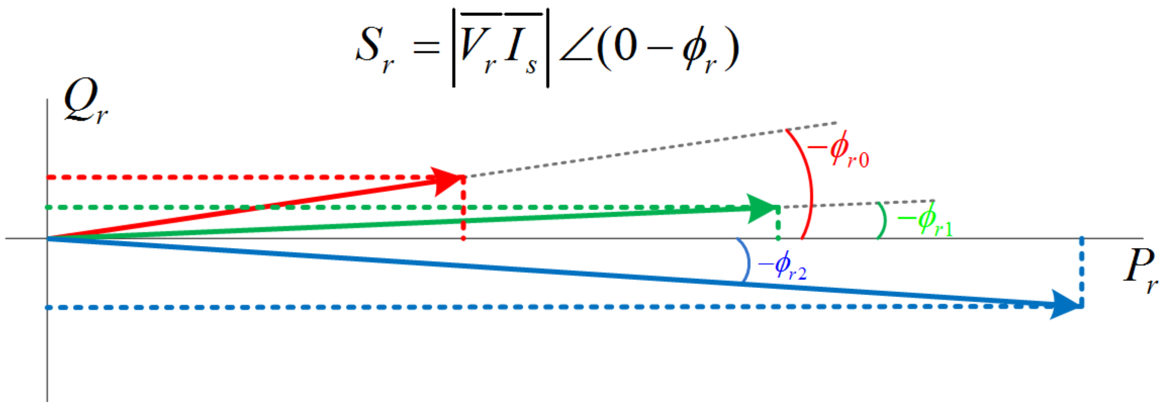

Figure 5.59. Sending voltage angle change on receiving real/reactive power in LV network.

It is clear from Figure 5.57 and Figure 5.59 that in a LV network, reactive power transferred to the common AC bus is fairly bounded despite large changes in sending voltage magnitude or angle. This is not the case with the transfer of real power which is affected significantly by changes in sending voltage magnitude or angle. This suggests that one, either, or both voltage magnitude and angle may be used to control real power transfer to the common AC bus. This is very different from conventional generator control which separates real and reactive power and must focus on both for power transfer. Using this concept to its advantage, for microgrid electrical network simulation, sending voltage magnitude is the primary control parameter for manipulating real power transfer from a generation asset to the common AC bus.

Power flow on the LV microgrid is simulated by phasor notation. The circuit diagram of the microgrid is shown in Figure 5.60. The grey items in Figure 5.60 indicate the expansion of additional circuits based on the actual configuration of the microgrid.

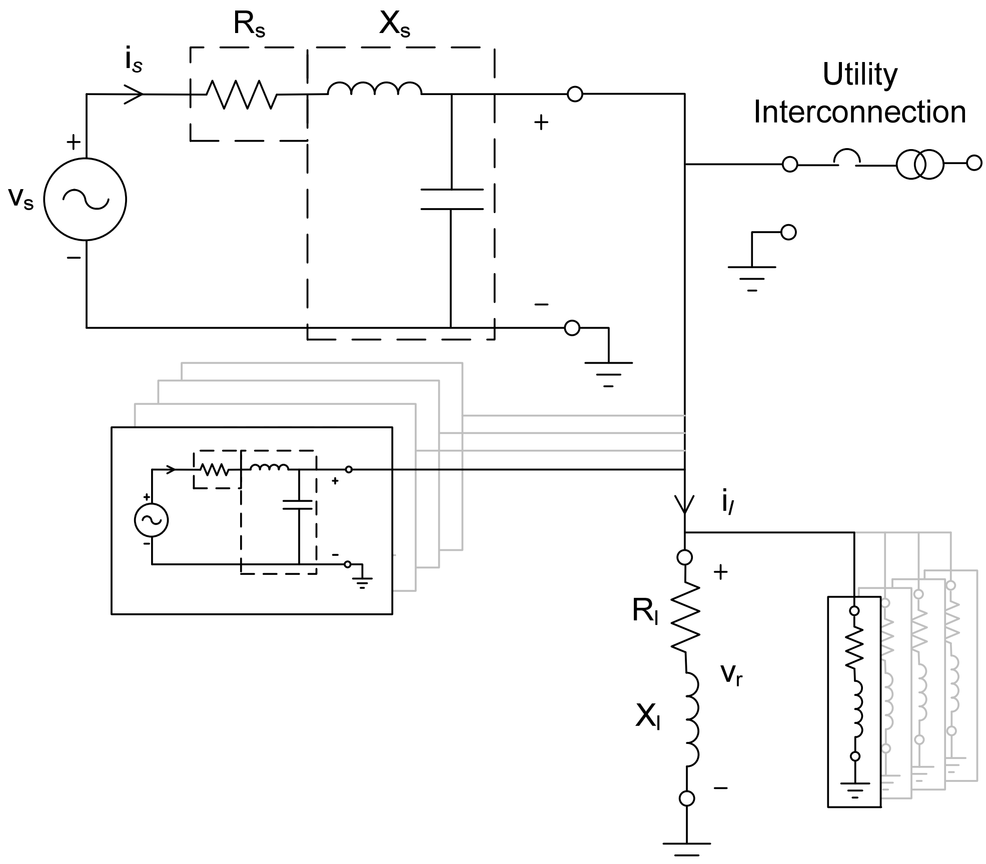

Figure 5.60. Circuit representation of microgrid generators and storage.

The common AC bus voltage serves as the benchmark quantity that guides each assets corresponding sending voltage through the asset's connection impedance. The voltage on the common AC bus may be determined by calculating the individual current contributions of each generation asset (V_s, I_s) according to:

$$\begin{bmatrix} I_1 \\ \vdots \\ I_n \end{bmatrix} = \begin{bmatrix} \dfrac{V_1 - V_{bus}}{R_1 + jX_1} \\ \vdots \\ \dfrac{V_n - V_{bus}}{R_n + jX_n} \end{bmatrix} \tag{5.124}$$

This can be converted to admittances (Y_i) and rearranged to:

$$\begin{bmatrix} I_1 \\ \vdots \\ I_n \end{bmatrix} = \begin{bmatrix} V_1 Y_1 \\ \vdots \\ V_n Y_n \end{bmatrix} - V_{bus} \begin{bmatrix} Y_1 \\ \vdots \\ Y_n \end{bmatrix} \qquad (5.125)$$

By recognizing that the sum of generator currents (I_i) is equal to the sum of current sourced by the utility (I_{grid}) and the current sunk in the load (I_L). In the islanded case, that leads to:

$$\sum_{i=1}^{n} V_i Y_i - V_{bus} \sum_{i=1}^{n} Y_i = V_{bus} Y_L \qquad (5.126)$$

where, V_{bus} is the unknown to be solved for. In the grid connected case, however, the utility grid is presumed to act as an infinite bus, regulating voltage and frequency [5.110]. It is noted for more than one load bank, the right side of (5.126) changes to V_{bus} times the sum of all load bank admittances. This modifies (5.125) somewhat and yields:

$$I_{grid} = \sum_{i=1}^{n} V_i Y_i - V_{bus} \sum_{i=1}^{n} Y_i - V_{bus} Y_L \qquad (5.127)$$

where, V_{bus} is known and the one unknown is the current sourced or sunk by the utility (I_{grid}). It is noted for more than one load bank, the load term on the right side of (5.127) changes to V_{bus} times the sum of all load bank admittances.

In either the grid-connected or islanded case, the real and reactive powers (P_i, Q_i) of each asset is known locally to the asset. This allows generator sending voltage angle to be obtained readily from (5.121):

$$\phi_s = \phi_{R+jX} + \cos^{-1}\left(\frac{|V_r|}{|V_s|}\cos\left(-\phi_{R+jX}\right) + \frac{P|Z|}{|V_s||V_r|} \right) \quad (5.128)$$

And, sending voltage magnitude may be obtained by observing that:

$$|S_r|^2 = |V_r|^2 |I_s^*|^2 = |V_r|^2 \left| \frac{V_s - V_r}{Z} \right|^2 = P^2 + Q^2 \quad (5.129)$$

Leads to:

$$|V_s| = \sqrt{\frac{|Z|^2}{|V_r|^2}\left(P^2 + Q^2\right) + |V_r|^2 + 2|Z|\left[P\cos(\phi_r) + Q\sin(\phi_r)\right]} \quad (5.130)$$

where: ϕ_r is the angular difference between the torque angle (ϕ_s) and the impedance angle (ϕ_{R+jX}). This angle, ϕ_r, represents the angular difference between the receiving voltage (V_r) and the branch current (I_s). The angular difference between receiving voltage and branch current is identical to the angular difference between real and reactive power, where the leading or lagging effects of current relative to voltage are expressed. The cosine of ϕ_r is known as the power factor (pf) and represents the relationship between the component of apparent power that is capable of performing real work on the electrical network and the imaginary component which describes the power consumed and released in magnetic and electrostatic processes within the electrical network, yielding no real work for the electrical network. More on this topic may be found in Appendix A.

These electrical parameters define power flow on the LV microgrid. The other major electrical parameter, frequency, is challenging to find especially in a network with predominantly inverted sources. In the grid connected case, the utility provides a rigid mains electrical frequency. In the islanded case, frequency regulation is akin to that for a large power system. For conventional power systems, power/frequency (Pf) droop methods are used to avoid synchronization signals passed between generators. However, as mentioned above, Vf- and Pf-droop methods are undesirable in the microgrid because of difficulty measuring frequency, especially very small changes on the LV microgrid network. This may not be problematic, however, for inverter AC output with a mains frequency output that is electronically regulated as opposed to mechanical governor controlled for combustion or steam generation in large conventional power plants. The question, therefore, is not how frequency is regulated so much as how power is shared amongst microgrid sources. Numerous variations on droop methods, most of which focus on voltage/power (VP) droop, have been presented for power sharing [5.111, 5.112, 5.113]. However, for this work, the use of automatic droop controls is supplanted by agent-based decision-making for power flow, explained in Chapter 4. However, different power sharing methods may be introduced, including droop methods, based on the flexible MAS framework, allowing the opportunity to more broadly investigate these methods in the future.

Overall, the electrical network model of microgrid parameters is simulated using a dedicated hierarchy of the MAS simulation environment, presented in Chapter 4. The aggregated power model information is not available to the assets themselves, except what they can sense locally (V_{bus}). This differentiation of electrical model information that is calculated centrally maintains the enhanced decentralized integrity of the MAS decision-making layer.

5.10 Other Models

5.10.1 Electrical End-use Load Profiles

As regulated utilities faced deregulatory forces and increased competition during the mid-1990s, the emphasis on demand-side management and load studies diminished. Increasingly, utilities and power marketers have kept any load-related studies limited and proprietary. As a result, the researcher today is left with very few options when they require real-world, end-use load information. By far the most common solution to the lack of information, especially regarding electricity consumption for the residential sector, is to model the load. Possibly because of the difficulty obtaining good data sets, recent studies have attempted to specifically model residential load composition, rather than obtain data from actual monitoring [5.114, 5.115, 5.116]. This process can be very accurate, but still requires detailed information about the consumer and load. Once the models are created they must be validated which often leads researchers back to the lack of available real-world data.

An alternative technique to load component modeling involves the development of aggregate load models at the medium voltage/low voltage (MV/LV) level to simulate a mix of commercial, residential, and industrial load connected to a particular substation. Often these aggregate models are more easily obtained because electrical utilities maintain information about energy consumption through billing. Unfortunately, when more detailed residential load information is desired, it is typically calculated as a percentage of the total aggregated load [5.117].

It was important to this work to find end-use electricity consumption profiles that were representative of real customer habits. For many reasons, not the least of which that a prime deployment location for future microgrids is residential subdivisions, realistic residential end-use information was highly desired. After an exhaustive literature search, as well as contacting numerous utilities and power marketers, little relevant and recent data was found. The viability of developing residential load models was explored, but was abandoned. Specifically, models were not pursued because of a lack of ability to validate them. Developing physically-based load models is straight-forward, but the key information about human behavior and actual usage of specific devices is not evident from feeder level consumption information. Reliance on out-of-date data, e.g. [5.118], was not recommended because such data sets do not accurately represent modern electrical component improvements that affect demand profiles.

Although very little publically available information is collected regarding end-use load, the scant amounts of consistently collected information, such as that maintained by the U.S. Energy Information Administration, can be used to update comprehensive studies conducted many years prior. Based on this trend information, the idea was conceived to project established customer behavior patterns, known from older end-use studies, along with updated the electrical profile information adapted with current mean annual unit energy consumption (UEC) data. This infers that consumer behavior has remained fairly constant while the mix and electrical characteristics of the load devices has changed. Results obtained indicate the suitability of the proposed method in updating end-use load profile information.

The largest and most comprehensive residential electrical demand study available was nearly 20 years old. The End-Use Load and Consumer Assessment Program (ELCAP) was large-scale data collection study conducted by the Bonneville Power Administration (BPA) between 1983 and 1991. The purpose of the ELCAP study was to collect specific electricity end-use information which would ultimately assist the achievement of a number of forecasting and engineering goals. Hourly end-use data was collected from 454 single-family, owner-occupied, electrically space-heated residences in the Pacific Northwest between 1986 and 1991. The richest data set from the ELCAP study focused on residential electricity consumption for homes built before 1983 and was reported in 1992 [5.118]. It is the most comprehensive end-use load study of the Pacific Northwest United States known. Though the methods and the data collected by the ELCAP study were solid, it was necessary to combine ELCAP information with more current end-use data to provide a more relevant load framework for their case study purposes.

A major challenge of any end-use load study is that the electrical ratings of similar devices used in the home vary widely from residence to residence. Investigators with the ELCAP study were interested in finding the average time-based electrical energy consumed by the appliances throughout the home. Their results clearly show a use patterns for each electrical device. Although the electrical ratings of home appliances change over time, the most compelling and lasting information that the ELCAP data suggests are the use signatures for each electrical device within the home. The two primary assumptions made were: the basic patterns for electrical appliance usage has not changed since the ELCAP study and the overall efficiency of electrical devices within residences has evolved. Although the ELCAP study did not record information about the ratings of individual electrical appliances or devices, the study did collect comprehensive information about mean annual UEC along with the hourly demand information. The UEC represents the average physical quantity of consumption per electrical device, per year. By comparison, the U.S. EIA periodically collects similar appliance UEC data nationally, but does not collect the key hourly end-use information inherent to the ELCAP [5.119]. The EIA average annual UEC information allows the authors to ratio the data presented in the 1992 ELCAP study with the most recent EIA data available from 2005. This combination of older and more recent data allows the authors to apply the unique end-use patterns with relevant manufactured electrical device characteristics. It is noted that scaling techniques of this type that update data curves based on more current data collections have been used in other investigations, e.g. [5.120]. However, the technique described above is unique in its application to residential load data and produces comprehensive end-use load profiles based on real data, not simulations. Table I shows UEC data for residences in the Pacific Northwest from the 1992 ELCAP UEC data and the 2005 EIA UEC data. It also presents a ratio of the data sets, meant to aid the authors in updating the hourly end-use patterns for more recent electrical devices.

Table 5.16. 1992 and 2005 end-use mean and ratio data sets.

End-Use Load	1992 ELCAP Mean Average UEC Data for the Pacific Northwest (kW)	2005 EIA Mean Average UEC Data for the Pacific Northwest (kW)	Ratio of EIA to ELCAP datasets
Space Heating	0.934	0.237	0.254
Air Conditioning	0.116	0.142	1.224
Water Heating	0.530	0.349	0.658
Refrigerator	0.416	0.139	0.334
Lighting and Appliances†	0.829	0.592	0.714
Total Residence	2.825	1.459‡	0.516

† The "Lighting and Appliances" category includes lighting, small appliances, clothes washer, clothes dryer, dishwasher, electric range, etc. The ELCAP study differentiated end-use by specific appliance, while the EIA dataset lumped all appliances together. For the purpose of this study, the ELCAP "Lighting and Convenience" data and all appliance categories were aggregated to derive an appropriate "Lighting and Appliances" category for comparison to the EIA dataset.
‡ It is noted that the sum of the five 2005 EIA load categories is approximately 1.459 kW, but the EIA reports that the total average UEC per Pacific Northwest household is 0.969 kW. This is far less than the sum of the reported electrical device consumption values and the EIA does not explain this discrepancy. As a result, the authors the larger empirical total has been used herein.

Comparing these two data sets yielded some unexpected observations. First, the large drop in refrigerator end-use (about 66%) is surprising. The National Appliance Energy Conservation Act of 1987 established minimum efficiency standards for major home appliances in the United States. Although most of the appliance standards were in effect by 1990, some appliances, such as refrigerators, were not required to achieve compliance until 1993. It is noted that almost none of the refrigerators on the market at the end of the ELCAP data collection period met the 1993 appliance standards [5.119]. This analysis shows that significant progress has been made in improving electrical device efficiency, significant numbers of less efficient refrigerators have been replaced, and correspondingly the end-use consumption dropped significantly. Additionally, it is noted that while the average household in the Pacific Northwest has achieved an approximately 48% overall reduction in the consumption of electricity for presumably the same use patterns, one category actually shows a rise in consumption (i.e., air conditioning). A broader investigation into the root causes of changes in consumption is has not been conducted here, but this could be an example of increased installation of devices such as central air conditioners which indicate a change in the appliance baselines. This highlights the fact that updated real-time end-use studies, like those conducted for the ELCAP, are needed to better understand how electricity is being consumed by consumers.

Based on the 1992 ELCAP data, the aggregated normalized residential electrical device use for typical winter and summer weekdays and weekends was calculated and are shown in Figure 5.61 through Figure 5.65. The use factor is a normalized, dimensionless figure that represents the intensity of end-use of that appliance based on the time-of-day. It represents the actual end-use patterns for residential customers, i.e. the actual kW consumed over the maximum peak kW consumed.

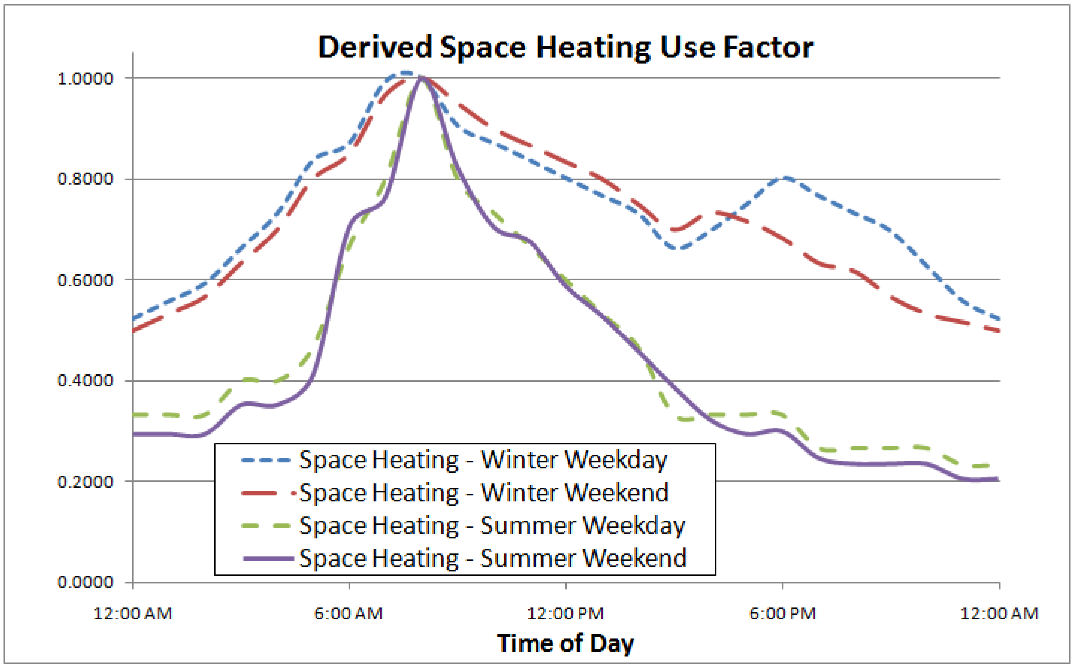

Figure 5.61. Space heating end-use load factor derived from 1992 ELCAP data.

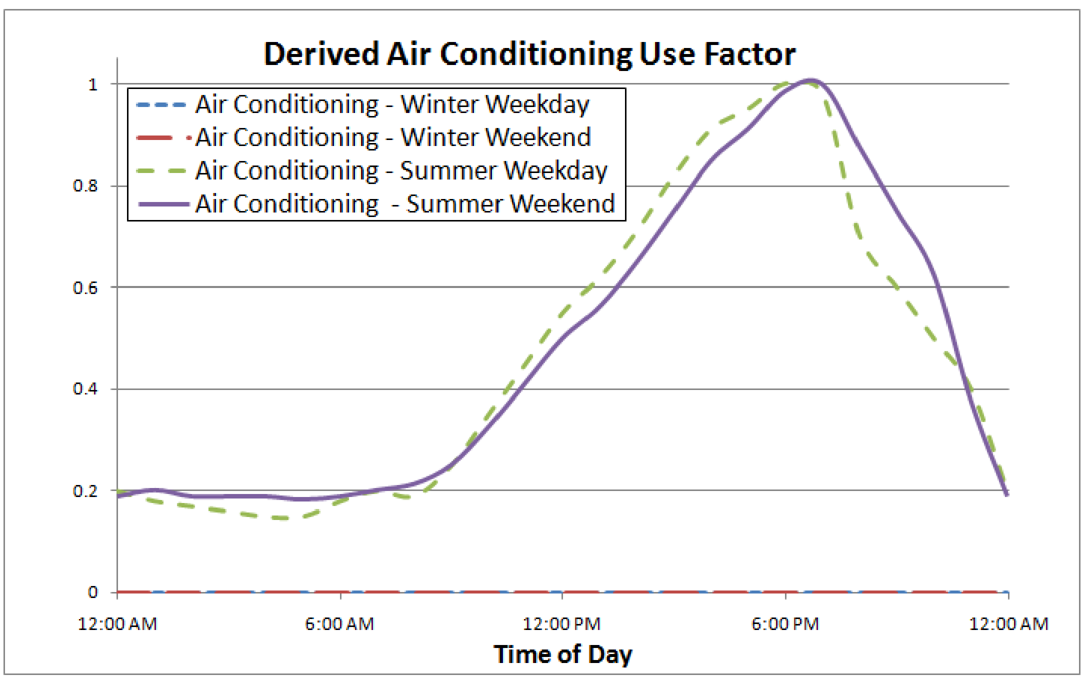

Figure 5.62. Air conditioning end-use load factor derived from 1992 ELCAP data.

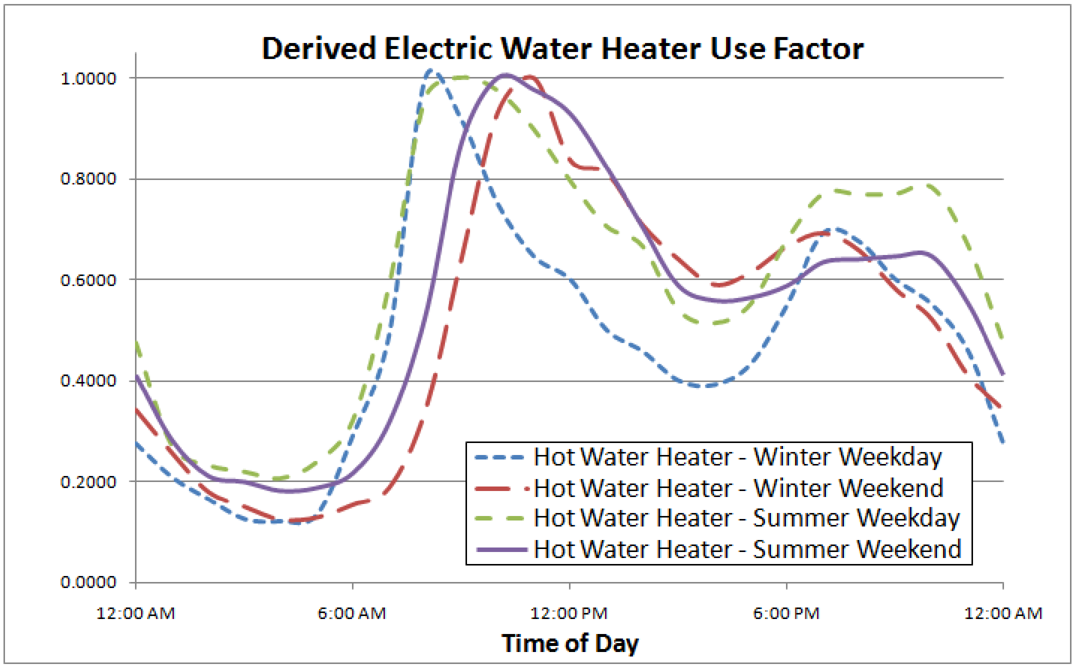

Figure 5.63. Water heater end-use load factor derived from 1992 ELCAP data.

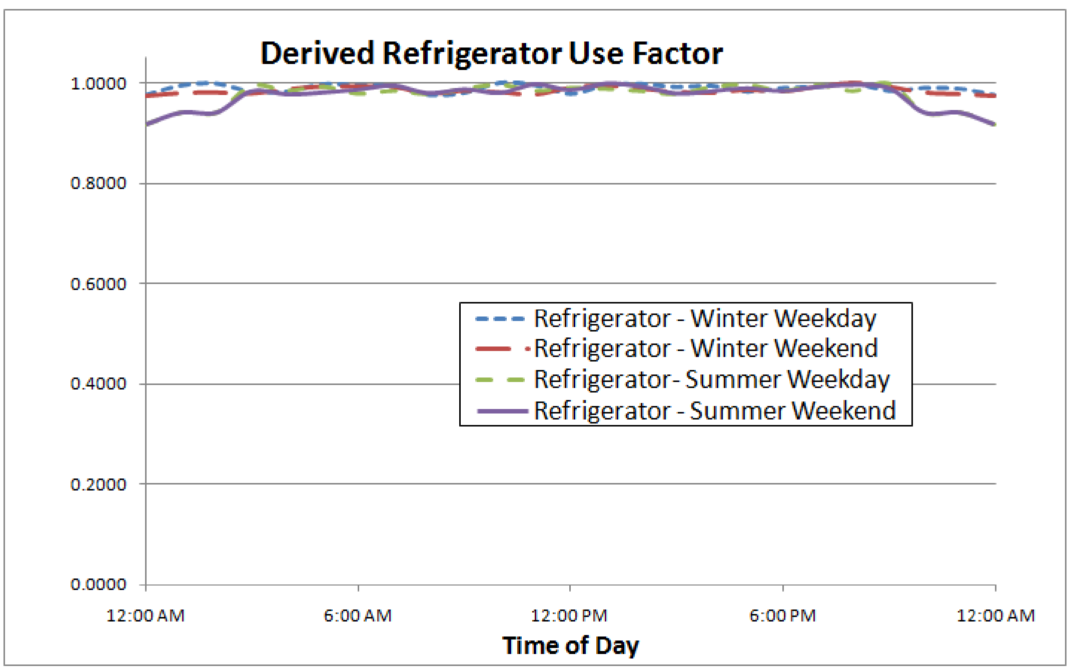

Figure 5.64. Refrigerator end-use load factor derived from 1992 ELCAP data.

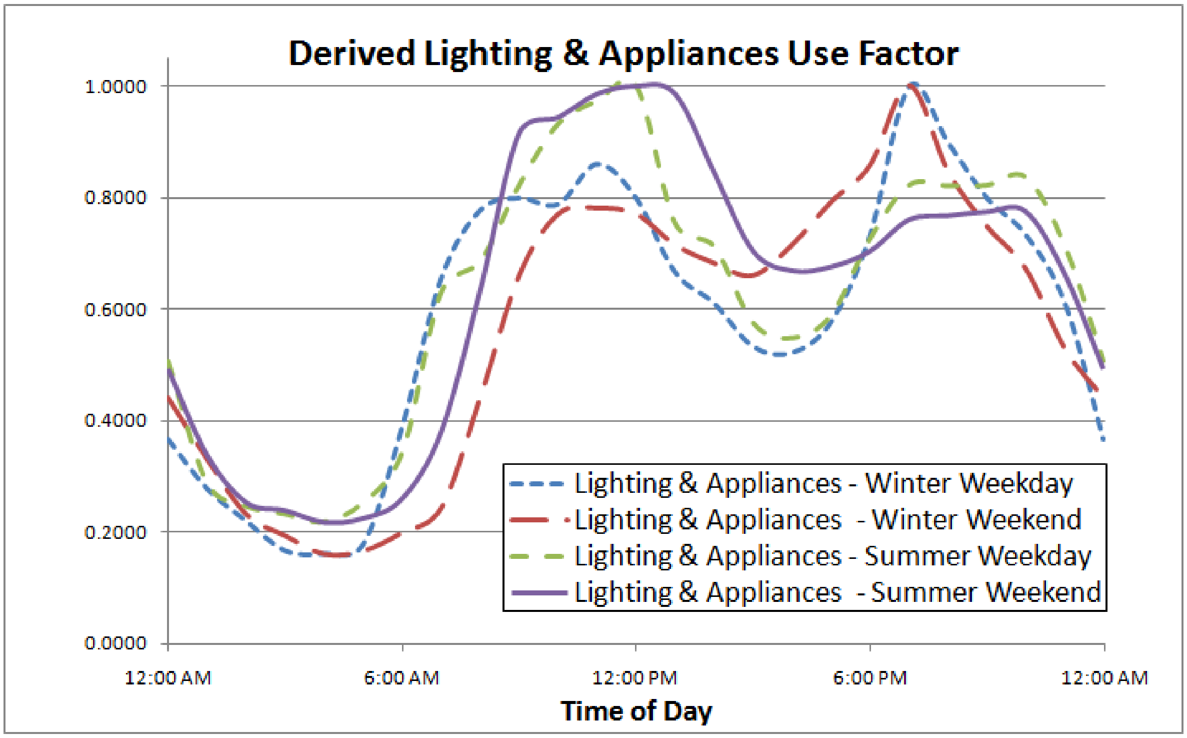

Figure 5.65. Lighting & appliance end-use load factor derived from ELCAP data.

By aggregating these end-use curves and updating them based on the ratios shown in Table 5.16, appropriate representations of total hourly electrical end-use information becomes available for use in this study. The seasonal updated aggregate curves are shown in. Due to a need to conduct a heat recovery analysis for the SOFC-CHP system, Figs. 6 and 7 show the inclusion and exclusion of electric water heater (EWH) usage.

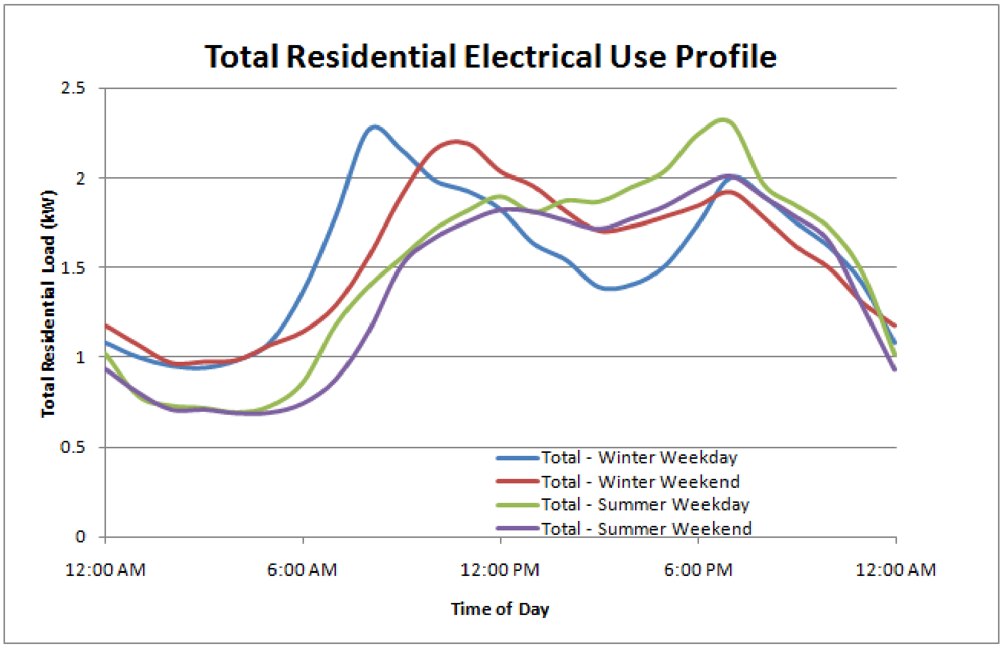

Figure 5.66. Aggregated total residential electrical use profile (with EHW usage included) based on 1992 ELCAP data and updated with ratios from Table I based on 2005 EIA Mean Average UEC Data for the Pacific Northwest.

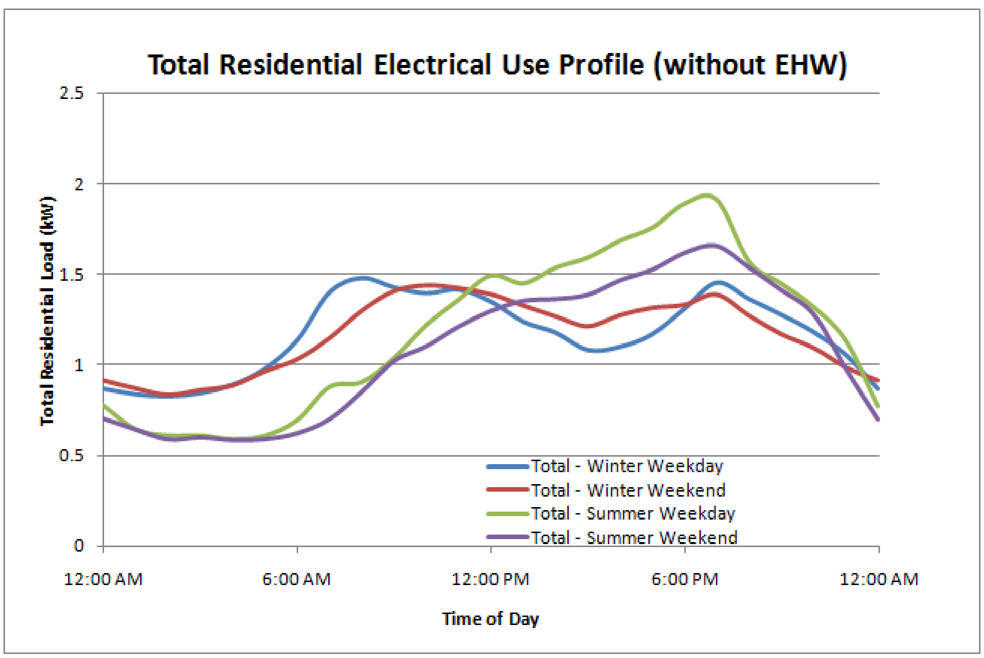

Figure 5.67. Aggregated total residential electrical use profile (without EHW usage included) based on 1992 ELCAP data and updated with ratios from Table I based on 2005 EIA Mean Average UEC Data for the Pacific Northwest.

The entering argument of this work is that current load profile data sets, especially for residential electrical customers, are unavailable. Correspondingly, it is difficult to validate the updated load curves derived above. However, two means were used to substantiate the accuracy of this method. First, because the load profiles describe daily seasonal customer behavior, by integrating time-of-day kW consumption for an annual basis this yields total energy consumed for an entire year. This end-use annual consumption information can be compared to aggregated data collected by the EIA. In this way, if the total consumed electricity profile for the residential customer is accurate, then the annual total should match with the EIA data. The correlation between the updated load curves developed above and the annual EIA data is shown in Table 5.17.

Table 5.17. Total annual electricity consumed per residence.

Source	Total Annual Electricity Consumed per Residence (kW-hrs)
1992 ELCAP Annual Average Residential Consumption	19,735.72
Updated Load Profiles (developed above)†	13,249.60
2005 EIA Annual Average Residential Consumption for the Pacific Northwest [5.119]	12,498.96

† A weighted average of the seasonal daily residential consumption is developed based on the appropriate ratio of weekends to weekdays.

The data presented in Table 5.17 shows only a 6% difference between the updated load profiles developed in this paper and the 2005 EIA data, whereas there is almost a 58% difference for the 1992 ELCAP data upon which the updated load profiles are based. This result demonstrates two factors: first, the outdated end-use information has been significantly improved, and second, the aggregation of the updated profiles is very closely correlated with current consumption information. Despite this good correlation between the load information developed, the obvious drawback is that this aggregation cannot validate the actual time-of-day load profile shapes, only the annual averages. Therefore, a recent total residential load study was used to verify the load profile. The residential load data was collected in 2002-2003 by the Market Surveillance Administrator (MSA), a regulatory agency established by the Alberta Utilities Commission Act; and represents the average daily demand for residential customers in the ENMAX utility service area around the Calgary, Alberta [5.121]. The MSA end-use profile for the residential consumer is based on a 730-day average for households that consumed, on average, 600 kW-hrs per year. A seasonally-aggregated daily load profile based on the in information from Figure 5.66 is shown with the MSA daily load profile in Figure 5.68. The MSA load basis is adjusted to match the load basis of the ELCAP data for the purpose of comparing equivalent households.

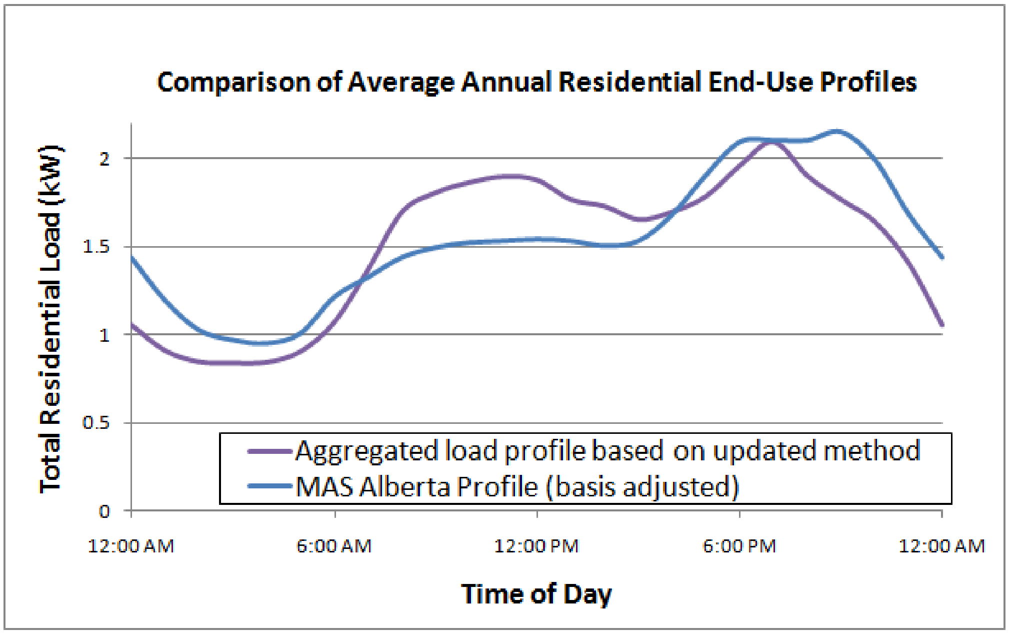

Figure 5.68. Comparison of average annual residential end-use profile shapes.

The data comparison, in Figure 5.68, shows very similar load profile shapes. Although both regions experience climate differences, Calgary, AB and the Pacific Northwest are roughly in the same geographic area (about 400 to 600 miles separation). The similarity in load profile shape helps to correlate the consumer behavior shown by the aggregation of the individual end-use curves upon which the updated curves rely. This shape correlation, along with the total annual consumption information (Table 5.17) helps justify this proposed method for developing updated load profiles.

Avoiding the need to develop and validate end-use load models for the purpose of simply obtaining data for other studies is a great benefit to researchers in the power engineering field. This methodology for updating of end-use load profile curves is applicable to demand datasets for all electrical sectors, including commercial and industrial. Eliminating the need for detailed load component modeling and allowing the researcher to update older data sets from comprehensive studies collected during an era of large regulated utilities may offset the significant lack of end-use load profile information available and serves as the basis for demand modeling in the work presented herein.

5.10.2 Residential Hot Water End-Use Profile

For simulation studies that involved CHP systems, it was important to have the best information about how consumers actually expend resources under real-world conditions. However, it was difficult to acquire end-use hot water consumption information for households in the United States, similar to the difficulty finding non-proprietary or publically available end-use electrical system information. The most ubiquitous resource available for residential hot-water consumption data came from the American Society of Heating, Refrigerating and Air Conditioning Engineers (ASHRAE), shown in Figure 5.69. Although originally published in 1990 [5.122], its data has been cited and validated in many publications [5.123, 5.124].

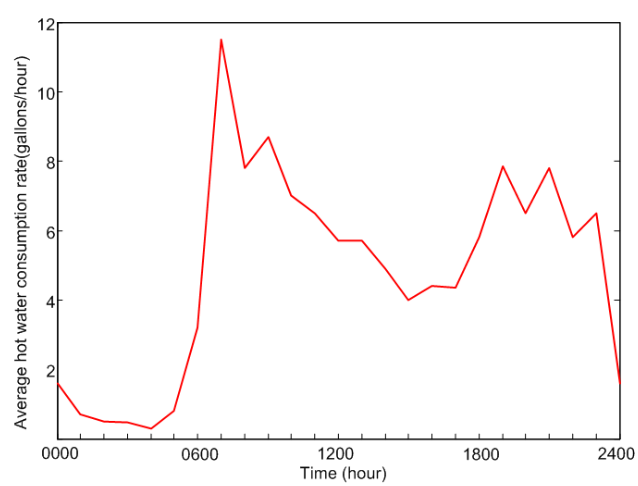

Figure 5.69. ASHRAE Residential Hot Water End-Use [5.122].

5.10.3 Vital and Non-Vital Loading.

An important concept for power management is the differentiation between vital and non-vital loading. Typically, in a residence or commercial building, there is no difference between electrical loads. However, clearly some electrical loads are more important than others. For example, in times of extremis, lighting, HVAC services, and communication systems may be the most important electrical loads. This is in stark contrast to extraneous loads such as clothes washers, copy machines, and other appliances that would not be considered critically important in an emergency. In this way, the load assigned to a microgrid can be differentiated by individual branch circuits whether vital or non-vital. Using rudimentary estimates, about 20% of LV loading is considered vital, while the rest is non-vital.

From a power management perspective, vital load is required to be energized at all times. If this incurs especially high costs of electricity or poorly performing generators to achieve continuous power to the vital loads, that is acceptable. Non-vital loads, on the other hand, are free to be denergized at any time, without warning. Examples of loads that may be denergized without concern are lighting (during the day), thermostatic loads (for a limited period of time), entertainment systems, some appliances, etc. [5.125]. Experience over the past decade has shown increased interest in utilizing non-vital loading as a flexible power system component, analogous to reserve margin [5.126]. At least a portion of non-vital loading may also be energized at any time, asynchronously, to aid in capitalizing on opportunities of low cost electricity or to assist in voltage and frequency regulation [5.125]. Examples of non-vital loads that may be energized or denergized at any time include water heating elements, irrigation pumps, exhaust fans, some lighting, and so on. The manipulation of load resources on a microgrid is considered to be of high importance for meeting customer goals and is considered a key component of comprehensive microgrid power management.

5.10.4 Utility Spot Market Price.

Retail utility prices in the U.S. are available by regulatory region from the EIA. To that end, for simulation the spot market price was bracketed by reasonable published retail prices for the Mountain West region. It is noted, that of all of the eighth NERC regions in the U.S., the Mountain West consistently enjoyed the lowest per kWh price for retail electricity in the nation. While this makes renewables sources increasingly less competitive with the predominance of hydroelectric and coal-combustion power, nonetheless the Mountain West was used for utility price benchmarks.

REFERENCES CITED

[5.1] Collected from numerous manufacturer's specification sheets and product literature.

[5.2] C.C. Lee and S. Dar Lin, Handbook of Environmental Engineering Calculations, McGraw-Hill, New York, 2000, pp. 2.46-2.48.

[5.3] D. Zhu, N. J. Nussbaum, H. D. Kuhns, M.-C. Chang, D. Sodeman, S. Uppapalli, H. Moosmuller, J. C. Chow, and J. G. Watson, "In-Plume Emission Test Stand 2: Emission Factors for 10- to 100-kW U.S. Military Generators", *Journal of Air & Waste Management Association*, Vol. 59, 2009, pgs. 1446–1457.

[5.4] S. Shah, D.Cocker III, K.Johnson, J. M. Lee, B. Soriano, and J. W. Miller, "Emissions of regulated pollutants from in-use diesel back-up generators", *Atmospheric Environment,* Vol. 40, 2006, pgs. 4199–4209.

[5.5] J. H. Seinfeld and S. N. Pandis, Atmospheric Chemistry And Physics - From Air Pollution to Climate Change (2nd Edition). John Wiley & Sons, 2006.

[5.6] U.S. Federal Register, "Control of Emissions of Air Pollution From Nonroad Diesel Engines and Fuel – Final Rule", Vol. 69, No. 124, June 29, 2004, pgs. 38958-38964.

[5.7] Code of U.S. Federal Regulations, Title 40: Protection of Environment, Chapter I – Environmental Protection Agency, Subchapter C: Air Programs, Part 50: National Primary And Secondary Ambient Air Quality Standards, available at: http://ecfr.gpoaccess.gov/

[5.8] L.N. Hannett, F.P. de Mello, G.H. Tylinski, and W.H. Becker, "Validation Of Nuclear Plant Auxiliary Power Supply By Test", *IEEE Transactions on Power Apparatus and Systems*, Vol. 101, No. 9, September 1982, pgs 3068-3075.

[5.9] K.E. Yeager and J.R. Willis, "Modeling Of Emergency Diesel Generators In An 800 Megawatt Nuclear Power Plant", *IEEE Transactions on Energy Conversion*, Vol. 8, No. 3, September 1993.

[5.10] L. Goldstein, "Gas-fired distributed energy resource technology characterizations," National Renewable Energy Laboratory (NREL), NREL/TP-620-34783, Nov. 2003.

[5.11] S. R. Guda, C. Wang, and M. H. Nehrir, "Modeling of Microturbine Power Generation Systems," *Electric Power Components and Systems*, Vol. 34, 2006, pgs. 1027-1041.

[5.12] M.R. Patel, Wind and Solar Power Systems – Second Edition, CRC Press, 2005.

[5.13] Solar Energy Research Institute, “Basic Photovoltaic Principles and Methods”, U.S. Department of Energy, SERI/SP-290-1448, February 1982.

[5.14] W. De Soto, S.A. Klein, and W.A. Beckman, “Improvement and validation of a model for photovoltaic array performance”, *Solar Energy*, Vol. 80, 2006, pgs. 78-88.

[5.15] T.U. Townsend, “A Method for Estimating the Long-Term Performance of Direct-Coupled Photovoltaic Systems”, MS thesis, University Of Wisconsin-Madison, 1989, pgs.24,64.

[5.16] W.H. Strehlow and E.L. Cook, “Compilation of Energy Band Gaps in Elemental and Binary Compound Semiconductors and Insulators”, *Journal of Physical Chemistry Reference Data*, Vol. 2, No.1, 1973.

[5.17] M. G. Villalva, J. R. Gazoli, and E. R. Filho, “Comprehensive Approach to Modeling and Simulation of Photovoltaic Arrays”, *IEEE Transactions On Power Electronics*, Vol. 24, No. 5, May 2009, pgs. 1198-1208.

[5.18] H. Tian, F. Mancilla-David, K. Ellis, E. Muljadi, and P. Jenkins, “A cell-to-module-to-array detailed model for photovoltaic panels”, *Solar Energy*, Vol. 86, 2012, pgs. 2695-2702.

[5.19] S.K. Kim, J. H. Jeon, C.H. Cho, E.S. Kim, and J.B. Ahn, “Modeling and simulation of a grid-connected pv generation system for electromagnetic transient analysis”, *Solar Energy,* Vol. 83, 2009, pgs. 664–678.

[5.20] H. P. Desai and H. K. Patel, “Maximum Power Point Algorithm In Pv Generation: An Overview”, *Proceedings of the 7th International Conference on Power Electronics and Drive Systems (PEDS)*, 2007, pgs. 624–630.

[5.21] N. Fermia, D. Granozio, G. Petrone, M. Vitelli, “Predictive & adaptive MPPT Perturb and Observe Method”, *IEEE Transactions on Aerospace Electronic Systems,* Vol. 43, No. 3, 2007, pgs. 934–950.

[5.22] L. Piegari and R. Rizzo, “Adaptive Perturb and Observe Algorithm for Photovoltaic Maximum Power Point Tracking”, *IET Renewable Power Generation*, Vol. 4, No. 4, 2010, pgs. 317–328.

[5.23] Y. Yusof, S.H. Sayuti, M.A. Latif, M. Wanik, “Modeling And Simulation Of Maximum Power Point Tracker for Photovoltaic System”, *Proceedings of the National Power and Energy Conference (PEC)*, 2004, pgs. 88–93.

[5.24] W. Xiao and W.G. Dunford, “A Modified Adaptive Hill Climbing MPPT Method for Photovoltaic Power Systems”, *IEEE 35th Annual Power Electronics Specialists Conference (PESC)*, Vol. 3, 2004, pgs. 1957–1963.

[5.25] M. Miyatake, M. Veerachary, F. Toriumi, N. Fujii, H. Ko, “Maximum Power Point Tracking of Multiple Photovoltaic Arrays: A PSO Approach”, *IEEE Transactions on Aerospace and Electronic Systems,* Vol. 47 , No. 1, 2011, pgs. 367-380.

[5.26] Hansen, M. Aerodynamics of Wind Turbines. Earthscan Press, 2008.

[5.27] F. D. Bianchi, H. D. Battista, and R. J. Mantz, Wind Turbine Control Systems – Principles, Modeling and Gain Scheduling Design. Springer-Verlag London Limited, 2007.

[5.28] Siegfried Heier, Grid Integration of Wind energy Conversion Systems, John Wiley & Sons, 1998.

[5.29] J. G. Slootweg, S.W.H. de Haan, H. Polinder & W.L. Kling, “General Model for Representing Variable Speed Wind Turbines in Power System Dynamics Simulations,” *IEEE Transactions on Power Systems*, Vol. 18, No. 1, Feb. 2003.

[5.30] M. R. Patel, Wind and Solar Power Systems, CRC Press, 1999.

[5.31] Ahmet Duran Sahin, “Progress and recent trends in wind energy”, *Progress in Energy and Combustion Science*, Vol. 30, 2004.

[5.32] E. Muljadi and C.P. Butterfield, “Pitch-Controlled Variable-Speed Wind Turbine Generation”, *1999 IEEE Industry Applications Society Annual Meeting*, October, 1999.

[5.33] K. E. Johnson, L. Y. Pao, M. J. Balas, L. J. Fingersh, “Control of variable-speed wind turbines: Standard and adaptive techniques for maximizing energy capture”, *IEEE Control Systems Magazine*, Vol. 26, No. 3, June 2006.

[5.34] F.D. Bianchi, R.J. Mantz and C.F. Christiansen. “Power regulation in pitch controlled variable speed WECS above rated wind speed”, *Renewable Energy*, Vol. 29, 2004.

[5.35] M.M. Hand, M.J. Balas, “Systematic controller design methodology for variable-speed wind turbines”, *Wind Engineering*, Vol. 24, No. 3, 2000.

[5.36] A.E. Fitzgerald, C. Kingsley Jr., S.D. Umans, Electric Machinery. McGraw Hill, Boston, 2003.

[5.37] P.W. Sauer. Power System Dynamics and Stability. Prentice Hall, Upper Saddle River, NJ, 1998.

[5.38] H. Huang & L. Chang. “Energy-Flow Direction Control of Grid-Connected IGBT Inverters for Wind Energy Extraction”, *Proceedings of Canadian Conf on Electrical & Computer Engineering*, Vol. 1, 2000.

[5.39] S. Li, T. A. Haskew, & L. Xu. “Conventional and novel control designs for direct driven PMSG wind turbines”, *Electric Power Systems Research,* Vol. 80, 2010.

[5.40] C. Wang, M.H. Nehrir, and H. Gao, “Control of PEM Fuel Cell Distributed Generation Systems,” *IEEE Transactions on Energy Conversion*, Vol. 21, No. 2, June 2006.

[5.41] Pacific Northwest Cooperative Agricultural Weather Network, AgriMet Historical Dayfile Data Access, Deer Lodge, MT (DRLM), available at: http://www.usbr.gov/pn/agrimet/webaghrread.html.

[5.42] W.D. Kellogg, M.H. Nehrir, G. Venkataramanan, V. Gerez, “Generation unit sizing and cost analysis for stand-alone wind, photovoltaic, and hybrid wind/PV systems,” *IEEE Transactions on Energy Conversion*, Vol. 13, No. 1, March 1998.

[5.43] J. Appleby and F.R. Foulkes, Fuel Cell Handbook, Van Nostrand Reinhold, New York, 1989.

[5.44] C. Wang and M.H. Nehrir, "A Physically-Based Dynamic Model for Solid Oxide Fuel Cells," *IEEE Transactions on Energy Conversion*, Vol. 22, No. 4, Dec. 2007, pgs. 864 - 872.

[5.45] N. Autissier, F. Palazzi, F. Marechal, J. van Herle, and D. Favrat, “Thermo-Economic Optimization of a Solid Oxide Fuel Cell, Gas Turbine Hybrid System”, *Journal of Fuel Cell Science and Technology*, Vol. 4, Iss. 2, 2007, pgs. 123-129.

[5.46].A. Laughton and D.F. Warne, Electrical Engineer's Reference Book (16th Edition), Elsevier, 2003, pgs. 26/18-20.

[5.47] Hsin-Sena Chu, F. Tsau, Yi-Yiea Yan, Kan-Lina Hsueh, and Fa-Lin Chen, “The development of a small PEMFC combined heat and power system”, *Journal of Power Sources*, Vol. 176, Iss. 2, 2008, pgs. 499-514.

[5.48] H. Zhu & R. J. Kee, “Thermodynamics of SOFC efficiency and fuel utilization as functions of fuel mixtures and operating conditions”, *Journal of Power Sources*, Vol. 161, Iss. 2, Oct 2006.

[5.49] Y. Tanaka, A. Momma, K. Kato, A. Negishi, K. Takano, K. Nozaki & T. Kato, "Development of electrical efficiency measurement techniques for 10 kW-class SOFC system: Part I. Measurement of electrical efficiency", *Energy Conversion and Management*, Vol. 50, Iss. 3, March 2009.

[5.50] S. Farhad & F. Hamdullahpur, "Developing fuel map to predict the effect of fuel composition on the maximum efficiency of solid oxide fuel cells", *Journal of Power Sources*, Vol. 193, Iss. 2, Sept 2009.

[5.51] Aidu Qi, Brant Pepply, and Kunal Karan, "Integrated fuel processors for fuel cell application: A review", *Fuel Processing Technology*, Vol. 88, 2007, pgs.. 3-22.

[5.52] F. Calise, M. Dentice d' Accadia, L. Vanoli, and Michael R. von Spakovsky, "Full load synthesis/design optimization of hybrid SOFC-GT power plant," *Energy*, Vol. 32, 2007, pgs. 446-458.

[5.53] A. Rao, J. Maclay, and S. Samuelsen, "Efficiency of electrochemical systems," *Journal of Power Sources*, Vol. 134, 2004, pgs. 181-184.

[5.54] N. Wouodstra, T.P. van der Stelt, and K. Hemmes, "The Thermodynamic Evaluation and Optimization of Fuel Cell Systems," *Journal of Fuel Cell Science and Technology*, Vol. 3, 2006, pgs. 155-164.

[5.55] Felder, R. and Rousseau, R. Elementary Principles of Chemical Processes, John Wiley & Sons, New York, 1978.

[5.56] A. E. Lutz, R. S. Larson, and J.O. Keller, "Thermodynamic comparison of fuel cells to the Carnot cycle," *International Journal of Hydrogen Energy*, Vol. 27, 2002, pgs. 1103–1111.

[5.57] S.E. Wright. "Comparison of the theoretical performance potential of fuel cells and heat engines," *Renewable Energy*, Vol. 29, 2004, pgs. 179-195.

[5.58] C. Haynes, "Clarifying reversible efficiency misconceptions of high temperature fuel cells in relation to reversible heat engines," *Journal of Power Sources*, Vol. 92, 2001, pgs. 199-203.

[5.59] H. Hassanzadeh and S.H. Mansouri, "Efficiency of ideal fuel cell and Carnot cycle from a fundamental perspective," *Proceedings of the Institution of Mechanical Engineers -- Part A -- Power & Energy*, Vol. 219, Iss. 4, 2005, pgs. 245-254.

[5.60] R. O'Hayre, Suk-Won Cha, W. Colella, F. B. Prinz, Fuel Cell Fundamentals, John Wiley & Sons, New York, 2006.

[5.61] I. Beausoliel-Morrison, A. Schatz, and F. Marechal. "A Model for Simulating the Thermal and Electrical Production of Small-Scale Solid-Oxide Fuel Cell Cogeneration Systems within Building Simulation Programs". *HVAC&R Research Special Issue*, Vol. 12, No. 3a, 2006, pgs. 641-667.

[5.62] P.J. Linstrom and W.G. Mallard, Eds., "NIST Chemistry WebBook - Gas phase thermochemistry data", NIST Standard Reference Database Number 69, June 2005, National Institute of Standards and Technology, (http://webbook.nist.gov).

[5.63]W. Jamsak, S. Assabumrungrat, P.L. Douglas, N.Laosiripojana, S. Charojrochkul, "Theoretical performance analysis of ethanol-fuelled solid oxide fuel cells with different electrolytes," *Chemical Engineering Journal*, Vol. 119, 2006, pgs. 11-18.

[5.64] F.A. Coutelieris, S. Douvartzides, P. Tsiakaras, "The importance of the fuel choice on the efficiency of a solid oxide fuel cell system," *Journal of Power Sources*, Vol. 123, 2003, pgs. 200-205.

[5.65] F. Calise, M. Dentice d'Accadia, A. Palombo, L. Vanoli, "Simulation and exergy analysis of a hybrid Solid Oxide Fuel Cell (SOFC)-Gas Turbine System," *Energy*, Vol. 31, 2006, pgs. 3278-3299.

[5.66] M. Bischoff, "Large Stationary Fuel Cell Systems: Status and Dynamic Requirements," *Journal of Power Sources*, Vol. 154, 2006, pgs. 461-466.

[5.67] Boyce, Meherwan P., Gas Turbine Engineering Handbook (3rd Edition). Elsevier, 2006, pgs. 86-91.

[5.68] M. C. Williams, J. P. Strakey, W. A. Surdoval, and L. C. Wilson, "Solid oxide fuel cell technology development in the U.S.," *Solid State Ionics*, Vol. 177, Iss. 19, 2006.

[5.69] W.A. Surdoval, "US DoE Fossil Energy Fuel Cell Program," presented at: 7th SECA Workshop & Peer Review, Philadelphia, PA, Sept 2006, available at: http://www.netl.doe.gov/publications/proceedings/06/seca.

[5.70] U.S. Department of Energy, "Annual Energy Outlook 2006", DOE/EIA-0383, Energy Information Administration, Washington, D.C., 2006.

[5.71] R. U. Ayres, L. W. Ayres, and B. Warr "Exergy, power and work in the US economy, 1900–1998", *Energy*, Vol. 28, Iss. 3, March 2003.

[5.72]. U. Ayres, H. Turton, and T. Casten, "Energy efficiency, sustainability and economic growth", *Energy*, Vol. 32, Iss. 5, May 2007.

[5.73] W. Graus & E. Worrell, "Trend in efficiency and capacity of fossil power generation in the EU", *Energy Policy*, Vol. 37, Iss.. 6, June 2009.

[5.74] P.B. Nigel and D. Thompsett (editors), Fuel Cells Compendium - Chapter 1 (US distributed generation fuel cell program), Elsevier, 2005.

[5.75] M.H. Nehrir and C. Wang, Modeling and Control of Fuel Cells: Distributed Generation Applications, Wiley-IEEE Press, 2009.

[5.76] C. Wang and M.H. Nehrir, "Load transient mitigation for stand-alone fuel cell power generation systems," *IEEE Transactions on Energy Conversion*, Vol. 22, No. 4, December 2007.

[5.77] K.P. Adzakpa, K. Agbossou, Y. Dube, M. Dostie, M. Fournier, A. Poulin, "PEM fuel cells modeling and analysis through current and voltage transient behaviors," *IEEE Transactions on Energy Conversion*, Vol. 23, No. 2, June 2008.

[5.78] C. Wang, M.H. Nehrir, and H. Gao, "Control of PEM Fuel Cell Distributed Generation Systems," *IEEE Transactions on Energy Conversion*, Vol. 21, No. 2, June 2006.

[5.79] C. Colson, M. Nehrir, M. Deibert, M. Amin, & C. Wang, "Efficiency Evaluation of Solid-Oxide Fuel Cells in Combined Cycle Operations", *ASME Journal of Fuel Cell Science &Technology*, Vol. 6, Iss. 2, Feb. 2009.

[5.80] F. Kreith & R. Emmett West, CRC Handbook of Energy Efficiency. CRC-Press, 1996.

[5.81] M. F. Serincan, U. Pasaogullari, and N. M. Sammes, "Effects of operating conditions on the performance of a micro-tubular solid oxide fuel cell (SOFC)", *Journal of Power Sources*, Vol. 192, Iss. 2, July 2009.

[5.82] A. Nakajo, Z. Wuillemin, J. Van herle, and D. Favrat, "Simulation of thermal stresses in anode-supported solid oxide fuel cell stacks. Part I: Probability of failure of the cells", *Journal of Power Sources*, Vol. 193, Iss. 1, August 2009.

[5.83] N. Lu and S. Katipamula, "Control strategies of thermostatically controlled appliances in a competitive electricity market", *Proceedings of 2005 IEEE Power Engineering Society General Meeting*, June, 2005.

[5.84] M.Haines, J.Davison, "Designing carbon capture power plants to assist in meeting peak power demand", *Energy Procedia,* Vol. 1, Iss. 1, Feb 09.

[5.85] M. Kintner-Meyer, K. Schneider, R. Pratt, "Impacts assessment of plug-in hybrid vehicles on electric utilities and regional US power grids, Part 1: technical analysis", Regional Grids and Plug-in Hybrids, Pacific Northwest National Laboratory - Richland, WA, 2007.

[5.86] Compiled from multiple Energy Information Administration spreadsheets including "Emissions Detail by State", "Table 5.1-Emissions from Energy Consumption at CPPs and CHPs, 1996 - 2007", and "Electric Power Annual 2007- State Tables", available at: http://www.eia.doe.gov.

[5.87] U. S. Department of Energy, "2005 Electric Sales, Revenue, Price: Tables 2 & 3", Energy Information Administration, Washington, D.C., 2005, available at: http://www.eia.doe.gov/cneaf/electricity/esr.

[5.88] D.H. Doughty, P. C. Butler, A. A. Akhil, N. H. Clark, and J. D. Boyes, "Batteries for Large-Scale Stationary Electrical Energy Storage", *Electrochemical Society Interface*, Vol. 19, No. 3, 2010, pgs. 49-53.

[5.89] K.C. Divya and J. Østergaard, "Battery energy storage technology for power systems—An overview", *Electric Power Systems Research*, Vol. 79, 2009, pgs. 511-520.

[5.90] Z.M. Salameh, M. A. Casacca, and W. A. Lynch, "A mathematical model for lead–acid batteries," *IEEE Transactions on Energy Conversion*, Vol. 7, No. 1, Mar. 1992, pgs. 93–98.

[5.91] M. A. Casacca, "Determination of lead–acid battery capacity via mathematical modeling techniques," *IEEE Transactions on Energy Conversion*, Vol. 7, No. 3, Sept. 1992, pgs. 442–446.

[5.92] M.H. Nehrir, B.J. LaMeres, G. Venkataramanan, V. Gerez, and L. A. Alvarado, "An Approach to Evaluate the General Performance of Stand-Alone Wind/Photovoltaic Generating Systems", *IEEE Transactions On Energy Conversion*, Vol. 15, No. 4, Dec. 2000, pgs. 433-439.

[5.93] M. Durr, A. Cruden, S. Gair, and J. R. McDonald, "Dynamic model of a lead–acid battery for use in a domestic fuel cell system," *Journal of Power Sources*, Vol. 161, No. 2, Oct. 2006, pgs. 1400–1411.

[5.94] N. K. Medora and A. Kusko, "Dynamic battery modeling of lead–acid batteries using manufacturers' data," *Proceedings of the 27th International Telecommunications Conference - INTELEC '05*, Sep. 2005, pgs. 227–232.

[5.95] M. Ceraolo, "New dynamical models of lead-acid batteries", *IEEE Transactions on Power Systems*, Vol. 15, No. 4, 2000, pgs. 1184–1190.

[5.96] C.S. Moo, K.S. Ng, Y.P. Chen, and Y.C. Hsieh, "State-of-Charge Estimation with Open-Circuit-Voltage for Lead-Acid Batteries", *Power Conversion Conference Proceedings*, April 2007, pgs. 758 – 762.

[5.97] S. Barsali and M. Ceraolo, "Dynamical Models of Lead-Acid Batteries: Implementation Issues", *IEEE Transactions on Energy Conversion*, Vol. 17, No. 1, 2002, pgs.16-23.

[5.98] R. Walawalkar and J. Apt, "Market Analysis of Emerging Electric Energy Storage Systems", prepared for National Energy Technology Laboratory, DOE/NETL-2008/1330, July, 2008.

[5.99] D. Rastler, "Electricity Energy Storage Technology Options", EPRI-2010/1020676, Dec. 2010

[5.100] S. B. Peterson, J.F. Whitacre, and J. Apt, "The economics of using plug-in hybrid electric vehicle battery packs for grid storage", *Journal of Power Sources,* Vol. 195, 2010, pgs. 2377-2384.

[5.101] S.A. Pourmousavi, R. K. Sharma, and B. Asghari, "A Framework for Real-Time Power Management of a Grid-Tied Microgrid to Extend Battery Lifetime and Reduce Cost of Energy", *Proceedings of IEEE PES Innovative Smart Grid Technologies (ISGT),* Jan. 2012

[5.102] H. Wenzl, I. Baring-Gould, R. Kaiser, B. Y. Liaw, P. Lundsager, J. Manwell, A. Ruddell, and V. Svoboda, "Life prediction of batteries for selecting the technically most suitable and cost effective battery", *Journal of Power Sources*, Vol. 144, 2005, pgs 373-384.

[5.103] S. Drouilhet and B.L. Johnson, "A Battery Life Prediction Method for Hybrid Power Applications", NREL/CP-440-21978, January 1997.

[5.104] Robert Lasseter and Joe Eto, "Value and Technology Assessment to Enhance the Business Case for the CERTS Microgrid", Final Project Report prepared by Consortium for Electric Reliability Technology Solutions (CERTS), DE-FC02-06CH11350, May 15, 2010.

[5.105] MK-Powered data sheet (LIT-SS1004), model ES10-12S, January 2009.

[5.106] IEEE Std 141-1993, IEEE Recommended Practice for Electric Power Distribution for Industrial Plants (The IEEE Red Book), pgs 62-63.

[5.107] A. Engler, "Applicability of Droops in Low Voltage Grids", *International Journal of Distributed Energy Resources*, Vol. 1, No. 1, 2005.

[5.108] P. Wan and M.D. Lemmon, "Optimal power flow in microgrids using event-triggered optimization", *Proceedings of the American Control Conference*, 2010, pgs. 2521-2526.

[5.109] P. Kundur, N. Balu, and M. Lauby, Power system stability and control, McGraw-Hill, 1994, pg. 209.

[5.110] A.J. Wood and B.F. Wollenberg, Power Generation Operation and Control (2nd Edition). John Wiley and Sons, Inc., New York, 1996.

[5.111] K. Debrabandere, B. Bolsens, J. Van den Keybus, A.Woyte, J. Driesen, and R. Belmans, "A voltage and frequency droop control method for parallel inverters," *IEEE Transactions on Power Electronics*, Vol. 22, No. 4, 2007, pgs. 1107–1115.

[5.112] A. Haddadi and G. Joos, "Load sharing of autonomous distribution-level microgrids", *Proceedings of the IEEE Power and Energy Society General Meeting*, 2011.

[5.113] T. L. Vandoorn, B. Meersman, L. Degroote, B. Renders, and L. Vandevelde, "A control strategy for islanded microgrids with DC-link voltage control", *IEEE Transactions on Power Delivery*, Vol. 26, No. 2, 2011, pgs. 703-713.

[5.114] S.W. Heunis and R. Herman, "A probabilistic model for residential consumer loads", *IEEE Transactions on Power Systems*, Vol. 17, Iss. 3, August 2002.

[5.115] R.T. Guttromson, D.P. Chassin, and S.E. Widergren, "Residential energy resource models for distribution feeder simulation", *2003 IEEE Power Engineering Society General Meeting Proceedings*, Vol. 1, July 2003.

[5.116] D.H.O. McQueen, P.R. Hyland, S.J. Watson, "Monte Carlo simulation of residential electricity demand for forecasting maximum demand on distribution networks", *IEEE Transactions on Power Systems*, Vol. 19, Iss. 3, August 2004.

[5.117] T. V. Cutsem and C. Vournas, Voltage Stability of Electric Power Systems, Springer, 1998.

[5.118] J.M. Cahill, K.G. Ritland, and W. Lin-Kelly, "Description of Electric Energy Use In Single Family Residences in the Pacific Northwest 1986-1992", End-Use Load and Consumer Assessment Program (ELCAP), Bonneville Power Administration, December 1992.

[5.119] United States Department of Energy – Energy Information Administration, "2005 Residential Energy Consumption Survey", released September 2008, available at: http://www.eia.doe.gov/emeu/recs/recs2005/c&e/detailed_tables2005c&e

[5.120] M. Kintner-Meyer, K. Schneider, R. Pratt, “Impacts assessment of plug-in hybrid vehicles on electric utilities and regional US power grids, Part 1: technical analysis”, Regional Grids and Plug-in Hybrids, Pacific Northwest National Laboratory Richland, WA, 2007.

[5.121] Market Surveillance Administrator, “MSA Report: Residential Load Profiles”, Calgary, Alberta, April 2004, available at: www.albertamsa.ca/files/ResidentialLoadProfiles042804.pdf

[5.122] B.R. Becker and K.E. Stogsdill, “Development of a hot water use data base”, *Proceedings of the Annual meeting of the American Society of Heating, Refrigerating and Air-Conditioning Engineers (ASHRAE)*, June 1990, pgs. 422-427.

[5.123] P. Fairey and D. Parker, “ A Review of Hot Water Draw Profiles Used in Performance Analysis of Residential Domestic Hot Water Systems”, Florida Solar Energy Center, FSEC-RR-56-04, July 2004.

[5.124] R. Hendron and J. Burch, “Development of Standardized Domestic Hot Water Event Schedules for Residential Buildings”, NREL/CP-550-40874, Originally presented at *Energy Sustainability 2007,* August 2008.

[5.125] D.J. Hammerstrom (PI), “Pacific Northwest GridWise Testbed Demonstration Project – Part II. Grid Friendly Appliance Project (Final Report)”, Pacific Northwest National Laboratory under U.S. DOE contract DE-AC05-76L01830, October 2007.

[5.126] A. Molderink, V. Bakker, M. G. C. Bosman, J. L. Hurink, and G. J. M. Smit, “Management and Control of Domestic Smart Grid Technology”, *IEEE Transactions On Smart Grid*, Vol. 1, No. 2, September 2010, pgs. 109-119.

CHAPTER 6

INTRA-MICROGRID SIMULATION

The microgrid power management MAS is an example of an automated decision-making system that must comprehensively consider complex factors that affects a differentiated system. To assist the decentralized agents self-organize, a system of informational metrics is used, as described in 4.5 . During MAS operation, each agent periodically determines two values that represent the individual asset's operational situation: cost and a performance measure. Cost, which is self-explanatory, is a direct representation of the monetary value of the real and reactive power produced or consumed at that instant; in other words, operational cost. A cost measure alone, however, is not adequate to assist agents determine proper operation. Subsequently, each agent computes a performance measure for its instantaneous operating point based on how well the agent is achieving optimal operation based on assigned goals. These metrics are communicated between agents and assists them in cooperating. To be clear, how cost and performance metrics are determined depends upon asset dynamics, owner/operator objectives, and asset's role within the microgrid. This chapter intends to highlight how a variety of these metrics is readily achievable with the enhanced decentralized MAS and how the development of specific metrics is important in governing the behavior of agents.

6.1 Energy System Arbitrage and Tradeoffs

Energy arbitrage, when used in a power systems context, refers to the use of energy as a commodity. Microgrids, and the generation assets within them, can produce energy at a certain price. That energy commodity may be sold immediately or, if storage is incorporated into the microgrid, the energy may be held and sold at a later time. Part of the decision-making process for microgrid assets is whether to generate power now or defer generation until the future, and whether to store energy or not.

Around the world, the most common energy arbitrage pairing actually in use are diesel genset and lead-acid battery hybrids. Primarily, the low cost of diesel generation and the ruggedness of the lead-acid battery make for a cost-effective and survivable hybrid system. Examples of these stationary power hybrids range from on-grid uninterruptible power supplies (UPS) [6.1], to off-grid rural community power [6.2, 6.3], to remote base transceiver stations (BTS) for critical telecommunications [6.4, 6.5, 6.6]. These diesel-battery hybrids are being used in a simple energy arbitrage arrangement. That is, the battery storage capacity allows the diesel to periodically shutdown, thereby conserving fuel and the associated operating expense. This operational control scheme is simple: when the diesel reaches a lower loading threshold and the battery is fully charged, it shuts down. When the battery reaches a low SOC threshold, the diesel restarts to power the load and fully charge the battery. This cycle repeats. Clearly, this hybrid configuration does not optimize diesel operation, nor does it consider battery cyclic round-trip efficiency. This scenario, and many other similar ones where assets are used in arbitrage configurations, demonstrates great opportunity for optimizing operational performance. Hence, a short discussion about the importance of considering multiple objectives in energy arbitrage arrangements is made in this section.

For most generation assets, minimizing the cost per unit energy of an asset's operation can be a useful objective. After all, it follows that the lowest cost per unit energy will coincide with operation at the highest efficiency. This is illustrated in Figure 6.1, which displays the cost per unit energy for a 40kW diesel genset (model described in 5.2) versus rated output power and a range of sales prices for generated electrical energy, given a diesel fuel price of $0.97USD per liter [6.7]. In a grid connected system, when the cost of energy supplied by the grid is more than energy supplied by the hybrid system, the net cost per unit energy is positive corresponding to a profit for the hybrid system. It is clear in Figure 6.1 that a significant region (below the plane of zero cost per unit energy) exists where it is costly to operate the diesel. However, above the plane, profit is derived from diesel operation. If dispatch decisions were made solely on the basis of maximizing cost per unit energy, the optimal solutions would lie at the maximum efficiency for each cost scenario, distinguished as the ridge of peaks that dominate the topology of the graph in Figure 6.1. However, when attempting to optimize multiple assets operating in conjunction, optimizing the cost per unit energy objective alone may create undesirable situations. This typically arises in constrained multiple objective optimizations where tradeoff opportunities arise for one or more assets to achieve better overall system results.

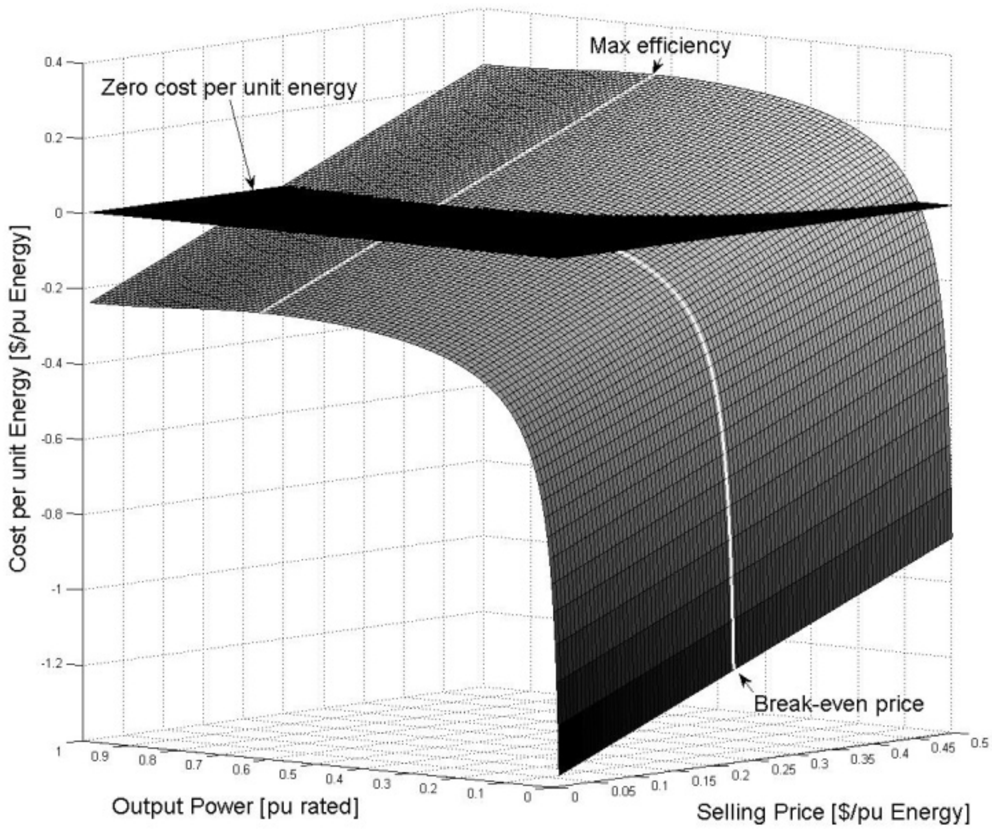

Figure 6.1. Diesel genset cost per unit energy cost vs. loading and selling price.

Different than cost per unit energy, net operational cost indicates an asset's temporal profit or loss, when accounting for all expenses and revenues derived from operation. In some cases, net operational cost may be positive indicating profitable operation, as may be expected from the sale of power. Consider, again, characteristics of the 40kW-rated diesel genset. In Figure 6.2, assuming a price ($0.42/kWh) allowing the genset to sell electricity profitably to the utility, the net operational cost (profit or loss) and genset efficiency are displayed. Note that the operating point to achieve optimal efficiency differs from the operating point to achieve optimal revenue. Whereas in Figure 6.1, if decisions were to be made regarding where to operate the diesel genset solely based on the highest per unit energy available, dispatch would always occur at the diesel's most efficient operating point. These decisions would neglect opportunities for higher revenue, as shown in Figure 6.2. This situation illustrates a case where a battery storage and genset hybrid may be exploited to achieve multiple objectives, given the right decision-making process.

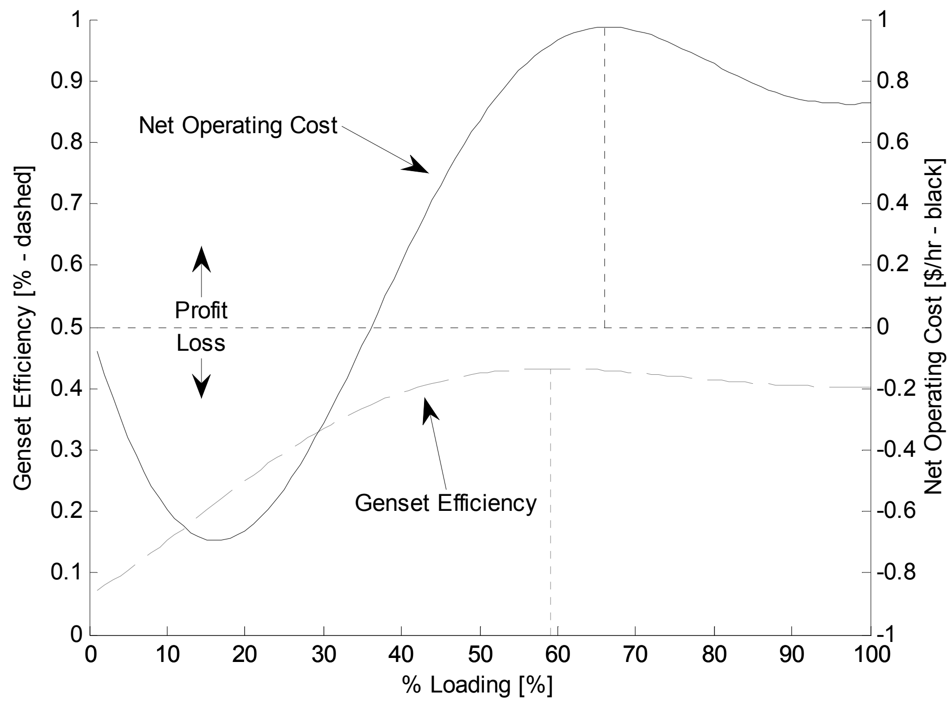

Figure 6.2. Diesel genset efficiency and net operating cost versus loading.

Clearly, having separate net operational cost and efficiency information allows decision-making to account for each of these factors separately. This discussion is applicable to not only dispatchable or storage assets, but all assets that transact energy on a hybrid system or microgrid. It is noted, however, that cost per unit energy can be a useful factor when weighting other deciding factors and is not intended to discount it when appropriate. This analysis of energy arbitrage and the recognition that considering multiple objectives can lead to better asset decisions justifies the interest in multi-objective power management and control for microgrids. Therefore, for the purposes of power and energy management decision-making, the methodology developed uses factors such as net operational cost and efficiency as separate decision-making criteria.

6.2 Simulations

The following two sections present simulations of the two modes microgrids operate in: grid-connected and islanded. The conditions for each simulation focus on unique aspects presented by the particular microgrid mode of operation.

6.2.1 Grid-Connected Operations

Many reported MAS have utilized a classic bid-award system for agent interaction [6.8, 6.9]. This process may include: a central call for economic bids to meet a proposed demand, collation and ranking of incoming bids, and awarding contracts based on bid ordering. This process may repeat indefinitely and works well with dispatching competing generators in real-time. Just as with conventional commodity auctions, the bid market is very effective at prioritizing based on lowest cost and dispatching the resulting configurations.

While in the interconnected mode, the spot market price of electricity is dictated by the utility alone. The microgrid is not a competitive participant in spot pricing. Therefore, the MAS methodology in this demonstration expands on the bid-award system. The availability and price of utility electrical power is taken as a benchmark.

MAS agents organize their dispatch based on this price threshold. In other words, using the spot price, agents decide whether it is in their best interest to operate or not, based on their locally-assigned goals.

In this demonstration, consumer agents assigned to control load are fully enabled to act according to grid price signals. In other words, the load agents may energize or shed load at will, based on the cost and performance functions shown in (6.1) and (6.2). The cost function represents the price the load consumer agent is willing to pay to energize increments of its load bank; vital load (0 to P_{vital}) is worth much more than the less critical non-vital load (P_{vital} to P_{rated}). The consumer agent will decide to energize load up to the cost effective threshold determined by the relationship between the load cost function and grid price, shown by the shaded region in Figure 6.3 for 100kW of total load installed in the bank.

$$C_i[k] = \begin{cases} C_{max}, & P_i[k] \le P_{vital} \\ \dfrac{C_{max}}{P_1} e^{-\frac{P_1}{P_{rated}}}, & P_i[k] > P_{vital} \end{cases} \tag{6.1}$$

$$\rho_i[k] = \begin{cases} 0.6\left(\dfrac{P_i}{P_{rated}}\right)^3 - 2.2\left(\dfrac{P_i}{P_{rated}}\right)^2 + 2.6\left(\dfrac{P_i}{P_{rated}}\right), & P_i[k] \le P_{rated} \\ 0, & \text{otherwise} \end{cases} \tag{6.2}$$

where, C_i is the cost function of the load bank i at increment k; C_{max} is the maximum cost defined by the user for the load; P_{vital} is the user-defined threshold below which power to the load is critical; ρ_i is the performance function of the load bank i at increment k; P_i is the operating power of load bank i at increment k; and P_{rated} is the total power rating of the installed load bank. The performance function shown in Figure 6.4 implies that the more load energized by the load consumer agent, the better the performance; at lower loading, the incremental improvement in performance is higher than for adding the same quantity of load at higher loading. The combination of the cost and performance functions allow the load consumer agent to make decisions for the local microgrid load bank, as well as participate with the other MAS agents in overall microgrid dispatch.

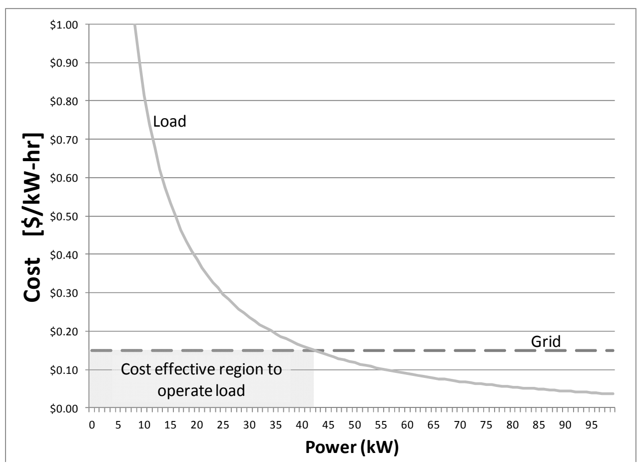

Figure 6.3. Load consumer agent cost function.

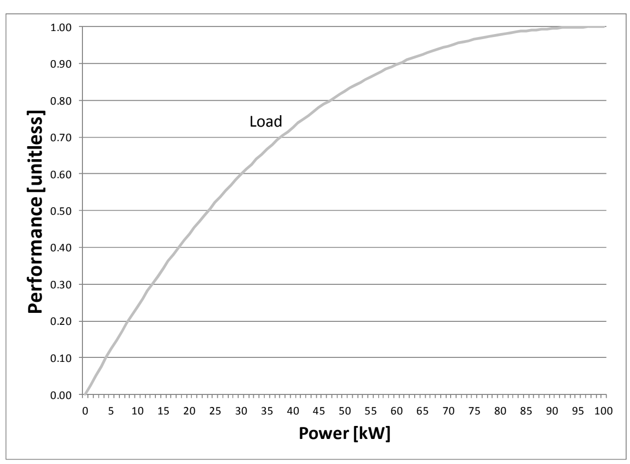

Figure 6.4. Load consumer agent performance function.

Renewable DER produce power that may vary moment to moment. For producer agents in charge of renewable DER assets, they must interpret and respond to rapid changes in renewable availability. To achieve this, the producer agent continuously updates the feasible regions of operation for the generation asset and correspondingly maintains cost and performance information for decision-making. An example of how the feasible region for a photovoltaic array changes with varying resource availability is shown in Figure 6.5 and Figure 6.6. The photovoltaic cost and performance metrics are defined by:

$$C_i[k] = \begin{cases} 0, & P_i[k] \in \{P_f[k]\} \\ C_{\max}, & P_i[k] \notin \{P_f[k]\} \end{cases} \tag{6.3}$$

$$\rho_i[k] = \begin{cases} 0.05\dfrac{P_i[k]}{P_{rated}[k]} + 0.95, & P_i[k] \in \{P_f[k]\} \\ 0, & P_i[k] \notin \{P_f[k]\} \end{cases} \tag{6.4}$$

where, C_i is the cost function of asset *i* at increment *k*; C_{max} is the maximum cost defined by the user for the asset; ρ_i is the performance function of asset *i* at increment *k*; P_i is the operating power of asset *i* at increment *k*; and $\{P_f\}$ is the set of discrete operating powers that make up the feasible region for asset *i* at increment *k* as a function of available resource, on the range of the low power limit ($P_{low\ limit}$) to asset rated power (P_{rated}). Having cost be zero within the feasible region indicates the incentive to utilize renewable energy when resources permit. This is applicable to each renewable asset such as wind, PV, or secondary CHP.

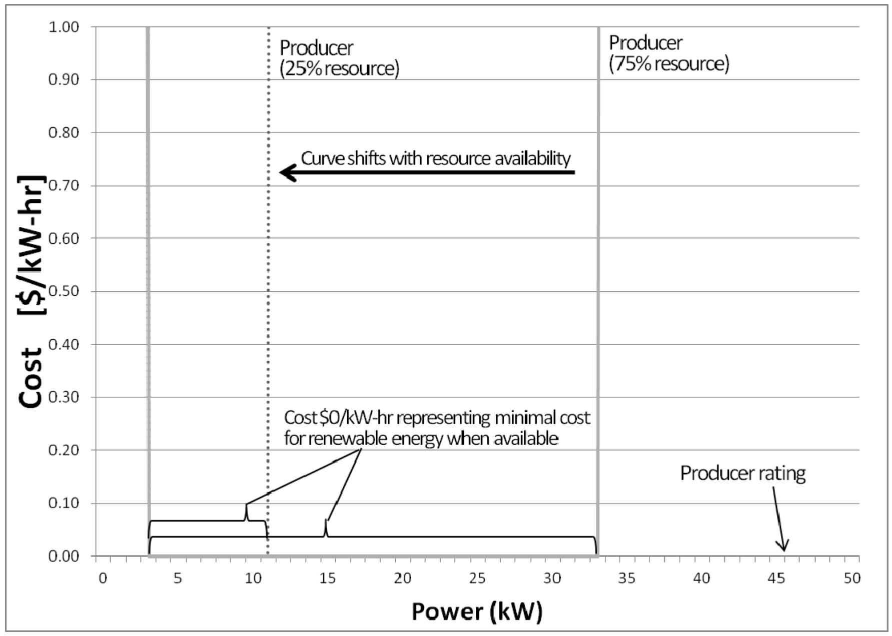

Figure 6.5. Producer agent cost information for renewable DER (PV).

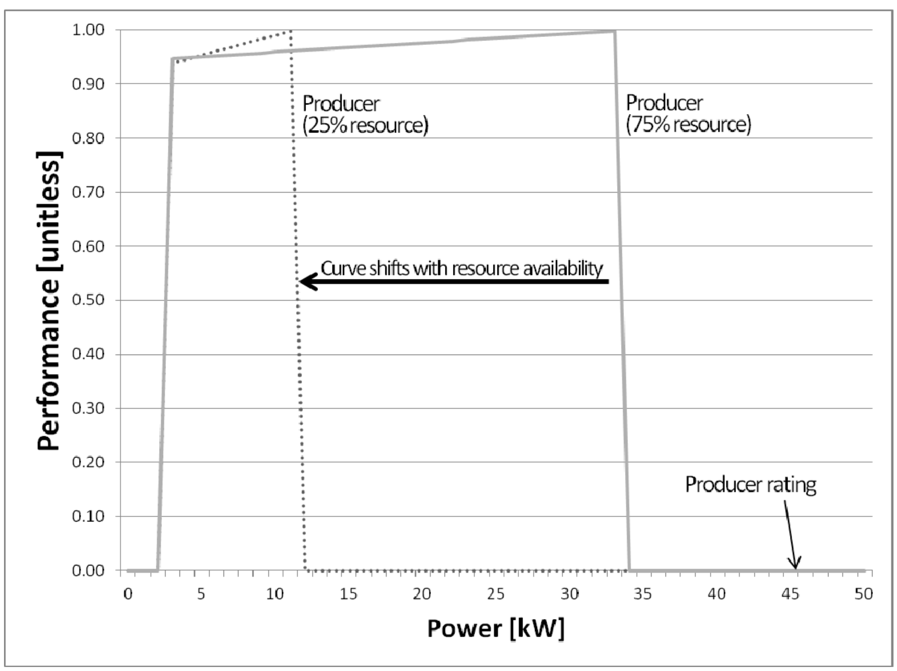

Figure 6.6. Producer agent performance information for renewable DER (PV).

The feasible region of operation ($\{P_f\}$) is defined by the asset's power rating (P_{rated}), the resource available to the asset, and additional constraints applicable to the asset. The levels of available resource for a renewable asset are analogous to wind speed, solar insolation, etc. In the case of the photovoltaic array example of Figure 6.5 and Figure 6.6, the rated capacity is 45kW and the available resource is shown at the 75% and the 25% levels. A constraint on the feasible region of operation ($P_{low\ limit}$) is imposed at low power levels (below 10% of rated capacity) to prevent asset power generation at low output, stressing the electronics. The combination of these parameters yields regions of feasible operation for the agent decision-making process of 4.5kW to 33kW and 4.5kW to 11kW for the 75% and 25% resource levels, respectively. Essentially the operational cost, shown on the y-axis of Figure 6.5, is zero within the region of feasible operation and very large (as dictated by the user) outside. The producer agent assigned to this asset uses this cost information in conjunction with the grid spot market price benchmark to make decisions how to operate the array. Within the feasible region of operation, the agent uses a performance metric, given in (6.4) and shown in Figure 6.6, to better refine asset operation. Outside the feasible region, the performance function is zero. In other words, the agent seeks to maximize performance within the feasible region of operation; for the photovoltaic array, maximum performance within the feasible region lies where maximum power is available. The performance function for the photovoltaic asset has a positive slope to encourage higher generation. Together, cost and performance information help guide the producer agent's decisions.

Storage assets are handled differently than generation and load assets. In the case of the latter two, one and only one agent is assigned to each asset connected to the microgrid; either a producer or consumer agent, as appropriate. Storage assets, on the other hand, are assigned two agents, one consumer and one producer. These agents are independent, but collectively allow the storage asset to be dispatched in two modes. When storage may be charged, it appears to the microgrid as a load. Alternatively, when additional energy is required by the microgrid, the storage asset can act as a generator. Similar to renewable assets, state-of-charge (SOC) is analogous to available renewable resource. SOC varies based on the energy discharged from or charged to the storage asset. Clearly, SOC will change based on charge/discharge rates and duration of these events. SOC dictates the performance functions for the consumer and producer agents and, at each increment, only one of the two storage agents is allowed to "win" negotiations, thereby dictating storage asset dispatch for that instant. The agent granted dispatch responsibility by the negotiations may also negotiate with other MAS agents towards other collective microgrid requirements.

In this demonstration, two fixed cost functions were used for the storage consumer and producer agents. This was intended to simulate costs during a short period in the storage assets life. In other words, for simplicity the cost function did not vary with predicted lifetime of the storage, as developed in 5.8.3 . This is appropriate for short-term simulation where the storage cost does not change appreciably. The cost functions for the storage consumer and producer agents, respectively, were:

$$C_{i,producer}[k]=\begin{cases}\beta_c P_i^4, & P_i[k]\le P_{rated}[k]\\ C_{\max}, & P_i[k]>P_{rated}[k]\end{cases} \tag{6.5}$$

$$C_{i,consumer}[k]=\begin{cases}C_{\max}, & P_i[k]_i\le 1\\ \dfrac{C_{\max}}{P_1}\left(1-\dfrac{P_i[k]}{P_{rated}[k]}\right), & 1\le P_i[k]\le P_{rated}[k]\\ C_{\max}, & P_i[k]_i>P_{rated}[k]\end{cases} \tag{6.6}$$

where, C_i is the cost function (either producer or consumer) of storage asset i at increment k; C_{max} is the maximum cost defined by the user for the asset; β_c is the producer shape coefficient defined by the user; P_i is the operating power of asset i at increment k; and P_{rated} is storage asset rated power at increment k. The cost functions, (6.5) and (6.6), reflect two aspects of desired storage behavior. First, discharges at low power, i.e. low discharge current, are more desirable because of the effects on battery lifetime (see 5.8.3). Therefore, it is less operationally costly to discharge at low rates rather than high. Secondly, charging at low rates is typically not cost effective (see 5.8.3). Therefore, it is less operationally costly to charge at the highest current possible within the storage rating. The cost functions are shown in Figure 6.7.

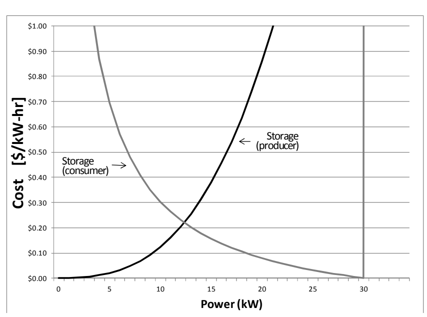

Figure 6.7. Storage producer and consumer agent cost functions.

The performance functions for storage producer and consumer agents, given in (5) and (6), are directly influenced by storage SOC. This implies that as SOC changes, the importance of charging the storage asset at low SOC and discharging at high SOC are emphasized.

$$\rho_{i,producer}[k]=\begin{cases} SOC[k]-\dfrac{P_i[k]}{3P_{rated}[k]}, & P_i[k]\in\{P_f[k]\} \\ 0, & P_i[k]\notin\{P_f[k]\} \end{cases} \tag{6.7}$$

$$\rho_{i,consumer}[k]=\begin{cases} \left(1-SOC[k]\right)+\dfrac{P[k]_i}{2P_{rated}[k]}, & P_i[k]\in\{P_f[k]\} \\ 0, & P_i[k]\notin\{P_f[k]\} \end{cases} \tag{6.8}$$

where, ρ_i is the performance function (either producer or consumer) of asset i at increment k; P_i is the operating power of asset i at increment k; and $\{P_f\}$ is the set of discrete operating powers that make up the feasible region for asset i at increment k; P_{rated} is rated power; and SOC is the storage asset state-of-charge at increment k. By using SOC in this way, at high SOC the performance of the producer (discharge) is best; at low SOC the performance of the consumer (charge) is favored. The positive slope in function (6.7) reflects the desire to discharge at lower currents (lower power sourced); the negative slope in (6.8) reflects the desire to charge at higher currents (higher power sunk). The producer and consumer performance functions for the storage asset are shown in Figure 6.8.

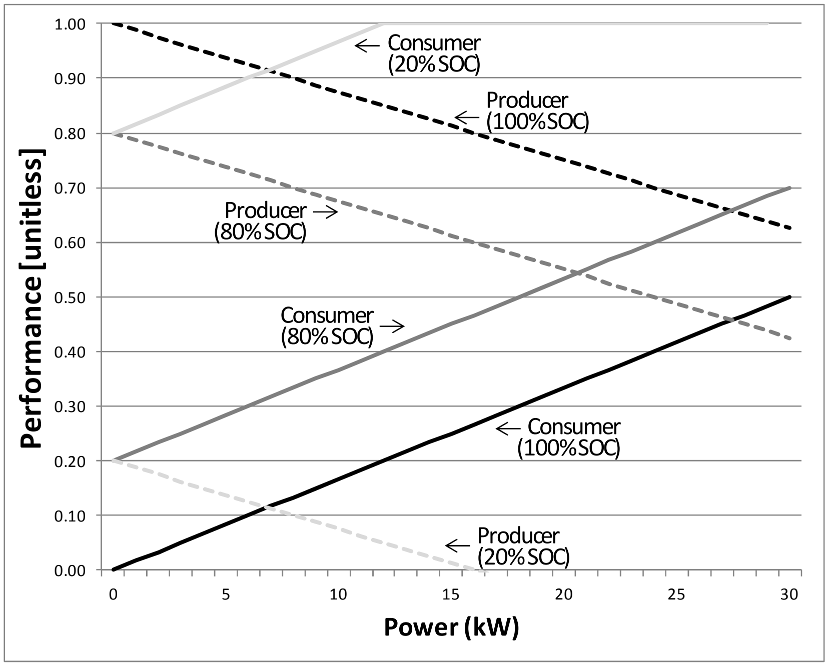

Figure 6.8. Storage producer and consumer agent performance functions.

In addition to the storage consumer and producer agent negotiation explained in Chapter 4, the storage producer agent may also conduct negotiations with the observer agent under special circumstances. For this demonstration, it is simulated that the user has established an additional rule for cases of high power flow from the utility to the microgrid (heavy purchases). In addition to the cost and performance measures that guide the storage producer agent's decisions, whenever the storage producer agent wins negotiation with the storage consumer agent (cases where the battery SOC is high), the storage producer agent must evaluate information communicated from the observer agent. The threshold to conduct negotiations with the observer agent is set at the lowest performance value for the storage producer agent; the value of ρ_i where P_i is equal to P_{rated} in increment k. The storage producer agent behavior is shown in Figure 6.9. This implementation represents the user adding an additional goal to the MAS decision-making: when the microgrid is consuming significant amounts of power across the PCC and the SOC of the battery is high, draw down the battery at a reasonable rate to mitigate some of the purchases from the utility. In other demonstrations, rather than the storage asset being the primary means of lowering the power sourced from the utility, the load consumer agent could be modified to shed load with a similar scheme. However, that method is not shown here as load shedding in periods of high demand is trivial and utilizing the storage asset in this way is potentially an effective means of energy arbitrage with the utility.

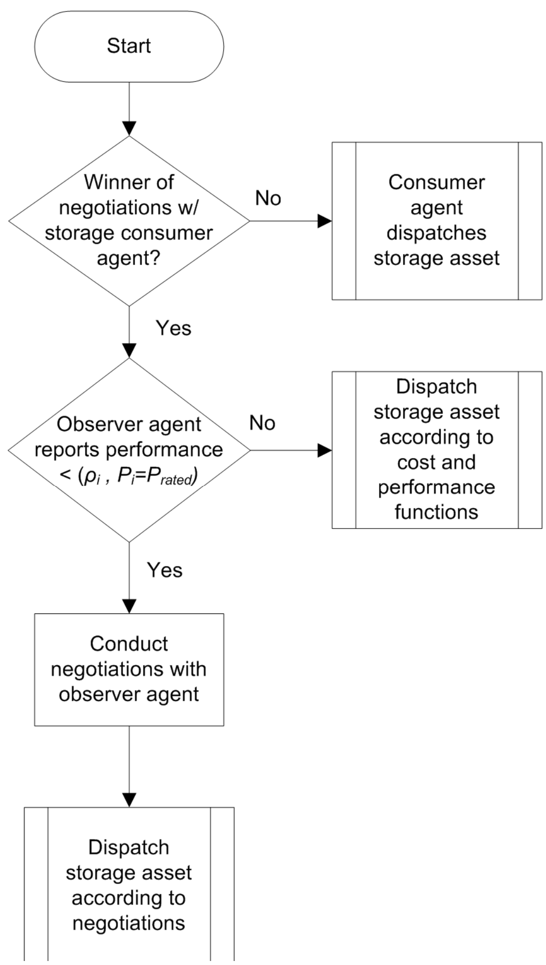

Figure 6.9. Storage consumer agent algorithm following negotiations with storage producer agent.

Finally, the last major agent that participates in the MAS for this demonstration is the observer agent. Here, the observer monitors the status of the interconnection between the microgrid and the utility at the PCC. Additionally, the observer agent is the receiver of grid price information from the utility, which it reports to the MAS. The observer agent develops a performance metric for the microgrid based on the quantity of power flow across the interconnection. For the observer agent, this is analogous to sensing AC bus voltage, as well as sensing current flow at the PCC. Positive current flow indicates the microgrid is sourcing power to the utility; negative flow means the microgrid is consuming power from the utility. This performance function is calculated according to:

$$\rho_o[k] = \begin{cases} 1, & P_{PCC}[k] \leq 0 \text{ \{Exporting\}} \\ 1 - \dfrac{P_{PCC}[k]}{\sum\limits_{dispatchable} P_{rated} - P_{rated,storage}}, & P_{PCC}[k] > 0 \text{ \{Importing\}} \end{cases} \tag{6.9}$$

where, ρ_o is the observer performance function at increment k; P_{PCC} is the power flow at the PCC at increment k; $\sum P_{rated}$ is the sum of the rated power of all dispatchable producer assets in the microgrid; and $P_{rated,storage}$ is the rated power of the storage asset. When the microgrid is exporting power to the utility, the observer performance function is 1 (100%); when importing power from the utility, the performance function is less than one (<100%). MAS agents, such as the storage producer agent in this demonstration, may use information from the observer to modify their decision-making with respect to their asset. This allows the agents the ability to aid overall microgrid performance if it is congruent with the performance functions established by the user.

For the purpose of demonstration, it was of primary importance to show the cooperative functions of the MAS; in other words, how an enhanced decentralized framework can achieve power management objectives. To simplify the discussion, the power system context for this MAS application was reduced to real power dispatch for the microgrid interconnected with the utility grid case only. By no means is this a restriction, as microgrid agent development is completely flexible allowing the incorporation of other factors such as reactive power dispatch, voltage and frequency regulation, synchronization concerns, economic factors, etc. Although decision-making domains have been limited for this demonstration, further functionality is readily implementable.

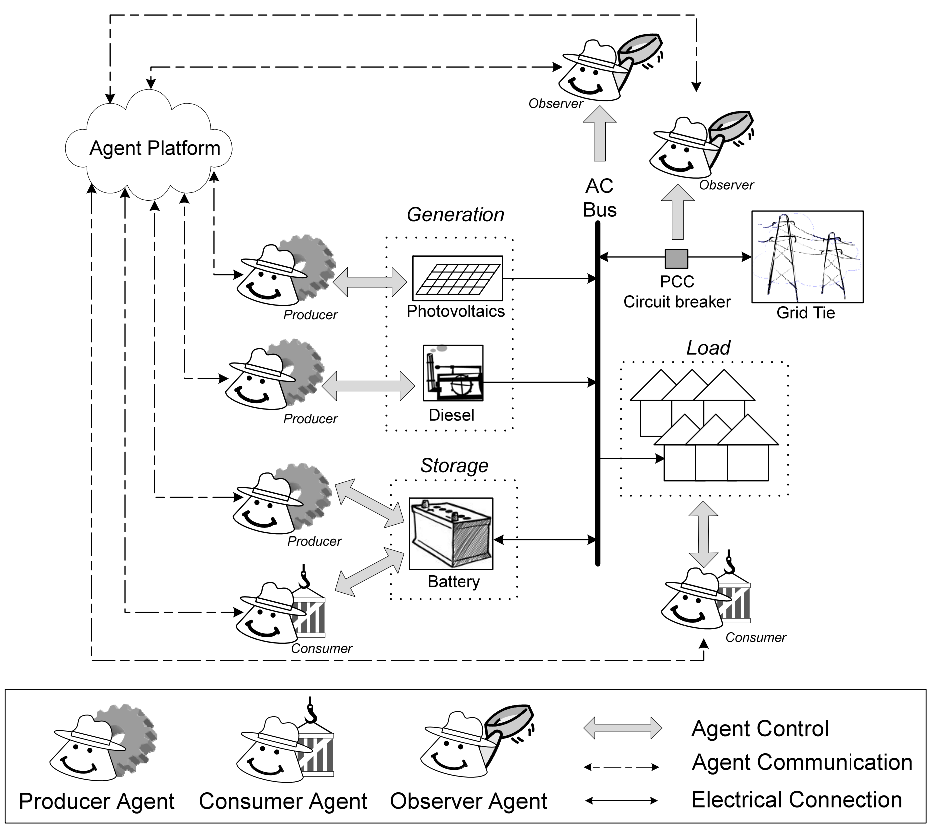

Figure 6.10. Concept of operations for scenarios A and B.

The demonstration results reflect the system parameters in two unique states: initially at steady state and at steady state following a disturbance. The results are shown this way to concisely present significant amounts of system information in a straightforward manner. Very simply, the scenarios show that each agent supervises its assigned asset to best achieve its assigned goals. Each agent's decisions rely on knowledge of its asset cost and performance, as well as utility market price information passed along by the agent observing the utility interconnection. The producer agents have the ability to ramp generation up or down based on the constraints of the generator and the available resources; the consumer agents may start or stop loads. Agents operate with a primarily self-interested protocol; however cooperation is encouraged through actions that would be mutually beneficial. The two simulated scenarios, shown below, are given to show the capabilities of decentralized MAS management of a microgrid with distributed control, including how cooperation can arise leading to better system-wide performance.

Table 6.1. Microgrid parameters for scenarios A and B.

Asset	**Rating**
Diesel Genset	75kW (Fuel price: $0.90/L)
Photovoltaic Array	45kW
Storage Battery Bank	12kWh (30kW @ 10 min rate)
Load Center	100kW (1kW increments)

The simulated microgrid is composed of two DER, a storage battery, and a load bank with controllable loads, parameters of which are shown in Table 6.1. The DERs are a non-renewable diesel genset and a renewable photovoltaic array. The microgrid is connected to the utility through a PCC and may supply or consume energy across the interconnection. Individual agents are assigned to each major asset or node in the microgrid for the purpose of managing operations, as shown in Figure 6.10.

6.2.1.1 Scenario A: Spot Market Price Change. The purpose of this simulation is to show how agents sense and respond to a system disturbance, using local cost and performance information to guide their decision-making. In this scenario, the microgrid is simulated at an initially stable condition, interconnected with the utility, at conditions given in Table 6.2.

Table 6.2. Scenario A parameters.

Initial Conditions	
Grid	Selling 8kW to microgrid at $0.15/kWh
Observer	Performance = 91.1%
Diesel	Off
Load	43kW of load energized
Storage	100% state of charge
PV	77% of maximum solar resource available, producing 35kW
Disturbance	
Grid	Selling price goes from $0.15/kWh to $0.30kWh
Final Conditions	
Grid	Purchasing 64kW from microgrid at $0.30/kWh
Observer	Performance = 100%
Diesel	Producing 55kW at $0.27/kWh
Load	26kW of load energized
Storage	100% state of charge
PV	77% of maximum solar resource available, producing 35kW

The utility grid has its supply of electricity available at $0.15/kWh, a relatively low spot price. Initially, the microgrid is buying energy from the utility to energize its loads, but the purchase is mostly mitigated by significant photovoltaic (PV) power produced locally. The initial status of the diesel genset and load cost and performance functions are shown in Figure 6.11 and Figure 6.12, respectively.

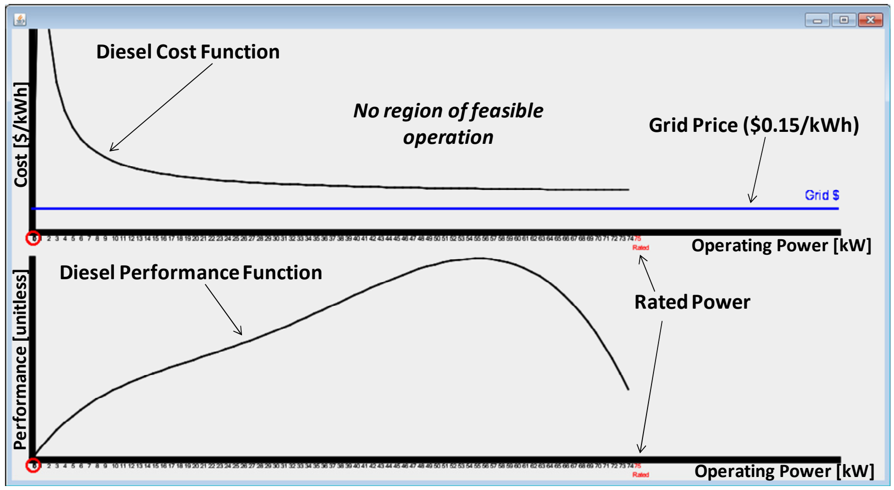

Figure 6.11. Screenshot showing diesel genset producer agent cost (top) and performance (bottom) functions prior to disturbance (note: no feasible region for operation).

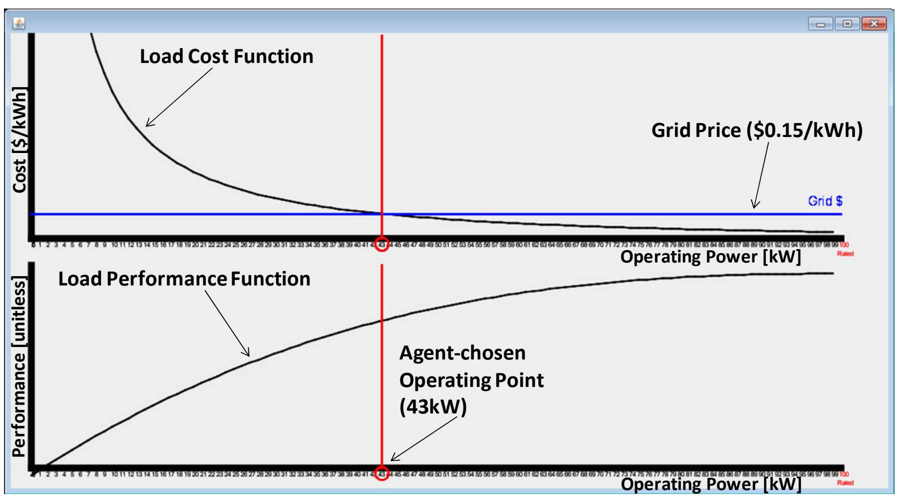

Figure 6.12. Screenshot showing load consumer agent cost (top) and performance (bottom) metrics prior to disturbance (the red line indicates chosen operating point).

The microgrid stable initial conditions are disturbed by a large spike in the market price of electricity supplied by the utility; rising from $0.15/kWh to $0.30/kWh. This rise could indicate a loss of utility generation, an increase in utility network loading, or a constrained transmission situation, each of which cause a significant rise in the spot price of electricity. From the microgrid's perspective, the reason for the utility price increase does not matter; the fact that it has risen indicates a new set of conditions that the microgrid agents must evaluate for new operating opportunities. Given the new benchmark price, the diesel producer agent senses an opportunity to operate its asset profitably. The agent searches the new feasible region (from 31kW to the genset P_{rated}) for the best operating point to maximize performance. The diesel producer agent decides to operate at 55kW (maximum performance within feasible range of operation) with an operational cost of \$0.27/kWh, as shown in Figure 6.13. It is noted that initially the observer agent performance value was 1.0 (100%) due to the export of power from the microgrid to the utility.

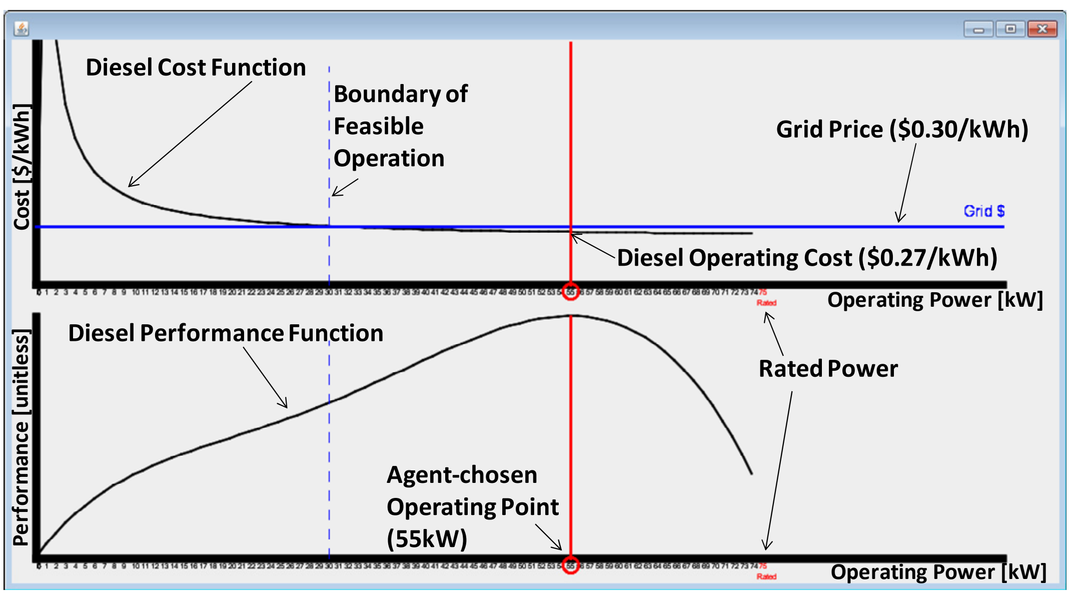

Figure 6.13. Screenshot showing diesel genset producer agent cost (top) and performance (bottom) functions after grid price disturbance (red line indicates chosen operating point).

Simultaneously, the load consumer agent senses the change in grid price. For the consumer agent, the price benchmark acts as a threshold, meaning that its feasible region is bounded by the loading level indicated by this price. In this case, the producer agent sheds load to achieve the maximum performance factor within its region of feasible operation to operate 26kW of load, shown in Figure 6.14.

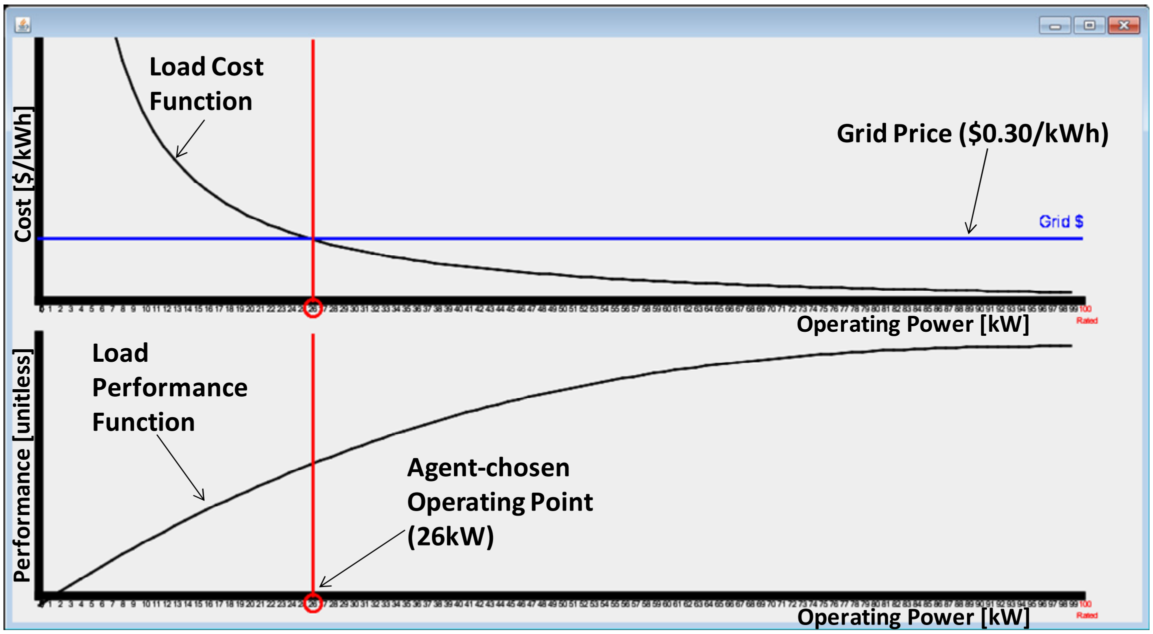

Figure 6.14. Screenshot showing load consumer agent cost (top) and performance (bottom) metrics after disturbance (the red line indicates chosen operating point).

In this scenario, the storage asset remains at or near 100% SOC throughout. As a result, neither the cost nor performance functions for the storage producer and consumer agents vary substantially during the disturbance or while the microgrid settles following it. Given the high grid price, the feasible regions of operation for both the storage producer and consumer agents is rather large. However, the SOC still being high allows the producer agent to dominate in negotiation. The end result is that the producer agent dictates storage operation in this case and desires to not discharge the battery based on maximizing performance. Of course, as SOC changes over time, so will the relationship between the storage producer and consumer agent performance functions which, in turn, will change the decision-making for the storage asset. Storage agent behavior will be further explored in scenario B, below.

The overall progression of events for scenario A is summarized in Table 6.2. This scenario has demonstrated how the microgrid agents respond independently to a shift in grid price.

6.2.1.2 Scenario B: Loss of Renewable Resource. The purpose of this demonstration is to show how agents can cooperate to raise the overall performance of the microgrid. This scenario builds upon the previous scenario, shown in 6.2.1.1 . Here, the demonstration explores how two agents interact, share information, and decide upon a collective action.

Initially, the microgrid is selling a small excess of power to the utility grid, resulting from maximum rated PV production of 45kW, shown in Table 6.3. Similar to the first scenario, the market price serves as a benchmark for microgrid agents ($0.15/kWh). Correspondingly, based on the grid price, the load consumer agent operates the load at 43kW, identical to Figure 6.12. Likewise, the diesel agent has determined it is not cost effective to operation and the diesel genset is off, identical to Figure 6.11. The storage battery is fully charged at the outset of the scenario (SOC = 100%), with the storage producer agent cost and performance functions shown in Figure 6.15.

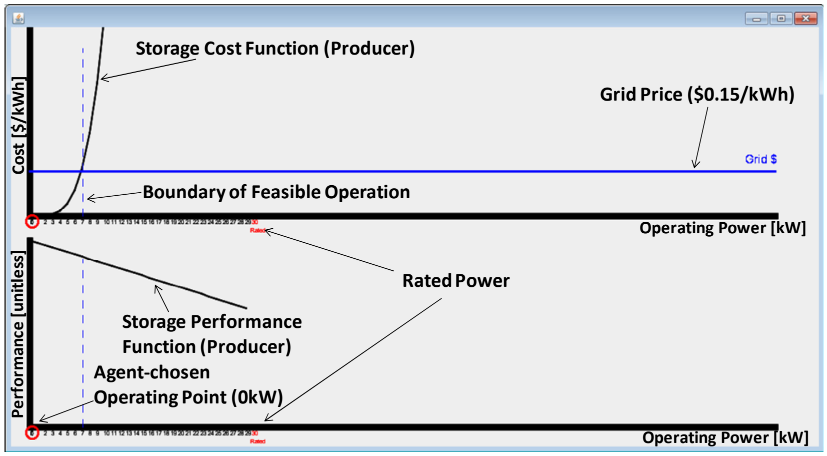

Figure 6.15. Screenshot showing storage producer agent cost (top) and performance (bottom) metrics prior to disturbance.

Table 6.3. Scenario B parameters.

Initial Conditions	
Grid	Purchasing 2kW from microgrid at $0.15/kWh
Observer	Performance = 100%
Diesel	Off
Load	43kW of load energized
Storage	100% state of charge
PV	100% of maximum solar resource available, producing 45kW
Disturbance	
PV	Available solar resource drops to 0%, produces 0kW
Final Conditions	
Grid	Selling 36kW to microgrid at $0.15/kWh
Observer	Performance = 60.0%
Diesel	Off
Load	43kW of load energized
Storage	99% state of charge, discharging 7kW (about 70 min rate)
PV	0% of maximum solar resource available, producing 0kW

The disturbance in this scenario is an environmental one. Simulating that a dense cloud system has moved into the sky over the microgrid's geographical area, the initially stable condition of the microgrid is disturbed by a complete loss of production from the PV array. Immediately following the disturbance, as the price benchmark did not change, load remains at 43kW. As the PV generation curtails, nearly instantaneously the microgrid shifts from selling 2kW of excess power to the utility to purchasing 43kW; a major reversal if storage were not available to somewhat mitigate the disturbance. The observer agent assigned to monitor parameters at the PCC senses the change in power flow, adjusts its performance metric accordingly (from 100% to 52% immediately after the disturbance), and reports this information to the storage producer agent. Despite the disturbance occurring, the storage producer agent desires to remain at or near 100% SOC where its performance metric is maximized, within the feasible region of operation, shown in. In this way, the storage producer agent is discouraged from discharging in order to support the massive import of power from the grid. However, according to its post-negotiation algorithm (Figure 6.9), the storage producer agent compares this reported observer performance to its own threshold (66% in this case). As the observer agent performance is so low (52%) relative to its own, the storage producer agent enters into negotiations with the observer agent. This negotiation involves a step-wise increase in the storage power produced resulting in less power received from the utility. This process of increasing the storage asset production continues until the storage producer agent reaches the limit of the feasible region dictated by grid price. By cooperating in this way, the storage producer agent discharges 7kW to support better overall microgrid performance, shown in Figure 6.16.

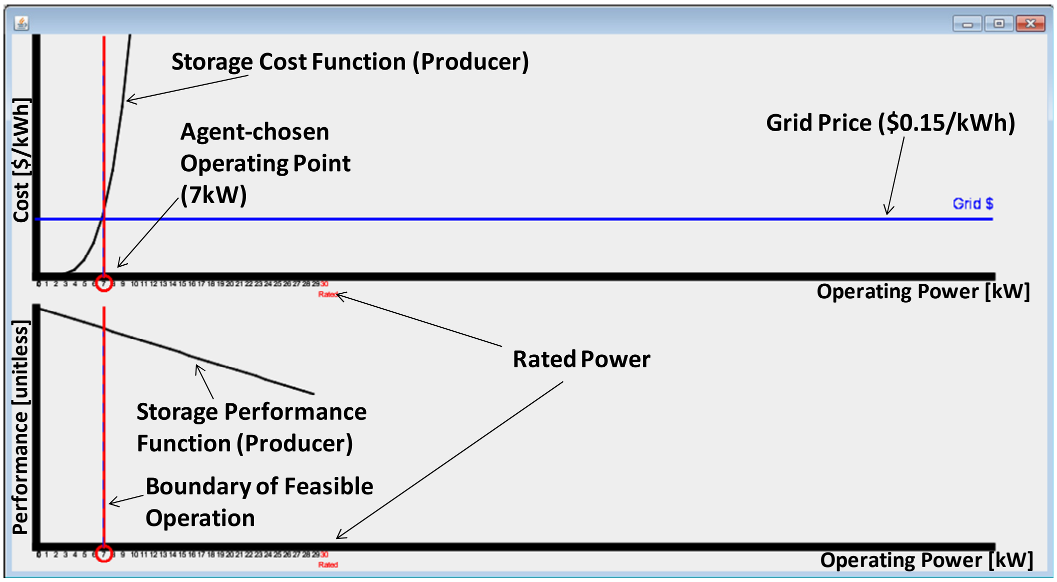

Figure 6.16. Screenshot showing storage producer agent cost (top) and performance (bottom) metrics after disturbance (the red line indicates chosen operating point).

Thus, the scenario ends with the microgrid purchasing 36kW from the utility, shown in Table 6.3. Although not shown here, as time continues, the SOC of the storage would degrade due to significant discharge, changing the performance information used by the storage consumer and producer agents. Ultimately, this effect would result in corresponding actions by the storage consumer agent to curtail discharging and recharge whether or not the PV resource has returned.

6.2.1.3 Scenario C: Grid-Connected Energy Arbitrage. In this scenario, the focus was on demonstrating an energy arbitrage scenario that is common worldwide, as explained in 6.1 . To reduce the microgrid complexity, three major changes were made to the microgrid shown in scenarios A and B. The first modification was to eliminate the influence of renewable generation on the revenue situation for the microgrid. Therefore, the PV array of scenarios A and B was eliminated for scenario C. Second, to eliminate the influence of load changes based on fluctuations in price and performance, the load bank was made to be fixed in scenario C. The third change made included enhancements to the battery cost and performance functions that took into account the operational cost and round-trip efficiency factors explained in 5.8 . The combination of these changes made for a more sophisticated simulation for the hybrid configuration of the diesel genset and lead-acid battery. The system diagram, therefore, for this scenario is shown in Figure 6.17. The microgrid parameters for scenario C are shown in Table 6.4.

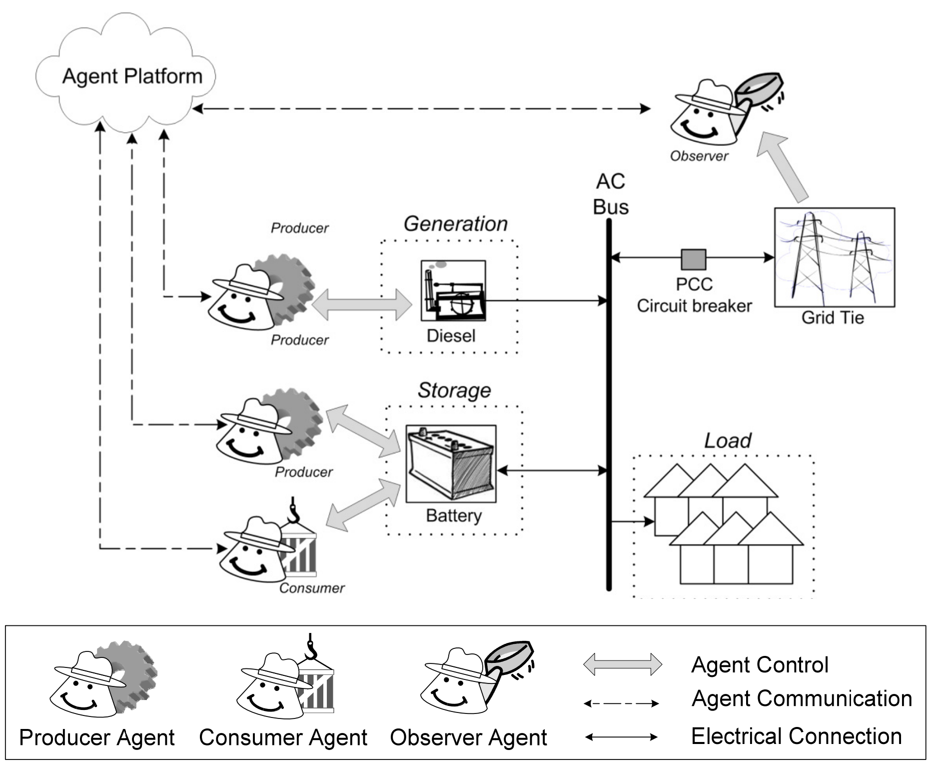

Figure 6.17. Concept of operations for scenario C.

Table 6.4. Microgrid parameters for scenario C.

Asset	Rating
Diesel Genset	125kW rated (Fuel price: $0.97/L)
Storage Battery Bank (Lead-Acid)	16kWh (25kW @ 10-min rate)
Load Center	100kW (fixed)

An additional feature that is introduced in this scenario attempts to qualify the value of the overall microgrid solution relative to the other possible solutions in each increment. Unfortunately, for microgrid systems conditions can change very rapidly changing the constraints and decision variables that make up the power management problem. This means that the Pareto set of solutions in one time increment may be dramatically different from the Pareto set in the next increment. Given that there is no known direct method to determine the Pareto set, the emphasis shifts to displaying the data visually to give the user a sense of how well the MAS is achieving proximate solutions to the Pareto front. In this demonstration, this added capability will be explored.

As the MAS operates, cost and performance functions are calculated by the agents for their respective assets at each computational increment. As discussed previously, a cost measure alone is not adequate to fully define the optimal operation of microgrid assets. Subsequently, each agent determines a performance measure that reflects how well its asset is achieving optimal operation based on its given objectives. The characteristics of the cost and performance functions vary dynamically depending on the asset and conditions including loading, state-of-charge (SOC), discharge history, etc. Cost and performance information may be shared between agents according to the decision cycle, described in 4.5 , to assist in cooperation. In order to solve for the best operating condition for an asset, the agent assigned to it first uses local information to develop its cost and performance functions, $f_c(\vec{x})$ and $f_p(\vec{x})$, respectively, where $\vec{x}$ is the n-length vector of variables to be optimized known as the decision variables. These functions are unique for every asset and depend on different decision variables ($\vec{x}$). For this demonstration, each agent's overall objective function followed:

$$F_a(\vec{x}) = w_1 f_c(\vec{x}) + w_2 f_p(\vec{x}) \tag{6.10}$$

where, F_a is the combinational objective function for agent a containing cost objective function (f_c) and performance objective function (f_c), weighted according to the user-defined w_1 and w_2. The details of the functions and variables have been previously discussed in 5.2 for the diesel genset and in 5.8 for the lead-acid battery. This linear sum of assigned objectives defines the decision-making search space which the agent must solve.

For scenario C, within the MAS framework two agents are assigned to a storage asset; one producer and one consumer, as in scenarios A and B. Each decision cycle, these agents independently seek solutions to the dispatch of their asset, guided by goal information provided by the user. User goals directly influenced the weights (w_1, w_2) assigned to the components of performance utilized by individual agents. However, because two agents are responsible for the same asset, negotiation is forced to arise each decision cycle. This ensures that merits of charging or discharging in each computational increment are properly evaluated. The result of storage agents' negotiations leads to an operating decision based upon a mutually agreed upon solution.

In this demonstration operational cost functions, $f_c(\vec{x})$, for the diesel and lead-acid battery were defined by fuel consumption and the cost of battery charge/discharge, respectively. Performance functions, $f_p(\vec{x})$, were defined by operational efficiency for the lead-acid battery and environmental emissions, namely total hydrocarbons (THC) and carbon dioxide (CO_2), for the diesel genset. More details about the modeling of these parameters may be found in 5.2 and 5.8 . As in scenarios A and B, the solutions decided by the agents translate into actual operation of their assets. For the purpose of evaluating the solution quality of the whole microgrid, the individual cost and performance results of each agent's solution was aggregated into total microgrid system measures, according to the following:

$$S_{microgrid}[k] = \left(P[k] f_c(x_{P[k]})\right)_{diesel} + \left(P[k] f_c(x_{P[k]})\right)_{battery} - P_{load} C_{grid}[k] \quad (6.11)$$

$$\rho_{microgrid}[k] = f_{p,diesel}(x_{P[k]}) + f_{p,battery}(x_{P[k]}) \quad (6.12)$$

where, $S_{microgid}$ is the total microgrid operational cost savings, either positive indicating savings or negative indicating loss, over the alternative of purchasing all power for the local microgrid load from the utility; $\rho_{microgid}$ is the total microgrid system performance, between 0 and 1 (0-100%); P is the operating power point chosen by the agent assigned to either the diesel or battery asset at increment k; $f_c(x_{P[k]})$ is the value of the cost function at the asset's operating power P at increment k; P_{load} is the power of the load (fixed in this scenario); and C_{grid} is the grid price of electricity at increment k. This information is highlighted by row-shading in.

It is important to note, that these overall measures of microgrid operation are a form of global knowledge that was only collected for testing and was not available to the agents. This preserves the enhanced decentralized nature of the MAS. While asset dispatch decisions were made exclusively by the agents, the user could impose their will upon the storage agents by specifying a relative importance (w_1, w_2) between revenue and battery health. The agents made dispatch decisions independently, but communicated as in scenarios A and B.

The purpose of scenario C was similar to scenario A, where microgrid agents sense and respond to a system disturbance (a grid price change), using local cost and performance information to guide their decision-making. As in scenario A, the microgrid was simulated at an initially stable condition, given in Table 6.5, interconnected with the utility and all objectives weighted equally ($w_1 = w_2$).

Table 6.5. Scenario C parameters.

Initial Conditions	
Grid	Purchasing 17kW from microgrid at $0.31/kWh
Diesel	Supplying 112kW
Load	100kW of load energized
Storage	80% state of charge, discharging 5kW
Microgrid	Operational savings: $0.412/hr System performance: 79.184%
Disturbance	
Grid	Selling price goes from $0.31/kWh to $0.38kWh
Final Conditions	
Grid	Selling 3kW to microgrid at $0.38/kWh
Diesel	Supplying 92kW
Load	100kW of load energized
Storage	80% state of charge, discharging 5kW
Microgrid	Operational savings: $6.462/hr System performance: 90.737%

Initially given the high cost of utility electricity supply, shown in Figure 6.18, the microgrid was both operating its diesel and discharging the battery to offset purchases from the utility required to power the local load. Then, system conditions were disturbed by a significant increase in the market price of electricity supplied by the utility, from $0.31 to $0.38 per kWh. Given a new price environment, the diesel producer agent realizes a broader feasible operating range and finds an operating point yielding the best performance within constraints, shown in Figure 6.18. During the short time period of grid price change, battery SOC did not change appreciably and, after communicating, the battery producer and consumer agents decide to continue discharging at pre-disturbance levels. Ultimately, as grid price rose in this scenario, a new diesel operating point determined by its agent leads to better overall microgrid performance and more cost savings than prior to the disturbance, shown by the shaded rows of Table 6.5. This may be counter-intuitive given that grid price went up and diesel generation went down. However, this result is explained by improved diesel performance after the disturbance given a larger feasible range of operations, shown in Figure 6.18, despite not selling power to the grid. Likewise, by continuing to avoiding large purchases from the utility to power the same local load at a new higher price, higher operational savings are achieved.

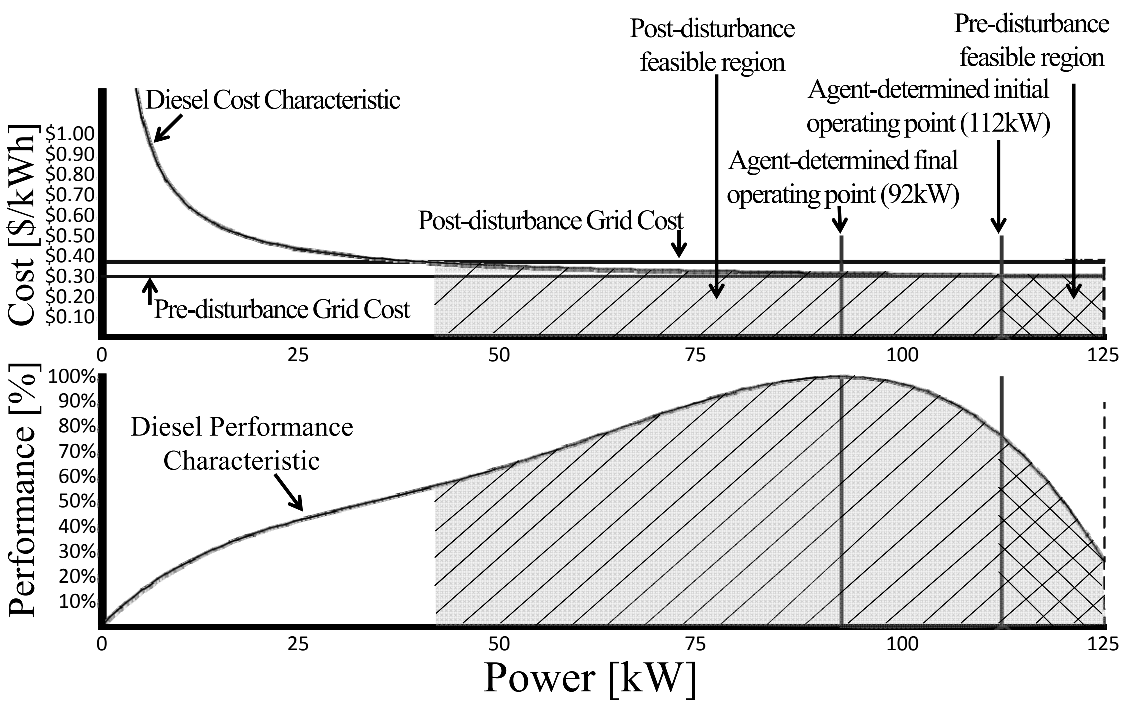

Figure 6.18. Diesel genset pre- and post-disturbance cost (top) and performance (bottom) functions for scenario C.

The aggregated solution can be difficult to see outside the context of the search space that the agents have available to them. Subsequently, in Figure 6.19, the initial overall search space is displayed, showing all possible discrete solutions for dispatch on the microgrid; an arrow points to the overall operating solution collectively found by microgrid agents. The objective functions (minimize cost, $f_c(\vec{x})$, and maximize performance, $f_p(\vec{x})$) form the axes; each circle represents a solution. The gaps in the search space result from the discrete values used to represent the decision variables. Clearly, as the increment between discrete values becomes smaller, the search space becomes closer to a continuously-valued search space. It is noted that, for simulations that include a global display of the search space, that the resolution of discrete decision variables affects the computational overhead (time and speed) of the simulation. Depending on the objectives of the researcher, the resolution may be expanded or condensed to improve simulation time.

In Figure 6.20, the post-disturbance search space is shown, reflecting the change in operational conditions that deepens the set of possible solutions (MAS overall operating solution shown by black arrow). In both cases, before and after the disturbance, the agents have settled upon operating decisions for their individual assets that yield a total microgrid solution that is along (or proximate) to the Pareto set. This evolves from the enhanced decentralized agents deciding operational dispatch for their asset independently, without being guided or dictated a solution by a central supervisor. The overall progression of events for scenario C is summarized in Table 6.5.

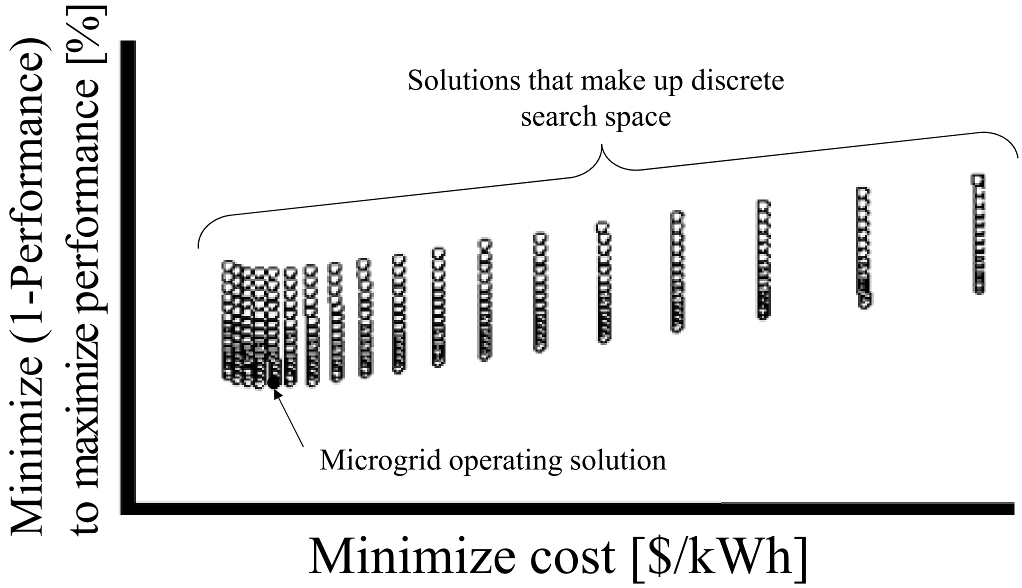

Figure 6.19. Screenshot showing the discrete search space for the pre-disturbance conditions of scenario C.

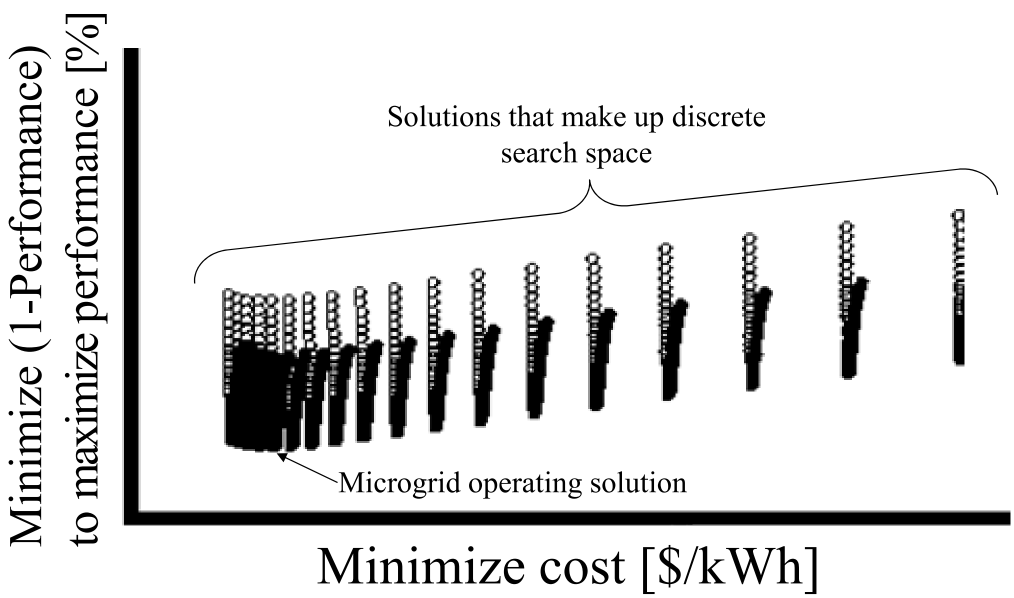

Figure 6.20. Screenshot showing the discrete search space for the post-disturbance conditions of scenario C.

6.2.1.4 Scenario D: Change in User Goals. One of the values of using the MAS framework for microgrid power management is the capability to dynamically incorporate changes in user goals into agent decision-making. The purpose of scenario D was to show how agents can not only incorporate changing operational conditions and constraints, but goals that adjust unpredictably, as well. Here, the user manipulates the relative importance of microgrid revenue to the health and longevity of the lead-acid battery (explained in 5.8). In other words, the user may influence MAS decision-making by conveying goals dynamically. The user accomplishes this by interacting with microgrid agents through a user interface, shown in Figure 6.21. The visual depiction of a weighing scale offers the user an intuitive sense of relative importance, choosing which goal to more heavily emphasize, thereby adjusting w_1 and w_2. The dollar sign (the left of the scale in Figure 6.21) represents revenue; the caduceus (the right of the scale) represents battery health and longevity. The scenario D initial conditions are on the left (balanced); disturbance conditions (favoring battery health/longevity) are on the right of Figure 6.21.

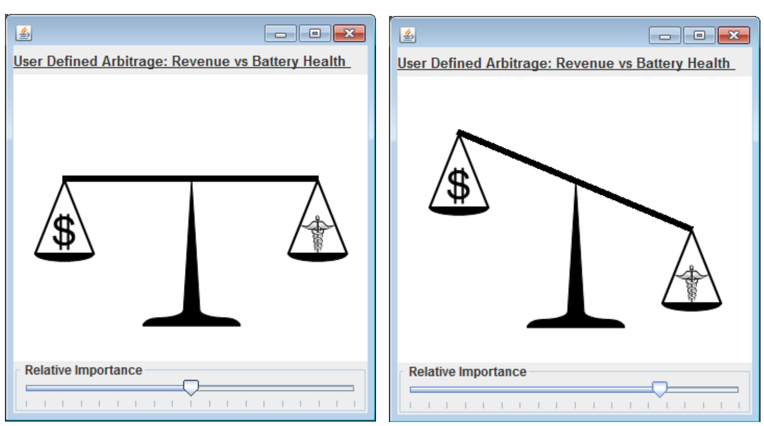

Figure 6.21. Screenshots of the user input interface for the relative importance of revenue versus battery health/longevity.

Under normal circumstances, it is sufficient to allow the storage producer and consumer agents to negotiate based on which as the best reported performance within their respective feasible ranges of operation. The winner of this negotiation then acquires the dispatch responsibility for the storage asset until the next round of negotiations. However, upon occasion, situations arise when the performance of the storage producer agent falls so low as to be undesirable, but the storage consumer agent does not have any feasible range of operations due to a high grid price of electricity. This situation may occur when both SOC and grid price are simultaneously low. To account for this situation and offer the storage agents the opportunity to reevaluate the feasible range of operations, the storage consumer agent undergoes an additional step in its decision-making, shown in Figure 6.22. Effectively, if charging operations are infeasible based on grid price, but the best reported performance for the storage producer agent is less than minimum performance for the storage consumer agent across its entire power range (0 to P_{rated}), then the storage consumer agent may override its feasible region and charge at the best performing point over its entire range. This behavior leads to more flexibility in the dispatch of the storage asset. Similarly, for the purpose of demonstration in scenario D, the interaction with the observer agent (Figure 6.9) is omitted for clarity.

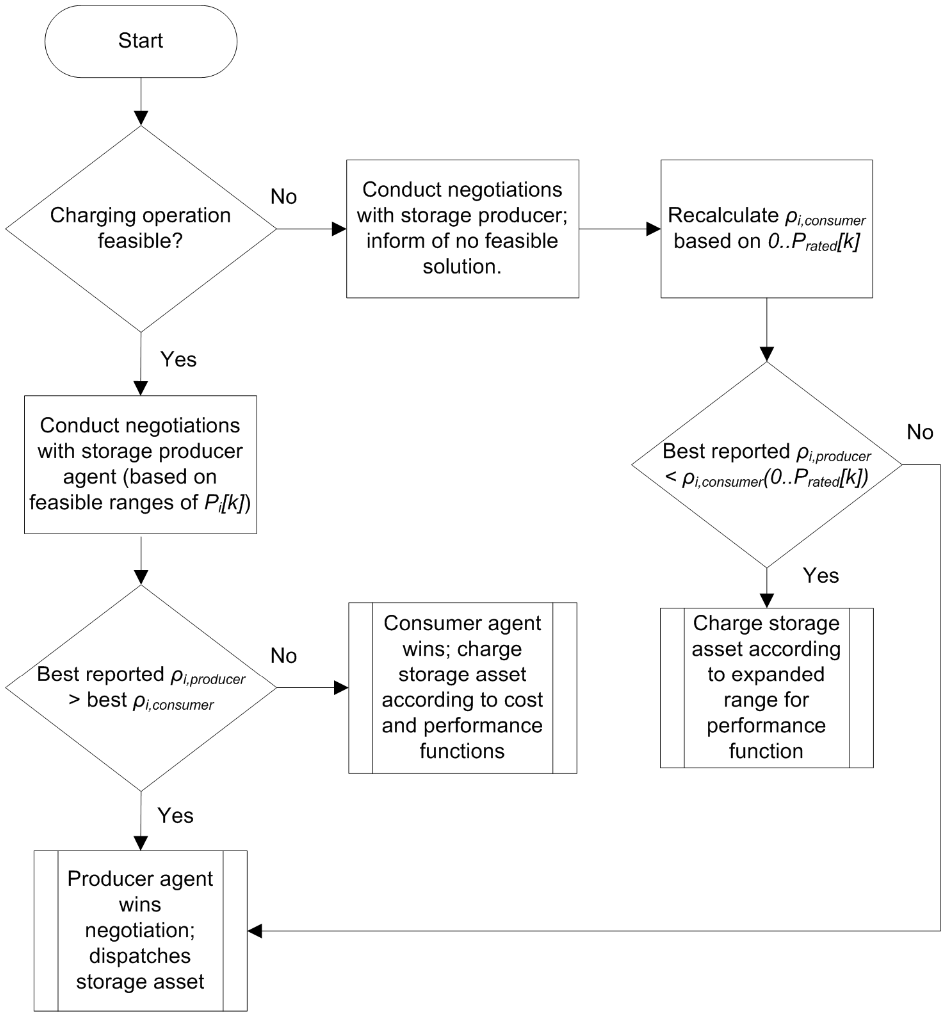

Figure 6.22. Storage consumer agent algorithm for negotiations with producer agent.

Initially, the microgrid conditions are identical to the final conditions from scenario C, shown in Table 6.5. The pre-disturbance cost and performance functions for the storage producer and consumer agents are shown in Figure 6.23. The solid vertical line in Figure 6.23 represents actual battery dispatch; the dotted vertical line represents the dispatch limit. SOC is in the middle of the operating band (60%) at the outset of scenario D and the storage consumer and producer agents, according to their negotiation, have decided upon the storage producer agent as the winner to dispatch the storage asset.

The storage producer agent has decided to discharge at 5kW according to the best performance achievable within the feasible operating range, shown in Figure 6.23.

The disturbance occurs when the user manipulates their goal interface (initially $w_1 = w_2$), shown on the left of Figure 6.21, making battery health more important than cost/profit ($w_1 < w_2$), shown on the right of Figure 6.21. Immediately, sensing a shift in objectives, the storage agents commence negotiations on how to best achieve them. Meanwhile, the grid price has not changed and the diesel genset, already operating at its optimal state given the conditions, does not modify its operation.

Table 6.6. Scenario D parameters.

Initial Conditions	
Grid	Selling 3kW to microgrid at $0.38/kWh
Diesel	Supplying 92kW
Load	100kW of load energized
Storage	60% state of charge, discharging 5kW
Microgrid	Operational savings: $6.462/hr System performance: 80.737%
Disturbance	
User	Changes relative importance of Revenue vs. Battery Health to heavily favor battery health.
Final Conditions	
Grid	Selling 33kW to microgrid at $0.38/kWh
Diesel	Supplying 92kW
Load	100kW of load energized
Storage	60% state of charge, charging 25kW
Microgrid	Operational savings: - $3.781/hr System performance: 99.079%

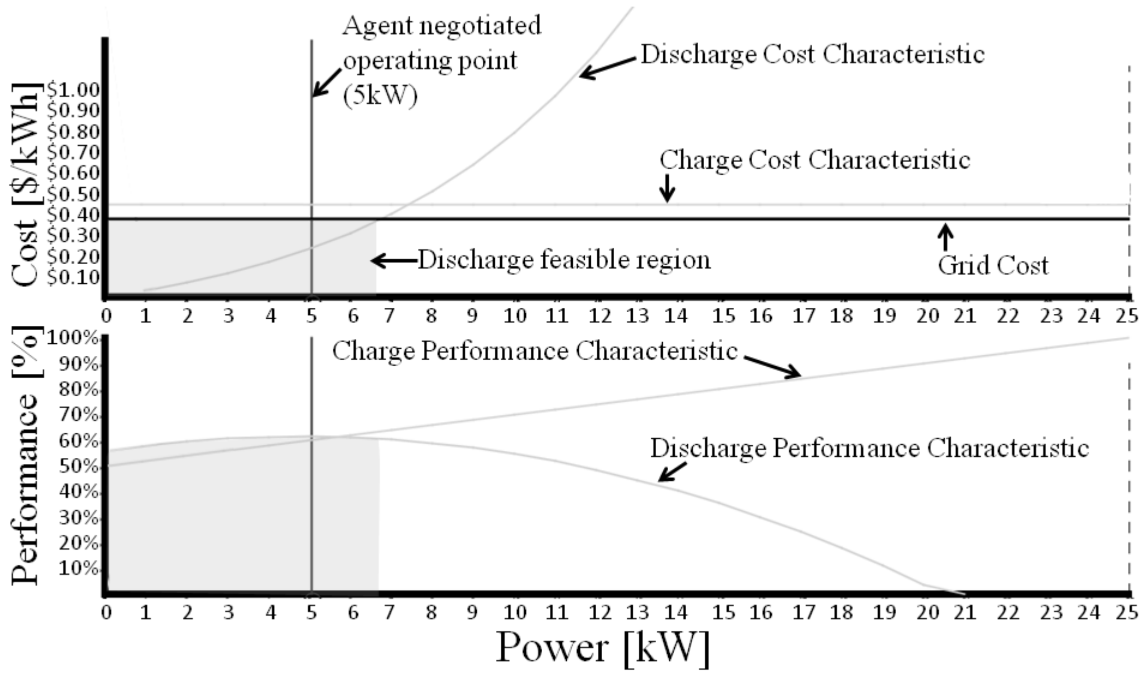

Figure 6.23. Screenshot showing the pre-disturbance cost (top) and performance (bottom) characteristics for the storage producer and consumer agents in scenario D.

In this demonstration, the grid cost ($0.38/kWh) remains below the charging cost threshold ($0.45/kWh). This presents the situation where SOC is low and the grid price is lower than allows feasible operation for charging dispatch by the storage consumer agent. During negotiations, the storage consumer agent reports infeasible operation, but determines that no discharging dispatch would offer a better performance value than the minimum charging performance over the expanded range of operation, according to Figure 6.22. This reveals a scenario where no point of discharge would yield better performance than any charging point. Illustrated in Figure 6.24, the producer agent's discharging performance curve, $f_{p,producer}(\vec{x})$ is less than the consumer agent's charging performance curve, $f_{p,consumer}(\vec{x})$, for all possible dispatch powers. This presents conditions where objectives of minimizing cost and maximizing performance are nearly directly opposed. In other words, because the user has emphasized the goal of battery health and there is no feasible solution that achieves a better objective function value, $F_a(\vec{x})$, for discharging than for charging, the battery must charge. Using the performance functions and through negotiation, the storage agents arrive at this conclusion collaboratively.

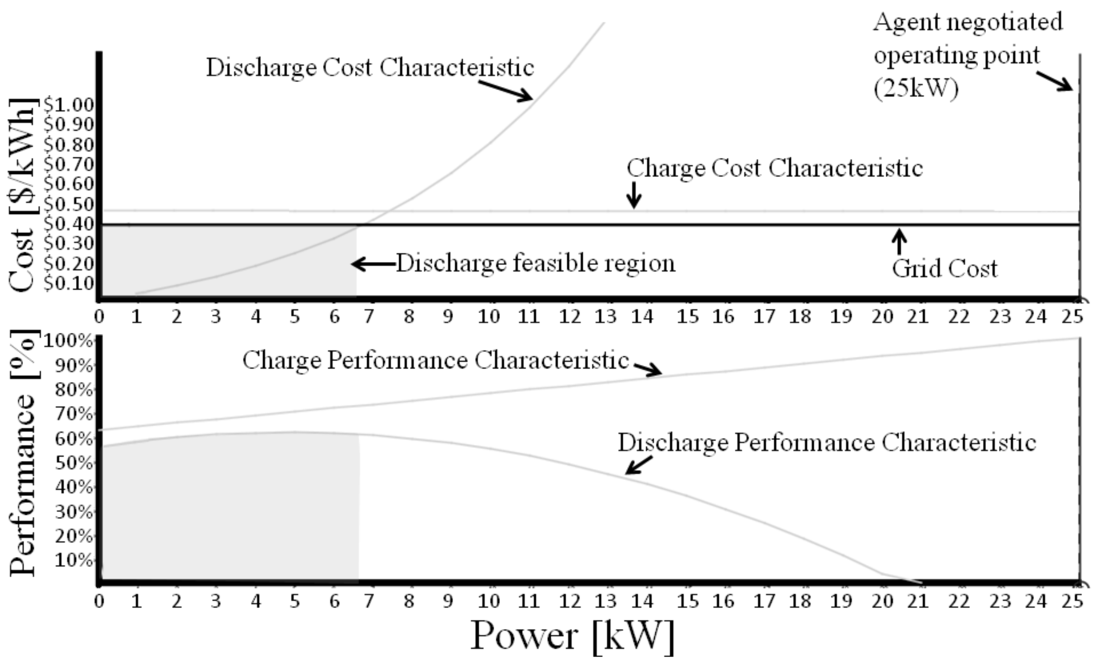

Figure 6.24. Screenshot showing the post-disturbance cost and performance characteristics for the storage producer and consumer agents in scenario D.

Despite being costly to charge, the storage agents' solution best achieves the user goals given the operating conditions. This decision is reflective of the user's intentions to maintain the battery health and longevity over cost implications, dictated by the user interface shown by Figure 6.21. Thus, when battery agent negotiation is completed, the initial 5kW battery discharge rate changes to charging at 25kW, indicating that the storage consumer agent has won negotiations and is responsible for the storage asset dispatch. In this scenario, as user goals changed to favor battery health, the overall system performance improved from 80% to 99%, while operational savings changes from $6/hr to -$3/hr, indicating a shift from savings to expense, shown in Table 6.6. In Figure 6.25, the post-disturbance search space has tightened compared to the pre-disturbance search space, identical to the post-disturbance of scenario C shown in Figure 6.20.

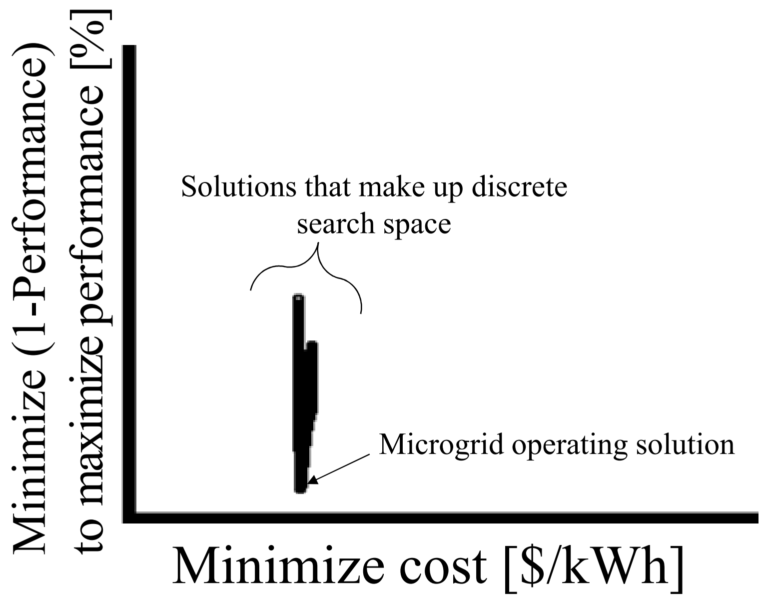

Figure 6.25. Screenshot showing the discrete search space for the post-disturbance conditions of scenario D.

In this scenario, the focus was on an isolated disturbance within a short period of time. Of course, as time moves ahead, the battery continues to charge until SOC improves to about 75% in this case, shown in Figure 6.26. At this point, the discharge performance measure, partially a function of SOC, contains operating points within its feasible region that represent performance values better than for charging. Following the algorithm of Figure 6.22 and given the new opportunity to improve battery operating performance, the storage consumer agent ceases its override behavior. The agents recognize that the storage producer agent now shows the best performance within the feasible operating range and conclude to resume discharging. In this way, using only local information, the agents autonomously follow the goals set forth by the user and dispatch the battery to best achieve them.

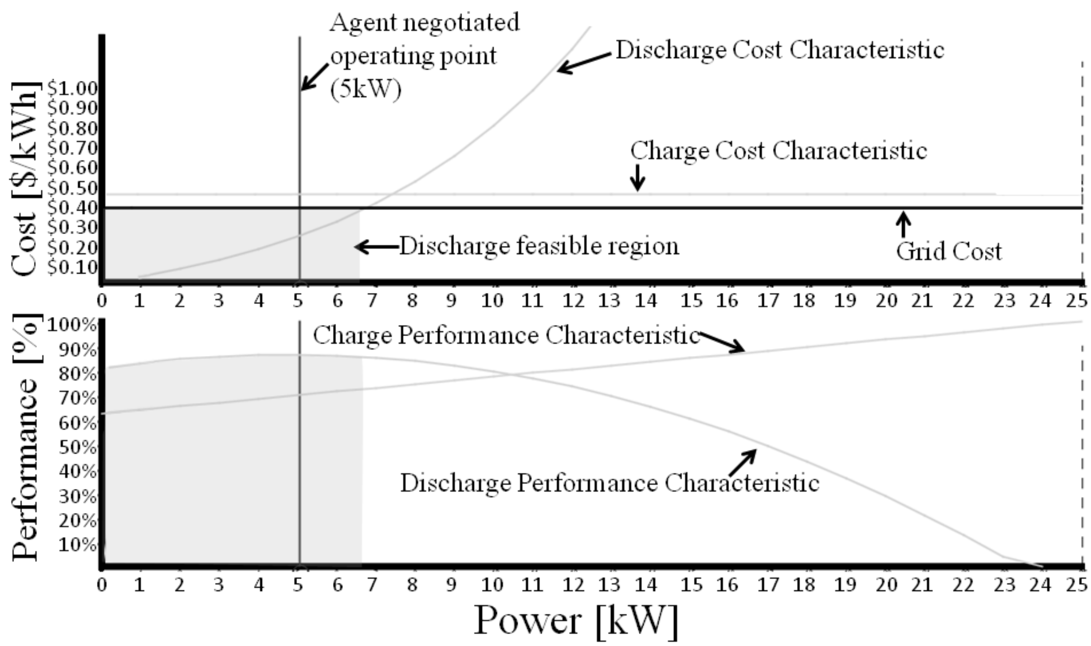

Figure 6.26. Screenshot showing the cost (top) and performance (bottom) characteristics for the storage producer and consumer agents after battery charging has recovered SOC to 75% from the post-disturbance conditions of scenario D.

6.2.2 Islanded Operations

Islanded operations, in some respects, are the least desirable from a microgrid power management perspective. Isolated from the utility grid, the microgrid cannot use the macrogrid as an infinite source or sink of power. Correspondingly, the microgrid must match its local generation exactly to its local load. This is a much more difficult constraint proposition, especially when attempting to optimize many other objectives. By demonstrating the islanded scenario here, there are two primary objectives. First, the objective is to illustrate the challenges the microgrid MAS faces when constrained to local load demand while attempting to optimize other objectives. Even a two asset microgrid faces difficult decision-making, as will be shown. Second, because there are relatively few actual microgrids currently operating worldwide, it is difficult to compare power management methods to evaluate strengths and weaknesses. Therefore, the microgrid simulated in this islanded scenario mimics diesel-battery hybrids, actually in use, that predominantly use a well understood power management method. In this way, microgrid MAS power management decision-making may be compared to a known conventional case. While many other issues could be approached by the MAS in the islanded case, the objective here is to highlight these two important topics.

In this scenario, the straight-forward diesel-battery microgrid from 6.2.1.3 and 6.2.1.4 is demonstrated in islanded mode. Without the utility supply of electrical power, the mix of individual agent's objectives has dramatic impacts on overall microgrid system operation. The difficulty in illustrating the computation that culminates in agent action as dictated by a single decision cycle was highlighted in the scenarios of 6.2.1 . These previous scenarios were presented for the purpose of showing how the MAS may respond to a disturbance. In this section, rather than focusing on an isolated disturbance, the MAS was simulated under constantly changing load conditions, as would be expected in a real-world situation. In this case, a grid-isolated (islanded) microgrid composed of a diesel genset and a lead-acid storage battery bank, serving a non-controllable load center, shown in Figure 6.27, was simulated over a full day. The load center was modeled as a residential neighborhood or village of 50 all-electric homes, daily load profiles of which were based on 5.10.1 and are shown in Figure 6.28. For brevity, only results from the Summer Weekend profile are given here, although overall simulation outcomes were similar for each daily profile.

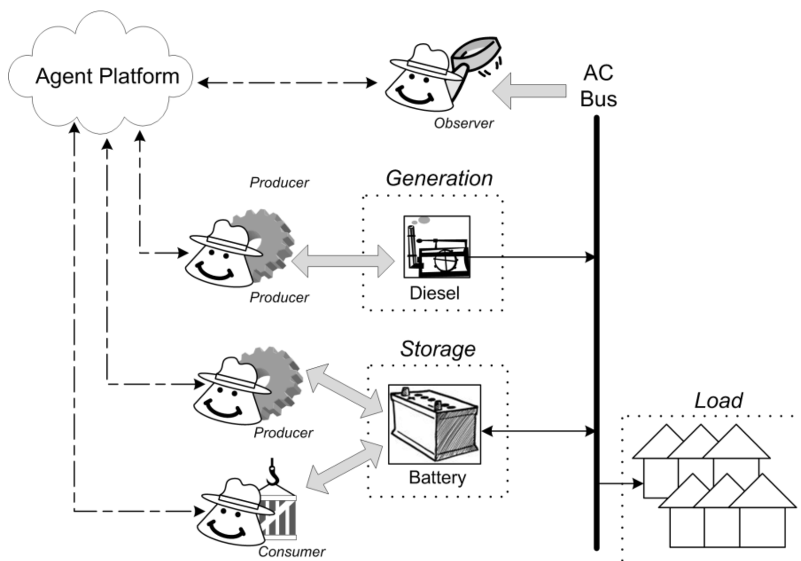

Figure 6.27. Concept of operations for microgrid islanded scenario.

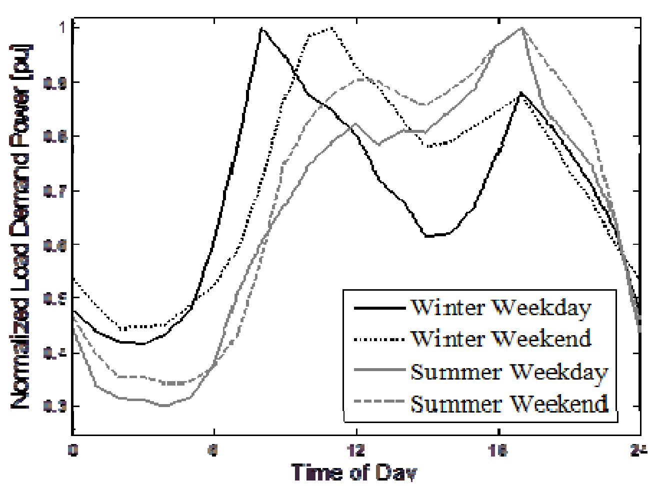

Figure 6.28. Normalized load demand profiles for 50-home village.

The MAS used for this islanded scenario was nearly identical to that used in 6.2.1 , with a major exception. In the grid-connected case, excess power produced locally by assets on the microgrid could be absorbed by the utility. Conversely, inadequate local supply could be supplemented with utility supply. In the islanded case, however, this is not possible and the local assets are constrained to meet demand at all times. The consequence of this constraint emphasizes the operational trade-offs between the diesel and battery assets that are not present in the grid-connected case. In other words, when grid-connected, each asset is fairly free to operate where the assigned agent determines the best operating point to be. However, in the islanded case, the agents must coordinate their operating points to precisely meet load demand. This presents a challenge for enhanced decentralized power management.

Clearly, the capacity ratings of the diesel and battery assets matter significantly in the islanded case. After all, the asset ratings determine how much energy storage is available to supplement dispatchable power, as well as how long it takes to replenish stored energy. To that end, two sizes of diesel gensets and two sizes of batteries were considered in this scenario. Using each possible combination of asset capacities, four unique scenarios were used for simulations:

- Large Diesel + Small Battery
- Large Diesel + Large Battery
- Small Diesel + Small Battery
- Small Diesel + Large Battery

Asset sizes were dictated by load demand, shown in Table 6.7. While many different sizes and combinations of assets are conceivable, the purpose of this scenario was not to evaluate sizing, but rather look at agent dispatch behavior and overall microgrid system results.

Table 6.7. Microgrid asset capacity options.

Asset	**Rating**
Large diesel genset	105% of peak load demand power + power of maximum rated battery charging
Small diesel genset	105% of peak load demand power
Large lead-acid battery bank	1/2 of daily load energy consumption
Small lead-acid battery bank	1/8 of daily load energy consumption

Note: daily load energy consumption is equal to $\int P_{load}\,dt$ over the simulated day.

Conventionally, diesel-battery hybrid systems operate with a fairly simple control strategy. In power management terms, the following rules summarize the method:

1) The battery supplies power to the load until reaching a low voltage threshold, indicating low SOC.
2) At the low voltage threshold, the diesel runs, powering the load in addition to fully recharging the battery.
3) As the battery charges, typically at a set rate, voltage rises and charging power decreases.
4) The diesel shuts off at a set low-load threshold.

This conventional control method for diesel-battery hybrid operations can be problematic [6.10], and clearly does not consider diesel or battery efficiency, emissions, or costs. For the purpose of comparison, this conventional power management scheme is used as the base case.

In the islanded microgrid, the diesel genset and storage battery must share the burden of the local load. Correspondingly, the diesel and battery agents must coordinate to properly manage power. This is accomplished through negotiation, but prioritization can be difficult. For this scenario, three methods of asset self-ordering were evaluated:

1) Battery operation is favored over the diesel.
2) Diesel operation is favored over the battery.
3) Neither asset is favored; dispatch optimization decisions are heuristically.

Each of these methods has merits and drawbacks. In the case of the battery favored over the diesel, this implies that when negotiating, the battery will be operated such that its operation is optimized (battery $max\, F_a(\vec{x})$). In other words, once the storage consumer and producer agents complete their negotiations, their dispatch decision takes priority over the optimal operation of the diesel genset. In this way, the diesel supplements optimal battery operation throughout simulated day. Conversely, when the diesel is favored over the battery, the diesel producer agent dispatches it such that its operation is optimized (diesel $max\, F_a(\vec{x})$). The feasible region of operation available for the battery agents decision-making is further limited by diesel operation. Finally, in the third case, neither asset has complete default priority over the other. Instead, during each decision cycle, negotiations determine how the assets will be dispatched according to a heuristical algorithm, shown in Figure 6.29. Within the middle operating range of the battery (35-75%), the dispatch priorities are blended together so that each asset operates according to its rating, found by:

$$P_{i,compromise}[k] = P_{load}[k]\left(\frac{P_{i,rated}[k]}{\sum_{assets} P_{rated}[k]}\right) \tag{6.13}$$

where, $P_{i,compromise}$ is the value of the operating point found by compromise for asset i at increment k; P_{load} is the load demand at increment k; $P_{i,rated}$ is the rated power of asset i at increment k (fixed for the diesel and battery assets in this scenario); and $\sum_{assets} P_{rated}$ is the sum of the rated powers for all microgrid generation assets at increment k. While this method does not guarantee optimal operation along the Pareto front when considering the six domains of objectives ($f_{c,diesel}(\vec{x})$, $f_{p,diesel}(\vec{x})$, $f_{c,battery\ producer}(\vec{x})$, and $f_{p,battery\ producer}(\vec{x})$, $f_{c,battery\ consumer}(\vec{x})$, and $f_{p,battery\ consumer}(\vec{x})$), it does facilitate finding a decent solution that shares the operational benefits and drawbacks of each asset according to its rating. Otherwise, in order to conduct a complete evaluation of the combined search space, significant information would have to be passed between agents or a centralized supervisor would have to be involved. This heuristical method keeps the interaction between the agents to a minimum and calculation fast, while still allowing good solutions.

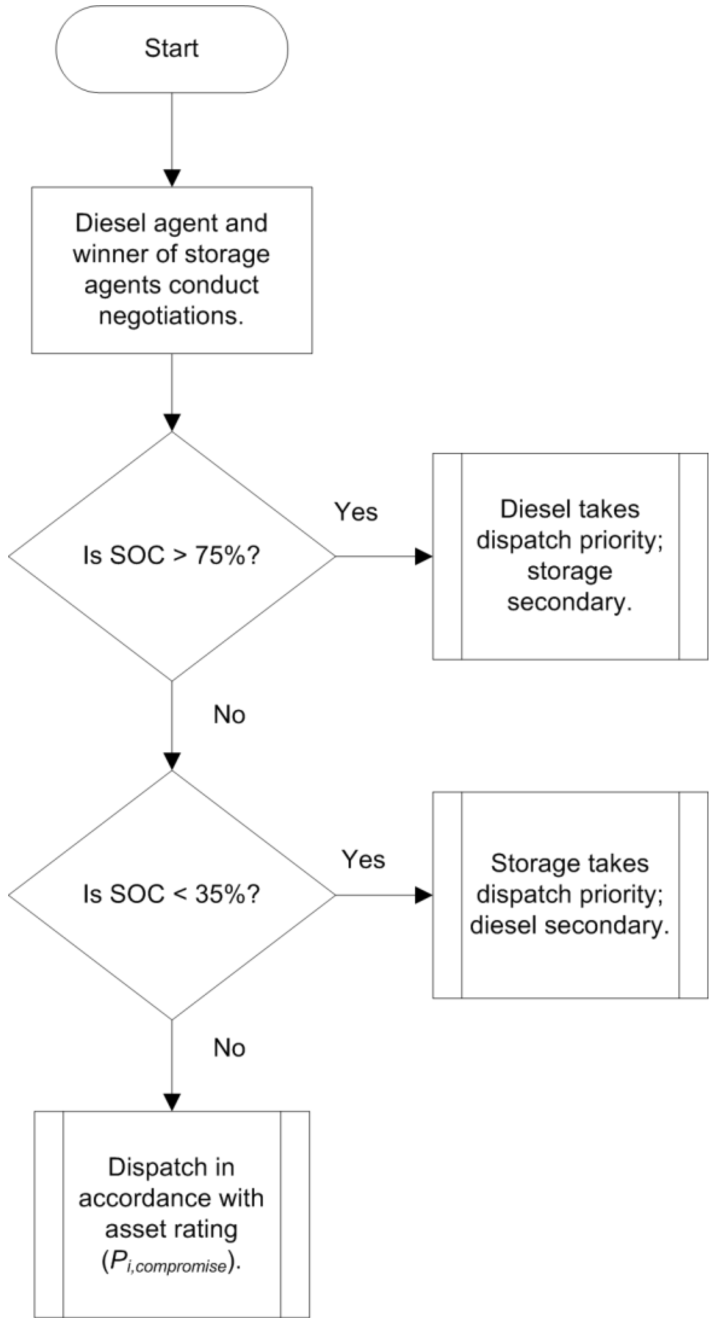

Figure 6.29. Blended priorities algorithm for agent negotiations in islanded scenario.

The results from the simulated 24-hour summer weekend day (time step = 1s) for the islanded microgrid are shown in Table 6.8.

Table 6.8. Islanded simulation scenarios for 24-hour summer weekend day.

	Large Diesel + Small Battery				Large Diesel + Large Battery				Small Diesel + Small Battery				Small Diesel + Large Battery			
Metric (over 24-hr period)	*Conv. Method*	*MAS - Battery favored*	*MAS - Diesel favored*	*MAS - heuristic objectives*	*Conv. Method*	*MAS - Battery favored*	*MAS - Diesel favored*	*MAS - heuristic objectives*	*Conv. Method*	*MAS - Battery favored*	*MAS - Diesel favored*	*MAS - heuristic objectives*	*Conv. Method*	*MAS - Battery favored*	*MAS - Diesel favored*	*MAS - heuristic objectives*
Diesel average efficiency	32.82%	30.87%	32.44%	32.44%	33.47%	30.22%	32.44%	32.44%	33.61%	33.15%	32.8%	32.63%	33.61%	33.61%	32.44%	32.44%
Battery average efficiency	87.49%	92.62%	89.24%	95.38%	94.38%	95.59%	94.35%	89.63%	93.18%	94.38%	91.94%	94.97%	96.85%	97.04%	96.81%	96.61%
Complete charge/ discharge cycles	6	6	5	0	2	2	2	0	3	4	1	0	0	0	0	0
Best Round-trip efficiency cycle	89.68% (Cycle: 1)	93.66% (Cycle: 2)	89.94% (Cycle: 2)	n/a	94.78% (Cycle: 1)	96.30% (Cycle: 1)	94.96% (Cycle: 1)	n/a	94.28% (Cycle: 3)	95.29% (Cycle: 4)	91.67% (Cycle: 1)	n/a	n/a	n/a	n/a	n/a
Worst Round-trip efficiency cycle	85.65% (Cycle: 6)	91.74% (Cycle: 5)	88.87% (Cycle: 3)	n/a	92.66% (Cycle: 2)	94.97% (Cycle: 2)	93.02% (Cycle: 2)	n/a	89.94% (Cycle: 1)	93.50% (Cycle: 1)	91.67% (Cycle: 1)	n/a	n/a	n/a	n/a	n/a
Average depth of discharge	56.68%	37.30%	59.47%	40.10%	70.01%	40.10%	70.01%	40.10%	61.32%	38.40%	70.10%	70.20%	70.01%	40.00%	70.10%	48.20%
Total cost to operate diesel	$501.30	$491.77	$465.36	$429.91	$479.44	$514.67	$505.37	$485.53	$450.78	$435.74	$435.60	$428.11	$353.89	$436.38	$309.21	$339.05
Total cost to operate battery	$4,498.04	$3,422.07	$3,799.07	$4,145.68	$4,825.78	$4,975.35	$4,170.31	$2,867.11	$2,076.62	$2,658.84	$1,155.16	$943.29	$1,834.65	$1,564.07	$1,820.27	$1,747.92
Total combined cost to operate	$4,999.34	$3,913.85	$4,264.43	$4,575.38	$5,305.22	$5,490.02	$4,675.68	$3,353.24	$2,527.40	$3,094.58	$1,590.76	$1,371.41	$2,188.54	$2,000.45	$2,129.48	$2,086.98
System combined average efficiency	60.15%	61.74%	60.84%	63.91%	63.92%	62.90%	63.40%	61.04%	63.39%	63.77%	62.37%	63.80%	65.23%	65.32%	64.62%	64.52%
Total THC emissions	122.19g	151.6g	106.7g	98.5g	125.81g	188.67g	115.8g	111.3g	131.43g	123.6g	98.7g	98.6g	103.18g	127.23g	70.9g	77.75g
Total CO2 emissions	1,276kg	1,215kg	1,170kg	1,081kg	1,237kg	1,257kg	1,270kg	1,220kg	1,168kg	1,120kg	1,105kg	1,081kg	917kg	1,131kg	777kg	852kg

The four power management methods are compared (conventional diesel-battery operation and the three MAS alternatives). In order to appropriately compare the operational results between the power management methods, metrics such as efficiency, cost, and emissions make up the rows of Table 6.8. The darkly shaded boxes indicate the power management method that achieved the best results within the summer weekend day scenario. Below the dark horizontal line, the last four rows of Table 6.8 give the combined microgrid results.

For each scenario, the best results within a row are highlighted with dark shading. It can be noted from Table 6.8 that the MAS that used a blend of both assets' cost and performance objectives to guide agent decisions (labeled as the MAS-heuristic objectives method in Table 6.8), rather than focus on attempting to optimize a single asset, consistently yielded the best results (achieves 10 of the 16 possible best solutions for system metrics across the four scenarios). However, some observations are important to note. For the multi-objective problem, there are many cases where conditions arise where superior results for one goal may be sacrificed for another. This finding is consistent with the Pareto-optimal discussions in 6.2.1.3 and 6.2.1.4 , and can be seen by some of the results. For example, in the Large Diesel + Large Battery scenario, the conventional dispatch method achieves the best system efficiency. However, the MAS using heuristics to incorporate mixed objectives showed better costs and emissions for the same scenario. In other words, in this case, although the MAS using the heuristical method had poorer efficiency, it had better results overall. This case highlights the importance of considering multiple objectives for power management and tailoring these objectives to the user's goals. Another example of this phenomenon is seen for the Large Diesel + Small Battery scenario. Although the MAS with the heuristical method yielded the best efficiency and emissions results, it does so at higher cost than other power management methods. Again, in most cases trade-offs exist when optimizing multiple objectives.

In order to compare the dispatch results of each method, the most extreme scenario of the four presented are shown in Figure 6.30. These results display how each asset was operated by its associated agent for the Small Diesel + Small Battery, summer weekend day islanded scenario. Although the MAS heuristical method yielded the best overall results of the four methods (see Table 6.8), one aspect of its behavior was not desirable, as revealed by the bottom right graph of Figure 6.30. The number of rapid restarts of the diesel genset early in the day may be an undesireable operational pattern from the perspective of other goal (minimize diesel noise, minimize short restart periods, minimize cycling, etc.). This is highlighted because it illustrates the difficulty in approaching the multi-objective problem for the microgrid. Despite achieving good results for minimizing cost and emissions, while maximizing efficiency, these goals that were incorporated into the MAS objective functions may omit other goals (such as genset cycling) that are also important. The importance of attempting to fully define the desired goals for microgrid to pursue is illustrated, and likewise emphasized, here.

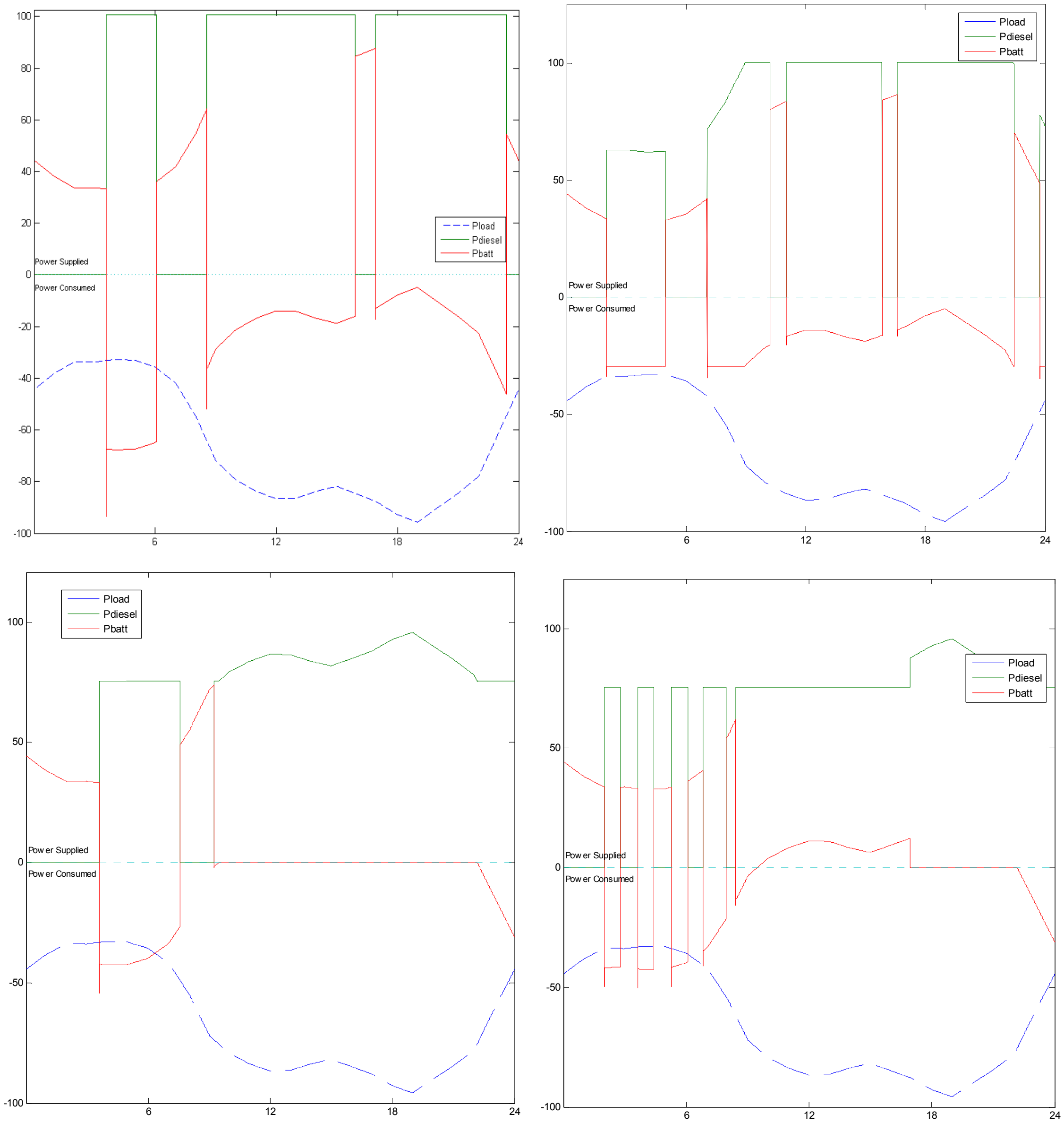

Figure 6.30. Dispatch results for islanded scenario on summer weekend day. (Top left) Conventional method. (Top right) MAS battery-favored method. (Bottom left) MAS diesel-favored method. (Bottom right) MAS heuristic method.

6.3 Discussion

Making the grid smarter requires advances on many fronts. Part of this advancement must be made in microgrid technology and operational management. In this chapter, some of the challenges involved with *intra*-microgrid power management have been explored. This has by no means covered the entire spectrum of decision-making topics facing *intra*-microgrid management, but the demonstrations shown illustrate the ability of the simulation environment developed for this purpose and the operation of the enhanced decentralized MAS. Power management scenarios for both grid connected and islanded conditions have been shown, along with common disturbances that affect system operation. Key enabling capabilities such as dynamically incorporating user goals into MAS decision-making, handling rapid changes in operational conditions, and factoring in multiple objectives, demonstrated here, indicate the potential of the approach investigated. Moreover, the simulation environment, as well as the MAS framework, are useful tools that can be of benefit to researchers and continue to offer insight into how tradeoffs between microgrid objectives affects the overall power management solution. It cannot be understated that in the emerging field of microgrid technology, simply understanding the power management and control issues involved with *intra*-microgrid decision-making is an enormous step. To provide a means (simulation environment) and a solution (enhanced decentralized MAS) is a significant contribution to the eventual realization of microgrid systems.

REFERENCES CITED

[6.1] C. V. Nayar, M. Ashari, and W. W. L. Keerthipala, "A Grid-Interactive Photovoltaic Uninterruptible Power Supply System Using Battery Storage and a Back Up Diesel Generator", *IEEE Transactions on Energy Conversion*, Vol. 15, No. 3, 2000, pgs. 348-353.

[6.2] R.W. Wies, R. A. Johnson, A. N. Agrawal, and T. J. Chubb, " Simulink Model for Economic Analysis and Environmental Impacts of a PV With Diesel-Battery System for Remote Villages", *IEEE Transactions On Power Systems*, Vol. 20, No. 2, 2005, pgs. 692-700.

[6.3] P. M. Crimp, S. Colt, and M. A. Foster, "Renewable Power in Rural Alaska: Improved Opportunities for Economic Deployment", Institute of the North – Arctic Energy Summit, Anchorage, AK, 2008.

[6.4] E.M. Nfah and J. M. Ngundam , "Evaluation of optimal power options for base transceiver stations of Mobile Telephone Networks Cameroon", *Solar Energy,* Vol. 86, 2012, pgs. 2935-2949.

[6.5] M.D. Bhawan and J.L.N. Marg, "Consultation Paper on Green Telecommunications", Telecom Regulatory Authority of India, New Delhi, No. 3/2011, Feb 2011.

[6.6] J. Rijssenbeek, H. Wiegman, D. Hall, C. Chuah, G. Balasubramanian, C. Brady, "Sodium-Metal Halide Batteries in Diesel-Battery Hybrid Telecom Applications", *Proceedings of the 33rd International IEEE Telecommunications Energy Conference (INTELEC)*, 2011.

[6.7] Energy Information Administration, "Gasoline & Diesel Fuel Update", retrieved 20 April 2012. Available at: www.eia.gov/petroleum/gasdiesel.

[6.8] A. L. Dimeas and N. D. Hatziargyriou, "Operation of a multiagent system for microgrid control," *IEEE Transactions on Power Systems*., Vol. 20, No. 3, 2005, pgs. 1447–1455.

[6.9] T. Logenthiran, D. Srinivasan, and A. M. Khambadkone "Multi-agent system for energy resource scheduling of integrated microgrids in a distributed system", *Electric Power Systems Research*, Vol. 81, 2011, pgs. 138-148.

[6.10] Bagen and R. Billinton, "Evaluation of Different Operating Strategies in Small Stand-Alone Power Systems", *IEEE Transactions on Energy Conversion*, Vol. 20, No. 3, Sept 2005, pgs. 654-660.

CHAPTER 7

EXTRA-MICROGRID SIMULATION

One of the most immediate ways that microgrid implementation could positively affect power system operation is by facilitating deliberate and controlled islanding. In fact, to pave the way for this new capability the IEEE Standard for Interconnecting Distributed Resources with Electric Power Systems (1547.4) "Guide for Design, Operation, and Integration of Distributed Resource Island Systems with Electric Power Systems" was revised in late 2011. This change to the 1547 standard allows portions of the grid to separate from the utility and operate independently; a mode that was previously discouraged [7.1]. The real value, therefore, that microgrids can provide with this added operational flexibility is the ability to maintain continuous operations during utility grid trouble by islanding itself from the broader power system. Additionally, when the utility network is no longer in distress, the microgrid may reconnect for interconnected normal operations.

When a fault occurs somewhere on the system, traditional power system protection systems such as fuses, over-current or under-voltage relay trips for circuit breakers, or distance relay trips quickly isolate the problem area [7.2]. When this occurs, portions of the power system may become islanded or disconnected from other sections. This presents an immediate problem if, prior to the fault, power flow from one area to serve load in another becomes infeasible. With numerous microgrids distributed throughout the utility power system, however, many customers could experience better continuity of service and reliability. By better distributing generation assets closer to the load they serve with microgrids, power flow to local loads travels over less of the power system thereby limiting the exposure to interruption due to faults. Additionally, microgrids formulated around the concept of deliberate islanding would have the capability to separate and reconnect smoothly.

In this chapter, the concept of power system reconfiguration and self-healing are explored. As microgrids represent a new infrastructure capability, how microgrids address these topics are of primary interest for utility operators and planners. To that end, the enhanced decentralized MAS framework is applied to the *extra*-microgrid problem of self-healing the broader power system network in cases of trouble. Results indicate the power of the MAS to evaluate, communicate, and execute power system reconfiguration that ensures the maximum level of service customers.

7.1 Self-healing

Simply, self-healing is defined as the capability for a system to automatically detect and recover functionality when faced with a single or many casualty events. For a power system, this definition is somewhat refined to include the rapid identification of problems, actions to minimize any adverse impacts from casualties, and the prompt recovery of the system to a stable operating state, if possible [7.3, 7.4]. Although sometimes not defined, there are two distinct periods for self-healing: first, the emergency reaction stage, followed by the restorative stage. During the first stage, a casualty condition is detected and the system reacts to minimize it, typically through isolation. Many emergency reactions may be automatic or predetermined, but have the effect of placing the system in a safer, less perilous condition. Once the system has transitioned beyond the initial emergency, restoration can begin. During restoration, a series of reconfigurations may take place improving overall system condition, involving breaker manipulations, generation startup or shutdown, load shedding or pickup, or other actions that change system operational posture. The restoration stage may be both a longer and more complicated self-healing stage, requiring more complex decisions. Typical performance measures of self-healing may include the speed a stable configuration is reached, the quantity of components that remain energized, and the minimization of equipment cycling during restoration.

Within the past decade and a half, the notion of resilient and self-healing power systems has become more prominent. Much of the self-healing literature and research within the power systems field is influenced by [7.5] and later additions, including [7.6] and [7.7]. In [7.5, 7.6, 7.7], a broad description of a comprehensive, multi-layered self-healing power system infrastructure is given. Subsequent literature has clarified and added to this initial vision, but a fundamental reliance on a strong centralized supervisory controller that encompasses global system awareness, in-depth pre-contingency analysis, and/or complex predictive planning cycles remains. Very little attention has been paid to truly decentralized and distributed decision-making that can accomplish similar self-healing objectives. While the reasons for this are unclear, two factors appear to have influenced the recent research direction. First, conglomerating communication, sensory, and control functions in a central manner allows decisions to be made with a global perspective. While it is cumbersome to centralize these functions, this facilitates the most complete information for decision-making. The second factor that may have discouraged development of capable distributed multi-agent systems is their difficulty. Without a dominant central supervisory force, achieving prioritization and cooperation for distributed control is a primary challenge. However, decentralizing decision-making has unique attributes that make it attractive from a resiliency perspective; chiefly because it can avoid the scenario where corruption or failure of the central supervisory node leads to total system collapse.

An example of a proposed multi-layered hierarchical system is given in [7.8]. Conceptually similar to [7.5], lower level agents perform reactive functions, while middle and higher level agents perform more complex forecasting and strategic functions. Clearly, architectures of this type have the potential to achieve self-healing objectives at the cost of significant computational, communication, and sensory complexity. Proposed self-healing schemes such as in [7.8] and [7.9] rely on large data flows of real-time power system monitoring information and predetermined network topologies to determine how to reconfigure the power system. In [7.10], a review of the challenges that conventional power system protection and control technology pose to self-healing objectives is given, but similarly propose a centrally-based architecture dependent upon significant amounts of system data to formulate global state estimations. These computationally intensive predictions of system-wide health guide reconfiguration decisions, but [7.10] acknowledges that centralizing system monitoring and decision-making is cumbersome, requiring surmounting numerous technical gaps. A key point made in [7.11] regarding centralized real-time decision-making is that courses of action based on predefined models of an unpredictable environment can have detrimental effects on system behavior.

In the method described in [7.11], when confronted with a power system emergency, network islands are formed first and subsequently load is shed within the islands to achieve stability. This method requires that islanding decisions be pre-scripted or determined in situ by a central supervisor with global knowledge.

A bottom-up approach utilizing intelligent switching components for a power system in a fault-prone area is described in [7.12]. Using dedicated VHF links for peer-to-peer communication, distributed controllers have responsibility for individual feeders with multiple reclosers and breakers to isolate areas of a power system during emergency situations. Primarily, [7.12] shows how effective delegating emergency reaction responsibility to a lower hierarchical level, closer to the affected area, can be as a self-healing method. This is an example of retaining self-healing capability without the need for centrally-dictated actions. Relatedly, in a move towards a diversified MAS, [7.13] outlines a complex hierarchy with both a central supervisory agent and many distributed agents that handle automatic emergency reactions. Different, however, from [7.12] and having intense reliance on information flows, the multiple control layers described by [7.13] depend on fast simulation and modeling to estimate future states, anticipate problems, and make system self-healing decisions.

Shipboard power system research has yielded interesting results for the self-healing question, but has commonality with methods described above. For example, in [7.14], the shipboard power system is modeled as a graph (edges and nodes) and formulated as a fixed charge (cost) network flow problem; the objective being to find the optimal post-event configuration using priority-weighted loads to maximize total shipboard load, while satisfying constraints such as unavailable equipment. Most shipboard self-healing methods rely on global knowledge by a central supervisor and therefore are similar to conventional power system self-healing methods. Even proposed shipboard self-healing methods that suggest multi-agent applications, such as [7.15], utilize hierarchical control and rely on central supervisory functions.

Clearly, for a power system to be effective at self-healing, it must encompass some fundamental traits, including: the ability to interpret emergencies, react promptly to abnormal situations, and a decision-making framework that guides the system to safe operation. While the majority of effort has been focused on centralizing these capabilities, an enhanced decentralized MAS may offer an alternative for computational and system complexity required by previous methods.

7.2 Formulation

In this *extra*-microgrid demonstration, the simulation environment is used to implement a MAS different than for *intra*-microgrid demonstrations. In this case, each agent is responsible for an individual microgrid in a broad utility power system, not individual assets within an *intra*-microgrid boundary. This is meant to simulate a higher hierarchical level, where many microgrids interact with each other, primarily through power flow and PCC status. While the *extra*-microgrid agents take on new roles governed by objectives that are different from the *intra*-microgrid demonstration, the fundamentals of their interaction and operation remain the same in both cases. Ultimately, it is conceivable that unifying the *intra*- and *extra*-microgrid concepts is achievable in a single microgrid MAS. This would be accomplished by additional agents that would take on the role of adjusting total microgrid system performance measures (such as the ones used by the *intra*-microgrid observer agent) based on *extra*-microgrid information from outside the microgrid. For lack of a better term, an additional agent that specifically looks for cooperative opportunities outside of the microgrid is called the "*extra*-microgrid liaison" agent. For example, if a microgrid on the macrogrid network were experiencing a loss of local generation, a neighboring microgrid's liaison agent may communicate with the microgrid experiencing trouble and offer to help. Based on direction from the liaison agent, the helper microgrid may modify the objectives for some of its agents, thereby increasing the quantity of real power exported. However, this may cause the microgrid as a whole to deviate from its user-defined objectives, such as minimizing operational costs and emissions. This is permissible however, if the user has authorized an *extra*-microgrid liason agent to modify microgrid objectives when trouble calls are received. This illustrates the exciting possibilities for more complex and layered hierarchical MAS systems built on the framework developed. The first step, of course, was the simulation of how *extra*-microgrid interactions could be conducted and what their effects on self-healing reconfigurations would be. The following two sections lay out how the agent algorithms were composed.

7.2.1 Normal Operation

For the purpose of this demonstration, it was of primary importance to show the cooperative functions of the MAS; in other words, how an enhanced decentralized framework can achieve self-healing objectives that have heretofore been primarily addressed in a centralized manner. To simplify the discussion, the power system context for this MAS application was reduced to real power flows only. By no means a restriction, microgrid agent development is completely flexible, allowing the incorporation of other factors such as reactive power flows, voltage and frequency, synchronization concerns, economic factors, etc. Although decision-making domains have been limited for this demonstration, further functionality is readily implementable.

Under normal circumstances, agents operate under a primarily self-interested protocol. Within each microgrid, a certain quantity of generation capacity (kW) is installed. The agent is not concerned with the type of generation resource explicitly, but instead relies on information regarding the status of local generation assets. Likewise, the quantity of installed load at each microgrid is known. For the purpose of experimentation, 20% of each microgrid's installed load is designated as vital and the rest is non-vital. This is arbitrary and can be modified depending on simulation requirements. Agents continuously assess the following primary variables:

- Instantaneous total generation capacity (kW)
- Current generation operating level (kW)
- Current load operating (kW)

The microgrid agent has the ability to ramp generation up or down based on the constraints of the generator and the available resources. Likewise, the microgrid agent can start or stop vital and non-vital loads based on the situation. The agent's prime objective is to maintain power to the vital loads within its microgrid at all times. If locally available power cannot sustain vital loads, then the agent will communicate to other agents seeking assistance. Clearly, this objective could be obviated if adequate dispatchable generation were mandated to be implemented at each microgrid, but this is not necessarily realistic. Under normal operations, if available generation capacity exceeds that which is required to power vital loads locally, then either non-vital loads are switched on incrementally or power is exported to neighboring microgrids who have requested it. The microgrid agent operates local generation and load based on the following priority hierarchy that incorporates both self-interest and cooperation:

- Local microgrid vital load requirements.
- Neighboring microgrid emergency vital load requirements.
- Local microgrid non-vital load requirements.
- Neighboring microgrid non-vital load requirements.

In this way, the microgrid agent seeks to energize the maximum number of local vital and non-vital loads based on local generation. If local generation is adequate to meet vital load requirements, but not to fully energize non-vital requirements, the microgrid can transmit a surplus request to other microgrids for assistance. Based on the priority hierarchy, a microgrid that receives the surplus request and has generation capacity in excess of its own vital and non-vital load requirements can export power to the another microgrid.

The microgrid agents interact as to utilize the maximum quantity of available generation possible. This is considered a maximum power utilization strategy. Specifically, each microgrid agent continuously attempts to fully energize local loads and, if conditions permit having accomplished this, will seek to export any excess power to other microgrids. In this way, microgrid agents are discouraged from curtailing generation if resources are available. This simulates the maximum utilization of available renewable sources, such as wind and photovoltaics, which are inherently intermittent, but desirable to operate maximally when available. In cases where the generation mix across microgrids includes both dispatchable and renewable sources, additional objectives come into play which compels modifying the maximum power utilization strategy, most commonly to account for costs. Clearly, the incremental generation cost for a unique microgrid, as well as the spot market clearing price, influences the normal operation priority hierarchy described above. However, for the purpose of this paper, demonstrating the cooperative effects of the multi-agent system were paramount and cost was neglected. Depending on desired complexity, the agent priority hierarchy can be modified to incorporate cost functions that account for changing costs and are fully integratable in the microgrid MAS framework.

Load prioritization across the power system is not considered in this demonstration. In other words, from the microgrid agent perspective, all non-vital loads of neighboring microgrids are equivalent. When a microgrid has excess power available, it broadcasts this fact to all agents. If a microgrid agent determines that it desires the surplus power, it responds to the sender. Responses to these broadcasts are handled on a "first come, first serve" assignment basis. For example, if microgrid A has an excess of 100 kW and microgrid B is first to submit a non-emergency request for 80 kW of the surplus, then 80kW is designated for microgrid B usage. Subsequently, microgrid A reissues a broadcast for the remaining 20kW. When negotiations between microgrids are finalized, a temporary contract is formed between supplier and receiver microgrids for a quantity of power. This contract can be modified at any time as conditions change. As instantaneous power generated or load demand changes, the contracted parties attempt to incorporate the changes into their existing contract, but if unable, the contract is released and the system-wide negotiation process repeats for supply to match demand. A common example of this occurs when microgrid A, who is generating excess power for microgrid B, experiences a curtailment of excess power. When this happens, the microgrid A informs the microgrid B that it can no longer supply at the previous quantity. Microgrid B decides whether to curtail its load demand to match the new excess power quantity or terminate the contract.

The multi-agent framework readily facilitates new microgrids joining the power system. As a new microgrid becomes operational, it communicates its presence, establishes connections with neighboring microgrids, and transitions immediately into normal cooperative behaviors as a participant in MAS decision-making.

7.2.2 Emergency Operation

An emergency situation is defined as either a failure of a microgrid resulting in its loss from the system or a faulted transmission line that results in the loss of that power flow path from the system. Following an emergency event, the remaining microgrids must respond with actions to restore the system to the maximum extent possible. Microgrid agent behavior upon a casualty event is characterized first by an emergency reaction stage, followed by the restorative stage. Once each microgrid has locally taken immediate reactive actions and placed itself in a safe condition, then a restorative stage can begin. The reaction stage is unique to emergencies; the restorative stage is very similar to normal operation.

The reaction stage is initiated by the microgrid that sends an emergency MAS message upon first sensing a fault or a neighboring microgrid failure. Upon receipt of that broadcast, microgrids make emergency reactions to stabilize system power flow. This is done according to the algorithm, shown in Figure 7.1, the primary objective of which is for each microgrid to transition to a self-sustaining state, therefore minimizing the transfer of power on the compromised power system. In this way, safe power system line connections are maintained and generation-to-load imbalances are minimized.

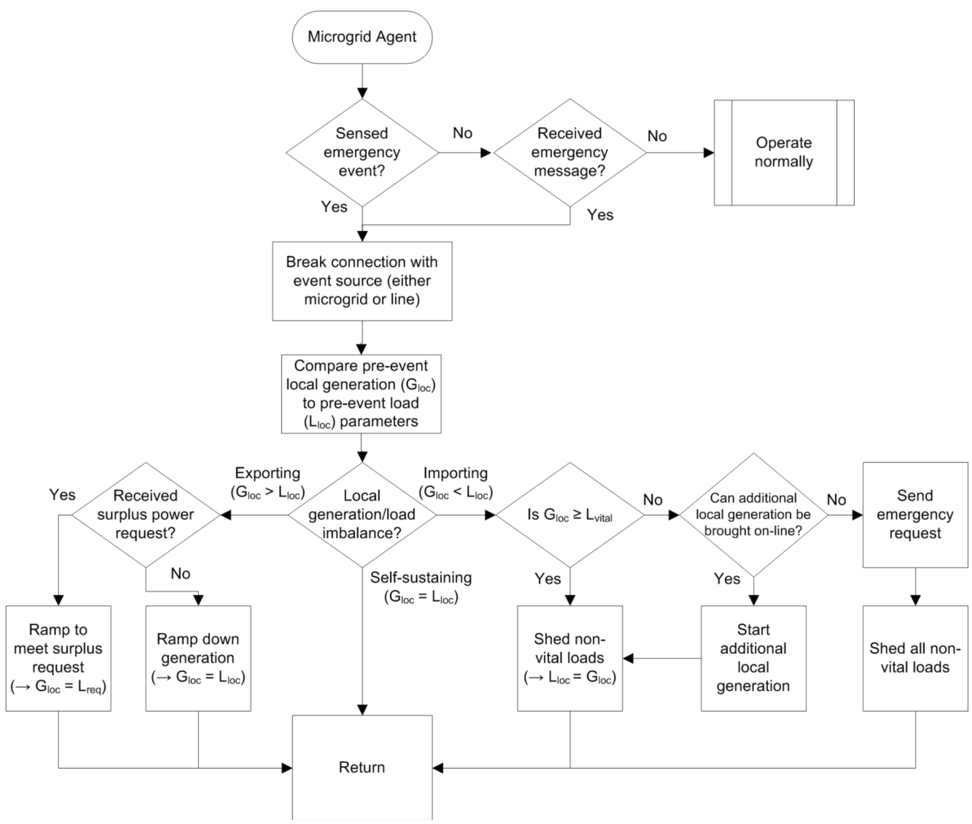

Figure 7.1. Agent algorithm for actions under normal and emergency conditions.

At the outset, if a microgrid has broadcasted an emergency message indicating that it cannot meet its local vital load requirements with local generation, then the multi-agent collective addresses this concern first according to the priorities listed in 7.2.1 . Each microgrid with available generation capacity in excess of its vital load requirements communicates its excess capacity and current list of available safe connections to the microgrid in trouble. By sending these emergency responses, the microgrid agents are declaring that they will forego supplying their own non-vital loads in order to help a neighboring microgrid power their vital ones. The microgrid in trouble determines which microgrid it will temporarily contract with for excess power based on the first positive response it receives.

Immediately following the emergency event and the completion of emergency reactions, it is very likely that some microgrids may have excess generation online. This is the beginning of the restorative stage. Microgrids that have shed non-vital load in the emergency transition transmit surplus requests, similar to normal operation, seeking additional power. During negotiation, the microgrids with excess generation pair with those that have shed load during the emergency. If the microgrids that enter into a temporary contract are connected by a transmission line that is safe, but not energized, they may determine to activate that line rather than wheeling power. Although not used in this demonstration, performance measures, such as the percentage of microgrid loads energized, can be used by the MAS for prioritization when negotiating temporary power contracts.

As the restorative stage winds down, the multi-agent collective is ready to restore operations to the maximum extent possible, considering the new system topology. The multi-agent system transitions to a normal operating condition, except that some microgrid nodes and connections are now unavailable to the system. Likewise, the newly reconfigured power system operates according to the normal cooperative protocols, described in 7.2.1 . The only exception is that, periodically, the microgrids that are nearest the faulted line or failed microgrid check to see whether the emergency condition has been rectified. If the emergency condition has cleared, the microgrids attempt to reestablish any prior connections with failed microgrids and incorporate them into normal operations.

7.3 Simulation

For the purpose of demonstration, a small power system incorporating eight microgrids is simulated, shown in Figure 7.2 (Figure 7.3 is the diagram key). This small power system represents a geographical area that contains about 5MW of total load; equivalent to peak loading experienced by about 3,500 residences. Within that network, the total sum of microgrid generation is matched with load to 5MW. However, the distribution of load and generation is widely discrepant from microgrid-to-microgrid throughout the geographical area, as shown in Table 7.1 (see Appendix C for more details about microgrid classification and citizenship).

At the start of the simulation, the small power system is operating according to the initial operating conditions shown in Table 7.2. The placement of interconnecting power lines and whether they are active of not was randomized at the start of the simulation. It is noted that, in this simulation, voltage and frequency transients are neglected, as are market economics and other objectives. This example is meant to highlight cooperative actions that microgrid agents initiate to restore the system to a semi-normal operating state following an emergency. There are no transmission constraints, so power can be wheeled without penalty.

In Figure 7.2, each microgrid is represented by two conjoined circles; the leftmost represents generation and the rightmost shows load (expanded in Figure 7.3). The relative size of each circle represents either the total installed generation capacity or the total installed load, respectively. Throughout operations, the proportion of instantaneous generation, in kW, and load consumption, in kW, is shown as the colored portion within each of the two microgrid circles, similar to a pie chart. Transmission lines interconnect the microgrids; dashed lines represent inactive transmission lines, i.e. the tie breakers are open, and the solid lines represent lines that are active. Each microgrid is operating within individual limits and were initialized to carry all of their native vital loads and 50% of their non-vital loads. Microgrids C2, C4, and C7 have excess power available that they are exporting to microgrids C1, C3, and C8 (Table 7.2).

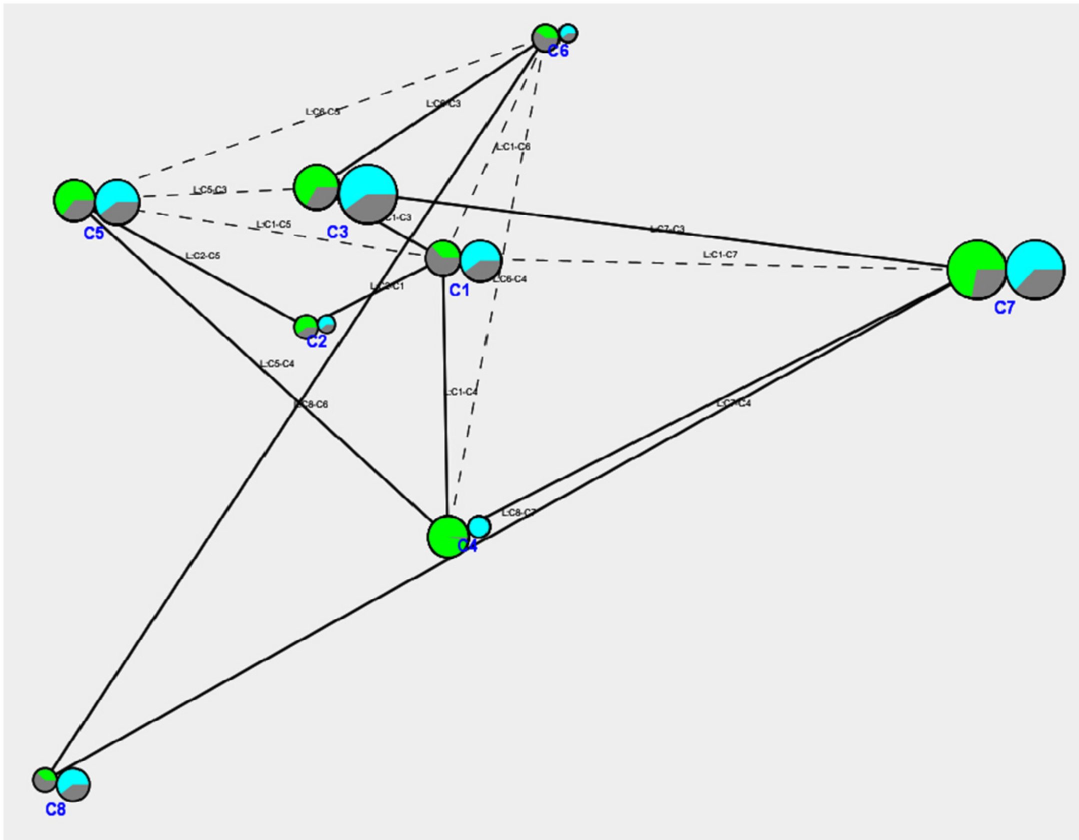

Figure 7.2. Geographical depiction of simulated power system prior to emergency.

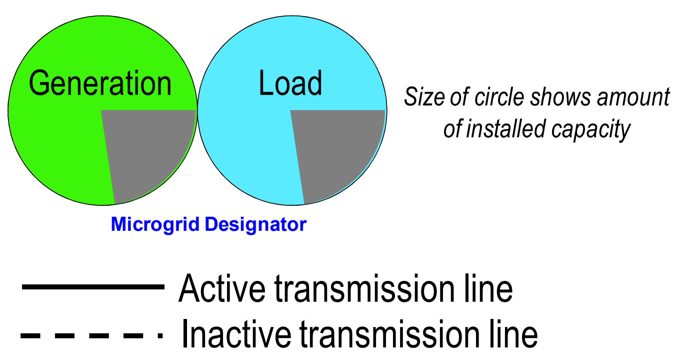

Figure 7.3. Diagram key for geographical depiction of power system.

Table 7.1. Parameters for small power system.

Microgrid Designator	**Total Installed Generation Capacity (kW)**	**Total Installed Vital Load (kW)**	**Total Installed Non-Vital Load (kW)**	**Microgrid Load-to-Generation Ratio**
C1	620	140	560	0.90
C2	400	60	240	0.60
C3	750	200	800	1.07
C4	680	70	280	0.41
C5	700	150	600	0.86
C6	450	60	240	0.53
C7	1000	210	840	0.84
C8	400	110	440	1.10
Total:	5,000 kW	1,000 kW	4,000 kW	

Table 7.2. Pre-emergency initial operating conditions.

Microgrid Designator	**Instantaneous Operating Generation (kW)**	**% of Vital Loads Operating**	**% of Non-Vital Loads Operating**	**Import / Export Power** (-kW in,+kW out)
C1	220	100%	50%	-200
C2	240	100%	50%	+60
C3	500	100%	50%	-100
C4	680	100%	100%	+330
C5	450	100%	50%	0
C6	180	100%	50%	0
C7	720	100%	50%	+90
C8	150	100%	50%	-180
Total:	3140 kW	1000 kW	2140 kW	0 kW

The small power system experiences a fault scenario that causes the complete loss of a system microgrid, designated C4. As a result, the remaining microgrids must react and recover operations to the maximum extent possible. The emergency event is initiated by tripping the interconnection breaker for microgrid C4. As is shown by Table 7.2, microgrid C4 was a significant contributor of surplus power to the power system. The loss of C4 causes system disruption and is a catalyzing event for the system to self-heal.

Immediately upon sensing the loss of C4, the MAS performs emergency reactions as described in 7.2.2 . In Table 7.3, power system conditions upon completion of the emergency reaction stage are shown: microgrids C1, C3, and C8 have reduced their operating non-vital loads to match their local generation; C2 and C7 with excess power available have transmitted surplus available messages to the MAS. Due to the emergency reactions, the power system is in a stable transitory state to begin restorative actions.

Table 7.3. Operating conditions immediately following the casualty to microgrid C4.

Microgrid Designator	**Instantaneous Operating Generation (kW)**	**% of Vital Loads Operating**	**% of Non-Vital Loads Operating**	**Import / Export Power** (-kW in,+kW out)
C1	220	100%	14%	0
C2	240	100%	50%	+60
C3	500	100%	38%	0
C4	0	0%	0%	0
C5	450	100%	50%	0
C6	180	100%	50%	0
C7	720	100%	50%	+90
C8	150	100%	9%	0
Total:	2440 kW	930 kW	1380 kW	150 kW surplus

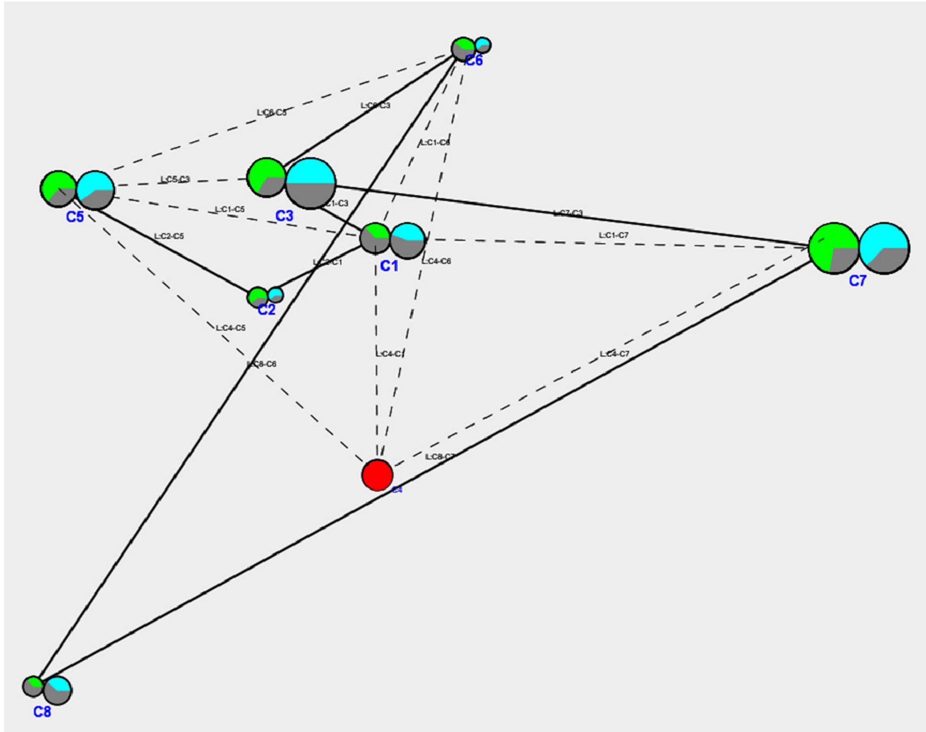

Figure 7.4. Geographical depiction of simulated power system post-restoration.

As the restoration phase begins, surplus availability messages are processed by microgrids C1, C3, and C8. In the cases of C1, C3, and C8, these microgrids have shed non-vital loading to match their operating generation level. When they receive surplus availability messages from C2 and C7, each responds seeking temporary supply contracts that will allow them to re-energize shed load with power produced from C2 or C7. Because these contracts are initiated on a "first come, first served basis", the order that contracts are awarded is random. In this demonstration, C1 and C8 are the first two microgrids to communicate with C2 and C7 and, therefore, win their temporary supply contracts. In this case, each of the microgrids with excess supply was able to contract all of their excess generation to individual microgrids in need. However, if the first microgrid to be awarded a contract could not accept all of the excess generation, the difference would be available to the next microgrid in the messaging queue, and so on. The results of the restoration actions are shown in Table 7.4. The impact of the temporary supply contracts are evident in Table 7.4, where C2 sources excess power to C8 and C7 does the same for C1. The system has now self-healed itself to the maximum extent possible. Operations continue without the failed microgrid C4, shown geographically in Figure 7.4.

When the restorative stage has concluded, system operation is as if the power network were in a normal state, except for the exclusion of C4 and the unavailability of transmission lines leading to it. As instantaneous generation or load fluctuates, the microgrids will respond and cooperate to meet their objectives in an identical manner to prior to the emergency, excluding the influence of microgrid C4. At the time that C4 is recovered, it may rejoin the system under the normal protocol.

Table 7.4. Operating conditions upon restoration without microgrid C4 operating.

Microgrid Designator	**Instantaneous Operating Generation (kW)**	**% of Vital Loads Operating**	**% of Non-Vital Loads Operating**	**Import / Export Power** (-kW in,+kW out)
C1	220	100%	30%	-90
C2	240	100%	50%	+60
C3	500	100%	38%	0
C4	0	0%	0%	0
C5	450	100%	50%	0
C6	180	100%	50%	0
C7	720	100%	50%	+90
C8	150	100%	23%	-60
Total:	2440 kW	930 kW	1530 kW	0 kW

7.4 Discussion

The purpose of this demonstration was two-fold. First, the *extra*-microgrid decision-making process is slightly different from that of the *intra*-microgrid, but the same MAS framework, when modified, can be applied to it. This indicates the possibility of developing hierarchical MAS structures that would allow self-interested *intra*-microgrid MAS power management and control systems to interact with and take into account *extra*-microgrid considerations. Second, the body of power systems research to date has not reported a self-healing methodology that was not based on centralized supervisory functionality. Here, an enhanced decentralized MAS without a central supervisor is capable of performing self-healing in the event of a power system fault. This, too, indicates the strong capabilities of decentralizing decision-making and opens the door to more sophisticated dynamic reconfiguration and electrical service sharing across the macrogrid; an important superlative of microgrids.

REFERENCES CITED

[7.1] "IEEE Guide for Design, Operation, and Integration of Distributed Resource Island Systems with Electric Power Systems", IEEE Standard 1547.4-2011, 2011.

[7.2] J.A. Aspinall, et. al. (editor). Power System Protection (Volume 2: Systems and Methods) – 2nd Edition. The Institution of Electrical Engineers, London, U.K., 2005.

[7.3] M. Amin and B.F. Wollenberg, "Toward a smart grid: power delivery for the 21st century", *IEEE Power and Energy Magazine*, Vol. 3 , No. 5, 2005, pgs. 34-41.

[7.4] K. Moslehi and R. Kumar, "Vision for a self-healing power grid", *ABB Review,* No. 4, 2006.

[7.5] M. Amin, "Toward Self-Healing Energy Infrastructure Systems", *IEEE Computer Applications in Power*, Vol. 14, No. 1, 2001, pp. 20-28.

[7.6] M. Amin, "Toward a self-healing energy infrastructure", *Proceedings of the IEEE Power Engineering Society General Meeting*, 2006.

[7.7] M. Amin, "Challenges in reliability, security, efficiency, and resilience of energy infrastructure: Toward smart self-healing electric power grid", *Proceedings of the IEEE Power and Energy Society General Meeting - Conversion and Delivery of Electrical Energy in the 21st Century*, 2008.

[7.8] Z. Noorian, H. Hosseini, and M. Ulieru, "An Autonomous Agent-based Framework for Self-Healing Power Grid", *Proceedings of the IEEE International Conference on Systems, Man, and Cybernetics*, 2009.

[7.9] P. Cox, "Self-Healing Networks Performance Improvement by Automated Switching Algorithm", *Proceedings of the CIRED Seminar 2008: SmartGrids for Distribution*, 2008.

[7.10] F. Li, Z. Chen, L. Fan, P. Zhang, "Toward a self-healing protection and control system", 40th North American Power Symposium, 2008.

[7.11] H. You, V. Vittal, and Z. Yang, "Self-Healing in Power Systems: An Approach Using Islanding and Rate of Frequency Decline-Based Load Shedding", *IEEE Transactions on Power Systems*, Vol. 18, No. 1, 2003.

[7.12] D. Macleman, W. Bik, and A. Jones, "Evaluation of a Self Healing Distribution Automation Scheme on the Isle Of Wight", *Proceedings of the CIRED 20th International Conference on Electricity Distribution*, 2009.

[7.13] A. Valenti, I. Bel, and S. Lee, “High Level Requirements of Fast Simulation and Modelling Suite Of Tools for Future ‘Self-Healing’ Distribution Power System”, *Proceedings of the CIRED 18th International Conference on Electricity Distribution*, 2005.

[7.14] K. L. Butler-Purry, and N. D. R. Sarma, “Self-Healing Reconfiguration for Restoration of Naval Shipboard Power Systems”, *IEEE Transactions on Power Systems*, Vol. 19, No. 2, 2004.

[7.15] K. L. Butler-Purry, “Multi-Agent Technology for Self-Healing Shipboard Power Systems”, *Proceedings of the 13th International Conference on Intelligent Systems Application to Power Systems*, 2005.

CHAPTER 8

CONCLUSIONS

This dissertation has covered the design and development of a microgrid simulation environment and an enhanced decentralized multi-agent system (MAS) for microgrid multi-objective power management. The primary content of this manuscript has focused on the framework for the simulation environment, its functionality, the modeling that supplements it, agent design and algorithms, as well as results from simulations. The conclusions drawn from this research work are summarized, as follows:

1. The electrical power system in the United States faces major challenges. Microgrids are an innovative solution and integral to a future smart grid that will, at least in part, rely upon microgrids.

2. Microgrid modeling demands more than just component models. Complex management and control of microgrids cannot be properly evaluated without a comprehensive simulation environment that incorporates operational concepts, electrical modeling, asset dynamics, and control conditions, as well as communications.

3. To address the lack of the comprehensive microgrid simulation, a software environment has been created with open-source tools and easily implementable on a wide range of hardware, is flexible and modular. The Java-based microgrid simulation architecture utilizes the JADE communication libraries to facilitate a software test bed

where microgrid components and control methods may be implemented and tested. This is a useful tool that can be used to improve research investigations into microgrid topics.

4. In support of the microgrid simulation environment, asset mathematical models have been investigated and developed, including five of the most common DER assets implementable in microgrids: a diesel generator model, a four- and five-factor photovoltaic model, a CHP model for thermal recovery, a wind turbine with PMSG, and lead-acid battery. In addition, models for power electronic interface and control have been investigated, as well as support models for microgrid topics, such as load demand. The key approach to all of these models was to identify aspects of the component that were previously un-modeled or existing models were inadequate for comprehensive microgrid modeling. These models can be used to aid research into DER topics, as well as their intended purpose of supplementing the microgrid simulation environment.

5. Enhanced decentralized methods for microgrid power management and control have been a central topic in this work. This departs from the conventional centralized methods commonly used for automated systems. This research has demonstrated that autonomous agents with limited visibility of microgrid information are capable of solving complex optimization problems comprising multiple objectives. Moreover, these agents have demonstrated the ability to self-organize under unpredictable circumstances, driving the microgrid system as a whole towards better overall outcomes for cost, environmental, efficiency, and other objectives. Decentralized control methods are inherently more difficult than centralized methods that have the

benefit of aggregated global system knowledge; the development of this functional enhanced decentralized MAS is proof to researchers that these methods have value and are extremely capable.

6. Making power management decisions for multiple assets within a microgrid is new. What is innovative about the work presented in this dissertation and represents a significant contribution to the decision-making field for microgrids is the focus on addressing multiple objectives simultaneously. This requires deeper knowledge of asset characteristics and operation (explored in the modeling chapter), but also a decision-making methodology capable of incorportating many goals and seeking solutions that address them comprehensively. This topic has been a main focus of the work presented.

7. The notion of real-time decision-making has been explored. Different than conventional centralized processing techniques, the new multi-agent agent-based approach to microgrid power management exhibits different attributes in real-time scenarios. The method has proved itself, rapidly finding local solutions that comprise fairly good overall solutions even before the agents negotiate for better performance. This is an important finding that demonstrates the value of breaking the microgrid power management problem into parts and distributing decision-making to the lowest hierarchical level with the MAS.

8. Renewable generation and enabling power system technologies can be directly incorporated into microgrids. Results from the *intra*-microgrid simulations demonstrate that unpredictable and unreliable renewable sources can add value to a

microgrid when paired with appropriate companion technology such as storage assets, demand response, or generation curtailment for wind turbines. Demonstrations of this type are important to affirming the use of renewable DERs in microgrids.

9. Trade-offs are very important for power management. Understanding this fact is critical to developing proper objectives for microgrids and, for that matter, any power or energy management system. This research has shown that in some cases counter-intuitive effects are experienced when attempting to raise the performance of one objective over another. This was seen in the *intra*-microgrid simulations with multiple agents each attempting to optimize their own assets. There, situations often arose where improving two objectives, such as cost and environmental emissions, led to poorer asset efficiency; a counter-intuitive, but consistent finding. Trade-offs were experienced in the *extra*-microgrid simulations, as well, where the desire to restore the interconnectedness of the system after a fault speedily can lead to stable by less desirable self-ordering amongst the MAS. The insights gained through this investigation will benefit researchers who attempt to develop effective power management methods.

Finally, the United States needs to take steps forward from an antiquated power system that was designed for primarily industrial customers over 100 years ago. While microgrids can achieve significant improvements for customers and utilities alike, prior to the work detailed in this manuscript, a comprehensive decentralized means of managing microgrid assets and controlling operations had not been realized. It is clear that without a safe, robust, and flexible power management, microgrids, along with their benefits, will not be adopted.

This dissertation has addressed a specific open question so far neglected by the power system community: how can microgrids be controlled in a decentralized way while optimizing the operation of local assets, providing electrical service customized for attached customers, and supporting the greater power system electrically? The primary goal has been to develop and demonstrate a novel, enhanced decentralized multi-agent power management architecture with the ability to manage multi-objective microgrid operations optimally under normal and emergency conditions. This has been achieved, along with the development of a microgrid simulation environment capable of expanding to whatever the needs of future researchers.

Microgrids are a way forward. Faced with the litany of hard choices bolstered by stark challenges, the United States needs power system innovation. By successfully completing the work detailed in this dissertation, an important step towards a stronger, more agile, better suited, and cleaner electrical future has been achieved. Without efforts, like annotated here, microgrids and the solutions they offer us will not come to pass. Now we are a bit closer.

REFERENCES CITED

[1.1] George Constable and Bob Somerville, “A Century of Innovation: Twenty Engineering Achievements that Transformed our Lives”, National Academies Press, 2003.

[1.2] Energy Information Administration, "Annual Energy Outlook 2012", U.S. Department of Energy, Report Number: DOE/EIA-0383, 2012.

[1.3] Energy Information Administration, "Electric Power Annual 2010 – Table 7.2", U.S. Department of Energy, Report Number: DOE/EIA-0348, revised 2012.

[1.4] Energy Information Administration, "Electric Power Annual 2010 – Table 7.3", U.S. Department of Energy, Report Number: DOE/EIA-0348, revised 2011.

[1.5] Energy Information Administration, "Electric Power Monthly, December 2010 – Table 5.1", U.S. Department of Energy, Report Number: DOE/EIA-0226, 2010.

[1.6] Energy Information Administration, “Annual Energy Outlook 2011 with Projections to 2035 - Table A8 (Revised Early Release)”, U.S. Department of Energy, DOE/EIA-0383, 2011.

[1.7] Energy Information Administration, “Annual Energy Outlook 2011 with Projections to 2035 - Tables A4, A5, and A6 (Revised Early Release)”, U.S. Department of Energy, DOE/EIA-0383, 2011.

[1.8] M. Chupka, R. Earle, P. Fox-Penner, and R. Hledik, “Transforming America’s Power Industry: The Investment Challenge 2010-2030”, The Edison Foundation, Nov. 2008, available at: http://www.edisonfoundation.net/.

[1.9] Energy Information Administration, "Electric Power Monthly, December 2010 – Table 1.1", U.S. Department of Energy, Report Number: DOE/EIA-0226, 2010.

[1.10] Energy Information Administration, "Electric Power Annual 2009 – Table 8.2", U.S. Department of Energy, Report Number: DOE/EIA-0348, revised 2011.

[1.11] E. Shuster, “Tracking New Coal-Fired Power Plants”, National Energy Technology Laboratory – Office of Systems Analyses and Planning, Jan. 2010, presentation available at: www.netl.doe.gov/coal/refshelf/ncp.pdf.

[1.12] Boyce, Meherwan P., “Gas Turbine Engineering Handbook (3rd Edition)”, Elsevier, 2006, pgs. 86-91.

[1.13] Energy Information Administration, "Electric Power Monthly, July 2012 – Table 4.13.A", U.S. Department of Energy, Report Number: DOE/EIA-0226, 2012.

[1.14] National Petroleum Council. “Balancing Natural Gas Policy - Fueling the Demands of a Growing Economy. Volume I: Summary of Findings and Recommendations”, 2003, available at: http://www.npc.org/reports.

[1.15] J.H. Harker and J.R. Backhurst, “Fuel and Energy”, Academic Press, London, 1981. (et al).

[1.16] 109th U.S. Congress, H.R. 6: Energy Policy Act of 2005, Public Law No: 109-58, Aug. 2005, available at: http://www.govtrack.us/congress/billtext.xpd?bill=h109-6.

[1.17] U.S. Nuclear Regulatory Commission, “Status of License Renewal Applications and Industry Activities - Expected New Nuclear Power Plant Applications”, Dec. 2010, available at: http://www.nrc.gov/reactors/new-reactors/new-licensing-files/expected-new-rx-applications.pdf

[1.18] Energy Information Administration, “Annual Energy Outlook 2011 with Projections to 2035 - Table A9 (Revised Early Release)”, U.S. Department of Energy, DOE/EIA-0383, 2011.

[1.19] Compiled from: Energy Information Administration, "Annual Energy Review – Chapter 8 Tables", U.S. Department of Energy, Report Number: DOE/EIA-0384, 2011.

[1.20] Energy Information Administration, "Electric Power Annual 2009 – Table 5.2", U.S. Department of Energy, Report Number: DOE/EIA-0348, revised 2011.

[1.21] Renewable Energy Research Laboratory, “Wind Power: Capacity Factor, Intermittency, and what happens when the wind doesn’t blow?”, University of Massachusetts at Amherst, available at: http://www.ceere.org/rerl/about_wind/RERL_Fact_Sheet_2a_Capacity_Factor.pdf

[1.22] Energy Information Administration, "Electric Power Annual 2011 – Table 2.1.B", U.S. Department of Energy, Report Number: DOE/EIA-0348, revised 2011.

[1.23] Office of Electric Transmission and Distribution, “Grid 2030 – A National Vision for Electricity’s Second 100 Years”, U.S. Department of Energy, 2003.

[1.24] A. Chopra, V. Kundra, and P. Weiser, editors "Policy Framework for the 21st Century Grid: Enabling Our Secure Energy Future", Executive Office of the President of the United States, National Science And Technology Council, June 2011.

[1.25] Energy Information Administration, "Electric Power Annual 2009 – Table 1.1", U.S. Department of Energy, Report Number: DOE/EIA-0348, revised 2011.

[1.26] Energy Information Administration, "Electric Power Annual 2009 – Table 1.6.C", U.S. Department of Energy, Report Number: DOE/EIA-0348, revised 2011.

[1.27] Energy Information Administration, "Electric Power Annual 2009 – Table 4.2", U.S. Department of Energy, Report Number: DOE/EIA-0348, revised 2011.

[1.28] Energy Information Administration - Office of Integrated Analysis and Forecasting, “Assumptions to the Annual Energy Outlook 2012”, U.S. Department of Energy, DOE/EIA-0554, 2012.

[1.29] Boyce, Meherwan P., “Gas Turbine Engineering Handbook (3rd Edition)”, Elsevier, 2006, pp. 86-91.

[1.30] National Petroleum Council. “Balancing Natural Gas Policy - Fueling the Demands of a Growing Economy. Volume I: Summary of Findings and Recommendations”, 2003.

[1.31] Statement of Guy Caruso, Administrator, Energy Information Administration, U.S. Department Of Energy, Before the Committee on Energy And Natural Resources, United States Senate, March 4, 2008.

[1.32] J.H. Harker and J.R. Backhurst, “Fuel and Energy”, Academic Press, London, 1981. (et al)

[1.33] Energy Information Administration, "U.S. Natural Gas Production and Imports", U.S. Department of Energy, DOE/EIA-Short-Term Energy and Winter Fuels Outlook, October 2012.

[1.34] Federal Energy Regulatory Commission, FERC Form 423, "Monthly Report of Cost and Quality of Fuels for Electric Plants - State of Montana”, 1999.

[1.35] Energy Information Administration, "Coal News and Markets Report", U.S. Department of Energy, October 2012.

[1.36] James G. Speight, “Handbook of Coal Analysis”, John Wiley & Sons, 2005.

[1.37] Damian Flynn, “Thermal Power Plant Simulation and Control”, Institution of Engineering and Technology, 2003.

[1.38] U.S. Federal Register, “Control of Emissions of Air Pollution From Nonroad Diesel Engines and Fuel – Final Rule”, Vol. 69, No. 124, June 29, 2004, pgs. 38958-38964.

[1.39] U.S. Department of Energy and the U.S. Environmental Protection Agency, “Carbon Dioxide Emissions from the Generation of Electric Power in the United States”, July 2000.

[1.40] U.S. Environmental Protection Agency, Emission Factor and Inventory Group (D205-01), “2002 Electric Generating Unit National Emissions Inventory”, September 2004.

[1.41] Available at: http://www.eia.doe.gov/cneaf/electricity/epa/epat1p1.html.

[1.42] Puget Sound Energy, “Colstrip Generating Station - Fact Sheet”, No: 4153_064, September, 2010.

[1.43] 2010 EPA Toxic Release Explorer, available at: http://iaspub.epa.gov/triexplorer.

[1.44] Commission for Environmental Cooperation (CEC), “North American Power Plant Air Emissions”, Montréal (Québec), Canada, 2011.

[1.45] M.L. Parry, O.F. Canziani, J.P. Palutikof, P.J. van der Linden and C.E. Hanson, “Summary for Policymakers. In: Climate Change 2007: Impacts, Adaptation and Vulnerability”, Intergovernmental Panel on Climate Change, Cambridge University Press, Cambridge, UK, 7-22.

[1.46] J.H. Harker and J.R. Backhurst, “Fuel and Energy”, Academic Press, London, 1981. (et al).

[1.47] Available at: http://www.naturalgas.org/naturalgas/distribution.asp

[1.48] Anne-Marie Borbely and Jan F. Kreider, “Distributed Generation: The Power Paradigm for the New Millennium”, CRC Press, Boca Raton, 2001.

[1.49] Available at: http://www.eere.energy.gov/de/microturbines.

[1.50] Michael Modell & Robert Reid, “Thermodynamics and Its Applications”, Prentice Hall, Englewood Cliffs, 1983.

[1.51] U.S. Department of Energy's (DoE) Distributed Energy Program, http://www.eere.energy.gov/de/microturbines.

[1.52] U.S. Energy Information Administration, “Electric Power Monthly – Table 1.17.A”, December 2011, available online at: http http://www.eia.gov/electricity/monthly.

[1.53] U.S. Energy Information Administration, “Electric Power Monthly – Table 1.1.A”, December 2011, available online at: http http://www.eia.gov/electricity/monthly.

[1.54] World Wind Energy Association (WWEA), “World Wind Energy Report 2009”, Bonn, Germany, March 2010.

[1.55] World Wind Energy Association (WWEA), "World Wind Energy Report 2011", Bonn, Germany, May 2012.

[1.56] Hansen, M. Aerodynamics of Wind Turbines. Earthscan Press, 2008.

[1.57] Emerging Energy Research (EER), "Wind Turbine Supply Chain Strategies 2009-2020", Cambridge, Massachusetts, July 2009.

[1.58] F. D. Bianchi, H. D. Battista, and R. J. Mantz, Wind Turbine Control Systems – Principles, Modeling and Gain Scheduling Design. Springer-Verlag London Limited, 2007.

[1.59] P. Fairley, "Wind Turbines Shed Their Gears", *Technology Review*, April 27, 2010.

[1.60] National Renewable Energy Laboratory (NREL), "U.S. Annual Average Wind Speed at 30m Map", available at: http://www.nrel.gov/gis/wind.html

[1.61] M. A. Green, K. Emery, Y. Hishikawa, W. Warta, E. D. Dunlop, "Solar cell efficiency tables (version 39)", *Progress in Photovoltaics: Research and Applications,* Vol. 20, No. 1, pgs. 12–20, January 2012.

[1.62] Mints, P. "Photovoltaic Manufacturer Shipments, Capacity & Competitive Analysis 2010/2011", Navigant Consulting Photovoltaic Service Program Report, NPS-Supply6, April 2011.

[1.63] Solarbuzz Consultants, "Solarbuzz Retail Pricing Environment", NPD Group, released: 07 January 2012, available at: http://www.solarbuzz.com/sites/default/files/facts_figs/SB_Retail_Pricing_120308.xlsx.

[1.64] C. Winneker (editor), "Global Market Outlook for Photovoltaics until 2016", European Photovoltaic Industry Associations, Brussels, Belgium, May 2012.

[1.65] R. Walawalkar and J. Apt, "Market Analysis of Emerging Electric Energy Storage Systems - Final Report", DOE/NETL-2008/1330, July 31, 2008.

[1.66] Electricity Storage Association, "System Ratings – Installed systems as of November 2008", available at: http://www.electricitystorage.org/technology.

[1.67] Energy Information Administration - Office of Coal, Nuclear, and Alternative Fuels, "Electric Trade in the United States - 1996", U.S. Department of Energy, DOE/EIA-0531/UC-950, 1998.

[1.68] Energy Information Administration, "2006 Generation Capacity Ownership", Form EIA-860 Database, 2006.

[1.69] Energy Information Administration, “2006 Electric Sales, Revenue, and Average Price Report - Table 10: Class of Ownership, Number of Consumers, Revenue, Sales, and Average Retail Price by State and Utility: All Sectors”, U.S. Department of Energy, 2006.

[1.70] Energy Information Administration, “2011 Generation Capacity Ownership”, Form EIA-860 Database, 2011.

[1.71] “Energy Independence and Security Act of 2007”, H. R. 6, One Hundred Tenth Congress of the United States of America, Dec. 2007.

[1.72] United States Combined Heat and Power Association, “USCHPA Policy Alert: New FERC Policies in Response to EPAct Amendments of PURPA”, Feb 10, 2006. (http://uschpa.admgt.com/press.htm).

[1.73] United States of America, Federal Energy Regulatory Commission, “Revised Regulations Governing Small Power Production and Cogeneration Facilities”, Feb 2, 2006. (http://ferc.gov/whats-new/comm-meet/020206/E-2.pdf)

[1.74] Database of State Incentives for Renewables and Efficiency, Quantitative RPS Data Project Spreadsheet, North Carolina State University, May 2011, available at: http://www.dsireusa.org/.

[1.75] J. Miller, S. Pullins, & S. Bossart, "The Modern Grid", Wisconsin Public Utility Institute & UW Energy Institute presentation to National Energy Technology Laboratory, 29 April 2008.

[1.76] Energy Information Administration, "Wholesale Market Data from Intercontinental Exchange (ICE)", U.S. Department of Energy, 2011, available at: http://www.eia.gov/cneaf/electricity/wholesale/.

[1.77] S. M. Amin, "U.S. Grid Gets Less Reliable", IEEE Spectrum, January 2011, pg. 80.

[1.78] Nikos Hatziargyriou, Hiroshi Asano, Reza Iravani, and Chris Marnay, “Microgrids,” IEEE Power & Energy Magazine, Vol. 5, Issue 4, July/August 2007.

[1.79] K. Forsten & R. Lordan, "Transmission Efficiency Initiative", Technical Report 1017894, Electric Power Research Institute, Oct 2009.

[1.80] U.S. Energy Information Administration, “Gasoline and Diesel Fuel Update”, July 2012, available online at: http http://www.eia.gov/petroleum/gasdiesel.

[1.81] “IEEE Guide for Design, Operation, and Integration of Distributed Resource Island Systems with Electric Power Systems”, IEEE Std 1547.4-2011, 2011.

[1.82] Collected via manufacturer's internet websites, February 2012.

[1.83] National Energy Technology Laboratory (NETL), "Smart Grid Principal Characteristics Provides Power Quality for the Digital Economy", DOE/NETL-2010/1412, 2010.

[1.84] United States Department of Energy, "2010 Smart Grid System Report - Report to Congress", February 2012, pg. 45.

[2.1] R. Ramakumar, J. J. Bzura, J. Eyer, J. Gutierrez-Vera, T. E. Hoff, C. Herig, J. Iannucci, and M.R. Milligan, "Renewable technologies and distribution systems", *IEEE Power Engineering Review*, Vol. 19, No. 11, 1999, pg. 5.

[2.2] S.N. Singh, "Emerging issues and new challenges in electric power systems", *International Energy Journal*, Vol. 2, No. 2, 2001, pgs. 53-66.

[2.3] X. Li, "Diversification and localization of energy systems for sustainable development and energy security", *Energy Policy*, Vol. 33, No. 17, 2005, pgs. 2237-2243.

[2.4] R. Lawrence, and S. Middlekauff, "The new guy on the block: Applying distributed generation tools in power design systems", *IEEE Industry Applications Magazine*, Vol. 11, No. 1, 2005, pgs. 54-59.

[2.5] L.S. Schell and S. Neff, "Solar Peaking: Distributed photovoltaic generation can ease utility demand", *Energy*, Vol. 30, No. 2, 2005, pgs. 40-42.

[2.6] Editorial, "Distributed generation: Embrace the change", *IEE Power Engineer*, Vol. 18, No. 2, 2004, pgs. 12-13.

[2.7] J. Guerrero, F. Blaabjerg, T. Zhelev, K. Hemmes, E. Monmasson, S. Jemeï, M. P. Comech, R. Granadino, and J. I. Frau, "Distributed generation: Toward a new energy paradigm", *IEEE Industrial Electronics Magazine*, Vol. 4, No. 1, 2010, pgs. 52-64.

[2.8] Y. Fujioka, H. Maejima, S. Nakamura, Y. Kojima, M. Okudera, and S. Uesaka, "Regional power grid with renewable energy resources: A demonstrative project in Hachinohe," *CIGRE 2006*, Paris, August 2006.

[2.9] G. Celli, F. Pilo, G. Pisano, V. Allegranza, R. Cicoria, and A. Iaria, "Meshed vs. Radial MV Distribution Network in Presence of Large Amount of DG", *Proceedings of the IEEE 2004 Power and Energy Society Power Systems Conference*, Vol. 2, Oct. 2004.

[2.10] W. Clark and W. Isherwood, "Distributed generation: Remote power systems with advanced storage technologies", *Energy Policy*, Vol. 32, No. 14, 2004, pgs. 1573-1589.

[2.11] F. Bouffard and D. Kirschen, "Centralised and distributed electricity systems", *Energy Policy*, Vol. 36, No. 12, 2008, pgs. 4504-4508.

[2.12] B. K. Sovacool, "Distributed generation (DG) and the American electric utility system: What is stopping it?", *ASME Transactions on Energy Resources Technology,* Vol. 130, No. 1, 2008, pgs. 120011-120018.

[2.13] T.J. Hammons, "Integrating renewable energy sources into European grids", *International Journal of Electrical Power and Energy Systems*, Vol. 30, No. 8, 2008, pgs. 462-475.

[2.14] A. Bayod-Rújula, "Future development of the electricity systems with distributed generation", *Energy*, Vol. 34, No. 3, 2009, pgs. 377-383.

[2.15] K. J. Holmes and L. Papay, "Prospects for electricity from renewable resources in the United States", *Journal of Renewable and Sustainable Energy*, Vol. 3, No. 4, 2011, pgs. 042701/1-042701/14.

[2.16] S. F. Rivera, "Distributed generation challenges: Air quality, siting, permitting", *Strategic Planning for Energy and the Environment*, Vol. 20, No. 3, 2000 pgs. 63-66 and 69-80.

[2.17] D. Trebolle, T. Gómez, R. Cossent, P. Frías, "Distribution planning with reliability options for distributed generation", *Electric Power Systems Research*, Vol. 80, No. 2, 2010, pgs. 222-229.

[2.18] F. Blaabjerg, R. Teodorescu, M. Liserre, & A. V. Timbus, "Overview of control and grid synchronization for distributed power generation systems", *IEEE Transactions on Industrial Electronics*, Vol. 53, No. 5, Oct 2006.

[2.19] M. Thomson, & D.G. Infield, "Impact of widespread photovoltaics generation on distribution systems", *IET Renewable Power Generation*, Vol. 1, No. 1, 2007.

[2.20] M. K. Donnelly, J. E. Dagle, D. J. Trudnowski, and G. J. Rogers, "Impacts of the distributed utility on transmission system stability", *IEEE Transactions on Power Systems*, Vol. 11, No. 2, May 1996.

[2.21] F. D. Kanellos & N. D. Hatziargyriou, "The Effect of Variable-Speed Wind Turbines on the Operation of Weak Distribution Networks *", IEEE Transactions on Energy Conversion*, Vol. 17, No. 4, Dec. 2002.

[2.22] H. Lund, "Electric grid stability and the design of sustainable energy systems", *International Journal of Sustainable Energy*, Vol. 24, No. 1, 2005, pgs. 45-54.

[2.23] J. Liu, Jianwei, M.M.A Salama, and R. R. Mansour, “Identify the impact of distributed resources on congestion management”, *IEEE Transactions on Power Delivery*, Vol. 20, No. 3, 2005, pgs. 1998-2005.

[2.24] V.V. Thong, J. Driesen, and R. Belmans, Ronnie “Interconnection of distributed generators and their influences on power system”, *International Energy Journal*, Vol. 6, No. 1, 2005, pgs. 3127-3140.

[2.25] C. Chompoo-Inwai, W.J. Lee, P. Fuangfoo, M. Williams, and J.R. Liao, “System impact study for the interconnection of wind generation and utility system”, *IEEE Transactions on Industry Applications*, Vol. 41, No. 1, 2005 pgs. 163-168.

[2.26] R. A. Walling, R. Saint, R.C. Dugan, J. Burke, and L. A. Kojovic, “Summary of distributed resources impact on power delivery systems”, *IEEE Transactions on Power Delivery*, Vol. 23, No. 3, 2008, pgs. 1636-1644.

[2.27] G. C. Bakos, “Distributed power generation: A case study of small scale PV power plant in Greece”, *Applied Energy*, Vol. 86, No. 9, 2009, pgs. 1757-1766.

[2.28] A. Y. Saber and G. K. Venayagamoorthy, “Efficient utilization of renewable energy sources by gridable vehicles in cyber-physical energy systems”, *IEEE Systems Journal*, Vol. 4, No. 3, 2010, pgs. 285-294.

[2.29] T. J. Hammons, “Dispersed generation in modern power systems and its impact in Europe on power system structure and secure operation”, *International Journal of Power and Energy Systems*, Vol. 30, No. 1, 2010, pgs. 36-46.

[2.30] T. Moore, “Emerging markets for distributed resources”, *EPRI Journal*, Vol. 23, No. 2, 1998, pgs. 8-17.

[2.31] N. I. Meyer, “Distributed generation and the problematic deregulation of energy markets in Europe”, *International Journal of Sustainable Energy*, Vol. 23, No. 4, 2003 pgs. 217-221.

[2.32] H.A. Gil & G. Joos, “Models for quantifying the economic benefits of distributed generation”, *IEEE Transactions on Power Systems*, Vol. 23, No. 2, May 2008.

[2.33] R. Priddy, “Distributed generation and energy management: Reducing energy costs”, *Cogeneration and Distributed Generation Journal*, Vol. 20, No. 3, 2005, pgs. 60-71.

[2.34] D. Mears, J. Iannucci, J. Eyer, and S. Eckroad, “Distributed electricity storage: Foundation for the business case”, *IEEE Power and Energy Magazine*, Vol. 3, No. 3, 2005, pgs. 20-24.

[2.35] J. Skea, D. Anderson, T. Green, R. Gross, P. Heptonstall, and M. Leach, "Intermittent renewable generation and the cost of maintaining power system reliability", *IET Generation, Transmission and Distribution*, Vol. 2, No. 1, 2008, pgs. 82-89.

[2.36] S. Wong, K. Bhattacharya, and J. D. Fuller, "Long-term effects of feed-in tariffs and carbon taxes on distribution systems", *IEEE Transactions on Power Systems*, Vol. 25, No. 3, 2010, pgs. 1241-1253.

[2.37] D. A. Ball, W. T. Hanna, and J. A. Stets, "Distributed generation for residential and small commercial markets", *Proceedings of the American Power Conference*, Vol. 61, 1999.

[2.38] O. Bailey, C. Creighton, R. Firestone, C. Marnay, and M. Stadler, "Distributed energy resources in practice: a case study analysis and validation of LBNL's customer adoption model", Lawrence Berkeley National Laboratory (LBNL), Feb. 2003.

[2.39] A. J. Conejo, J. M. Morales, and J. A. Martinez,"Tools for the analysis and design of distributed resources-Part III: Market studies", *IEEE Transactions on Power Delivery*, Vol. 26, No. 3, 2011, pgs.1663-1670.

[2.40] M. Manfren, P. Caputo, G. Costa, "Paradigm shift in urban energy systems through distributed generation: Methods and models", *Applied Energy*, Vol. 88, No. 4, 2011, pgs. 1032-1048.

[2.41] A. G. Tsikalakis and N. D. Hatziargyriou, "Environmental benefits of distributed generation with and without emissions trading", *Energy Policy*, Vol. 35, No. 6, 2007, pgs. 3395-3409.

[2.42] M . Dicorato, G. Forte, and M. Trovato, "Environmental-constrained energy planning using energy-efficiency and distributed-generation facilities", *Renewable Energy*, Vol. 33, No. 6, 2008, pgs. 1297-1313.

[2.43] S. Karki, M.D. Mann, and H. Salehfar, "Environmental implications of renewable distributed generation technologies in rural electrification", *Energy Sources, Part B: Economics, Planning and Policy*, Vol. 3, No. 2, 2008, pgs. 186-195.

[2.44] M. F. Akorede, H. Hizam, and E. Pouresmaeil, "Distributed energy resources and benefits to the environment", *Renewable and Sustainable Energy Reviews*, Vol. 14, No. 2, 2010, pgs. 724-734.

[2.45] R.T. Guttromson, "Modeling distributed energy resource dynamics on the transmission system", *IEEE Transactions on Power Systems*, Vol. 17, No. 4, 2002, pgs. 1148-1153.

[2.46] K. Sedghisigarchi & A. Feliachi, "Dynamic and Transient Analysis of Power Distribution Systems with Fuel Cells - Part II: Control and Stability Enhancement", *IEEE Transactions on Energy Conversion*, Vol. 19, No. 2, June 2004.

[2.47] Z. Chen, Y. Hu, and F. Blaabjerg, "Control of Distributed Power Systems" *Proceedings from the CES/IEEE 5th International Power Electronics and Motion Control Conference, IPEMC '06*, Vol. 3, Aug. 2006.

[2.48] J. M. Guerrero, L. Hang, and J. Uceda, "Control of distributed uninterruptible power supply systems", *IEEE Transactions on Industrial Electronics*, Vol. 55, No. 8, 2008,
pgs. 2845-2859.

[2.49] M. Kim, R. Hara, and H. Kita, "Design of the optimal ULTC parameters in distribution system with distributed generations", *IEEE Transactions on Power Systems*, Vol. 24, No. 1, 2009, pgs. 297-305.

[2.50] K. J. P. Macken, K. Vanthournout, J. Van den Keybus, G. Deconinck, and R. J. M. Belmans, "Distributed control of renewable generation units with integrated active filter", *IEEE Transactions on Power Electronics*, Vol. 19, No. 5, 2004, pgs. 1353-1360.

[2.51] W. Wongsaichua, W.J. Lee, S. Oraintara, C. Kwan, and F. Zhang, "Integrated high-speed intelligent utility tie unit for disbursed/renewable generation facilities", *IEEE Transactions on Industry Applications*, Vol. 41, No. 2, 2005, pgs. 507-513.

[2.52] M. A. Kashem, and G. Ledwich, "Energy requirement for distributed energy resources with battery energy storage for voltage support in three-phase distribution lines", *Electric Power Systems Research*, Vol. 77, No. 1, 2007, pgs. 10-23.

[2.53] J. A. P. Lopes, N. Hatziargyriou, J. Mutale, P. Djapic, and N. Jenkins, "Integrating distributed generation into electric power systems: A review of drivers, challenges and opportunities", *Electric Power Systems Research*, Vol. 77, No. 9, 2007, pgs. 1189-1203.

[2.54] J. Arai, K. Iba, T. Funabashi, Y. Nakanishi, K. Koyanagi, and R. Yokoyama, "Power electronics and its applications to renewable energy in Japan", *IEEE Circuits and Systems Magazine*, Vol. 8, No. 3, 2008, pgs. 52-66.

[2.55] C. L. Trujillo, D. Velasco, E. Figueres, and G. Garcerá,Analysis of active islanding detection methods for grid-connected microinverters for renewable energy processing", *Applied Energy*, Vol. 87, No. 11, 2010, pgs. 3591-3605.

[2.56] M. Liserre, T. Sauter, and J. Y. Hung, "Future energy systems: Integrating renewable energy sources into the smart power grid through industrial electronics", *IEEE Industrial Electronics Magazine*, Vol. 4, No. 1, 2010, pgs. 18-37.

[2.57] Y. Liao, and C. Lai, “Newly-constructed simplified single-phase multistring multilevel inverter topology for distributed energy resources”, *IEEE Transactions on Power Electronics*, Vol. 26, No. 9, 2011, pgs. 2386-2392.

[2.58] Y. Zhu and K. Tomsovic, “Optimal distribution power flow for systems with distributed energy resources”, *International Journal of Electrical Power and Energy Systems*, Vol. 29, No. 3, 2007, pgs. 260-267.

[2.59] D. Yazdani, M. Mojiri, A. Bakhshai, G. Joós, “A fast and accurate synchronization technique for extraction of symmetrical components”, *IEEE Transactions on Power Electronics*, Vol. 24, No. 3, 2009, pgs. 674-684.

[2.60] J. S. Savier, and D. Das, “Energy loss allocation in radial distribution systems: A comparison of practical algorithms”, *IEEE Transactions on Power Delivery*, Vol. 24, No. 1, 2009, pgs. 260-267.

[2.61] A. Moreno-Munoz, J. J. G. De-La-Rosa, M .A. Lopez-Rodriguez, J. M. Flores-Arias, F. J. Bellido-Outerino, M. Ruiz-De-Adana, “Improvement of power quality using distributed generation”, *International Journal of Electrical Power and Energy Systems*, Vol. 32, No. 10, 2010, pgs. 1069-1076.

[2.62] R. Noroozian, M. Abedi, G. B. Gharehpetian, S. H. Hosseini, “Distributed resources and DC distribution system combination for high power quality”, *International Journal of Electrical Power and Energy Systems*, Vol. 32, No. 7, 2010, pgs. 769-781.

[2.63] C. J. Dent, L. F. Ochoa, G. P. Harrison, “Network distributed generation capacity analysis using OPF with voltage step constraints”, *IEEE Transactions on Power Systems*, Vol. 25, No. 1, 2010, pgs. 296-304.

[2.64] C. Lee, C. Hsu, and P. Cheng, “A low-voltage ride-through technique for grid-connected converters of distributed energy resources”, *IEEE Transactions on Industry Applications*, Vol. 47, No. 4, 2011, pgs. 1821-1832.

[2.65] G. Celli, E. Ghiani, S. Mocci, and F. Pilo, “A multiobjective evolutionary algorithm for the sizing and siting of distributed generation”, *IEEE Transactions on Power Systems*, Vol. 20, No. 2, 2005, pgs. 750-757.

[2.66] A. K. Akella, M. P. Sharma, and R. P. Saini, “Optimum utilization of renewable energy sources in a remote area”, *Renewable and Sustainable Energy Reviews*, Vol. 11, No. 5, 2007, pgs. 894-908.

[2.67] A. Alarcon-Rodriguez, E. Haesen, G. Ault, J. Driesen, R. Belmans, “Multi-objective planning framework for stochastic and controllable distributed energy resources”, *IET Renewable Power Generation*, Vol. 3, No. 2, 2009, pgs. 227-238.

[2.68] Y. P. Cai, G. H. Huang, Z.F. Yang, Q.G. Lin, Q. Tan, "Community-scale renewable energy systems planning under uncertainty-An interval chance-constrained programming approach", *Renewable and Sustainable Energy Reviews*, Vol. 13, No. 4, 2009, pgs. 721-735.

[2.69] A. Alarcon-Rodriguez, G. Ault, and S. Galloway, "Multi-objective planning of distributed energy resources: A review of the state-of-the-art", *Renewable and Sustainable Energy Reviews*, Vol. 14, No. 5, 2010, pgs. 1353-1366.

[2.70] H. Ren, and W. Gao, "A MILP model for integrated plan and evaluation of distributed energy systems", *Applied Energy*, Vol. 87, No. 3, 2010, pgs 1001-1014.

[2.71] Y. M. Atwa, E. F. El-Saadany, M. M. A. Salama, and R. Seethapathy, "Optimal renewable resources mix for distribution system energy loss minimization", *IEEE Transactions on Power Systems*, Vol. 25, No. 1, 2010, pgs. 360-370.

[2.72] W. Ouyang, H. Cheng, X. Zhang, L. Yao, and M. Bazargan, "Distribution network planning considering distributed generation by genetic algorithm combined with graph theory", *Electric Power Components and Systems*, Vol. 38, No. 3, 2010, pgs. 325-339.

[2.73] T. Niknam, S. I. Taheri, J. Aghaei, T. Jamshid; S. Tabatabaei, M. Nayeripour, "A modified honey bee mating optimization algorithm for multiobjective placement of renewable energy resources", *Applied Energy*, Vol. 88, No. 12, 2011, pgs. 4817-4830.

[2.74] H. Oh, "Optimal planning to include storage devices in power systems", *IEEE Transactions on Power Systems*, Vol. 26, No. 3, 2011, pgs. 1118-1128.

[2.75] S. M. Moghaddas-Tafreshi, H. A. Zamani, S. M. Hakimi, "Optimal sizing of distributed resources in micro grid with loss of power supply probability technology by using breeding particle swarm optimization", *Journal of Renewable and Sustainable Energy*, Vol. 3, No. 4, 2011, pgs. 043105/1-043105/17.

[2.76] D. Alfonso, A. Pérez-Navarro, N. Encinas, C. Álvarez, J. Rodríguez, and M. Alcázar, "Methodology for ranking customer segments by their suitability for distributed energy resources applications", *Energy Conversion and Management*, Vol. 48, No. 5, 2007, pgs. 1615-1623.

[2.77] S. Iniyan, K. Sumathy, L. Suganthi, and A. A. Samuel, "Sensitivity analysis of optimal renewable energy mathematical model on demand variations", *Energy Conversion and Management*, Vol. 41, No. 2, 2000, pgs.199-211.

[2.78] H. Ren, W. Gao, W. Zhou, K. Nakagami, "Multi-criteria evaluation for the optimal adoption of distributed residential energy systems in Japan", *Energy Policy*, Vol. 37, No. 12, 2009, pgs. 5484-5493.

[2.79] M. D. Ilic, J. Joo, L. Xie, M. Prica, N. Rotering, "A decision-making framework and simulator for sustainable electric energy systems", *IEEE Transactions on Sustainable Energy*, Vol. 2, No. 1, 2011, pgs. 37-49.

[2.80] S. Sakai, Y. Hayashi, S. Kawasaki, J. Matsuki, Y. Fuwa, and K. Mori, "Experimental multi-objective evaluation of radial and loop distribution network configuration using distribution network equipment", *IEEJ Transactions on Electrical and Electronic Engineering*, Vol. 3, No. 5, 2008, pgs. 530-539.

[2.81] H. Ko, K.Y. Lee, M. Kang, and H. Kim, "Power quality control of an autonomous wind-diesel power system based on hybrid intelligent controller", *Neural Networks*, Vol. 21, No. 10, 2008, pgs. 1439-1446.

[2.82] I. Wasiak, M. C. Thoma, C. E. T. Foote, R. Mienski, R. Pawelek, P. Gburczyk, and G. M. Burt, "A power-quality management algorithm for low-voltage grids with distributed resources", *IEEE Transactions on Power Delivery*, Vol. 23, No. 2, 2008, pgs. 1055-1062.

[2.83] A. Borghetti, M. Bosetti, S. Grillo, S. Massucco, C. A. Nucci, M. Paolone, and F. Silvestro, "Short-term scheduling and control of active distribution systems with high penetration of renewable resources", *IEEE Systems Journal*, Vol. 4, No. 3, 2010 pgs. 313-322.

[2.84] H. Li, F. Li, X. Fangxing; Y. Xu, D. T. Rizy, and J. D. Kueck, "Adaptive voltage control with distributed energy resources: Algorithm, theoretical analysis, simulation, and field test verification", *IEEE Transactions on Power Systems*, Vol. 25, No. 3, 2010, pgs. 1638-1647.

[2.85] N. El Halabi, M. García-Gracia, J. Borroy, and J. L. Villa, "Current phase comparison pilot scheme for distributed generation networks protection", *Applied Energy*, Vol. 88, No. 12, 2011, pgs. 4563-4569.

[2.86] M. A. Pedrasa, T. D. Spooner, and I. F. MacGill, "A novel energy service model and optimal scheduling algorithm for residential distributed energy resources", *Electric Power Systems Research*, Vol. 81, No. 12, 2011, pgs. 2155-2163.

[2.87] W. W. Weaver, "Dynamic energy resource control of power electronics in local area power networks", *IEEE Transactions on Power Electronics*, Vol. 26, No. 3, 2011, pgs. 852-859.

[2.88] A. Keane and M. O'Malley, "Optimal allocation of embedded generation on distribution networks", *IEEE Transactions on Power Systems*, Vol. 20, No. 3, 2005, pgs. 1640-1646.

[2.89] A. Poullikkas "Implementation of distributed generation technologies in isolated power systems", *Renewable and Sustainable Energy Reviews*, Vol. 11, No. 1, 2007, pgs. 30-56.

[2.90] D. Pudjianto, C. Ramsay, and G. Strbac, "Virtual power plant and system integration of distributed energy resources", *IET Renewable Power Generation*, Vol. 1, No. 1, 2007, pgs. 10-16.

[2.91] L. F. Ochoa, A. Padilha-Feltrin, and G. P. Harrison, "Time-series-based maximization of distributed wind power generation integration", *IEEE Transactions on Energy Conversion*, Vol. 23, No. 3, 2008, pgs. 968-974.

[2.92] Y. Chen, C. Shen, and J. Wang, "Distributed transient stability simulation of power systems based on a Jacobian-free Newton-GMRES method", *IEEE Transactions on Power Systems*, Vol. 24, No. 1, 2009, pgs. 146-156.

[2.93] M. A. A. Pedrasa, T. D. Spooner, I. F. MacGill, "Coordinated scheduling of residential distributed energy resources to optimize smart home energy services", *IEEE Transactions on Smart Grid*, Vol. 1, No. 2, 2010, pgs. 134-143.

[2.94] M. Reza, G. Papaefthymiou, P. Schavemaker, W. Kling, and L. Van Der Sluis, "Distributed generation impact on power system transient stability: A stochastic approach", *International Energy Journal*, Vol. 11, No. 2, 2010, pgs. 93-100.

[2.95] B. Klöckl and G. Papaefthymiou, "Multivariate time series models for studies on stochastic generators in power systems", *Electric Power Systems Research*, Vol. 80, No. 3, 2010, pgs. 265-276.

[2.96] A. Schroeder, "Modeling storage and demand management in power distribution grids", *Applied Energy*, Vol. 88, No. 12, 2011, pgs. 4700-4712.

[2.97] C. Cecati, C. Citro, and P. Siano, "Combined operations of renewable energy systems and responsive demand in a smart grid", *IEEE Transactions on Sustainable Energy*, Vol. 2, No. 4, 2011, pgs. 468-476.

[2.98] A. Keane, L. F. Ochoa, E. Vittal, C. J. Dent, and G. P. Harrison, "Enhanced utilization of voltage control resources with distributed generation", *IEEE Transactions on Power Systems*, Vol. 26, No. 1, 2011, pgs. 252-260.

[2.99] C. Marnay, F. Javier Rubio, and A. S. Siddiqui, "Shape of the microgrid", *Proceedings of the IEEE Power Engineering Society Transmission and Distribution Conference*, Vol. 1, 2001, pgs. 150-153.

[2.100] R. H. Lasseter, "MicroGrids", *Proceedings of the IEEE Power Engineering Society Transmission and Distribution Conference*, Vol. 1, 2002, pgs. 305-308.

[2.101] J. M. Carrasco, L.G. Franquelo, J.T. Bialasiewicz, E. Galvan, R.C.P. Guisado, M. Prats, J.I. Leon, and N. Moreno-Alfonso, "Power-electronic systems for the grid integration of renewable energy sources: a survey", *IEEE Transactions on Industrial Electronics*, Vol. 53, No. 4, 2006, pgs. 1002-1016.

[2.102] D. Salomonsson, L. Soder, and A. Sannino, "An adaptive control system for a DC microgrid for data centers", *IEEE Transactions on Industry Applications*, Vol. 44, No. 6, 2008, pgs. 1910-1917.

[2.103] K. Kurohane, A. Uehara, T. Senjyu, A. Yona, N. Urasaki, T. Funabashi, and C. Kim, "Control strategy for a distributed DC power system with renewable energy", *Renewable Energy*, Vol. 36, No. 1, 2011, pgs. 42-49.

[2.104] L. Xu and D. Chen, "Control and operation of a DC microgrid with variable generation and energy storage", *IEEE Transactions on Power Delivery,* Vol. 26, No. 4, 2011, pgs. 2513-22.

[2.105] S.K Sul, I. Alan and T.A. Lipo, "Performance testing of a high frequency link converter for space station power distribution system," *Proceedings of the 24th Intersociety: Energy Conversion Engineering Conference*, Vol. 1, No. 6-11, 1989, pgs. 617 – 623.

[2.106] I .S. Roth, M. Gaudreau, M. A. Kempkes, T. J. Hawkey, and M. J. Mulvaney, "Solid-state high frequency power converters", *Proceedings of the IASTED Multi-Conference- Power and Energy Systems*, Vol. 7, 2003, pgs. 322-326.

[2.107] Z. Ye, Zhihong, T. Wang, G. Sinha, and R. Zhang, "Efficiency comparison for microturbine power conditioning systems", *PESC Record - IEEE Annual Power Electronics Specialists Conference*, Vol. 4, 2003, pgs. 1551-1556.

[2.108] C. Lai, C. Pan, and M. Cheng, "High-efficiency modular high step-up interleaved boost converter for dc-microgrid applications", *IEEE Transactions on Industry Applications*, Vol. 48, No. 1, 2012, pgs. 161-171.

[2.109] D. Jacob, K. Nithiyananthan, "Smart and micro grid model for renewable energy based power system", *International Journal for Engineering Modelling*, Vol. 22, No. 1-4, 2009, pgs. 89-94.

[2.110] X. Zhang, G.G. Karady, and Y. Guan, "Design methods investigation for residential microgrid infrastructure", *European Transactions on Electrical Power*, Vol. 21, No. 8, 2011, pgs 2125-2141.

[2.111] J. Jimeno, J. Anduaga, J. Oyarzabal, and A.G. De Muro, "Architecture of a microgrid energy management system", *European Transactions on Electrical Power*, Vol. 21, No. 2, 2011, pgs. 1142-1158.

[2.112] A. Vaccaro, M. Popov, D. Villacci, and V. Terzija, "An integrated framework for smart microgridsmodeling, monitoring, control, communication, and verification", *Proceedings of the IEEE*, Vol. 99, No. 1, 2011, pgs. 119-132.

[2.113] D. Pudjianto, C. Ramsay, and G. Strbac, "Microgrids and virtual power plants: Concepts to support the integration of distributed energy resources", *Proceedings of the Institution of Mechanical Engineers, Part A: Journal of Power and Energy*, Vol. 222, No. 7, 2008, pgs. 731-741.

[2.114] H. Jiayi, J. Chuanwen, and X. Rong, "A review on distributed energy resources and MicroGrid", *Renewable and Sustainable Energy Reviews*, Vol. 12, No. 9, 2008, pgs. 2465-2476.

[2.115] N.S. Wade, P. C. Taylor, P. D. Lang, and P. R. Jones, "Evaluating the benefits of an electrical energy storage system in a future smart grid", *Energy Policy*, Vol. 38, No. 11, 2010, pgs. 7180-7188.

[2.116] E. Mashhour, and S.M. Moghaddas-Tafreshi, "Integration of distributed energy resources into low voltage grid: A market-based multiperiod optimization model", *Electric Power Systems Research*, Vol. 80, No. 4, 2010, pgs. 473-480.

[2.117] M.K. Deshmukh, and S. S. Deshmukh, "Modeling of hybrid renewable energy systems", *Renewable and Sustainable Energy Reviews*, Vol. 12, No. 1, 2008, pgs. 235-249.

[2.118] A. A. Hussein, S. Harb, N. Kutkut, J. Shen, I. Batarseh, "Design considerations for distributed micro-storage systems in residential applications", *Proceedings of the International Telecommunications Energy Conference*, 2010.

[2.119] W. Prommee and W. Ongsakul, "Optimal multiple distributed generation placement in microgrid system by improved reinitialized social structures particle swarm optimization", *European Transactions on Electrical Power*, Vol. 21, No. 1, 2011, pgs. 489-504.

[2.120] A. S. Siddiqui, C. Marnay, J. L. Edwards, R. Firestone, S. Ghosh, and M. Stadler, "Effects of carbon tax on microgrid combined heat and power adoption", *Journal of Energy Engineering*, Vol. 131, No. 1, 2005, pgs. 2-25.

[2.121] N. J. Kelly, J. A. Clarke, A. Ferguson, and G. Burt, "Developing and testing a generic micro-combined heat and power model for simulations of dwellings and highly distributed power systems", *Proceedings of the Institution of Mechanical Engineers, Part A: Journal of Power and Energy*, Vol. 222, No. 7, 2008, pgs. 685-695.

[2.122] Y. Yamagishi, H. Sugihara, O. Saeki, and K. Tsuji, "An operational algorithm for residential cogeneration systems based on the monitored daily-basis energy demand", *Electrical Engineering in Japan*, (English translation by Denki Gakkai Ronbunshi), Vol. 170, No. 2, 2010, pgs. 37-45.

[2.123] A. K. Basu, S. Chowdhury, and S. P. Chowdhury, “Impact of strategic deployment of CHP-based DERs on microgrid reliability”, *IEEE Transactions on Power Delivery*, Vol. 25, No. 3, 2010, pgs. 1697-1705.

[2.124] M. Jovanovic, V. Turanjanin, V. Bakic, M. Pezo, B. Vucicevic, “Sustainability estimation of energy system options that use gas and renewable resources for domestic hot water production”, *Energy*, Vol. 36, No. 4, 2011, pgs. 2169-2175.

[2.125] Y. Ono, N. Uchiyama, T. Nakamura, and Y. Fujita, “Short-term balanced supply and demand control system for microgrids”, *Hitachi Review*, Vol. 54, No. 3, 2005, pgs. 141-144.

[2.126] A. G. Tsikalakis, and N. D. Hatziargyriou, “Centralized control for optimizing microgrids operation”, *IEEE Transactions on Energy Conversion*, Vol. 23, No. 1, 2008, pgs. 241-248.

[2.127] Y. W. Li, and C. Kao, “An accurate power control strategy for power-electronics-interfaced distributed generation units operating in a low-voltage multibus microgrid”, *IEEE Transactions on Power Electronics*, Vol. 24, No. 12, 2009, pgs. 2977-2988.

[2.128] E. Serban and H. Serban, “A control strategy for a distributed power generation microgrid application with voltage- and current-controlled source converter”, *IEEE Transactions on Power Electronics*, Vol. 25, No. 12, 2010, pgs. 2981-2992.

[2.129] K. Jong-Yul, J. Jin-Hong, K. Seul-Ki, C. Changhee, H.P. June, K. Hak-Manand N. Kee-Young, “Cooperative Control Strategy of Energy Storage System and Microsources for Stabilizing the Microgrid during Islanded Operation”, *IEEE Transactions on Power Electronics*, Vol. 25, No. 12, 2010, pgs. 3037-3048.

[2.130] T. L. Vandoorn, B. Meersman, L. Degroote, B. Renders, and L. Vandevelde, “A control strategy for islanded microgrids with DC-link voltage control”, *IEEE Transactions on Power Delivery*, Vol. 26, No. 2, 2011, pgs. 703-713.

[2.131] M. A. Sofla, and G. B. Gharehpetian, “Dynamic performance enhancement of microgrids by advanced sliding mode controller”, *International Journal of Electrical Power and Energy Systems*, Vol. 33, No. 1, 2011, pgs.1-7.

[2.132] C. Cho, J. Jeon, J. Kim, S. Kwon, K. Park, and S. Kim, “Active synchronizing control of a microgrid”, *IEEE Transactions on Power Electronics*, Vol. 26, No. 12, 2011, pgs. 3707-3719.

[2.133] H. Karimi, E. J. Davison, and R. Iravani, “Multivariable servomechanism controller for autonomous operation of a distributed generation unit: Design and performance evaluation", *IEEE Transactions on Power Systems*, Vol. 25, No. 2, 2010, pgs. 853-865.

[2.134] E. Sortomme, S.S. Venkata, and J. Mitra, "Microgrid protection using communication-assisted digital relays", *IEEE Transactions on Power Delivery*, Vol. 25, No. 4, 2010, pgs. 2789-2796.

[2.135] S. Khomfoi, W. Sae-Kok, I. Ngamroo, "An open circuit fault diagnostic technique in IGBTS for ac to dc converters applied in microgrid applications", *Journal of Power Electronics*, Vol. 11, No. 6, 2011, pgs. 801-810.

[2.136] C. Álvarez Bel, M. A. Ortega, G.E. Escrivá, and A. G. Marín, "Technical and economical tools to assess customer demand response in the commercial sector", *Energy Conversion and Management*, Vol. 50, No. 10, 2009, pgs. 2605-2612.

[2.137] S. A. Pourmousavi and M. H. Nehrir, "Demand response for smart microgrid: Initial results", *IEEE PES Innovative Smart Grid Technologies Conference Europe*, 2011.

[2.138] M. A. Abido, "Environmental/economic power dispatch using multiobjective evolutionary algorithms," *IEEE Transactions on Power Systems*, Vol. 18, No. 4, 2003, pgs. 1529–1537.

[2.139] A. Ahuja, S. Das, and A. Pahwa, "An AIS-ACO Hybrid Approach for Multi-Objective Distribution System Reconfiguration", *IEEE Transactions on Power Systems*, Vol. 22, No. 3, 2007, pgs. 1101-1111.

[2.140] X. Li, Y. Song, and S. Han, "Frequency control in micro-grid power system combined with electrolyzer system and fuzzy PI controller", *Journal of Power Sources*, Vol. 180, No. 1, 2008, pgs. 468-475.

[2.141] B. Ramachandran, S. K. Srivastava, D. A. Cartes, and C. S. Edrington, "Distributed energy resource management in a smart grid by risk based auction strategy for profit maximization", *Proceedings of the IEEE PES General Meeting*, 2010.

[2.142] B. Ramachandran, S. K. Srivastava, C. S. Edrington, D. A. Cartes, "An intelligent auction scheme for smart grid market using a hybrid immune algorithm", *IEEE Transactions on Industrial Electronics*, Vol. 58, No. 10, 2011, pgs. 4603-4612.

[2.143] A. Mazza and G. Chicco, "Multi-Objective Distribution System Optimization Using Euclidean Distance Calculations In The Genetic Operators", *Proceedings of the International Conference on Power and Energy Systems*, 2012, pgs. 14-19.

[2.144] H. Frank and S. Mesentean, "Effcient communication interfaces for distributed energy resources", *International Journal of Grid and High Performance Computing*, Vol. 2, No. 2, 2010, pgs. 23-36.

[2.145] B. Yoo, S. Yang, H. Yang, W. Kim, Y. Jeong, B. Han, and K. Jang, "Communication architecture of the IEC 61850-based micro grid system", *Journal of Electrical Engineering and Technology*, Vol. 6, No. 5, 2011, pgs. 605-612.

[2.146] M. Erol-Kantarci, B. Kantarci, and H. T. Mouftah, "Reliable overlay topology design for the smart microgrid network", *IEEE Network*, Vol. 25, No. 5, 2011, pgs. 38-43.

[2.147] H. Nikkhajoei and R. Iravani, "Steady-state model and power flow analysis of electronically-coupled distributed resource units", *IEEE Transactions on Power Delivery*, Vol. 22, No. 1, 2007, pgs. 721-728.

[2.148] Z. Yanping and L. Yuping, "A novel newton current equation method on power flow analysis in microgrid", *IEEE Power & Energy Society General Meeting*, 2009.

[2.149] M. Z. Kamh and R. Iravani, "Unbalanced model and power-flow analysis of microgrids and active distribution systems", *IEEE Transactions on Power Delivery*, Vol. 25, No. 4, 2010, pgs. 2851-2858.

[2.150] H. Ren, W. Zhou, K. Nakagami, W. Gao, and Q. Wu, "Multi-objective optimization for the operation of distributed energy systems considering economic and environmental aspects", *Applied Energy*, Vol. 87, No. 12, 2010, pgs. 3642-3651.

[2.151] A.A. Moghaddam, A. Seifi, Alireza; T. Niknam, M. Z. A. Pahlavani, "Multi-objective operation management of a renewable MG (micro-grid) with back-up micro-turbine/fuel cell/battery hybrid power source", *Energy*, Vol. 36, No. 11, 2011, pgs. 6490-6507.

[2.152] C. Schwaegerl, L. Tao, P. Mancarella, and G. Strbac, "A multi-objective optimization approach for assessment of technical, commercial and environmental performance of microgrids", *European Transactions on Electrical Power*, Vol. 21, No. 2, 2011, pgs. 1271-1290.

[2.153] K. Hopkinson, X. Wang, R. Giovanini, J. Thorp, K. Birman, and D. Coury, "EPOCHS: a platform for agent-based electric power and communication simulation built from commercial off-the-shelf components", *IEEE Transactions on Power Systems*, Vol. 21, No. 2, 2006, pgs. 548 –558.

[2.154] R.H. Lasseter, J. H. Eto, B. Schenkman, J. Stevens, H. Vollkommer, D. Klapp, E. Linton, H. Hurtado, J. Roy, "CERTS Microgrid Laboratory Test Bed", *IEEE Transactions on Power Delivery*, Vol. 26, No. 1, 2011, pgs. 325-332.

[2.155] J. Jeon, J. Kim, H. Kim, S. Kim, C. Cho, J. Kim, J. Ahn, K. Nam, "Development of Hardware In-the-Loop Simulation System for Testing Operation and Control Functions of Microgrid", *IEEE Transactions on Power Electronics*, Vol. 25, No. 12, 2010, 2919-2929.

[3.1] R.A. Walling, R. Saint, R.C. Dugan, J. Burke, and L.A. Kojovic, “Summary of distributed resources impact on power delivery systems”, *IEEE Transactions on Power Delivery*, Vol. 23, 2008, pgs. 1636 – 1644.

[3.2] P. Denholm, “Enabling Technologies for High Penetration of Wind and Solar Energy”, *Proceedings, ASME 5th International Conference on Energy Sustainability,* 2011, pgs. 1451-1458.

[3.3] K. Sedghisigarchi, and A. Feliachi, “Dynamic and Transient Analysis of Power Distribution Systems with Fuel Cells-Part II: Control & Stability Enhancement”, *IEEE Transactions on Energy Conversion*, Vol. 19, 2004, pgs.429-434.

[3.4] E.A. DeMeo, W. Grant, M.R. Milligan, and M.J. Schuerger, “Wind Plant Integration”, *IEEE Power and Energy Magazine*, Vol. 3, 2005, pgs. 38-46.

[3.5] T. Basso and R. DeBlasio, “IEEE 1547 series of standards: interconnection issues”, *IEEE Transactions on Power Electronics*, Vol. 19, 2004, pgs. 1159–1162.

[3.6] J. Zhenhua and R.A. Dougal, “Hierarchical microgrid paradigm for integration of distributed energy resources”, *Proceedings, IEEE Power and Energy Society General Meeting: Conversion and Delivery of Electrical Energy in the 21st Century*, Vol. 1, 2008.

[3.7] G. Celli, F. Pilo, G. Pisano, V. Allegranza, R. Cicoria, and A. Iaria, “Meshed vs. Radial MV Distribution Network in Presence of Large Amount of DG”, *Proceedings, IEEE Power and Energy Society Power Systems Conference*, Vol. 2, 2004 pgs. 709-714.

[3.8] C. Langbort, “Distributed control of complex interconnected systems: a convex approach”, Doctoral Dissertation, Cornell University, Ithaca, NY, 2005.

[3.9] IEEE/CIGRE Joint Task Force on Stability Terms and Definitions, "Definition and Classification of Power System Stability", *IEEE Transactions On Power Systems*, Vol. 19, No. 2, May, 2004.

[3.10] P. Kundur, Power System Stability and Control. New York: McGraw-Hill, 1994.

[3.11] Foundation for Intelligent Physical Agents (FIPA), 2010, available at: http://www.fipa.org/.

[3.12] K. Huang, S.K. Srivastava, D.A. Cartes, and L. Sun, “Market-based multiagent system for reconfiguration of shipboard power systems”, *Electric Power Systems Research*, Vol. 79, 2009, pgs. 550-556.

[3.13] F.L. Bellifemine, G. Caire, D. Greenwood, Developing Multi-Agent Systems with JADE. John Wiley & Sons, West Sussex, England, 2007, chapters 3-4.

[3.14] Gerhard Weiss (Editor), Multiagent Systems, MIT Press, Cambridge, MA, 1999.

[3.15] K. Barnes, B. Johnson, R. Nickelson, "Review Of Supervisory Control And Data Acquisition (SCADA) Systems", Idaho National Engineering and Environmental Laboratory, INEEL/EXT-04-01517, January 2004.

[3.16] A.G. Bruce, "Reliability analysis of electric utility SCADA systems", *IEEE Transactions on Power Systems*, Vol. 13 , No. 3, 1998, pgs: 844-849.

[3.17] K. Stouffer, J. Falco, and K. Kent, "Guide to Supervisory Control and Data Acquisition (SCADA) and Industrial Control Systems Security - Recommendations of the National Institute of Standards and Technology", NIST Special Publication 800-82, Computer Security Division - Information Technology Laboratory, National Institute of Standards and Technology, September 2006.

[3.18] By direction of Section 1302 of Title XIII of the Energy Independence and Security Act (EISA), "2010 Smart Grid System Report - Report to Congress", U.S. Department of Energy, February 2012.

[3.19] H. You, V. Vittal, and Z. Yang, "Self-Healing in Power Systems: An Approach Using Islanding and Rate of Frequency Decline-Based Load Shedding", *IEEE Transactions on Power Systems*, Vol. 18, No. 1, 2003.

[3.20] P. Mittra and G.K. Venayagamoorthy, "Implementation of an Intelligent Reconfiguration Algorithm for an Electric Ship Power System", *IEEE Transactions on Industry Applications*, Vol. 47, No. 5, 2011, pgs. 2292-2300.

[3.21] R. F. Yu, P. Zhang, W. Xiao, and P. Choudhury, "Communication systems for grid integration of renewable energy resources", *IEEE Network*, Vol. 25, No. 5, 2011, pgs. 22-29.

[3.22] H. Liang, B. J. Choi, W. Zhuang, X. Shen, and A. S. A. Awad, "Multiagent Coordination in Microgrids via Wireless Networks", *IEEE Wireless Communications*, Vol. 19, No. 3, 2012, pgs. 14-22.

[3.23] H. Kopetz, "Software engineering for real-time: a roadmap", *Proceedings of the Conference on the Future of Software Engineering,* 2000, pgs. 201-211.

[3.24] R. Zurawski (editor). The Industrial Communication Technology Handbook. CRC Press, Boca Raton, FL, 2005.

[3.25] Z. Wang. Internet QOS – Architectures and Mechanisms for Quality of Service. Academic Press, San Diego, CA, 2001.

[3.26] J.F. Kurose and K.W. Ross. Computer Networking – A Top-Down Approach (5th Edition). Addison-Wesley, New York, NY, 2010.

[3.27] S. Ci, J. Qian, D. Wu, and A. Keyhani, “Impact of wireless communication delay on load sharing among distributed generation systems through smart microgrids” *IEEE Wireless Communications*, Vol. 19, No. 3, 2012, pgs. 24-29.

[3.28] Available at: http://jns.sourceforge.net/

[3.29] Available at: http://www.isi.edu/nsnam/ns/

[3.30] G. N. Ericsson, “Cyber security and power system communication - essential parts of a smart grid infrastructure”, *IEEE Transactions on Power Delivery*, Vol. 25, No. 3, 2010, pgs. 1501-1507.

[3.31] S. Clements and H. Kirkham, “Cyber-security considerations for the smart grid”, *Proceedings of the IEEE PES General Meeting*, 2010.

[3.32] I. L. G. Pearson, “Smart grid cyber security for Europe”, *Energy Policy*, Vol. 39, No. 9, 2011, pgs. 5211-5218.

[3.33] X. Li, X. Liang, R. Lu, X. Shen, X. Lin, and H. Zhu, “Securing smart grid: Cyber attacks, countermeasures, and challenges”, *IEEE Communications Magazine*, Vol. 50, No. 8, 2012, pgs. 38-45.

[3.34] S. Sridhar, A. Hahn, and M. Govindarasu, “Cyber-physical system security for the electric power grid”, *Proceedings of the IEEE*, Vol. 100, No. 1, 2012, pgs. 210-224.

[3.35] D. Dolezilek and L. Hussey, “Requirements or recommendations? Sorting out NERC CIP, NIST, and DOE cybersecurity”, *Proceedings of the 64th Annual Conference for Protective Relay Engineers*, 2011, pgs. 328-333.

[3.36] Y. Yan, Y. Qian, H. Sharif, and D. Tipper, “A Survey on Cyber Security for Smart Grid Communications”, *IEEE Communications Surveys & Tutorials*, In press, 2012.

[3.37] X. Li, X. Liang, R. Lu, X. Shen, X. Lin, and H. Zhu, “Securing smart grid: cyber attacks, countermeasures, and challenges”, *IEEE Communications Magazine*, Vol. 50, No. 8, 2012, pgs. 38 – 45.

[3.38] A.H. Mohsenian-Rad and A. Leon-Garcia, “Distributed Internet-Based Load Altering Attacks Against Smart Power Grids,” *IEEE Transactions on Smart Grid*, Vol. 2, No. 4, 2011, pgs. 667–674.

[4.1] G. Weiss. Multiagent Systems. MIT Press, Cambridge, MA, 1999.

[4.2] S. McArthur, E. Davidson, V. Catterson, A. Dimeas, N. Hatziargyriou, F. Ponci, and T. Funabashi, “Multi-Agent Systems for Power Engineering Applications—Part I: Concepts, Approaches, and Technical Challenges”, *IEEE Transactions on Power Systems*, Vol. 22, 2007, pgs. 1743-1759.

[4.3] L.Vig and J. Adams, “Multi-robot coalition formation”, *IEEE Transactions on Robotics*, Vol. 22, No. 4, pgs. 637-649.

[4.4] F.L. Bellifemine, G. Caire, and D. Greenwood. Developing Multi-Agent Systems with JADE. John Wiley & Sons, West Sussex, England, 2007.

[4.5] Java Agent Development Framework (Telecom Italia), 2012, available at: http://jade.tilab.com/

[4.6] Foundation for Intelligent Physical Agents (FIPA), 2011, available at: http://www.fipa.org/.

[4.7] J. Bloch. Effective Java (Second Edition). Sun Microsystems, Inc., Santa Clara, CA, 2008.

[4.8] H. Fakham, A. Doniec, F. Colas, and X. Guillaud, “A Multi-agents System for a Distributed Power Management of Micro Turbine Generators Connected to a Grid”, *IFAC CMTEE*, Vol. 1, 2010.

[4.9] B. Ramachandran, S.K. Srivastava, D.A. Cartes, C.S. Edrington, “Distributed energy resource management in a smart grid by risk based auction strategy for profit maximization”, *Proceedings, IEEE Power and Energy Society General Meeting*, 2010.

[4.10] Saul Gass, Linear Programming: Methods and Applications - 5th Edition, Dover Publications, Inc. 2003, pgs. 224-250.

[5.1] Collected from numerous manufacturer’s specification sheets and product literature.

[5.2] C.C. Lee and S. Dar Lin, Handbook of Environmental Engineering Calculations, McGraw-Hill, New York, 2000, pp. 2.46-2.48.

[5.3] D. Zhu, N. J. Nussbaum, H. D. Kuhns, M.-C. Chang, D. Sodeman, S. Uppapalli, H. Moosmuller, J. C. Chow, and J. G. Watson, “In-Plume Emission Test Stand 2: Emission Factors for 10- to 100-kW U.S. Military Generators”, *Journal of Air & Waste Management Association*, Vol. 59, 2009, pgs. 1446–1457.

[5.4] S. Shah, D.Cocker III, K.Johnson, J. M. Lee, B. Soriano, and J. W. Miller, “Emissions of regulated pollutants from in-use diesel back-up generators”, *Atmospheric Environment,* Vol. 40, 2006, pgs. 4199–4209.

[5.5] J. H. Seinfeld and S. N. Pandis, Atmospheric Chemistry And Physics - From Air Pollution to Climate Change (2nd Edition). John Wiley & Sons, 2006.

[5.6] U.S. Federal Register, “Control of Emissions of Air Pollution From Nonroad Diesel Engines and Fuel – Final Rule”, Vol. 69, No. 124, June 29, 2004, pgs. 38958-38964.

[5.7] Code of U.S. Federal Regulations, Title 40: Protection of Environment, Chapter I – Environmental Protection Agency, Subchapter C: Air Programs, Part 50: National Primary And Secondary Ambient Air Quality Standards, available at: http://ecfr.gpoaccess.gov/

[5.8] L.N. Hannett, F.P. de Mello, G.H. Tylinski, and W.H. Becker, "Validation Of Nuclear Plant Auxiliary Power Supply By Test", *IEEE Transactions on Power Apparatus and Systems*, Vol. 101, No. 9, September 1982, pgs 3068-3075.

[5.9] K.E. Yeager and J.R. Willis, "Modeling Of Emergency Diesel Generators In An 800 Megawatt Nuclear Power Plant", *IEEE Transactions on Energy Conversion*, Vol. 8, No. 3, September 1993.

[5.10] L. Goldstein, "Gas-fired distributed energy resource technology characterizations," National Renewable Energy Laboratory (NREL), NREL/TP-620-34783, Nov. 2003.

[5.11] S. R. Guda, C. Wang, and M. H. Nehrir, "Modeling of Microturbine Power Generation Systems," *Electric Power Components and Systems*, Vol. 34, 2006, pgs. 1027-1041.

[5.12] M.R. Patel, Wind and Solar Power Systems – Second Edition, CRC Press, 2005.

[5.13] Solar Energy Research Institute, "Basic Photovoltaic Principles and Methods", U.S. Department of Energy, SERI/SP-290-1448, February 1982.

[5.14] W. De Soto, S.A. Klein, and W.A. Beckman, "Improvement and validation of a model for photovoltaic array performance", *Solar Energy*, Vol. 80, 2006, pgs. 78-88.

[5.15] T.U. Townsend, "A Method for Estimating the Long-Term Performance of Direct-Coupled Photovoltaic Systems", MS thesis, University Of Wisconsin-Madison, 1989, pgs.24,64.

[5.16] W.H. Strehlow and E.L. Cook, "Compilation of Energy Band Gaps in Elemental and Binary Compound Semiconductors and Insulators", *Journal of Physical Chemistry Reference Data*, Vol. 2, No.1, 1973.

[5.17] M. G. Villalva, J. R. Gazoli, and E. R. Filho, "Comprehensive Approach to Modeling and Simulation of Photovoltaic Arrays", *IEEE Transactions On Power Electronics*, Vol. 24, No. 5, May 2009, pgs. 1198-1208.

[5.18] H. Tian, F. Mancilla-David, K. Ellis, E. Muljadi, and P. Jenkins, "A cell-to-module-to-array detailed model for photovoltaic panels", *Solar Energy*, Vol. 86, 2012, pgs. 2695-2702.

[5.19] S.K. Kim, J. H. Jeon, C.H. Cho, E.S. Kim, and J.B. Ahn, "Modeling and simulation of a grid-connected pv generation system for electromagnetic transient analysis", *Solar Energy,* Vol. 83, 2009, pgs. 664–678.

[5.20] H. P. Desai and H. K. Patel, "Maximum Power Point Algorithm In Pv Generation: An Overview", *Proceedings of the 7th International Conference on Power Electronics and Drive Systems (PEDS)*, 2007, pgs. 624–630.

[5.21] N. Fermia, D. Granozio, G. Petrone, M. Vitelli, "Predictive & adaptive MPPT Perturb and Observe Method", *IEEE Transactions on Aerospace Electronic Systems,* Vol. 43, No. 3, 2007, pgs. 934–950.

[5.22] L. Piegari and R. Rizzo, "Adaptive Perturb and Observe Algorithm for Photovoltaic Maximum Power Point Tracking", *IET Renewable Power Generation*, Vol. 4, No. 4, 2010, pgs. 317–328.

[5.23] Y. Yusof, S.H. Sayuti, M.A. Latif, M. Wanik, "Modeling And Simulation Of Maximum Power Point Tracker for Photovoltaic System", *Proceedings of the National Power and Energy Conference (PEC)*, 2004, pgs. 88–93.

[5.24] W. Xiao and W.G. Dunford, "A Modified Adaptive Hill Climbing MPPT Method for Photovoltaic Power Systems", *IEEE 35th Annual Power Electronics Specialists Conference (PESC)*, Vol. 3, 2004, pgs. 1957–1963.

[5.25] M. Miyatake, M. Veerachary, F. Toriumi, N. Fujii, H. Ko, "Maximum Power Point Tracking of Multiple Photovoltaic Arrays: A PSO Approach", *IEEE Transactions on Aerospace and Electronic Systems,* Vol. 47 , No. 1, 2011, pgs. 367-380.

[5.26] Hansen, M. Aerodynamics of Wind Turbines. Earthscan Press, 2008.

[5.27] F. D. Bianchi, H. D. Battista, and R. J. Mantz, Wind Turbine Control Systems – Principles, Modeling and Gain Scheduling Design. Springer-Verlag London Limited, 2007.

[5.28] Siegfried Heier, Grid Integration of Wind energy Conversion Systems, John Wiley & Sons, 1998.

[5.29] J. G. Slootweg, S.W.H. de Haan, H. Polinder & W.L. Kling, "General Model for Representing Variable Speed Wind Turbines in Power System Dynamics Simulations," *IEEE Transactions on Power Systems*, Vol. 18, No. 1, Feb. 2003.

[5.30] M. R. Patel, Wind and Solar Power Systems, CRC Press, 1999.

[5.31] Ahmet Duran Sahin, "Progress and recent trends in wind energy", *Progress in Energy and Combustion Science*, Vol. 30, 2004.

[5.32] E. Muljadi and C.P. Butterfield, "Pitch-Controlled Variable-Speed Wind Turbine Generation", *1999 IEEE Industry Applications Society Annual Meeting*, October, 1999.

[5.33] K. E. Johnson, L. Y. Pao, M. J. Balas, L. J. Fingersh, "Control of variable-speed wind turbines: Standard and adaptive techniques for maximizing energy capture", *IEEE Control Systems Magazine*, Vol. 26, No. 3, June 2006.

[5.34] F.D. Bianchi, R.J. Mantz and C.F. Christiansen. "Power regulation in pitch controlled variable speed WECS above rated wind speed", *Renewable Energy*, Vol. 29, 2004.

[5.35] M.M. Hand, M.J. Balas, "Systematic controller design methodology for variable-speed wind turbines", *Wind Engineering*, Vol. 24, No. 3, 2000.

[5.36] A.E. Fitzgerald, C. Kingsley Jr., S.D. Umans, Electric Machinery. McGraw Hill, Boston, 2003.

[5.37] P.W. Sauer. Power System Dynamics and Stability. Prentice Hall, Upper Saddle River, NJ, 1998.

[5.38] H. Huang & L. Chang. "Energy-Flow Direction Control of Grid-Connected IGBT Inverters for Wind Energy Extraction", *Proceedings of Canadian Conf on Electrical & Computer Engineering*, Vol. 1, 2000.

[5.39] S. Li, T. A. Haskew, & L. Xu. "Conventional and novel control designs for direct driven PMSG wind turbines", *Electric Power Systems Research,* Vol. 80, 2010.

[5.40] C. Wang, M.H. Nehrir, and H. Gao, "Control of PEM Fuel Cell Distributed Generation Systems," *IEEE Transactions on Energy Conversion*, Vol. 21, No. 2, June 2006.

[5.41] Pacific Northwest Cooperative Agricultural Weather Network, AgriMet Historical Dayfile Data Access, Deer Lodge, MT (DRLM), available at: http://www.usbr.gov/pn/agrimet/webaghrread.html.

[5.42] W.D. Kellogg, M.H. Nehrir, G. Venkataramanan, V. Gerez, "Generation unit sizing and cost analysis for stand-alone wind, photovoltaic, and hybrid wind/PV systems," *IEEE Transactions on Energy Conversion*, Vol. 13, No. 1, March 1998.

[5.43] J. Appleby and F.R. Foulkes, Fuel Cell Handbook, Van Nostrand Reinhold, New York, 1989.

[5.44] C. Wang and M.H. Nehrir, "A Physically-Based Dynamic Model for Solid Oxide Fuel Cells," *IEEE Transactions on Energy Conversion*, Vol. 22, No. 4, Dec. 2007, pgs. 864 - 872.

[5.45] N. Autissier, F. Palazzi, F. Marechal, J. van Herle, and D. Favrat, "Thermo-Economic Optimization of a Solid Oxide Fuel Cell, Gas Turbine Hybrid System", *Journal of Fuel Cell Science and Technology*, Vol. 4, Iss. 2, 2007, pgs. 123-129.

[5.46].A. Laughton and D.F. Warne, Electrical Engineer's Reference Book (16th Edition), Elsevier, 2003, pgs. 26/18-20.

[5.47] Hsin-Sena Chu, F. Tsau, Yi-Yiea Yan, Kan-Lina Hsueh, and Fa-Lin Chen, "The development of a small PEMFC combined heat and power system", *Journal of Power Sources*, Vol. 176, Iss. 2, 2008, pgs. 499-514.

[5.48] H. Zhu & R. J. Kee, "Thermodynamics of SOFC efficiency and fuel utilization as functions of fuel mixtures and operating conditions", *Journal of Power Sources*, Vol. 161, Iss. 2, Oct 2006.

[5.49] Y. Tanaka, A. Momma, K. Kato, A. Negishi, K. Takano, K. Nozaki & T. Kato, "Development of electrical efficiency measurement techniques for 10 kW-class SOFC system: Part I. Measurement of electrical efficiency", *Energy Conversion and Management*, Vol. 50, Iss. 3, March 2009.

[5.50] S. Farhad & F. Hamdullahpur, "Developing fuel map to predict the effect of fuel composition on the maximum efficiency of solid oxide fuel cells", *Journal of Power Sources*, Vol. 193, Iss. 2, Sept 2009.

[5.51] Aidu Qi, Brant Pepply, and Kunal Karan, "Integrated fuel processors for fuel cell application: A review", *Fuel Processing Technology*, Vol. 88, 2007, pgs.. 3-22.

[5.52] F. Calise, M. Dentice d' Accadia, L. Vanoli, and Michael R. von Spakovsky, "Full load synthesis/design optimization of hybrid SOFC-GT power plant," *Energy*, Vol. 32, 2007, pgs. 446-458.

[5.53] A. Rao, J. Maclay, and S. Samuelsen, "Efficiency of electrochemical systems," *Journal of Power Sources*, Vol. 134, 2004, pgs. 181-184.

[5.54] N. Wouodstra, T.P. van der Stelt, and K. Hemmes, "The Thermodynamic Evaluation and Optimization of Fuel Cell Systems," *Journal of Fuel Cell Science and Technology*, Vol. 3, 2006, pgs. 155-164.

[5.55] Felder, R. and Rousseau, R. Elementary Principles of Chemical Processes, John Wiley & Sons, New York, 1978.

[5.56] A. E. Lutz, R. S. Larson, and J.O. Keller, "Thermodynamic comparison of fuel cells to the Carnot cycle," *International Journal of Hydrogen Energy*, Vol. 27, 2002, pgs. 1103–1111.

[5.57] S.E. Wright. "Comparison of the theoretical performance potential of fuel cells and heat engines," *Renewable Energy*, Vol. 29, 2004, pgs. 179-195.

[5.58] C. Haynes, "Clarifying reversible efficiency misconceptions of high temperature fuel cells in relation to reversible heat engines," *Journal of Power Sources*, Vol. 92, 2001, pgs. 199-203.

[5.59] H. Hassanzadeh and S.H. Mansouri, "Efficiency of ideal fuel cell and Carnot cycle from a fundamental perspective," *Proceedings of the Institution of Mechanical Engineers -- Part A -- Power & Energy*, Vol. 219, Iss. 4, 2005, pgs. 245-254.

[5.60] R. O'Hayre, Suk-Won Cha, W. Colella, F. B. Prinz, Fuel Cell Fundamentals, John Wiley & Sons, New York, 2006.

[5.61] I. Beausoliel-Morrison, A. Schatz, and F. Marechal. "A Model for Simulating the Thermal and Electrical Production of Small-Scale Solid-Oxide Fuel Cell Cogeneration Systems within Building Simulation Programs". *HVAC&R Research Special Issue*, Vol. 12, No. 3a, 2006, pgs. 641-667.

[5.62] P.J. Linstrom and W.G. Mallard, Eds., "NIST Chemistry WebBook - Gas phase thermochemistry data", NIST Standard Reference Database Number 69, June 2005, National Institute of Standards and Technology, (http://webbook.nist.gov).

[5.63]W. Jamsak, S. Assabumrungrat, P.L. Douglas, N.Laosiripojana, S. Charojrochkul, "Theoretical performance analysis of ethanol-fuelled solid oxide fuel cells with different electrolytes," *Chemical Engineering Journal*, Vol. 119, 2006, pgs. 11-18.

[5.64] F.A. Coutelieris, S. Douvartzides, P. Tsiakaras, "The importance of the fuel choice on the efficiency of a solid oxide fuel cell system," *Journal of Power Sources*, Vol. 123, 2003, pgs. 200-205.

[5.65] F. Calise, M. Dentice d'Accadia, A. Palombo, L. Vanoli, "Simulation and exergy analysis of a hybrid Solid Oxide Fuel Cell (SOFC)-Gas Turbine System," *Energy*, Vol. 31, 2006, pgs. 3278-3299.

[5.66] M. Bischoff, "Large Stationary Fuel Cell Systems: Status and Dynamic Requirements," *Journal of Power Sources*, Vol. 154, 2006, pgs. 461-466.

[5.67] Boyce, Meherwan P., Gas Turbine Engineering Handbook (3rd Edition). Elsevier, 2006, pgs. 86-91.

[5.68] M. C. Williams, J. P. Strakey, W. A. Surdoval, and L. C. Wilson, "Solid oxide fuel cell technology development in the U.S.," *Solid State Ionics*, Vol. 177, Iss. 19, 2006.

[5.69] W.A. Surdoval, "US DoE Fossil Energy Fuel Cell Program," presented at: 7th SECA Workshop & Peer Review, Philadelphia, PA, Sept 2006, available at: http://www.netl.doe.gov/publications/proceedings/06/seca.

[5.70] U.S. Department of Energy, "Annual Energy Outlook 2006", DOE/EIA-0383, Energy Information Administration, Washington, D.C., 2006.

[5.71] R. U. Ayres, L. W. Ayres, and B. Warr "Exergy, power and work in the US economy, 1900–1998", *Energy*, Vol. 28, Iss. 3, March 2003.

[5.72]. U. Ayres, H. Turton, and T. Casten, "Energy efficiency, sustainability and economic growth", *Energy*, Vol. 32, Iss. 5, May 2007.

[5.73] W. Graus & E. Worrell, "Trend in efficiency and capacity of fossil power generation in the EU", *Energy Policy*, Vol. 37, Iss.. 6, June 2009.

[5.74] P.B. Nigel and D. Thompsett (editors), <u>Fuel Cells Compendium - Chapter 1 (US distributed generation fuel cell program)</u>, Elsevier, 2005.

[5.75] M.H. Nehrir and C. Wang, <u>Modeling and Control of Fuel Cells: Distributed Generation Applications</u>, Wiley-IEEE Press, 2009.

[5.76] C. Wang and M.H. Nehrir, "Load transient mitigation for stand-alone fuel cell power generation systems," *IEEE Transactions on Energy Conversion*, Vol. 22, No. 4, December 2007.

[5.77] K.P. Adzakpa, K. Agbossou, Y. Dube, M. Dostie, M. Fournier, A. Poulin, "PEM fuel cells modeling and analysis through current and voltage transient behaviors," *IEEE Transactions on Energy Conversion*, Vol. 23, No. 2, June 2008.

[5.78] C. Wang, M.H. Nehrir, and H. Gao, "Control of PEM Fuel Cell Distributed Generation Systems," *IEEE Transactions on Energy Conversion*, Vol. 21, No. 2, June 2006.

[5.79] C. Colson, M. Nehrir, M. Deibert, M. Amin, & C. Wang, "Efficiency Evaluation of Solid-Oxide Fuel Cells in Combined Cycle Operations", *ASME Journal of Fuel Cell Science &Technology*, Vol. 6, Iss. 2, Feb. 2009.

[5.80] F. Kreith & R. Emmett West, <u>CRC Handbook of Energy Efficiency</u>. CRC-Press, 1996.

[5.81] M. F. Serincan, U. Pasaogullari, and N. M. Sammes, "Effects of operating conditions on the performance of a micro-tubular solid oxide fuel cell (SOFC)", *Journal of Power Sources*, Vol. 192, Iss. 2, July 2009.

[5.82] A. Nakajo, Z. Wuillemin, J. Van herle, and D. Favrat, "Simulation of thermal stresses in anode-supported solid oxide fuel cell stacks. Part I: Probability of failure of the cells", *Journal of Power Sources*, Vol. 193, Iss. 1, August 2009.

[5.83] N. Lu and S. Katipamula, "Control strategies of thermostatically controlled appliances in a competitive electricity market", *Proceedings of 2005 IEEE Power Engineering Society General Meeting*, June, 2005.

[5.84] M.Haines, J.Davison, "Designing carbon capture power plants to assist in meeting peak power demand", *Energy Procedia,* Vol. 1, Iss. 1, Feb 09.

[5.85] M. Kintner-Meyer, K. Schneider, R. Pratt, "Impacts assessment of plug-in hybrid vehicles on electric utilities and regional US power grids, Part 1: technical analysis", Regional Grids and Plug-in Hybrids, Pacific Northwest National Laboratory - Richland, WA, 2007.

[5.86] Compiled from multiple Energy Information Administration spreadsheets including "Emissions Detail by State", "Table 5.1-Emissions from Energy Consumption at CPPs and CHPs, 1996 - 2007", and "Electric Power Annual 2007- State Tables", available at: http://www.eia.doe.gov.

[5.87] U. S. Department of Energy, "2005 Electric Sales, Revenue, Price: Tables 2 & 3", Energy Information Administration, Washington, D.C., 2005, available at: http://www.eia.doe.gov/cneaf/electricity/esr.

[5.88] D.H. Doughty, P. C. Butler, A. A. Akhil, N. H. Clark, and J. D. Boyes, "Batteries for Large-Scale Stationary Electrical Energy Storage", *Electrochemical Society Interface*, Vol. 19, No. 3, 2010, pgs. 49-53.

[5.89] K.C. Divya and J. Østergaard, "Battery energy storage technology for power systems—An overview", *Electric Power Systems Research*, Vol. 79, 2009, pgs. 511-520.

[5.90] Z.M. Salameh, M. A. Casacca, and W. A. Lynch, "A mathematical model for lead–acid batteries," *IEEE Transactions on Energy Conversion*, Vol. 7, No. 1, Mar. 1992, pgs. 93–98.

[5.91] M. A. Casacca, "Determination of lead–acid battery capacity via mathematical modeling techniques," *IEEE Transactions on Energy Conversion*, Vol. 7, No. 3, Sept. 1992, pgs. 442–446.

[5.92] M.H. Nehrir, B.J. LaMeres, G. Venkataramanan, V. Gerez, and L. A. Alvarado, "An Approach to Evaluate the General Performance of Stand-Alone Wind/Photovoltaic Generating Systems", *IEEE Transactions On Energy Conversion*, Vol. 15, No. 4, Dec. 2000, pgs. 433-439.

[5.93] M. Durr, A. Cruden, S. Gair, and J. R. McDonald, “Dynamic model of a lead–acid battery for use in a domestic fuel cell system,” *Journal of Power Sources*, Vol. 161, No. 2, Oct. 2006, pgs. 1400–1411.

[5.94] N. K. Medora and A. Kusko, “Dynamic battery modeling of lead–acid batteries using manufacturers’ data,” *Proceedings of the 27th International Telecommunications Conference - INTELEC '05*, Sep. 2005, pgs. 227–232.

[5.95] M. Ceraolo, “New dynamical models of lead-acid batteries”, *IEEE Transactions on Power Systems*, Vol. 15, No. 4, 2000, pgs. 1184–1190.

[5.96] C.S. Moo, K.S. Ng, Y.P. Chen, and Y.C. Hsieh, “State-of-Charge Estimation with Open-Circuit-Voltage for Lead-Acid Batteries”, *Power Conversion Conference Proceedings*, April 2007, pgs. 758 – 762.

[5.97] S. Barsali and M. Ceraolo, “Dynamical Models of Lead-Acid Batteries: Implementation Issues”, *IEEE Transactions on Energy Conversion*, Vol. 17, No. 1, 2002, pgs.16-23.

[5.98] R. Walawalkar and J. Apt, “Market Analysis of Emerging Electric Energy Storage Systems”, prepared for National Energy Technology Laboratory, DOE/NETL-2008/1330, July, 2008.

[5.99] D. Rastler, “Electricity Energy Storage Technology Options”, EPRI-2010/1020676, Dec. 2010

[5.100] S. B. Peterson, J.F. Whitacre, and J. Apt, “The economics of using plug-in hybrid electric vehicle battery packs for grid storage”, *Journal of Power Sources,* Vol. 195, 2010, pgs. 2377-2384.

[5.101] S.A. Pourmousavi, R. K. Sharma, and B. Asghari, “A Framework for Real-Time Power Management of a Grid-Tied Microgrid to Extend Battery Lifetime and Reduce Cost of Energy”, *Proceedings of IEEE PES Innovative Smart Grid Technologies (ISGT),* Jan. 2012

[5.102] H. Wenzl, I. Baring-Gould, R. Kaiser, B. Y. Liaw, P. Lundsager, J. Manwell, A. Ruddell, and V. Svoboda, “Life prediction of batteries for selecting the technically most suitable and cost effective battery”, *Journal of Power Sources*, Vol. 144, 2005, pgs 373-384.

[5.103] S. Drouilhet and B.L. Johnson, “A Battery Life Prediction Method for Hybrid Power Applications”, NREL/CP-440-21978, January 1997.

[5.104] Robert Lasseter and Joe Eto, “Value and Technology Assessment to Enhance the Business Case for the CERTS Microgrid”, Final Project Report prepared by Consortium for Electric Reliability Technology Solutions (CERTS), DE-FC02-06CH11350, May 15, 2010.

[5.105] MK-Powered data sheet (LIT-SS1004), model ES10-12S, January 2009.

[5.106] IEEE Std 141-1993, IEEE Recommended Practice for Electric Power Distribution for Industrial Plants (The IEEE Red Book), pgs 62-63.

[5.107] A. Engler, "Applicability of Droops in Low Voltage Grids", *International Journal of Distributed Energy Resources*, Vol. 1, No. 1, 2005.

[5.108] P. Wan and M.D. Lemmon, "Optimal power flow in microgrids using event-triggered optimization", *Proceedings of the American Control Conference*, 2010, pgs. 2521-2526.

[5.109] P. Kundur, N. Balu, and M. Lauby, Power system stability and control, McGraw-Hill, 1994, pg. 209.

[5.110] A.J. Wood and B.F. Wollenberg, Power Generation Operation and Control (2nd Edition). John Wiley and Sons, Inc., New York, 1996.

[5.111] K. Debrabandere, B. Bolsens, J. Van den Keybus, A.Woyte, J. Driesen, and R. Belmans, "A voltage and frequency droop control method for parallel inverters," *IEEE Transactions on Power Electronics*, Vol. 22, No. 4, 2007, pgs. 1107–1115.

[5.112] A. Haddadi and G. Joos, "Load sharing of autonomous distribution-level microgrids", *Proceedings of the IEEE Power and Energy Society General Meeting*, 2011.

[5.113] T. L. Vandoorn, B. Meersman, L. Degroote, B. Renders, and L. Vandevelde, "A control strategy for islanded microgrids with DC-link voltage control", *IEEE Transactions on Power Delivery*, Vol. 26, No. 2, 2011, pgs. 703-713.

[5.114] S.W. Heunis and R. Herman, "A probabilistic model for residential consumer loads", *IEEE Transactions on Power Systems*, Vol. 17, Iss. 3, August 2002.

[5.115] R.T. Guttromson, D.P. Chassin, and S.E. Widergren, "Residential energy resource models for distribution feeder simulation", *2003 IEEE Power Engineering Society General Meeting Proceedings*, Vol. 1, July 2003.

[5.116] D.H.O. McQueen, P.R. Hyland, S.J. Watson, "Monte Carlo simulation of residential electricity demand for forecasting maximum demand on distribution networks", *IEEE Transactions on Power Systems*, Vol. 19, Iss. 3, August 2004.

[5.117] T. V. Cutsem and C. Vournas, Voltage Stability of Electric Power Systems, Springer, 1998.

[5.118] J.M. Cahill, K.G. Ritland, and W. Lin-Kelly, "Description of Electric Energy Use In Single Family Residences in the Pacific Northwest 1986-1992", End-Use Load and Consumer Assessment Program (ELCAP), Bonneville Power Administration, December 1992.

[5.119] United States Department of Energy – Energy Information Administration, "2005 Residential Energy Consumption Survey", released September 2008, available at: http://www.eia.doe.gov/emeu/recs/recs2005/c&e/detailed_tables2005c&e

[5.120] M. Kintner-Meyer, K. Schneider, R. Pratt, "Impacts assessment of plug-in hybrid vehicles on electric utilities and regional US power grids, Part 1: technical analysis", Regional Grids and Plug-in Hybrids, Pacific Northwest National Laboratory Richland, WA, 2007.

[5.121] Market Surveillance Administrator, "MSA Report: Residential Load Profiles", Calgary, Alberta, April 2004, available at: www.albertamsa.ca/files/ResidentialLoadProfiles042804.pdf

[5.122] B.R. Becker and K.E. Stogsdill, "Development of a hot water use data base", *Proceedings of the Annual meeting of the American Society of Heating, Refrigerating and Air-Conditioning Engineers (ASHRAE)*, June 1990, pgs. 422-427.

[5.123] P. Fairey and D. Parker, " A Review of Hot Water Draw Profiles Used in Performance Analysis of Residential Domestic Hot Water Systems", Florida Solar Energy Center, FSEC-RR-56-04, July 2004.

[5.124] R. Hendron and J. Burch, "Development of Standardized Domestic Hot Water Event Schedules for Residential Buildings", NREL/CP-550-40874, Originally presented at *Energy Sustainability 2007,* August 2008.

[5.125] D.J. Hammerstrom (PI), "Pacific Northwest GridWise Testbed Demonstration Project – Part II. Grid Friendly Appliance Project (Final Report)", Pacific Northwest National Laboratory under U.S. DOE contract DE-AC05-76L01830, October 2007.

[5.126] A. Molderink, V. Bakker, M. G. C. Bosman, J. L. Hurink, and G. J. M. Smit, "Management and Control of Domestic Smart Grid Technology", *IEEE Transactions On Smart Grid*, Vol. 1, No. 2, September 2010, pgs. 109-119.

[6.1] C. V. Nayar, M. Ashari, and W. W. L. Keerthipala, "A Grid-Interactive Photovoltaic Uninterruptible Power Supply System Using Battery Storage and a Back Up Diesel Generator", *IEEE Transactions on Energy Conversion*, Vol. 15, No. 3, 2000, pgs. 348-353.

[6.2] R.W. Wies, R. A. Johnson, A. N. Agrawal, and T. J. Chubb, " Simulink Model for Economic Analysis and Environmental Impacts of a PV With Diesel-Battery System for

Remote Villages", *IEEE Transactions On Power Systems*, Vol. 20, No. 2, 2005, pgs. 692-700.

[6.3] P. M. Crimp, S. Colt, and M. A. Foster, "Renewable Power in Rural Alaska: Improved Opportunities for Economic Deployment", Institute of the North – Arctic Energy Summit, Anchorage, AK, 2008.

[6.4] E.M. Nfah and J. M. Ngundam , "Evaluation of optimal power options for base transceiver stations of Mobile Telephone Networks Cameroon", *Solar Energy,* Vol. 86, 2012, pgs. 2935-2949.

[6.5] M.D. Bhawan and J.L.N. Marg, "Consultation Paper on Green Telecommunications", Telecom Regulatory Authority of India, New Delhi, No. 3/2011, Feb 2011.

[6.6] J. Rijssenbeek, H. Wiegman, D. Hall, C. Chuah, G. Balasubramanian, C. Brady, "Sodium-Metal Halide Batteries in Diesel-Battery Hybrid Telecom Applications", *Proceedings of the 33rd International IEEE Telecommunications Energy Conference (INTELEC)*, 2011.

[6.7] Energy Information Administration, "Gasoline & Diesel Fuel Update", retrieved 20 April 2012. Available at: www.eia.gov/petroleum/gasdiesel.

[6.8] A. L. Dimeas and N. D. Hatziargyriou, "Operation of a multiagent system for microgrid control," *IEEE Transactions on Power Systems*., Vol. 20, No. 3, 2005, pgs. 1447–1455.

[6.9] T. Logenthiran, D. Srinivasan, and A. M. Khambadkone "Multi-agent system for energy resource scheduling of integrated microgrids in a distributed system", *Electric Power Systems Research*, Vol. 81, 2011, pgs. 138-148.

[6.10] Bagen and R. Billinton, "Evaluation of Different Operating Strategies in Small Stand-Alone Power Systems", *IEEE Transactions on Energy Conversion*, Vol. 20, No. 3, Sept 2005, pgs. 654-660.

[7.1] "IEEE Guide for Design, Operation, and Integration of Distributed Resource Island Systems with Electric Power Systems", IEEE Standard 1547.4-2011, 2011.

[7.2] J.A. Aspinall, et. al. (editor). Power System Protection (Volume 2: Systems and Methods) – 2nd Edition. The Institution of Electrical Engineers, London, U.K., 2005.

[7.3] M. Amin and B.F. Wollenberg, "Toward a smart grid: power delivery for the 21st century", *IEEE Power and Energy Magazine*, Vol. 3 , No. 5, 2005, pgs. 34-41.

[7.4] K. Moslehi and R. Kumar, "Vision for a self-healing power grid", *ABB Review,* No. 4, 2006.

[7.5] M. Amin, "Toward Self-Healing Energy Infrastructure Systems", *IEEE Computer Applications in Power*, Vol. 14, No. 1, 2001, pp. 20-28.

[7.6] M. Amin, "Toward a self-healing energy infrastructure", *Proceedings of the IEEE Power Engineering Society General Meeting*, 2006.

[7.7] M. Amin, "Challenges in reliability, security, efficiency, and resilience of energy infrastructure: Toward smart self-healing electric power grid", *Proceedings of the IEEE Power and Energy Society General Meeting - Conversion and Delivery of Electrical Energy in the 21st Century*, 2008.

[7.8] Z. Noorian, H. Hosseini, and M. Ulieru, "An Autonomous Agent-based Framework for Self-Healing Power Grid", *Proceedings of the IEEE International Conference on Systems, Man, and Cybernetics*, 2009.

[7.9] P. Cox, "Self-Healing Networks Performance Improvement by Automated Switching Algorithm", *Proceedings of the CIRED Seminar 2008: SmartGrids for Distribution*, 2008.

[7.10] F. Li, Z. Chen, L. Fan, P. Zhang, "Toward a self-healing protection and control system", 40th North American Power Symposium, 2008.

[7.11] H. You, V. Vittal, and Z. Yang, "Self-Healing in Power Systems: An Approach Using Islanding and Rate of Frequency Decline-Based Load Shedding", *IEEE Transactions on Power Systems*, Vol. 18, No. 1, 2003.

[7.12] D. Macleman, W. Bik, and A. Jones, "Evaluation of a Self Healing Distribution Automation Scheme on the Isle Of Wight", *Proceedings of the CIRED 20th International Conference on Electricity Distribution*, 2009.

[7.13] A. Valenti, I. Bel, and S. Lee, "High Level Requirements of Fast Simulation and Modelling Suite Of Tools for Future 'Self-Healing' Distribution Power System", *Proceedings of the CIRED 18th International Conference on Electricity Distribution*, 2005.

[7.14] K. L. Butler-Purry, and N. D. R. Sarma, "Self-Healing Reconfiguration for Restoration of Naval Shipboard Power Systems", *IEEE Transactions on Power Systems*, Vol. 19, No. 2, 2004.

[7.15] K. L. Butler-Purry, "Multi-Agent Technology for Self-Healing Shipboard Power Systems", *Proceedings of the 13th International Conference on Intelligent Systems Application to Power Systems*, 2005.

APPENDICES

APPENDIX A

FUNDAMENTALS OF POWER SYSTEM OPERATION

A voltage source induces a current through a conductor. When an alternating voltage source varies sinusoidally with respect to time, the induced current will also vary sinusoidally according to the following:

$$v(t) = V_{peak}\sin(\omega t + \phi_V) \text{ may be transformed to phasor form,} \tag{A.1}$$

$$\vec{V} = V_{peak}e^{i(\omega t+\phi_V)} = V_{peak}\angle\phi_V; \tag{A.2}$$

$$i(t) = I_{peak}\sin(\omega t + \phi_I) \text{ may be transformed to phasor form,} \tag{A.3}$$

$$\vec{I} = I_{peak}e^{i(\omega t+\phi_I)} = I_{peak}\angle\phi_I; \tag{A.4}$$

And, these give rise to impedance:

$$|Z|\angle\phi_Z = \frac{V_{peak}}{I_{peak}}e^{i(\phi_V-\phi_I)} \tag{A.5}$$

These phasor expressions for complex voltage and current sinusoids can be shown by their real component in the time domain. The series of examples below demonstrate how electrical parameters vary as the angular difference (ϕ_V- ϕ_I) is adjusted.

Example #1: In-phase 1.0 pu voltage and 1.0 pu current.

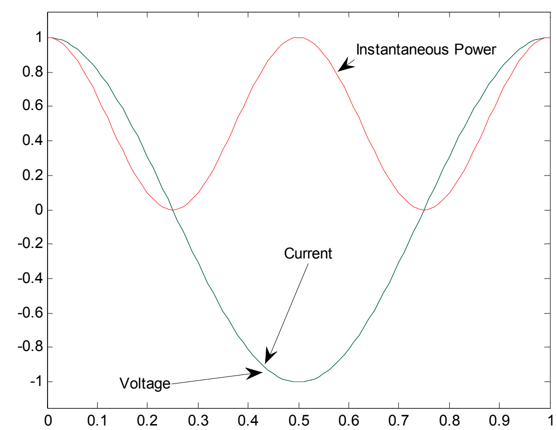

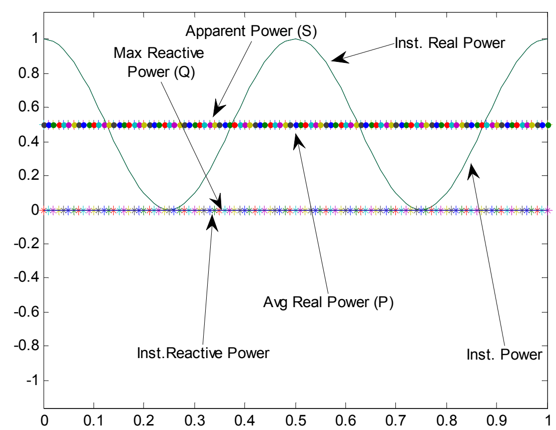

Voltage (1 pu) and current (1 pu) in phase (power factor = 1).
Peak inst. power = 1 pu (average inst. power = 0.5pu).
Peak real power = 1 pu (average real power = 0.5pu)
Peak reactive power = 0 pu (average reactive power = 0pu).
Apparent power (=Vrms*Irms) = 0.5.

Example #2: Leading 1.0 pu voltage and 1.0pu current.

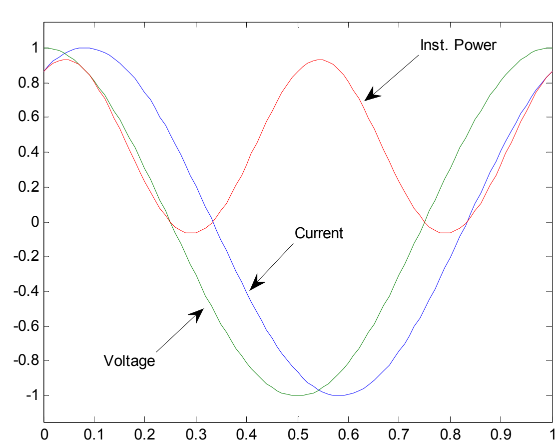

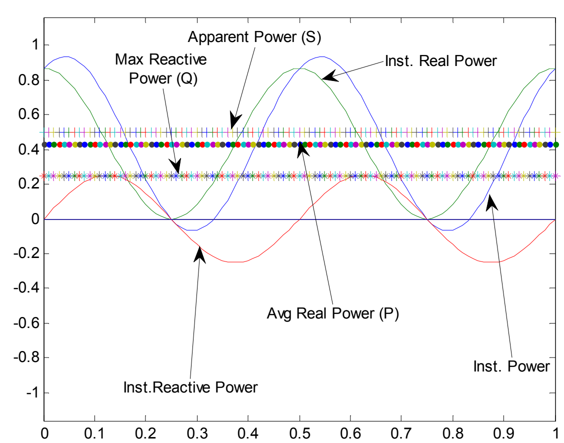

Voltage (1 pu) and current (1 pu) out of phase (power factor = 0.85).
Peak inst. power= 0.93pu (avg inst. = 0.44pu).
Peak real power = 0.86 pu (average real power = 0.44pu)
Peak reactive power = 0.25 pu (average reactive power = 0pu).
Apparent power = 0.5.
Instantaneous peak power occurs at intervals of $\omega t = \theta/2 + 2\pi$.

<u>Example #3: Leading 1.0 pu voltage and 1.15 pu current.</u>

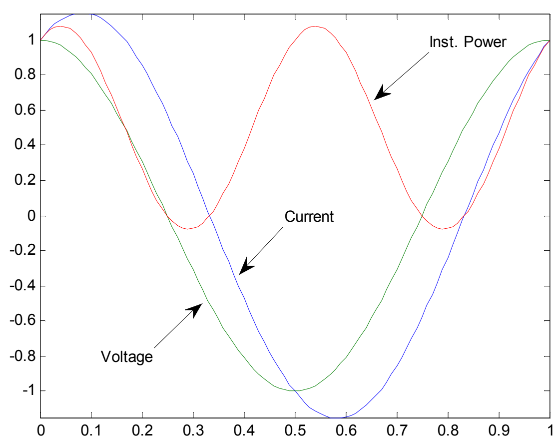

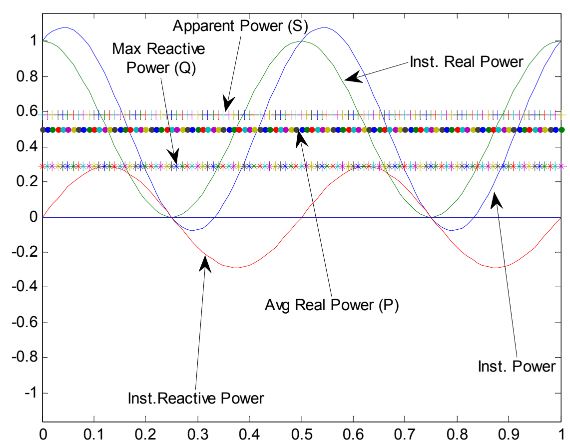

Voltage (1 pu) and current (1.15 pu) out of phase (power factor = 0.85).
Peak inst. power= 1.07pu (avg inst. = 0.5pu).
Peak real power = 1.0 pu (average real power = 0.5pu).
Peak reactive power = 0.29 pu (average reactive power = 0pu).
Apparent power = 0.58.

APPENDIX B

PER UNIT CONVERSION

Per unit values are commonly used for relating power system parameters. These per unit quantities are especially useful for relating phasor information between two interconnected circuits having different voltage levels. Current and voltage phase angles and the circuit power factor are not affected by the conversion to per unit values. In general, per unit values are calculated by:

$$per\ unit\ value = \frac{actual\ value}{base\ value} \tag{B.1}$$

Often, manufacturers will specify equipment rated voltage and power as base voltage and power. Base current and impedance can be calculated according to the specified base voltage and power by:

$$I_{base} = \frac{S_{base}}{V_{base}} \tag{B.2}$$

$$Z_{base} = \frac{V_{base}^2}{S_{base}} \tag{B.3}$$

Equipment impedances are usually given by percentage of the equipment's Z_{base} [Ω] by:

$$Z_{\%} = \frac{Z_{actual}}{Z_{base}} \times 100\% \tag{B.4}$$

Manufacturers often rate transformers according to a high side voltage and low side voltage, as well as rated power and internal impedance as measured on a particular side (either high or low). The currents and the internal impedance can be reflected across the transformer according to:

$$I_{HV} V_{HV} = S_{base} = I_{LV} V_{LV} \tag{B.5}$$

$$\frac{\vec{Z}_{HV}}{V_{HV}^{2}} = \frac{\vec{Z}_{LV}}{V_{LV}^{2}} \tag{B.6}$$

For equipment of different ratings, impedances must be converted to a common base. This implies that for any actual impedance, Z [Ω], that:

$$Z = Z_{a,p.u.}\ Z_{a,base} = Z_{b,p.u.}\ Z_{b,base} = Z_{c,p.u.}\ Z_{c,base}\text{ , and so on.}$$

Therefore, when converting bases:

$$Z_{a,p.u.} \frac{V_{a,base}^{2}}{S_{a,base}} = Z_{b,p.u.} \frac{V_{b,base}^{2}}{S_{b,base}} \tag{B.7}$$

Which, in a more useful form for conversion:

$$Z_{a,p.u.} = Z_{b,p.u.} \frac{MVA_{a,base}}{MVA_{b,base}} \cdot \frac{(kV_{b,base})^{2}}{(kV_{a,base})^{2}} \tag{B.8}$$

To illustrate the use of per unit values for circuit analysis, consider a series circuit which a load impedance of $\vec{Z}_L = 10 + j20\ \Omega$. The no load voltage of the source is

$\vec{E}_S = 10V\angle 0^o$ with an internal resistance of $\vec{Z}_S = j5\ \Omega$. The total impedance of the circuit is $\vec{Z}_T = 10 + j25\ \Omega$. The load current through the circuit is:

$$\vec{I}_L = \frac{\vec{E}_S}{\vec{Z}_T} = \frac{10\angle 0^o}{10 + j25} = 0.4A\angle -68^o \tag{B.9}$$

The apparent power produced by the source is:

$$\vec{S}_S = \vec{E}_S \cdot \vec{I}_L^{\,*} = 10\angle 0^o \cdot 0.4\angle 68^o = 4VA\angle 68^o \tag{B.10}$$

Arbitrarily, the base values are established for parameter magnitudes as: V_{base} = 10 V, Z_{base} = 100 Ω, I_{base} = 10 A, S_{base} = 10 VA. Once established as the reference bases, they apply to the system analyzed. Any circuit quantity may be referenced to these base values. These per unit values are phasors due to their reference to circuit values. Thus, the magnitude of the voltage across the load is:

$$V_L = E_S \frac{Z_L}{Z_T} = 10 \cdot \frac{22.4}{100} = 2.24V \tag{B.11}$$

In terms base voltage, the load voltage is:

$$\frac{V_L}{V_{base}} = \frac{2.24V}{10V} = 0.224 \text{ or 22.4\% of the base voltage.}$$

Any ohmic value can be described in terms of the base impedance. The per unit resistance and reactance of the load are:

$$R_{Lp.u.} = \frac{R_L}{Z_{base}} = \frac{10}{100} = 0.1 p.u.(\Omega) \tag{B.12}$$

$$X_{Lp.u.} = \frac{X_L}{Z_{base}} = \frac{20}{100} = 0.2\ p.u.(\Omega) \tag{B.13}$$

The real and reactive power of the load can be found by:

$$\begin{aligned} P_{p.u.} + jQ_{p.u.} &= \frac{P}{S_{base}} + j\frac{Q}{S_{base}} = \frac{R_L I_L{}^2}{S_{base}} + j\frac{X_L I_L{}^2}{S_{base}} \\ &= \frac{10 \cdot 0.4^2}{10} + j\frac{20 \cdot 0.4^2}{10} \\ &= 0.16 p.u.VA + j0.32 p.u.VAR \end{aligned} \tag{B.14}$$

APPENDIX C

MICROGRID CITIZENSHIP ASSESSMENT TOOL

The implementation of a microgrid onto a utility feeder introduces broad uncertainty for the bulk power system operator. Given that a microgrid can both receive and supply electrical power, support and encumber voltage profile, and acts in an unpredictable manner (due to DER generation variability), how will a microgrid "appear" to the utility side of the PCC? From a planning perspective, the microgrid has a maximum aggregate generation capacity based on nameplate ratings of the installed DERs. The same is true for microgrid storage assets. However, the actual capacity of the microgrid to supply real/reactive power at any given instant is impossible to predict because of the variable nature of some types of "green" DERs. Additionally, planners can make assessments of the quantity of aggregated load attached within the microgrid framework, both dispatchable and non-controllable. The overall effect of an interconnected microgrid is very different than a typical load termination on a feeder: an interconnected microgrid can act as a load at one instant (e.g. due to cloud cover, photovoltaic DER generation is low) and reverse power the utility the next (e.g. wind DER generation ramps up due to gusting). A desirable aspect of microgrids is the ability to act independently from the utility without a burdensome and vast communication infrastructure that shares information with the utility. In this way, the microgrid must be viewed as an autonomous entity that accepts real and reactive power from the utility when it needs it, but will support the utility with real and reactive power when it can. In this view, the microgrid is sometimes a taker, sometimes giver, but always self-interested in meeting its local load demand. When interconnected, the utility is sometimes a giver, sometimes forced to take, and in this way has a different relationship to the microgrid than typical load centers.

Based on the key microgrid characteristics of nameplate generation capacity, installed storage, and load, a three axis qualitative tool for judging the "grid citizenship" of a microgrid is presented in Figure C.1. Grid citizenship can be described as the way that an interconnected component interacts with the greater power system. Good "citizenship" is seen as contributing positively to the larger system by presenting a consistent profile. That profile may include dependable real/reactive power support, having adequate storage resources to mitigate power flow reversal across the interconnection, or appearing as a typical distribution load. Examples of poor "citizenship" can be seen as introducing large and intermittent power flow transients, frequent reversals, or causing a transient voltage profile on the feeder.

The component ratio (CR) is defined as:

$$\frac{G_{max} - L}{G_{max} + L}, G_{max} \geq 0, L \geq 0, G_{max} + L \geq 0 \qquad \text{(C.1)}$$

where, G_{max} is the aggregated nameplate capacity of generation and L is the aggregated load, attached to the microgrid. The component ratio offers a qualitative scale (between -1 and +1) for the degree of generation-to-load. The storage ratio (SR) is defined as:

$$\frac{G_{max} - S}{G_{max} + S}, G_{max} \geq 0, S \geq 0, G_{max} + S > 0 \qquad \text{(C.2)}$$

where, S is the aggregated nameplate storage capacity attached to the microgrid. The storage ratio gives a measure of how well the installed microgrid generation is supported by its own storage. It is presumed that storage capacity will be far less than generation ($S << G_{max}$), but a zero or negative ratio indicates a significant storage resource. The intermittency ratio (IR) is defined as:

$$\frac{G_{daily\ avg} + S}{G_{max} + S}, G_{max} > 0, S \geq 0, G_{daily\ avg} \geq 0 \qquad \text{(C.3)}$$

where, $G_{daily\ avg}$ is a measure of the average amount of generated energy divided by the average number hours the DER was generating power per day. This ratio is intended to give a qualitative indication as to how "dependable" the microgrid is at supplying power. The intermittency ratio can vary between 0 and 1 (indicating constant availability of microgrid generation assets).

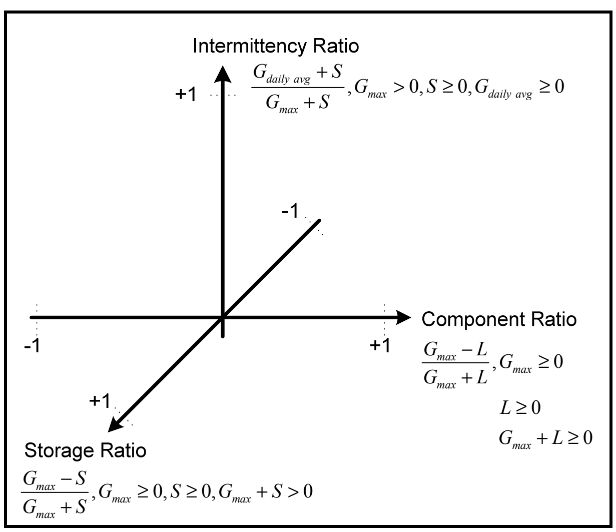

Figure C.1. Quantitative tool for judging microgrid "grid citizenship".

These ratios are meant to assist in high level power system planning. They offer a means of quickly classifying microgrid systems attached to the power systems and qualifying them by their contributions to, or burden upon, the greater utility grid. Using Figure C.1, the relative distribution of connected systems any given feeder can be displayed in such a way as to indicate qualitative measures of stability, power quality, and reliability. For example, given a rural radial medium voltage (MV) feeder with a weak voltage profile, power system planners can use the tool described above to assess the effect of adding one or more microgrid systems to the feeder. A power system planner is presented with a single microgrid system with parameters specified in Table C.1 for consideration.

Table C.1: Example of the grid citizenship tool applied to a weak rural feeder.

Parameter	Design Specification
Proposed Microgrid	
DC Bus Voltage (nominal)	400V
Installed Nameplate Capacity (G_{max})	5.0 MW
Installed Generation Mix	Photovoltaic / Wind
Daily average generation availability	22%
Installed Rated Load (*L*)	350 kW
Storage Rating (1-hr discharge rate)	225 A-hr
Storage Capacity (*S*, fully charged to discharged, 1.0 hr.)	90 kW
Ratios	
Component Ratio (CR)	0.869
Storage Ratio (SR)	0.965
Intermittency Ratio (IR)	0.234

This proposed microgrid has a component ratio near 1.0 and an intermittency ratio near zero. Using this information, the planner can easily recognize that this microgrid may not be a “good” grid citizen. Correspondingly, the planner could use this qualitative analysis to establish heuristics for evaluating attributes of the microgrid. One such heuristic is proposed in Figure C.2, where the planner might establish that an IR larger than +0.5 contributes to voltage support, while a IR less than +0.5 would adversely affect feeder voltage stability. Using simple heuristics and the plot of the ratios on the citizenship tool graph, the planner can quickly recognize that this proposed microgrid could cause large power reversals at the interconnection and contribute to a worse voltage profile on the weak feeder. However, a different microgrid system, or a combination of microgrids could yield aggregated ratios that would indicate to the system planner that they were better suited to supporting the weak feeder. In this way, the qualitative tool described above can assist in power system planning and analysis.

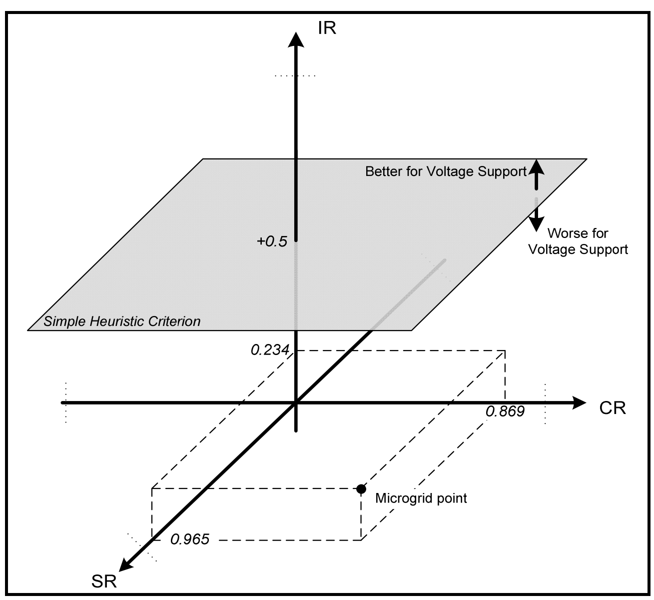

Figure C.2. Grid citizen plot of proposed microgrid and a sample heuristic criterion.

APPENDIX D

INTELLIGENT COMPUTATIONAL METHODS

Microgrids will exist in an environment where system elements are controlled through automated means by control entities that make decisions computationally. The information available for making decisions will be extensive and change rapidly in real-time. Therefore, microgrids will require viable and innovative techniques to manage their operations given the multi-objective, multi-constraint decision environment. In this chapter, two computational intelligence methods, particle swarm optimization (PSO) and ant colony optimization (ACO), are explored to aid the speed and computational efficiency for the microgrid power management problem.

D.1. Computational Challenges

The practice of decision-making is a very familiar process for humans. However, attempting to codify the decision-making process in a meaningful, efficient, and useful way is often very challenging. Subsequently, implementing effective autonomous decision-making for automated systems can be difficult. Additionally, implementation is complicated by the need to make judgments rapidly and to seek an ideal conclusion amongst a field of many options and factors. The microgrid power management system is an example of an automated decision-making framework that must comprehensively consider complex factors that affect a complex system.

Typically, when attempting to decide between simple options, say whether to purchase a bus ticket or walk to a destination, there is often more than a single factor that influences the decision. In this way, the travel choice via bus or on foot can be considered the "variable" which has two possibilities, or a "domain" of two. However, many related "constraints" may exist, such as: available change to pay the cost of the bus ticket, time allowed to reach the destination, etc. Assuming that decisions are made towards a certain goal or collection of goals, this interrelated combination of variables, their domains, and constraints are compiled according to the decision-making framework towards the development of a solution. In this broad context, the process of evaluating decision components and seeking the best solution available is incorporated within the extensive field of optimization analysis. In optimization, when objectives are described as mathematical formulations, a single or multiple objective functions may result. Although many possible solutions exist within the space of possibilities, the ultimate prize is the single solution that either "maximizes" or "minimizes" the objective function across all possible solutions. In other words, when an objective function is maximized or minimized, it has achieved the largest possible "satisfaction" for the decision-maker. In a local solution space, the solution that is the best of all local possibilities is considered the "local" best; the solution that is the very best of all possible solutions across the entire solution space is considered the "global" best.

Often, decision-making situations arise that require analysis of numerous competing objectives, simultaneously. The pursuit of an ideal solution given this more complex scenario is described as a multi-objective optimization, where the goal is to seek an optimal solution amidst many objectives. In such problems, the satisfaction of the objective functions becomes a combination of vector "maximizations" or "minimizations". However, in most cases, a global best of any particular individual objective function may not be a satisfactory solution for the remaining objectives [D.1].

Similar to economic systems, a Pareto optimum can be reached where the solution represents a state of satisfaction for one objective that cannot be raised further without lowering another objective's satisfaction. In other words, many "optimal" solutions exist when considering multiple objectives. The mathematical expression for this problem is shown in 4.8 . To illustrate this concept, consider two decision variables (x_1, x_2), three constraints (dashed lines), and two objective functions ($f_1(\vec{x})$, $f_2(\vec{x})$) shown in Figure D.1. A particular solution in the region of feasible solutions, shown on the top graph of Figure D.1, maps to the objective functions graph, projection shown by the dotted line to the bottom graph of Figure D.1, where the particular solution's relative achievement of each objective is shown. The Pareto front represents the combinational minimization of the two objective functions, shown by the dark line in Figure D.1. Along this front, $F(\vec{x})$ is at a minimum, where $F(\vec{x})=[f_1(\vec{x}), f_2(\vec{x})]$. It is noted that no direct method to derive the Pareto set of solutions is known.

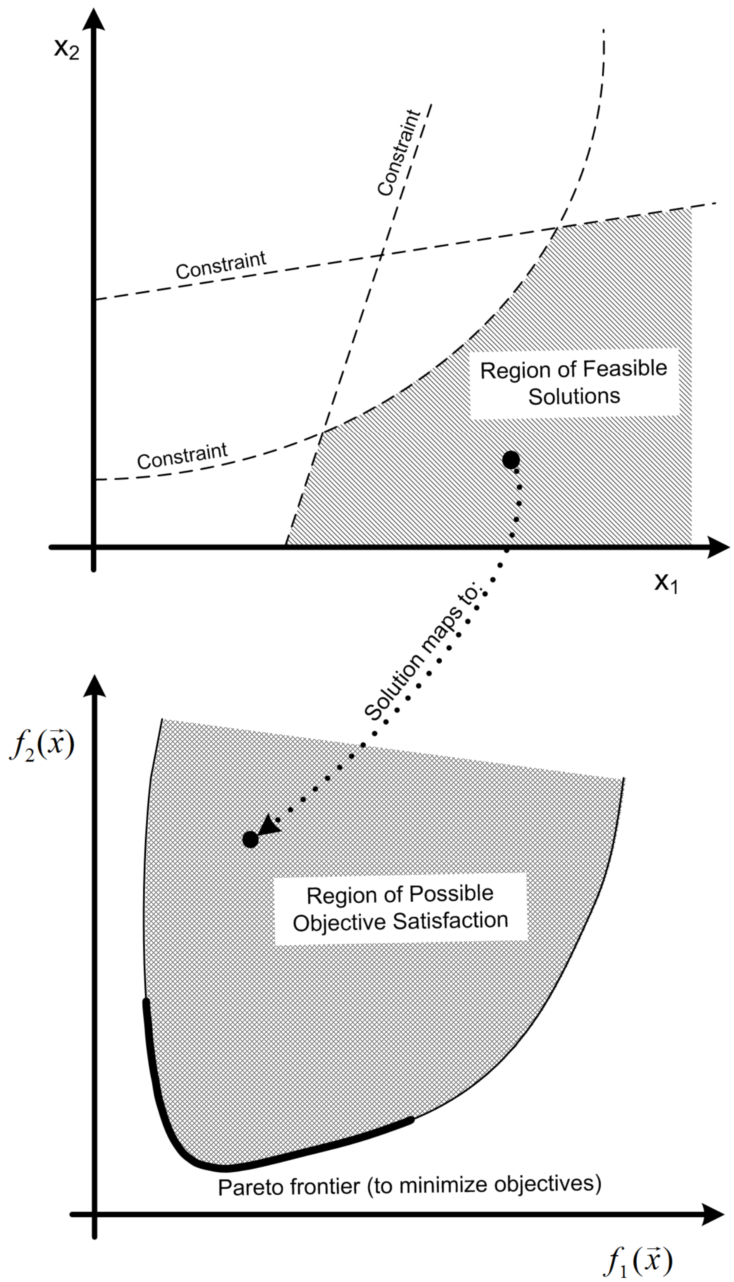

Figure D.1. Representation of a multi-objective, multi-constrait optimization problem and resulting Pareto frontier.

As is described above, there are no direct methods for developing the solution set that lies along the Pareto front. However, two primary formal mathematical techniques exist to derive Pareto solutions. The first technique involves aggregating the various objective functions into a single objective function expression [D.2]. In effect, by combining objective functions, the issues of simultaneously handling multiple objective functions is side-stepped. This technique is straight-forward, but requires the decision-maker to assign the relative weights of the constituent objective functions within the aggregation. It is noted that this is achievable and demonstrated in Chapter 6 using the input of the microgrid user. The second broad category for addressing multiple objectives involves the class of intelligent methods. The intelligent methods category incorporates a diverse range of techniques including: evolutionary, heuristic, and non-classical algorithms. The primary advantage of these intelligent methods is that they can address many objective functions simultaneously while requiring less computational resources to derive solutions in less time [D.3].

In Figure D.2, a survey of intelligent computational concepts is presented. While often considered “artificial intelligence”, computational intelligence methods encompass a broad array of subjects, clearly seen in Figure D.2. Additionally, a differentiation is made between what is considered a method or technique, and what is considered an implementation. An artificially intelligent application, such as a robot, may implement a computationally intelligent method, such as a fuzzy logic, in an algorithm operating on a computing platform, such as a field-programmable gate array (FPGA). While sometimes confusing, Figure D.2 attempts to hierarchically discriminate terminology.

For more than a decade, intelligent methods have proven themselves for a variety of computational challenges. Power management of microgrid operations clearly fits into the broad field of multi-objective optimization problems of interest today. The mathematical class of multi-objective optimization problems has not been proven to be solvable in strongly polynomial-time, or in other words, present verifiably global solutions rapidly. Because of the slower nature of traditional iterative techniques, alternative intelligent methods have shown promise. Ultimately, the interest in computational alternatives to traditional iterative techniques is manifested by the desire to derive near-optimum results in short periods of time [D.4]. Therefore, their application to microgrids for real-time power management is a ready area of challenge.

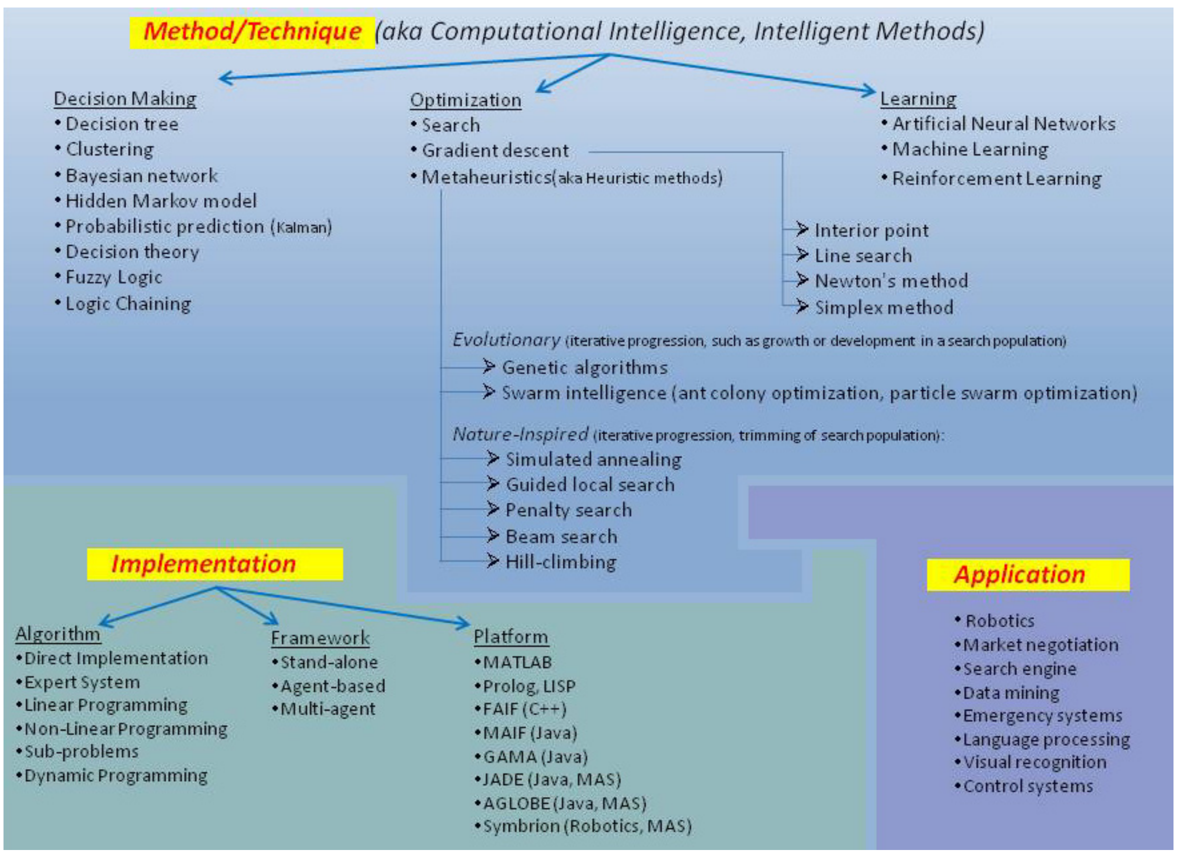

Figure D.2. Hierarchical classification of computational intelligence.

The formulation of the multi-objective, multi-constraint microgrid power management problem begins by identifying the desired attributes of the microgrid. These factors encompass many of the objectives currently sought by the power system, but go beyond conventional operations in many key ways. Inherently, these objectives are entirely dependent upon the relative importance to the consumer. Much of the prior chapters have been dedicated to this discussion; the remainder of this chapter presents how intelligent methods may be incorporated into microgrid decision-making.

To date, the majority of power system research applications utilizing intelligent computational methods have primarily investigated off-line problem solving [D.5, D.6, D.7, D.8, D.9, D.10, D.11, D.12, D.13]. This involves the use of computational resources to solve a problem, not in real-time, and have those solutions used later. These previous works have demonstrated the effectiveness of computational intelligence methods for power system application. For the microgrid PM&C, however, the desire was to build upon prior research to support the concept that these techniques can be used for both off-line and real-time applications. The ultimate advantage of applying intelligent methods to the microgrid power management problem is to capitalize on their most powerful demonstrated property: rapid convergence. That characteristic, coupled with the capability of computationally intelligent methods to handle multiple objectives simultaneously makes them of considerable interest for microgrid power management.

D.2. Metaheuristical Methods

This section seeks to introduce emerging computational techniques for application in agents of the microgrid PM&C architecture. Metaheuristical methods are a class of stochastically-based algorithms that combine certain degrees of randomization with local search capabilities to find quality solutions to difficult, complex, or large problems [D.14]. Specifically, two representative emerging intelligent methods, particle swarm optimization (PSO) and ant colony optimization (ACO) are presented.

D.2.1. Particle Swarm Optimization

For the purpose of introducing the topic of a commonly employed intelligent method, a brief description of particle swarm optimization is made here. The PSO computational method was inspired by biological social swarming behavior such as exhibited by birds flocking or fish schooling. Since its introduction in 1995, PSO has been shown as a powerful tool for solving many classes of problems including nonlinear optimization, control, and artificial intelligence [D.15, D.16, D.17, D.18]. PSO is amongst the heuristic class of intelligent methods and it shares many similarities with evolutionary computation techniques such as genetic algorithms (GA). However, PSO is easier and faster to implement PSO than GA in that the former does not have evolutionary operators such as crossover and mutation. Similar to other evolutionary algorithms, PSO requires a fitness evaluation function assesses each solution according to its value. At each iteration, the solution developed with the highest fitness value amongst all solutions thus far developed is retained as the global best. PSO is an iterative method, so the best retained solution at the end of assigned iterations is returned as final best solution.

The primary premise of PSO is the use of computational entities, referred to as particles here, which are distributed throughout the search space. Within the search space, each position location represents a solution to the posed problem. Each particle is initialized with a random position and random velocity. At each computational increment, the particles travel through the search space, checking the fitness of each position they traverse. They retain information about the best location (P_{best}) they have visited. Additionally, by communicating information about their search results to the total swarm of particles, the collective group can converge upon the globally best solution within the available possible solutions. At each increment in computation, each particle within the n-dimensional search space has their velocity accelerated towards the swarm's global best and the local particle's personal best position based on [D.18]:

$$v_j^{t+1} = \omega v_j^t + c_1 rand\left(P_{best,j} - s_j^t\right) + c_2 rand\left(G_{best} - s_j^t\right) \qquad \text{(D.1)}$$

where: v_j^t is the velocity of particle j at iteration t; c_1 and c_2 are weighting factors which can be fixed or changed during iterations; *rand* is a random number between 0 and 1, s_j^t is the current position of particle j at iteration t; $P_{best,j}$ is the personal best value of particle j so far; G_{best} is the swarm's best solution so far, ω is the inertial weight of the particle. Upon each successive iteration, the search position (s_j) of each particle is obtained by the following equation [D.18]:

$$s_j^{t+1} = s_j^t + v_j^{t+1} \qquad \text{(D.2)}$$

At the beginning of the search, the inertial weight of each particle within the swarm is large. This compels a greater emphasis on the randomly initialized particle velocities and causes greater exploration of the solution space. As the number of iterations increases, inertial values decrease allowing the particles to better converge on the "best" solution. The process for steering the particle particles as they travel through the search space according to (D.1) is illustrated in Figure D.3.

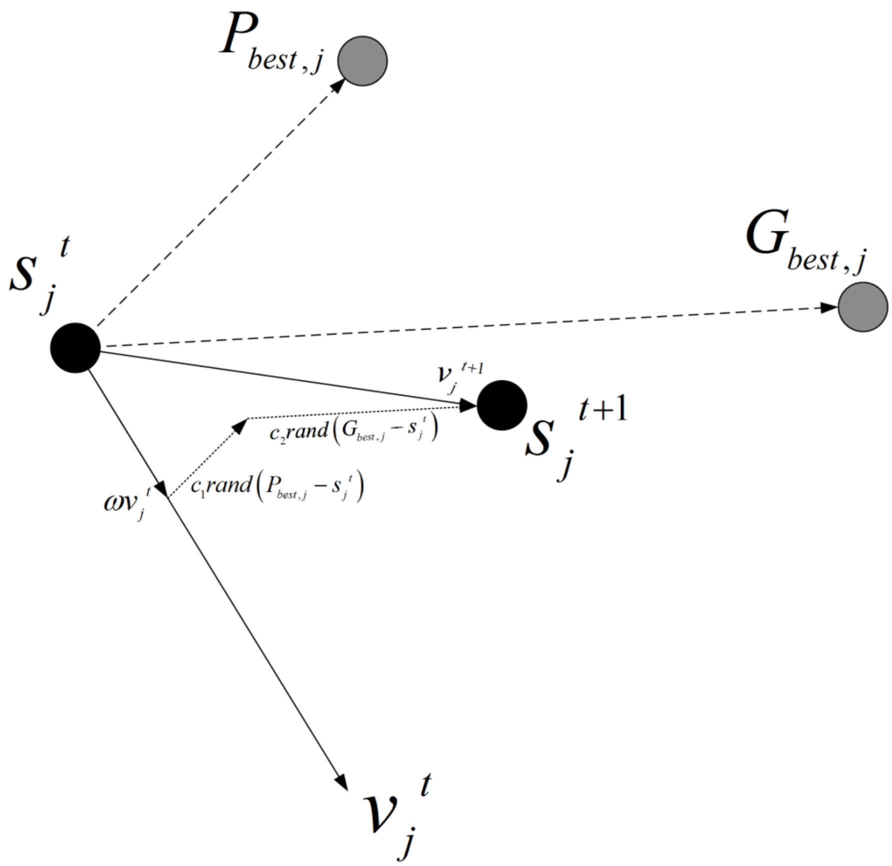

Figure D.3. PSO particle update.

As a computational technique, PSO is well-suited for handling multi-objective optimization problems. In the microgrid formulation, solutions that satisfy simultaneous objectives, and therefore define the Pareto optimal set, must be found from an expansive set of possibilities. The PSO algorithm, because of its strong search capabilities and quick convergence upon best solutions, can be used to rapidly find the Pareto set. These characteristics make it of keen interest for addressing the temporal demands imposed by performing microgrid power management in real-time. The PSO algorithm could be implemented into any microgrid agent for the purpose of finding a local solution rapidly.

D.2.1. Ant Colony Optimization

The ACO algorithm is also a nature-inspired metaheuristic optimization method, proposed by Dorigo, et al. [D.4], for solving NP-hard combinatorial optimization problems such as the benchmark traveling salesman problem (TSP), scheduling problems, subset problems, and a host of others. This intelligent computational technique is of particular interest because it has been shown to develop Pareto-optimal solutions with short time complexity [D.19]. Additionally, the ACO algorithm has been shown to outperform other general purpose optimization algorithms including genetic algorithms (GA) when applied to a number of benchmark combinatorial optimization problems, although this claim is widely interpretational [D.4]. The ACO algorithm has been investigated for power system-related applications, but exclusively for off-line computation only [D.5, D.8, D.20, D.21, D.22, D.23].

Within the ACO algorithm, colonies of artificial ants cooperate in a similar manner as PSO, to search the space of possible solutions to find the ones that are optimal. However, the framework for ACO is very different than PSO, as well as the use of heuristics to guide searching. The mathematical formulations for optimization problems are generally represented within ACO as construction graphs, where each node in the graph corresponds to a component of the solution. The goal is to find the solution with the minimum cost or distance path, which ultimately represents the best solution. Each ant "walks" on this graph and incrementally builds a solution. In this way, ACO is different from PSO in that at each computational increment, the PSO particle calculates the fitness of an actual problem solution. In ACO, each node represents an incremental part of the actual problem solution and it is not until after an ant has completed their "walk" that an actual solution is available. Modeled after real ants, the behavior of the artificial ants is governed by two primary factors: stigmergic tendency and random exploration. Stigmergy, or indirect communication facilitated by the environment, is accomplished in nature through the deposit of chemical pheromones. The pheromones reinforce good solutions and guide the search. For the ACO algorithm, a simulated ant uses artificial pheromones at each step in the construction graph, along with other problem specific heuristics, to randomly select the next solution component.

The algorithmic framework for ACO depends on the construction graph representation, is typically simplified as: $G = (N,A,C)$. For the graph G, the set of nodes $N = \{d_1,d_2, . . . ,d_n\}$ represents where path decisions must be made; the set of arcs $A =\{l_{ij}\}$ link the nodes i to j; and (optionally) $C = \{c_{ij}\}$ is the set of costs associated with arcs A. The elements of sets N and A are typically constrained. Depending on the particular problem formulation, the order of the solution sequence is not important. Figure D.4 shows an example of a construction graph that the ACO algorithm would attempt to solve. Nodes d_1 through d_3 are shown in Figure D.1, as well as how additional nodes (d_n) would be added to the construction graph. A complete path on the graph passes through each node once, contains a set of arcs (represented as dashed lines in Figure D.5), and is called a solution (s). The minimum cost path is called the best solution (s*) and is represented by the darkened arcs in Figure D.5 as the shortest complete path, and thus the best solution.

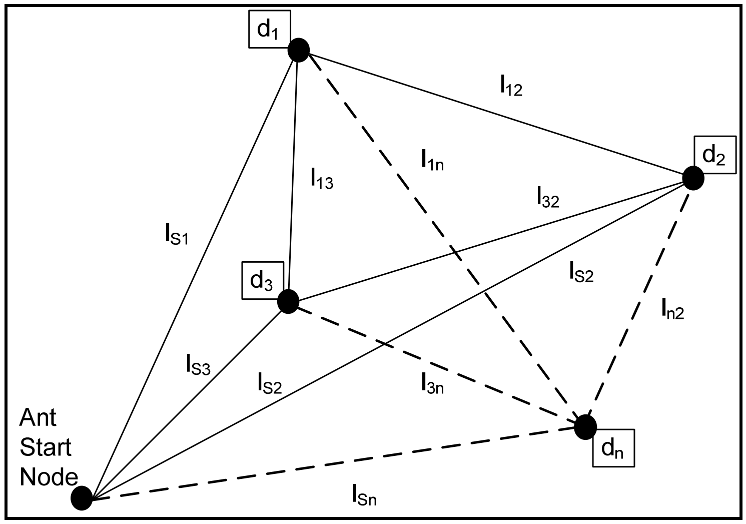

Figure D.4. Typical ACO construction graph.

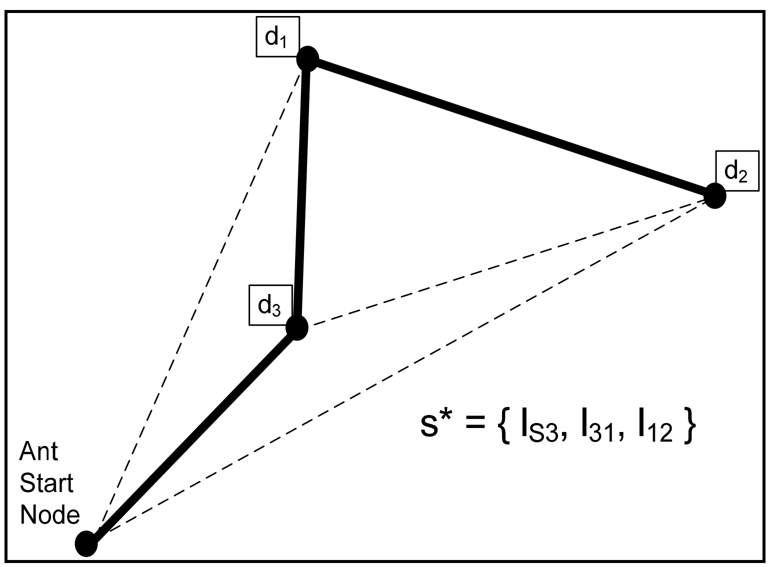

Figure D.5. Optimal solution (s*) representation.

The path an ant takes is constructed based on a probabilistic function. At each construction step, an ant must "choose" the next node to visit in pursuit of a complete solution. The probability of choosing node j from node i, is a combination of pheromone weighting and random exploration, expressed by:

$$p_{ij}^{k} = \frac{[\tau_{ij}]^{\alpha}[n_{ij}]^{\beta}}{\sum_{l \epsilon N_i^k}[\tau_{il}]^{\alpha}[n_{il}]^{\beta}} \tag{D.3}$$

where: τ_{ij} is the pheromone on arc ij, α is the pheromone weighting factor, n_{ij} is the heuristic value on arc ij, β is the heuristic weighting factor, and N_i is the feasible neighborhood of options for the ant, k, to traverse from node i. In addition to global heuristics that help improve the simulated ant's capabilities, pheromones associated with the construction graph are "deposited" on the arc chosen and globally "evaporate" over time. Pheromone decay on the construction graph arcs are accomplished by:

$$\tau_{ij}^{f} = (1-\rho)\tau_{ij}^{o} \tag{D.4}$$

where: $\tau_{ij}{}^{o}$ is the current step pheromone value on arc ij, $\tau_{ij}{}^{f}$ is the updated pheromone value on arc ij, and ρ is the decay factor. This combined effect allows for the artificial stigmergic effect which leads to better solution convergence.

As with PSO, there are numerous modifications to the ACO algorithm that can be made to allow customization for particular problems. Specific heuristics and factors such as the number of particles or ants per iteration, as well as the influence of inertia, pheromones, and decay affect the speed and accuracy of the solutions derived. In a similar manner to PSO, ACO can outperform gradient-based methods when faced with multi-objective optimization problems. The ants of ACO can find solutions that satisfy many simultaneous objectives rapidly and minimizing computational resources. As with PSO, the computational characteristics that make ACO attractive for deriving Pareto optimal solutions make it desirable for addressing the diverse objectives and constraints inherent to agent-based power management for the microgrids.

D.3. Example and Results

Using a three-asset microgrid framework, shown in Figure D.6, a centrally-based intelligent power management system was developed and evaluated. The purpose of this evaluation was to examine how an individual computational entity could handle a fairly complex optimization problem. Although the individual computational entity in this simulation is responsible for an entire microgrid, the use of the ACO metaheuristic is applicable to the optimization problem faced by an individual agent, described in the previous chapters.

By using information about generator characteristics, resource availability, and power demand, the ACO-based power management supervisor sought optimal dispatch solutions given two objectives: minimize environmental emissions and minimize the cost of generation. The primary constraints were dictated by the generator characteristics, power flow characteristics, and a 0.05 per unit deadband about the microgrid bus voltage, to which the customer load is connected. The customer load was modeled as a constant impedance; the changes in power consumed by the load were dictated in simulation by changing load current. The electrical configuration for the simple microgrid is shown in Figure D.7.

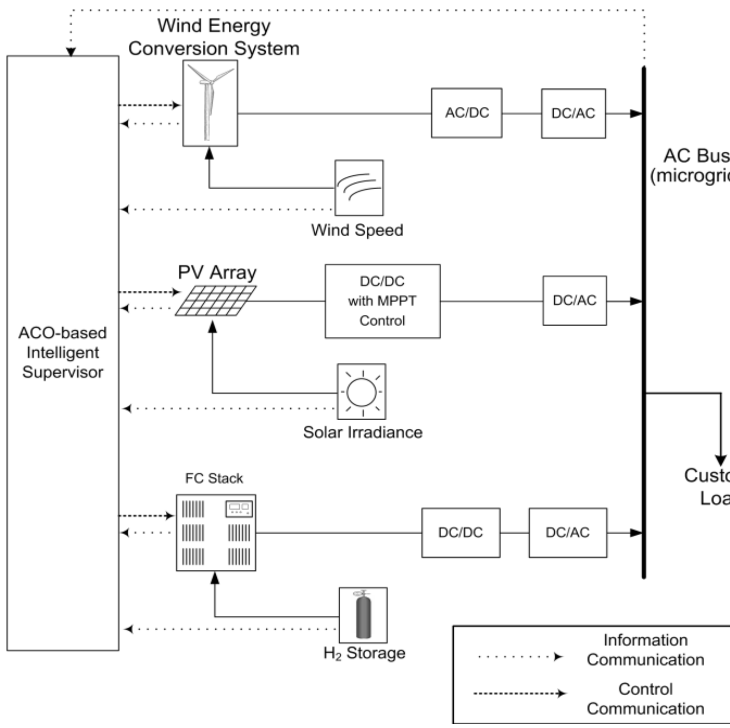

Figure D.6. Simulated microgrid and ACO-based power management supervisor.

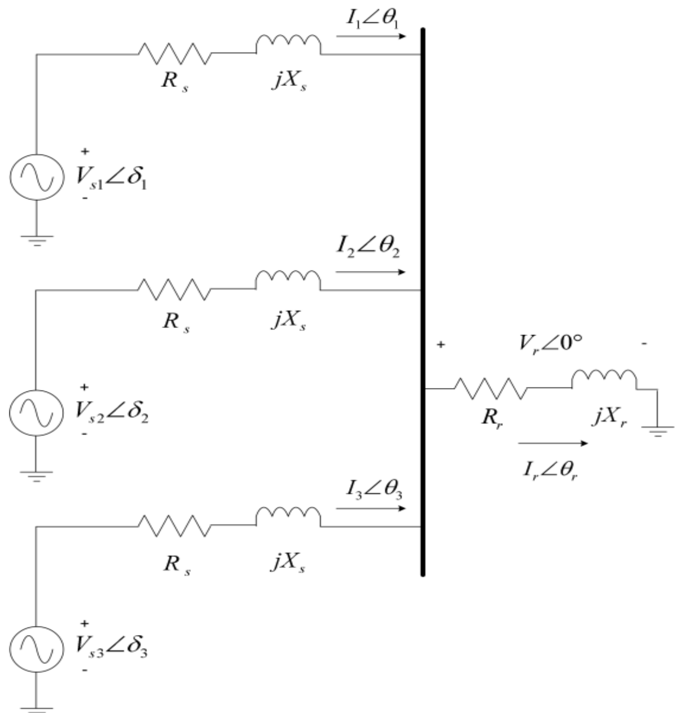

Figure D.7. Simulated three-generator microgrid electrical configuration.

The power management algorithm evaluated conditions on the microgrid every 30 seconds. At each sampling instant, the power management supervisor perceived power demand and the local conditions (e.g. wind speed and solar insolation) that dictated the ability of the renewable generators to produce power. Based on this information, the algorithm (within the sampling interval) developed and searched the construction graph for optimal dispatch solutions for the three microgrid generators. The mathematical formulation of the optimization problem is shown in equations (D.5-D.11), below:

Minimize:

$$\sum_m f_{1,m}(\sigma_m, V_m) = E_m \qquad \text{(D.5)}$$

$$\sum_m f_{2,m}(\mu_m, V_m) = C_m \tag{D.6}$$

Subject to:

$$V_{deadband}^{low} \leq V_r = Z_r I_r \leq V_{deadband}^{high} \tag{D.7}$$

Given:

$$I_1 + I_2 + I_3 - I_r = 0 \tag{D.8}$$

$$V_{sm} - V_r = Z_m I_m \tag{D.9}$$

$$Z_1 = Z_2 = Z_3 = Z_s \tag{D.10}$$

$$P_m = f_{p,m}(V_m) \tag{D.11}$$

where: m is the generator index, f_1 and f_2 are the objective functions, σ is the environmental impact factor, V is the nodal voltage, μ is the cost factor, Z is the component impedance, I is the branch current, and P is the instantaneous power generated by the generator, as determined by f_p. The voltage V_{sm} refers to the sending voltage of generator m; V_r refers to the receiving bus voltage to which the customer loads are connected; E_m is the environmental objective; and C_m is the cost objective. Both σ and μ factors are functions of the operating point of the given generator, e.g. the operating cost of the fuel cell is based on the fuel it consumes at a given output power.

Established by equations (D.5) through (D.11) and the known generator characteristics, the construction graph was formed, shown in Figure D.8. During the sampling interval, the ACO-based algorithm searched the construction graph for the optimal dispatch solution of each generator. The construction graph contained a node

($x_{sm,n}$; where, sm is the specific generator and n is the node index) for every possible variable assignment ($V_{n,sm}$). In other words, the construction graph represents the entire scope of available operating conditions for the microgrid, during a sampling interval; each node represents an operating point for an individual generator and its associated objective function values ($f_{1,sm}$ and $f_{2,sm}$). The graph is fully connected except for nodes of the same generator (e.g., $x_{s1,1}$ cannot be connected to $x_{s1,2}$). This prescribed constraint enforces the stipulation that only one instantiation for each variable (variable selection) is allowed in a solution set. For the microgrid power management formulation, this is analogous to selecting one operating point for an individual generator (it is invalid to select two or more operating points for the same generator). Only one generator operating characteristic was modeled for this example (e.g., voltage), but there is no limit to generator properties, such as frequency, that can be added as domains in this formulation. The ants walk the graph until a value has been selected for each variable, resulting in dispatch positions for each generator attached to the microgrid. Stigmergic information relating to the best solutions developed by colonies of ants was retained between sampling instances, although decayed over time, on the construction graph. This improved the ants' performance upon subsequent sampling intervals because lower fitness solutions were discriminated against. Although the search space is large, the constraints trim the construction graph preventing the inclusion of every possible variable assignment. It should be noted that not all nodal connections are indicated on the construction graph in Figure D.8 for clarity.

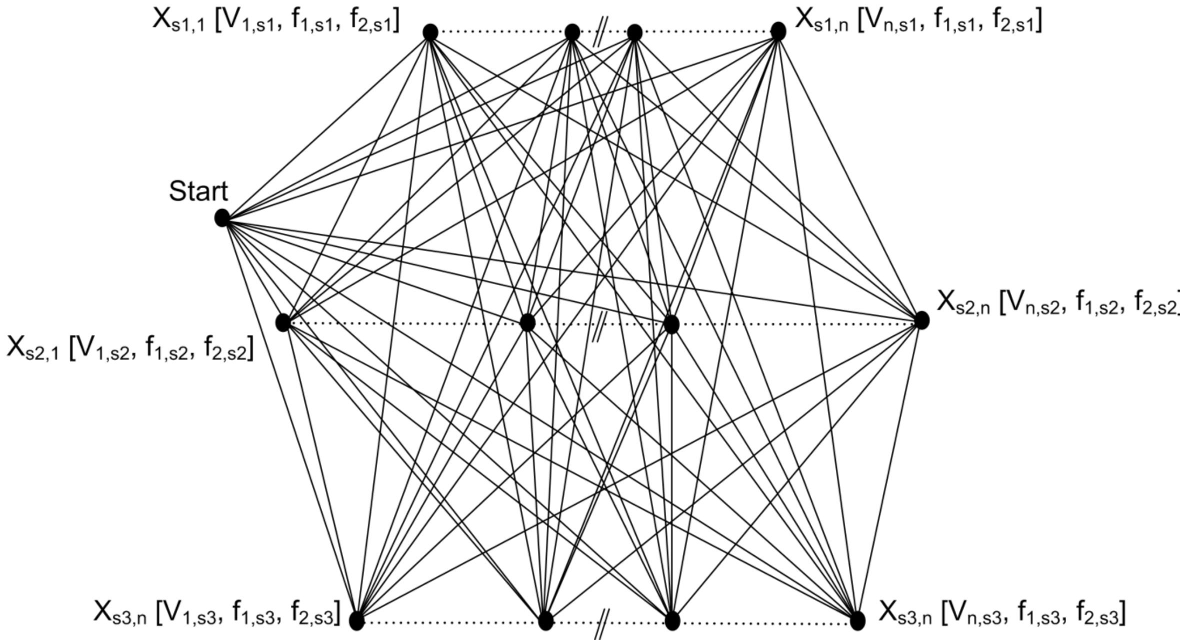

Figure D.8. Construction graph.

Using the ACO-based power management algorithm for the three-generator microgrid, Pareto-optimal dispatch solutions were developed during each sampling interval. A typical result based on the resource availability at a sampling instance is shown in Figure D.9. In Figure D.9, the power characteristic curves for each microgrid generator are shown, as well as the best operating power points for each generator selected by the power management algorithm after searching the construction graph. Results similar to those shown in Figure D.9 were produced during each sampling interval facilitating near real-time power management for the simulated microgrid.

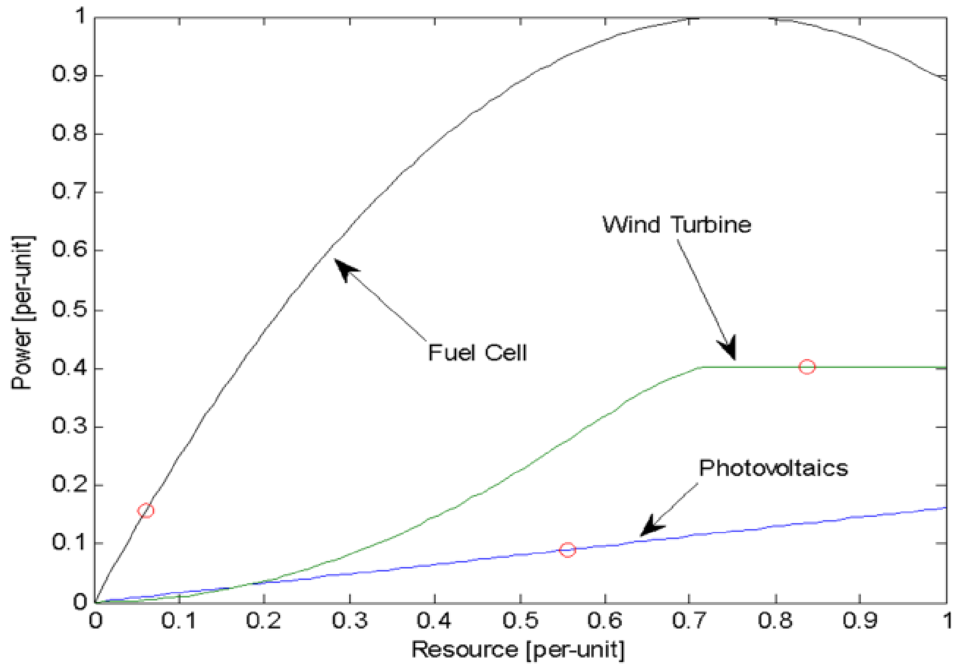

Figure D.9. Example results for dispatch based on available resources.

One of the primary reasons intelligent methods are of interest for microgrid multi-objective optimization is the desire to derive solutions quickly, facilitating real-time power management. Towards this goal, the ACO-based algorithm functioned well and after a series of experiments, its performance was characterized, as shown by Figure D.10 and Figure D.11. Simulation results show that in this case, there was not a direct correlation between increasing the computational resources (e.g. the number of ant colonies that search the construction graph) and the achievement of corresponding gains in finding better solutions. In other words, as shown by Figure D.10, given a fixed number of computational iterations, significant improvement in the satisfaction of the objectives was not achieved by utilizing more than 5-20 colonies of 50 ants. Simply put, the considerable additional time spent by more than 5-20 colonies of ants searching for better solutions does not show great benefit. This is not a new discovery [D.4] and supports the concept of tuning the algorithm for the particular application. Moreover, by using 5-20 colonies of 50 ants per colony, strong solutions for the microgrid power management problem could easily be derived within the 30-second sampling interval. This is important because the ability to find near-optimal solutions quickly represents a significant result towards achieving solutions truly in real-time.

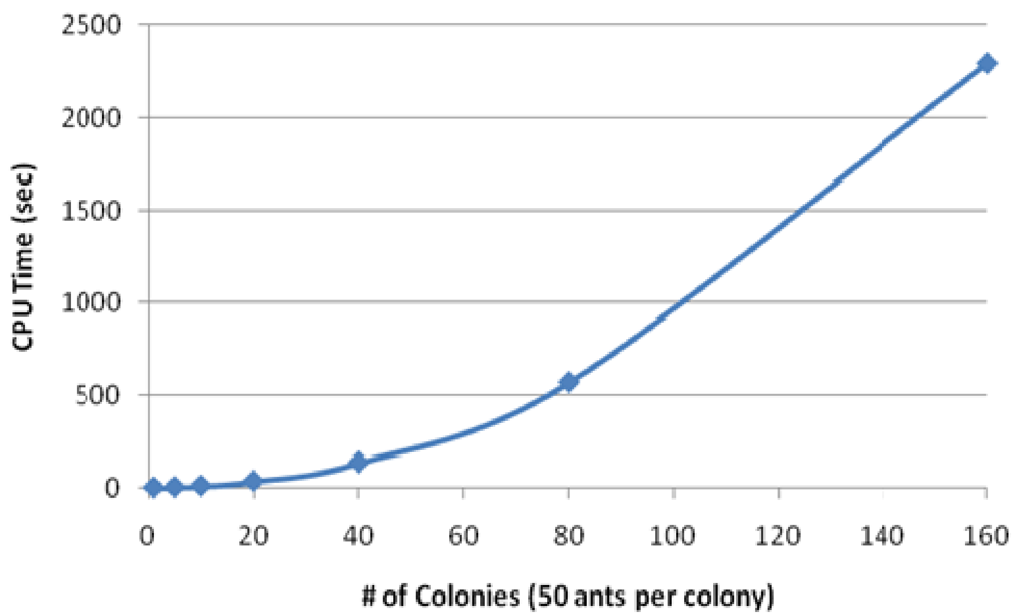

Figure D.10. Computation time required by increased numbers of algorithm colonies.

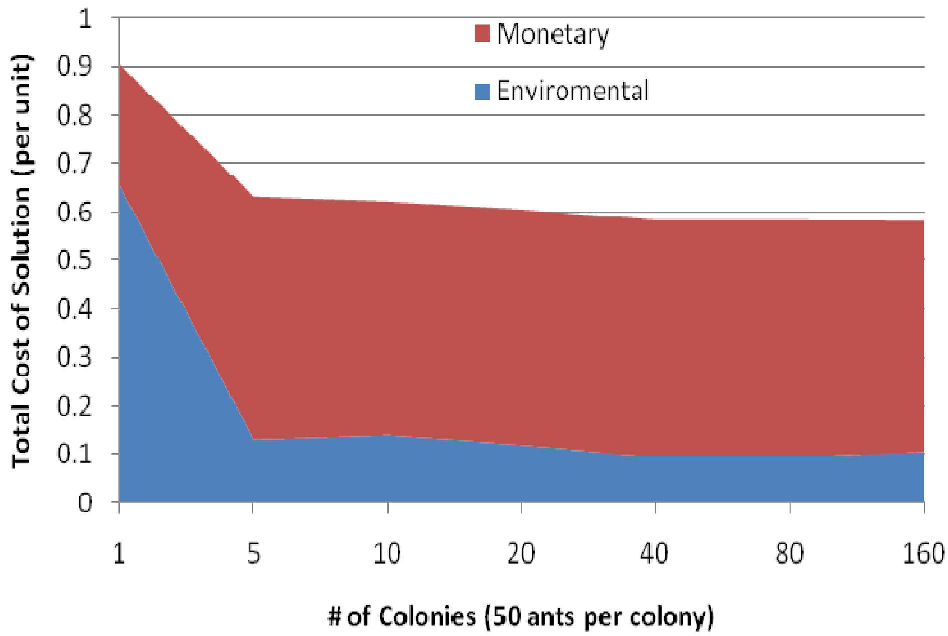

Figure D.11. Average performance (five runs) after a fixed number of iterations, varying the number of algorithm colonies.

D.4. Discussion

Even if approached from a centralized supervisory perspective that aggregates all microgrid information centrally, the multi-objective optimization problem for microgrid power management is not expected to be solvable in polynomial-time. Therefore, as the complexity and size of the search space broadens, along with the consideration of multiple objectives, computational techniques such as PSO and ACO are expected to perform significantly better than traditional gradient-based optimization methods. This is primarily because of the computational expense suffered by traditional means of solving optimization problems. For gradient-based methods, including Newton's method, the set of first-order partial derivatives of the objective function, called the Jacobian matrix, must be obtained. In some cases, the set of second-order partial derivatives, called the

Hessian matrix, or an approximation of it, must also be obtained. Finding the inverse of a matrix of appreciable size requires a significant amount of computational time and resource. On the other hand, computationally intelligent methods do not explicitly derive large matrix inverses because they remain within the search domain only. The result from attacking the optimization problem with ACO or PSO is a much more rapid convergence to a near-optimal solution, especially as the complexity of the microgrid problem grows.

In addition to computational burdens, when seeking a solution, gradient-based methods rely heavily on an initial guess of the solution. Correspondingly, they suffer from pitfalls which may lead them towards local best solutions rather than global best solutions. Alternatively, the general performance of the PSO and ACO algorithms is independent of the quality of particle or ant initialization. Inherent to intelligent methods are heuristical and stochastic terms that minimize the possibility of the search becoming fixed upon a solution that is not globally best.

For any computationally intelligent method, there will always be practical and theoretical tradeoffs that are incorporated into the algorithmic formulation. For example, the choice of how many ants per colony, or how many particles per stage, directly affects solution development. It is difficult to know, except through experience and educated-guessing how to best formulate the intelligent method for a particular problem. While these are practical considerations for the development of computationally intelligent methods, they offer the opportunity to tune the algorithms in more customizable ways than with traditional methods.

In this chapter, algorithmic details for two metaheuristic methods and their advantages over traditional gradient-based techniques have been shown, as well as the performance of a simulated microgrid implementation. The microgrid power management problem is complicated greatly by the demand for robust and rapid solutions. Ultimately, intelligent methods may offer the best opportunity to quickly derive "good enough" solutions that agents can use for microgrid power management. Regardless if the emphasis is on enhanced decentralized agent techniques, as in the previous chapters, or centralized techniques, the advantages of intelligent methods are clear. This opens the door for far more research into advanced microgrid agent designs that incorporate fast intelligent methods, such as the metaheuristics discussed in this chapter.

REFERENCES CITED

[D.1] Saul Gass, Linear Programming: Methods and Applications - 5th Edition, Dover Publications, Inc. 2003, pgs. 224-250.

[D.2] A. Osyczka, "Multicriteria optimization for engineering design", Design Optimization edited by J. Gero, Academic Press Inc., 1985.

[D.3] C.M. Fonseca and P.J. Fleming, "Multiobjective optimization and multiple constraint handling with evolutionary algorithms - Part I: a unified formulation", *IEEE Transactions on Systems, Man, and Cybernetics Part A:Systems and Humans*, Vol. 28, No. 1, Jan 1998.

[D.4] M. Dorigo and T. Stutzle, Ant Colony Optimization. MIT Press, 2004.

[D.5] P. Korosec and J. Silc, "The distributed multilevel ant-stigmergy algorithm used at the electric-motor design" *Engineering Applications of Artificial Intelligence*, Vol. 21, No. 6, September 2008.

[D.6] M. Lopez-Ibanez, T.D. Prasad, and B. Paechter, "Ant colony optimization for optimal control of pumps in water distribution networks" *Journal of Water Resources Planning and Management*, Vol. 134, No. 4, July/August 2008.

[D.7] S.K. Chaharsooghi and A.H. Meimand Kermani, "An effective ant colony optimization algorithm (ACO) for multi-objective resource allocation problem (MORAP)", *Applied Mathematics and Computation*, Vol. 200, No. 1, Jun 15, 2008.

[D.8] A. Ahuja, S. Das, and A. Pahwa. "An AIS-ACO Hybrid Approach for Multi-Objective Distribution System Reconfiguration", *IEEE Transactions on Power Systems,* Vol. 22, No. 3, August 2007.

[D.9] H. Bai, P. Zhang, and V. Ajjarapu, "A novel parameter identification approach via hybrid learning for aggregate load modeling", *IEEE Transactions on Power Systems*, Vol. 24, No. 3, 2009.

[D.10] P. Maghouli, S. H. Hosseini, M.O. Buygi, and M. Shahidehpour, "A multi-objective framework for transmission expansion planning in deregulated environments", *IEEE Transactions on Power Systems*, Vol.24, No.2, 2009.

[D.11] Y. Yare, G.K. Venayagamoorthy, and U.O. Aliyu, "Optimal generator maintenance scheduling using a modified discrete PSO", *IET Generation, Transmission & Distribution*, Vol. 2, No. 6, Nov. 2008.

[D.12] A.H. Shahirinia, A. Hajizadeh, and A.R. Moghaddamjoo, "Genetic-based size optimization of renewable energy sources", *International Journal of Power and Energy Systems*, Vol. 28, No. 3, 2008.

[D.13] A. Pregelj, M. Begovic, and A. Rohatgi, "Recloser allocation for improved reliability of DG-enhanced distribution networks", *IEEE Transactions on Power Systems*, Vol. 21, No. 3, August 2006.

[D.14] X. Yang. Nature-Inspired Metaheuristic Algorithms (Second Edition). Luniver Press, Frome, U.K., 2010.

[D.15] K.Y. Lee and M.A. El-Sharkawi, Modern Heuristic Optimization Techniques – Theory and Application to Power Systems, IEEE Press, Piscataway, NJ, 2008.

[D.16] J. Kennedy and R.C. Eberhart, "Particle Swarm Optimization," *Proceedings, 1995 IEEE Conference on Neural Networks*, Vol. 4, 1995.

[D.17] X. Hu, R. Eberhart, and Y. Shi. "Recent advances in particle swarm", *Proceedings from the IEEE Congress on Evolutionary Computation* , 2004.

[D.18] Maurice Clerc, Particle Swarm Optimization, Wiley, 2008.

[D.19] B. Fox, W. Xiang, and H.P. Lee, "Industrial applications of the ant colony optimization algorithm", *International Journal of Advanced Manufacturing Technology*, Vol. 31, No. 7-8, January 2007.

[D.20] E. Carpaneto, "Distribution system minimum loss reconfiguration in the Hyper-Cube Ant Colony Optimization framework", *Electric Power Systems Research*, Vol. 78, No. 12, Dec. 2008.

[D.21] W. Tippachon and D. Rerkpreedapong, "Multiobjective optimal placement of switches and protective devices in electric power distribution systems using ant colony optimization", *Electric Power Systems Research*, Vol. 79, No. 7, July 2009.

[D.22] L. Wang & C. Singh, "Reliability-constrained optimum placement of reclosers and distributed generators in distribution networks using an ant colony system algorithm", *IEEE Transactions on Systems, Man and Cybernetics Part C (Applications & Review)*, Vol. 38, No. 6, Nov. 2008.

[D.23] Chung-Fu Chang, "Reconfiguration and capacitor placement for loss reduction of distribution systems by ant colony search algorithm", *IEEE Transactions on Power Systems*, Vol. 23, No. 4, Nov. 2008.

APPENDIX E

AUTHOR PEER-REVIEWED PUBLICATIONS

The following annotates peer-reviewed publications by the author that have been used in the preparation of this dissertation.

Journal publications

C. Colson and M. Nehrir, "Comprehensive Real-Time Microgrid Power Management & Control with Distributed Agents", *IEEE Transactions on Smart Grid–Special Issue*, July 2012, revised and submitted for final review.

C. Colson, M. Nehrir, R. Sharma, & B. Asghari, "Improving Sustainability of Hybrid Energy Systems - Part I: Incorporating Battery Round-trip Efficiency & Operational Cost", *IEEE Transaction on Sustainable Energy*, submitted Sept 2012.

C. Colson, M. Nehrir, R. Sharma, & B. Asghari, "Improving Sustainability of Hybrid Energy Systems - Part II: Managing Multiple Objectives with a Multi-agent System", *IEEE Transactions on Sustainable Energy*, submitted Sept 2012.

C. Colson and M. Nehrir, "Evaluating the Benefits of a Hybrid Solid Oxide Fuel Cell Combined Heat & Power Plant for Energy Sustainability and Emissions Avoidance", *IEEE Transactions on Energy Conversion*, Vol. 26, Iss. 1, March 2011.

S. Pourmousavi, M. Nehrir, C. Colson, & C. Wang, "Real-Time Energy Management of a Stand-Alone Hybrid Wind-MT System Using Particle-Swarm Optimization", *IEEE Transactions on Sustainable Energy*, Vol. 1, Iss. 3, Oct 2010.

C. Colson, M. Nehrir, M. Deibert, M. Amin, & C. Wang, "Efficiency Evaluation of Solid-Oxide Fuel Cells in Combined Cycle Operations", *ASME Journal of Fuel Cell Science and Technology*, Vol. 6, Iss. 2, Feb 2009.

W. Rickerson and C. Colson, "Montana firefighters see benefit of PV", *Renewable Energy Focus*, Elsevier Ltd., Kidlington, GB, Vol. 8, Iss. 6, Nov. 2007.

Conference publications

C. Colson, M. Nehrir, and R. Gunderson, "Distributed Multi-Agent Microgrids: A Decentralized Approach to Resilient Power System Self-healing", *Proceedings of the International Symposium on Resilient Control Systems*, August 2011.

C. Colson, M. Nehrir, and R. Gunderson, "Multi-agent Microgrid Power Management", *Proceedings of the International Federation of Automatic Control (IFAC) World Congress*, August 2011.

C. Colson and M. Nehrir, “Agent-based Power Management of Microgrids including Renewable Energy Power Generation”, *Proceedings of the IEEE Power & Energy Society General Meeting*, July 2011.

C. Colson and M. Nehrir, “Algorithms for Distributed Decision-Making for Multi-agent Microgrid Power Management”, *Proceedings of the IEEE Power & Energy Society General Meeting*, July 2011.

S.A.P. Kani, M.H. Nehrir, C. Colson, and C. Wang, “Real-time energy management of a stand-alone hybrid wind-microturbine energy system using PSO”, *Proceedings of the IEEE Power & Energy Society General Meeting*, July 2011.

C. Colson and M. Nehrir, “Load-following for Wind Turbines with Permanent Magnet Synchronous Generators”, *Proceedings of the 42nd North American Power Symposium*, October 2010.

J. Wilson and C. Colson, “Cost and Unit-sizing Analysis of a Hybrid SOFC/Microturbine Generation System for Residential Loads”, *Proceedings of the 42nd North American Power Symposium*, October 2010.

C. Colson, M. Nehrir, and S. Pourmousavi, “Towards Real-time Microgrid Power Management using Computational Intelligence Methods”, *Proceedings of the IEEE Power & Energy Society General Meeting*, July 2010.

C. Colson and M. Nehrir, “An Alternative Method to Load Modeling for Obtaining End-Use Load Profiles”, *Proceedings of the 41st North American Power Symposium*, Sept 2009.

C. Colson and M. Nehrir, “A Review of Challenges to Real-Time Power Management of Microgrids”, *Proceedings of the IEEE PES General Meeting*, July 2009.

C. Wang, C. Colson, M. Nehrir, & J. Li. “Power Management of a Stand-Alone Hybrid Wind-MT Distributed Generation System”, *Proceedings of the IEEE Power Electronics & Machines in Wind Applications*, June 2009.

C. Colson, M. Nehrir, C. Wang, “Ant Colony Optimization for Microgrid Multi-Objective Power Management”, *Proceedings of the IEEE PES Power Systems Conference*, March 2009.

C. Colson, C. Wang, M. Nehrir, S. Guda, & J. Li, “Stand-alone Hybrid Wind-Microturbine Distributed Generation System: A Case Study”, *Proceedings of the 39th North American Power Symposium*, August 2007.